

OPEN ACCESS

A holographic map of action onto entropy

To cite this article: D Acosta *et al* 2012 *J. Phys.: Conf. Ser.* **361** 012027

View the [article online](#) for updates and enhancements.

You may also like

- [Urea oxidation in a paper-based microfluidic fuel cell using *Escherichia coli* anode electrode](#)
L C Castillo-Martínez, D M Amaya-Cruz, J Gachuz et al.
- [Optical fibres for a mini-dish/Stirling system: thermodynamic optimization](#)
O A Jaramillo and J A del Río
- [Consequences of a generalized Ohm's law for magnetic transport in conducting media](#)
S Cuevas, J A del Río and M López de Haro

PRIME
PACIFIC RIM MEETING
ON ELECTROCHEMICAL
AND SOLID STATE SCIENCE

HONOLULU, HI
Oct 6–11, 2024

Abstract submission deadline:
April 12, 2024

Learn more and submit!

Joint Meeting of
The Electrochemical Society
•
The Electrochemical Society of Japan
•
Korea Electrochemical Society

A holographic map of action onto entropy

D Acosta^{1,a}, P Fernández de Córdoba^{2,b}, J M Isidro^{2,c}, J L G Santander^{3,d}

¹Departamento de Matemáticas, Universidad de Pinar del Río, Pinar del Río, Cuba

²Instituto Universitario de Matemática Pura y Aplicada, Universidad Politécnica de Valencia, Valencia 46022, Spain

³Cátedra Energesis de Tecnología Interdisciplinar, Universidad Católica de Valencia, Guillem de Castro 94, Valencia 46003, Spain

E-mail: ^adago@mat.upr.edu.cu

E-mail: ^bpfernandez@mat.upv.es

E-mail: ^cjoissan@mat.upv.es

E-mail: ^dmartinez.gonzalez@ucv.es

Abstract. We propose a holographic correspondence between the action integral I describing the mechanics of a finite number of degrees of freedom in the bulk, and the entropy S of the boundary (a holographic screen) enclosing that same volume. The action integral must be measured in units of (i times) Planck's constant, while the entropy must be measured in units of Boltzmann's constant. In this way we are led to an intriguing relation between the second law of thermodynamics and the uncertainty principle of quantum mechanics.

1. Introduction

There are compelling reasons to believe that quantum mechanics must be an emergent phenomenon [2, 10, 11, 14, 15, 18, 19, 20, 21, 23, 24]. Actually not just quantum mechanics, but also gravity and spacetime appear to be emergent phenomena as well (for a comprehensive review see [31] and refs. therein). The guiding principle in all emergent theories is the fact that they provide a coarse-grained description of some underlying theory [9]. Due to our ignorance of a full microscopic description, emergent phenomena are in principle amenable to a thermodynamical description.

It is the purpose of this contribution to develop an approach to emergent quantum mechanics from the *entropic* point of view presented in ref. [1]. We take the view that, apart from other important reasons [3, 16, 25, 26, 28, 29, 32], quantum theory must be an emergent phenomenon *also* because the spacetime it is defined on is an emergent concept. There exist in the literature a number of different approaches to account for the emergent nature of spacetime, too numerous to quote here in detail. Here we will follow the holographic [22, 34] proposal presented in ref. [35]. Thus gravity and quantum mechanics share the common feature of being effective, thermodynamical descriptions of their respective underlying theories.

We should point out that quantum mechanics can be recast in thermodynamical terms [30], although without making use of the properties of emergence and holography used here. On the contrary, our approach hinges crucially on the notions of emergence and holography.

Altogether, our approach will provide us with a *holographic, entropic picture of emergent quantum mechanics*.

2. The correspondence

2.1. The main result

Our main result can be summarised in the holographic correspondence

$$\text{(bulk)} \frac{iI}{\hbar} \leftrightarrow \frac{S}{k_B} \text{(boundary)}. \quad (1)$$

This correspondence can be explained as follows. Let a finite 3-dimensional volume \mathcal{V} be given, such that it is bounded by a closed 2-dimensional surface \mathcal{S} (a holographic screen, see [35]). Let a finite number of quantum-mechanical degrees of freedom be defined within \mathcal{V} , described by the action integral I . The screen \mathcal{S} is assumed to carry N information bits. These bits encode the holographic projection, onto \mathcal{S} , of the degrees of freedom within \mathcal{V} . Since we do not know the specific mechanism whereby the holographic principle projects the mechanics within \mathcal{V} onto its boundary $\mathcal{S} = \partial\mathcal{V}$, we assign the screen an entropy S , which measures our ignorance about the specific nature of the degrees of freedom on the surface. Thus I describes a mechanical system in the bulk, while S describes its corresponding thermodynamics on the boundary. In this setup, space merely plays the role of a *storage device for information*; space has already emerged within \mathcal{S} , while it does not yet exist outside \mathcal{S} [35]. It will be observed that each side of the dimensionless correspondence (1) is measured in units of the corresponding quantum—the quantum of action (Planck’s constant \hbar) on the mechanical side, the quantum of entropy (Boltzmann’s constant k_B) on the thermodynamical side. Finally, there is a relative factor of i , whose origin will be elucidated presently. For the moment we note that the semiclassical limit $\hbar \rightarrow 0$ in the bulk corresponds to letting $k_B \rightarrow 0$ on the boundary. Last but not least, the two quantities I and S separately obey a corresponding extremum principle. Eqn. (1) differs from an ana! logous correspondence, presented in [1], by a factor of 2, to be explained later.

2.2. A quantum of entropy

The starting point in ref. [35] is a classical point particle of mass M approaching a holographic screen \mathcal{S} , from that side of the latter on which spacetime has already emerged. At a distance from \mathcal{S} equal to 1 Compton length, the particle causes the entropy S of the screen to increase by the amount

$$\Delta S = 2\pi k_B, \quad (2)$$

where k_B is Boltzmann’s constant. The above can also be understood as meaning that $2\pi k_B$ is the *quantum* by which the entropy of the screen increases, whenever a particle crosses \mathcal{S} . The factor 2π on the right-hand side is conventional. Relevant is only the fact that the entropy increase of the screen appears quantised in units of k_B .

2.3. Two thermodynamical languages

Thermodynamics can be conveniently expressed in either of two equivalent languages, respectively called the energy representation and the entropy representation [8]. Any given thermodynamical system can be completely described if one knows its *fundamental equation*. The latter contains all the thermodynamical information one can obtain about the system. The fundamental equation can be expressed in either of two equivalent ways, respectively called the *energy representation* and the *entropy representation*. In the energy representation one has a fundamental equation $E = E(S, \dots)$, where the energy E is a function of the entropy S , plus of whatever additional variables may be required. In the entropy representation one solves for the entropy in terms of the energy to obtain a fundamental equation $S = S(E, \dots)$.

Here we will argue that quantum mechanics as we know it (*i.e.*, on spacetime) corresponds to the energy representation, while quantum mechanics on a holographic screen (*i.e.*, in the absence of spacetime) will correspond to the entropy representation. Our goal is to describe the laws of *entropic quantum mechanics*, that is, the thermodynamical laws on the boundary \mathcal{S} that correspond to the quantum mechanics within $\mathcal{S} = \partial\mathcal{V}$.

One must bear in mind, however, that standard thermodynamical systems admit both representations (energy and entropy) simultaneously, which representation one uses being just a matter of choice. In our case this choice is dictated, for each fixed observer, by that side of the screen on which the observer wants to study quantum mechanics. For example there is no energy variable beyond the screen, as there is no time variable, but an observer can assign the screen an entropy, measuring the observer's ignorance of what happens beyond the screen. This notwithstanding, the analogy with thermodynamical systems we have just sketched can be quite useful.

2.4. A (classical) holographic dictionary

Assume that we are given a foliation of 3-space by 2-dimensional holographic screens \mathcal{S}_j : $R^3 = \cup_{j \in \mathcal{J}} \mathcal{S}_j$, where the index j runs over some (continuous) set \mathcal{J} . For reasons to be explained presently we will restrict our attention to potentials such that the \mathcal{S}_j are all closed surfaces; we denote the finite volume they enclose by \mathcal{V}_j , so $\partial\mathcal{V}_j = \mathcal{S}_j$.

One can formulate a *holographic dictionary* between gravitation, on the one hand, and thermodynamics, on the other [35]. Let V_G denote the gravitational potential created by a total mass $M = \int_{\mathcal{V}} d^3V \rho_M$ within the volume \mathcal{V} . Then the following two statements are equivalent: *i*) there exists a gravitational potential V_G satisfying Poisson's equation $\nabla^2 V_G = 4\pi G \rho_M$, such that a test mass m in the background field created by the mass distribution ρ_M experiences a force $\mathbf{F} = -m\nabla V_G$;

ii) given a foliation of 3-space by holographic screens, $R^3 = \cup_{j \in \mathcal{J}} \mathcal{S}_j$, there are two scalar quantities, called entropy S and temperature T , such that the force acting on a test mass m is given by $F\delta x = \int_{\mathcal{S}} T \delta dS$. The latter integral is taken over a screen that does not enclose m . Moreover, the thermodynamical equivalent of the gravitational theory includes the following *dictionary entries* [35]:

$$\frac{1}{k_B} S(x) = \frac{-1}{4\hbar c L_P^2} V_G(x) A(V_G(x)), \quad (3)$$

$$2\pi k_B T(x) = \frac{dV_G}{dn}, \quad (4)$$

$$\frac{k_B}{2} \int_{\mathcal{S}} d^2a T = L_P^2 M c^2. \quad (5)$$

In (3), (4) and (5) we have placed all thermodynamical quantities on the left, while their mechanical analogues are on the right. As in ref. [35], the area element d^2a on \mathcal{S} is related to the infinitesimal number of bits dN on it through $d^2a = L_P^2 dN$. We denote the area of the equipotential surface passing through the point x by $A(V_G(x))$, while dV_G/dn denotes the derivative of V_G along the normal direction to the same equipotential. The above expressions tell us how, given a gravitational potential $V_G(x)$ and its normal derivative dV_G/dn , the entropy S and the temperature T can be defined *as functions of space*.

Specifically, eqn. (3) expresses the proportionality between the area A of the screen \mathcal{S} and the entropy S it contains. This proportionality implies that gravitational equipotential surfaces get translated, by the holographic dictionary, as *isoentropic surfaces*, above called holographic screens \mathcal{S} .

Equation (4) expresses the Unruh effect: an accelerated observer experiences the vacuum of an inertial observer as a thermal bath at a temperature T that is proportional to the observer's acceleration dV_G/dn .

Finally, eqn. (5) expresses the first law of thermodynamics and the equipartition theorem. The right-hand side of (5) equals the total rest energy of the mass enclosed by the volume \mathcal{V} , while the left-hand side expresses the same energy content as spread over the bits of the screen $\mathcal{S} = \partial\mathcal{V}$, each one of them carrying an energy $k_B T/2$. It is worthwhile noting that equipartition need not be postulated. Starting from (4) one can in fact prove the following form of the equipartition theorem [1]:

$$\frac{k_B}{2} \int_{\mathcal{S}} d^2a T = \frac{A(\mathcal{S})}{4\pi} U(\mathcal{S}), \quad A(\mathcal{S}) = \int_{\mathcal{S}} d^2a. \quad (6)$$

Above, U can be an arbitrary potential energy, subject only to the requirement that its equipotential surfaces are closed. We will henceforth mean eqn. (6) when referring to the first law and the equipartition theorem. In all the above we are treating the area as a continuous variable, but in fact it is quantised [35]. If $N(\mathcal{S})$ denotes the number of bits of the screen \mathcal{S} , then

$$A(\mathcal{S}) = N(\mathcal{S})L_P^2. \quad (7)$$

However, in the limit $N \rightarrow \infty$, when $\Delta N/N \ll 1$, this approximation of the area by a continuous variable is accurate enough. We will see later on that letting $N \rightarrow \infty$ is equivalent to the semiclassical limit in quantum mechanics.

3. The emergence of quantum mechanics

We intend to write a holographic dictionary between quantum mechanics, on the one hand, and thermodynamics, on the other. This implies that we will need to generalise eqns. (3), (4) and (6) so as to adapt them to our quantum-mechanical setup. Thus we will replace the classical particle of [35] with a quantum particle, subject to some potential energy U of nongravitational origin, but we will take (2) to hold for a quantum particle as well. We will assume U to be such that its equipotential surfaces \mathcal{S}_j are closed, in agreement with our assumptions about the foliation. Let $H = K + U$ be the classical Hamiltonian function on R^3 whose quantisation leads to the quantum Hamiltonian operator $\hat{H} = \hat{K} + \hat{U}$ that governs our quantum particle.

3.1. A (quantum) holographic dictionary

Inside the screen, spacetime has already emerged. This gives us the energy representation of quantum mechanics—the one we are used to: a time variable with a conserved Noether charge, the energy, and wavefunctions depending on the spacetime coordinates. We have the uncertainty relation

$$\Delta\hat{Q} \Delta\hat{P} \geq \frac{\hbar}{2}. \quad (8)$$

Expectation values are computed as functional integrals, with a density function d_I given by

$$d_I = \exp\left(\frac{i}{\hbar} I\right). \quad (9)$$

Above, $I = \int dt L$ is the action integral satisfying the Hamilton–Jacobi equation.

We can now posit the quantum-mechanical analogues of eqns. (3), (4) and (6). In the energy representation these analogues read, respectively,

$$\frac{1}{k_B} \hat{S}(x) = \frac{1}{4\hbar c L_P} A(U(x)) |\hat{U}(x)|, \quad (10)$$

$$2\pi k_B \hat{T}(x) = L_P \frac{d\hat{U}}{dn}, \quad (11)$$

$$\frac{k_B}{2} \int_{\mathcal{S}} d^2 a \hat{T} = \frac{A(\mathcal{S})}{4\pi} \hat{U}(\mathcal{S}). \quad (12)$$

3.2. Emergence of the holographic correspondence

It is well known, in the theory of thermodynamical fluctuations, that the probability density function d_S required to compute expectation values of thermodynamical quantities is given by the exponential of the entropy [8]:

$$d_S = \exp\left(\frac{S}{k_B}\right). \quad (13)$$

Comparing (13) with (9) we arrive at the holographic correspondence (1)

$$\frac{iI}{\hbar} \leftrightarrow \frac{S}{k_B} \quad (14)$$

between the energy representation and the entropy representation.

We would like to point out that an analogous correspondence has been given in [1], the only difference being a factor of 2 in the denominator on the right-hand side. This factor of 2 is easy to account for. In [1], one compares the semiclassical wavefunction in the energy representation, given by $\psi = \exp(iI/\hbar)$, with the square root of the probability density function d_S in the entropy representation, given by $\sqrt{d_S} = \exp(S/2k_B)$. Instead, here we are equating the probability densities d_I and d_S rather than the wavefunctions. See refs. [4, 5] for specific instances of the correspondence (14).

3.3. Emergence of the wavefunction

The equation $U(x^1, x^2, x^3) = U_0$, where U_0 is a constant, defines an equipotential surface in R^3 . As U_0 runs over all its possible values, we obtain a foliation of R^3 by equipotential surfaces. Following [35], we will identify equipotential surfaces with holographic screens. Hence forces will arise as entropy gradients.

Assume that ψ is nonvanishing at a certain point in space. Consider an infinitesimal cylinder around this point, with height L_P and base area equal to the area element $d^2 a$. Motivated by the proportionality between area and entropy, already mentioned, we postulate that there is an infinitesimal entropy flow dS from the particle to the area element $d^2 a$:

$$dS = C 2\pi k_B L_P |\psi|^2 d^2 a. \quad (15)$$

Here C is a dimensionless numerical constant, to be determined presently. A closed surface Σ receives an entropy flux $S(\Sigma)$:

$$S(\Sigma) = C(\Sigma) 2\pi k_B L_P \int_{\Sigma} d^2 a |\psi|^2. \quad (16)$$

The constant $C(\Sigma)$ will in general depend on the particular surface chosen; the latter may, but need not, be a holographic screen. The key notion here is that the integral of the scalar field $|\psi|^2$ over any surface carries an entropy flow associated. When the surface Σ actually coincides with a holographic screen \mathcal{S} , and when the latter is not a nodal surface of ψ , the constant $C(\mathcal{S})$ may be determined by the requirement that the entropy flux from the particle to the screen equal the quantum of entropy (2). Thus

$$\frac{1}{C(\mathcal{S})} = L_P \int_{\mathcal{S}} d^2 a |\psi|^2. \quad (17)$$

Let us now read eqn. (17) in reverse, under the assumption that one knows the proportionality constants $C(\mathcal{S}_j)$ for a given foliation $R^3 = \cup_{j \in \mathcal{J}} \mathcal{S}_j$. This amounts to a knowledge of the integrands, *i.e.*, of the probability density $|\psi|^2$ within the surface integral (17) on each and every \mathcal{S}_j . From these tomographic sections of all probability densities *there emerges the complete wavefunction ψ on all of R^3* , at least up to a (possibly point-dependent) phase $e^{i\alpha}$.

Thus the integrand of (17) gives the surface density of entropy flow into the holographic screen \mathcal{S}_j , and the wavefunction ψ becomes (proportional to) the square root of this flow. The collection of all these tomographic sections of ψ along all possible screens amounts to a knowledge of the complete wavefunction. Hence *a knowledge of the different surface densities of entropy flux across all possible screens is equivalent to a knowledge of the quantum-mechanical wavefunction ψ* . This is how the quantum-mechanical wavefunction ψ emerges from the holographic screens.

4. The Unruh equation of state

In this section we will rewrite the dictionary entries (10), (11) and (12), postulated to hold in the energy representation of quantum mechanics, in the entropy representation. For this purpose we first need to solve the eigenvalue equation $\hat{S}\phi = S\phi$ on the screen, so the latter will be kept fixed. That is, we will not consider a variable surface \mathcal{S}_j of the foliation, but rather a specific surface corresponding to a fixed value of the index j . Observe also a difference in notation: ϕ instead of ψ . This is to stress the fact that, by (10), entropy eigenstates ϕ cannot be eigenstates of the complete Hamiltonian \hat{H} , but only of the potential energy \hat{U} . Once we have solved the eigenvalue equation

$$\hat{U}\phi = U\phi, \quad (18)$$

then the same ϕ diagonalise \hat{S} :

$$\hat{S}\phi = S\phi, \quad S = \frac{k_B}{4\hbar c L_P} A(\mathcal{S})|U(\mathcal{S})|. \quad (19)$$

Thermodynamical quantities will now arise as expectation values of operators in the entropic eigenstates $\phi(\mathcal{S})$.

We first deal with (10). Clearly its reexpression in the entropy representation will be the thermodynamical fundamental equation $S = S(A)$, since the extensive parameter corresponding to the holographic screen is the area A . Then we have

$$\langle \hat{S} \rangle = \frac{k_B}{4\hbar c L_P} A(\mathcal{S})|U(\mathcal{S})|. \quad (20)$$

Availing ourselves of the freedom to pick the origin of potentials at will, let us set $|U(\mathcal{S})| = \hbar c/L_P$. Thus

$$\langle \hat{S} \rangle = \frac{k_B}{4L_P^2} A, \quad (21)$$

which is the celebrated Bekenstein–Hawking law. It arises as a thermodynamical fundamental equation in the entropy representation.

Our holographic screen is treated thermodynamically as a stretched membrane, so the generalised force conjugate to the extensive parameter A is the surface tension σ . Then the equation of state corresponding to (21) is

$$\sigma = \frac{k_B \langle \hat{T} \rangle}{4L_P^2}. \quad (22)$$

Rewrite the above as $2\pi k_B \langle \hat{T} \rangle = 8\pi L_P^2 \sigma$ and recall that σ is the normal component of force per unit length on the screen. Since force is proportional to acceleration, the above equation of state turns out to be equivalent to the Unruh law.

Finally we turn to the first law of thermodynamics and the equipartition theorem. Taking the expectation value, in the entropic eigenstates ϕ , of the operator equation (12), produces the thermodynamical expression for the equipartition theorem:

$$\frac{k_B}{2} \int_{\mathcal{S}} d^2a \langle \hat{T} \rangle = \frac{A(\mathcal{S})}{4\pi} \langle \hat{U}(\mathcal{S}) \rangle. \quad (23)$$

5. The second law of thermodynamics, revisited

The second law of thermodynamics,

$$\Delta S \geq 0, \quad (24)$$

has been related to the Heisenberg uncertainty principle in ref. [30]. In ref. [13] it has been argued that the second law of thermodynamics has a quantum–mechanical reexpression in the Bell inequalities. In ref. [1] we have established a link between (24) and the Hilbert space of entropic quantum mechanics. Here we would like to propose yet another quantum–mechanical interpretation of the second law, one that combines the uncertainty principle with the notion of emergence.

From eqn. (2) one derives the obvious inequality

$$\Delta S \geq \pi k_B \quad (25)$$

which looks like some refinement of the second law (24)—the latter would be recovered in the semiclassical limit $k_B \rightarrow 0$. Therefore let us, for the sake of the argument, consider eqn. (25) as a more precise statement of the second law than (24). As such (25) is reminiscent the uncertainty principle (8) of quantum mechanics. However the left–hand side of (25) contains just one uncertainty, instead of a product of two uncertainties as usual. This reflects the fact that the variable on the left, S , is *selfconjugate*—its dimension equals that of the quantum k_B on the right–hand side¹. We can include a dimensionless formal parameter! τ in the left–hand side that will make (25) resemble the uncertainty principle in its standard form. This can be done as follows.

Let N denote the total number of bits on \mathcal{S} . Whenever a quantum particle hits the screen we have $\Delta N = 1$, and the ratio $\Delta N/N$ will be small if N is large enough. In this limit we can treat N as a continuous variable, that we re-denote by τ in order to interpret it as a continuous, dimensionless parameter:

$$\tau := N, \quad \text{when} \quad \frac{\Delta N}{N} \ll 1. \quad (26)$$

This is the limit $N \rightarrow \infty$ referred to in (7). Compatibility with all the above requires this limit to correspond to $k_B \rightarrow 0$ or, equivalently, to $\hbar \rightarrow 0$. In other words, the large area limit for a holographic screen corresponds to the semiclassical approximation in quantum mechanics.

We have $\Delta\tau \geq 1$, the inequality allowing for the possibility of more than just one particle hitting \mathcal{S} . Thus multiplying the two inequalities $\Delta\tau \geq 1$ and $\Delta S \geq \pi k_B$ together we arrive at the following uncertainty principle *on the holographic screen*:

$$\Delta S \Delta\tau \geq \pi k_B. \quad (27)$$

The fact that k_B , though small, is nonvanishing, leads to the impossibility of having strictly reversible processes; reversibility is possible only in the limiting case of a vanishing value for

¹ Compare this situation with (q, p) and (H, t) , which are conjugate pairs: the product of the two components of each pair has the dimension of \hbar . Angular momentum L is selfconjugate, in the sense that it carries the dimension of \hbar , but one writes the corresponding uncertainty principle as $\Delta L \Delta\varphi \geq \hbar/2$, where the dimensionless variable φ is an angle.

the quantum k_B . We conclude that quantisation appears as dissipative mechanism. The notion that information loss leads to a quantum behaviour lies at the heart of the notion of emergence [6, 7, 14, 15, 18, 19, 20, 21, 23, 24, 33].

We have derived the uncertainty principle (27) starting from the second law of thermodynamics (24). Let us now prove that the reverse path is also possible: from the uncertainty principle to the second law of thermodynamics. We start from (8) in the bulk rewritten as $\Delta I/\hbar \geq 1$, where $I = \int pdq$ is the action. On the boundary, the correspondence (1) allows to reexpress the above inequality as in (25). Along the way we have dropped irrelevant numerical factors.

Altogether, we have an equivalence between the uncertainty principle of quantum mechanics (either in the bulk (8) or on the boundary (27)), and a refined version of the second law of thermodynamics, one that includes a small but nonvanishing value of the corresponding quantum (\hbar or k_B) on the right-hand side. This is in agreement with the results of [30]—now with the added bonus that our equivalence has the properties of emergence and holography.

6. Discussion

The entropy representation of quantum mechanics, as presented here, is a holographic projection of the energy representation of the same theory, as defined on spacetime. Our central claim, summarised by eqn. (1), expresses this holographic property.

There is, however, one additional property of quantum mechanics that is deeply encoded in eqn. (1); as such it is not immediately recognised. Namely, quantum mechanics is an emergent phenomenon *also* because quantum mechanics is defined on spacetime, and spacetime itself is an emergent phenomenon. Let us analyse this latter point in more detail.

Any model of emergent gravity must ultimately account for the laws governing the motion of material bodies. Thus, *e.g.*, the proposal made in [35] allows for a (somewhat heuristic) derivation of Newton's law of motion, $F = ma$, and of the relativistic generalisations thereof, as emergent, thermodynamical laws. Moreover, the intriguing presence of Planck's constant \hbar [12] in the purely classical setup of ref. [35] makes one suspect that quantum mechanics also has a role to play in that setup. On the other hand, it is well known that Newton's law $F = ma$ can be recovered in the semiclassical limit of quantum mechanics, as being satisfied by the expectation values of certain operators (Ehrenfest's theorem). Last but not least, thermodynamics is the paradigm of emergent phenomena.

All these different pieces of evidence point toward one and the same conclusion—*viz.*, that if classical mechanics follows from the emergence property of spacetime, then the same should be true of quantum mechanics. Here and in ref. [1] we have exploited this point of view. We would like to stress that this conclusion is ultimately independent of the precise mechanism whereby spacetime emerges. Thus, although the holographic dictionary presented in previous sections hinges crucially on the emergence mechanism being precisely that of ref. [35], the holographic correspondence (1) is independent of that mechanism. As such, the holographic correspondence (1) should hold just as well in any other specific model for the emergence of spacetime (say, loop quantum gravity or any alternative thereto such as [17, 27]).

Acknowledgments

J.M.I. heartily thanks the organisers of the *5th International Heinz von Foerster Congress: Emergent Quantum Mechanics*, Vienna, Nov. 11-13, 2011, for the opportunity to present this talk, and for providing a congenial environment for scientific discussions. This work has been supported by Universidad Politécnic de Valencia under grant PAID-06-09.

Handle stets so, daß weitere Möglichkeiten entstehen.

—Heinz von Foerster.

References

- [1] Acosta D, Fernández de Córdoba P, Isidro J M and Santander J L G 2011 An entropic picture of emergent quantum mechanics *Preprint* 1107.1898 [hep-th]
- [2] Adler S 2004 *Quantum theory as an emergent phenomenon* (Cambridge: Cambridge University Press)
- [3] Allahverdyan A, Balian R and Nieuwenhuizen T 2011 Understanding quantum measurement from the solution of dynamical models *Preprint* 1107.2138 [quant-ph]
- [4] Banerjee R and Majhi B 2010 Statistical origin of gravity *Phys. Rev. D* **81** 124006 (*Preprint* 1003.2312 [gr-qc])
- [5] Banerjee R 2010 From black holes to emergent gravity *Int. J. Mod. Phys. D* **19** 2365 (*Preprint* 1005.4286 [gr-qc])
- [6] Blasone M, Jizba P and Vitiello G 2001 Dissipation and quantization *Phys. Lett. A* **287** 205 (*Preprint* hep-th/0007138)
- [7] Blasone M, Jizba P and Vitiello G 2004 *Dissipation, Emergent Quantization, and Quantum Fluctuations in Decoherence and Entropy in Complex Systems, Selected Lectures from DICE 2002*, ed Elze H T, Lecture Notes in Physics **633** (Berlin: Springer)
- [8] Callen H 1960 *Thermodynamics* (New York: John Wiley)
- [9] Carroll R 2010 *On the Emergence Theme of Physics* (Singapore: World Scientific)
- [10] Carroll R 2011 Remarks on osmosis, quantum mechanics and gravity *Preprint* 1104.0383 [gr-qc]
- [11] Carroll R 2011 Thermodynamics and scale relativity *Preprint* 1110.3059 [math-ph]
- [12] Chen P and Wang C H 2011 Where is \hbar hiding in entropic gravity? *Preprint* 1112.3078 [gr-qc]
- [13] Durham I 2011 The necessity of entanglement and the equivalence of Bell's theorem with the second law of thermodynamics *Preprint* 1111.1746 [quant-ph]
- [14] Elze H T 2009 The attractor and the quantum states, *Int. J. Qu. Info.* **7** 83 (*Preprint* 0806.3408 [quant-ph])
- [15] Elze H T 2011 Linear dynamics of quantum–classical hybrids *Preprint* 1111.2276 [quant-ph]
- [16] Faraggi A and Matone M 2009 The equivalence postulate of quantum mechanics: main theorems *Preprint* 0912.1225 [hep-th]
- [17] Finster F and Grotz A 2011 A Lorentzian quantum geometry *Preprint* 1107.2026 [math-ph]
- [18] Groessing G 2008 On the thermodynamic origin of the quantum potential *Physica A* **388** 811 (*Preprint* 0808.3539 [quant-ph])
- [19] Groessing G, Mesa Pascasio J and Schwabl H 2011 A classical explanation of quantization *Found. Phys.* **41** 1437 (*Preprint* 0812.3561 [quant-ph])
- [20] Groessing G 2010 Sub–quantum thermodynamics as a basis of emergent quantum mechanics *Entropy* **12** 1975
- [21] Groessing G, Fussy S, Mesa Pascasio J and Schwabl H 2011 An explanation of interference effects in the double slit experiment: classical trajectories plus ballistic diffusion caused by zero–point fluctuations *Ann. Phys.* **327** (2012) 421. *Preprint* 1106.5994 [quant-ph]
- [22] 't Hooft G 1993 Dimensional reduction in quantum gravity, *Preprint* gr-qc/9310026
- [23] 't Hooft G 2007 Emergent quantum mechanics and emergent symmetries *Preprint* 0707.4568 [hep-th]
- [24] 't Hooft G 2011 How a wavefunction can collapse without violating Schroedinger's equation, and how to understand Born's rule *Preprint* 1112.1811 [quant-ph]
- [25] Kauffman L 2011 Eigenforms and quantum physics *Preprint* 1109.1892 [math-ph]
- [26] Khrennikov A 2010 An analog of Heisenberg uncertainty relation in prequantum classical field theory *Physica Scripta* **81** 065001 (*Preprint* 0912.1565 [quant-ph])
- [27] Mäkelä J 2010 Notes concerning “On the origin of gravity and the laws of Newton” by E. Verlinde *Preprint* 1001.3808 [gr-qc]
- [28] Munkhammar J 2010 Is holographic entropy and gravity the result of quantum mechanics? *Preprint* 1003.1262 [hep-th]
- [29] Munkhammar J 2011 Canonical relational quantum mechanics from information theory *Preprint* 1101.1417 [physics.gen-ph]
- [30] Olah N 2011 *Einsteins Trojanisches Pferd: eine Thermodynamische Deutung der Quantentheorie* (Wien: Springer)
- [31] Padmanabhan T 2011 Lessons from classical gravity about the quantum structure of spacetime *J. Phys. Conf. Ser.* **306** 012001 (*Preprint* 1012.4476 [gr-qc])
- [32] de la Peña L, Cetto A, Valdés–Hernández A and França H 2011 Origin and meaning of quantum nonlocality *Preprint* 1110.4641 [quant-ph]
- [33] Sakellariadou M, Stabile A and Vitiello G 2011 Noncommutative spectral geometry, algebra doubling and the seeds of quantization *Phys. Rev. D* **84** 045026 (*Preprint* 1106.4164 [math-ph])
- [34] Susskind L 1994 The world as a hologram *Preprint* hep-th/9409089
- [35] Verlinde E 2011 On the origin of gravity and the laws of Newton *JHEP* **1104** 029 (1001.0785 [hep-th])

AN ENTROPIC PICTURE OF EMERGENT QUANTUM MECHANICS

D. Acosta^{1,a}, P. Fernández de Córdoba^{2,b}, J.M. Isidro^{2,c} and J.L.G. Santander^{3,d}

¹Departamento de Matemáticas, Universidad de Pinar del Río,
Pinar del Río, Cuba

²Instituto Universitario de Matemática Pura y Aplicada,
Universidad Politécnica de Valencia, Valencia 46022, Spain

³Cátedra Energesis de Tecnología Interdisciplinar, Universidad Católica de Valencia,
C/ Guillem de Castro 94, Valencia 46003, Spain

^adago@mat.upr.edu.cu, ^bpfernandez@mat.upv.es

^cjoissan@mat.upv.es, ^dmartinez.gonzalez@ucv.es

Abstract Quantum mechanics emerges *à la* Verlinde from a foliation of \mathbb{R}^3 by holographic screens, when regarding the latter as entropy reservoirs that a particle can exchange entropy with. This entropy is quantised in units of Boltzmann's constant k_B . The holographic screens can be treated thermodynamically as stretched membranes. On that side of a holographic screen where spacetime has already emerged, the *energy representation* of thermodynamics gives rise to the usual quantum mechanics. A knowledge of the different surface densities of entropy flow across all screens is equivalent to a knowledge of the quantum–mechanical wavefunction on \mathbb{R}^3 . The *entropy representation* of thermodynamics, as applied to a screen, can be used to describe quantum mechanics in the absence of spacetime, that is, quantum mechanics beyond a holographic screen, where spacetime has not yet emerged. Our approach can be regarded as a formal derivation of Planck's constant \hbar from Boltzmann's constant k_B .

Contents

1	Introduction	2
2	Holographic screens as entropy reservoirs	3
2.1	A quantum of entropy	3
2.2	Two thermodynamical representations	4
2.3	A holographic dictionary	5
3	The energy representation	7
4	The entropy representation	8
4.1	Action <i>vs.</i> entropy	8
4.2	Quantum states <i>vs.</i> holographic screens	9
4.3	The entropic uncertainty principle	10
4.4	The entropic Schroedinger equation	11
4.5	The fundamental equation, the equation of state, and equipartition	13

4.6	Planck vs. Boltzmann, or \hbar vs. k_B	15
4.7	The second law of thermodynamics, revisited	15
5	Discussion	16
5.1	Quantum mechanics as a holographic, emergent phenomenon	16
5.2	Quantum mechanics in the absence of spacetime	17
5.3	Open questions	18

1 Introduction

Groundbreaking advances in our understanding of gravity have led to profound new insights into its nature (see [50, 51, 52, 53, 54, 69] and refs. therein). Perhaps the most relevant insight is the recognition that gravity cannot a fundamental force, but rather must be an effective description of some underlying degrees of freedom. As such, gravity is amenable to a thermodynamical description. Although this fact had already been suspected for some time [4, 5, 33, 67, 41, 34], it is only more recently that it has been given due attention. The derivation of Newton’s laws of motion and of Einstein’s gravity, presented in ref. [69] from an entropic perspective, has triggered off an avalanche of research into the subject, ensuing papers being too numerous to quote here in detail; see however [47, 8, 65, 18, 46, 25, 26]. A feature of these developments is that, while offering insights into the quantum structure of spacetime, the treatment is largely classical, in that no specific microscopic model of spacetime is assumed. In other words, these developments refer not to the (microscopic) statistical mechanics of gravity and spacetime, but to its (macroscopic) thermodynamics instead. In this sense, notions usually considered to be *a priori*, such as inertia, force and spacetime, appear as phenomena arising from some underlying theory whose minutiae are largely unknown—but fortunately also irrelevant for a thermodynamical description. Such *emergent* phenomena are no longer *a priori*, but derived. We refer readers to the comprehensive overview of emergent physics presented in the nice book [11]. Spacetime itself appears as an emergent phenomenon, with the holographic principle playing a key role [35, 63]. Developments in string theory also point in this direction [6, 57].

It has also been conjectured that quantum mechanics itself must be an emergent theory [49, 1, 62, 36, 37, 19, 20, 21, 22, 42]; see also [45, 23, 9, 10, 12, 13, 14, 43] for its close link with gravity theories, and [29, 30, 31, 32] for an interpretation in thermodynamical terms. The guiding principle at work in many of these approaches is the notion that quantum mechanics provides some coarse-grained description of an underlying deterministic theory. In some of these models [36], quantum states arise as equivalence classes of classical, deterministic states, the latter being grouped together into equivalence classes, or quantum states, due to our ignorance of the full microscopic description. Quantisation thus appears to be some kind of dissipation mechanism for information. In the presence of dissipation, entropy immediately comes to mind [15, 16, 17].

Thus the two research lines mentioned above, gravity and quantum mechanics, share the common feature of being effective, thermodynamical descriptions of their respective underlying theories. It is the purpose of this paper to develop an approach to

emergent quantum mechanics from the *entropic* point of view pioneered in ref. [69], with a quantum–mechanical particle replacing the classical particle considered in ref. [69]. Additionally, this will contribute towards clarifying the role played by Planck’s constant \hbar in the entropic derivation of classical gravity (Newton’s and Einstein’s) presented in [69]. Indeed, our results can be regarded as an entropic derivation of Planck’s constant \hbar from Boltzmann’s constant k_B —at least conceptually if not numerically. Altogether, our approach will provide us with a *holographic, entropic picture of emergent quantum mechanics*.

Finally let us say a word on notation. Awkward though the presence of \hbar, c, G, k_B in our equations may seem, our purpose of exhibiting how \hbar emerges from k_B renders natural units inconvenient. Quantum operators will be denoted as \hat{f} , with f being the corresponding classical function.

2 Holographic screens as entropy reservoirs

2.1 A quantum of entropy

The starting point in ref. [69] is a classical point particle of mass M approaching a holographic screen \mathcal{S} , from that side of the latter on which spacetime has already emerged. At a distance from \mathcal{S} equal to 1 Compton length, the particle causes the entropy S of the screen to increase by the amount

$$\Delta S = 2\pi k_B, \tag{1}$$

where k_B is Boltzmann’s constant. The above can also be understood as meaning that $2\pi k_B$ is the *quantum* by which the entropy of the screen increases, whenever a particle crosses \mathcal{S} . The factor 2π on the right–hand side is conventional. Relevant is only the fact that the entropy increase of the screen appears quantised in units of k_B .

We call *bright* that side of the holographic screen on which spacetime has already emerged, whereas the other side might well be termed *dark*. One can also think of the holographic screen as being the horizon of some suitably picked observer \mathcal{O} in spacetime. For example, in the relativistic case, one can think of this observer as being a Rindler observer. The dark side might well be identified with the screen itself, as there is literally no spacetime beyond the bright side—this assertion is to be understood as relative to the corresponding observer, since different observers might perceive different horizons. In this way, for each fixed value of the time variable, a collection of observers \mathcal{O}_j , with the index j running over some (continuous) set \mathcal{J} , gives rise to a foliation of 3–space by 2–dimensional holographic screens \mathcal{S}_j : $\mathbb{R}^3 = \cup_{j \in \mathcal{J}} \mathcal{S}_j$. For reasons to be explained presently we will mostly restrict our attention to potentials such that the \mathcal{S}_j are all closed surfaces; we denote the finite volume they enclose by \mathcal{V}_j , so $\partial \mathcal{V}_j = \mathcal{S}_j$.

2.2 Two thermodynamical representations

We will take (I) to hold for a quantum particle as well. A quantum particle hitting the holographic screen¹ exchanges entropy with the latter, *i.e.*, the wavefunction ψ exchanges information with \mathcal{S} . Just as information is quantised in terms of bits, so is entropy quantised, as per eqn. (I). The only requirement on this exchange is that the holographic screen act as an entropy reservoir. (See refs. [44, 48] for related proposals, with the mechanical action integral replacing the entropy).

Describing the quantum particle on the bright side of the screen we have the standard wavefunction ψ_+ , depending on the spacetime coordinates and obeying the usual laws of quantum mechanics. On the other hand, the *entropic* wavefunction ψ_- describes the same quantum particle, as seen by an observer on the dark side of the holographic screen. If imagining an observer on the dark side of \mathcal{S} , where spacetime has not yet emerged, raises some concern, one can also think of ψ_- as being related, in a way to be made precise below, to the flow of entropy across the horizon \mathcal{S} , as measured by an observer on the bright side of the same horizon.

Our goal is to describe the laws of *entropic quantum mechanics*, that is, the laws satisfied by the entropic wavefunction ψ_- , and to place them in correspondence with those satisfied by the standard wavefunction ψ_+ on spacetime. The relevant thermodynamical formalism needed here can be found, *e.g.*, in the classic textbook [7]. However, for later use, let us briefly summarise a few basics. Any given thermodynamical system can be completely described if one knows its *fundamental equation*. The latter contains all the thermodynamical information one can obtain about the system. The fundamental equation can be expressed in either of two equivalent ways, respectively called the *energy representation* and the *entropy representation*. In the energy representation one has a fundamental equation $E = E(S, \dots)$, where the energy E is a function of the entropy S , plus of whatever additional variables may be required. In the entropy representation one solves for the entropy in terms of the energy to obtain a fundamental equation $S = S(E, \dots)$.

As an example, let there be just one extensive parameter, the volume V . Then the fundamental equation in the entropy representation will be an expression of the form $S = S(E, V)$, hence $dS = (\partial S/\partial E) dE + (\partial S/\partial V) dV$. We know that $\delta Q = T dS$, while the first law of thermodynamics reads, in this case, $\delta Q = dE + p dV$, with p the pressure. It follows that $T^{-1} = \partial S/\partial E$ and $p = T(\partial S/\partial V)$. This latter equation is the equation of state. For example, in the case of an ideal gas we have $S(E, V) = k_B \ln(V/V_0) + f(E)$, with $f(E)$ a certain function of the energy and V_0 a reference volume (that can be regarded as a constant contribution to S and thus neglected). It follows from $\partial S/\partial V = k_B V^{-1}$ that pV is proportional to T , as expected of an ideal gas.

In a sense to be made more precise presently, the bright side of the holographic screen corresponds to the energy representation, while the dark side corresponds to the entropy representation. Thus the energy representation will give us quantum mechanics on spacetime as we know it. One must bear in mind, however, that standard thermo-

¹Due to quantum delocalisation, statements such as *a quantum particle hitting the holographic screen* must be understood as meaning *a quantum-mechanical wavepacket, a substantial part of which has nonzero overlap with the screen*.

dynamical systems admit both representations (energy and entropy) simultaneously, which representation one uses being just a matter of choice. In our case this choice is dictated, for each fixed observer, by that side of the screen on which the observer wants to study quantum mechanics. For example there is no energy variable on the dark side, as there is no time variable, but an observer can assign the screen an entropy, measuring the observer’s ignorance of what happens beyond the screen. By the same token, on the bright side we have an energy but there is no entropy². In this case these two representations cannot be simultaneous.

The situation just described changes somewhat as soon as one considers two or more observers, each one of them perceiving a different horizon or holographic screen. Consider, for simplicity, two observers $\mathcal{O}_1, \mathcal{O}_2$ with their respective screens $\mathcal{S}_1, \mathcal{S}_2$, and assume the latter to be such that \mathcal{S}_2 gets beyond \mathcal{S}_1 , in the sense that \mathcal{S}_2 encloses more emerged volume than \mathcal{S}_1 . That is, the portion of emerged spacetime perceived by \mathcal{O}_2 includes all that perceived by \mathcal{O}_1 , plus some volume that remains on the dark side of \mathcal{S}_1 . Call \mathcal{V}_{12} this portion of spacetime that appears dark to \mathcal{O}_1 but bright to \mathcal{O}_2 . Clearly, quantum mechanics on \mathcal{V}_{12} will be described in the energy representation by \mathcal{O}_2 and in the entropy representation by \mathcal{O}_1 . In this case the two representations can coexist simultaneously—not as corresponding to one observer, as in standard thermodynamics, but each one of them as *pertaining to a different observer*.

The differences just mentioned, as well as some more that will arise along the way, set us somewhat apart from the standard thermodynamical formalism. Nevertheless, the thermodynamical analogy can be quite useful if one bears these differences in mind.

2.3 A holographic dictionary

Let us recall that one can formulate a *holographic dictionary* between gravitation, on the one hand, and thermodynamics, on the other [50, 51, 52, 53, 54]. Let V_G denote the gravitational potential created by a total mass $M = \int_{\mathcal{V}} d^3V \rho_M$ within the volume \mathcal{V} enclosed by the holographic screen $\mathcal{S} = \partial\mathcal{V}$. Then the following two statements are equivalent [69, 38]:

- i) there exists a gravitational potential V_G satisfying Poisson’s equation $\nabla^2 V_G = 4\pi G \rho_M$, such that a test mass m in the background field created by the mass distribution ρ_M experiences a force $\mathbf{F} = -m\nabla V_G$;
- ii) given a foliation of 3-space by holographic screens, $\mathbb{R}^3 = \cup_{j \in \mathcal{J}} \mathcal{S}_j$, there are two scalar quantities, called entropy S and temperature T , such that the force acting on a test mass m is given by $F\delta x = \int_{\mathcal{S}} T\delta dS$. The latter integral is taken over a screen that does not enclose m .

Moreover, the thermodynamical equivalent of the gravitational theory includes the following *dictionary entries* [69]:

$$\frac{1}{k_B} S(x) = \frac{-1}{4\hbar c L_P^2} V_G(x) A(V_G(x)), \quad (2)$$

$$2\pi k_B T(x) = \frac{dV_G}{dn}, \quad (3)$$

²We are considering the simplified case of a pure quantum state. Were our quantum state to be described by a density matrix, there would of course be an entropy associated.

$$\frac{k_B}{2} \int_S d^2a T = L_P^2 M c^2. \quad (4)$$

In (2), (3) and (4) we have placed all thermodynamical quantities on the left, while their mechanical analogues are on the right. As in ref. [69], the area element d^2a on \mathcal{S} is related to the infinitesimal number of bits dN on it through $d^2a = L_P^2 dN$. We denote the area of the equipotential surface passing through the point x by $A(V_G(x))$, while dV_G/dn denotes the derivative of V_G along the normal direction to the same equipotential. The above expressions tell us how, given a gravitational potential $V_G(x)$ and its normal derivative dV_G/dn , the entropy S and the temperature T can be defined as functions of space.

Specifically, eqn. (2) expresses the proportionality between the area A of the screen \mathcal{S} and the entropy S it contains. This proportionality implies that gravitational equipotential surfaces get translated, by the holographic dictionary, as *isoentropic surfaces*, above called holographic screens \mathcal{S} .

Equation (3) expresses the Unruh effect: an accelerated observer experiences the vacuum of an inertial observer as a thermal bath at a temperature T that is proportional to the observer's acceleration dV_G/dn .

Finally, eqn. (4) expresses the first law of thermodynamics and the equipartition theorem. The right-hand side of (4) equals the total rest energy of the mass enclosed by the volume \mathcal{V} , while the left-hand side expresses the same energy content as spread over the bits of the screen $\mathcal{S} = \partial\mathcal{V}$, each one of them carrying an energy $k_B T/2$. It is worthwhile noting that equipartition need not be postulated. Starting from (3) one can in fact prove the following form of the equipartition theorem:

$$\frac{k_B}{2} \int_S d^2a T = \frac{A(\mathcal{S})}{4\pi} U(\mathcal{S}), \quad A(\mathcal{S}) = \int_S d^2a. \quad (5)$$

The details leading up to (5) from (3) will be given in section 4.5. Above, U can be an arbitrary potential energy³. We will henceforth mean eqn. (5) when referring to the first law and the equipartition theorem. In all the above we are treating the area as a continuous variable, but in fact it is quantised [69]. If $N(\mathcal{S})$ denotes the number of bits of the screen \mathcal{S} , then

$$A(\mathcal{S}) = N(\mathcal{S}) L_P^2. \quad (6)$$

However, in the limit $N \rightarrow \infty$, when $\Delta N/N \ll 1$, this approximation of the area by a continuous variable is accurate enough. We will see later on that letting $N \rightarrow \infty$ is equivalent to the semiclassical limit in quantum mechanics.

We intend to write a holographic dictionary between quantum mechanics, on the one hand, and thermodynamics, on the other. This implies that we will need to generalise eqns. (2), (3) and (5) so as to adapt them to our quantum-mechanical setup. Thus we will replace the classical particle of [69] with a quantum particle, subject to some potential energy U of nongravitational origin.

³The gravitational potential V_G appearing above is the gravitational energy U_G per unit test mass m .

3 The energy representation

Let $H = K + U$ be the classical Hamiltonian function on \mathbb{R}^3 whose quantisation leads to the quantum Hamiltonian operator $\hat{H} = \hat{K} + \hat{U}$ that governs our quantum particle. The Hamiltonian \hat{H} will be assumed to possess normalisable states. This condition on the potential was already reflected in the gravitational case of eqn. (2), where the negative sign of the gravitational potential led to a positive definite entropy.

On the bright side of the screen, spacetime has already emerged. This gives us the energy representation of quantum mechanics—the one we are used to: a time variable with a conserved Noether charge, the energy, and wavefunctions depending on the spacetime coordinates. We have the uncertainty relation

$$\Delta\hat{Q}\Delta\hat{P} \geq \frac{\hbar}{2}. \quad (7)$$

In the semiclassical limit we have a wavefunction

$$\psi_+ = \exp\left(\frac{i}{\hbar}I\right), \quad (8)$$

where $I = \int dtL$ is the action integral satisfying the Hamilton–Jacobi equation.

Let \mathcal{V} denote the finite portion of 3–space bounded by the closed holographic screen $\mathcal{S} = \partial\mathcal{V}$. We can now posit the quantum–mechanical analogues of eqns. (2), (3) and (5). In the energy representation these analogues read, respectively,

$$\frac{1}{k_B}\hat{S}(x) = \frac{1}{4\hbar cL_P}A(U(x))|\hat{U}(x)|, \quad (9)$$

$$2\pi k_B\hat{T}(x) = L_P\frac{d\hat{U}}{dn}, \quad (10)$$

$$\frac{k_B}{2}\int_{\mathcal{S}}d^2a\hat{T} = \frac{A(\mathcal{S})}{4\pi}\hat{U}(\mathcal{S}). \quad (11)$$

Some comments are in order. We are considering the nonrelativistic limit, in which the rest energy of the particle can be ignored. We also neglect all gravitational effects, relativistic or not; we will limit ourselves to the external potential \hat{U} . Quantum operators such as \hat{U} , initially defined to act on wavefunctions in $L^2(\mathbb{R}^3)$, must now be restricted to act on wavefunctions in $L^2(\mathcal{V})$. Denote this restriction by $\hat{U}_{\mathcal{V}}$. By definition, its matrix elements $\langle f_+|\hat{U}_{\mathcal{V}}|g_+\rangle$ are

$$\langle f_+|\hat{U}_{\mathcal{V}}|g_+\rangle := \int_{\mathcal{V}}d^3Vf_+^*\hat{U}g_+, \quad (12)$$

the integral extending over the finite volume \mathcal{V} instead of all \mathbb{R}^3 . For simplicity we have suppressed the subindex \mathcal{V} in (9), (10) and (11), but it must be understood that all operators are to be restricted as specified.

The right–hand side of (9) deserves more attention. $|\hat{U}|$ denotes the operator whose matrix elements are the absolute values of those of \hat{U} . Taking the absolute value ensures

that the entropy is positive definite, given that the potential U need not have a constant sign, contrary to the gravitational case of (2).

It will also be observed that no carets stand above $A(U(x))$, $A(S)$, because they are c -numbers. They denote the area of the equipotential surface passing through the point x and the area of the screen S , respectively. Also, the integral on the left-hand side of (11) is a standard surface integral, even if the integrand is the operator \hat{T} , because the latter depends on the c -number-valued coordinate functions x .

As a final remark, let us point out that the above equations (9), (10) and (11), as well as their classical counterparts (2), (3) and (5), are correctly understood as being expressed in the energy representation of thermodynamics. This is so despite the fact that one writes the entropy as an explicit function of the potential energy—would this not be the defining property of the entropy representation? The answer is negative for two reasons. First, one would need to express the entropy as a function of the total energy H , rather than as a function of just the potential energy U . Second, all the above expressions are functions defined on the emerged portion of space, where there exists a conserved Noether charge, the energy H , and its conjugate variable, the time t . The entropy representation will be introduced later on, when the absence of spacetime will make it necessary to eliminate the space dependence of quantities such as entropy and temperature. Such will be the case beyond the holographic screen.

4 The entropy representation

The entropy representation can also be thought of as quantum mechanics in the absence of spacetime, as we will come to recognise presently.

4.1 Action vs. entropy

It is well known, in the theory of thermodynamical fluctuations [7], that the probability density function d required to compute expectation values of thermodynamical quantities is given by the exponential of the entropy:

$$d = \exp\left(\frac{S}{k_B}\right). \quad (13)$$

Its square root, that one may call the amplitude for the probability density d , can therefore be identified with an entropic wavefunction $\psi_-^{(d)}$:

$$\psi_-^{(d)} = \exp\left(\frac{S}{2k_B}\right). \quad (14)$$

This identification is made up to a (possibly point-dependent) phase $e^{i\alpha}$, plus a normalisation. Comparing (14) with (8) we arrive at the correspondence

$$\frac{iI}{\hbar} \leftrightarrow \frac{S}{2k_B} \quad (15)$$

between the energy representation and the entropy representation, *both of them taken in the semiclassical limit*. This amounts to the statement that quantum–mechanical fluctuations can be understood thermodynamically, at least in the semiclassical limit.

We should note that the correspondence (15) is holographic in nature, because the action integral I is defined on space, while the entropy S is defined on the screen bounding it. Moreover, the above correspondence also implies that, in the entropic representation, the semiclassical limit (the one considered in (8)) corresponds to letting $k_B \rightarrow 0$.

The wavefunction (14) describes an *incoming* wave, from the point of view of the screen. An *outgoing* wave, from the point of view of the screen, would be described by $\exp(-S/2k_B)$.

It is reassuring to observe that the same correspondence (15) has been found in the context of gravity and black–hole thermodynamics [2, 3].

4.2 Quantum states vs. holographic screens

The equation $U(x^1, x^2, x^3) = U_0$, where U_0 is a constant, defines an equipotential surface in \mathbb{R}^3 . As U_0 runs over all its possible values, we obtain a foliation of \mathbb{R}^3 by equipotential surfaces. Following [69], we will identify equipotential surfaces with holographic screens. Hence forces will arise as entropy gradients.

Assume that ψ_+ is nonvanishing at a certain point in space. Consider an infinitesimal cylinder around this point, with height L_P and base area equal to the area element d^2a . Motivated by the proportionality between area and entropy, already mentioned, we postulate that there is an infinitesimal entropy flow dS from the particle to the area element d^2a :

$$dS = C 2\pi k_B L_P |\psi_+|^2 d^2a. \quad (16)$$

Here C is a dimensionless numerical constant, to be determined presently. A closed surface Σ receives an entropy flux $S(\Sigma)$:

$$S(\Sigma) = C(\Sigma) 2\pi k_B L_P \int_{\Sigma} d^2a |\psi_+|^2. \quad (17)$$

The constant $C(\Sigma)$ will in general depend on the particular surface chosen; the latter may, but need not, be a holographic screen. The key notion here is that the integral of the scalar field $|\psi_+|^2$ over any surface carries an entropy flow associated. When the surface Σ actually coincides with a holographic screen \mathcal{S} , and when the latter is not a nodal surface of ψ_+ , the constant $C(\mathcal{S})$ may be determined by the requirement that the entropy flux from the particle to the screen equal the quantum of entropy (1). Thus

$$\frac{1}{C(\mathcal{S})} = L_P \int_{\mathcal{S}} d^2a |\psi_+|^2. \quad (18)$$

We should point out the following. Given a wavefunction ψ_+ , the probability density $|\psi|^2$ on \mathbb{R}^3 gives rise to a natural definition of entropy, namely,

$$-k_B \int d^3V |\psi_+|^2 \log |\psi_+|^2. \quad (19)$$

However, (19) is the entropy associated with our uncertainty in the position of the particle in 3–space. As such it should not be confused with the entropy (17) associated with the particle traversing the surface Σ . It is this latter entropy that we are interested in.

Let us now read eqn. (18) in reverse, under the assumption that one knows the proportionality constants $C(\mathcal{S}_j)$ for a given foliation $\mathbb{R}^3 = \cup_{j \in \mathcal{J}} \mathcal{S}_j$. This amounts to a knowledge of the integrands, *i.e.*, of the probability density $|\psi_+|^2$ within the surface integral (18) on each and every \mathcal{S}_j . From these tomographic sections of all probability densities *there emerges the complete wavefunction ψ_+ on all of \mathbb{R}^3* , at least up to a (possibly point–dependent) phase $e^{i\alpha}$.

Thus the integrand of (18) gives the surface density of entropy flow into the holographic screen \mathcal{S}_j , and the wavefunction ψ_+ becomes (proportional to) the square root of this flow. The collection of all these tomographic sections of ψ_+ along all possible screens amounts to a knowledge of the complete wavefunction. Hence *a knowledge of the different surface densities of entropy flux across all possible screens is equivalent to a knowledge of the quantum–mechanical wavefunction ψ_+* . This is how the quantum–mechanical wavefunction ψ_+ emerges from the holographic screens. Close ideas concerning the wavefunction in relation to foliations of space have been put forward in ref. [9].

4.3 The entropic uncertainty principle

Let us define the dimensionless variable

$$s := \frac{S}{2\pi k_B}, \quad (20)$$

that we will call the *reduced entropy*. It is nonnegative: $s \geq 0$. For example, the semiclassical entropic wavefunction (14) can be expressed in terms of s as $\psi_-^{(d)}(s) = e^{\pi s}$. We can consider arbitrary functions $f(s)$ on which we let the following operators \hat{Q}_S, \hat{P}_S act:

$$\hat{Q}_S f(s) := s f(s), \quad \hat{P}_S f(s) := 2\pi k_B \frac{df(s)}{ds}. \quad (21)$$

For reasons that will become clear presently, \hat{Q}_S will also be called the *normal, or entropic, position operator*, while \hat{P}_S will be called the *normal, or entropic, momentum*⁴. One finds that $i\hat{P}_S$ and \hat{Q}_S are Hermitian on $L^2[0, \infty)$. Unlike the usual case on $L^2(\mathbb{R})$, the Hermitian property of position and momentum on the semiaxis involves some nontrivial mathematical subtleties that will not be touched upon here; see [64]. Now the above operators satisfy the Heisenberg algebra

$$[\hat{Q}_S, \hat{P}_S] = 2\pi k_B \mathbf{1}. \quad (22)$$

Therefore the following *entropic uncertainty principle* holds:

$$\Delta \hat{Q}_S \Delta \hat{P}_S \geq \pi k_B. \quad (23)$$

The above uncertainty principle has been derived rather than postulated; this is in the spirit of refs. [27, 28].

⁴The missing factor of i in the definition of \hat{P}_S is due to the correspondence (15).

4.4 The entropic Schroedinger equation

Since the screens \mathcal{S}_j are isoentropic surfaces, the reduced entropy s can be regarded as a dimensionless coordinate orthogonal to all the \mathcal{S}_j . Multiplication by L_P gives a dimensionful coordinate ρ :

$$\rho := L_P s. \quad (24)$$

Modulo multiplication by a dimensionless numerical factor, and the possible addition of a constant, the above is an equivalent reexpression of the equation [69]

$$\Delta S = 2\pi k_B \frac{Mc}{\hbar} \Delta x, \quad (25)$$

where x is the distance measured normally to the screen—in turn, (25) is the same as (11). We can exploit this fact if we assume that the time-independent Schroedinger equation

$$-\frac{\hbar^2}{2M} \nabla^2 \psi_+ + U \psi_+ = E \psi_+ \quad (26)$$

is separable in a coordinate system that includes ρ as one of its coordinate functions. So let us supplement ρ with two additional coordinates ξ, χ such that the triple ρ, ξ, χ provides an orthogonal set of curvilinear coordinates⁵ in which (26) separates as per (28) below. Then the Euclidean line element on \mathbb{R}^3 will be given by

$$ds^2 = h_\rho^2 d\rho^2 + h_\xi^2 d\xi^2 + h_\chi^2 d\chi^2, \quad (27)$$

where the metric coefficients h_ρ, h_ξ, h_χ are functions of all three coordinates ρ, ξ, χ . We will call ρ the *normal coordinate* to the foliation, while ξ, χ will be called *tangential coordinates* to the foliation. A more physical terminology, based on (24) and (10), could be *entropic coordinate* for ρ and *isothermal coordinates* for ξ, χ .

We recall that U depends only on the normal coordinate ρ , so equipotential surfaces are defined by $U(\rho) = U_0$, for any constant U_0 . The tangential dimensions ξ, χ are purely spatial constructs: they encode the geometry of the equipotential surfaces. For example, in the particular case of a Coulomb potential, or also of an isotropic harmonic oscillator, the \mathcal{S}_j are a family of concentric spheres of increasing radii. Then ρ can be identified with the usual radial coordinate r on \mathbb{R}^3 , while ξ, χ can be taken as the usual polar angles θ, φ . In the general case ρ, ξ, χ need not coincide with any of the standard coordinate functions on \mathbb{R}^3 . However, each screen \mathcal{S}_j can be univocally identified by the equation $\rho = \rho_j$. The uncertainty principle (23) holds on the phase space corresponding to ρ , and the operator \hat{Q}_S defined in (21) is nothing but *the position operator along the normal, or entropic, coordinate*.

Thus separating variables as per

$$\psi_+(\rho, \xi, \chi) = R(\rho)Y(\xi, \chi), \quad (28)$$

⁵In general, ρ, ξ, χ are only local coordinates, and need not cover all of \mathbb{R}^3 . In particular, ξ, χ need not cover a complete screen \mathcal{S}_j , nor need they be simultaneously defined on different screens $\mathcal{S}_j, \mathcal{S}_k$. However, to simplify our notation, we omit all the indices that would be necessary in order to take all these possibilities into account.

and substituting into (26) leads to

$$\begin{aligned} \frac{1}{h_\rho h_\xi h_\chi} \left[\frac{1}{R} \frac{\partial}{\partial \rho} \left(\frac{h_\xi h_\chi}{h_\rho} \frac{\partial R}{\partial \rho} \right) + \frac{1}{Y} \frac{\partial}{\partial \xi} \left(\frac{h_\rho h_\chi}{h_\xi} \frac{\partial Y}{\partial \xi} \right) + \frac{1}{Y} \frac{\partial}{\partial \chi} \left(\frac{h_\rho h_\xi}{h_\chi} \frac{\partial Y}{\partial \chi} \right) \right] \\ + \frac{2M}{\hbar^2} (E - U) = 0. \end{aligned} \quad (29)$$

The precise way in which (29) separates into a ρ -dependent piece and a ξ, χ -dependent piece cannot be written down in all generality, as it varies according to the particular choice made for ρ, ξ, χ . This is due to our ignorance of the specific way in which the metric coefficients h_ρ, h_ξ, h_χ depend on all three variables ρ, ξ, χ . One can, however, outline some general features of the final outcome. Terms involving the Laplacian ∇^2 will decompose as a sum $\nabla_\rho^2 + \nabla_{\xi, \chi}^2$, where subindices indicate the variables being differentiated in the corresponding operators. Calling the separation constant λ , there will be two separate equations. The first equation will involve the normal Laplacian ∇_ρ^2 , the potential energy $U(\rho)$, the energy eigenvalue E , the mass M and the separation constant λ . All these elements (with the exception of ∇_ρ^2) appear as a certain function F of ρ :

$$\nabla_\rho^2 R(\rho) + F(\rho, U(\rho), E, M, \lambda) R(\rho) = 0. \quad (30)$$

The unknown function F is explicitly computable once a specific choice has been made for the coordinates ξ, χ . The second equation involves only the tangential Laplacian $\nabla_{\xi, \chi}^2$ and the separation constant λ :

$$\nabla_{\xi, \chi}^2 Y(\xi, \chi) + \lambda Y(\xi, \chi) = 0. \quad (31)$$

It is important to note that (31) can be solved independently of (30)⁶. The eigenfunctions $Y(\xi, \chi)$ constitute a complete orthonormal system of eigenfunctions of the tangential Laplacian within the *tangential Hilbert space* $L^2(\mathcal{S}_j)$. Moreover, since we have assumed the screens to be closed surfaces, the eigenvalues λ will be quantised. Once these eigenvalues have been determined, substitution into (30) allows the latter to be completely solved.

We are finally in a position to define the entropic wavefunction ψ_- in terms of its partner ψ_+ . We take the entropic wavefunction to be the ρ -dependent piece in the factorisation (28),

$$\psi_-(\rho) := R(\rho). \quad (32)$$

Clearly the *entropic, or normal, Hilbert space* corresponding to the screen \mathcal{S}_j will be $L^2[0, \rho_j]$. The latter is considered with respect to an integration measure that includes a certain Jacobian factor $J(\rho)$. In order to compute this Jacobian we proceed as follows. Apply the factorisation (28) to the normalisation condition for ψ_+ on \mathcal{V}_j :

$$\int_{\mathcal{V}_j} d^3V |\psi_+|^2 = \int_0^{\rho_j} d\rho \int_{\mathcal{S}_j} d\xi d\chi h_\rho h_\xi h_\chi |R(\rho)|^2 |Y(\xi, \chi)|^2. \quad (33)$$

⁶Needless to say, in the case of a Coulomb field, (30) becomes the standard radial wave equation, while (31) becomes that satisfied by the usual spherical harmonics, with $\lambda = l(l+1)$.

In general, the product $h_\rho h_\xi h_\chi$ depends on all three coordinates ρ, ξ, χ . The sought-for Jacobian $J(\rho)$ equals the ρ -dependent factor in the integration measure after the integral over ξ, χ has been carried out. As ρ_j becomes larger and larger, we obtain the entropic Hilbert space $L^2[0, \infty)$. The latter would correspond to an observer who perceives no horizon at all, thus extending his normalisation integral (33) over all of \mathbb{R}^3 . We will come back to the issue of the different realisations of the entropic Hilbert space ($L^2[0, \rho_j]$ vs. $L^2[0, \infty)$) in section 5.2

In the passage from the energy representation to the entropy representation we appear to have lost the information corresponding to the holographic screens one integrates over. However the screens carry no dynamics, because the force at point x is orthogonal to the screen passing through x . Thus a knowledge of the entropic wavefunction ψ_- , *plus of the foliation itself*, is equivalent to a knowledge of the wavefunction ψ_+ in the energy representation. That the foliation is a piece of information belonging to the entropy representation, was stated in assertion *ii*) of our section 2.3 following [69, 38].

It remains to identify the wave equation satisfied by the entropic wavefunction ψ_- . Obviously this equation is (30), which may thus be regarded as *the entropy-representation analogue of the time-independent Schroedinger equation* $\hat{H}\psi_+ = E\psi_+$ on space. Recalling (9) and (24), this entropic Schroedinger equation reads

$$\nabla_s^2 \psi_-(s) + G(s, A(s), E, M, \lambda) \psi_-(s) = 0. \quad (34)$$

We have called $G(s, A(s), E, M, \lambda)$ the function that results from expressing the potential U as a function of the entropy S and the area A , and writing everything in terms of the reduced entropy s . As was the case with F in (30), the unknown function G is explicitly computable once a specific choice has been made for the coordinates ξ, χ .

4.5 The fundamental equation, the equation of state, and equipartition

In this section we will rewrite the dictionary entries (9), (10) and (11), found to hold in the energy representation, in the entropy representation. For this purpose we first need to solve the eigenvalue equation $\hat{S}\phi_- = S\phi_-$ on the screen, so the latter will be kept fixed. That is, we will not consider a variable surface \mathcal{S}_j of the foliation, but rather a specific surface corresponding to a fixed value of the index j . Observe also a difference in notation: ϕ instead of ψ . This is to stress the fact that, by (9), entropy eigenstates ϕ cannot be eigenstates of the complete Hamiltonian \hat{H} , but only of the potential energy \hat{U} . Once \hat{U} is diagonalised by a set of ϕ_+ defined on the bright side, *i.e.*, once we have solved the eigenvalue equation⁷

$$\hat{U}\phi_+ = U\phi_+, \quad (35)$$

⁷Obviously the ϕ_+ are the well-known eigenfunctions of the position operator on the bright side, but this property is immaterial for our purposes.

then the corresponding ϕ_- on the screen are defined per continuity: $\phi_-(\mathcal{S}) = \phi_+(\mathcal{S})$. By (9), the same ϕ_- then diagonalise \hat{S} :

$$\hat{S}\phi_- = S\phi_-, \quad S = \frac{k_B}{4\hbar c L_P} A(\mathcal{S})|U(\mathcal{S})|. \quad (36)$$

Thermodynamical quantities will now arise as expectation values of operators in the entropic eigenstates $\phi_-(\mathcal{S})$.

We first deal with (9). Clearly its reexpression in the entropy representation will be the thermodynamical fundamental equation $S = S(A)$ in the sense of ref. [7], since the extensive parameter corresponding to the holographic screen is the area A . Then we have

$$\langle \hat{S} \rangle = \frac{k_B}{4\hbar c L_P} A(\mathcal{S})|U(\mathcal{S})|. \quad (37)$$

Availing ourselves of the freedom to pick the origin of potentials at will, let us set $|U(\mathcal{S})| = \hbar c/L_P$. Thus

$$\langle \hat{S} \rangle = \frac{k_B}{4L_P^2} A, \quad (38)$$

which is the celebrated Bekenstein–Hawking law. It arises as a thermodynamical fundamental equation in the entropy representation.

Our holographic screen is treated thermodynamically as a stretched membrane, so the generalised force conjugate to the extensive parameter A is the surface tension σ . Then the equation of state corresponding to (38) is

$$\sigma = \frac{k_B \langle \hat{T} \rangle}{4L_P^2}. \quad (39)$$

Rewrite the above as $2\pi k_B \langle \hat{T} \rangle = 8\pi L_P^2 \sigma$ and recall that σ is the normal component of force per unit length on the screen. Since force is proportional to acceleration, the above equation of state turns out to be equivalent to the Unruh law.

Finally we turn to the first law of thermodynamics and the equipartition theorem. As already mentioned in section 2.3, it turns out that the equipartition theorem can be derived from the Unruh law. Since this fact is valid both in the classical case (5) and in its quantum counterpart (11), the derivation being exactly the same whatever the case, we will provide the details pertaining to the derivation of (11) from (10). Integrate the latter over a thin 3-dimensional slice of width dn bounded by two equipotentials \mathcal{S}_1 and \mathcal{S}_2 . Now the Planck length L_P is extremely small, so we can safely set $dn = L_P$, while the two screens \mathcal{S}_1 and \mathcal{S}_2 will not differ appreciably in their surface area. Then the volume integral of the left-hand side of (10) very approximately equals $2\pi k_B L_P \int_{\mathcal{S}} d^2 a \hat{T}$. On the right-hand side, let us first integrate $d\hat{U}/dn$ along the normal direction, to obtain $L_P \hat{U}(\mathcal{S}_2) - L_P \hat{U}(\mathcal{S}_1)$. We can take the origin for the potential function such that it will vanish on \mathcal{S}_1 . The remaining term is the surface integral $L_P \int_{\mathcal{S}} d^2 a \hat{U}(\mathcal{S})$. The integrand can be pulled past the integration sign because \mathcal{S} is an equipotential surface, thus yielding $L_P \hat{U}(\mathcal{S}) \int_{\mathcal{S}} d^2 a$. This latter integral equals the surface area $A(\mathcal{S})$ of the screen, and (11) follows as claimed.

Taking the expectation value, in the entropic eigenstates ϕ_- , of the operator equation (11), produces the thermodynamical expression for the equipartition theorem:

$$\frac{k_B}{2} \int_S d^2a \langle \hat{T} \rangle = \frac{A(S)}{4\pi} \langle \hat{U}(S) \rangle. \quad (40)$$

4.6 Planck vs. Boltzmann, or \hbar vs. k_B

Planck’s quantum of action \hbar gets replaced, in the entropic picture, with Boltzmann’s constant k_B . This explains the presence of \hbar in the entropic derivation of classical gravity (Newton’s and Einstein’s) given in ref. [69]: by the correspondence (15), *the presence of \hbar is an unavoidable consequence of the presence of k_B , and vice-versa*. We find this dichotomy between the energy and the entropy representations very suggestive—it appears to be a sort of complementarity principle, in Bohr’s sense of the word. For example, this dichotomy allows one to write a quantum of energy in the form $E = \hbar\omega$, or else in the alternative form $E = Ck_B T$ (C being a dimensionless number). It also allows one to express a quantum of entropy in the form $S = \hbar\omega/T$, or else as $S = 2\pi k_B$. This dichotomy exchanges frequency ω with temperature T , thus time t maps to inverse temperature T^{-1} , which is reminiscent of the Tolman–Ehrenfest relation [66] and also of thermal time [56].

4.7 The second law of thermodynamics, revisited

As a minor technical point, we have restricted our analysis to closed holographic screens enclosing a finite 3–dimensional volume. Quantum–mechanically this corresponds to normalisable states in the energy representation. Nonnormalisable states correspond to open holographic screens without a boundary (thus having an infinite surface area and enclosing an infinite volume). Our analysis can be extended to the latter by replacing absolute quantities with densities (per unit surface or unit volume as the case may be). The connection with the second law of thermodynamics comes about as follows. The second law of thermodynamics, $\Delta S \geq 0$, lies hidden within the quantum theory. Of course, one can derive it from statistical mechanics, but our purpose here is the opposite. We have seen that the domain of the reduced entropy s is the half axis $s \geq 0$, and that this fact led to the entropic Hilbert space $L^2[0, \infty)$ (instead of $L^2(\mathbb{R})$) for the wavefunctions $\psi_-(s)$. All this is a quantum–mechanical rewriting of the second law. One could ask, under what conditions will the entropic coordinate ρ be nonnegative? This is certainly the case when the holographic screens are all closed, but what happens in case they are open? The geometry of the screens is dictated by the potential U . If the latter has flat directions, then its equipotentials will no longer be closed surfaces—instead they will have an infinite surface area and will enclose an infinite volume. As mentioned above, one appropriately replaces quantities like entropy and energy with the corresponding densities. However, the corresponding screens must be such that the normal coordinate to their bright side, ρ , runs over the half axis $\rho \geq 0$. This latter condition will be satisfied whenever the potential is such that it possesses a centre of force, or an axis, or a plane, or possibly a more general surface of symmetry, with respect to which one can define a nonnegative normal coordinate. This appears to

be the case in all physically interesting situations, thus staying in agreement with the second law of thermodynamics. Only the free particle lacks a *canonical* definition of a normal coordinate—but then again the second principle holds in the form $\Delta S = 0$, due to the absence of forces.

5 Discussion

5.1 Quantum mechanics as a holographic, emergent phenomenon

Classical thermodynamics can be conveniently expressed in either of two equivalent languages, respectively called the energy representation and the entropy representation [7]. Here we have argued that quantum mechanics as we know it (*i.e.*, on spacetime) corresponds to the energy representation, while quantum mechanics beyond a holographic screen (*i.e.*, in the absence of spacetime) corresponds to the entropy representation. In this paper we have developed the formalism of entropic quantum mechanics and placed it in correspondence with that of standard quantum mechanics on spacetime.

In particular, we have formulated the entropic uncertainty principle (23) for the (reduced) entropy variable s that the entropic wavefunction $\psi_-(s)$ (sometimes also denoted $R(\rho)$) depends on; see (24). The latter arises as the result of factoring out the part of the wavefunction that depends on the tangential coordinates to the screen, the normal coordinate being proportional to the entropy itself. We have also written down a differential equation satisfied by the entropic wavefunction, that one may well call the entropic Schroedinger equation; see (34).

Moreover, we have identified the explicit expression (14) as corresponding to the entropic wavefunction in the semiclassical limit $k_B \rightarrow 0$. There is a nice map, given by (15), between the semiclassical wavefunction in the energy representation and the corresponding semiclassical wavefunction in the entropy representation. This map exchanges the classical action integral with the entropy of the screen, while at the same time introducing a relative factor of i . It also exchanges Planck’s constant \hbar with Boltzmann’s constant k_B . In so doing, this map succeeds in explaining why Planck’s constant \hbar had to appear in the derivation of classical gravity (Newton’s and Einstein’s) given in ref. [69]. Namely, the presence of \hbar is an inescapable consequence of the presence of k_B , and viceversa, since \hbar is required by the energy representation, while k_B is required by the entropy representation.

If spacetime is an emergent phenomenon, then everything built on it necessarily becomes emergent [24]. This applies to quantum mechanics in particular. However, in the entropy representation developed here, the emergence property of quantum mechanics becomes a much sharper feature. Indeed, one usually associates entropy with lack of information, while energy (*e.g.*, a sharp energy eigenvalue) is thought of as providing definite information. Now the correspondence (15) implies that, if the entropy representation is emergent, then so is the energy representation, and viceversa. In this sense, the information content carried by entropy is no more diffuse than that carried by energy, nor is the information encoded by energy more sharply defined than that encoded in entropy. In other words, the correspondence (15) confirms what we already knew from other sources—namely, that quantum mechanics is definitely an emergent

phenomenon.

We have also succeeded in writing a holographic dictionary between quantum mechanics, on the one hand, and thermodynamics, on the other. An analogous holographic dictionary was presented, in the gravitational case, in ref. [69]. Some key entries in this gravitational/thermodynamical dictionary are summarised in eqns. (2), (3) and (5), preceded by the equivalence between statements *i*) and *ii*) of section 2.3. As a novelty, here we have presented the corresponding entries in our quantum–mechanical/thermodynamical dictionary. These entries include the equivalence between the analogues of statements *i*) and *ii*) of section 2.3. In our setup, this is expressed in the assertion that the energy representation of quantum mechanics (statement *i*)) is equivalent to the entropy representation of quantum mechanics (statement *ii*)). Further entries in this dictionary of equivalences are the analogues of eqns. (2), (3) and (5), respectively given by our eqns. (9), (10) and (11) when working in the energy representation. Our eqns. (9), (10) allow one to define an entropy field and a temperature field as (operator–valued) functions on \mathbb{R}^3 , whereas (11) is a reexpression of the first law of thermodynamics and of the equipartition theorem. Their respective vacuum expectation values give rise to the corresponding equations in the entropy representation, (38), (39) and (40), where the space dependence disappears. Their respective interpretations are the proportionality between the area and the entropy of the screen (the Bekenstein–Hawking law), the thermodynamical equation of state of the screen (the Unruh law), and the equipartition theorem.

5.2 Quantum mechanics in the absence of spacetime

Entropic quantum mechanics can be thought of as describing quantum mechanics *in the absence of spacetime*. This latter statement must be understood as meaning that the tangential coordinates to the holographic screens, as well as functions thereof, have been factored out, while the normal coordinate and functions thereof remain—though no longer as a *spatial coordinate*, but rather as a *measure of entropy*. This viewpoint is motivated in eqn. (25), that we have borrowed directly from [69]. Now in the absence of time there is no Hamiltonian. In the absence of space there are also no paths to sum over *à la* Feynman. One might thus conclude that there can be no quantum mechanics in the absence of spacetime. This is however not true, as shown here and as shown also by independent analyses. For example, quantum mechanics without spacetime has been proposed as a case for noncommutative geometry [58, 59, 40]. Without resorting to noncommutative geometry, one can also argue as follows.

We have seen that the Hilbert space of entropic quantum states is $L^2[0, \rho_j]$ for an observer who perceives space terminating at the screen \mathcal{S}_j , and $L^2[0, \infty)$ for an observer who perceives no screen at all, or horizon. Given the two screens \mathcal{S}_j and \mathcal{S}_k , respectively located at $\rho = \rho_j$ and $\rho = \rho_k$ with $\rho_j < \rho_k$, it holds that the two spaces $L^2[0, \rho_j]$ and $L^2[0, \rho_k]$ are unitarily isomorphic because both are infinite–dimensional and separable [64]. Now let $\rho_k \rightarrow \infty$. The isomorphism between $L^2[0, \rho_j]$ and $L^2[0, \infty)$, plus the identification (24) between entropy and normal coordinate, allows the observer who perceives the screen \mathcal{S}_j to extend his wavefunctions $R(\rho)$ beyond his boundary at ρ_j . His wavefunctions are now understood as $\psi_-(s)$, *i.e.*, as functions of the reduced entropy s —indeed the latter is not bounded from above. It is in this sense

that this second observer can be said to be doing *quantum mechanics in the absence of spacetime*.

It is right to observe that the unitary isomorphism between the two different realisations of the entropic Hilbert space, $L^2[0, \infty)$ and $L^2[0, \rho_j)$, need not map the semi-classical regime of the one into the semiclassical regime of the other, nor the strong-quantum regime of the one into the corresponding regime of the other. An analogous statement applies to the spaces $L^2[0, \rho_j)$ and $L^2[0, \rho_k)$ corresponding to the screens $\mathcal{S}_j, \mathcal{S}_k$. The observation just made will become relevant in section [5.3](#).

5.3 Open questions

We can summarise our conclusions so far with the assertion that entropic quantum mechanics is a holographic phenomenon, as emergent as spacetime itself. To round up our discussion we would like to present some thoughts of a more speculative nature.

As a first thought we would like to state that *entropic quantum mechanics is an observer-dependent phenomenon*. That measurement disturbs any quantum system is, of course, a basic tenet of quantum mechanics. The statement just made, however, refers to something different. The concept that quantum mechanics is observer-dependent has also appeared, in different guises, in [\[68, 60, 61\]](#) under the name of *duality*. Under duality one understands that *the notion of classical vs. quantum is relative to which theory one measures from* (see section 6 of ref. [\[68\]](#)). This is also the interpretation advocated in refs. [\[39\]](#) by one of the present authors.

An idea that lies close to the above notions is the statement that *the entropy of a horizon is an observer-dependent quantity* (see section 3 of ref. [\[52\]](#)). In view of our correspondence [\(15\)](#), this latter assertion turns out to be equivalent to the one above defining duality.

Thus the statement that quantum mechanics is observer-dependent, is an equivalent reexpression of duality, *i.e.*, of the relativity of the notion of a quantum. In the entropic picture developed here, this relativity presents itself as the different realisations of the entropic Hilbert space, explained in section [5.2](#). Equivalently, this relativity of the notion of a quantum arises here as the relativity of the entropy.

The previous statements may at first sound surprising. Classic treatises such as, *e.g.*, ref. [\[66\]](#), teach that the Lorentz transformation laws for the heat energy and the temperature are such that their ratio (the entropy) is a scalar. Moreover, in principle one expects physical constants such as k_B and \hbar to be observer-independent. However, let us note that a totally analogous phenomenon has been reported in refs. [\[50, 51, 52, 53, 54\]](#), where the entropy of the screen has been argued to be an observer-dependent quantity. That the entropy of a thermodynamical system becomes an observer-dependent quantity has also been concluded in an information-theoretical context [\[55\]](#). Upon transforming back to the energy representation, the dependence just described can be recast as the dependence of Planck's constant \hbar upon the observer. Exactly this latter conclusion concerning \hbar has been reported in [\[70\]](#).

Given that the equations of motion for Einstein's gravity can be recast as thermodynamical equations of state, it has been claimed that the canonical quantisation of gravity makes as little sense as *quantising sound waves in air* [\[41\]](#). This remark makes it clear that quantising Einstein's gravity may be attempting to quantise the wrong

classical theory, but it casts no doubt yet on the validity of quantum theory. However, doubts concerning the microscopic fundamentality of the latter arise once one realises that *quantum theory, too, is a thermodynamics in disguise...*

Acknowledgements J.M.I. thanks Max–Planck–Institut für Gravitationsphysik, Albert–Einstein–Institut (Golm, Germany), for hospitality extended a number of times over the years. This work has been supported by Universidad Politécnica de Valencia under grant PAID-06-09.

*Dich störe nichts, wie es auch weiter klinge,
schon längst gewohnt der wunderbarsten Dinge.
—Goethe.*

References

- [1] S. Adler, *Quantum Theory as an Emergent Phenomenon*, Cambridge University Press, Cambridge (2004).
- [2] R. Banerjee and B. Majhi, *Statistical Origin of Gravity*, Phys. Rev. **D81** (2010) 124006, arXiv:1003.2312 [gr-qc].
- [3] R. Banerjee, *From Black Holes to Emergent Gravity*, Int. J. Mod. Phys. **D19** (2010) 2365, arXiv:1005.4286 [gr-qc].
- [4] J. Bardeen, B. Carter and S. Hawking, *The Four Laws of Black Hole Mechanics*, Comm. Math. Phys. **31** (1973) 161.
- [5] J. Bekenstein, *Black Holes and Entropy*, Phys. Rev. **D7** (1973) 2333.
- [6] M. Blau and S. Theisen, *String Theory as a Theory of Quantum Gravity: a Status Report*, Gen. Rel. Grav. **41** (2009) 743.
- [7] H. Callan, *Thermodynamics*, Wiley, New York (1960).
- [8] F. Caravelli and L. Modesto, *Holographic Effective Actions from Black Holes*, arXiv:1001.4364 [gr-qc].
- [9] R. Carroll, *Remarks on Gravity, Entropy and Information*, arXiv:physics/0602036.
- [10] R. Carroll, *Fluctuations, Information, Gravity and the Quantum Potential*, Springer, New York (2006).
- [11] R. Carroll, *On the Emergence Theme of Physics*, World Scientific, Singapore (2010).
- [12] R. Carroll, *Remarks on Gravity and Quantum Geometry*, arXiv:1007.4744 [mat-ph].
- [13] R. Carroll, *On some Toy Quantum Cosmology*, arXiv:1010.1732 [gr-qc].

- [14] R. Carroll, *Remarks on Osmosis, Quantum Mechanics and Gravity*, arXiv:1104.0383 [gr-qc].
- [15] A. Caticha, *Entropic Dynamics*, arXiv:gr-qc/0109068.
- [16] A. Caticha, *From Entropic Dynamics to Quantum Theory*, arXiv:0907.4335 [quant-ph].
- [17] A. Caticha, *Entropic Dynamics, Time and Quantum Theory*, arXiv:1005.2357 [quant-ph].
- [18] H. Culetu, *Comments on “On the Origin of Gravity and the Laws of Newton”, by Erik Verlinde*, arXiv:1002.3876 [hep-th].
- [19] H.-T. Elze, *Note on the Existence Theorem in “Emergent Quantum Mechanics and Emergent Symmetries”*, arXiv:0710.2765 [quant-ph].
- [20] H.-T. Elze, *The Attractor and the Quantum States*, arXiv:0806.3408 [quant-ph].
- [21] H.-T. Elze, *Spacetime and Matter — a Duality of Partial Orders*, arXiv:1001.3964 [gr-qc].
- [22] H.-T. Elze, *Introduction: Quantum Theory and Beneath*, in *Decoherence and Entropy in Complex Systems*, H.-T. Elze (ed.), Lect. Notes in Phys. **633** (2004) 119.
- [23] A. Faraggi and M. Matone, *The Equivalence Postulate of Quantum Mechanics: Main Theorems*, arXiv:0912.1225 [hep-th].
- [24] P. Freund, *Emergent Gauge Fields*, arXiv:1008.4147 [hep-th].
- [25] S. Ghosh, *Planck Scale Effect in the Entropic Force Law*, arXiv:1003.0285 [hep-th].
- [26] S. Ghosh, *Black Hole Entropy: from Shannon to Bekenstein*, arXiv:1008.0946 [hep-th].
- [27] M. de Gosson, *The Symplectic Camel and the Uncertainty Principle: the Tip of an Iceberg?*, Found. Phys. **39** (2009) 194.
- [28] M. de Gosson and F. Luef *Symplectic Capacities and the Geometry of Uncertainty: the Irruption of Symplectic Topology in Classical and Quantum Mechanics*, Phys. Rep. **484** (2009) 131.
- [29] G. Groessing, *The Vacuum Fluctuation Theorem: Exact Schroedinger Equation via Nonequilibrium Thermodynamics*, Phys. Lett. **A372** (2008) 4556, arXiv:0711.4954 [quant-ph].
- [30] G. Groessing, *On the Thermodynamic Origin of the Quantum Potential*, Physica **A388** (2009) 811, arXiv:0808.3539 [quant-ph].

- [31] G. Groessing, J. Mesa Pascasio and H. Schwabl, *A Classical Explanation of Quantization*, arXiv:0812.3561 [quant-ph].
- [32] G. Groessing, *Sub-Quantum Thermodynamics as a Basis of Emergent Quantum Mechanics*, Entropy **2010**, 12, 1975.
- [33] S. Hawking, *Particle Creation by Black Holes*, Comm. Math. Phys. **43** (1975) 199.
- [34] G. 't Hooft, *On the Quantum Structure of a Black Hole*, Nucl. Phys. **B256** (1985) 727.
- [35] G. 't Hooft, *Dimensional Reduction in Quantum Gravity*, arXiv:gr-qc/9310026.
- [36] G. 't Hooft, *The Mathematical Basis for Deterministic Quantum Mechanics*, J. Phys. Conf. Ser. **67** (2007) 012015, arXiv:quant-ph/0604008.
- [37] G. 't Hooft, *Emergent Quantum Mechanics and Emergent Symmetries*, arXiv:0707.4568 [hep-th].
- [38] S. Hossenfelder, *Comments and Comments on Comments on Verlinde's Paper "On the Origin of Gravity and the Laws of Newton"*, arXiv:1003.1015 [gr-qc].
- [39] J.M. Isidro, *Quantum Mechanics as a Spontaneously Broken Gauge Theory on a $U(1)$ Gerbe*, Int. J. Geom. Meth. Mod. Phys. **5** (2008) 233, arXiv:0708.0720 [hep-th].
- [40] J.M. Isidro, P. Fernández de Córdoba, J. Rivera-Rebolledo and J.L.G. Santander, *On the Noncommutative Eikonal*, Int. J. Geom. Meth. Mod. Phys. **8** (2011) 621, arXiv:1007.4929 [hep-th].
- [41] T. Jacobson, *Thermodynamics of Spacetime: the Einstein Equation of State*, Phys. Rev. Lett. **75** (1995) 1260, arXiv:gr-qc/9504004.
- [42] A. Khrennikov, *An Analog of Heisenberg Uncertainty Relation in Pre-quantum Classical Field Theory*, Physica Scripta **81** (6) (2010) 065001, arXiv:0912.1565 [quant-ph].
- [43] B. Koch, *Quantizing Geometry or Geometrizing the Quantum?*, arXiv:1004.2879 [hep-th].
- [44] A. Lisi, *Quantum Mechanics from a Universal Action Reservoir*, arXiv:0605068 [physics.pop-ph].
- [45] M. Matone, *Equivalence Postulate and Quantum Origin of Gravitation*, Found. Phys. Lett. **15** (2002) 311, arXiv:hep-th/0005274.
- [46] L. Modesto and A. Randono, *Entropic Corrections to Newton's Law*, arXiv:1003.1998 [hep-th].

- [47] J. Munkhammar, *Is Holographic Entropy and Gravity the Result of Quantum Mechanics?*, arXiv:1003.1262 [hep-th].
- [48] J. Munkhammar, *Canonical Relational Quantum Mechanics from Information Theory*, arXiv:1101.1417 [physics.gen-ph].
- [49] E. Nelson, *Quantum Fluctuations*, Princeton University Press, Princeton (1985).
- [50] T. Padmanabhan, *Thermodynamics and/of Horizons: a Comparison of Schwarzschild, Rindler and de Sitter Spacetimes*, Mod. Phys. Lett. **A17** (2002) 923, arXiv:gr-qc/0202078.
- [51] T. Padmanabhan, *Is Gravity an Intrinsically Quantum Phenomenon? Dynamics of Gravity from the Entropy of Spacetime and the Principle of Equivalence*, Mod. Phys. Lett. **A17** (2002) 1147, arXiv:hep-th/0205278.
- [52] T. Padmanabhan, *A Dialogue on the Nature of Gravity*, arXiv:0910.0839 [gr-qc].
- [53] T. Padmanabhan, *Thermodynamical Aspects of Gravity: New Insights*, arXiv:0911.5004 [gr-qc].
- [54] T. Padmanabhan, *Lessons from Classical Gravity about the Quantum Structure of Spacetime*, arXiv:1012.4476 [gr-qc].
- [55] L. del Río, J. Aberg, R. Renner, O. Dahlsten and V. Vedral, *The Thermodynamic Meaning of Negative Entropy*, arXiv:1009.1630 [quant-ph].
- [56] C. Rovelli and M. Smerlak, *Thermal Time and Tolman–Ehrenfest Effect: Temperature as the “Speed of Time”*, arXiv:1005.2985 [gr-qc].
- [57] N. Seiberg, *Emergent Spacetime*, arXiv:hep-th/0601234.
- [58] T. Singh, *Quantum Mechanics without Spacetime—a Case for Noncommutative Geometry*, Bulg. J. Phys. **33** (2006) 217, arXiv:gr-qc/0510042.
- [59] T. Singh, *String Theory, Quantum Mechanics and Noncommutative Geometry*, Int. J. Mod. Phys. **D15** (2006) 2153, arXiv:hep-th/0605112.
- [60] T. Singh, *Noncommutative Gravity, a ‘No Strings Attached’ Quantum–Classical Duality, and the Cosmological Constant Puzzle*, Gen. Rel. Grav. **40** (2008) 2037, arXiv:0805.2124 [gr-qc].
- [61] T. Singh, *Quantum Theory, Noncommutative Gravity, and the Cosmological Constant Problem*, Adv. in Astronomy 2009 (2009) 632064, arXiv:0901.0978 [gr-qc].
- [62] L. Smolin, *Could Quantum Mechanics be an Approximation to Another Theory?*, arXiv:quant-ph/0609109.
- [63] L. Susskind, *The World as a Hologram*, arXiv:hep-th/9409089.

- [64] W. Thirring, *Quantum Mathematical Physics*, Springer, Berlin (2002).
- [65] Y. Tian and X. Wu, *Thermodynamics of Black Holes from Equipartition of Energy and Holography*, arXiv:1002.1275 [hep-th].
- [66] R. Tolman, *Relativity, Thermodynamics and Cosmology*, Dover, New York (1987).
- [67] W. Unruh, *Notes on Black Hole Evaporation*, Phys. Rev. **D14** (1976) 870.
- [68] C. Vafa, *Lectures on Strings and Dualities*, arXiv:hep-th/9702201.
- [69] E. Verlinde, *On the Origin of Gravity and the Laws of Newton*, JHEP **1104** (2011) 029, arXiv:1001.0785[hep-th].
- [70] G. Volovik, *\hbar as Parameter of Minkowski Metric in Effective Theory*, JETP Lett. **90** (2009) 697, arXiv:0904.1965 [gr-qc].

EMERGENT QUANTUM MECHANICS AS A CLASSICAL, IRREVERSIBLE THERMODYNAMICS

D. Acosta^{1,a}, P. Fernández de Córdoba^{2,b}, J.M. Isidro^{2,c} and J.L.G. Santander^{3,d}

¹Departamento de Matemáticas, Universidad de Pinar del Río,

Pinar del Río, Cuba

²Instituto Universitario de Matemática Pura y Aplicada,

Universidad Politécnica de Valencia, Valencia 46022, Spain

³Cátedra Energesis de Tecnología Interdisciplinar, Universidad Católica de Valencia,

C/ Guillem de Castro 94, Valencia 46003, Spain

^adago@mat.upr.edu.cu, ^bpfernandez@mat.upv.es

^cjoissan@mat.upv.es, ^dmartinez.gonzalez@ucv.es

Abstract We present an explicit correspondence between quantum mechanics and the classical theory of irreversible thermodynamics as developed by Onsager, Prigogine *et al.* Our correspondence maps irreversible Gaussian Markov processes into the semi-classical approximation of quantum mechanics. Quantum–mechanical propagators are mapped into thermodynamical probability distributions. The Feynman path integral also arises naturally in this setup. The fact that quantum mechanics can be translated into thermodynamical language provides additional support for the conjecture that quantum mechanics is not a fundamental theory but rather an emergent phenomenon, *i.e.*, an effective description of some underlying degrees of freedom.

Contents

1	Introduction	2
2	The Chapman–Kolmogorov equation in quantum mechanics	2
3	Fluctuations and irreversible processes	4
3.1	Thermodynamic forces	4
3.2	Fluctuations	6
3.3	Markov processes	7
3.4	Gaussian processes	8
4	The map between quantum mechanics and irreversible thermodynamics	9
4.1	Path integrals in irreversible thermodynamics	9
4.2	Propagators from thermodynamical distributions	10
4.3	Integrability vs. square–integrability	11
4.4	Entropy vs. action	14
5	Discussion	15

1 Introduction

Emergent physics as a research topic has drawn a lot of attention recently [10, 25]. The very spacetime we live in, as well as the gravitational force that governs it, both appear to be emergent phenomena [24, 39, 49]. Quantum mechanics has also been conjectured to be the emergent theory of some underlying deterministic model, in part because of its long-standing conflict with general relativity. There exists a large body of literature on emergent quantum mechanics, some basic references being [2, 21, 33]; see also [3, 11, 12, 14, 19, 22, 29, 30, 34, 43, 44, 45] for more recent work. The hypothesis of emergence and the holographic principle [20, 46] have been hailed as landmarks in the endeavour to arrive at a consistent theory of quantum gravity.

Without touching on the difficulties facing quantum gravity, a number of interpretational questions and foundational issues arise and remain within a purely quantum-mechanical setup (or, eventually, within a quantum field theory setup, see [23]). In this article, following earlier work [1], we will focus on *the emergent aspects of quantum mechanics applying a thermodynamical approach*. In fact the classical thermodynamics of irreversible processes and fluctuation theory will turn out to share many common features with quantum mechanics—surprisingly, with Feynman’s path integral approach to quantum mechanics. Some basic references on the subject of fluctuations and irreversible thermodynamics are [28, 37, 38, 40, 48]; intriguing questions such as the emergence of macroscopic irreversibility from microscopic reversibility, the arrow of time, and other related puzzles are analysed in [31, 41]. A more complete list of references can be found in [36].

Specifically, the purpose of this article is twofold:

- i*) to establish an explicit correspondence between quantum mechanics on the one hand, and the classical thermodynamics of irreversible processes on the other. We claim validity for this correspondence at least in the Gaussian approximation (which corresponds to the linear response regime in thermodynamics, and to the semiclassical approximation in quantum mechanics);
- ii*) to use the correspondence just mentioned in order to provide an independent proof of the statement that *quantum mechanics is an emergent phenomenon, at least in the semiclassical limit*.

With hindsight, once one has realised that quantum mechanics in the Gaussian approximation is a classical thermodynamics in disguise, the emergent nature of quantum theory becomes selfevident—after all, thermodynamics is a paradigm of emergent theories.

2 The Chapman–Kolmogorov equation in quantum mechanics

To begin with we present a collection of *purely* quantum-mechanical expressions, for which there will be *purely* thermodynamical reexpressions using the correspondence we are about to develop. Although the material of this section is standard, a good general reference is [50]. For simplicity we will restrict to a 1-dimensional configuration space X coordinatised by x .

The quantum–mechanical propagator $K(x_2, t_2|x_1, t_1)$ is defined as the amplitude for the conditional probability that a particle starting at (x_1, t_1) end at (x_2, t_2) :

$$K(x_2, t_2|x_1, t_1) = \langle x_2|U(t_2 - t_1)|x_1\rangle, \quad U(t) = \exp\left(-\frac{i}{\hbar}tH\right). \quad (1)$$

Above, $U(t)$ is the unitary time–evolution operator, and H is the quantum Hamiltonian operator. The time–evolution operators satisfy *the group property*,

$$U(t_1)U(t_2) = U(t_1 + t_2), \quad (2)$$

an equation known in statistics already since the 1930’s as *the Chapman–Kolmogorov equation* [I3]. Its solutions satisfy the differential equation

$$i\hbar\frac{dU}{dt} = HU(t), \quad H = i\hbar\frac{dU}{dt}\Big|_{t=0}. \quad (3)$$

Using (II) we obtain an alternative reexpression of the Chapman–Kolmogorov equation:

$$K(x_3, t_3|x_1, t_1) = \int dx_2 K(x_3, t_3|x_2, t_2) K(x_2, t_2|x_1, t_1). \quad (4)$$

Since wavefunctions ψ are *unconditional* probability amplitudes, they are related to propagators K (which are *conditional* probability amplitudes) as follows:

$$\psi(x_2, t_2) = \int dx_1 K(x_2, t_2|x_1, t_1) \psi(x_1, t_1). \quad (5)$$

Propagators can be computed via path integrals over configuration space X ,

$$K(x_2, t_2|x_1, t_1) = \int_{x(t_1)=x_1}^{x(t_2)=x_2} Dx(t) \exp\left\{\frac{i}{\hbar} \int_{t_1}^{t_2} dt L[x(t), \dot{x}(t)]\right\}, \quad (6)$$

where L is the classical Lagrangian function. Two simple examples in which the path integral (6) can be evaluated exactly are the free particle and the harmonic potential. For a free particle we have

$$K^{(\text{free})}(x_2, t_2|x_1, t_1) = \sqrt{\frac{m}{2\pi i\hbar(t_2 - t_1)}} \exp\left[\frac{im}{2\hbar} \frac{(x_2 - x_1)^2}{t_2 - t_1}\right], \quad (7)$$

while for a harmonic potential we have, ignoring the caustics,

$$K^{(\text{harmonic})}(x_2, t_2|x_1, t_1) = \sqrt{\frac{m\omega}{2\pi i\hbar \sin(\omega(t_2 - t_1))}} \times \exp\left\{\frac{im}{2\hbar} \frac{\omega}{\sin(\omega(t_2 - t_1))} [(x_2^2 + x_1^2) \cos(\omega(t_2 - t_1)) - 2x_1x_2]\right\}. \quad (8)$$

When the path integral (6) cannot be computed exactly, an approximate evaluation can still be helpful. For $\hbar \rightarrow 0$ we have the semiclassical approximation to the propagator, denoted by K_{cl} :

$$K_{\text{cl}}(x_2, t_2|x_1, t_1) = Z^{-1} \exp\left\{\frac{i}{\hbar} \int_{t_1}^{t_2} dt L[x_{\text{cl}}(t), \dot{x}_{\text{cl}}(t)]\right\}, \quad (9)$$

where $x_{\text{cl}}(t)$ stands for the classical trajectory between (x_1, t_1) and (x_2, t_2) , and Z^{-1} is some normalisation factor¹

3 Fluctuations and irreversible processes

For the benefit of the reader, with an eye on later applications, we include below a summary of ref. [38].

3.1 Thermodynamic forces

Let a thermodynamical system be given. If we are interested in only a single instant, the probability P of a given state is given by Boltzmann's principle,

$$k_B \ln P = S + \text{const}, \quad (10)$$

where S is the entropy of that state. If we are interested in two instants widely separated in time, the probability of given states at each instant is equal to the product of the individual probabilities. A long time lapse makes the states statistically independent. Hence the joint probability of the succession is related to the sum of the two entropies. But if the time lapse is not long, the states will be statistically correlated. It is precisely the laws for irreversible behaviour which tell us the correlations.

Let the thermodynamical state of our system be defined by a set of extensive variables y^1, \dots, y^N . The entropy $S = S(y^1, \dots, y^N)$ will be a function of all the y^k . Its maximum (equilibrium) value will be denoted by S_0 , and the y^k will be redefined to vanish for the equilibrium state: $S_0 = S(0, \dots, 0)$. The tendency of the system to seek equilibrium is measured by the *thermodynamic forces* Y_k defined as

$$Y_k = \frac{\partial S}{\partial y^k}, \quad k = 1, \dots, N. \quad (11)$$

The Y_k are *restoring forces* that vanish with the y^k .

Fluxes are measured by the time derivatives of the y^k . The essential physical assumption made here is that *irreversible processes are linear, i.e., they depend linearly on the forces that cause them*. Therefore we have²

$$\dot{y}^i = \frac{dy^i}{d\tau} = \sum_{j=1}^N L^{ij} Y_j, \quad i = 1, \dots, N. \quad (12)$$

Onsager's reciprocity theorem states that L is a symmetric matrix [37],

$$L^{ij} = L^{ji}. \quad (13)$$

¹We will henceforth use the collective notation Z^{-1} to denote all the different normalisation factors that we will not keep track of.

²We use τ to denote time in the theory of irreversible thermodynamics, and t to denote time in the quantum theory. As will be seen in [44], τ and t are related by a Wick rotation.

Further assuming that L is nonsingular one can solve for the forces in terms of the fluxes:

$$Y_i = \sum_{j=1}^N R_{ij} \dot{y}^j, \quad i = 1, \dots, N. \quad (14)$$

Thus the rate of production of entropy,

$$\dot{S} = \sum_{j=1}^N \frac{\partial S}{\partial y^j} \dot{y}^j = \sum_{j=1}^N Y_j \dot{y}^j, \quad (15)$$

can be expressed in either of two equivalent ways:

$$\dot{S} = \sum_{i,j=1}^N R_{ij} \dot{y}^i \dot{y}^j = \sum_{i,j=1}^N L^{ij} Y_i Y_j. \quad (16)$$

One defines the *dissipation function* Φ as the following quadratic form in the fluxes³

$$\Phi := \frac{1}{2} \sum_{i,j=1}^N R_{ij} \dot{y}^i \dot{y}^j. \quad (17)$$

This function is a potential for the Y_k , because $\partial\Phi/\partial\dot{y}^j = R_{jk} Y_k$. The corresponding quadratic form of the forces,

$$\Psi := \frac{1}{2} \sum_{i,j=1}^N L^{ij} Y_i Y_j, \quad (18)$$

has a similar property, but it should be noticed that it is a function of the *state* (since the Y_k depend only on the y^j), whereas the numerically equal Φ is a function of its *rate of change*.

If we expand the entropy in a Taylor series around equilibrium we have

$$S = S_0 - \frac{1}{2} \sum_{i,j=1}^N s_{ij} y^i y^j + \dots \quad (19)$$

The matrix s_{ij} is symmetric and positive definite. Neglect of the higher terms in y^k means the assumption that fluctuations are Gaussian: for Boltzmann's principle (10) states that the logarithm of the probability of a given fluctuation is proportional to its entropy, or

$$P(y^1, \dots, y^N) = Z^{-1} \exp\left(\frac{S}{k_B}\right) = Z^{-1} \exp\left(-\frac{1}{2k_B} \sum_{i,j=1}^N s_{ij} y^i y^j\right). \quad (20)$$

³We assume R_{ij} to be positive definite. This ensures that $\dot{S} > 0$ as expected of a dissipative process. Indeed, the dissipation function Φ can be identified with a kinetic energy, $T = \sum_{i,j=1}^N g_{ij} \dot{x}^i \dot{x}^j / 2$, where g_{ij} is a certain Riemannian metric on the space spanned by the velocities \dot{x}^j . Identifying \dot{x}^j with \dot{y}^j we have $g_{ij} = R_{ij}$.

The assumption of Gaussianity (I9) then implies that the Y_i are linear in the y^j :

$$Y_i = - \sum_{j=1}^N s_{ij} y^j. \quad (21)$$

Thus the phenomenological laws (I4) become

$$\sum_{j=1}^N (R_{ij} \dot{y}^j + s_{ij} y^j) = 0. \quad (22)$$

3.2 Fluctuations

Let us now modify the deterministic equations (I4) to include fluctuations by the addition of a random force ξ_i ,

$$\sum_{j=1}^N R_{ij} \dot{y}^j = Y_i + \xi_i, \quad (23)$$

which turns (I4) into the set of stochastic equations (23). We require that the ξ_i have zero means, which implies that the right-hand side of (23) is a random force with means Y_i . For simplicity, as in the quantum-mechanical case, let us set $N = 1$, so we have a single variable y obeying the stochastic equation

$$R\dot{y} + sy = \xi. \quad (24)$$

We will be concerned with the path of y in time under the influence of these random forces. Our aim is to calculate the probability of any path. For n instants of time $\tau_1 < \tau_2 < \dots < \tau_n$ we denote the *cumulative distribution function* by F_n :

$$F_n \left(\begin{matrix} y_1 \cdots y_n \\ \tau_1 \cdots \tau_n \end{matrix} \right) = P(y(\tau_k) \leq y_k, k = 1, \dots, n). \quad (25)$$

The function F_n tells the probability that the thermodynamical path $y(\tau)$ lie below the barriers y_1, \dots, y_n at the corresponding instants τ_1, \dots, τ_n . A *stationary* process is defined as one whose cumulative distribution function F_n is invariant under arbitrary time shifts $\delta\tau$:

$$F_n \left(\begin{matrix} y_1 \cdots y_n \\ \tau_1 \cdots \tau_n \end{matrix} \right) = F_n \left(\begin{matrix} y_1 & \cdots & y_n \\ \tau_1 + \delta\tau & \cdots & \tau_n + \delta\tau \end{matrix} \right), \quad \forall \delta\tau \in \mathbb{R}. \quad (26)$$

Physically this describes an *aged* system, one that has been left alone long enough that any initial conditions have worn off, or been forgotten. Thus we consider entropy creation as a loss of information: a dissipative system forgets its past.

Alongside F_n , the *probability density function* f_n is defined such that the product

$$f_n \left(\begin{matrix} y_1 \cdots y_n \\ \tau_1 \cdots \tau_n \end{matrix} \right) dy_1 \cdots dy_n \quad (27)$$

gives the probability that a thermodynamical path pass through gates of width dy_k .

We will also be interested in conditional probabilities. The *conditional probability function* for the $(n + 1)$ th event given the previous n ,

$$F_1 \left(\begin{matrix} y_{n+1} \\ \tau_{n+1} \end{matrix} \middle| \begin{matrix} y_1 \cdots y_n \\ \tau_1 \cdots \tau_n \end{matrix} \right) = P \left(y(\tau_{n+1}) = y_{n+1} \mid y(\tau_k) = y_k, k = 1, \dots, n \right), \quad (28)$$

is defined implicitly as follows:

$$\begin{aligned} & F_{n+1} \left(\begin{matrix} y_1 \cdots y_{n+1} \\ \tau_1 \cdots \tau_{n+1} \end{matrix} \right) \\ &= \int_{-\infty}^{y_1} d\tilde{y}_1 \cdots \int_{-\infty}^{y_n} d\tilde{y}_n F_1 \left(\begin{matrix} y_{n+1} \\ \tau_{n+1} \end{matrix} \middle| \begin{matrix} \tilde{y}_1 \cdots \tilde{y}_n \\ \tau_1 \cdots \tau_n \end{matrix} \right) dF_n \left(\begin{matrix} \tilde{y}_1 \cdots \tilde{y}_n \\ \tau_1 \cdots \tau_n \end{matrix} \right). \end{aligned} \quad (29)$$

Correspondingly, the *conditional probability density function* f_1 is defined such that

$$f_1 \left(\begin{matrix} y_k \\ \tau_k \end{matrix} \middle| \begin{matrix} y_{k-1} \\ \tau_{k-1} \end{matrix} \right) dy_k dy_{k-1} \quad (30)$$

equals the probability that a thermodynamical path pass through a gate of width dy_k at time τ_k , *given* that it passed through a gate of width dy_{k-1} at time τ_{k-1} .

3.3 Markov processes

A Markov process is defined as one whose conditional probabilities are independent of all but the immediately preceding instant [13]:

$$F_1 \left(\begin{matrix} y_{n+1} \\ \tau_{n+1} \end{matrix} \middle| \begin{matrix} y_1 \cdots y_n \\ \tau_1 \cdots \tau_n \end{matrix} \right) = F_1 \left(\begin{matrix} y_{n+1} \\ \tau_{n+1} \end{matrix} \middle| \begin{matrix} y_n \\ \tau_n \end{matrix} \right). \quad (31)$$

Intuitively: a Markov system has a short memory. For a Markov process (29) and (31) imply

$$f_n \left(\begin{matrix} y_1 \cdots y_n \\ \tau_1 \cdots \tau_n \end{matrix} \right) = f_1 \left(\begin{matrix} y_n \\ \tau_n \end{matrix} \middle| \begin{matrix} y_{n-1} \\ \tau_{n-1} \end{matrix} \right) \cdots f_1 \left(\begin{matrix} y_2 \\ \tau_2 \end{matrix} \middle| \begin{matrix} y_1 \\ \tau_1 \end{matrix} \right) f_1 \left(\begin{matrix} y_1 \\ \tau_1 \end{matrix} \right). \quad (32)$$

Now $f_1 \left(\begin{matrix} y_1 \\ \tau_1 \end{matrix} \right)$ is known from Boltzmann's principle (10). Hence, by stationarity, all that is needed in order to obtain the distribution function for an arbitrary number of gates is to evaluate the conditional probability density function

$$f_1 \left(\begin{matrix} y_2 \\ \tau + \delta\tau \end{matrix} \middle| \begin{matrix} y_1 \\ \tau \end{matrix} \right), \quad (33)$$

which depends only on $\delta\tau$, being independent of τ . Thus the n -gate problem reduces to the 2-gate problem.

3.4 Gaussian processes

A Gaussian stochastic process is one whose probability density function is a Gaussian distribution. Let us set, in (24),

$$\gamma := \frac{s}{R}. \quad (34)$$

Then the conditional probability function for a Gaussian process is given by (38)

$$f_1 \left(\begin{array}{c} y_2 \\ \tau + \delta\tau \end{array} \middle| \begin{array}{c} y_1 \\ \tau \end{array} \right) = \frac{1}{\sqrt{2\pi}} \frac{s/k_B}{\sqrt{1 - e^{-2\gamma\delta\tau}}} \exp \left[-\frac{s}{2k_B} \frac{(y_2 - e^{-\gamma\delta\tau}y_1)^2}{1 - e^{-2\gamma\delta\tau}} \right]. \quad (35)$$

Now eqn. (35), together with (32), constitutes the solution to the problem of finding the probability of any path in a Gaussian Markov process. We also remark that (35) correctly reduces to the one-gate distribution function (20) for $\delta\tau \rightarrow \infty$.

Next let us divide the interval $(\tau, \tau + \delta\tau)$ into n equal subintervals of length $\delta\tau/n$:

$$\tau_1 = \tau, \quad \tau_2 = \tau_1 + \frac{\delta\tau}{n}, \quad \dots, \quad \tau_{n+1} = \tau + \delta\tau. \quad (36)$$

Then we have

$$f_1 \left(\begin{array}{c} y_{n+1} \\ \tau_{n+1} \end{array} \middle| \begin{array}{c} y_1 \\ \tau_1 \end{array} \right) = \int dy_n \cdots \int dy_2 f_1 \left(\begin{array}{c} y_{n+1} \\ \tau_{n+1} \end{array} \middle| \begin{array}{c} y_n \\ \tau_n \end{array} \right) \cdots f_1 \left(\begin{array}{c} y_2 \\ \tau_2 \end{array} \middle| \begin{array}{c} y_1 \\ \tau_1 \end{array} \right). \quad (37)$$

This is again the Chapman–Kolmogorov equation. The integral above extends over all the $n - 1$ intermediate gates. Using (37) one can reexpress (35) in the following alternative form (38):

$$f_1 \left(\begin{array}{c} y_{n+1} \\ \tau_{n+1} \end{array} \middle| \begin{array}{c} y_1 \\ \tau_1 \end{array} \right) = Z^{-1} \exp \left\{ -\frac{1}{4k_B} \int_{\tau_1}^{\tau_{n+1}} d\tau R [\dot{y}(\tau) + \gamma y(\tau)]^2 \right\}_{\min}, \quad (38)$$

subject to $y(\tau_1) = y_1$, $y(\tau_{n+1}) = y_{n+1}$. The subscript *min* refers to the fact that argument of the exponential is to be evaluated along the trajectory that minimises the integral.

The one-gate distribution is obtained from the conditional distribution $f_1 \left(\begin{array}{c} y_2 \\ \tau_2 \end{array} \middle| \begin{array}{c} y_1 \\ \tau_1 \end{array} \right)$ by taking $\tau_1 = -\infty$ and $y_1 = 0$ (because the aged system certainly was at equilibrium long ago). Thus we set $n = 1$ in (38) and define the *thermodynamical Lagrangian function* \mathcal{L} as

$$\mathcal{L} [\dot{y}(\tau), y(\tau)] := \frac{R}{2} [\dot{y}(\tau) + \gamma y(\tau)]^2. \quad (39)$$

The dimension of \mathcal{L} is entropy per unit time, instead of energy. However, our map between mechanics and thermodynamics will justify the denomination ‘‘Lagrangian’’. The Euler–Lagrange equation for a minimum value of the integral in (38) is

$$\ddot{y} - \gamma^2 y = 0. \quad (40)$$

The solution to the above that satisfies the boundary conditions $y(\tau = -\infty) = 0$ and $y(\tau = \tau_2) = y_2$ is

$$y(\tau) = y_2 e^{\gamma(\tau - \tau_2)}. \quad (41)$$

Evaluating the integral in (38) along this extremal trajectory leads to

$$f_1 \left(\begin{array}{c} y_2 \\ \tau_2 \end{array} \middle| \begin{array}{c} 0 \\ -\infty \end{array} \right) = f_1 \left(\begin{array}{c} y_2 \\ \tau_2 \end{array} \right) = Z^{-1} \exp \left[-\frac{s}{2k_B} (y_2)^2 \right]. \quad (42)$$

This result is in agreement with what one expects from Boltzmann's principle (10) in the Gaussian approximation (19).

Finally substituting (42) into (37), we obtain the thermodynamical analogue of the quantum–mechanical relation (5):

$$f_1 \left(\begin{array}{c} y_2 \\ \tau_2 \end{array} \right) = \int dy_1 f_1 \left(\begin{array}{c} y_2 \\ \tau_2 \end{array} \middle| \begin{array}{c} y_1 \\ \tau_1 \end{array} \right) f_1 \left(\begin{array}{c} y_1 \\ \tau_1 \end{array} \right). \quad (43)$$

This concludes our summary of ref. [38].

4 The map between quantum mechanics and irreversible thermodynamics

The Wick rotation

$$\tau = it \quad (44)$$

between the thermodynamical evolution parameter τ and the quantum–mechanical time variable t is the first entry in our dictionary between classical irreversible thermodynamics and quantum mechanics.

4.1 Path integrals in irreversible thermodynamics

The concept of a path integral can be traced back to the Chapman–Kolmogorov equation. Indeed letting $n \rightarrow \infty$ in (36) and using (37), the right–hand side of (38) becomes a path integral *over the thermodynamical configuration space* Y :

$$f_1 \left(\begin{array}{c} y_2 \\ \tau_2 \end{array} \middle| \begin{array}{c} y_1 \\ \tau_1 \end{array} \right) = \int_{y(\tau_1)=y_1}^{y(\tau_2)=y_2} Dy(\tau) \exp \left\{ -\frac{1}{4k_B} \int_{\tau_1}^{\tau_2} d\tau R [\dot{y}(\tau) + \gamma y(\tau)]^2 \right\}. \quad (45)$$

Thus it turns out that (38) actually equals the semiclassical approximation (as per (9)) to the path integral (45). This latter expression for the distribution function f_1 in terms of a path integral is implicit in ref. [38]—but actually never written down explicitly in that paper; see however [18].

Dropping in (39) the term proportional to $\dot{y}y$ (a total derivative), we redefine the thermodynamical Lagrangian function \mathcal{L} to be

$$\mathcal{L} [\dot{y}(\tau), y(\tau)] = \frac{R}{2} [\dot{y}^2(\tau) + \gamma^2 y^2(\tau)]. \quad (46)$$

We observe that $\dot{y}^2(\tau)$ and $y^2(\tau)$ in \mathcal{L} carry the same relative sign. Similarly dropping in (45) the term proportional to $\dot{y}y$, we can rewrite the path integral using (46) as

$$f_1 \left(\begin{array}{c} y_2 \\ \tau_2 \end{array} \middle| \begin{array}{c} y_1 \\ \tau_1 \end{array} \right) = \int_{y(\tau_1)=y_1}^{y(\tau_2)=y_2} Dy(\tau) \exp \left\{ -\frac{1}{2k_B} \int_{\tau_1}^{\tau_2} d\tau \mathcal{L} [\dot{y}(\tau), y(\tau)] \right\}. \quad (47)$$

The path integral (47) is the thermodynamical analogue of the path integral (6) that defines the quantum–mechanical propagator. Thus setting $n = 1$ in (38), dropping the total derivative $\dot{y}y$, and replacing the integrand with the thermodynamical Lagrangian (46) leads to the Gaussian approximation to (47):

$$f_1 \left(\begin{array}{c} y_2 \\ \tau_2 \end{array} \middle| \begin{array}{c} y_1 \\ \tau_1 \end{array} \right) = Z^{-1} \exp \left\{ -\frac{1}{2k_B} \int_{\tau_1}^{\tau_2} d\tau \mathcal{L} [\dot{y}_{\text{cl}}(\tau), y_{\text{cl}}(\tau)] \right\}. \quad (48)$$

Here $\mathcal{L} [\dot{y}_{\text{cl}}(\tau), y_{\text{cl}}(\tau)]$ stands for the evaluation of (46) along the classical trajectory $y_{\text{cl}}(\tau)$ that satisfies the equations of motion (40). In this way (48) is seen to correspond to the semiclassical approximation for the quantum–mechanical propagator, given in (9). On the thermodynamical side, the quantum–mechanical semiclassical approximation translates as the assumption of Gaussianity for the stochastic forces ξ and for the entropy S , as well as the assumption of linearity between forces and fluxes (which leads up to the quadratic forms (17) and (18)).

4.2 Propagators from thermodynamical distributions

The next entry in our dictionary relates quantum–mechanical wavefunctions and propagators to thermodynamical distribution functions. Within the Gaussian approximation we use throughout, this entry will refer to the free particle and the harmonic oscillator. We first we need to identify certain mechanical variables with their thermodynamical partners. Specifically, we will make the following replacements⁴

$$\omega \leftrightarrow \gamma, \quad \frac{m\omega}{\hbar} \leftrightarrow \frac{s}{2k_B}, \quad x \leftrightarrow y. \quad (49)$$

To begin with, one expects the squared modulus of the wavefunction $|\psi|^2$ to be related to the 1–gate distribution function $f_1 \left(\begin{array}{c} y \\ \tau \end{array} \right)$, while the propagator K must correspond to a 2–gate distribution function $f_1 \left(\begin{array}{c} y_2 \\ \tau_2 \end{array} \middle| \begin{array}{c} y_1 \\ \tau_1 \end{array} \right)$. Indeed the 1–gate distribution function (42) gives the squared modulus of the ground state $\psi_0(x) = \exp(-m\omega x^2/2\hbar)$ of the harmonic oscillator once the replacements (44), (49) are applied:

$$f_1 \left(\begin{array}{c} x \\ it \end{array} \right) = Z^{-1} \exp \left(-\frac{m\omega}{\hbar} x^2 \right) = |\psi_0^{\text{(harmonic)}}(x)|^2. \quad (50)$$

With the appropriate choices for the constants m and ω , (50) can also represent a free wavepacket. Next we turn to propagators K . Elementary algebra brings the conditional probability function for a Gaussian process (35) into the form

$$f_1 \left(\begin{array}{c} y_2 \\ \tau \end{array} \middle| \begin{array}{c} y_1 \\ 0 \end{array} \right) = \frac{s}{2k_B} \frac{e^{\gamma\tau/2}}{\sqrt{\pi \sinh(\gamma\tau)}} \exp \left[-\frac{s}{2k_B} \frac{(e^{\gamma\tau/2}y_2 - e^{-\gamma\tau/2}y_1)^2}{2 \sinh(\gamma\tau)} \right]. \quad (51)$$

We will also be interested in the limit $\gamma \rightarrow 0$ of the above:

$$f_1 \left(\begin{array}{c} y_2 \\ \tau \end{array} \middle| \begin{array}{c} y_1 \\ 0 \end{array} \right)_{\gamma \rightarrow 0} \simeq \frac{s}{2k_B} \frac{1}{\sqrt{\pi \gamma\tau}} \exp \left[-\frac{s}{2k_B} \frac{(y_2 - y_1)^2}{2\gamma\tau} \right]. \quad (52)$$

⁴A dimensionful conversion factor must be understood as implicitly contained in the replacement $x \leftrightarrow y$, whenever needed.

Using (44) and (49), the free quantum–mechanical propagator (7) follows from (52):

$$K^{(\text{free})}(x_2, t|x_1, 0) = \sqrt{\frac{k_B}{s}} f_1 \left(\begin{array}{c|c} x_2 & x_1 \\ it & 0 \end{array} \right)_{\gamma \rightarrow 0}. \quad (53)$$

The case when γ is nonvanishing requires some more work. Again (44) and (49) allow one to relate the conditional probability (51) to the harmonic propagator (8) as follows:

$$f_1 \left(\begin{array}{c|c} x_2 & x_1 \\ it & 0 \end{array} \right) = \exp \left(\frac{i\omega t}{2} - \frac{\Delta V}{\hbar\omega} \right) \sqrt{\frac{2m\omega}{\hbar}} K^{(\text{harmonic})}(x_2, t|x_1, 0), \quad (54)$$

where $V(x) = kx^2/2$ is the harmonic potential and $\Delta V = V(x_2) - V(x_1)$. As had to be the case, (54) correctly reduces to (53) when $\omega \rightarrow 0$. The square roots present in (53) and (54) ensure that these two equations are dimensionally correct.

4.3 Integrability vs. square–integrability

Under our correspondence, the squared modulus of the wavefunction $|\psi|^2$ gets mapped into the *unconditional* probability density $f_1 \left(\begin{array}{c} y_1 \\ \tau_1 \end{array} \right)$, while the propagator K gets mapped into the *conditional* probability density $f_1 \left(\begin{array}{c|c} y_2 & y_1 \\ \tau_2 & \tau_1 \end{array} \right)$. One should bear in mind, however, that the quantum–mechanical objects ψ, K are probability *amplitudes*, while the thermodynamical objects f_1 are true probabilities. Therefore quantum mechanics is not just the Wick rotation of classical, irreversible thermodynamics—it is also the *square root* thereof, so to speak, because of the Born rule. In order to address this question in more detail we need to recall some background mathematics; see ref. [47] for a physics–oriented approach, and also [5] for a recent discussion of some of the issues analysed later in this section.

Let M be a measure space, and denote by $L^p(M)$ the Banach space⁵

$$L^p(M) = \{f : M \rightarrow \mathbb{C}, \|f\|_p < \infty\}, \quad \|f\|_p := \left(\int_M |f|^p \right)^{1/p}, \quad 0 < p < \infty. \quad (55)$$

It turns out that $L^p(M)$ is a Hilbert space only when $p = 2$. Moreover, $L^p(M)$ and $L^q(M)$ are linear duals of each other whenever $1/p + 1/q = 1$. Two particular cases of this duality will interest us. The first one is $p = 2, q = 2$, the other one is $p = 1, q = \infty$.

When $p = 2$ we have that $L^2(M)$ is selfdual, the duality being given by the scalar product: $\langle \cdot | \cdot \rangle : L^2(M) \times L^2(M) \rightarrow \mathbb{C}$. The corresponding algebra of bounded operators is $\mathcal{L}(L^2(M))$, a noncommutative C^* –algebra with respect to operator multiplication. Complex conjugation in $\mathcal{L}(L^2(M))$ consists in taking the adjoint operator, while the noncommutativity is that of matrix multiplication.

The operator algebra $\mathcal{L}(L^p(M))$ is also a Banach algebra for any $p > 0$, and not just for $p = 2$. However, only when $p = 2$ is a $\mathcal{L}(L^p(M))$ a C^* –algebra, because only when $p = 2$ does $\mathcal{L}(L^p(M))$ possess a complex conjugation.

⁵The space $L^p(M)$ is complex or real according to whether its elements f are taken to be complex–valued or real–valued functions on M . For quantum–mechanical applications we will consider the complex case, while thermodynamical applications require the real case. For generality, this summary assumes all spaces complex.

Set now $p = 1$. The dual of $L^1(M)$ is $L^\infty(M)$. Elements of the latter are measurable, essentially bounded functions f with a finite norm $\|f\|_\infty$:

$$L^\infty(M) = \{f : M \rightarrow \mathbb{C}, \|f\|_\infty < \infty\}, \quad \|f\|_\infty := \sup_{z \in M} \{|f(z)|\}. \quad (56)$$

The duality between $L^1(M)$ and $L^\infty(M)$ is

$$(\cdot|\cdot) : L^\infty(M) \times L^1(M) \longrightarrow \mathbb{C}, \quad (f|\rho) := \int_M f \rho, \quad (57)$$

for any $f \in L^\infty(M)$ and any $\rho \in L^1(M)$. Now $L^\infty(M)$ also qualifies as a C^* -algebra, the multiplication law being pointwise multiplication of functions (hence commutative), and the complex conjugation being that of the functions f . An important difference with respect to the previous case is that $\mathcal{L}(L^2(M))$ is noncommutative, whereas $L^\infty(M)$ is commutative.

We will henceforth write X for the space M when dealing with the mechanical configuration space, and Y when referring to the thermodynamical configuration space.

Textbook quantum mechanics regards quantum states as unit rays within $L^2(X)$, while physical observables \mathcal{O} are represented by selfadjoint operators $\mathcal{O} \in \mathcal{L}(L^2(X))$ ⁶. On the other hand, the natural framework for the theory of irreversible thermodynamics is the *real* Banach space $L^1(Y)$ and its dual, the *real* Banach algebra $L^\infty(Y)$. Thermodynamical states are probability distributions $\rho \in L^1(Y)$, that is, *real* functions, normalised as per $\int_Y \rho = 1$. Thermodynamical observables are *real* functions $f \in L^\infty(Y)$. Thus $\int_Y f \rho$ in (57) equals the average value of the physical quantity f in the state described by ρ .

Clearly the thermodynamical setup is not quite as sophisticated as its mechanical counterpart. As opposed to the *complex* Hilbert space $L^2(X)$, the *real* Banach space $L^1(Y)$ does not know about the existence of the imaginary unit i . In the absence of a complex conjugation to implement time reversal, the thermodynamical setup necessarily describes *irreversible* processes. Moreover, there exists no scalar product on $L^1(Y)$. Correspondingly there is no notion of a selfadjoint operator in $\mathcal{L}(L^1(Y))$ —in fact, thermodynamical observables are elements of a very different space, $L^\infty(Y)$ ⁷.

The previous differences notwithstanding, we can establish a map between quantum-mechanical states/observables and their thermodynamical counterparts, as we do next. We treat observables first, and discuss states later.

It is reasonable to identify real thermodynamical averages $(f|\rho)$ with quantum mechanical expectation values $\langle \psi | \mathcal{O} | \psi \rangle$ of selfadjoint operators \mathcal{O} , something like

$$\int_Y f \rho = (f|\rho) \leftrightarrow \langle \psi | \mathcal{O} | \psi \rangle = \int_X \psi^* \mathcal{O} \psi, \quad (58)$$

where the correspondence denoted by \leftrightarrow has yet to be given a precise meaning. For this we can assume diagonalising \mathcal{O} by a (complete, orthonormal) set of eigenstates $\psi_i \in L^2(X)$, so we can replace the right-hand side of (58) with the corresponding

⁶We ignore the mathematical subtleties due to the fact that \mathcal{O} is generally an unbounded operator, hence generally not an element of $\mathcal{L}(L^2(X))$, because this fact is immaterial to the discussion.

⁷In particular, the *real* space $L^\infty(Y)$ is a Banach algebra but not a C^* -algebra.

eigenvalue λ_i . We want to define a functional f for the left-hand side of (58). A sensible definition actually involves a collection of constant functionals f_i , each one of them equal to the corresponding eigenvalue λ_i :

$$f_i : Y \longrightarrow \mathbb{R}, \quad f_i(y) = \lambda_i, \quad \forall y \in Y. \quad (59)$$

Since the eigenvalues λ_i are constants and the density ρ can be normalised to unity, the imprecise correspondence (58) can be replaced with the precise dictionary entry

$$\int_Y f_i \rho = (f_i | \rho) = \lambda_i = \langle \psi_i | \mathcal{O} | \psi_i \rangle = \int_X \psi^* \mathcal{O} \psi. \quad (60)$$

This generalises in the obvious way to the case of a set of commuting observables \mathcal{O}_k . Noncommuting observables, not being simultaneously diagonalisable, lead to the impossibility of simultaneously defining the corresponding thermodynamical functionals f on the left-hand side of (60). We will examine the thermodynamical analogue of quantum commutators in a forthcoming publication.

So much for the observables; now we turn to the states. Since thermodynamical probabilities are elements of $L^1(Y)$ while quantum-mechanical amplitudes belong to $L^2(X)$, we would like to define some map of $L^2(X)$ into $L^1(Y)$, or viceversa. Given $\psi \in L^2(X)$, one's first instinct is to set $\rho := |\psi|^2$ because then $\rho \in L^1(X)$; this is of course the Born rule. The attentive reader will have noticed that we actually need $\rho \in L^1(Y)$: it is generally meaningless to equate ρ to $|\psi|^2$ —or to any other function of ψ , for that matter. We will proceed ahead under the simplifying assumption that $X = Y$.

The usual Born map b is defined as

$$b : L^2(X) \longrightarrow L^1(X), \quad b(\psi) := |\psi|^2. \quad (61)$$

This map is obviously not 1-to-1, so it fails to be an injection. As such it possesses no inverse. We will however use the formal notation b^{-1} to denote the map

$$b^{-1} : L^1(X) \longrightarrow L^2(X), \quad b^{-1}(\rho) := \sqrt{\rho} e^{\frac{i}{\hbar} \varphi}, \quad (62)$$

where φ is taken as the solution to the continuity equation

$$\dot{\rho} + \nabla \cdot (\rho \nabla \varphi) = 0 \quad (63)$$

that is well known from the Madelung transformation. Moreover, if $b^{-1}(\rho)$ satisfies the Schroedinger equation, then φ must of course equal the action integral $I = \int dt L$, and thus satisfy the *quantum* Hamilton-Jacobi equation [16]. Although the map b^{-1} also fails to be an injection, we use the notation b^{-1} because $bb^{-1}(\rho) = \rho$. Aside from this difficulty about the lack of injectivity, b and b^{-1} provide us with the required maps from quantum-mechanical states into thermodynamical distribution functions, and viceversa.

The Chapman-Kolmogorov equation (37), written below for $n = 2$,

$$f_1 \left(\begin{array}{c} y_3 \\ \tau_3 \end{array} \middle| \begin{array}{c} y_1 \\ \tau_1 \end{array} \right) = \int dy_2 f_1 \left(\begin{array}{c} y_3 \\ \tau_3 \end{array} \middle| \begin{array}{c} y_2 \\ \tau_2 \end{array} \right) f_1 \left(\begin{array}{c} y_2 \\ \tau_2 \end{array} \middle| \begin{array}{c} y_1 \\ \tau_1 \end{array} \right), \quad (64)$$

is the thermodynamical analogue of the quantum–mechanical equation (4). This leads us to the following point. Our correspondence maps $f_1 \left(\begin{smallmatrix} y_2 \\ \tau_2 \end{smallmatrix} \middle| \begin{smallmatrix} y_1 \\ \tau_1 \end{smallmatrix} \right)$, which is a conditional probability, into $K(x_2, t_2 | x_1, t_1)$, which is an *amplitude* for a conditional probability. In other words, under our correspondence, the Born rule does *not* apply to the map between conditional probabilities, although it does apply to the map between unconditional probabilities. There is nothing wrong with this. Indeed, f_1 and K satisfy the respective Chapman–Kolmogorov equations (64) and (4). Regarding the latter as matrix equations (which is what they are), they read formally $f_1 \times f_1 = f_1$ and $K \times K = K$. That is, squaring f_1 and K as matrices (which is how they should be squared, since f_1 and K are operators), they are idempotent. It therefore makes sense *not* to impose the Born rule on the map between K and f_1 .

4.4 Entropy vs. action

To complete our dictionary between quantum mechanics and irreversible thermodynamics we postulate the following correspondence between the action integral I and the entropy S :

$$\text{(mechanics)} \quad \frac{i}{\hbar} I \leftrightarrow \frac{1}{k_B} S \quad \text{(thermodynamics)}, \quad (65)$$

up to a numerical, dimensionless factor. Now the Wick rotation (44) replaces iI with the Euclidean action I_E , so we could just as well write

$$\text{(mechanics)} \quad \frac{1}{\hbar} I_E \leftrightarrow \frac{1}{k_B} S \quad \text{(thermodynamics)}, \quad (66)$$

again up to a numerical, dimensionless factor. We observe that both I and S independently satisfy an extremum principle. We also note that the respective fluctuation theories⁸ in the Gaussian approximation are obtained upon taking the exponential. Thus exponentiating (65) we arrive at the wavefunction

$$\psi = \sqrt{\rho} \exp \left(\frac{i}{\hbar} I \right) \quad (67)$$

and at the Boltzmann distribution function (10):

$$\rho_B = Z^{-1} \exp \left(\frac{1}{k_B} S \right). \quad (68)$$

We should point out that the correspondence (65), (66) has also been found to hold in independent contexts, long ago by de Broglie [9] and more recently *e.g.* in [1, 6].

Applying the Born rule we set the Boltzmann probability density ρ_B equal to the quantum–mechanical probability density $|\psi|^2$:

$$\rho_B = |\psi|^2 = \rho. \quad (69)$$

⁸These fluctuations are of course measured with respect to the corresponding mean values of I and S as given by their extremals.

(See ref. [4] for distributions other than the *squared* modulus). Hence

$$\rho = Z^{-1} \exp\left(\frac{1}{k_B} S\right). \quad (70)$$

Substitution of (70) into (67) yields an elegant expression for the wavefunction

$$\psi = Z^{-1/2} \exp\left(\frac{1}{2k_B} S\right) \exp\left(\frac{i}{\hbar} I\right), \quad (71)$$

combining thermodynamics and quantum mechanics into a single formula.

Implicitly assumed in (71) is the identification of mechanical variables x and thermodynamical variables y , as already done in (49). One can now define the *complex-valued action* $\mathcal{I}(x)$ ⁹

$$\mathcal{I}(x) := \frac{1}{2k_B} S + \frac{i}{\hbar} I. \quad (72)$$

in order to write

$$\psi(x) = Z^{-1/2} \exp(\mathcal{I}(x)) \quad (73)$$

as the semiclassical wavefunction (71), where

$$Z = \int dx |\exp(\mathcal{I}(x))|^2. \quad (74)$$

We realise that the correspondence (65), (66) leads naturally to the existence of a complexified action such as (72), which expresses a *fundamental symmetry between entropy and mechanical action*.

Finally we would like to point out that complexified action functionals have also been considered recently in ref. [32].

5 Discussion

We can summarise this article in the following statements:

- i)* we have succeeded in formulating a correspondence between standard quantum mechanics, on the one hand, and the classical thermodynamics of irreversible processes, on the other;
- ii)* this correspondence holds at least in the Gaussian approximation (the latter being defined in quantum mechanics as the semiclassical limit, and in thermodynamics as the regime of linearity between forces and fluxes);
- iii)* this possibility of encoding of quantum–mechanical information in thermodynamical terms provides an independent proof of the statement that quantum mechanics is an emergent phenomenon.

Specifically, our correspondence between semiclassical quantum mechanics and Gaussian irreversible thermodynamics includes the following points of section 4:

⁹While the entropy S is a true function of x , the action integral I is actually a *functional* of $x(t)$. However, in (72) we need I within the exponential defining ψ . To this end, I is to be evaluated along *the* classical trajectory starting at a certain given point and ending at a variable endpoint x . This amounts to regarding I as a true function of x and no longer as a functional.

- i*) we have shown that the path–integral representation for quantum–mechanical propagators is already present in the thermodynamical description of classical dissipative phenomena (section 4.1);
- ii*) we have mapped thermodynamical distribution functions into quantum–mechanical propagators (section 4.2);
- iii*) we have constructed an explicit correspondence between quantum–mechanical states and thermodynamical states, and also an analogous correspondence between quantum–mechanical observables and thermodynamical observables (section 4.3);
- iv*) we have grounded our correspondence in the existence of a fundamental symmetry between mechanical action and entropy (section 4.4).

In order to make this paper selfcontained we have also included, in section 3, a crash course in classical irreversible thermodynamics, the latter considered in the linear approximation. Presumably, the theory of irreversible thermodynamics beyond the linear regime should allow one to extend the present correspondence beyond the semiclassical approximation of quantum mechanics.

Having mapped *quantum* mechanics into *classical* irreversible thermodynamics raises another old question, *viz.*, the issue of how sharply, how univocally defined is the divide between *quantumness* and *classicality*. This issue has also been addressed, from the viewpoint of emergent theories, in ref. [15]; we defer our own contribution to the subject until a forthcoming publication. However we would like to briefly touch upon the emergence property of *spacetime*—not from a gravitational perspective, but from a purely quantum–mechanical viewpoint. If spacetime is an emergent phenomenon, as widely conjectured, then everything that makes use of spacetime concepts must necessarily be emergent, too. Quantum mechanics is no exception, unless one succeeds in constructing a quantum–mechanical formalism that is entirely free of spacetime notions. Progress towards this latter goal has been achieved along lines based on noncommutative geometry (see [17] and references therein). A more modest approach is to try and directly map quantum mechanics into thermodynamics, as done here and elsewhere. It turns out that spacetime arises as an emergent concept *also* in our quantum–mechanical approach, if only because our correspondence has required replacing space variables x with thermodynamical variables y . Thus, indirectly, we have also furnished (admittedly circumstantial) evidence of the emergence property of spacetime.

It was Einstein’s dream to see quantum mechanics formulated as an ensemble theory in which uncertainties would *not* have a fundamental ontological status. Instead, Einstein would have uncertainties and fluctuations arise as a consequence of *the statistical nature* of the description of an underlying *deterministic* system (see [27, 35] and refs. therein). Thermodynamical fluctuation theory thus appears to be the archetypal example that Einstein would presumably have liked for quantum mechanics to be modelled upon.

Actually it has been known since the early days of quantum mechanics that the (free) Schroedinger equation can be interpreted as the standard heat equation in imaginary time, so the thermodynamical connection has always existed. An unavoidable consequence of imaginary time is that real (decaying) exponentials replace imaginary (oscillatory) exponentials. This is the hallmark of dissipation. Thus quantum mechanics can be thought of as a dissipative phenomenon that becomes conservative only in

stationary states [7, 8, 21]—that little i in the Schroedinger equation makes a big difference [26].

After completion of this work we became aware of ref. [42], where topics partially overlapping with those treated here are discussed.

Acknowledgements J.M.I. would like to thank the organisers of the Heinz von Foerster Congress on Emergent Quantum Mechanics (Vienna, Austria, Nov. 2011) for stimulating a congenial atmosphere of scientific exchange, and for the interesting discussions that followed.

Willst Du erkennen? Lerne zu handeln!—Heinz von Foerster.

References

- [1] D. Acosta, P. Fernández de Córdoba, J.M. Isidro and J.L.G. Santander, *An Entropic Picture of Emergent Quantum Mechanics*, Int. J. Geom. Meth. Mod. Phys. **9** (2012) 1250048, arXiv:1107.1898 [hep-th].
- [2] S. Adler, *Quantum Theory as an Emergent Phenomenon*, Cambridge University Press, Cambridge (2004).
- [3] S. Adler, *Quantum Theory as an Emergent Phenomenon: Foundations and Phenomenology*, J. Phys. Conf. Ser. **361** (2012) 012002.
- [4] G. Bacciagaluppi, *Non-Equilibrium in Stochastic Mechanics*, J. Phys. Conf. Ser. **361** (2012) 012017.
- [5] J. Baez and B. Fong, *A Noether Theorem for Markov Processes*, arXiv:1203.2035 [math-ph].
- [6] R. Banerjee, *From Black Holes to Emergent Gravity*, Int. J. Mod. Phys. **D19** (2010) 2365, arXiv:1005.4286 [gr-qc].
- [7] M. Blasone, P. Jizba and G. Vitiello, *Dissipation and Quantization*, Phys. Lett. **A287** (2001) 205, arXiv:hep-th/0007138.
- [8] M. Blasone, P. Jizba and G. Vitiello, *Dissipation, Emergent Quantization, and Quantum Fluctuations*, in *Decoherence and Entropy in Complex Systems, Selected Lectures from DICE 2002*, H.-T. Elze (ed.), Lecture Notes in Physics **633**, Springer, Berlin (2004).
- [9] L. de Broglie, *La Thermodynamique de la Particule Isolée*, Gauthier-Villars, Paris (1964).
- [10] R. Carroll, *On the Emergence Theme of Physics*, World Scientific, Singapore (2010).
- [11] R. Carroll, *Remarks on Osmosis, Quantum Mechanics, and Gravity*, J. Phys. Conf. Ser. **361** (2012) 012010, arXiv:1104.0383 [gr-qc].



- [12] A. Cetto, L. de la Peña and A. Valdés–Hernández, *Quantization as an Emergent Phenomenon Due to Matter–Zeropoint Field Interaction*, J. Phys. Conf. Ser. **361** (2012) 012013.
- [13] J. Doob, *Stochastic Processes*, Wiley, New York (1953).
- [14] H.-T. Elze, *The Attractor and the Quantum States*, Int. J. Qu. Info. **7** (2009) 83, arXiv:0806.3408 [quant-ph].
- [15] H.-T. Elze, *Linear Dynamics of Quantum–Classical Hybrids*, Phys. Rev. **A85** (2012) 052109, arXiv:1111.2276 [quant-ph];
Four Questions for Quantum–Classical Hybrid Theory, J. Phys. Conf. Ser. **361** (2012) 012004, arXiv:1202.3448 [quant-ph].
- [16] A. Faraggi and M. Matone, *The Equivalence Postulate of Quantum Mechanics: Main Theorems*, arXiv:0912.1225 [hep-th].
- [17] G. Giachetta, L. Mangiarotti and G. Sardanashvily, *Geometric and Algebraic Topological Methods in Quantum Mechanics*, World Scientific, Singapore (2005).
- [18] R. Graham, *Path Integral Formulation of General Diffusion Processes*, Z. Phys. **B26** (1977) 281.
- [19] G. Groessing, S. Fussy, J. Mesa Pascasio and H. Schwabl, *The Quantum as an Emergent System*, J. Phys. Conf. Ser. **361** (2012) 012008, arXiv:1205.3393 [quant-ph].
- [20] G. 't Hooft, *Dimensional Reduction in Quantum Gravity*, arXiv:gr-qc/9310026.
- [21] G. 't Hooft, *Emergent Quantum Mechanics and Emergent Symmetries*, AIP Conf. Proc. **957** (2007) 154, arXiv:0707.4568 [hep-th].
- [22] G. 't Hooft, *Quantum Mechanics from Classical Logic*, J. Phys. Conf. Ser. **361** (2012) 012024;
Relating the Quantum Mechanics of Discrete Systems to Standard Canonical Quantum Mechanics, arXiv:1204.4926 [quant-ph].
- [23] G. 't Hooft, *Duality between a Deterministic Cellular Automaton and a Bosonic Quantum Field Theory in $1 + 1$ Dimensions*, arXiv:1205.4107 [quant-ph].
- [24] B. Hu, *Gravity and Nonequilibrium Thermodynamics of Classical Matter*, Int. J. Mod. Phys. **D20** (2011) 697, arXiv:1010.5837 [gr-qc].
- [25] B. Hu, *Emergence: Key Physical Issues for Deeper Philosophical Enquiries*, J. Phys. Conf. Ser. **361** (2012) 012003, arXiv:1204.1077 [physics.hist-ph].
- [26] L. Kauffman, *Eigenforms, Discrete Processes and Quantum Processes*, J. Phys. Conf. Ser. **361** (2012) 012034, arXiv:1109.1892 [math-ph].

- [27] A. Khrennikov, “Einstein’s Dream” – *Quantum Mechanics as Theory of Classical Random Fields*, arXiv:1204.5172 [quant-ph].
- [28] L. Landau and E. Lifschitz, *Statistical Physics, Part I*, vol. 5 of *Course of Theoretical Physics*, Pergamon Press, Oxford (1980).
- [29] J.-W. Lee, *Quantum Mechanics Emerges from Information Theory Applied to Causal Horizons*, Found. Phys. **41** (2011) 744, arXiv:1005.2739 [hep-th].
- [30] J. Mesa Pascasio, S. Fussy, H. Schwabl and G. Groessing, *Classical Simulation of Double Slit Interference via Ballistic Diffusion*, J. Phys. Conf. Ser. **361** (2012) 012041, arXiv:1205.4521 [quant-ph].
- [31] B. Misra, I. Prigogine and M. Courbage, *From Deterministic Dynamics to Probabilistic Descriptions*, Proc. Natl. Acad. Sci. USA **76** (1979) 3607;
Lyapounov Variable: Entropy and Measurement in Quantum Mechanics, Proc. Natl. Acad. Sci. USA **76** (1979) 4768.
- [32] K. Nagao and H. Nielsen, *Formulation of Complex Action Theory*, arXiv:1104.3381 [quant-ph];
Theory Including Future not Excluded—Formulation of Complex Action Theory II—, arXiv:1205.3706 [quant-ph].
- [33] P. Nelson, *Derivation of the Schroedinger Equation from Newtonian Mechanics*, Phys. Rev. **150** (1966) 1079.
- [34] P. Nelson, *Review of Stochastic Mechanics*, J. Phys Conf. Ser. **361** (2012) 012011.
- [35] T. Nieuwenhuizen, *Towards Einstein’s Dream of a Unified Field Theory: Reports from a Journey on a Long and Winding Road*, J. Phys. Conf. Ser. **361** (2012) 012036.
- [36] N. Olah, *Einsteins Trojanisches Pferd: eine Thermodynamische Deutung der Quantentheorie*, Springer, Wien (2011).
- [37] L. Onsager, *Reciprocal Relations in Irreversible Processes. I.*, Phys. Rev. **37** (1931) 405;
Reciprocal Relations in Irreversible Processes. II., Phys. Rev. **38** (1931) 2265.
- [38] L. Onsager and S. Machlup, *Fluctuations and Irreversible Processes*, Phys. Rev. **91** (1953) 1505;
Fluctuations and Irreversible Processes. II. Systems with Kinetic Energy, Phys. Rev. **91** (1953) 1512.
- [39] T. Padmanabhan, *Lessons from Classical Gravity about the Quantum Structure of Spacetime*, J. Phys. Conf. Ser. **306** (2011) 012001, arXiv:1012.4476 [gr-qc].

- [40] I. Prigogine, *Introduction to Thermodynamics of Irreversible Processes*, Interscience, New York (1961);
Time, Structure and Fluctuations, Nobel Prize Lecture (1977).
- [41] I. Prigogine and Cl. George, *The Second Law as a Selection Principle: The Microscopic Theory of Dissipative Processes in Quantum Systems*, Proc. Natl. Acad. Sci. USA **80** (1983) 4590.
- [42] A. Ruuge, *Pauli Problem in Thermodynamics*, arXiv:1208.2919 [math-ph].
- [43] M. Sakellariadou, A. Stabile and G. Vitiello, *Noncommutative Spectral Geometry, Dissipation and the Origin of Quantization*, J. Phys. Conf. Ser. **361** (2012) 012025.
- [44] H. Schwabl, J. Mesa Pascasio, S. Fussy and G. Groessing, *Quantum Features Derived from the Classical Model of a Bouncer–Walker Coupled to a Zero–Point Field*, J. Phys. Conf. Ser. **361** (2012) 012021, arXiv:1205.4519 [quant-ph].
- [45] L. Smolin, *Could Quantum Mechanics be an Approximation to Another Theory?*, arXiv:quant-ph/0609109.
- [46] L. Susskind, *The World as a Hologram*, J. Math. Phys. **36** (1995) 6377, arXiv:hep-th/9409089.
- [47] W. Thirring, *Quantum Mathematical Physics*, 2nd edition, Springer, Berlin (2002).
- [48] L. Tisza and I. Manning, *Fluctuations and Irreversible Thermodynamics*, Phys. Rev. **105** (1957) 1695.
- [49] E. Verlinde, *On the Origin of Gravity and the Laws of Newton*, JHEP **1104** (2011) 029, arXiv:1001.0785 [hep-th].
- [50] J. Zinn–Justin, *Path Integrals in Quantum Mechanics*, Oxford University Press, Oxford (2005).

Article

On the van der Waals Gas, Contact Geometry and the Toda Chain

Diego Alarcón, P. Fernández de Córdoba , J. M. Isidro *  and Carlos Orea

Instituto Universitario de Matemática Pura y Aplicada, Universidad Politécnica de Valencia, 46022 Valencia, Spain; diealcor@doctor.upv.es (D.A.); pfernandez@mat.upv.es (P.F.d.C.); carorhue@etsii.upv.es (C.O.)

* Correspondence: joissan@mat.upv.es

Received: 7 June 2018; Accepted: 16 July 2018; Published: 26 July 2018



Abstract: A Toda-chain symmetry is shown to underlie the van der Waals gas and its close cousin, the ideal gas. Links to contact geometry are explored.

Keywords: van der Waals gas; contact geometry; Toda chain

1. Introduction

The contact geometry of the classical van der Waals gas [1] is described geometrically using a five-dimensional contact manifold \mathcal{M} [2] that can be endowed with the local coordinates U (internal energy), S (entropy), V (volume), T (temperature) and p (pressure). This description corresponds to a choice of the fundamental equation, in the energy representation, in which U depends on the two extensive variables S and V . One defines the corresponding momenta $T = \partial U / \partial S$ and $-p = \partial U / \partial V$. Then, the standard contact form on \mathcal{M} reads [3,4]

$$\alpha = dU + TdS - pdV. \quad (1)$$

One can introduce Poisson brackets on the four-dimensional Poisson manifold \mathcal{P} (a submanifold of \mathcal{M}) spanned by the coordinates S, V and their conjugate variables $T, -p$, the nonvanishing brackets being

$$\{S, T\} = 1, \quad \{V, -p\} = 1. \quad (2)$$

Given now an equation of state

$$f(p, T, \dots) = 0, \quad (3)$$

one can make the replacements $T = \partial U / \partial S$, $-p = \partial U / \partial V$ in order to obtain

$$f\left(-\frac{\partial U}{\partial V}, \frac{\partial U}{\partial S}, \dots\right) = 0. \quad (4)$$

In Ref. [5], we have called Equation (4) a partial differential equation of state (PDE of state for short). It plays a role analogous to that played by the Hamilton–Jacobi equation in classical mechanics [2,6,7]. With respect to the latter, however, there is one fundamental difference. While in mechanics the Hamilton–Jacobi equation is just one equation (regardless of the number of degrees of freedom), in thermodynamics, we have one PDE of state per degree of freedom because the defining equation of each momentum qualifies as an equation of state.

2. The PDEs of State of the van der Waals Gas

Let us consider one mole of particles of van der Waals gas (i.e., Avogadro's number N of particles). The fundamental equation in the energy representation $U = U(S, V)$ reads [1]

$$U(S, V) = U_0 \left(\frac{V_0}{V-b} \right)^{2/3} \exp \left(\frac{2S}{3Nk_B} \right) - \frac{a}{V}, \quad (5)$$

with U_0, V_0 certain fiducial values; setting $a = 0$ and $b = 0$, one recovers the ideal gas. The variables T and $-p$, conjugate to S and V , are

$$T = \frac{\partial U}{\partial S} = U_0 \left(\frac{V_0}{V-b} \right)^{2/3} \exp \left(\frac{2S}{3Nk_B} \right) \frac{2}{3Nk_B} \quad (6)$$

and

$$p = -\frac{\partial U}{\partial V} = \frac{2}{3} U_0 \exp \left(\frac{2S}{3Nk_B} \right) \frac{V_0^{2/3}}{(V-b)^{5/3}} - \frac{a}{V^2}. \quad (7)$$

Equations (6) and (7) lead to the van der Waals equation of state

$$\left(p + \frac{a}{V^2} \right) (V-b) = Nk_B T \quad (8)$$

and the equipartition theorem:

$$U(T, V) = \frac{3}{2} Nk_B T - \frac{a}{V}. \quad (9)$$

The first PDE of state follows from Equation (8),

$$\left(\frac{\partial U}{\partial V} - \frac{a}{V^2} \right) (V-b) + Nk_B \frac{\partial U}{\partial S} = 0, \quad (10)$$

while, from Equation (9), we obtain the second PDE of state:

$$U - \frac{3}{2} Nk_B \frac{\partial U}{\partial S} + \frac{a}{V} = 0. \quad (11)$$

when $a = 0$ and $b = 0$, systems (10) and (11) correctly reduce to the corresponding system of PDEs for the ideal gas, obtained in Ref. [5]. One readily verifies that integration of the systems (10) and (11) lead back to the fundamental Equation (5) we started off with.

3. Relation to the Toda Chain

Although well studied in the literature [8–10], for the benefit of the reader, we very briefly summarise the essentials of Toda lattices needed for our purposes here. The Toda chain is a model for a nonharmonic lattice describing the motion of a chain of particles subject to nearest-neighbour interactions. The statement that interactions are restricted to nearest neighbours translates into an equation of motion for the n -th particle

$$m_n \ddot{x}_n(t) = \nabla V(x_{n+1}(t) - x_n(t)) - \nabla V(x_n(t) - x_{n-1}(t)), \quad (12)$$

where $x_n(t)$ is its displacement from equilibrium, and V is a certain potential function. Toda assumes the latter to be given by the exponential of the relative displacements:

$$V = \exp(-(x_n - x_{n-1})). \quad (13)$$

Although the resulting model turns out to exhibit many interesting properties, integrability being one of them, the succinct summary just given is all we will need for our purposes.

Returning now to our problem, a succession of changes of variables in configuration space \mathcal{C} (the submanifold of \mathcal{M} spanned by the extensive coordinates S, V) will relate the fundamental Equation (5) for the van der Waals gas to the potential energy of the Toda chain. We define the new variables S', V'

$$S' := S, \quad V' := V - b, \tag{14}$$

and s, v

$$s := \frac{S'}{Nk_B}, \quad v := \ln\left(\frac{V'}{V_0}\right), \tag{15}$$

in terms of which the fundamental Equation (5) reads

$$U(s, v) = U_0 \exp\left[\frac{2(s-v)}{3}\right] - \frac{a}{V_0 e^v + b}. \tag{16}$$

The transformations (14) and (15) are both diffeomorphisms: they can be inverted, regardless of the values of the van der Waals parameters a, b . However, the final change of variables

$$x := s - v, \quad U_0 \exp\left(\frac{2y}{3}\right) := \frac{a}{V_0 e^v + b} \tag{17}$$

becomes singular when $a = 0$. For the moment, we proceed under the assumption that $a \neq 0$, so Equation (17) is invertible. Then, the fundamental Equation (16) becomes

$$U(x, y) = U_0 \left[\exp\left(\frac{2x}{3}\right) - \exp\left(\frac{2y}{3}\right) \right] = W(x) - W(y), \tag{18}$$

where we have defined the new function

$$W(z) := U_0 \exp\left(\frac{2z}{3}\right). \tag{19}$$

The function $W(z)$ coincides with the potential function of the Toda chain; we have already encountered it in Ref. [5] in the context of the ideal gas. Since the latter has $a = 0$, which causes the change of variables (17) to be singular, one must proceed differently in this case. Instead of Equation (17), a nonsingular change of variables to consider for the ideal gas is

$$x' := s - v, \quad y' := s + v. \tag{20}$$

As already seen in Ref. [5], this yields a fundamental equation depending on x' , but not on y' :

$$U_{\text{ideal}}(x') = W(x'). \tag{21}$$

On the other hand, from Ref. [8], we know that, in the limit of small wave amplitudes, the time average of the momentum variable in a thermal ensemble of Toda chains is directly proportional to the product of Boltzmann's constant k_B times the temperature T (see Equation (3.20) of Ref. [8], the right-hand side of which is independent of the lattice site n). We conclude that, *in the limit of small amplitudes, a thermal ensemble of waves in the Toda chain behaves exactly as an ideal gas.*

Returning now to the van der Waals gas in Equation (18), the new canonical momenta read

$$p_x = \frac{\partial U}{\partial x} = \frac{2}{3}W(x), \quad p_y = \frac{\partial U}{\partial y} = -\frac{2}{3}W(y). \tag{22}$$

While the momentum p_x is the same as for the ideal gas, the negative sign in p_y can be traced back to the reduction in energy, with respect to the ideal case, due to the van der Waals parameter a . The PDEs of state read, in the new variables x, y ,

$$\frac{\partial U}{\partial x} - \frac{2U_0}{3} \exp\left(\frac{2x}{3}\right) = 0, \quad \frac{\partial U}{\partial y} + \frac{2U_0}{3} \exp\left(\frac{2y}{3}\right) = 0. \quad (23)$$

Compared to Equations (10) and (11), we see that, in the new variables x, y , the PDEs of state decouple into a system of two identical equations (up to a sign), one for each independent variable. Moreover, the equation corresponding to the variable x equals that PDE of the ideal gas, which expresses the equipartition theorem. Finally the contact form (1) reads, in terms of x, y and the corresponding momenta p_x, p_y ,

$$\alpha = dU + p_x dx + p_y dy. \quad (24)$$

In the limit when the gas is ideal, the momentum p_y vanishes identically [5], and the physics is described in terms of the three-dimensional contact submanifold \mathcal{N} spanned by x, p_x and U .

4. Discussion

The physics of the classical van der Waals gas is usually described by a five-dimensional contact manifold \mathcal{M} endowed with the contact form given in Equation (1). In this paper, we have identified one particular diffeomorphism that neatly disentangles the (rather abstruse) fundamental Equation (5) to the much more manageable form given by Equations (18) and (19). This latter form is not just easier to work with; it is also more inspiring. Namely, the fundamental equation of the van der Waals gas now equals the difference of two terms (one term per independent variable x, y), each one of which is a copy of the Toda potential function [8–10].

From the point of view of contact geometry, the only difference between the van der Waals gas and the ideal gas lies in the fact that the contact manifold describing the van der Waals gas remains five-dimensional, instead of reducing to the three-dimensional contact submanifold \mathcal{N} we found in the ideal case [5]. However, as we have proved in Equation (18), the fundamental equation can be expressed in terms of the Toda potential function in both cases.

Why the precisely Toda potential should arise in this thermodynamical context, instead of some other potential function, is a question that arises naturally. We believe the answer is the following. The distinguishing feature of the Toda potential is the exponential function. In thermodynamics, the exponential function arises naturally through Boltzmann's principle: the number of microstates that are compatible with a given macrostate specified by the value S of the entropy is proportional to $\exp(S/k_B)$. That the latter factor is present in the fundamental Equation (5) should come as no surprise, since the internal energy should be an extensive variable of the system.

Another intriguing feature of the above correspondence between the fundamental equation of a gas (either ideal or van der Waals) and the Toda potential function is the following. The small-amplitude limit considered in Ref. [8] is the limit of vanishing kinetic energy; this fact is reflected in the vanishing (to first order of approximation) of the time average of the generalised velocities \dot{s}_n in Ref. [8]. This limit has been called *the topological limit* in Ref. [11]; roughly speaking, it amounts to cancelling the kinetic term while keeping only the potential term in the Hamiltonian. This fact allows us to sharpen our previous correspondence, which we can now state more precisely as follows: *the classical thermodynamics of the (ideal or van der Waals) gas has a dual theory which, to first order of approximation, coincides with the topological limit of a thermal ensemble of waves in the Toda chain.* Surprising here is the fact that, for the ideal gas, all energy is purely kinetic, and the potential energies introduced by the van der Waals parameters a, b are almost negligible compared to the kinetic energy. Thus, *the theory of gases, where energies are completely or mostly kinetic, is mapped by this correspondence into a dual theory in which kinetic energies are negligible.* Vanishing or at least negligible kinetic energies are strongly reminiscent of topological field theory [12]; we hope to report on this issue in the future, as well as on its relation to Riemannian fluctuation theory [13,14].

Author Contributions: All authors contributed equally to the paper.

Funding: This research was supported by Grant No. ENE2015-71333-R (Spain) and Convocatoria Abierta 2015 para Cursar Estudios de Doctorado, SENESCYT (Ecuador).

Acknowledgments: J.M.I. wishes to thank the organisers of the congress “Entropy 2018: From Physics to Information Sciences and Geometry”, Barcelona, for the opportunity to present a preliminary version of this work.

Conflicts of Interest: The authors declare no conflict of interest.

References

1. Callen, H. *Thermodynamics*; Wiley: New York, NY, USA, 1960.
2. Arnold, V. *Mathematical Methods of Classical Mechanics*. In *Graduate Texts in Mathematics*; Springer: Berlin, Germany, 1989.
3. Bravetti, A. Contact Hamiltonian Dynamics: The Concept and its Use. *Entropy* **2017**, *19*, 535. [[CrossRef](#)]
4. Mrugala, R.; Nulton, J.; Schön, J.; Salamon, P. Contact Structure in Thermodynamic Theory. *Rep. Math. Phys.* **1991**, *29*, 109–121. [[CrossRef](#)]
5. Isidro, J.M.; de Córdoba, P.F. On the Contact Geometry and the Poisson Geometry of the Ideal Gas. *Entropy* **2018**, *20*, 247. [[CrossRef](#)]
6. Rajeev, G. Quantization of Contact Manifolds and Thermodynamics. *Ann. Phys.* **2008**, *323*, 768–782. [[CrossRef](#)]
7. Rajeev, G. A Hamilton–Jacobi Formalism for Thermodynamics. *Ann. Phys.* **2008**, *323*, 2265–2285. [[CrossRef](#)]
8. Toda, M. Vibration of a Chain with Nonlinear Interaction. *J. Phys. Soc. Jpn.* **1967**, *22*, 431–436. [[CrossRef](#)]
9. Toda, M. Wave Propagation in Anharmonic Lattices. *J. Phys. Soc. Jpn.* **1968**, *23*, 501–506. [[CrossRef](#)]
10. Toda, M. Waves in Nonlinear Lattice. *Prog. Theor. Phys. Suppl.* **1970**, *45*, 174–200. [[CrossRef](#)]
11. Cabrera, D.; de Córdoba, P.F.; Isidro, J.M.; Molina, J.V. Entropy, Topological Theories and Emergent Quantum Mechanics. *Entropy* **2017**, *19*, 87. [[CrossRef](#)]
12. Schwarz, A. *Quantum Field Theory and Topology*. In *Grundlehren der Mathematischen Wissenschaften*; Springer: Berlin, Germany, 2010.
13. Ruppeiner, G. Riemannian Geometry in Thermodynamic Fluctuation Theory. *Rev. Mod. Phys.* **1995**, *67*, 605. [[CrossRef](#)]
14. Velázquez, L. Curvature of Fluctuation Geometry and its Implications on Riemannian Fluctuation Theory. *J. Phys. A Math. Theor.* **2013**, *46*, 345003. [[CrossRef](#)]



© 2018 by the authors. Licensee MDPI, Basel, Switzerland. This article is an open access article distributed under the terms and conditions of the Creative Commons Attribution (CC BY) license (<http://creativecommons.org/licenses/by/4.0/>).

Document downloaded from:

<http://hdl.handle.net/10251/43259>

This paper must be cited as:

García March, MA.; Gimenez Palomares, F.; Villatoro, FR.; Pérez Quiles, MJ.; Fernández De Córdoba Castellá, PJ.; Fernández De Córdoba (2011). Unisolvency for Multivariate Polynomial Interpolation in Coatsmèlec Configurations of Nodes. *Applied Mathematics and Computation*. 217(18):7427-7431. doi:10.1016/j.amc.2011.02.034.



The final publication is available at

<http://dx.doi.org/10.1016/j.amc.2011.02.034>

Copyright Elsevier

Unisolvency for Multivariate Polynomial Interpolation in Coatsmèlec Configurations of Nodes

Miguel-Ángel García-March^a, Fernando Giménez^b,
Francisco R. Villatoro^c, Jezabel Pérez^{b,*}, and
Pedro Fernández de Córdoba^b

^a*Department of Physics, Colorado School of Mines, Golden, Colorado (USA)*

^b*Instituto Universitario de Matemática Pura y Aplicada - IUMPA. Universidad Politécnica de Valencia. Valencia (SPAIN)*

^c*Departamento de Lenguajes y Ciencias de la Computación
E.T.S.I. Industriales, Universidad de Málaga
Málaga (SPAIN)*

Abstract

A new and straightforward proof of the unisolvability of the problem of multivariate polynomial interpolation based on Coatsmèlec configurations of nodes, a class of properly posed set of nodes defined by hyperplanes, is presented. The proof generalizes a previous one for the bivariate case and is based on a recursive reduction of the problem to simpler ones following the so-called Radon-Bézout process.

Key words: multivariate interpolation, properly posed set of nodes, geometric characterization, Coatsmèlec lattices

1 Introduction

The problem of polynomial interpolation of one-dimensional data has a widely known solution. However, despite its apparent simplicity, multivariate polynomial interpolation remains a topic of current research [1–3]. The existence and uniqueness of the interpolation polynomial strongly depends on the geometrical distribution of the interpolation points. The distribution of points

* Corresponding author. Tel: (+34) 963-877-007 (Ext. 76648)
Email address: jperezq@mat.upv.es (Jezabel Pérez).

for which the interpolation problem is unsolvable is referred to as properly posed set of nodes (PPSN).

The mathematical characterization of the most general PPSN is not currently known. The configurations of nodes based on algebraic varieties, such as those of Bos [4] and Liang et al. [5,6], are very general but non-constructive. In a computational setting, configurations based on hyperplanes, such as those of Coatmèlec [7] and Chung and Yao [8], are preferred.

Surprisingly, the configuration of nodes introduced by Coatmèlec [7] in the plane has received several names: DH-set [2], straight line type node configuration [5], PPSN with node configuration A [9], straight line type node configuration A [10], PPSN by the recursive construction theorem using lines [11], and PPSN by line-superposition process [12].

In this paper, a new proof of the unsolvability of the interpolation problem for Coatmèlec configuration of nodes in arbitrary dimensions is presented. The proof is based on a Bézout-Radon process [13,14]. Chui and Lai [9] present a proof for the bivariate case only, state the result in arbitrary dimension, but did not prove it because of complications in their notation. Multidimensional interpolation is the basis to develop different numerical methods. The results of this paper permit to design, for example, generalized finite difference methods in irregular meshes based on Coatmèlec configuration of nodes in two [15] or more dimensions.

The contents of this paper are as follows. The definitions and notation required to set our main theorem are presented in the next section. The proof of this theorem is detailed in Section 3. Finally, in the last section, the main conclusions are summarized.

2 Presentation of the problem

Let $\Pi_m(\mathbb{R}^k)$ be the vector space of multivariate polynomials of degree not greater than m with k variables. Let $w = (x_1, \dots, x_k)^\top \in \mathbb{R}^k$, where \top denotes transpose, $\mathbb{N}_0 = \mathbb{N} \cup \{0\}$, $j = (j_1, \dots, j_k)^\top \in \Gamma := \mathbb{N}_0^k$, $|j| = j_1 + \dots + j_k$, $w^j = x_1^{j_1} x_2^{j_2} \dots x_k^{j_k}$, and $\Gamma_m := \{j \in \Gamma : |j| \leq m\}$. The set of multivariate monomials $\{w^j\}_{j \in \Gamma_m}$ is a basis of $\Pi_m(\mathbb{R}^k)$, i.e., every polynomial $p_m(w)$ may be written uniquely as $\sum_{j \in \Gamma_m} a_j w^j$, with $a_j \in \mathbb{R}$. Hence, the vector space $\Pi_m(\mathbb{R}^k)$ has dimension $N = C_{k+m}^k$, where C_n^k is the binomial coefficient $\binom{n}{k}$.

Let $\Gamma^s := \{j \in \Gamma_m : |j| = s\}$, $s = 0, 1, \dots, m$. Note that $\Gamma_m = \cup_{s=0}^m \Gamma^s$, the cardinal $\#\Gamma^s = C_{k-1+s}^{k-1}$, and $\#\Gamma_m = \sum_{s=0}^m C_{k-1+s}^{k-1} = N$. The set of s -th degree monomials may be represented as a column vector of length $\#\Gamma^s$

given by $w^{(s)} := (x_1^s, x_1^{s-1} x_2^1, \dots, x_{i_1} x_{i_2} \cdots x_{i_s}, \dots, x_{k-1}^1 x_k^{s-1}, x_k^s)^\top$, for all $i = (i_1, \dots, i_s)^\top \in \mathbb{N}_0^s$, and $1 \leq i_1 \leq i_2 \leq \dots \leq i_s \leq k$. Note that $w^{(0)} = (1) \in \mathbb{R}$, $w^{(1)} = w \in \mathbb{R}^k$, and each component of the vector $w^{(s)}$ corresponds to a unique monomial w^j with $j \in \Gamma^s$. Using this notation, every polynomial $p_m(w) \in \Pi_m(\mathbb{R}^k)$ may be written as $\sum_{s=0}^m \sum_{j \in \Gamma^s} a_j w^j$.

Here on, a node refers to a point in \mathbb{R}^k and a configuration of nodes (CN) is a set of pairwise distinct nodes $X_m = \{w_i\}_{i=1}^N$ where $w_i \equiv (x_{(1,i)}, x_{(2,i)}, \dots, x_{(k,i)})^\top \in \mathbb{R}^k$.

The Lagrange interpolation problem may be stated as follows: Given a CN X_m and an arbitrary set of real numbers $\{f_i \in \mathbb{R}\}_{i=1}^N$, find a polynomial $p_m(w) \in \Pi_m(\mathbb{R}^k)$ such that

$$p_m(w_i) := \sum_{j \in \Gamma_m} a_j w_i^j = f_i, \quad i = 1, 2, \dots, N. \quad (1)$$

This problem is *properly posed* with respect to X_m if it has a unique solution (unisolvability) for every set $\{f_i\}_{i=1}^N$. Compared with the one-dimensional case where the solvability is always assured, the solvability of multivariate interpolation depends strongly on the geometrical distribution of the nodes. A CN X_m is said to be a *properly posed set of nodes* (PPSN) if the Lagrange interpolation problem is properly posed with respect to X_m .

Equation (1) is a system of N linear equations with a multivariate Vandermonde matrix V_m , i.e., $(V_m)_{ij} = w_i^j$, where $j \in \Gamma_m$, $w_i \in X_m$, and $1 \leq i \leq N$. Note that this matrix looks a little bit bizarre since rows and columns are indexed by different structural entities. A graded lexicographical order in the set of multiindices Γ_m may be introduced to enhance the notation (see Ref. [16]) but this is not required in this paper.

The following theorem summarizes some previously known results.

Theorem 1 *Let $X_m = \{w_i\}_{i=1}^N$ be a CN in k dimensions and V_m the corresponding multivariate Vandermonde matrix, then the following expressions are equivalent:*

- (i) X_m is a PPSN in \mathbb{R}^k .
- (ii) V_m is a nonsingular matrix, i.e., $\det(V_m) \neq 0$.
- (iii) $\text{rank}(V_m) = N$.

Let $X_m \equiv X_{(m,k)} = \{w_i\}_{i=1}^N \subset \mathbb{R}^k$ be a CN with $N = C_{m+k}^k$ nodes in k dimensions. Let us define by induction on k the following CNs, first introduced by Coatmèlec [7,9].

Definition 2 *A CN $X_m \equiv X_{(m,k)} \subset \mathbb{R}^k$ is Coatmèlec in k dimensions if $X_{(m,k)} = \bigcup_{p=0}^m X_{(p,k-1)}$ with $\#X_{(p,k-1)} = C_{p+k-1}^{k-1}$ and there exists $m+1$ hyper-*

planes $\gamma_0, \gamma_1, \dots, \gamma_m$ such that $X_{(m,k-1)} \subset \gamma_m$ and $X_{(p,k-1)} \subset \gamma_p \setminus \bigcup_{q=p+1}^m \gamma_q$, for $0 \leq p \leq m-1$, with each $X_{(p,k-1)}$ being Coatmèlec in $(k-1)$ dimensions by identifying each hyperplane γ_p with \mathbb{R}^{k-1} .

Note that, in one dimension, every CN $X_m \equiv X_{(m,1)} \subset \mathbb{R}$ is Coatmèlec because all its nodes are pairwise distinct, i.e., $w_i \neq w_j$, if $i \neq j$. Note also that, in Definition 2, only one node belongs to the hyperplane γ_m .

The main result of this paper is a proof of the following theorem.

Theorem 3 *Every Coatmèlec CN X_m in k dimensions is a properly posed set of nodes in \mathbb{R}^k .*

3 Proof of the main theorem

Our proof makes use of the following lemmas.

Lemma 4 *Let us take the CN X_m where the nodes $\{w_i\}_{i=1}^N$ are represented as column vectors in \mathbb{R}^k , and the CN \hat{X}_m whose nodes are $\hat{w}_i = w_0 + H w_i$, $i = 1, \dots, N$, where w_0 is an arbitrary vector and H is a non-singular matrix of dimension k . Let V_m and \hat{V}_m be the Vandermonde matrices associated to the CNs X_m and \hat{X}_m , respectively. If $\text{rank}(V_m) = N$, then $\text{rank}(\hat{V}_m) = N$.*

Proof of Lemma 4. For every set of real numbers $\{f_i \in \mathbb{R}\}_{i=1}^N$, there exists one and only one interpolating polynomial such that $\hat{p}_m(\hat{w}_i) = f_i$, given by $\hat{p}_m(\hat{x}) = p_m(H^{-1}(x - w_0))$ where $p_m(x)$ is the unique interpolating polynomial for X_m given by Theorem 1. Therefore, $\text{rank}(\hat{V}_m) = N$.

Lemma 5 *Let $\{\hat{x}_i : i = 1, \dots, k\}$ be an orthonormal basis of \mathbb{R}^k , and n_1 an arbitrary vector. There always exists an orthogonal matrix H , representing a rotation in \mathbb{R}^k , which transform the vector \hat{x}_1 onto $H \hat{x}_1 = \hat{n}_1 = n_1 / \|n_1\|$.*

Proof of Lemma 5. If $\hat{n}_1 = \hat{x}_1$, then $H = I$, the identity matrix. Otherwise, let us apply the procedure of Gram-Schmidt orthonormalization to vectors $\{\hat{x}_1, n_1\}$, yielding

$$\hat{q}_1 = \hat{x}_1, \quad q_2 = n_1 - (n_1 \cdot \hat{q}_1) \hat{q}_1, \quad \hat{q}_2 = \frac{q_2}{\sqrt{q_2 \cdot q_2}} = \frac{q_2}{\|q_2\|},$$

where the dot is the ordinary Euclidean dot product. An arbitrary vector q can be written as $q = q_\perp + q_\parallel$, where $q_\parallel = (q \cdot \hat{q}_1) \hat{q}_1 + (q \cdot \hat{q}_2) \hat{q}_2 = Q Q^\top q$, where $Q = [\hat{q}_1; \hat{q}_2]$ is the rectangular matrix whose columns are the vectors \hat{q}_i ; note that $Q^\top Q$ is the identity matrix of dimension 2. Taking the vector $q_\perp = q - q_\parallel$ as the rotation axis for the rotation matrix H results in $H q = q_\perp + H q_\parallel =$

$(I - Q Q^\top) q + Q R Q^\top q$, where R is the standard two-dimensional rotation matrix

$$R = \begin{pmatrix} \cos \theta & -\sin \theta \\ \sin \theta & \cos \theta \end{pmatrix}, \quad \cos \theta = \hat{x}_1 \cdot \hat{n}_1, \quad \sin \theta = \sqrt{1 - (\hat{x}_1 \cdot \hat{n}_1)^2}.$$

Hence, $H = I - Q Q^\top + Q R Q^\top$ is a rotation matrix ($H H^\top = H^\top H = I$ and $\det(H) = 1$) such that $H \hat{x}_1 = \hat{n}_1$.

Proof of Theorem 3. Let us use the induction principle over m and k . Let us first consider $m = 0$ and any $k \in \mathbb{N}$. Clearly $X_0 = w_1$ and $\text{rank}(V_0) = 1 = N$. We consider next $k = 1$ and $m \neq 0$. The corresponding CN is Coatsmèlec in one dimension and the coefficient matrix is a (one-dimensional) Vandermonde matrix with maximal rank $C_{m+1}^1 = m + 1 = N$, since the nodes are pairwise distinct.

By the induction hypothesis, let us assume that the theorem holds for either $m - 1$ or $k - 1$, and let us prove that it holds for m and k . Here on, let us take $n = m + k$. Since X_m is a Coatsmèlec CN in k dimensions, the following conditions are fulfilled

$$\begin{aligned} X_{(m,k-1)} &= \{w_1, w_2, \dots, w_{C_{n-1}^{k-1}}\} \subset \gamma_m, \\ X_{(m-1,k-1)} &= \{w_{C_{n-1}^{k-1}+1}, \dots, w_{C_{n-1}^{k-1}+C_{n-2}^{k-1}}\} \subset \gamma_{m-1} \setminus \gamma_m, \\ X_{(m-2,k-1)} &= \{w_{C_{n-1}^{k-1}+C_{n-2}^{k-1}+1}, \dots, w_{C_{n-1}^{k-1}+C_{n-2}^{k-1}+C_{n-3}^{k-1}}\} \\ &\quad \subset \gamma_{m-2} \setminus \gamma_{m-1} \cup \gamma_m, \\ &\quad \vdots \\ X_{(0,k-1)} &= \{w_N\} \subset \gamma_0 \setminus \gamma_1 \cup \dots \cup \gamma_m, \end{aligned}$$

where

$$X_m = X_{(m,k-1)} \cup X_{(m-1,k-1)} \cup \dots \cup X_{(0,k-1)}.$$

The multivariate Vandermonde matrix associated to the Lagrange interpolation problem in the CN X_m may be written as

$$V_m = \begin{pmatrix} 1 & 1 & \cdots & 1 \\ w_1^{(1)} & w_2^{(1)} & \cdots & w_{C_n^k}^{(1)} \\ w_1^{(2)} & w_2^{(2)} & \cdots & w_{C_n^k}^{(2)} \\ \vdots & \vdots & & \vdots \\ w_1^{(m)} & w_2^{(m)} & \cdots & w_{C_n^k}^{(m)} \end{pmatrix}.$$

Let us apply the affine transformation $\hat{w} = w_0 + H w$ to all the nodes of the CN, where H is the orthogonal matrix given in Lemma 5, that transforms the x_k coordinate axis in \mathbb{R}^k into the normal vector to the hyperplane γ_m , and w_0 is the distance between the intersection point of the (new) rotated x_k axis and the hyperplane γ_m .

The application of the affine transformation nullifies the k -th coordinates of the vectors $\{\hat{w}_1, \hat{w}_2, \dots, \hat{w}_{C_{n-1}^{k-1}}\}$, hence $\hat{w}_i = (\hat{x}_{(1,i)}, \hat{x}_{(2,i)}, \dots, \hat{x}_{(k-1,i)}, 0)^\top$. Let \hat{V}_m , where $(\hat{V}_m)_{ij} = \hat{w}_i^j$, be the coefficient matrix of the transformed linear system of equations. From Lemma 4, $\text{rank}(V_m) = \text{rank}(\hat{V}_m)$.

The rows and columns of the matrix \hat{V}_m may be sorted by renaming the nodes \hat{w}_i to \tilde{w}_i , in order to group all its zero elements into its left-bottom part. This process preserves the rank. The resulting matrix \tilde{V}_m has the following structure

$$\begin{pmatrix} A & B \\ 0 & A' D \end{pmatrix}, \quad (2)$$

where A is the $C_{n-1}^{k-1} \times C_{n-1}^{k-1}$ matrix given by

$$A = \begin{pmatrix} 1 & 1 & \cdots & 1 \\ \tilde{w}_1^{(1)} & \tilde{w}_2^{(1)} & \cdots & \tilde{w}_{C_{n-1}^{k-1}}^{(1)} \\ \tilde{w}_1^{(2)} & \tilde{w}_2^{(2)} & \cdots & \tilde{w}_{C_{n-1}^{k-1}}^{(2)} \\ \vdots & \vdots & \ddots & \vdots \\ \tilde{w}_1^{(m)} & \tilde{w}_2^{(m)} & \cdots & \tilde{w}_{C_{n-1}^{k-1}}^{(m)} \end{pmatrix},$$

B is the $C_{n-1}^{k-1} \times C_{n-1}^k$ matrix

$$B = \begin{pmatrix} 1 & 1 & \cdots & 1 \\ \tilde{w}_{C_{n-1}^{k-1}+1}^{(1)} & \tilde{w}_{C_{n-1}^{k-1}+2}^{(1)} & \cdots & \tilde{w}_{C_n^k}^{(1)} \\ \tilde{w}_{C_{n-1}^{k-1}+1}^{(2)} & \tilde{w}_{C_{n-1}^{k-1}+2}^{(2)} & \cdots & \tilde{w}_{C_n^k}^{(2)} \\ \vdots & \vdots & \ddots & \vdots \\ \tilde{w}_{C_{n-1}^{k-1}+1}^{(m)} & \tilde{w}_{C_{n-1}^{k-1}+2}^{(m)} & \cdots & \tilde{w}_{C_n^k}^{(m)} \end{pmatrix},$$

D is the $C_{n-1}^k \times C_{n-1}^k$ diagonal matrix

$$D = \begin{pmatrix} \hat{x}_{(k, C_{n-1}^{k-1}+1)} & 0 & \cdots & 0 \\ 0 & \hat{x}_{(k, C_{n-1}^{k-1}+2)} & \cdots & 0 \\ \vdots & \vdots & \ddots & \vdots \\ 0 & 0 & \cdots & \hat{x}_{(k, C_n^k)} \end{pmatrix},$$

A' is the $C_{n-1}^k \times C_{n-1}^k$ matrix given by

$$A' = \begin{pmatrix} 1 & 1 & \cdots & 1 \\ \tilde{w}_{C_{n-1}^{k-1}+1}^{(1)} & \tilde{w}_{C_{n-1}^{k-1}+2}^{(1)} & \cdots & \tilde{w}_{C_n^k}^{(1)} \\ \vdots & \vdots & \ddots & \vdots \\ \tilde{w}_{C_{n-1}^{k-1}+1}^{(m)} & \tilde{w}_{C_{n-1}^{k-1}+2}^{(m)} & \cdots & \tilde{w}_{C_n^k}^{(m)} \end{pmatrix},$$

and finally 0, cf. Eq. (2), represents the null matrix of dimensions $C_{n-1}^k \times C_{n-1}^{k-1}$. We recall that $C_n^k = C_{n-1}^{k-1} + C_{n-1}^k$.

The square matrix A is a multivariate Vandermonde matrix in $(k-1)$ variables and the C_{n-1}^{k-1} nodes $\{\tilde{w}_i\}$ are a Coatsmèlec CN in $(k-1)$ dimensions. Therefore, by the induction hypothesis, $\text{rank}(A) = C_{n-1}^{k-1}$.

The diagonal matrix D is nonsingular, i.e., $\hat{x}_{k,i} \neq 0$, for $i = C_{n-1}^{k-1} + 1, \dots, C_n^k$, because if there existed at least an i with $\hat{x}_{k,i} = 0$, then there would be at least $C_{n-1}^{k-1} + 1$ different nodes lying in the hyperplane γ_m , but this is not possible because X_m is a Coatsmèlec CN. Hence, $\text{rank}(A'D) = \text{rank}(A')$. Moreover, the matrix A' is also a multivariate Vandermonde matrix corresponding to the C_{n-1}^k nodes that do not belong to the hyperplane γ_m . Since the Coatsmèlec property of a CN does not change under either rotation or translation of all the nodes, the CN $\{\tilde{w}_i\}$, $i = C_{n-1}^{k-1} + 1, \dots, C_n^k$, is also a Coatsmèlec CN. The induction hypothesis yields that the rank of matrix A' is C_{n-1}^k .

Finally, the rank of the $C_n^k \times C_n^k$ matrix \tilde{V}_m is $\text{rank}(A) + \text{rank}(A') = C_{n-1}^{k-1} + C_{n-1}^k = C_n^k$, and the theorem is proved.

4 Conclusions

The unisolvency of the problem of multivariate polynomial interpolation in a Coatmèlec CN, a kind of properly posed set of nodes defined by hyperplanes, has been shown through a new and straightforward proof. This proof uses elementary techniques from linear algebra. This fact permits the understanding of the topic by nonexperts and opens the possibility of it being incorporated in numerical analysis textbooks.

The geometrical condition characterizing Coatmèlec CNs is one of the most general conditions currently available for the characterization of properly posed set of nodes defined by hyperplanes, which is easier and more efficient to be checked by an automatic computational software than the widely known geometrical characterization of Chung and Yao [8]. Therefore, Coatmèlec CNs are useful in mesh generation for the numerical solution of partial differential equations in irregular domains, such as generalized finite difference methods.

Acknowledgements

The authors thank to Drs. Mariano Gasca and Juan I. Ramos for pointing us some references and for their useful comments which have greatly improved the presentation. The authors also thank a reviewer for pointing out a mistake in the original proof of Lemma 5. The research reported in this paper was partially supported by Project MTM2010-19969 from the Ministerio de Ciencia e Innovación of Spain and Grant PAID-06-09-2734 from the Universidad Politècnica de Valencia.

References

- [1] M. GASCA AND T. SAUER, *On the history of multivariate polynomial interpolation*, J. Comput. Appl. Math., 122 (2000), pp. 23–35.
- [2] M. GASCA AND T. SAUER, *Polynomial interpolation in several variables*, Advances Comput. Math., 12 (2000), pp. 377–410.
- [3] R.A. LORENTZ, *Multivariate Hermite interpolation by algebraic polynomials: A survey*, J. Comput. Appl. Math., 122 (2000), pp. 167–201.
- [4] L. BOS, *On certain configurations of points in \mathbb{R}^n which are unisolvent for polynomial interpolation*, J. Approx. Theor., 64 (1991), pp. 271–280.

- [5] X.-Z. LIANG, C.-M. LÜ, AND R.-Z. FENG, *Properly posed sets of nodes for multivariate Lagrange interpolation in C^s* , SIAM J. Numer. Anal., 39 (2001), pp. 587–595.
- [6] X.-Z. LIANG, R.-H. WANG, L.-H. CUI, J.-L. ZHANG, AND M. ZHANG, *Some researches on trivariate Lagrange interpolation*, J. Comput. Appl. Math., 195 (2006) pp. 192–205.
- [7] C. COATMÈLEC, *Approximation et interpolation des fonctions différentiables de plusieurs variables*, Ann. Sci. École Norm. Sup., 83 (1966), pp. 271–341.
- [8] K. C. CHUNG AND T. H. YAO, *On lattices admitting unique Lagrange interpolation*, SIAM J. Numer. Anal., 14 (1977), pp. 735–743.
- [9] C. K. CHUI AND M. J. LAI, *Vandermonde determinant and Lagrange interpolation in R^s* , in Nonlinear and Convex Analysis, B. L. Lin and S. Simon, eds., Marcel Dekker, New York, 1987, pp. 23–35.
- [10] P. ZHU, *On Birkhoff interpolation by polynomials in several variables*, J. Comput. Appl. Math., 85 (1997), pp. 263–270.
- [11] X.-Z. LIANG AND C.-M. LU, *Properly posed set of nodes for bivariate Lagrange interpolation*, in Approximation Theory IX, Volume 1: Theoretical Aspects, C.K. Chui and L.L. Schumacker, eds., Vanderbilt University Press, Nashville, TN, 1998, pp. 189–196.
- [12] X.-Z. LIANG, L.-H. CUI, AND J.-L. ZHANG, *The application of Cayley-Bacharach theorem to bivariate Lagrange interpolation*, J. Comput. Appl. Math., 163 (2004), pp. 177–187.
- [13] J. RADON, *Zur mechanischen Kubatur*, Monatshefte für Mathematik, 52 (1948), pp. 286–300.
- [14] R. B. GUENTHER AND E. L. ROETMAN, *Some observations on interpolation in higher dimensions*, Math. Comput., 24 (1970), pp. 517–522.
- [15] GARCÍA-MARCH, M.A., AREVALILLO-HERRÁEZ, M., VILLATORO, F.R., GIMÉNEZ, F., AND FERNÁNDEZ DE CÓRDOBA, P., *A generalized finite difference method using Coatmèlec lattices*, Comput. Phys. Comm., 180 (2009) pp. 1125–1133.
- [16] D. A. COX, J. B. LITTLE, AND D. B. O’ SHEA, *Ideals, Varieties, and Algorithms: An Introduction to Computational Algebraic Geometry and Commutative Algebra*, Second ed., Springer Verlag, New York, 1996.

TEMPERATURE STABILIZATION OF HIGH-POWER LED CHIPS USING LOW-COST PASSIVE HEAT SINKS

Eduardo Balvís (1), Ricardo Bendaña (2), Humberto Michinel (3), Pedro Fernández de Córdoba (4)

(1) Innebo, Lugar do Penedo, 32910 S. Cibrao das Viñas, Spain, +34653887252, ebalvis@innebo.es

(2) Facultad de Ciencias, Universidade de Vigo, As Lagoas s/n 32004 Ourense, Spain, +34988387220, ricardobjb@uvigo.es

(3) Área de Óptica, Universidade de Vigo, As Lagoas s/n 32004 Ourense, Spain, +34988387220, hmichinel@uvigo.es

(4) IUMPA, Universitat Politècnica de València, Camino de Vera 14 46022 València Spain, +34963877007, pfernandez@mat.upv.es

Abstract: We present a numerical analysis and experimental measurements of the temperature stabilization of high-power LED chips that we have obtained by employing an aluminium passive heat sink, designed to be used in a compact light bulb configuration. We demonstrate that our system keeps the temperature of the LED chip well-below 60°C yielding long-term operation of the device. Our simulations have been performed for a device of low fabrication costs and which enables an easy installation in public streetlights. The experimental measurements performed in different configurations show a nice agreement with the numerical calculations.

1. Introduction

The use of high-power light emitting diodes (HP-LED) for public illumination is an emerging subject, triggered by recent developments of different technologies including semiconductor materials [1], fluorescence techniques [2], driver electronics [3], or thermal control [4], among others [5].

One of the key aspects concerning the performance and durability of HP-LED lighting systems is the adequate control of the temperature of the LED chip [6]. As it has been pointed by recent studies [7], LEDs have a high energy efficiency and long lifespan, however, a large amount of heat is dissipated during operation due to Joule effect; thus, cooling HP-LEDs is an important challenge in package designs, where a correct evacuation of the heat will substantially enlarge the lifetime of the device.

Besides the previous constraint, other practical aspects like a compact design, low cost, mass production or even aesthetic considerations can play an important role in market-oriented products. Thus, in this paper we present a numerical analysis of the thermal stabilization of a 50W LED chip attached to a passive heat sink, yielding a compact light bulb design that can be used for commercial purposes in the street lighting market. The system we propose keeps the temperature of the LED chip well-below 60°C under all circumstances, yielding long-term operation of the bulb.

After the numerical calculations performed, a practical device has been implemented in a compact and easy-to-install design in order to compare the results of the computational simulations with experimental measurements taken under realistic conditions, finding a nice agreement.

2. Numerical Model

Our first aim is to calculate the steady-state temperature distribution over the surface of a heat sink with

translational symmetry along, say the z -axis. This configuration is ideal for mass production via metal extrusion process. In our model, we have assumed that the heat sink is made of black anodized Al surrounded by a laminar air flow with constant properties except the density of air (ρ), given by the ideal gas law. Thus, in the air side the first formula is the continuity equation:

$$\nabla \cdot (\rho \vec{v}) = 0, \quad (1)$$

being \vec{v} the velocity of air. In addition we have the energy equation [8]:

$$\rho \frac{\partial \vec{v}}{\partial t} = -\nabla P + \mu \nabla^2 \vec{v} - \rho g, \quad (2)$$

where t is the time, P the pressure, μ the dynamic viscosity and g the acceleration of gravity. One more formula needed is the moment equation:

$$\rho C_p \frac{\partial T}{\partial t} = \nabla \cdot (k \nabla T) + \frac{\partial P}{\partial t}, \quad (3)$$

being C_p the specific heat, T the absolute temperature and k the thermal conductivity. On the heat sink we have the condition $\nabla^2 T = 0$. For a black anodized surface with high emissivity (>0.8), we can neglect at the interface the effect of the incoming radiation heat flux (W/m^2) and thus, the outgoing flux (\dot{q}) is given by the Stefan-Boltzmann law:

$$\dot{q} = \varepsilon \sigma T^4, \quad (4)$$

where ε is the emissivity of the wall is the Stefan-Boltzmann constant and T is the absolute temperature of the heat sink. We want to solve the previous problem for a heat sink made of black-anodized aluminum (Al6061) with the geometry shown in Fig. 1. To numerically integrate the previous set of equations, we have used COMSOL Multiphysics^R, which is a finite element analysis solver commercial package for various physics and engineering applications. As it can be appreciated in

Fig. 1, the steady-state temperature distribution ranges from 53°C to 42°C .

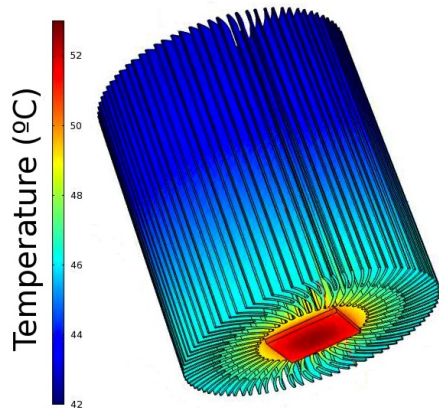


Fig. 1. Numerical simulation of the steady-state temperature distribution over the heat sink. The size is 10cm height and 6cm diameter. The LED (red square) power is 50W .

3. Experimental results and discussion

In order to check the validity of our numerical model, a series of experiments were made. As shown in Fig. [2] an Al6061 black anodized heat sink 10cm length was attached to a 50W LED chip in a light-bulb configuration. The emissivity of the heat sink with the surface treatment was 0.8 . The geometric parameters of the experimental model are the same as in the numerical simulations described before.

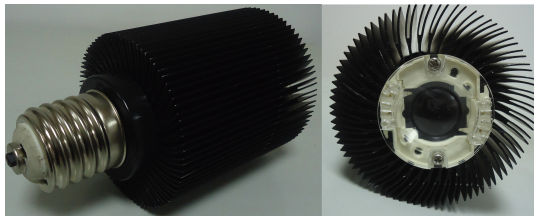


Fig. 2. Lateral (left) and front (right) view of the real system composed of a black anodized aluminum structure in a compact LED bulb configuration.

A temperature sensor with three different probe heads (DAQ-9172, NI9211), a power supply, a wattmeter, and a laptop were used in order to collect data. To minimize the thermal contact resistance between the LED chip and the heat sink a graphite film of high thermal conductivity ($240\text{Wm}^{-1}\text{K}^{-1}$) was used. As it can be seen in Fig. 3 the steady state temperature of the LED chip shows a nice agreement with the numerical calculations.

4. Conclusions

We have presented a numerical study of the steady-state temperature distribution of a practical high-power light emitting diode (HP-LED) bulb. Our results have been compared with experimental data obtained in a physical device fabricated for market purposes. From our analysis

we can derive that low-cost passive heat sinks fabricated for 50W HP-LED chips can keep the temperature of the device below 60°C , thus making it possible to reach lifetimes of 55.000h .

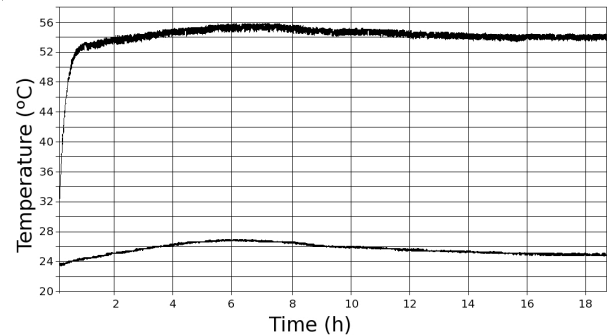


Fig. 3. Experimental measurement of the temperature distribution of the LED chip (top curve) and the environment (bottom curve).

Acknowledgement

HM thanks funding from projects K133131H64102 and K044131H64502 Xunta de Galicia. PF-C thanks Universitat Politècnica de València funding via project SP20120909.

References

- [1] R. Mueller-Mach, G. Mueller, M. Krames, T. Trotter, "High-power phosphor-converted light-emitting diodes based on iii-nitrides," *IEEE J. Sel. Topics Quantum Electron.*, **8**, 339–345 (2002).
- [2] Y. Narukawa, J. Narita, T. Sakamoto, K. Deguchi, T. Yamada, T. Mukai, "Ultra-high efficiency white light emitting diodes," *Jpn. J. Appl. Phys.*, **45**, L1084–L1086 (2006).
- [3] A. Krost, A. Dadgar, "Gan-based devices on Si," *Phys. Status Solidi*, **A 194**, 361–375 (2002).
- [4] H. Luo, J. K. Kim, E. F. Schubert, J. Cho, C. Sone, Y. Park, "Analysis of high-power packages for phosphor-based white-light-emitting diodes," *Appl. Phys. Lett.*, **86**, 243505 (2005).
- [5] H.-J. Chiu, Y.-K. Lo, J.-T. Chen, S.-J. Cheng, C.-Y. Lin, S.-C. Mou, "A high-efficiency dimmable led driver for low-power lighting applications," *IEEE Trans. Ind. Electron.*, **57**, 735–743 (2010).
- [6] A. Efremov, N. Bochkareva, R. Gorbunov, D. Lavrinovich, Y. Rebane, D. Tarkhin, Y. Shreter, "Effect of the Joule heating on the quantum efficiency and choice of thermal conditions for high-power blue ingan/gan leds," *Semiconductors*, **40**, 605–610 (2006).
- [7] H. Y. Chen, W. Y. Lam, J. D. Luo, Y. L. Ho, B. Z. Tang, D. B. Zhu, M. Wong, H. S. Kwok, "Highly efficient organic light-emitting diodes with a silole-based compound," *Appl. Phys. Lett.*, **81**, 574–576 (2002).

PAPER • OPEN ACCESS

Analysis of a passive heat sink for temperature stabilization of high-power LED bulbs

To cite this article: Eduardo Balvis *et al* 2015 *J. Phys.: Conf. Ser.* **605** 012005

View the [article online](#) for updates and enhancements.

You may also like

- [Effect of n-Type AlGaAs Layer on Efficiency of Reflective 590-nm AlGaInP Light Emitting Diodes](#)
Hyung Joo Lee, Jae Hoon Kim and Choong Hun Lee
- [A Numerical Study of Thermal and Electrical Effects in a Vertical LED Chip](#)
Farn-Shiun Hwu, Jyh-Chen Chen, Sheng-Han Tu et al.
- [Vertical Structure GaN-Based Light Emitting Diodes with Electrochemically Deposited Stress-Free Nickel Substrate](#)
Kim Sunjung

PRIME
PACIFIC RIM MEETING
ON ELECTROCHEMICAL
AND SOLID STATE SCIENCE

HONOLULU, HI
Oct 6–11, 2024

Abstract submission deadline:
April 12, 2024

Learn more and submit!

Joint Meeting of
The Electrochemical Society
•
The Electrochemical Society of Japan
•
Korea Electrochemical Society

Analysis of a passive heat sink for temperature stabilization of high-power LED bulbs

Eduardo Balvís¹, Ricardo Bendaña², Humberto Michinel^{2,1} Pedro Fernández de Córdoba³ and Angel Paredes²

¹Innebo Ingeniería, Lugar do Penedo, S. Cibrao das Viñas, Ourense, 32910 Spain

²Facultade de Ciencias, Universidade de Vigo, As Lagoas s/n, Ourense, 32004 Spain

³IUMPA, Universitat Politècnica de València, Camino de Vera 14, Valencia, 46022 Spain

E-mail: hmichinel@uvigo.es

Abstract. In this paper we present a numerical analysis and experimental measurements of the temperature stabilization of high-power LED chips that we have obtained by employing an aluminum passive heat sink, designed to be used in a compact light bulb configuration. We demonstrate that our system keeps the temperature of the LED chip well-below 70°C yielding long-term operation of the device. Our simulations have been performed for a low-cost device ready to install in public streetlights. The experimental measurements performed in different configurations show a nice agreement with the numerical calculations.

1. Introduction

The use of high-power light emitting diodes (HP-LED) for public illumination is an emerging subject, triggered by recent developments of different technologies including semiconductor materials[1, 2, 3], fluorescence techniques[4], driver electronics[5] or thermal control[6] among others[7, 8].

One of the key aspects concerning the performance and durability of HP-LED lighting systems is the adequate control of the temperature of the LED chip[9]. As it has been pointed by recent studies[10], LEDs have a high energy efficiency and long lifespan, however, a large amount of heat is dissipated during operation due to Joule effect; thus, cooling HP-LEDs is an important challenge in package designs, where a correct evacuation of the heat will substantially enlarge the lifetime of the device[11].

Besides the previous constraint, other practical aspects like a compact configuration, low cost, mass production or even esthetic considerations can play an important role in market-oriented products. Thus, in this paper we present a numerical analysis of the thermal stabilization of 30W – 50W LED chips attached to passive heat sinks, yielding a compact light bulb design that can be used for commercial purposes in the street lighting market. The system we propose keeps the temperature of the LED chip well-below 70°C under realistic conditions, yielding long-term operation of the bulb, with the corresponding savings in energy consumption and maintenance.

After the numerical calculations performed, in order to compare the results of the computational simulations with experimental measurements taken in standard systems, a set of prototypes has been constructed in a compact and ready-to-install configuration. As we will



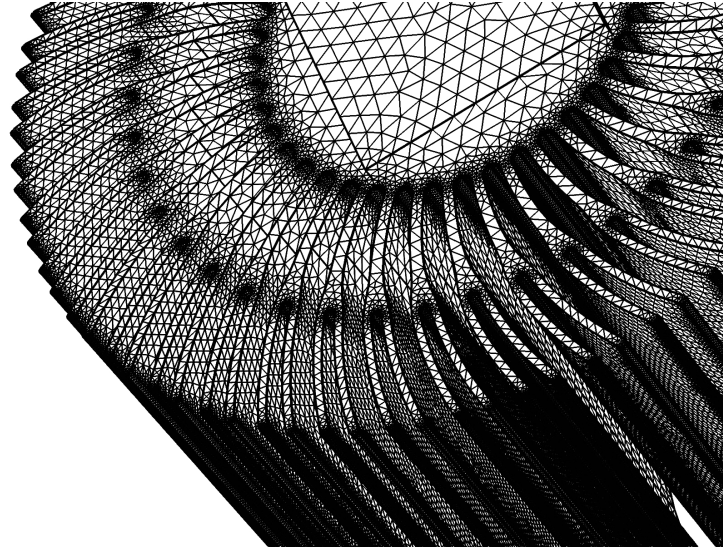


Figure 1. Detail of the computational grid used for the numerical simulations. The size of the real devices was 5cm and 10cm height and 9cm diameter. Details of the calculations are given in the text.

demonstrate, there is a nice agreement between the numerical simulations and the corresponding data obtained.

2. Numerical model

Our first aim is to calculate the steady-state temperature distribution over the surface of a heat sink with translational symmetry along one axis. This configuration is ideal for mass production at a very low cost via metal extrusion process. In our theoretical model, we have assumed that the heat sink is made of black anodized aluminum (Al 16061), which is surrounded by a laminar air flow of density (ρ) given by the ideal gas law. Thus, in the air side, the first expression that we formulate is the continuity equation:

$$\nabla \cdot (\rho \vec{v}) = 0, \quad (1)$$

being \vec{v} the velocity of air. In addition we have the energy equation[12]:

$$\rho \frac{\partial \vec{v}}{\partial t} = -\nabla P + \mu \nabla^2 \vec{v} - \rho \vec{g}, \quad (2)$$

where t is the time, P the pressure and μ the dynamic viscosity of air. We assume that the acceleration of gravity \vec{g} , is parallel to the z -axis. Another formula to be added to the model is the moment equation:

$$\rho C_P \frac{\partial T}{\partial t} = \nabla \cdot (k \nabla T) + \frac{\partial P}{\partial t}, \quad (3)$$

being C_P the specific heat, T the absolute temperature and k the thermal conductivity. On the heat sink we have the condition $\nabla^2 T = 0$. At the interface, for a black anodized surface with high emissivity (≥ 0.8), we can neglect the effect of the incoming radiation heat flux (W/m^2) and thus the outgoing flux (\dot{q}) is given by the Stefan-Boltzmann law:

$$\dot{q} = \epsilon \sigma T^4, \quad (4)$$

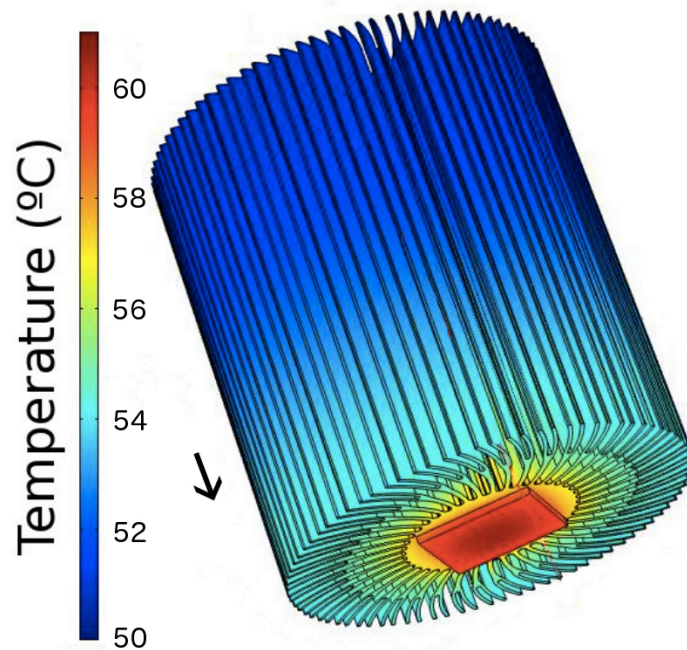


Figure 2. Numerical simulation of steady-state temperature distribution over the surface of a passive heat sink in vertical configuration corresponding to the geometry of Fig. 1. The color scale ranges from 50°C (blue) to 61°C (red). The arrow indicates the direction of the gravitational force, which in this case is parallel to the axis of symmetry of the heat sink. The system modeled is black anodized Al and the size used for the calculations was 10cm height and 9cm diameter. The LED power in this simulation is 50W . Other details of the simulation are given in the text.

where ϵ is the emissivity of the aluminum wall, σ is the Stefan-Boltzmann constant and T is the absolute temperature of the heat sink.

We want to solve the previous problem for a heat sink made of black-anodized aluminum (Al6061) with the geometry shown in Fig. 1. To numerically integrate the previous set of equations, we have used COMSOL Multiphysics[®], which is a finite element analysis solver commercial package for various physics and engineering applications, especially coupled phenomena. In addition to conventional physics-based user interfaces, this software also allows for entering coupled systems of partial differential equations (PDEs). In particular, we have used the Heat Transfer Module which provides user interfaces for heat transfer by conduction, convection and radiation.

We have modeled the LED chip as a 1mm -thick aluminum square plate which provides a constant heat flux at the base of the heat sink. For the chips under consideration the amount of waste heat can be estimated as 70% of the LED power[13]. The dependence on the grid density was investigated by changing the number of points. The final selection is shown in Fig. 1. The simulation corresponds to a heat sink 10cm height with a diameter of 9cm . The diameter of the solid internal core is 4cm .

The results of the numerical calculations are shown in Fig. 2 for a vertical configuration (i.e.: the symmetry axis of sink parallel to the direction of the acceleration of gravity \vec{g}) and simulating the effect of a 50W LED chip placed at the bottom of the heat sink. As it can be appreciated in the picture, the maximum of the temperature distribution is obviously located at the LED

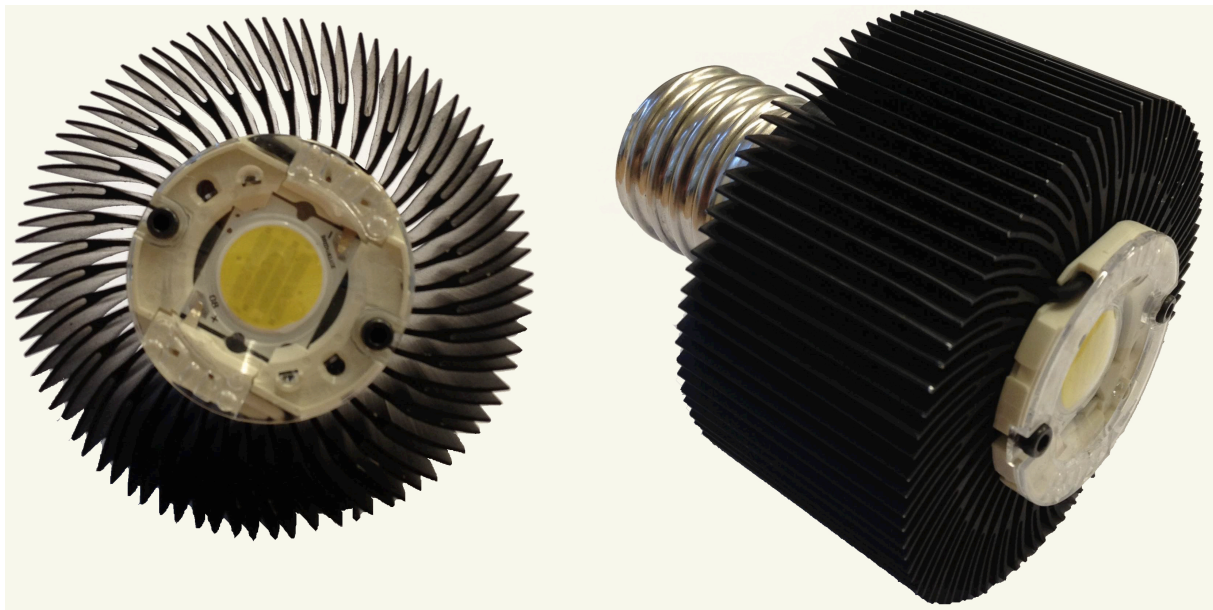


Figure 3. Front (left) and lateral (right) view of the real system composed of a black anodized aluminum structure in a compact LED bulb configuration. The height of the sink is 5cm and its diameter is 9cm the corresponding simulations and experiments for horizontal and vertical orientations with a 25W LED chip are shown in Fig.5 and Fig. 6, respectively.

chip and the values of T gradually diminish with the distance from the chip, showing a radially symmetric distribution around the axis of the cylinder. For an ambient temperature of 21°C , the maximum of the resulting steady-state distribution calculated is 60.8°C , well below the critical damage temperature provided by the LED manufacturer, providing thus a maximal lifetime of the device. As we will show below, this result is in good agreement with the experimental measurements performed in a real system. Of course, for higher ambient temperatures our predictions are still valid and in this case the gap with respect to the damage threshold is reduced accordingly[11].

3. Experimental Setup

In order to check the validity of our numerical model, a series of experiments were made. Aluminum (Al6061) black anodized heat sinks with the same geometry as in Fig 1 and two different lengths (5.0cm and 10.0cm) were attached to a 25W and 50W LED chips respectively. In Fig. 3 we show a photo of one of the prototypes that we constructed to perform the experimental measurements.

In all the cases, to minimize the thermal contact resistance between the LED chip and the heat sink a graphite film of high thermal conductivity ($240\text{Wm}^{-1}\text{K}^{-1}$) was used. Finally, the light bulbs were mounted in several orientations in order to reproduce different operation conditions. The emissivity of the heat sink with the black-anodized surface treatment is 0.8. The geometric parameters of the experimental model are the same as in the numerical simulation described above and below. A temperature sensor with three different probe heads (DAQ-9172, NI9211), a power supply, a wattmeter, and a laptop were used in order to collect data.

The overall pattern for the air flow could be described as follows: the cooling air enters from the outer region of the heat sink and is heated while passing through the fins. The heated air rises upward in the inner regions of the heat sink due to the fact that the density of the air in

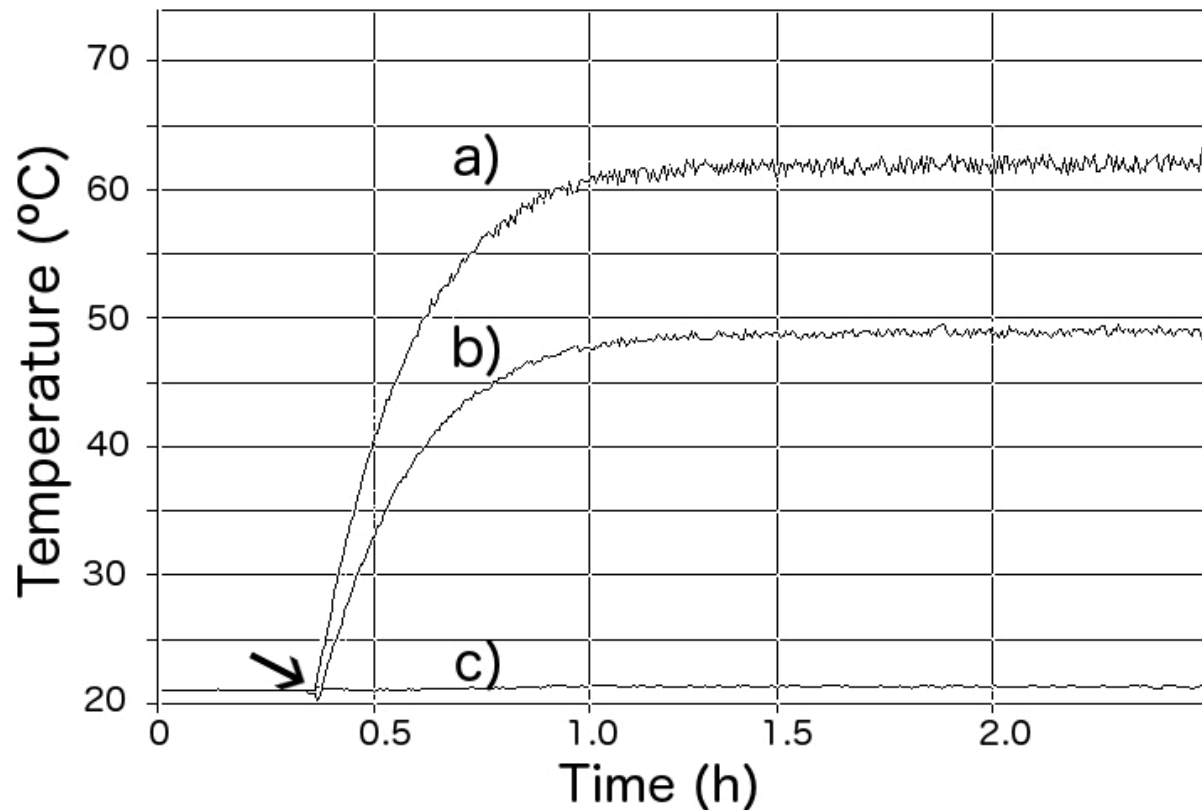


Figure 4. Experimental measurement of the temperature distribution in the vertical configuration (the axis of symmetry of the sink is parallel to the gravity force) corresponding to the numerical simulation of Fig.2. Curves a), b) and c) correspond respectively to the LED chip, the center of the top side of the heat sink and the ambient. Details of the experiment are given in the text. The arrow points to the instant when the power is switched on.

this zones became less than that of the surrounding air. In addition, a thermal boundary layer develops discontinuously, after some delay. Thus, a relatively high local heat transfer coefficient is expected in the inner regions of the heat sink.

The pin-fin heat sink will show uniform cooling performance in the case of natural convection considered. Repeated leading-edge effects will appear in the outer regions of the heat sink because the fins are arranged to keep the flow at a certain distance in the radial direction.

4. Results and discussion

In Fig. 4, we plot the experimental measurement of temperature values measured for a 50 – W LED chip in vertical configuration (the axis of symmetry of the sink is parallel to the gravity force) corresponding to the numerical simulation of Fig.2 with the chip placed at the bottom of the heat-sink. Curves a), b) and c) correspond respectively to the temperatures measured at the LED chip, the center of the top side of the heat sink and the ambient.

As it can be appreciated in the curves, once the power is switched on (indicated by an arrow) the temperature increases until saturation after less than one hour. The maximum values measured in curves a) and b) are respectively 63°C and 49°C which are in very good agreement with the numerical simulation of Fig. 2.

To determine the optimum configuration and the precision of the numerical model, we have simulated and measured different orientations and lengths of the heat sink. The results of the numerical calculations can be seen in fig. 5 for a 25W HPLED and 5cm height heat sink. The results show the simulation of the steady-state temperature for vertical (a) and horizontal (b) configuration, meaning these names that the acceleration of gravity (\vec{g}) is parallel or perpendicular to the symmetry axis of the heat sink, respectively.

The comparison of the numerical simulations of Fig. 5 with experimental values is shown in Fig. 6. In this figure we plot the temperature measured at the chip (a) and at the center of the opposite side of the heat sink (b). Line c) shows the ambient temperature during the experiment.

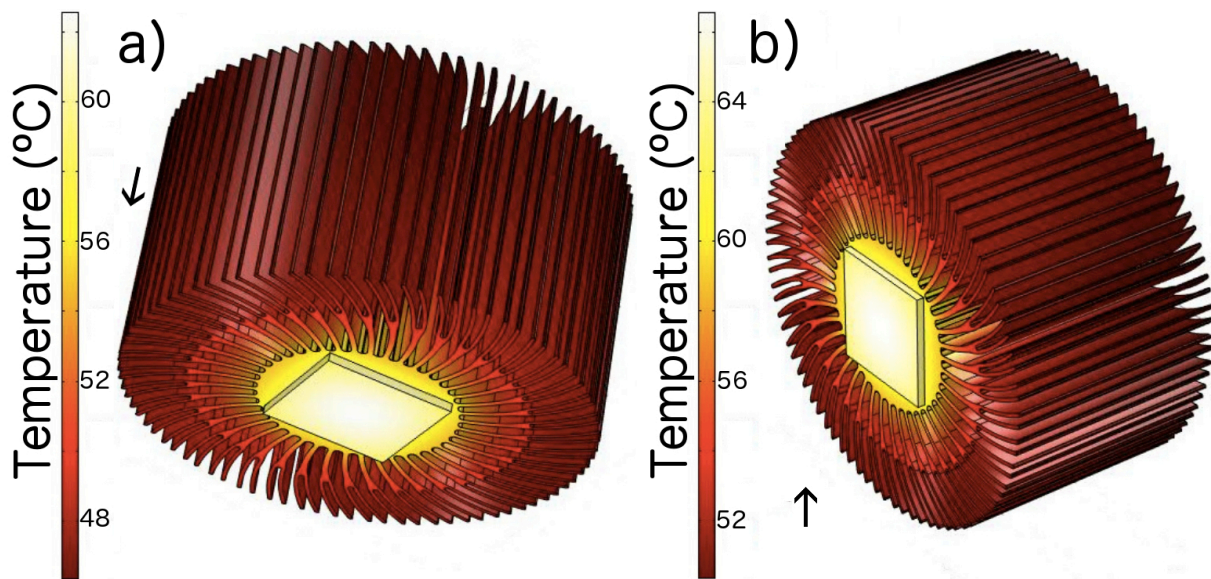


Figure 5. Numerical simulation of steady-state temperature distribution over the passive heat sink in horizontal (left) and vertical (right) configuration. The arrows indicate the direction of the gravitational force in each case. The color scale ranges are plotted in the left side of each simulation. The system modeled is black anodized Al as in Fig. 2. In this case the size used for the calculations was 5cm height and 9cm of diameter. The LED power is 25W. Other details of the simulation are given in the text.

As it can be appreciated in the left non-shaded zone of Fig. 6, after less than one hour of operation of the LED, the system reaches a thermal steady state with a maximum temperature in the chip of 63°C, in excellent agreement with the simulations of Fig. 5-a. Once the temperature is stabilized, we rotate the system 90° which corresponds to a perpendicular orientation of the axis of symmetry of the heat sink with respect to the force of gravity (see Fig. 5-a). This situation is indicated by a dark-grey shading in the graph. It is obvious that this configuration is not the optimal one, yielding an increase of about 8°C in the chip temperature.

Then, we rotate the sink another 90° and thus, the axis of symmetry of the sink is aligned with the gravity force as in 5-b, however the chip is placed now at the top of the chip instead of the bottom. As it can be appreciated the temperature slightly decreases showing the important contribution of air convection along the pin-fins.

Finally, we restore the initial position and the temperature asymptotically recovers the steady-state value of the first zone of the graph. All the measurements made are in very good agreement with the numerical simulations shown in Fig. 5 for two different orientations.

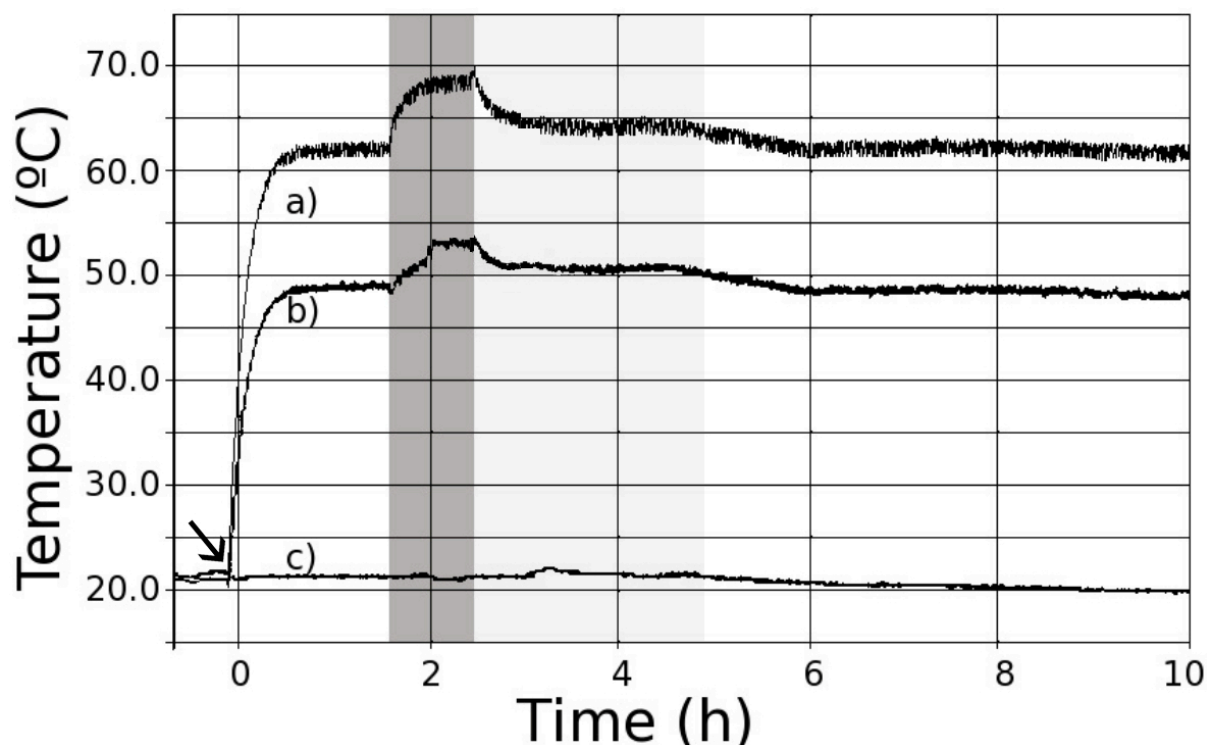


Figure 6. Experimental measurement of the temperature distribution measured at: a) the LED chip, b) the center of the back side of the heat sink, and c) the ambient. The non-shaded parts of the graph correspond to measurements made for parallel orientation of the symmetry axis of the heat sink with respect to the force of gravity and with the LED chip placed at the bottom of the heat sink corresponding to Fig. 5-a. The dark-gray zone displays the values obtained for perpendicular orientation (Fig. 5-b) and the light-gray region corresponds to the same orientation Fig. 5-a but with the LED chip placed at the top of the sink. The rest of the parameters of the experiment are given in the text.

5. Conclusions

We have presented a numerical study of the steady-state temperature distribution of a realistic high-power light emitting diode (HP-LED) bulb. Our results have been compared with experimental data measured in a prototype fabricated under market considerations. A nice agreement has been found between the computer simulations and the measurements performed.

Therefore, from our analysis we can derive that aluminum low-cost passive heat sinks can be used to keep the temperature of 30W – 50W HP-LED chips below 70°C, thus making it possible to reach life-times of 55.000h with the corresponding savings in energy consumption and maintenance.

Acknowledgments

HM thanks funding from projects K133131H64102 and K044131H64502 Xunta de Galicia. PF-C thanks Universitat Politècnica de València funding under project SP20120909.

References

- [1] Mueller-Mach R, Mueller G, Krames M and Trottier T 2002 *Selected Topics in Quantum Electronics, IEEE Journal of* **8** 339 –345 ISSN 1077-260X

- [2] Narukawa Y, Narita J, Sakamoto T, Deguchi K, Yamada T and Mukai T 2006 *Japanese Journal of Applied Physics* **45** L1084–L1086
- [3] Krost A and Dadgar A 2002 *physica status solidi (a)* **194** 361–375 ISSN 1521-396X
- [4] Luo H, Kim J K, Schubert E F, Cho J, Sone C and Park Y 2005 *Applied Physics Letters* **86** 243505 (pages 3)
- [5] Chiu H J, Lo Y K, Chen J T, Cheng S J, Lin C Y and Mou S C 2010 *Industrial Electronics, IEEE Transactions on* **57** 735 –743 ISSN 0278-0046
- [6] Efremov A, Bochkareva N, Gorbunov R, Lavrinovich D, Rebane Y, Tarkhin D and Shreter Y 2006 *Semiconductors* **40**(5) 605–610 ISSN 1063-7826
- [7] Chen H Y, Lam W Y, Luo J D, Ho Y L, Tang B Z, Zhu D B, Wong M and Kwok H S 2002 *Applied Physics Letters* **81** 574–576
- [8] Gardner N F, Kim J C, Wierer J J, Shen Y C and Krames M R 2005 *Applied Physics Letters* **86** 111101 (pages 3)
- [9] Yu S H, Lee K S and Yook S J 2010 *International Journal of Heat and Mass Transfer* **53** 2935 – 2938 ISSN 0017-9310
- [10] Narendran N and Gu Y 2005 *Display Technology, Journal of* **1** 167 – 171 ISSN 1551-319X
- [11] Tan C M and Singh P 2014 *Device and Materials Reliability, IEEE Transactions on* **14** 742 – 750
- [12] Jang D, Yu S H and Lee K S 2012 *International Journal of Heat and Mass Transfer* **55** 515 – 521 ISSN 0017-9310
- [13] Arik M and Setlur A 2010 *International Journal of Energy Research* **34** 1195–1204 ISSN 1099-114X

Document downloaded from:

<http://hdl.handle.net/10251/67992>

This paper must be cited as:

Bandos, T.; Montero Reguera, ÁE.; Fernández De Córdoba Castellá, P.J.; Urchueguía Schölzel, JF. (2011). Improving parameter estimates obtained from thermal response tests: Effect of ambient air temperature variations. *Geothermics*. 40(2):136-143.
doi:10.1016/j.geothermics.2011.02.003.



The final publication is available at

<http://dx.doi.org/10.1016/j.geothermics.2011.02.003>

Copyright Elsevier

Additional Information

Improving Parameter Estimates Obtained from Thermal Response Tests: Effect of Ambient Air Temperature Variations

T.V. Bandos^{1*}, Á. Montero², P. Fernández de Córdoba¹, J.F. Urchueguía¹

¹ *Instituto Universitario de Matemática Pura y Aplicada, Universidad Politécnica de Valencia, Camino de Vera s/n, 46022 Valencia, Spain*

² *Instituto de Ingeniería Energética, Universidad Politécnica de Valencia, Camino de Vera s/n, 46022 Valencia, Spain*

ABSTRACT

This paper presents a method of subtracting the effect of atmospheric conditions from thermal response test (TRT) estimates by using data on the ambient air temperature. The method assesses effective ground thermal conductivity within 10% of the mean value from the test, depending on the time interval chosen for the analysis, whereas the estimated value can vary by a third if energy losses outside the borehole are neglected. Evaluating the same test data using the finite line-source (FLS) model gives lower values for the ground thermal conductivity than for the infinite line-source (ILS) model, whether or not heat dissipation to ambient air is assumed.

Keywords: Borehole heat exchangers, Heat transfer, Finite line-source method, Ground-source heat pumps, Thermal response test

*Corresponding author. Tel.: +34 963877007/85247. E-mail address: tbandos@uv.es.

Nomenclature

$C(C_f)$	volumetric heat capacity of ground (fluid) ($\text{Jm}^{-3}\text{K}^{-1}$)
D	length along the piping between the temperature probe location and the borehole inlet or outlet (see Fig. 1) (m)
Ei	exponential integral
$g(t) = \frac{2\pi\lambda}{q_z}(T - T_0)$	thermal response function
G	fluid volume flow rate (m^3s^{-1})
H	depth of the borehole heat exchanger (BHE) (m)
r	radial coordinate (m)
$p = \langle Q_{air} \rangle / Qt$	part of the total heat rate transmitted to the ambient air
r_b	radius of the BHE (m)
R_a	thermal resistance between fluid and ambient air (KmW^{-1})
R_b	borehole thermal resistance (KmW^{-1})
$q_z = \frac{GC_f}{H}(T_{in} - T_{out})$	heat flow per unit length (Wm^{-1})
Q_{air}	heat dissipation rate to the ambient air (W)
$Q_t = GC_f(T_{in}^* - T_{out}^*)$	total produced heat rate (W)
s	coordinate along the pipe in the range from 0 to D (m)
$t_0 (t_1)$	start (end) point of the time interval (s)
$t_r = r_b^2/\alpha$	short time scale for the BHE (s)
$t_s = H^2/(9\alpha)$	Eskilson (1987) steady-state time scale (s)
$t_z = H^2/\alpha$	large time scale for the BHE (s)
T	temperature of ground (K or °C)
T_a	ambient air temperature (K or °C)
T_f	temperature of heat carrier fluid (K or °C)
T_0	undisturbed ground temperature (K or °C)
T_{in}	inlet temperature of BHE (K or °C)
T_{out}	outlet temperature of BHE (K or °C)
T_{in}^*	measured inlet temperature of BHE (K or °C)
T_{out}^*	measured outlet temperature of BHE (K or °C)

z vertical axial coordinate (m)

Greek letters

$\alpha = \lambda/C$ ground thermal diffusivity (m²/s)

γ Euler's constant

λ ground thermal conductivity (W(Km)⁻¹)

$\eta [= D/(R_a C_f G)]$ dimensionless parameter

Superscripts

—
..... arithmetic mean

$\langle \dots \rangle (= \int_0^H \dots dz/H)$ integral mean

$\langle \dots \rangle_t$ time average

$\dots \uparrow (\dots \downarrow)$ up (down) directions for heat carrier fluid circulation

Subscripts

a ambient air

1. Introduction

Nowadays, ground-source heat pumps (GHPs) are a solid alternative as choice of system for heating and cooling in buildings (Omer, 2008; Sanner et al., 2005; Urchueguía et al., 2008). By comparison with standard technologies, they offer competitive levels of comfort, reduced noise levels, savings of greenhouse gas emissions, and reasonable environmental safety. Furthermore, their electrical consumption and maintenance requirements are lower than those required by conventional systems and, consequently, the annual cost is lower (Lund, 2000). Ground-source systems are recognized by the Environmental Protection Agency as being among the most efficient and comfortable heating and cooling systems available today.

A thermal response test (TRT) is a method of determining the effective on-site ground thermal conductivity in order to design ground coupled heat pump systems. These in-situ tests are based on the ILS theory of heat transfer by thermal conduction (Ingersoll et al., 1954; Reuß et al., 2009). Due to its two-dimensional nature, the ILS theory cannot describe axial temperature variations around geothermal borehole heat exchanger.

Fig. 1 represents a typical TRT test to measure the temperature response of the borehole heat exchanger (BHE) to a constant heat injection or extraction. A U-tube loop, through which a heat carrier fluid circulates, is inserted inside the borehole to approximately the same depth as the BHE planned for the site. To provide a constant heat flux to the ground, the fluid flow rate in the borehole loop and the temperature difference between inlet and outlet are kept constant during the testing. The outputs of the TRT are the inlet (T_{in}) and outlet (T_{out}) temperatures of the heat carrier fluid as a function of time (see **Fig.1**). The difference between the temperatures T_{in} and T_{out} , measured at the end points of the U-tube, is used to determine the rate at which heat is transferred by thermal conduction into the ground.

The BHE, which consists of two tubes separated by filling material, can be modeled as a heat source in the form of a line or cylinder. The effective thermal resistance of the borehole (Mogensen, 1983) defines the temperature drop between the BHE surface and an average temperature of the fluid. The temperature of heat carrier fluid circulating through the loop varies with depth, as do the ground thermal properties. A weighted average of T_{in} and T_{out} measured at the end points of the U-tube is assumed to be the mean temperature of the heat carrier fluid over the loop length (Marcotte and Pasquier, 2008). Typically, their arithmetic average is compared with a reference temperature of the borehole surface from the ILS model, around which the TRT is designed. From these experimental data and with an appropriate model for average temperature around the BHE, the effective thermal conductivity of the surroundings is inferred.

Different analytical and numerical methods have been developed for determining ground thermal properties from the TRT output data. The cylinder heat source (Ingersoll et al., 1954) and line heat source (Carslaw and Jaeger, 1959) model for BHE with parameter-estimating techniques are commonly applied in Europe (Claesson and Eskilson, 1988; Gehlin and Hellström, 2003; Sanner et al., 2005; Witte et al., 2002) and North America (Austin, 1998; Beier and Smith, 2002; Beier, 2008; Shonder and Beck, 2000). Kelvin's ILS model is among the most widely used models for evaluation of response test data at sufficiently large times because of the fact that the TRT was actually devised on the basis of ILS theory (Ingersoll et al., 1954; Mogensen, 1983).

The FLS model overcomes some limitations of the ILS model: its solution has been expressed as an integral (Eskilson, 1987), given zero temperature at the boundary of the semi-infinite medium. The temperature response functions, so-called "g-functions" introduced by Eskilson (1987), are based on the solution of this model for the BHE temperature field at a constant heat load. The g-functions are computed for moderate times (Javed et al., 2009) and provide an asymptotic approach to the steady-state limit, which is not reached within the ILS model. The FLS solution for the ground temperature in the vicinity of the midpoint of the BHE depth was shown to be approximately the same as the classical result of the traditional ILS during the TRT (Bandos et al., 2009).

However, the best solution for applications is given by the mean integral temperature (Lamarche and Beauchamp, 2007; Zeng et al., 2002). This is because the average or effective thermal properties of the ground are used in the design. An exact solution for the temperature averaged over the borehole depth has been approximated, providing analytical formulae for a wide time range (Bandos, et al., 2009) that account for the edge effects due to the vertical heat transfer along the borehole. These simple asymptotic expressions for the mean borehole temperature allow flexibility in parametric analysis of the test data. It is important to take account of the finite depth of the BHE because there is an incentive to install the minimum possible length and so decrease the cost of the ground source systems.

Evaluating TRT data based on the ILS model assumes that there is no heat transfer between the heat carrier fluid and the ambient air, and that there are no significant effects of boundary conditions for the vertical temperature profile in the ground surrounding the BHE. In practice, the inlet and outlet temperatures T_{in}^* and T_{out}^* are measured at some distance D from the ground surface; Fig.1 shows location of the temperature probes. The data analysis is based on solution of a purely conductive problem in the ground, which depends on T_{in} and T_{out} temperatures inferred from T_{in}^* and T_{out}^* (see **Fig.1**). The above-surface part of the TRT system is thermally insulated. However, it is difficult to insulate the external pipes completely; the exchange of heat between the ambient air and fluid is often inevitable. Depending on air temperature, the heat carrier fluid can gain or lose some heat to the ambient. Furthermore, even a small flow of heat through the

insulation may influence the ground conductivity estimate, causing instability (i.e., the dependence of the estimate on the time interval used for evaluation). That complicates the analysis of the TRT.

Experiments have demonstrated that the evaluation of thermal conductivity is affected by ambient air temperature changes. The influence of diurnal temperature changes on the measured fluid temperature has been reported several times (Austin, 1998; Esen and Inalli, 2009; Florides and Kalogirou, 2008; Fujii et al., 2009; Signorelli et al., 2007). In particular, the cooling effect of the ambient conditions has been observed (Gehlin and Nordell, 2003). The observation of atmospheric effects in numerous experiments prompts a quest for a method that would allow the influence of air temperature variation to be subtracted from the dependence of the ground conductivity estimate on the time interval chosen for analysis. Being complementary to the efforts to increase the accuracy of the test (Sanner et al., 2005; Witte et al., 2002) such a technique would allow the already existing data, whose acquisition is fairly costly, to be used more efficiently.

This paper addresses the heat transfer in the above-ground and subsurface parts of the TRT system shown in **Fig. 1**. It presents (i) a new method for subtracting the atmospheric effect on the test parameters by using data of ambient air temperature in the estimation; (ii) analysis of test data on the basis of the formula for average borehole temperature, accounting for the edge effects from the FLS model; and (iii) comparison of these thermal conductivity estimates to those from the ILS model, accounting for heat losses to the ambient.

The rest of the paper is organized as follows: Section 2 reviews the results from the classical infinite and finite line-source models. Section 3 introduces the heat balances for the heat carrier fluid and proposes a method to account for climatic influence and efficiently subtract it from the data. Section 4 compares the proposed model with experimental dependence of the temperature of the circulating fluid on time and summarizes results for the test estimates with and without heat losses to the atmosphere. Finally, Section 5 concludes and discusses directions for further investigation.

2. Line-source theory

Within the ILS framework commonly applied for the evaluation of thermal response test data, the ground is assumed to be a homogeneous infinite medium characterized by its thermal conductivity λ . In the vicinity of the borehole, for sufficiently large time values, the ILS model gives (Ingersoll et al., 1954):

$$T(r, t) = T_0 - \frac{q_z}{4\pi\lambda} Ei\left(-\frac{r^2}{4\alpha t}\right) \\ \approx \frac{Q_z}{4\pi\lambda} \left\{ \ln \frac{4\alpha t}{r^2} - \gamma + O\left(\frac{r^2}{4\alpha t}\right) \right\} + T_0, \quad \text{for } \frac{4\alpha t}{r^2} \gg 1 \quad (1)$$

where $Ei(u)$ denotes the exponential integral (Carslaw and Jaeger, 1959) q_z as the heat flux density per length unit, γ as Euler's constant, α as ground thermal diffusivity, and T_0 as the undisturbed ground temperature. It is usually assumed that the heat is released at a constant rate from the BHE, in the "radial" direction orthogonal to it, and is transferred by the mechanism of thermal conduction. The ILS solution is applicable to the temperature around a midpoint of BHE, modeled as an FLS of the same constant heat flow, and only for moderate times ($t < t_z$) (because a physically reasonable steady-state solution is beyond its scope). It has been shown

analytically that the classical result of the traditional ILS is reproduced by the FLS solution for the ground temperature about the midpoint depth (up to the exponentially small correction terms $e^{-t_z/t}$) at times that are comparable with the duration of the TRTs (Bandos et. al, 2009). That is precisely the reason why the simplifying assumption about an infinitely long heat source in an infinite medium provides a good approximation and is commonly used for the TRT analysis (Mogensen, 1983) and for the design standards of the International Ground Source Heat Pump Association (Bose et al., 1985). This is also why the ILS is used as a benchmark model for comparison with new proposals.

Approximate expressions for average borehole temperature (instead of temperatures at the midpoint of the borehole) were derived to apply over a wide range of time values (Bandos et. al, 2009). In the frame of the FLS in the semi-infinite region, the approximation of the average ground temperature for the times corresponding to the TRT (i.e., for $t_z \gg t \gg r^2/4\alpha$) is given by:

$$\langle T(r, z, t) - T_0 \rangle = \frac{q_z}{4\pi\lambda} \left\{ \ln \frac{4\alpha t}{r^2} - \gamma - \frac{3}{\sqrt{\pi}} \sqrt{\frac{4t}{t_z}} + \frac{3r}{H} - \frac{3}{\sqrt{\pi}} \frac{r^2}{H^2} \sqrt{\frac{t_z}{4t}} \right\} \quad (2)$$

$$\langle T(r, z, t) - T_0 \rangle = \frac{1}{H} \int_0^H (T(r, z, t) - T_0) dz$$

This expression for the average temperature of the BHE differs from the classical one (**Eq. 1**) by the finite-size corrections, which vanish in the limiting case of $H \rightarrow \infty$. Notice that for both models ILS (1) and FLS (2), the heat flux density q_z is implied to be the same and constant along the borehole, assuming a purely conductive heat transport. The effects of the finite source size are described by the last three terms in the right-hand side of **Eq. 2**. Their contribution to the transient temperature at various radial distances from the borehole center is significant for shallow boreholes as calculated numerically (Philippe et al., 2009). Indeed, **Eq. 2** shows that, for $H = 25\text{m}$ and for $t/t_z \approx 0.16$ and $t/t_z \approx 0.0016$, corresponding approximately to 4 months and 1 day respectively, the relative difference between the results from the ILS and FLS model reaches 30% and 6.5% at $r = 1\text{m}$.

Early time, $t < 5t_r$, values are in the order of one day (Eskilson, 1987), whereas typical thermal test durations range from 40 to over 200 hours (Signorelli et al., 2007). The latter fall within $t_r < t < t_z$, termed medium times to distinguish them from very long time values $t > t_z$ corresponding to the approach to the steady-state (Claesson and Eskilson, 1988). In this case, the integral average temperature change at the radial distance r from the borehole center is given by (Bandos et al., 2009):

$$\frac{q_z}{4\pi\lambda} \left\{ 4 \sinh^{-1} \frac{H}{r} - 2 \sinh^{-1} \frac{2H}{r} + 3 \frac{r}{H} - 4 \sqrt{1 + \frac{r^2}{H^2}} + \sqrt{4 + \frac{r^2}{H^2}} - \frac{t_z^{3/2}}{12\sqrt{\pi}t^{3/2}} \left(1 - \frac{3t_z(1+r^2/H^2)}{20t} \right) \right\}, \quad t \gg \max(H^2, r^2) \quad (3)$$

where $\sinh^{-1} a = \ln(a + \sqrt{1+a^2})$.

Eq. 3 describes the time-asymptotic approach to the steady-state temperature of the designed geothermal system, whereas **Eq. 2** is applicable to the data of the test within the medium time interval. The following section shows how to account for the atmospheric effect that influences the time dependence of the temperature of heat carrier fluid.

3. Analysis of TRT data

3.1 The response test

The test described here was carried out in Castellon (Spain) in January 2007, to obtain design values for the planned geothermal pump. In the data acquisition system, the apparatus used to monitor the thermal response was connected to the BHE by thermally insulated 4-m-long tubes. The field test was performed on a borehole with radius r_b of 0.15m, and $H = 25$ m (See Fig. 1). Bentonite grout filled the space between the U-loop tube and the inner BHE wall, and water was used as the heat carrier fluid. By measuring the plug flow temperature before the test, the undisturbed temperature was determined to be $18.4 \pm 0.2^\circ\text{C}$.

The test apparatus worked in heat injection mode: the water entering the BHE was warmer than that exiting. The test parameters were monitored every three minutes by a data logger. **Fig 2** presents plots of the 1,418 data readings of ambient air temperature and average water temperature, defined by the arithmetic mean of the inlet and outlet temperatures, as a function of time during the 71-hour experiment.

To provide a constant heat rate (about 1.04 kW, as shown by the gray line of **Fig. 3**), the difference between the temperatures of the circulating fluid at the input and output of the ground loop was held constant (at about 3°C), as was the volume flow rate of water, $G \approx 0.3 \text{ m}^3/\text{h}$. High-frequency oscillations of the total heat rate were due to the control system for the temperature of water entering borehole. The flow rate was measured by a Coriolis meter with an accuracy limited to 1%, while the temperature sensors were four-wire PT100 with an accuracy of $\pm 0.1^\circ\text{C}$.

Although pipes connecting the test device with the borehole were well thermally insulated, an undesirable correlation between the air temperature and the mean temperature of the fluid was also observed in our test, as in other cases. Just visible in **Fig. 2** are small jumps in average water temperature at 15, 30, and 54 hours that are related to significant variations of the temperature of the ambient air around its average value of 14°C . This implies some heat transfer through the above-ground pipes between the borehole and data acquisition instrument (Sanner et al., 2005).

The relationship between the time dependence of the carrier fluid temperature and the ambient air temperature has been observed during TRTs carried out by different groups (Esen and Inalli, 2009; Florides and Kalogirou, 2008; Fujii et al., 2009; Gehlin and Nordell, 2003; Sanner et al., 2005; Shonder and Beck, 2000; Signorelli et al., 2007; Spitler, 2000). This may indicate that it is often difficult to completely remove the atmospheric effect by means of insulation. The fact that, in practice, the ambient air and the fluid temperatures are correlated strongly affects the stability of the ground conductivity estimate, making it dependent on the chosen time interval (Austin, 1998; Gehlin and Hellström, 2003; Shonder and Beck, 2000; Signorelli et al., 2007; Witte et al., 2002). On the other hand, the observation of such correlations in numerous experiments suggests that it is necessary to consider heat transfer processes in the geothermal system as a whole in order to handle test data that is influenced by the ambient air temperature variation.

3.2 Climatic effect on the heat transferred to the ground: interpretation model

Heat exchange between the ambient air and the fluid in the above-ground pipe work changes the heat transferred to the borehole. Then, the total heat rate Q_t can be written as a sum of the heat dissipation rate to the ambient air (Q_{air}) and the actual heat rate transferred to the ground (q_zH):

$$Q_t = Q_{air} + q_zH \quad (4)$$

Besides diurnal variations of the air temperature, the interior temperatures of the test rig affect the efficiency of the system operation (Sanner et al., 2005). In many practical circumstances, the inlet and the outlet temperatures are measured using temperature probes on the above-ground connection pipes, as implied in **Fig. 1**. The thermal influence on the borehole temperature of the heat carrier fluid in the above-ground piping has been recorded (Gehlin and Nordell, 2003).

The fluid temperature changes with the s coordinate along the pipes outside the borehole due to the undesirable heat exchange with the ambient air. In the quasi steady-state case, the heat transport by the fluid in the tube, accompanied by the transverse heat flux to the air, is governed by the convection equations (Claesson and Eskilson, 1988; Hellström, 1991):

$$GC_f \frac{dT_f^\downarrow(s, t)}{ds} = (T_a(t) - T_f^\downarrow(s, t))/R_a, \quad T_f^\downarrow(s=0) = T_{in}^* \quad (5)$$

$$-GC_f \frac{dT_f^\uparrow(s, t)}{ds} = (T_a(t) - T_f^\uparrow(s, t))/R_a, \quad T_f^\uparrow(s=0) = T_{out}^* \quad (6)$$

$$0 \leq s \leq D$$

The measured temperatures T_{out}^* and T_{in}^* related to the borehole input and output are required to estimate the total amount of the heat rate:

$$Q_t = C_f G (T_{in}^* - T_{out}^*) \quad (7)$$

Heat dissipation to the ambient air causes temperature variation along the connection pipe. As a result, the actual heat rate transferred to the ground is not Q_t , but q_zH (see **Eq. 4**). In fact, the heat convection by fluid balances the radial heat flux to the ground and determines the heat rate q_zH through the temperatures near the surface level as:

$$q_zH = C_f G (T_{in} - T_{out}) \quad (8)$$

The BHE input and output temperatures, $T_{in} = T_f^\downarrow(s=D)$ and $T_{out} = T_f^\uparrow(s=D)$, need to be found. Here, D is the length of piping along the zone of thermal contact of fluid with the ambient air (i.e., between the point of measurement and the point of input (output) to the BHE, as **Fig. 1** shows). The effective length D may also include the uppermost part of the borehole.

The solution of the system of **Eq. 5** and **6** with the boundary conditions at the points of measurement can be written as:

$$T_{in} = T_{in}^* e^{-\eta} + T_a (1 - e^{-\eta}) \quad (9)$$

$$T_{out} = T_{out}^* e^{\eta} + T_a (1 - e^{\eta})$$

$$\eta = D / (R_a C_f G) \quad (10)$$

The above solutions depend on thermal characteristics of the flow system through the model parameter η . Its physical meaning can be inferred from physical parameters entering **Eq. 10**: flow rate, heat capacity of fluid, piping dimensions; its value can be calculated based on an assumed thermal resistance R_a . Notice that this model parameter η takes non-zero values in actual conditions of penetrating ambient influence, while its zero value is reached for the limiting case of perfect thermal insulation of the connecting pipes $R_a = \infty$ or $G \rightarrow \infty$. Therefore, $\eta = 0$ corresponds to the ideal test conditions without heat dissipation to the ambient and is used for comparison with the proposed model hereafter. A non-zero value of the dimensionless parameter η from **Eq. 10** accounts for the climatic influence. It can be calculated using physically observable properties, as in **Eq. 10**, or estimated from the test data as described below.

The outputs of the exterior problem, **Eq. 9**, influence both the heat rate to the ground and mean fluid temperature. Indeed, substituting **Eq. 9** into **Eq. 8**, one finds:

$$q_z(\eta, t)H = C_f G (2T_a(t) \sinh \eta - e^{\eta} T_{out}^* + e^{-\eta} T_{in}^*) \quad (11)$$

and then

$$\bar{T}_f(\eta, t) = (T_{out}(t) + T_{in}(t))/2 = T_a(t)(1 - \cosh \eta) + (e^{\eta} T_{out}^* + e^{-\eta} T_{in}^*)/2 \quad (12)$$

The inputs for the conduction problem, related to T_{in} and T_{out} at the top of the borehole are now expressed using measured fluid temperatures T_{in}^* and T_{out}^* .

Notice that if the connecting pipes were ideally insulated (i.e., $\eta = 0$, neither T_{out} , T_{in} , or q_z would depend on the ambient air temperature. In the test, the temperature probes are to be immersed directly into the flow (Witte et al., 2002), where, presumably, the outside heat influence should not penetrate. However, under real conditions, there exist heat losses to the ambient outside the borehole, and so the parameter η takes small but non-zero values.

The question then arises of how to select parameter η in order to filter out the effect of air temperature variation. The energy rate balance, **Eq. 7** and **11** set the correspondence between η and the fraction p of the total heat rate transmitted to the ambient air

$$\langle Q_{air} \rangle_t = p \langle Q_t \rangle_t \quad (13)$$

as:

$$(p - 1 + \cosh \eta) \langle T_{in}^*(t) - T_{out}^*(t) \rangle_t = \langle T_{out}^*(t) + T_{in}^*(t) - 2T_a(t) \rangle_t \sinh \eta \quad (14)$$

Note that the thermal resistance $R_a = D / (\eta C_f G)$ between the fluid and the air is independent of the flow direction due to the fact that above equation is invariant under $\eta \rightarrow -\eta$ if this is supplied by $T_{in}^*(t) \leftrightarrow T_{out}^*(t)$. If the heat loss to the ambient air is a small part of the total produced heat rate ($p \ll 1$), the leading terms in the series expansion in η in **Eq. 14** give:

$$\eta = p \frac{\langle T_{in}^*(t) - T_{out}^*(t) \rangle_t}{\langle T_{out}^*(t) + T_{in}^*(t) - 2T_a(t) \rangle_t} \quad (15)$$

Then, the values of η turn out to be small as long as $p \ll 1$; these parameters are proportional, and the case of $\eta = 0$ corresponds to $p = 0$. (**Eq. 15** does not mean that the flow parameter should be considered as a function of the measured temperatures.) One can use **Eq. 15** to select η .

The idea behind the proposed method of handling TRT data is to use the freedom in choosing η to suppress the influence of the air temperature oscillations. The algorithm to determine the model parameter η can be summarized as follows:

1. Choose an initial guess for p (for instance, use an acceptable energy loss to the ambient, and calculate η from **Eq. 15**)
2. Apply the three-parameter scheme, described in section 4.1 below, varying estimates of λ , R_b , and T_0
3. Compare the value T_0 thus obtained with the experimental value T_0^{exp}
4. If $T_0 - T_0^{exp}$ is less than some tolerance threshold, then stop iteration: the value of η is sufficiently accurate; otherwise, choose another value for p

As a sample application of the above proposed algorithm for determining η using T_0^{exp} , consider the TRT data. For the initial guess of p , the optimal choice happens to be $p = 0.055$, or 5.5% of heat dissipated to the ambient during the heat injection. With this value for p , **Eq. 15** gives $\eta = 0.006$. Then, as a result of steps 2 and 3, the estimate of T_0 (what is the value) appears to be close enough to the value T_0^{exp} determined from the experiment before the test.

Fig. 3 plots the variable heat rates $q_z H$ and Q_{air} calculated using **Eq. 11** and **17** with $p = 0.055$, $\eta = 0.006$; it is seen that the heat rate Q_t remains roughly the same by keeping the temperature difference $T_{in}^* - T_{out}^*$ constant during the TRT. There are minor variations of the resulting heat input during this TRT (in accordance to hardly discernable fluctuations of fluid temperature caused by the daily air temperature fluctuations; see **Fig. 2**.)

In the next stage, the total heat flow from the fluid to ground through the borehole wall is considered. When fitting the temperature at the lateral surface of the borehole $T_b = T(r = r_b, t)$ to the experimental data \bar{T}_f for the mean heat carrier temperature, the thermal resistance R_b between the borehole wall and the fluid must be taken into account (Mogensen, 1983):

$$R_b C_f G (T_{in} - T_{out}) = R_b (Q_t - Q_{air}(t)) / H = \bar{T}_f(\eta, t) - T_b(t) \quad (16)$$

Notice that the temperature drop, $T_f(\eta, t) - T_b(t)$, is influenced by the ambient air temperature $T_a(t)$ through the heat rate $Q_{air}(t)$ that is given by:

$$Q_{air}(t) = C_f G (\sinh \eta (T_{in}^* + T_{out}^* - 2T_a(t)) + (1 - \cosh \eta) (T_{in}^* - T_{out}^*)) \quad (17)$$

or, for small values of η ($\ll 1$):

$$Q_{air}(t) \approx 2\eta C_f G (\bar{T}_f(\eta, t) - T_a(t)) \quad (18)$$

Besides determination of the ground thermal conductivity, an evaluation of the borehole thermal resistance, R_b , is another objective of the test. This test estimate is very sensitive to the value of undisturbed temperature T_0 (Marcotte and Pasquier, 2008).

The proposed formulae for subtraction of climatic influence from the TRT data, using a multivariate parameter estimation analysis, is described in the next section and the results are compared with the test estimates from new models.

4. Results and discussion

4.1 Parameter estimation algorithm

The data obtained from the TRT are evaluated and compared by making use of the ILS and FLS models, along with the above described method of accounting for the heat rate transmitted to ambient air, characterized by η . To find suitable model parameters, **Eq. 1** and **2** (in the time interval of their validity) have been matched, using a regression technique, to the experimental data for the mean temperature of the water as a function of time.

Parameter estimation minimizes some measure of discrepancy between the measured fluid temperature $\overline{T_f^{exp}}$ and its prediction from **Eq. 16**, which can be rewritten as:

$$\overline{T_f(t)} = \langle q_z(t) \rangle_t \frac{g(t)}{2\pi\lambda} + q_z(t)R_b + T_0, \quad (19)$$

Here, $\langle \dots \rangle_t$ denotes time averaging, and the g -function is defined by the models in **Eq. 1** and **2**. To find optimal test estimates, the measure of loss, which is proportional to the error $\overline{T_f} - \overline{T_f^{exp}}$, is minimized by adjusting test parameters. The model parameter η was fixed by applying two or three parameter schemes based on the multivariate regression method. In the three-parameter estimation procedure, T_0 was allowed to vary, along with the variables of the two-parameter scheme: ground thermal conductivity and borehole thermal resistance.

Note that the approximation for the average temperature in **Eq. 2** differs from the linear logarithmic time dependence for the ILS (**Eq. 1**) by the extra terms that are proportional to $1/H$. Both approximate functions remain linear in the test parameters $1/\lambda$, R_b , and T_0 . However, the general regression technique is valid regardless of the functional form of the time dependence of the model (Hastie et al., 2001). The optimization procedure was performed using the best estimates of the three or two variables (i.e., variable or fixed T_0) for both the model proposed here, $Q_{air}(\eta \neq 0) \neq 0$, and the traditional version, $Q_{air}(\eta = 0) = 0$ (i.e., with and without energy loss in the connections).

4.2 Test parameter estimates with four models

Fig. 4 compares the results of FLS and ILS models with the results of the benchmark ILS model, $q_z(\eta = 0)$, using $\alpha = 1.21 \times 10^{-6} \text{m}^2/\text{s}$ throughout the numerical calculations. Four different models were developed from the data measured (in situ) by applying two- and three-parameter estimation methods. These are FLS and ILS for $\eta = 0$ and FLS and ILS for $\eta \neq 0$ models: i.e., two models incorporating measured temperatures of the ambient air, $q_z(\eta \neq 0)$, and two models without it, $q_z(\eta = 0)$.

The classical ILS and FLS approaches are applied to the data set obtained from the test after the first few hours. Transient early-time data ($t \ll r_b^2/\alpha$) are influenced by the borehole itself (i.e., by its radius, length, etc.), thermal properties of the grout, tubes, and convective resistance between inside their walls and the fluid. Therefore, these early-time data are ignored in the analysis of the thermal properties of ground.

Fig. 4 shows the thermal conductivity as a function of length of the time interval $[t_0, t_1]$ chosen for the estimation, where t_0 is the time the measurement starts and t_1 is the overall time of the measurement. Then, the length of the estimation interval (t_1-t_0) corresponds to time on the x-axis of **Fig. 4** and **6**.

Fig. 4 plots the thermal conductivity estimates obtained by using the data in the intervals: from the [46–71] hours to the [1–71] hours (thus, t_0 varies from 1 hour to 46 hours). The length of estimation interval is changed by 1 hour in a step-wise manner from 25 to 70 hours; the former interval corresponds to the late times of the test. These sequential plots can indicate whether the estimate converges to a particular value over the time intervals chosen for the analysis and provides a check for groundwater flow (Sanner et al., 2005).

Firstly, **Fig. 4** compares the thermal conductivities on different length-of-time intervals estimated from both the ILS and FLS models for $\eta = 0$ (i.e., assuming zero energy losses to the ambient air) for the same test. When assuming no heat losses in the above-ground piping and the uppermost part of the vertical BHE, the instability of the effective thermal conductivity may mask a convergent value of the TRT estimate. Indeed, **Fig. 4** reveals the cyclic nature of the temperature response for $\eta = 0$ because of the influence of the outside perturbation; very small and hardly noticeable changes in the mean fluid temperature curve in **Fig. 2** are significantly amplified for λ , which is inversely proportional to its time derivative.

As **Fig.4** demonstrates, conventional data analysis (i.e., assuming no heat exchange between the ambient air and the fluid) gives significant differences between thermal conductivity estimates within the selected time intervals (when varying t_0 from 1 hour to 46 hours, while t_1 is fixed). In contrast to this TRT estimate, which is hardly interpretable, one can find convergence if the heat exchange through the connection pipes is taken into account by setting a non-zero value for the parameter η (see **Eq. 10**). And if the model accurately represents the heat transfer processes in the whole system, the thermal conductivity curves are expected to flatten out below and above the ground surface for large estimation intervals .

Secondly, **Fig. 4** compares the λ values estimated from both the ILS and FLS models, for $\eta = 0.006$, on different time intervals from the same test data. In this case, the injected heat rate varies with time, but without clear decreasing or increasing trends that can distort the estimate of ground conductivity (Beier and Smith, 2003). A superposition technique or a method proposed by Beier and Smith (2003) can provide a solution for the case of non-constant heat flow. However, if q_z weakly changes with time, $\Delta q_z/q_z \ll 1$, acceptable results can also be obtained through averaging the heat load over the TRT time. This is just the case, because the maximum variation of q_z (caused by the ambient temperature variations) is less than 5.5% of average heat flow. Therefore, to fit the model to the water temperature data, when the variations of $q_z(\eta;t)$ are caused by $T_a(t)$ fluctuations, the average component of the heat rate density, $\langle q_z(\eta;t) \rangle_t$, is used. As can be seen from **Eq. 19**, the mean heat rate is the key factor in the g-function, whereas the time variation of $q_z(\eta;t)$ accounts for the atmospheric effect which it turns out to be proportional to the time dependence of the air temperature attenuated by the small multiplier η in Eq. 18 and is therefore small. In this case, $\eta \neq 0$, **Fig. 4** also demonstrates that the ground conductivity curve

approaches a horizontal line with increasing length of time series. In addition, these sequential plots in **Fig. 4** allow assessment of the time interval that is necessary to obtain an accurate parameter estimate. **Fig. 4** shows that fluctuations in ground thermal conductivity estimates from the both ILS and FLS models with $\eta = 0$ almost disappear when using three-parameter regression for the value of $\eta \neq 0$ determined previously. Indeed, as **Fig. 4** demonstrates, the effective ground thermal conductivity estimate from the ILS (FLS) is constant to within 10%.

Fig. 5 shows that the FLS temperature curve ($\eta \neq 0$) (solid line) calculated in such a way (with the converged values of the test estimates found by using the three-parameter scheme) lies perfectly on a line of the measured temperature of fluid (ignoring high frequency fluctuations). This excellent agreement between the two curves is reached by taking into account the rate of heat losses $Q_{\text{air}}(t)$. The temperature curve (solid line) with the underlying atmospheric trend corresponds to $\lambda = 2.57 \text{ W}/(\text{m}^\circ\text{C})$ and $R_b = 0.174 \text{ m}^\circ\text{C}/\text{W}$, $T_0 \approx 18.32^\circ\text{C}$, estimated from the three-parameter scheme for the proposed model with $\eta = 0.006$ in the time interval range from 6 to 71 hours. The straight dashed line in **Fig. 5** corresponds to a thermal conductivity of $2.66 \text{ W}/(\text{m}^\circ\text{C})$ and borehole resistance of $0.163 \text{ m}^\circ\text{C}/\text{W}$ found from two parameters fitting at the same effective undisturbed ground temperature of $T_0 \approx 18.32^\circ\text{C}$ without heat dissipation to the ambient (i.e., at $\eta = 0$). **Fig. 5** demonstrates the ability of the proposed model to predict the temperature of the heat carrier fluid as function of time.

After ground thermal conductivity, thermal resistance of the borehole is the most important test estimate for the design of a vertical BHE. The borehole resistance values are also estimated from the field data and are plotted versus the time evaluation interval in **Fig. 6**. In fact, **Fig. 6** shows that the borehole, filled with thermally enhanced grout, yielded values within the range from 0.151 to $0.185 \text{ m}^\circ\text{C}/\text{W}$. The estimate of the undisturbed ground temperature (from the three-parameter estimation scheme) varies from 19.4 to 17.9°C for the same time intervals. This range includes the T_0 value used for determination of the model parameter p in **Eq. 13** and **14**. Therefore, the developed method successfully filters out the main part of the cyclic distortions of test estimates caused by the diurnal temperature cycle and smoothens their dependencies on the length of time interval chosen for the assessment.

When neglecting energy losses to the ambient air ($p = 0$), the values of λ calculated from both ILS and FLS models are higher than ones evaluated with the proposed method of suppressing the climatic influence from the TRT data; this is because of the cooling effect. For $\eta \neq 0$ ($p \neq 0$), as well as for $\eta = 0$ ($p = 0$), the comparison between the numerical results of FLS and ILS models applied to the same experimental data shows that, as predicted by Bandos et al. (2009), the effective thermal conductivity value of the ground is overestimated by the ILS model (**Fig. 4**).

5. Conclusions

The ground thermal conductivity has been estimated from the TRT data by modeling a BHE as a finite and infinite line-source of constant heat flow. A method of subtracting the influence of outside perturbations has been developed and applied in the estimation process. The removal of the climatic effect successfully damps the oscillations of the ground conductivity estimates from the test data with increasing length of the time series. Application to the borehole test demonstrates that the atmospheric effect can distort the estimate of ground conductivity by a factor of one-third, while the proposed method estimates ground conductivity to within a 10% interval of the mean value. It has been shown that this proposed method of using the ambient temperature data in the analysis allows suppression of the influence of diurnal atmospheric conditions on the estimates of thermal conductivity and borehole resistance.

Parameter estimation from the test data yields a lower value for ground thermal conductivity when some energy dissipates from the above-ground pipes in the heat injection mode. This holds true for calculations in the framework of both infinite and finite line-source models. The results confirm that the finite depth corrections for the mean borehole temperature result in decreasing the ground thermal conductivity estimate from test data and improve accuracy of the evaluation. The proposed method is model-independent and is valid for data analysis with the line-source or cylindrical model for BHE.

Acknowledgments

This paper has been supported by the European Union Commission under projects GROUND-MED FP7-ENERGY-2007-2-TREN-218895, 043340, and Geotrinet - IEE/ 07/581; the Spanish Ministry of Education and Science under projects “Modelado y simulación de sistemas energéticos complejos” (Programa Ramón y Cajal 2005) and ENE2008-00599/CON; by the Government of Valencia under project GV/2008/292; and by PAID-06-09/2734.

References

- Austin, W. A., 1998. Development of an In situ System for Measuring Ground Thermal Properties. MS thesis, Oklahoma State University, Stillwater, Oklahoma, 177 pp.
- Bandos, T.V., Montero, Á., Fernández, E., Santander, J.L.G., Isidro, J.M., Pérez, J., Fernández de Córdoba, P.J., and Urchueguía, J.F., 2009. Finite line-source model for borehole heat exchangers: Effect of vertical temperature variations. *Geothermics* 38, 263–270.
- Beier, R.A. and Smith, M.D., 2002. Borehole Resistance from Line-Source Model of In situ Tests. *American Society of Heating, Refrigerating and Air Conditioning Engineers Transactions* 108(2), pp. 212–219.
- Beier, R.A. and Smith, M.D., 2003. Removing Variable Heat Rate Effects from Borehole Tests. *American Society of Heating, Refrigerating and Air Conditioning Engineers Transactions* 109(2), pp. 463–474.
- Beier, R.A., 2008. Equivalent time for interrupted tests on borehole heat exchangers. *International Journal of Heating Ventilating, and Airconditioning Research* 14, 489–503.
- Bose, J. E., Parker, J. D., and McQuiston, F. C., 1985. Design/Data Manual for Closed Loop Ground Coupled Heat Pump Systems. American Society of Heating, Refrigerating, and Air Conditioning Engineers, Atlanta, Georgia, 16 pp.
- Carslaw, H. S. and Jaeger, J. C., 1959. *Conduction of Heat in Solids*. Oxford University Press, New York, NY, 510 pp.
- Claesson, J. Eskilson, P., 1988. Conductive heat extraction to a deep borehole, thermal analysis and dimensioning rules. *Energy* 13, 509– 527.
- Eskilson, P., 1987. *Thermal Analysis of Heat Extraction Boreholes*. PhD dissertation, Department of Mathematical Physics, University of Lund, Lund, Sweden, 264 pp.
- Esen, H., and Inalli, M., 2009. In-Situ thermal response test for ground source heat pump system heat exchanger in Elazig, Turkey. *Energy and Buildings* 41, 395–401.
- Florides, G. and Kalogirou S., 2008. First In-Situ determination of the thermal performance of a U-Pipe borehole heat exchanger in Cyprus. *Applied Thermal Engineering* 28, 157–163.

- Fujii, G., Okubo, H., Nishi, K., Itoi, R., Ohyama, K., and Shibata, K., 2009. An improved thermal response test for U-Tube ground heat exchanger based on optical fiber thermometers. *Geothermics* 38(4), 399–406.
- Gehlin, S. and Hellström, G., 2003. Comparison of Four Models for Thermal Response Test Evaluation. *American Society of Heating, Refrigerating American Engineers Transactions* 109, pp. 131–142.
- Gehlin, S. and Nordell, B., 2003. Determining Undisturbed Ground Temperature for Thermal Response Test. *American Society of Heating, Refrigerating American Engineers Transactions* 107, pp. 151–156.
- Hastie, T., Tibishirani, R., and Friedman, J., 2001. *The Elements of Statistical Learning*. Springer-Verlag, New York, NY, 536 pp.
- Hellström, G., 1991. *Thermal Analysis of Duct Storage System*. Department of Mathematical Physics, University of Lund, Lund, Sweden, 262 pp.
- Ingersoll, L.R., Zohel, O.J., and Ingersoll, A.C., 1954. *Heat Conduction with Engineering Geological and Other Applications*. University of Wisconsin Press, Madison, Wisconsin, 342 pp.
- Javed, S., Fahlén, P., and Claesson, J., 2009. Vertical Ground Heat Exchangers: A Review of Heat Flow Models. In: *Proceedings of 11th International Congress on Thermal Energy Storage for Efficiency and Sustainability*, Stockholm, Sweden, 8 pp.
- Lamarche, L. and Beauchamp, B., 2007. A new contribution to the finite line-source model for geothermal boreholes. *Energy and Buildings* 39, 188–198.
- Lund, J. W., 2000. Ground Source (Geothermal) Heat Pumps. in: Lineau, P. J. (Ed.), *Course on Heating with Geothermal Energy: Conventional and New Schemes*. World Geothermal Congress Short Courses. Kazuno, Tohuko district, Japan, pp. 1–21.
- Marcotte, D. and Pasquier, P., 2008. On the estimation of thermal resistance in borehole thermal conductivity test. *Renewable Energy* 33, 2407–2415.
- Mogensen, P., 1983. Fluid to Duct Wall Heat Transfer in Duct System Heat Storage. In: *Proceedings of the International Conference on Surface Heat Storage in Theory and Practice*, Stockholm, Sweden, pp. 652–657.
- Omer, A.M., 2008. Ground-source heat pump systems and applications. *Renewable and Sustainable Energy Reviews* 12(2), 344–371.
- Philippe, M., Bernier, M., Marchio, D., 2009. Validity ranges of three analytical solutions to heat transfer in the vicinity of single boreholes. *Geothermics* 38, 407–413.
- Reuß, M., Proell, M., Nordell, J., 2009. IEA ECES-ANNEX 21 THERMAL RESPONSE TEST. In: *Proceedings of 11th International Congress on Thermal Energy Storage for Efficiency and Sustainability*, Stockholm, Sweden, 8 pp.
- Sanner, B., Hellström, G., Spitler, J. Gehlin, S., 2005. Thermal Response Test-Current Status and World-Wide Application. In: *Proceedings World Geothermal Congress*, Antalya, Turkey, pp. 1436–1445.

- Signorelli, S., Bassetti, S., Pahud, D., Kohl, T., 2007. Numerical evaluation of thermal response tests. *Geothermics* 36, 141–166.
- Shonder, J.A., Beck, J.V., 2000. Field Test of a New Method for Determining Soil Formation Thermal Conductivity and Borehole Resistance. *American Society of Heating, Refrigerating American Engineers ASHRAE Transactions* 106(1), pp. 843–850.
- Spitler, J. D., 2000. GLHEPRO: A Design Tool for Commercial Building Ground Loop Heat Exchangers. In: *Proceedings of the Fourth International Heat Pumps in Cold Climates Conference*, Aylmer, Queb'ec, pp. 1–26.
- Urchueguía, J.F., Zacarés, M., Corberán, J.M., Montero, Á, Martos, J., Witte, H., 2008. Comparison between the energy performance of a ground coupled water to water heat pump system and an air to water heat pump system for heating and cooling in typical conditions of the European Mediterranean coast. *Energy Conversion and Management* 49, pp. 2917–2923.
- Witte, H.J.L., van Gelder, G.J., and Spitler, J.D., 2002. In situ measurement of ground thermal conductivity: A Dutch perspective. *American Society of Heating, Refrigerating American Engineers ASHRAE Transactions* 108, pp. 1–10.
- Zeng H., Diao N., Fang Z., 2002. A finite line-source model for boreholes in geothermal heat exchangers. *Heat Transfer Asian Research* 31, 558–567.

Figure captions

Figure 1. Schematic of field test to measure ground properties.

Figure 2. Daily variations of the air temperature (black line) and the average fluid temperature (gray line) versus the time of the thermal response test at constant heat injection rate.

Figure 3. Time variation of the measured total heat rate, Q_t (gray line) and variable heat rate, $q_z H$, transferred to ground (black line). Q_{air} calculated with the fitting parameter $\eta = 0.006$ corresponding to 5.5% heat losses ($p = 0.055$) to ambient air (dashed black line).

Figure 4. Comparison between dependence of thermal conductivity on the time interval length from the ILS (gray line) and FLS (black line) models for the same test data. Estimates of thermal conductivity are from the ILS and FLS models when the end of the evaluation interval is fixed while its starting point increases: (i) without outside heat losses to the ambient air ($p = 0$, $\eta = 0$) and (ii) with 5.5% heat losses ($p = 0.055$, $\eta = 0.006$) to the ambient air.

Figure 5. Measured (gray line) and calculated mean fluid temperature versus the natural log of time (hrs) from two FLS models with (solid black line) and without ($p = 0$, dashed black line) external heat dissipation for the converged test parameters values.

Figure 6. Comparison between dependence of borehole thermal resistance on the time interval length from the ILS (black line) and FLS (gray line) models for the same test data assuming 5.5% heat losses ($p = 0.055$, $\eta = 0.006$) to the ambient. Estimates of BHE thermal resistance are from the ILS and FLS models when the end of the evaluation interval is fixed while its starting point increases

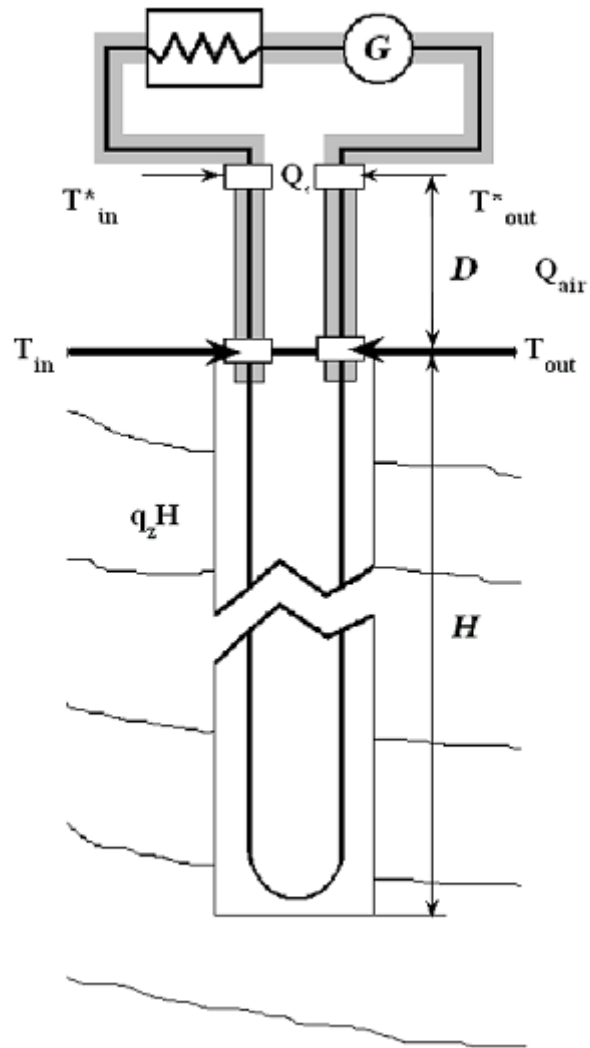


FIGURE 1

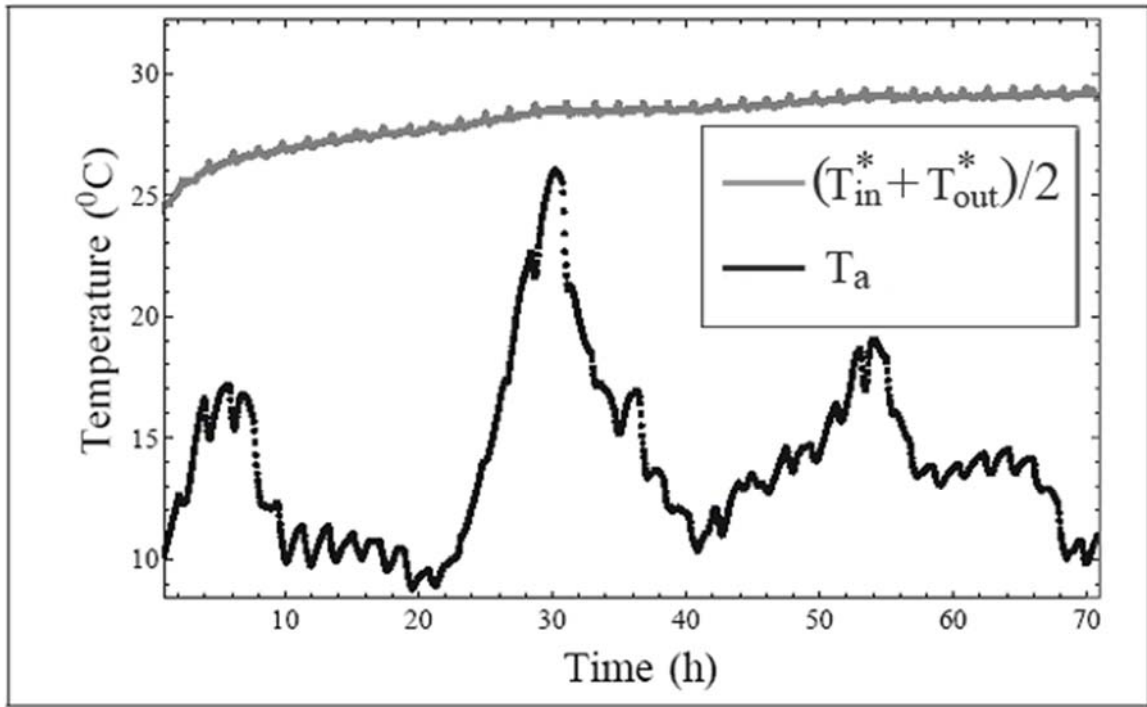


FIGURE 2

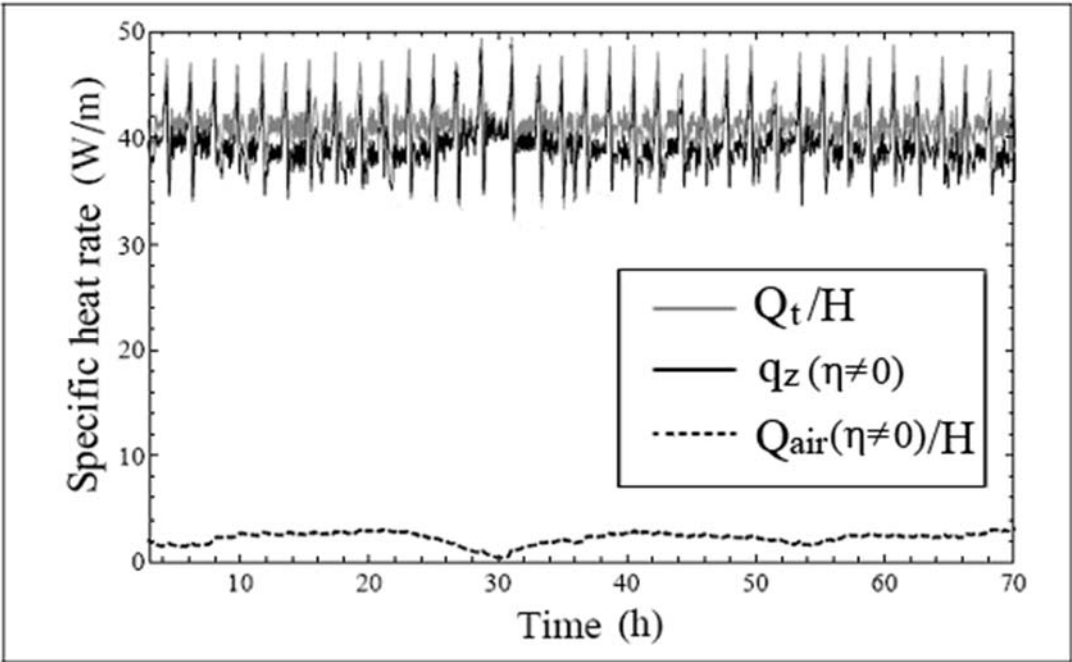


FIGURE 3

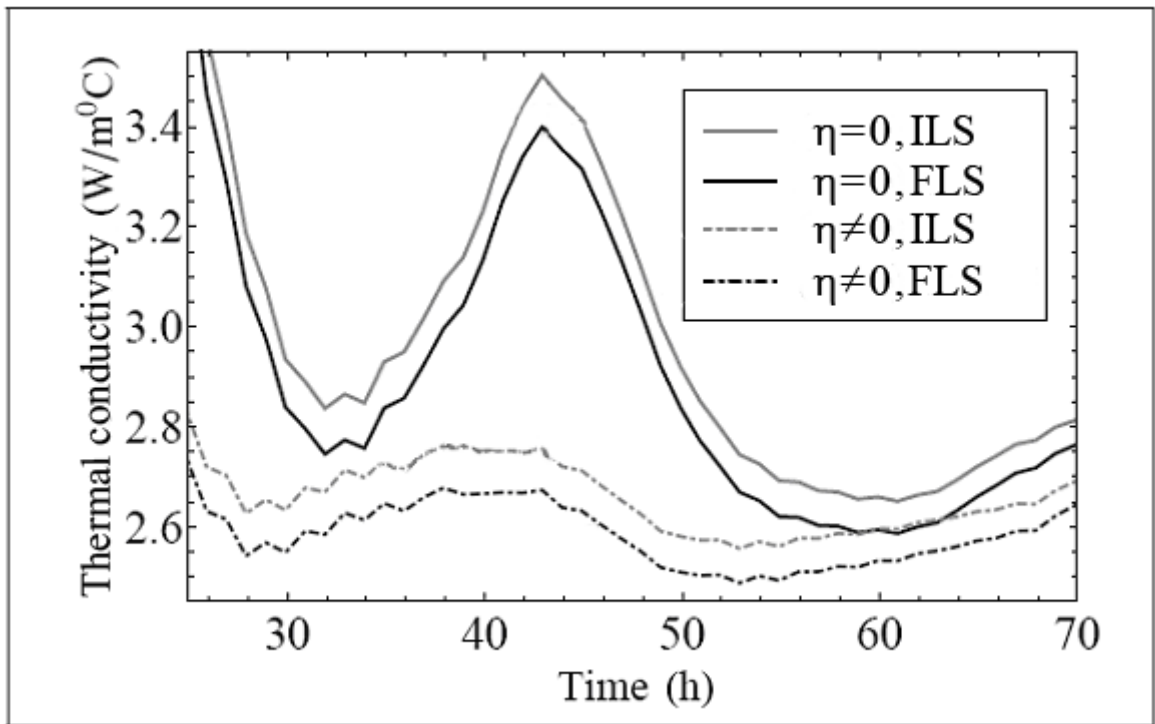


FIGURE 4

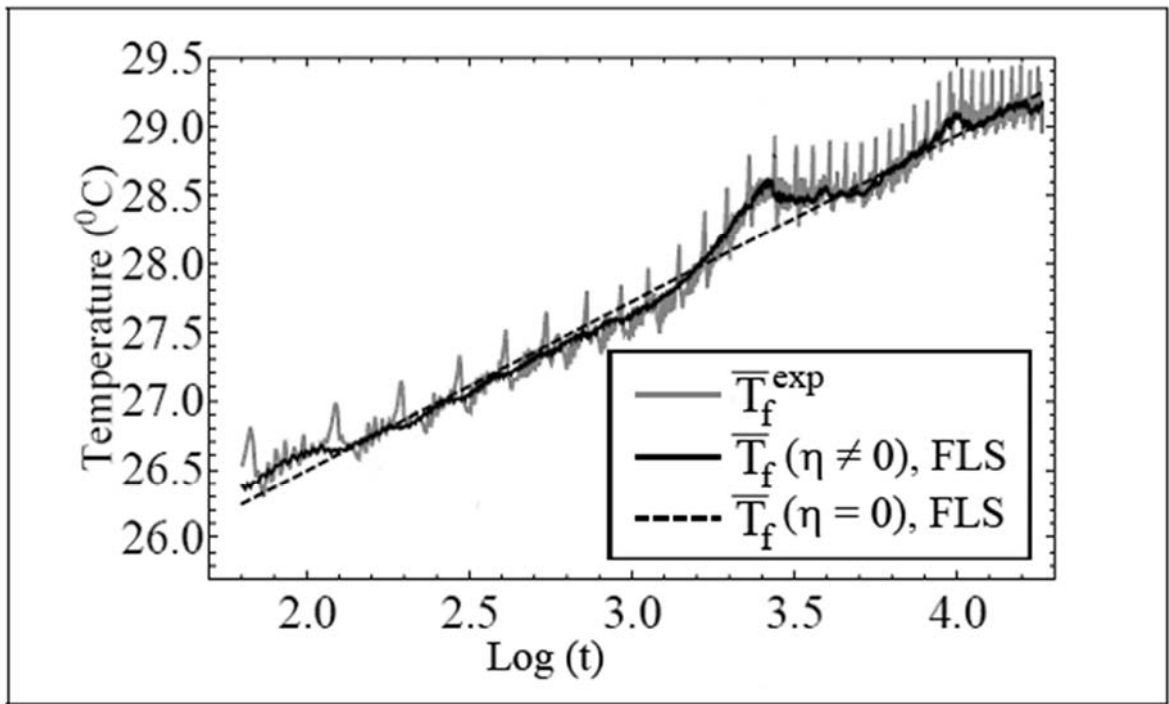


FIGURE 5

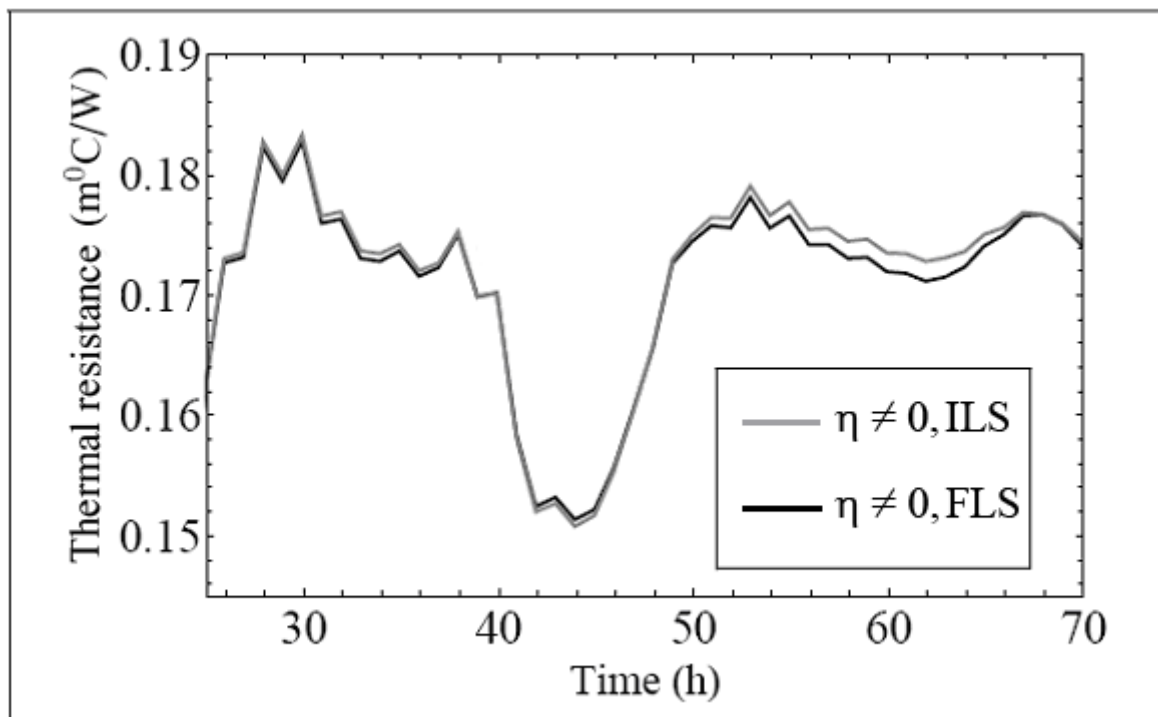


FIGURE 6

Document downloaded from:

<http://hdl.handle.net/10251/83904>

This paper must be cited as:

Bandos, T.; Montero Reguera, ÁE.; Fernández De Córdoba Castellá, P.J.; Urchueguía Schölzel, JF. (2011). Use of thermal conductivity from thermal response test for estimating steady-state temperatures in rock and stratified soil near a line source of heat. HVAC&R Research. 17(6):1030-1043. doi:10.1080/10789669.2011.625349.



The final publication is available at

<http://doi.org/10.1080/10789669.2011.625349>

Copyright Taylor & Francis

Additional Information

Use of Thermal Conductivity from Thermal Response Test for Estimating Steady State Temperatures in Rock and Stratified Soil near Line Source of Heat

ABSTRACT

This paper addresses anisotropic dependence of effective thermal conductivity measured by a field thermal response test (TRT). That is a key parameter in the design of Ground-Coupled Heat Pumps (GCHP) to heat and cool buildings.

First, the paper provides a brief overview of the current technique of estimating thermal conductivity from a data obtained in TRT based on predictions for temperature from line source of heat in an isotropic ground. Then, the solutions for isotropic medium are used to develop this temperature transient method for stratified medium, where the angle between the ground surface and the sedimentary strata is arbitrary. In addition, the paper provides a new analytical exact solution for temperatures around finite line source (FLS) of heat in an anisotropic semi-infinite medium. Approximate expressions for the temperature evolution during the test duration and for the steady state temperature are presented.

The limitations of the FLS method in stratified medium and recommendations for layout of multiple vertical or horizontal ground coupled heat exchangers or waste canisters in repository rock are discussed.

INTRODUCTION

Thermal conductivity of the ground is a key property when sizing of the ground coupled heat pump (GCHP) air-conditioning systems. For large commercial installations it is measured on a field borehole in a thermal response test (TRT) the scheme of which is shown in Figure 1. Figure 1 represents a typical TRT test to measure the temperature response of the borehole heat exchanger (BHE) to a constant heat injection or extraction. A U-tube loop, through which a heat carrier fluid circulates, is inserted inside the borehole to approximately the same depth as the BHE planned for the site. The outputs of the TRT are the inlet (T_{in}) and outlet (T_{out}) temperatures of the heat carrier fluid as a function of time (see Figure 1). The average change of fluid temperature is directly related to the rock/soil thermal conductivity around the well. To determine the rate at which heat is transferred into the ground its model is necessary that may account for underground water flows, temperature dependency of thermal conduction, variable thickness of the strata, d_i see Figure 1. The temperatures T_{in} and T_{out} , measured at the end points of the U-tube, are used to determine a mean value of thermal conductivity, averaged over the length of shallow BHE. The effective thermal conductivity represents a number of the model parameters, when fitting the TRT data.

From the experimental data, and with an appropriate model describing the heat transfer between the fluid and the ground, the effective thermal conductivity of the surroundings is inferred. Thermal conduction of ground from a TRT data can be estimated with different models. The measured thermal conductivity of the ground depends on parameters of the model for the ground chosen for analysis through the effective thermal conductivity.

The Kelvin's solution for temperature of the ground surrounding the borehole heat exchanger (BHE) modeled as an infinite line source (ILS), is the basis for the TRT in estimating the thermal properties of the ground. This approach is used further in the GCHP design standards of the International Ground Source Heat Pump Association (Bose et al. 1985). The cylinder heat source and line heat source (Carslaw and Jaeger 1959) model for BHE with parameter-estimating techniques are commonly applied for the design and analysis of vertical ground coupled systems (Bernier 2001).

The Kelvin's concept assumes a homogeneous isotropic media surrounds the heat line source of a constant heat rate. However, vertical BHE systems are often installed in ground of multiple dipping layers

(of rock or soil) with different thermal conductivities. For stratified media effective thermal conductivity in the ILS theory represents average thermal conductivity.

An algorithm proposed in (Sutton et al. 2001) for the performance of vertical BHE is based on analytical solution of an infinite cylindrical heat source model for horizontally stratified geologic formations. These models for the BHE describe radial heat flow that implies only transverse conductivity to its axis.

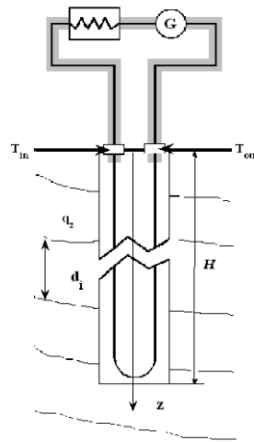


Figure 1. In-situ TRT schematic and formation layers.

In general, the ground is an anisotropic medium whose thermal conductivity depends on the direction. Typically, the sedimentary soil or rock formations have the conductivity in one direction greater than in another: the heat flow passes more easily along the planes of deposition than across them and, thus, direction of heat flow does not coincide with the direction of the imposed temperature gradient. The heat flow and temperature gradient are vector quantities related by the thermal conductivity tensor in anisotropic media instead of scalar thermal conductivity in isotropic one.

It is necessary to determine thermal conductivity tensor of the ground with application to the estimation of temperature field. On a large scale it depends upon the average thermal conductivities parallel and perpendicular to bedding and its spatial orientation to the surface.

A geophysical logging of wells is one of the methods presently used for identification of type of the ground, and establishment of thermal conductivity distribution in depth (Pribnow and Sass, 1995; Davis

et al., 2007). In-plane thermal conductivity λ_{\parallel} and thermal conductivity λ_{\perp} normal to the bedding can be determined from parallel and series models, applicable for bedded sediments.

Data on thermal conductivities and anisotropy values, assembled from different areas around the world are available from literature (Deming, 1994). These data are classified by rock name and origin. Thermal properties of samples extracted from identified layers are available from review articles (Pribnow and Sass, 1995).

There are areas where only data on borehole cuttings are available. The typical approach to the estimation of thermal conductivities is to carry out measurements in the laboratory on samples. The thermal conductivity tensor and the anisotropy (defined as $a^2 = \frac{\lambda_{\parallel}}{\lambda_{\perp}}$) can be obtained on oriented core, when measuring by line source probe on the same sample face at multiply angles to bedding (Pribnow and Sass, 1995; Popov et al., 1999).

Laboratory results are normally combined with in situ thermal conductivity measurements. Assessments of the thermal conductivities by laboratory methods are difficult to extrapolate to in-situ conditions for deep boreholes (Pribnow and Sass, 1995).

The line source method, used for thermal conductivity determination in both field and laboratory, provides ground thermal conductivity in the direction perpendicular to the line.

In addition, the mean dip angle between bedding and surface is required for practical applications to define the average thermal conductivity tensor. Small variations of dip in wells can be viewed in borehole imaging logs (Borehole Televiewer, Formation Micro Scanner) (Pribnow and Sass, 1995). In practice, the value of dip angle can be estimated simply by examining the in situ cross section.

When no data are available on the dip angle between the bedding formations and the earth's surface, assessment of the temperature in the BHE surroundings may be useful in the limiting cases of horizontal and vertical stratification. Such estimation defines upper and lower limits for average temperature field for the intermediate angle values from 0 to $\frac{\pi}{2}$.

For geologic applications, to measure thermal conductivity in vertical direction, normal to the earth's surface, the model was developed for arbitrary angle between the ILS and the principal direction of heat flow in an infinite anisotropic medium (Grubbe et al. 1983).

However, infinite-source models have some limitations. For long time periods the finite size effects need to be taken into account; otherwise the ILS models predict unlimited increase of the temperature when time tends to infinity. The very introduction of the surface boundary has the effect of setting a steady-state (Bandos et al., 2009); this is beyond the scope of the infinite line-source models either for isotropic or anisotropic media. Three dimensional finite line source (FLS) model of the BHE in a semi-infinite medium (Carslaw and Jaeger, 1959) does account for vertical heat transfer with both the soil surface and deep earth.

Design tools use the so called “*g-function*” introduced by Eskilson (1987), which represents the thermal response factor of the borehole to a constant heat pulse at the borehole periphery, i.e. $r = r_b$. It is estimated at the BHE mid-point in simulations of GCHP systems because ILS method implies the temperature at the point far away from the BHE ends. After Zeng et al. (2002), Lamarche and Beauchamp (2007) extended the *g-function* concept of Eskilson to analytical integral average *g-function*. Further, the mean *g-function* has been approximated for a wide time range, providing its explicit steady state limit at any point and the finite size corrections during the test for $H \gg r \geq r_b$, i.e. in the borehole vicinity (Bandos et al. 2009). The edge effects are due to the vertical heat flow along the borehole from the deep earth and its surface. The thermal response of a borehole is proportional to the ratio of $\frac{q_z}{\lambda_{eff}}$ of two significant factors in almost all analytical *g-functions* for the short and long term time analysis of the BHE response (Javed et al., 2009).

These FLS models have been limited in application to the infinite ground of either isotropic or anisotropic thermal properties, whereas to the best of author knowledge, solution for the temperature in the semi-infinite anisotropic medium has never been known. To assess properly the steady state temperature of the underground installation one needs to account for principal directions of the heat flow in the ground. It may be relevant to guarantee stability of operating the ground coupled installation as well as the time of investment return. The financial reward of installing a geothermal system comes after

the long term. The anisotropy effect on temperature in borehole surroundings also becomes significant for very long time values.

In this context, line-source methods to estimate thermal conductivity include conducting laboratory experiments on rock and soil samples and/or performing field tests (Davis et al. 2007; Popov et al. 1999). It should be noted, however, that the ILS based method was developed for rocks layered non perpendicular to the ILS (Grubbe et al. 1983). In geologic applications it is widely used for calculation of terrestrial heat flow density, while in geothermal applications it is necessary to determine the borehole temperature for the design purposes. However, for both applications of this method do not account for the fact that the earth's surface can make arbitrary angle with the sedimentary bedding. The ILS method in an infinite anisotropic medium was proposed to determine the vertical component of thermal conductivity along the ILS embedded in rocks layered non perpendicular to it (Grubbe et al. 1983). However, this method cannot describe exactly the temperature field in an anisotropic half-space without accounting for a boundary condition on the ground surface.

Further refinement of the FLS approach is desirable for anisotropic semi-infinite medium; anisotropic corrections to the g-function reveal how rocks are layered to the surface. Moreover, bedding angle dependence on temperature response is of significant importance for long-term underground energy systems. It may be important, when estimating maximum temperatures tolerated in nuclear waste repositories or aquifer thermal energy storages (Hörmark and Claesson 2005; Sundberg and Helström 2009).

The effect of anisotropy of heat flow in a multi-layer geological formation on the temperature around the vertical line heat source at an arbitrary dip angle of the strata to the earth surface is the subject of this paper. It has practical implications for the estimate of test data, the steady-state temperature field and for the selection of orientation of vertical bore field.

This paper presents (I) exact solution for the FLS thermal response function of a borehole that takes into account the geometrical disposition of the earth surface and the sedimentary bedding; (II) approximate expressions for the mean temperature of the vertical BHE for the times corresponding to the TRT duration as well as to the long times in the limiting cases of horizontal and vertical stratification to the earth's

surface. Results on the time-series expansion for the temperature around the finite line-source in an anisotropic semi-infinite medium - including the existence of a steady-state limit – are also discussed.

PROBLEM STATEMENT

For the line-source analysis of TRT data, the ground is assumed to be a homogeneous isotropic medium characterized by scalar thermal conductivity λ . For the stratified geologic regime, this assumption is extended to the thermal conductivity tensor that characterizes anisotropic medium. The heat flow and temperature gradient are vector quantities related by the thermal conductivity tensor Λ_{ik} (Carslaw and Jaeger, 1959). The heat flow in the i -th direction Q_i at a given point of the anisotropic medium is given by

$$Q_i = -\sum_{k=1}^3 \Lambda_{ik} \partial T / \partial x_k$$

It is assumed that the heat flow in the stratified ground proceeds as if the media were homogeneous, i.e. the thermal conductivity tensor is homogeneous, but anisotropic.

This paper considers heat flow along the vertical z - axis, which is perpendicular to the surface of the semi-infinite region, as shown in Figure 1. The heat is realised at a constant rate along the z -axis of the Borehole Heat Exchanger (BHE), modelled as the Finite Line- Source (FLS), and is transferred by thermal conduction along the preferential directions in the semi-infinite region. In the anisotropic model the equation of heat diffusion, generally, is not invariant under spatial rotation about the z -axis of the vertical BHE. The subsurface temperature, T , is governed by the heat conduction equation:

$$C \frac{\partial T(\vec{x}, t)}{\partial t} = \sum_{i=1}^3 \sum_{k=1}^3 \Lambda_{ik} \frac{\partial^2 T(\vec{x}, t)}{\partial x_i \partial x_k} + q_z \delta(x) \delta(y) (\theta(z) - \theta(z-H)), \quad \text{for } t \geq 0, z \geq 0 \quad (1)$$

where $\vec{x} = (x_1, x_2, x_3) = (x, y, z)$ is the coordinate vector, and q_z is the heat flux density per length unit of the BHE of radius r_b , where $\delta(x)$ is the Dirac delta function characterized by the property

$$\int_{-\infty}^{\infty} \delta(x) f(x) dx = f(0) \text{ for all functions } f, \theta(z) \text{ is the unit step function, which is zero for } z < 0 \text{ and unity for } z > 0$$

. The initial condition and boundary condition on the surface are given by:

$$T(\vec{x}, t=0) = T_0, \quad T(x, y, z=0, t) = T_0 \quad (2)$$

Typically, the line-source of heat is introduced as boundary condition on the cylindrical surface

$$\frac{q_z}{2\pi r_b} = [-\Lambda_{11}\partial T / \partial x - \Lambda_{22}\partial T / \partial y - \Lambda_{13}\partial T / \partial z]_s$$

and not as a heat generation term of Equation (1) in this equivalent formulation of problem (Carlaw and Jaeger, 1959).

We address the simplest case of anisotropy in which the thermal conductivity is the same for all directions of a plane X'Y and differs in the Z' direction noted in Figure 2. Two components of the thermal conductivity for heat flow through the ground in a direction perpendicular and parallel to the bedding plane are denoted by λ_{\perp} and λ_{\parallel} , respectively. The in-plane thermal conductivity λ_{\parallel} is larger than orthogonal component of thermal conductivity tensor λ_{\perp} (Davis et al. 2007; Popov et al. 1999), but this study is valid for any anisotropy ratio.

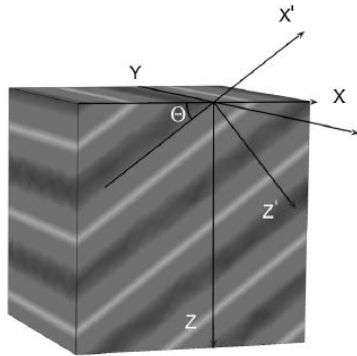


Figure 2. Direction of X', Y, Z' principal axes of the thermal conductivity tensor. The XY plane represents the ground surface at the dip angle Θ from the X'Y plane.

In order to formulate the problem around the BHE inserted into the ground so that its surface is at angle Θ to the bedding plane one needs to find the conductivity tensor in the chosen axes. The thermal conductivity tensor is diagonal in the X', Y, Z' coordinates shown in Figure 2. These three directions are called the principal axes of the thermal conductivity tensor:

$$\sum_{k=1}^3 \lambda_k \delta_{ik} \quad (3)$$

with the $\lambda_1 = \lambda_{\parallel}$, $\lambda_2 = \lambda_{\parallel}$ and $\lambda_3 = \lambda_{\perp}$ components.

To find the conductivity tensor Λ_{ij} in the chosen axes X, Y and Z (so that the BHE axis is at angle Θ to the Z' axis) one performs a rotation of tensor in Equation 3:

$$\Lambda_{ij} = \sum_{m=1}^3 \sum_{k=1}^3 R_{ki} \lambda_k \delta_{mk} R_{mj} \quad (4)$$

by the orthogonal matrix R_{mj} describing the rotation between two sets of axes shown in Figure 2. This is given by (Hastie et. al 2001):

$$R = \begin{pmatrix} \cos \Theta & 0 & \sin \Theta \\ 0 & 1 & 0 \\ -\sin \Theta & 0 & \cos \Theta \end{pmatrix} \quad (5)$$

Making use of the transformation defined above one gets

$$\Lambda = \begin{pmatrix} \lambda_{\perp} \sin^2 \Theta + \lambda_{\parallel} \cos^2 \Theta & 0 & (-\lambda_{\perp} + \lambda_{\parallel}) \sin 2\Theta / 2 \\ 0 & \lambda_{\parallel} & 0 \\ (-\lambda_{\perp} + \lambda_{\parallel}) \sin 2\Theta / 2 & 0 & \lambda_{\perp} \cos^2 \Theta + \lambda_{\parallel} \sin^2 \Theta \end{pmatrix} \quad (6)$$

The coefficient Λ_{11} is the thermal conductivity coefficient for the heat flow in the X direction due to a gradient in the direction X. It also gives rise to a heat flow in the vertical direction due to the presence of the off-diagonal coefficient Λ_{13} .

$$Q_3 = -\Lambda_{31} \partial T / \partial x - \Lambda_{33} \partial T / \partial z$$

The anisotropy factor causes the distortion of the temperature gradient at the surface of multilayered ground and around the BHE bottom, because the heat flow is not normal to the isotherms.

Throughout the paper the following normalization was used

$$\varepsilon_{ij} = \Lambda_{ij} / \Lambda_{33}, \quad i, j = 1, 2, 3 \quad (7)$$

The temperature field is thus defined by the solution of Equations 1, 2 with the above Λ matrix in Equation 6. If the angle $\Theta = 0$ (or $\Theta = \pi/2$), the axes coincide with appropriate symmetry directions of a multilayered ground, this matrix Λ becomes diagonal one, where $\Theta = 0$ (or $\Theta = \pi/2$) correspond to horizontal (or vertical) stratification of the ground.

In the following the grounds of these types will be considered as well as the ground strata at any dip angle to the surface.

ANISOTROPIC DIFFUSION IN SEMI-INFINITE MEDIUM. LINE HEAT SOURCE THEORY

This section is focused on the generalization of the analytical solutions of the thermal conduction problem for isotropic medium to the solutions for anisotropic semi-infinite medium representing multi-layered ground.

We introduce the common methods for TRT estimations and highlight their limitations due to the isotropy assumption.

Solution for Finite Line Heat Source in Isotropic Medium

The exact solution for temperature response from the isotropic ground, where the thermal tensor is diagonal, $\Lambda_{ik} = \lambda \delta_{ik}$, can be written (Bandos et. al 2009):

$$T(r, z, t) - T_0 = \frac{q_z}{4\pi\lambda} \int_{r/\sqrt{4\alpha t}}^{\infty} \left\{ 2\operatorname{erf}\left(\frac{z}{r}\right) - \operatorname{erf}\left(\frac{H+z}{r}\right) + \operatorname{erf}\left(\frac{H-z}{r}u\right) \right\} e^{-u^2} u du \quad (8a)$$

and its integration over the length of the BHE gives:

$$\langle T(r, t) - T_0 \rangle = \frac{q_z}{2\pi\lambda} \hat{g}(h, t), \quad \langle T \rangle = \frac{1}{H} \int_0^H T(z) dz \quad (8b)$$

$$\hat{g}(h, t) = \frac{1}{2} \int_{r/\sqrt{4\alpha t}}^{\infty} \left\{ 4\operatorname{erf}(hu) - 2\operatorname{erf}(2hu) - (3 + e^{-4h^2u^2} - 4e^{-h^2u^2}) \frac{1}{\sqrt{\pi}hu} \right\} \frac{e^{-u^2}}{u} du$$

Both the exact solution and its average represented in such a form recover straightforwardly the ILS result in the limit $H \rightarrow \infty$

$$-\frac{q_z}{4\pi\lambda} \operatorname{Ei}\left(-\frac{r^2}{4\alpha t}\right) \approx \frac{q_z}{4\pi\lambda} \left\{ \ln \frac{4\alpha t}{r^2} - \gamma \right\}, \quad \text{for } 5\frac{r^2}{\alpha} \ll t \ll \frac{H^2}{\alpha} \quad (9)$$

There are some approaches of deriving analytical expressions for Equation 8a (Eskilson, 1987) to overcome time consuming numerical calculation of the above integrals and to get insight on physical interpretation of the heat transfer processes. It can be seen that there are two characteristic scales of time,

namely, $t_z = H^2/\alpha$, $t_r = r_b^2/\alpha$. Early time values (i.e. $t < 5t_r$) are of the order of one day, whereas typical thermal test durations range from 40 to over 200 hours (Sutton et al., 2001). Thus, the duration of TRTs conform to what are called intermediate times ($t_r < t < t_z$) to distinguish them from very long times ($t > t_z$) that would approach those corresponding to steady-state conditions. Time of steady-state attainment is infinite and finite for the ILS and FLS, respectively. Furthermore, the approximation of the average ground temperature for the times corresponding to the TRT (i.e., for $5t_r < t < t_z$) is given by:

$$\langle T(r,t) - T_0 \rangle = \frac{q_z}{4\pi\lambda} \left(\ln \frac{4\alpha t}{r^2} - \gamma - 3 \left\{ \sqrt{\frac{4t}{\pi t_z}} - \frac{r}{H} + \frac{r^2}{H^2} \sqrt{\frac{t_z}{4\pi t}} \right\} \right) \quad \text{for } r_b \leq r \ll H \quad (10)$$

This expression for the average temperature of the BHE differs from the classical one by the finite-size corrections, which vanish in the limiting case of $H \rightarrow \infty$. The comparison between the numerical results of FLS and ILS models applied to the same experimental data showed that, as predicted by Bandos et al. (2009), the thermal conductivity value of the ground is overestimated by the ILS model (Bandos et al., 2011). In addition, error in estimating the thermal conductivity between two models can be found analytically.

Evaluating TRT is based on the linear logarithmic time dependence for the temperature from the ILS theory. From Equations 9 and 10 one can find

$$\frac{\lambda^{FLS}}{\lambda^{ILS}} = 1 - \frac{3}{\sqrt{\pi}} \sqrt{\frac{t}{t_z}} \left(1 - \frac{r_b^2}{4\alpha t}\right) \quad \text{for } \frac{r_b}{H} \ll 1, \quad 5t_r \leq t \ll t_z \quad (11)$$

$$\lambda^{FLS} = \frac{q_z}{4\pi} \frac{\partial \ln t}{\partial \langle T(r_b, t) \rangle}, \quad \lambda^{ILS} = \frac{q_z}{4\pi} \frac{\partial \ln t}{\partial T(r_b, t)}$$

Here λ^{ILS} and λ^{FLS} are the effective thermal conductivities estimated with the ILS and the approximation of the mean FLS models, respectively. Therefore, the estimate from the TRT with the mean FLS model gives a lower value for the log-derived thermal conductivity than the one predicted by the ILS model; the relative error is proportional to the square root of the small parameter $\frac{t}{t_z} \ll 1$ for test durations.

The explicit steady state borehole temperature was derived amid the approximate expressions for the mean ground temperature over a wide range of time values (Bandos et al. 2009).

$$\lim_{t \rightarrow \infty} \langle T(r,t) - T_0 \rangle = \frac{q_z}{2\pi\lambda} \hat{g}_s\left(\frac{H}{r}\right), \quad \lim_{t \rightarrow \infty} \hat{g}(h,t) = \hat{g}_s(h)$$

$$\hat{g}_s(h) = \ln \frac{(h + \sqrt{1+h^2})^2}{2h + \sqrt{1+4h^2}} - \frac{1}{2h} (3 + 4\sqrt{1+h^2} - \sqrt{1+4h^2}) \quad (11)$$

To proceed further, the anisotropy effect on the TRT estimate and the long time temperature profile are considered for horizontally and vertically alternating formations and in general case for layers non-parallel to the ground surface.

Solution for Finite Line Heat Source in Anisotropic Medium

This section, firstly, addresses to the simple case when a main direction of the thermal conductivity coincides with the vertical direction, perpendicular to the surface, while in-plane bedding plane is horizontal, i.e. parallel to the surface. Secondly, we introduce mean temperature method for the horizontal strata, $\Theta = 0$, i.e. parallel to the surface, present the closed form temperature solution around FLS for strata at any dip angle to it and conclude with the limiting case of vertical stratification, $\Theta = \pi/2$.

Mean temperature approximations at horizontal stratification

It is assumed that the thermal conductivity of horizontally stratified ground takes on different values in the horizontal (in-plane) direction, $\lambda_1 = \lambda_2 = \lambda_{\parallel}$, and in the vertical z direction, $\lambda_3 = \lambda_{\perp}$, which are the diagonal components of the thermal conductivity tensor with zero off-diagonal elements, $\Lambda_{ik} = \lambda_k \delta_{ik}$, $k = 1, 2, 3$. The problem of heat diffusion in horizontally stratified geologic regime ($\Theta = 0$) is subject to the conditions specified in Equation 2. Its solution is invariant under spatial rotation about the axis of the vertical BHE as it is in the case of the isotropic medium. Furthermore, after a transformation $z \rightarrow z\sqrt{\lambda_{\parallel}/\lambda_{\perp}}$, Equation 1 takes the same form as the equation for the isotropic homogeneous ground with the thermal conductivity λ_{\parallel} as for the primary line source model. This transformation reduces the heat conduction problem in the horizontally stratified anisotropic ground to the one in the isotropic semi-infinite medium of the thermal conductivity λ_{\parallel} and diffusivity $\alpha_{\parallel} = \lambda_{\parallel}/C$. Thus the solutions for the

anisotropic ground can be obtained from Equations 8a, 8b for the isotropic soil by substituting $z \rightarrow z\sqrt{\lambda_{\parallel}/\lambda_{\perp}}$ supplemented by the $H \rightarrow H\sqrt{\lambda_{\parallel}/\lambda_{\perp}}$ rescaling; hence, the resulting depth is stretched for the horizontal stratification for $\lambda_{\parallel} \geq \lambda_{\perp}$.

Approximate expressions for ground temperature, averaged over the BHE depth, were derived to use (instead of temperature at the mid-point) over a wide range of time values (Bandos et al. 2009). Then, after applying the above described transformations, the average ground temperature response for the time in the interval corresponding to the TRT (i.e. for $r^2/4\alpha_{\parallel} \ll t \ll H^2a^2/4\alpha_{\parallel}$) can be written as:

$$\langle T(r,t) - T_0 \rangle = \frac{q_z}{4\pi\lambda_{\parallel}} \left[\ln(4Fo_{\parallel}) - \gamma - \frac{3r}{\sqrt{\pi}aH} \left\{ \sqrt{4Fo_{\parallel}} - \sqrt{\pi} + \frac{1}{\sqrt{4Fo_{\parallel}}} \right\} \right] \quad \text{for } r \ll aH \quad (12)$$

where $a^2 = \lambda_{\parallel}/\lambda_{\perp}$ is the in-plane conductivity scaled by the normal conductivity, $Fo_{\parallel} = \frac{t\alpha_{\parallel}}{r^2}$ is the Fourier number that refers to a radial distance r from the borehole center, not to the borehole radius r_b , which defines characteristic time t_r . The TRT measures a multiplier for logarithm of time that is a function of model parameters. Effective thermal conductivity is such a function that is inversely proportional to logarithmic derivative from the temperature in the intermediate-time interval. From the above equation effective thermal conductivity λ_{eff} measured by the line source method equals to the thermal conductivity in direction parallel to bedding (to the ground surface for horizontal stratification) λ_{\parallel} . Note that the log-derived thermal conductivity is equal to the only parameter of the isotropic model of the ground: $\lambda_{eff} = \lambda$.

The effects of the finite source size (described by the last three terms in the right hand side of Equation 12 for intermediate time values) depend on the anisotropy a , vanish in the limiting case $H \rightarrow \infty$ and are smaller than those in the isotropic model ($a=1$) for $\lambda_{\parallel} > \lambda_{\perp}$.

Application of the same scale transformations to the approximation derived for the long times (Bandos et al. 2009), when approaching the steady-state conditions, the integral average temperature response at the radial distance r from the borehole center is given by:

$$\langle T(r,t) - T_0 \rangle = \frac{q_z}{2\pi\lambda_{\parallel}} \left\{ \hat{g}_s \left(\frac{aH}{r} \right) - \frac{(t_{\parallel}a^2/t)^{3/2}}{24\sqrt{\pi}} \left[1 - 3t_{\parallel}a^2 \frac{1+r^2/(Ha)^2}{20t} \right] \right\}, \quad t_{\parallel} = \frac{H^2}{\alpha_{\parallel}}, \quad t \gg \frac{\max(a^2H^2, r^2)}{\alpha_{\parallel}} \quad (13)$$

This equation provides time-asymptotic approach to the steady-state of the designed geothermal system, whereas Equation 12 is applicable to analysis of the TRT data in the intermediate-time interval. It is noteworthy to mention that the effective thermal conductivity $\lambda_{eff} = \lambda_{\parallel}$ defines thermal response of the BHE embedded in horizontally stratified ground in the the intermediate and the long-time intervals. Furthermore, both above approximations for the mean BHE response depend on anisotropy through the ratio $\frac{aH}{r}$. There are two characteristic times $\frac{r^2}{\alpha_{\parallel}}$ and $\frac{H^2 a^2}{\alpha_{\parallel}} = \frac{H^2 C}{\lambda_{\perp}}$ for anisotropic diffusion in the radial and axial directions, respectively; these directions coincide with the Λ principal axes for horizontal stratification.

Exact solution for the mean steady-state temperature in the dimensionless form of $\hat{g}_s(\frac{aH}{r})$ reveals anisotropy effect at any radial distance from borehole center. Using the expansion we arrive at the following result for anisotropy correction to the steady state temperature from isotropic and anisotropic models, which can be used in the vicinity of borehole, i.e. $r \ll H$

$$\left\langle T(r)_{|a=1} - T(r)_{|a \neq 1} \right\rangle = \frac{q_z}{2\pi\lambda_{eff}} \left[\hat{g}_s\left(\frac{H}{r}\right) - \hat{g}_s\left(\frac{Ha}{r}\right) \right] = \frac{q_z}{2\pi\lambda_{\parallel}} \left[-2\ln a + \frac{3r}{H}(1-a^{-1}) + O\left(\frac{r}{H}\right) \right] \quad \text{for } \frac{H}{r} \rightarrow \infty \quad (HS)$$

The symbol $O(x)$ denotes terms proportional to x and higher powers of x . This comparison is done for $\lambda_{eff} = \lambda = \lambda_{\parallel}$.

Throughout the paper the following parameters were used in the numerical calculations: $a = 1.4$ for the anisotropy case (Davis et. al 2007) and $\alpha = 1.16 \times 10^{-6} \text{ m}^2/\text{s}$, $\lambda = 4.3 \text{ W}/(\text{mK})$. How anisotropy of the ground thermal conductivity influences the time dependence of the temperature distribution around the vertical BHE penetrating strata is shown in Figure 3. Exact temperature profiles along the borehole calculated for the horizontal stratification are presented in Figure 3a at various time values from 1.5 months to 12 years. Figure 3a shows that maximum temperature along the BHE for $\lambda_{\parallel} / \lambda_{\perp} > 1$ (anisotropic case) becomes noticeably higher than that for $a = 1$ (isotropic case) as the time increases. That is due to decreased heat transfer from the bottom of the borehole.

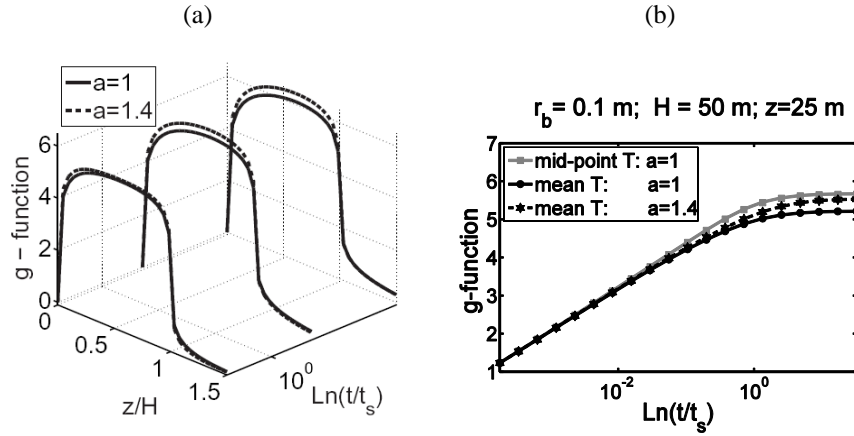


Figure 3. Comparison between thermal response g -functions at $r = r_b = 0.1$ m around the borehole penetrating horizontal strata ($\Theta = 0$) from two models: isotropic model ($\lambda_{\parallel} = \lambda_{\perp} = \lambda$) and anisotropic model ($\lambda_{\parallel} = a^2 \lambda_{\perp}$, $\Theta = 0$; $\lambda = \lambda_{\parallel}$) of the ground. (a) Profiles of the g -function versus the natural logarithm of time t/t_s and the dimensionless coordinate z/H along the borehole; (b) Mid-point ($z=H/2$) (gray line) and mean g -functions from the isotropic model and mean g -function from the anisotropic model versus the natural logarithm of time. Exact solutions calculated for constant heat injection are shown in the range: $5r_b^2 / \alpha_{\parallel} < t < H^2 a^2 / \alpha_{\parallel}$, $\alpha = \alpha_{\parallel}$. The time is scaled by $t_s = H^2 / (9\alpha)$ (Eskilson, 1987).

Figure 3b shows that the g -function estimated at the BHE mid-point (Eskilson, 1987) and averaged response function are rather close to each other for the isotropic medium ($\lambda = \lambda_{\parallel}$) and to the mean temperature response function for the anisotropic medium in the intermediate-time interval. There is the increase of the mean temperature evaluated from Equation 13 for the horizontal stratification of sufficiently low λ_{\perp} value: $a = 1.4$ compared to the mean temperature, but this temperature remains lower than mid-point temperature at $z = H/2$ for the isotropic case.

Notice that the higher the scaled thermal conductivity $\lambda_{\parallel} / \lambda_{\perp}$ in the horizontal direction, the later is the onset of the asymptotic behavior when attaining steady state. Therefore, evaluation of thermal conductivity from the TRTs provides primarily effective thermal conductivity in the horizontal direction, while thermal conductivity in the vertical direction noticeably manifests itself for the long time values.

Temperature solution for FLS in a half-space of axial anisotropy at arbitrary dip angle

The problem for ground layered non-parallel to the surface can be solved by using exact correspondences between the isotropic and anisotropic solutions. It is easy to check that the transformation of coordinates

$$\{x, y, z\} \rightarrow \left\{ \frac{x - \varepsilon_{13}}{\sqrt{\Delta \Lambda_{33}}}, \frac{y}{\sqrt{\Lambda_{22}}}, \frac{z}{\sqrt{\Lambda_{33}}} \right\}, \quad \Delta = \varepsilon_{11} - \varepsilon_{13}^2 \quad (14)$$

reduces Equation 2 to the heat conduction equation in an isotropic medium. Formulation in the new coordinates $\bar{y} = (y_1, y_2, y_3)$ is given by:

$$C \frac{\partial T(\bar{y}, t)}{\partial t} = \sum_{k=1}^3 \frac{\partial^2 T(\bar{y}, t)}{\partial y_k^2} + q'_z \delta(y_1 + y_3 \tan \vartheta) \delta(y_2) (He(y_3) - He(y_3 - \frac{H}{\Lambda_{33}})), \quad (15)$$

for $t \geq 0, y_3 \geq 0$

where

$$\tan \vartheta = \sqrt{\frac{\varepsilon_{13}^2}{\varepsilon_{11}}}, \quad \cos \vartheta = \sqrt{\frac{\Delta}{\varepsilon_{11}}}$$

with exactly the same initial and boundary conditions :

$$T(\bar{y}, t = 0) = T_0, \quad T(y_1, y_2, y_3 = 0, t) = T_0 \quad (16)$$

Equations 15, 16 formulate the problem for an inclined line-source of heat strength $q'_z = q_z \sqrt{\frac{\Lambda_{33}}{\det \Lambda}}$ in the semi-infinite medium of the unit thermal conductivity, where ϑ denotes tilting angle of the line source with the y_3 axis (Cui et al., 2006) in the mapped space (not shown in Figure 2).

Since its solution is known (Cui et al., 2006), the solution in the physical space \bar{x} can be obtained directly by back transformation from the \bar{y} coordinate space as:

$$T - T_0 = \frac{q_z}{4\pi\sqrt{\lambda\Lambda_{11}}} \int_0^{H/\cos\vartheta} \left\{ \operatorname{erfc} \frac{r_+}{\sqrt{4\alpha_{33}t}} - \operatorname{erfc} \frac{r_-}{\sqrt{4\alpha_{33}t}} \right\} dz', \quad \alpha_{33} = \frac{\Lambda_{33}}{C} \quad (17)$$

where

$$r_+^2 = \sum_{i,j=1}^3 (\bar{x} - \bar{x}')_i \Lambda_{ij}^{-1} (\bar{x} - \bar{x}')_j \Lambda_{33}, \quad r_-^2 = r_+^2 + 4z z' \cos\vartheta \quad (18)$$

and $\bar{x}' = \{0, 0, z' \cos\vartheta\}$ is the vector along the line-source of the length $H/\cos\vartheta$.

Note also that the tilting angle ϑ in the transformed space can be expressed through the dip angle Θ as follows

$$\vartheta = \arctan \left(\left(\frac{1}{\lambda_{\perp}} - \frac{1}{\lambda_{\parallel}} \right) \frac{\sin 2\Theta}{2\sqrt{2}} \right) \quad (19)$$

For the TRT analysis the above solution $T(\bar{x}, t)$ obtained for the finite-line source in anisotropic medium was approximated and compared with that from the isotropic FLS model in a wide time range starting from the intermediate times.

We proceed to derive expression that allows the calculation of an effective thermal conductivity as a function of bedding direction.

Effective thermal conductivity, measured by the vertical line-source method: the layers are non parallel to the ground surface. To compare the results of evaluating the thermal conductivity for isotropic medium with that developed here for anisotropic medium, the ground temperature in the vicinity of the mid-point of the finite depth BHE was calculated.

Series of $T(\bar{x}, t)$ in time about a mid-point depth (up to the exponentially small correction terms) can be written as:

$$T - T_0 = -\frac{q_z}{4\pi\sqrt{\Lambda_{11}\lambda_{\parallel}}} \operatorname{Ei} \left(-\frac{\tilde{r}^2}{4\alpha_{33}t} \right) \approx \frac{q_z}{4\pi\sqrt{\Lambda_{11}\lambda_{\parallel}}} \left\{ \ln \frac{4\alpha_{33}t}{\tilde{r}^2} - \gamma \right\} \quad (20)$$

$$T - T_0 \approx \frac{q_z}{4\pi\lambda_{\text{eff}}} \left(\ln t + \ln 4\alpha_{33} / \tilde{r}^2 - \gamma \right)$$

where

$$\tilde{r}^2 = \frac{x^2}{\varepsilon_{11}} + \frac{y^2}{\varepsilon_{22}} \quad (21)$$

and

$$\lambda_{eff} = \sqrt{\Lambda_{11} \lambda_{\parallel}} = \sqrt{\lambda_{\parallel} (\lambda_{\perp} + (\lambda_{\parallel} - \lambda_{\perp}) \cos^2 \Theta)} \quad (22)$$

This expansion is valid for time values in the interval

$$\tilde{r} \ll \sqrt{\alpha_{33} t} \ll L / \cos \vartheta, \quad L = \min(z, H - z) \quad (23)$$

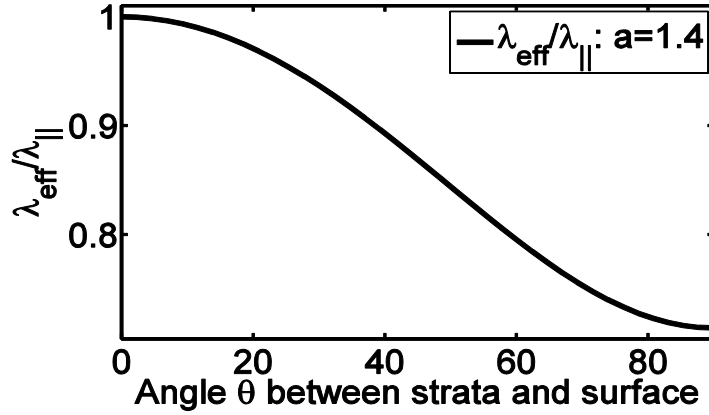


Figure 4. Effective scaled thermal conductivity versus the angle Θ between the ground surface and sedimentary planes, see Figure 2, for $a = 1.4$.

Equation 22 represents that effective thermal conductivity as a function of the thermal conductivity components and the structure of ground (dip angle). Effective thermal conductivity λ_{eff} depends on the angle Θ between the FLS and the axis of symmetry, as it is shown in Figure 4. This result for the λ_{eff} at the intermediate time values is consistent with the ILS prediction for the perpendicular thermal conductivity measured in ground bedding non-parallel to the surface (Grubbe et. al 1983). In geologic applications, the interpretation of Equation 22 enables determination of the thermal conductivity in a certain direction from the tensor components, when measuring anisotropy of rock samples in the laboratory at various angles (Pribnow and Sass, 1995).

Let us stress that the estimate of thermal conductivity is defined by the logarithmic derivative of the TRT data and should be identified with the effective conductivity from a model. So, using anisotropic model one should write

$$\lambda_{eff} = \sqrt{\Lambda_{11}\lambda_{\parallel}} = \frac{q_z}{4\pi} \frac{\ln(t_2/t_1)}{T(t_2) - T(t_1)} \quad (24)$$

while for isotropic model the right hand side is equal just to λ .

Figure 4 illustrates that the ground thermal conductivity from the TRT varies significantly from the maximum value $\lambda_{eff} = \lambda_{\parallel}$ for the horizontal stratification to the minimum value $\lambda_{eff} = \sqrt{\lambda_{\parallel}\lambda_{\perp}}$ as angle Θ tends from 0 to $\pi/2$.

The following shows how the anisotropy influences the steady-state temperature distribution around the line-heat source and long-term performance of underground installation due to vertical heat transfer effects with the surface and the deep earth.

Steady-state temperature field around LS penetrating layers at any angle to the ground surface. Retaining the first leading term in the expansion of the integral in Equation 17 we arrive at the following result for FLS, which can be used for the long-time values (i.e. for $\sqrt{\alpha_{33}t} \gg H/\cos\vartheta$):

$$T - T_0 = \frac{q_z}{4\pi\lambda_{eff}} \left\{ \ln[z - \eta_+ + \sqrt{\tilde{r}^2 \cos^2 \vartheta + (z - \eta_+)^2}] + \ln \frac{H + \eta_+ - z + \sqrt{\tilde{r}^2 \cos^2 \vartheta + (H + \eta_+ - z)^2}}{H + \eta_- + z + \sqrt{\tilde{r}^2 \cos^2 \vartheta + (H + \eta_- + z)^2}} [z + \eta_- + \sqrt{\tilde{r}^2 \cos^2 \vartheta + (z + \eta_-)^2}] \right\} \quad (25)$$

Here

$$z + \eta_- = z \cos 2\vartheta + \frac{x}{2\varepsilon_{13}} (1 - 2 \cos 2\vartheta), \quad z - \eta_+ = z - \frac{x}{2\varepsilon_{13}} (1 - 2 \cos 2\vartheta) \quad (26)$$

$$\tilde{r}_-^2 = \tilde{r}_+^2 + 4 \sin^2 \vartheta z \left(\frac{x}{\varepsilon_{13}} - z \right), \quad \varepsilon_{13} = \frac{\lambda_{\parallel} - \lambda_{\perp}}{\lambda_{\perp} \cot^2 \Theta + \lambda_{\parallel} \tan^2 \Theta} \quad (27)$$

This result, describing the steady state temperature field of one borehole, embedded in multilayered semi-infinite medium at arbitrary angle of the bedding relative to the surface, agree with the result derived from the isotropic FLS model (Zeng et al. 2002). In the limiting case, when λ_{\perp} tends to λ_{\parallel} ,

the proposed Equation 25 recovers the well known result for the steady state limit (SSL) of the temperature in the isotropic model.

One can see that the steady state temperature is proportional to the $\frac{q_z}{\lambda_{eff}}$ in addition to the BHE response function on anisotropy, dip angle and borehole depth. The effect of anisotropy manifests itself in the steady state conditions, whereas thermal conductivity values obtained by fitting the same TRT data to anisotropic solution, Equation (20), and isotropic solution, Equation (9), are identical. The steady state BHE response is strongly influenced by anisotropy.

Figure 3 shows that the steady state temperature profile along the borehole depth at the horizontal stratification exceeds that for the isotropic ground, as one might expect for $\lambda_{\perp} \leq \lambda_{\parallel}$.

The following section addresses the specific case of vertically stratified geologic regime, i.e. for $\Theta = \pi/2$ and thus $\varepsilon_{13} = 0$.

Mean temperature approximations at vertical stratification

The effect of anisotropy on vertical temperature dependencies increases with increasing of the dip angle for typical situation: $\lambda_{\perp} \leq \lambda_{\parallel}$. Indeed, let there be strata parallel to the plane YZ depicted in Figure 2. The thermal conductivity of such vertically stratified ground takes smaller values in the X direction, $\lambda_1 = \lambda_{\perp}$, than in the in-plane direction, $\lambda_2 = \lambda_3 = \lambda_{\parallel}$ (Polubaronova-Kochina 1962). These define the principal components of the thermal tensor. The exact temperature solution is presented by Equation 17 at $\vartheta = 0$; it is not invariant under spatial rotation about the axis of the vertical BHE as at the horizontal stratification of the previous section. Notice that the effective thermal conductivity attains minimum value: $\lambda_{eff} = \sqrt{\lambda_{\parallel}\lambda_{\perp}}$. Furthermore, substituting $x \rightarrow x\sqrt{\lambda_{\parallel}/\lambda_{\perp}}$ and $r \rightarrow \tilde{r} = \sqrt{x^2 a^2 + y^2}$ into Equation 8b one can also get the solution for the temperature field integrated along the same borehole depth H . Indeed, under the conditions in Equation 23, the mean thermal response at $\vartheta = 0$ is represented by the approximation in the transient regime .

$$\langle T - T_0 \rangle = \frac{q_z}{4\pi\sqrt{\lambda_{\perp}\lambda_{\parallel}}} \left(\ln \frac{4\alpha t}{\tilde{r}^2} - \gamma - 3 \left\{ \sqrt{\frac{4t}{\pi t_{\parallel}}} - \frac{r}{H} + \frac{r^2}{H^2} \sqrt{\frac{t_{\parallel}}{4\pi t}} \right\} \right), \quad \tilde{r} = \sqrt{x^2 a^2 + y^2} \quad \text{for } r_b \leq \tilde{r} \ll H \quad (28)$$

Here $t_{\parallel} = H^2 / \alpha_{\parallel}$, $\alpha_{\parallel} = \lambda_{\parallel} / C$ and \tilde{r} is defined by Equation 21 at $\varepsilon_{11} = 1/a^2$, $\varepsilon_{22} = 1$. Notice that isotherms of the mean thermal response function around the borehole, where \tilde{r} is constant. Furthermore, due to $a > 1$ ($\tilde{r} > r$) the effective ratio of the BHE depth to \tilde{r} is shortened for the vertical stratification with respect to H/r for the isotropic medium and the edge corrections become more pronounced. The steady state limit from Equation 8b or 21 for $t \gg \max(H^2, \tilde{r}^2) / \alpha_{\parallel}$ can be written in the following form.

$$\langle T - T_0 \rangle = \frac{q_z}{2\pi\sqrt{\lambda_{\perp}\lambda_{\parallel}}} \left\{ \hat{g}_s\left(\frac{H}{\tilde{r}}\right) - \frac{(t_{\parallel}/t)^{3/2}}{24\sqrt{\pi}} \left[1 - 3t_{\parallel} \frac{1 + \tilde{r}^2 / H^2}{20t} \right] \right\}, \quad t_{\parallel} = \frac{H^2}{\alpha_{\parallel}}, \quad t \gg \frac{\max(H^2, \tilde{r}^2)}{\alpha_{\parallel}} \quad (29)$$

There are two characteristic times $\frac{\tilde{r}^2}{\alpha_{\parallel}}$ and $\frac{H^2}{\alpha_{\parallel}} = \frac{H^2 C}{\lambda_{\parallel}}$ for anisotropic diffusion in the radial and axial directions, respectively.

Exact solution for the mean steady-state temperature in the dimensionless form of $\hat{g}_s\left(\frac{H}{\tilde{r}}\right)$ is valid at any distance from borehole center. Using the expansion of the $\hat{g}_s\left(\frac{H}{\tilde{r}}\right)$ for large values of the $\frac{H}{\tilde{r}}$ we arrive at the following result for anisotropy correction to the steady state temperature from isotropic and anisotropic models

$$\langle T(x, y)_{|a=1} - T(x, y)_{|a \neq 1} \rangle = \frac{q_z}{2\pi\lambda_{eff}} \left[\hat{g}_s\left(\frac{H}{\tilde{r}}\right) - \hat{g}_s\left(\frac{H}{r}\right) \right] = \frac{q_z}{2\pi\lambda_{eff}} \left[-2 \ln \frac{r}{\tilde{r}} + \frac{3(r - \tilde{r})}{H} + O\left(\frac{r}{H}\right) \right] \text{ for } \frac{H}{\tilde{r}} \rightarrow \infty \text{ (VS)}$$

This correction is derived for $\lambda_{eff} = \lambda = \sqrt{\lambda_{\perp}\lambda_{\parallel}}$ and valid in the vicinity of borehole. Equations HS and VS provide anisotropy corrections for the mean borehole temperature in explicit form in the limiting cases of horizontal and vertical stratifications, respectively

Figure 5 presents the time-dependence of the exact mid-point g -function and average g -functions for isotropic ground and average g -functions for the vertical stratification at $\alpha_{\parallel} = \alpha$. Furthermore, as shown in Figure 5, point $x=0.1\text{m}$; $y=0$ has lower value of mean thermal response function than point $x=0$; $y=0.1\text{m}$ in the uniform in-plane direction y . Notice that, although the physical distance is the same as

derived from the line heat source, the ratio \tilde{r}/H is different at these two points causing splitting mean \hat{g} function curve calculated for an isotropic ground in two branches shown in Figure 5.

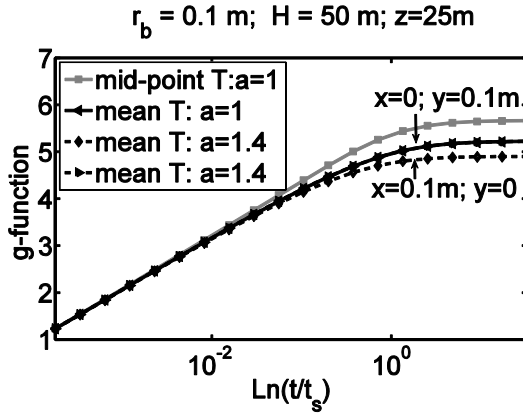


Figure 5. Comparison between the borehole response functions from two models of medium with vertical strata. Mid-point ($z=H/2$) (gray line) and mean g -functions from the isotropic model ($\lambda_{\parallel} = \lambda_{\perp} = \lambda$) and mean \hat{g} -functions in the X and Y directions from the anisotropic model ($\lambda_{\parallel} = a^2 \lambda_{\perp}$, $\Theta = \pi/2$) versus the natural logarithm of time. Exact solutions calculated for constant heat injection are shown in the range: $5r_b^2 / \alpha_{\parallel} < t < a^2 H^2 / \alpha_{\parallel}$, $\alpha = \alpha_{\parallel}$.

This behavior attributed to the fact that the thermal conductivity parallel to the layers is higher than that perpendicular to the bedding plane, suggests that row of boreholes should be aligned along the direction X to enhance conditions of the heat exchange with a multilayered ground as comparison shows also in Figure 6.

Many sedimentary and metamorphic laminated rocks are strongly anisotropic (Davis et al., 2007): the thermal conductivity in parallel to bedding planes of these rocks is 2-3 times higher than that perpendicular to bedding (Deming, 1994; Popov et al., 1995). This proposal on layout of the borehole raw is not referred to the anisotropy values less than unity also reported (Davis et al., 2007).

Although anisotropy value: $a=1.4$ in the given examples is common, our solution is valid for any thermal conductivity anisotropy.

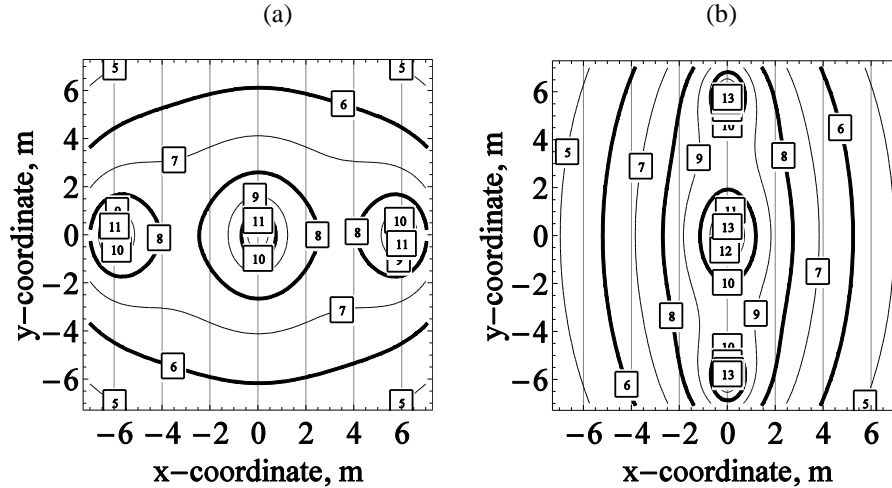


Figure 6. Comparison between isotherms curves of steady-state \hat{g} -functions from two 3 borehole configurations (with an inter-borehole distance of 3 m and $H=50$ m) at the $\Theta = \pi/2$: (a) along the direction X; (b) along the direction Y, shown in Figure 2.

CONCLUDING REMARKS, SUMMARY AND DISCUSSION

Results have been presented of a study of the thermal response from multilayered ground modeled as an anisotropic medium to constant heat pulse from the finite line source. This study discusses anisotropic dependence of both effective thermal conductivity measured by TRT and the steady state temperature field around vertical FLS in the arbitrary oriented strata with respect to the surface of the semi-infinite medium.

What is actually measured for the intermediate time values of the TRTs is the effective thermal conductivity of the soil/rock formation in the direction perpendicular to the borehole axis. We have provided effective conductivity as a function of the inclination angle, which should prove to be useful for the geothermal applications. In addition, we have shown that the dip angle and the anisotropy factor influence the steady-state temperature field of the designed installation. Therefore, it may be a discrepancy between the real temperature spatial distribution around vertical or horizontal GCHP systems in the steady state conditions and its prediction of the isotropic model with thermal conductivity value obtained from the short time TRT, but without using the data of anisotropy and dip of the bedding.

The exact solution accounting for anisotropy, its asymptotic behavior and the steady state expression for the temperature obtained here for any dip angle between the surface and the bedding should prove to be useful for designing multiple borehole configurations in stratified medium.

Analytical formulae have been obtained for the asymptotic behavior of the average temperature in horizontally and vertically stratified ground for intermediate- and long- time scales. The suggested corrections for anisotropic effects (Equations HS and VS) may give errors, when estimating the steady state average temperature by the isotropic model.

In these limiting cases the proposed response functions in Equations 13, 29 can be easily applied to estimate maximum and minimum of the mean steady state temperature field of an arbitrary borehole configuration using the superposition principle.

Due to the fact that the thermal conductivity of ground is higher along the layers the average thermal response method provides the lowest estimation for the dimensionless response function approaching steady-state limit; that is reached in the direction across the layers at the vertical stratification. This conclusion is relevant when choosing a proper configuration to minimize temperature between vertical sources of heat from data about the geometrical disposition of the layers and the surface. To this objective the proposal consists in disposing a row of vertical heat sources normally to the lines of strata intersection with the surface rather than along them at any values of the dip angle. This recommendation regards also selection of orientation for horizontal GCHP systems. The analytical formulae for the temperature allow flexibility in the estimation of the temperatures within and around a repository of nuclear waste in anisotropic rock.

NOMENCLATURE

$a = \sqrt{\frac{\lambda_{\parallel}}{\lambda_{\perp}}}$	= thermal conductivity anisotropy factor
C	= volumetric heat capacity of ground, $\text{Jm}^{-3}\text{K}^{-1}$
Ei	= exponential integral
$\hat{g} = \frac{2\pi\lambda_{\text{eff}}}{q_z} \langle T(r, t) - T_0 \rangle$	= generalized thermal response function for $r \geq r_b$

$Fo_{\parallel} = \frac{t\alpha_{\parallel}}{r^2}$ = in-plane Fourier number

H = depth of the borehole heat exchanger (BHE), m

r = radial coordinate, m

r_b = radius of the BHE, m

\vec{r} = coordinate vector, m

q_z = heat flow per unit length, Wm^{-1}

\vec{Q} = vector of heat density per unit area, Wm^{-2}

$t_r = r_b^2 / \alpha$ = short time scale for the BHE, s

$t_s = \frac{H^2}{\alpha}$ = steady-state time scale, s

$t_z = H^2 / \alpha$ = isotropic time scale for the BHE, s

$t_{\parallel} = H^2 / \alpha_{\parallel}$ = in-plane time scale for the BHE, s

T = temperature of ground (K or °C)

T_0 = undisturbed ground temperature (K or °C)

z = vertical axial coordinate, m

Greek letters

$\alpha = \lambda / C$ = isotropic thermal diffusivity, m^2/s

$\alpha_{\parallel} = \lambda_{\parallel} / C$ = in-plane thermal diffusivity, m^2/s

δ = delta function

$\Delta = \varepsilon_{11} - \varepsilon_{13}^2$ = dimensionless parameter

$\varepsilon = \Lambda / \Lambda_{33}$ = dimensionless thermal conductivity tensor

γ = Euler's constant

λ_{eff} = Equation 20, effective thermal conductivity, $W (Km)^{-1}$

λ_{\parallel} = in-plane thermal conductivity (parallel to bedding plane), $W (Km)^{-1}$

λ_{\perp} = normal thermal conductivity (normal to bedding plane), $W (Km)^{-1}$

Λ = three-dimensional thermal conductivity tensor, $W (Km)^{-1}$

$He(z)$ = unit step function

Θ = angle between the surface and strata, °

$\mathcal{G} = \arccos \sqrt{\frac{\varepsilon_{13}}{\Delta}}$ = dimensionless parameter

Subscripts

|| = direction parallel to bedding

s = steady-state

Superscripts

$\langle \dots \rangle (= \frac{1}{H} \int_0^H \dots dz)$ = integral mean

REFERENCES

- Bandos, T.V., Montero, Á., Fernández, E., Santander, J.L.G., Isidro, J.M., Pérez, J., Fernández de Córdoba, P.J., and Urchueguía, J.F. 2009. Finite line-source model for borehole heat exchangers: effect of vertical temperature variations, *Geothermics* 38: 263-270.
- Bandos, T.V., Montero, Á., Fernández de Córdoba P., and Urchueguía J.F. 2011. Improving parameter estimates obtained from thermal response tests: effect of ambient air temperature variations. *Geothermics* 40: 136-143.
- Bernier, M. A. 2001. Ground-coupled heat pump system simulation. *American Society of Heating, Refrigerating and Air Conditioning Engineers Transactions* 106(1): pp. 605–616.
- Bose, J. E., Parker, J. D., and McQuiston, F. C. 1985. Design/Data Manual for Closed Loop Ground Coupled Heat Pump Systems. *American Society of Heating, Refrigerating, and Air Conditioning Engineers*, Atlanta, Georgia: 16 pp.
- Carslaw, H.S., and Jaeger, J.C. 1959. *Conduction of Heat in Solids*. 510 pp. New York: Oxford University Press.
- Claesson, J., and Eskilson, P. 1988. Conductive heat extraction to a deep borehole, thermal analysis and dimensioning rules, *Energy* 13: 509-527.
- Cui, P., Yang, H., and Fang, Z. 2006. Heat transfer analysis of ground heat exchangers with inclined boreholes, *Applied Thermal Engineering* 26: 1169-1175.
- Davis, M. G., Chapman, D. S., Van Wagoner, T. M., and Armstrong P. A. 2007. Thermal conductivity anisotropy of metasedimentary and igneous rocks, *Journal of Geophysical Research* 112: B05216-B0523.
- Deming, D. 1994. Estimation of the thermal conductivity anisotropy of rock with application of terrestrial heat flow, *Journal of Geophysical Research* 99(B11): 22087-22091.
- Eskilson, P. 1987. *Thermal Analysis of Heat Extraction Boreholes*. PhD. Thesis, Department of Mathematical Physics, University of Lund, Lund, Sweden: 264 pp.
- Grubbe, K., Haenel, R., Zoth, G. 1983. Determination of the vertical component of thermal conductivity by line source methods. *Zentralblatt für Geologie und Paläontologie. Teil, Allgemeine, angewandte, regionale und historische* 1: 49-56.
- Hastie, T., Tibshirani, R., Friedman, J. 2001. *The Elements of Statistical Learning*. 536 pp. NY: Springer-Verlag.
- Hörmark, H., and Claesson, J. 2005. Use of an analytical solution for calculating temperatures in repository host rock. *Engineering Geology* 81: 353-364.
- Kavanaugh, S.P. 2000. Field tests for ground thermal properties- methods and impact on ground-source heat pump design. *ASHRAE Transactions* 106: 1-5.

- Lamarche, L., Beauchamp, B., 2007. A new contribution to the finite line-source model for geothermal boreholes. *Energy and Buildings* 39, 188-198.
- Sundberg, J., and Helström, G., 2009. Inverse modelling of thermal conductivity from temperature measurements at the Prototype Repository, Äspö HRL. *International Journal of Rock Mechanics and Mining Sciences* 46: 1029-1041.
- Polubarinova-Kochina, P. Ya. 1962. *Theory of Ground-Water Movement*. 613 pp. Princeton: Princeton University Press.
- Popov, Y. A., Pribnow, D. F. C., Sass, J. H., Williams, C. F., and Burkhardt, H. 1999. Characterization of rock thermal conductivity by high-resolution optical scanning. *Geothermics* 28: 253-276.
- Pribnow, D. F. C. and Sass J. H. 1995. Determination of thermal conductivity for deep boreholes, *Journal of Geophysical Research* 100(B6): 9981-9994.
- Sutton, M.G., Couvillion, R.J., Nutter, D.W., Davis R.K. 2001. An algorithm of approximating the performance of vertical bore heat exchangers installed in a stratified geologic regime. *ASHRAE Transactions* 106: 177-184.
- Zeng, H., Diao, N., Fang, Z. 2002. A finite line-source model for boreholes in geothermal heat exchangers. *Heat Transfer Asian Research* 31: 558-567.

Figure captions

Figure 1. In-situ TRT schematic and formations layers.

Figure 2. Direction of X' , Y , Z' principal axes of the thermal conductivity tensor. The XY plane represents the ground surface at the dip angle Θ from the $X'Y$ plane.

Figure 3. Comparison between thermal response g -functions at $r = r_b = 0.1\text{m}$ around the borehole penetrating horizontal strata ($\Theta = 0$) from two models: isotropic model ($\lambda_{\parallel} = \lambda_{\perp}$) and anisotropic model ($\lambda_{\parallel} = a^2 \lambda_{\perp}$) of the ground. (a) Profiles of the g -function versus the natural logarithm of time t/t_s and the dimensionless coordinate z/H along the borehole; (b) Mid-point ($z=H/2$) (gray line) and mean g -functions from the isotropic model and mean g -function from the anisotropic model versus the natural logarithm of time. Exact solutions calculated for constant heat injection are shown in the range: $5r_b^2 / \alpha_{\parallel} < t < H^2 a^2 / \alpha_{\parallel}$. The time is scaled by $t_s = H^2 / (9\alpha)$ (Eskilson, 1987).

Figure 4. Effective scaled thermal conductivity versus the angle Θ between the ground surface and sedimentary planes, see Figure 2, for $a = 1.4$.

Figure 5. Comparison between thermal response g -functions around the borehole penetrating vertical strata from two models of medium. Mid-point ($z=H/2$) (gray line) and mean g -functions from the isotropic model ($\lambda_{\parallel} = \lambda_{\perp}$) and mean \hat{g} -functions in the X and Y directions from the anisotropic model ($\lambda_{\parallel} = a^2 \lambda_{\perp}$) versus the natural logarithm of time. Exact solutions calculated for constant heat injection are shown in the range: $5r_b^2 / \alpha_{\parallel} < t < a^2 H^2 / \alpha_{\parallel}$.

Figure 6. Comparison between isotherms curves of generalized steady-state \hat{g} -functions from two 3 borehole configurations (with an inter-borehole distance of 3 m and $H=50$ m) at the $\Theta = \pi/2$: (a) along the direction X ; (b) along the direction Y , shown in Figure 2.

Article

Boltzmann Entropy of a Newtonian Universe

D. Cabrera, Pedro Fernández de Córdoba and J.M. Isidro *

Instituto Universitario de Matemática Pura y Aplicada, Universidad Politécnica de Valencia, Valencia 46022, Spain; dacabur@upvnet.upv.es (D.C.); pfernandez@mat.upv.es (F.d.C.)

* Correspondence: joissan@mat.upv.es; Tel.: +34-96-387-7000

Academic Editor: Remo Garattini

Received: 5 April 2017; Accepted: 4 May 2017; Published: 6 May 2017

Abstract: A dynamical estimate is given for the Boltzmann entropy of the Universe, under the simplifying assumptions provided by Newtonian cosmology. We first model the cosmological fluid as the probability fluid of a quantum-mechanical system. Next, following current ideas about the emergence of spacetime, we regard gravitational equipotentials as isoentropic surfaces. Therefore, gravitational entropy is proportional to the vacuum expectation value of the gravitational potential in a certain quantum state describing the matter contents of the Universe. The entropy of the matter sector can also be computed. While providing values of the entropy that turn out to be somewhat higher than existing estimates, our results are in perfect compliance with the upper bound set by the holographic principle.

Keywords: newtonian cosmology; emergent quantum theory

1. The Approach via Emergent Quantum Theory

In this article, we will argue in favour of *emergent* quantum mechanics as providing an appropriate framework to estimate thermodynamical quantities of the Universe, such as the entropy.

The notion that *quantum mechanics is an emergent theory* has been discussed at length in the literature [1–7]. Combined with the idea that *spacetime is also an emergent phenomenon* [8–12], this paves the way for *a computation of some thermodynamical properties of spacetime in quantum-mechanical terms*. We would like to remark that a quantum-mechanical approach to the expansion of the Universe was called for long ago in Reference [13], where it was suggested to regard the expansion of the Universe as a scattering problem in quantum mechanics.

The expansion of the Universe is a long-standing experimental observation [14] that has in recent years been refined thanks to very precise measurements [15,16]. In the Newtonian approximation, this receding behaviour of the galaxies can be easily modelled by a phenomenological potential—namely, an isotropic harmonic potential carrying a negative sign:

$$U_{\text{Hubble}}(\mathbf{r}) = -\frac{H_0^2}{2} \mathbf{r}^2. \quad (1)$$

As the angular frequency, we take the current value of Hubble's constant H_0 . Thus, U_{Hubble} has the dimensions of energy per unit mass, or velocity squared.

In the emergent approach to spacetime presented in Reference [12], gravity qualifies as an entropic force. If gravitational forces are entropy gradients, gravitational equipotential surfaces can be identified with isoentropic surfaces. Recalling the arguments of Reference [12], a classical point particle approaching a holographic screen causes the entropy of the latter to increase by one quantum k_B . Here we will analyse a quantum-mechanical model in which the forces driving the galaxies away from each other can be modelled by the Hubble potential (1). We will replace the classical particle of Reference [12] with a collection of quantum particles (the matter contents of the Universe) described

by the wavefunction ψ . Let U denote the gravitational potential. Once dimensions are corrected using \hbar and k_B , the expectation value $\langle \psi|U|\psi \rangle$ becomes the quantum-mechanical analogue of the entropy increase caused by a classical particle approaching a holographic screen. Thus, *the expectation value $\langle \psi|U|\psi \rangle$ is a measure of the gravitational entropy of the Universe when the matter of the Universe is described by the wavefunction ψ .*

The potential U_{Hubble} of Equation (1) encodes the combined effect of the gravitational attraction, and of the repulsion caused by the dark energy on the matter content of the Universe (baryonic and dark matter). We can therefore identify the Hubble potential U_{Hubble} of Equation (1) with the gravitational potential U in the previous paragraph. Let us briefly recall why U_{Hubble} in fact combines a Newtonian gravitational attraction plus a harmonic repulsion. In the Newtonian limit considered throughout in this paper, the gravitational attraction is computed by applying Gauss' law to a sphere filled with a homogeneous isotropic density of matter. Then, the gravitational field *within the sphere* turns out to be proportional to the position vector, so the corresponding potential becomes a quadratic function of the position. Altogether, the total potential at any point within the cosmological fluid is the sum of two harmonic potentials; Hubble's constant H_0 is the frequency of this total harmonic potential.

We will first start with a flat Euclidean space governed by nonrelativistic Newtonian cosmology. The latter leads to the same equation that governs the scale factor of general-relativistic Robertson–Walker models [17]. On the other hand, it circumvents the mathematical sophistication required by general relativity. The advantage of first performing a nonrelativistic treatment is that it bears out the deep connection existing between the cosmological fluid and the Madelung approach to Schroedinger quantum mechanics; this is done in Section 2.1. In Section 2.2, we obtain a perturbative estimate for the entropy of the Universe; finally, this analysis is carried out nonperturbatively in Section 2.3. As a next level of sophistication, we move on to a flat Friedmann–Lemaître–Robertson–Walker (FLRW) four-dimensional spacetime; due to the great length of the calculations involved, the corresponding results will be presented in an upcoming publication [18].

We would finally like to stress the following points:

(i) The wavefunction ψ we will be concerned with here is meant to provide a *phenomenological* description of the receding matter in its recessional motion *within a fixed spacetime*.

(ii) We will comply with the cosmological principle, the latter stated in either one of the following two (inequivalent) ways. In its first formulation, given the wave function ψ , the volume density of matter $|\psi|^2$ is spatially constant. In its second formulation, given ψ and the three-dimensional volume element $d^3V = \sqrt{|g|} dx^1 dx^2 dx^3$, the particle number $|\psi|^2 d^3V$ is spatially constant. This second formulation is weaker than—and implied by—the first one.

(iii) A quantum-mechanical wavefunction ψ for the matter contents of the Universe will be used to obtain an estimate of the gravitational entropy of the Universe.

(iv) Invoking Boltzmann's principle, the same wavefunction ψ can be used to obtain an estimate of the entropy of the matter of the Universe (baryonic and dark matter).

(v) All entropies referred to in this paper are Boltzmann entropies.

We would like to thank the referees for drawing our attention to a number of issues and papers where points related to those analysed here are dealt with from different perspectives. Specifically, a wavefunction of the Universe was first considered in Reference [19]; the quantum potential was shown to generate gravitational attraction between particles in Reference [20]; the Hubble potential possesses no groundstate when considered on all of \mathbb{R}^3 [21]; the nonexistence of a stable groundstate has consequences on quantum fields on an expanding spacetime [22]. Since we are considering the Hubble potential on a finite Universe (with radius R_0), the existence of a stable groundstate is guaranteed. Additionally, the Hubble expansion is considered to maintain the Universe close to equilibrium, so we can apply standard thermodynamical relations.

2. Newtonian Cosmology à la Madelung

Newtonian cosmology represents a first step that succeeds in capturing some essential physics of the Universe, while avoiding the technical difficulties of general relativity [17,23].

2.1. The Ideal-Fluid Description

In this section, we will establish that Newtonian cosmology can be conveniently regarded as a nonrelativistic quantum mechanics.

In Newtonian cosmology, the matter content of the Universe is modelled as an ideal fluid satisfying the continuity equation and the Euler equation,

$$\frac{\partial \rho}{\partial t} + \nabla \cdot (\rho \mathbf{v}) = 0, \quad \frac{\partial \mathbf{v}}{\partial t} + (\mathbf{v} \cdot \nabla) \mathbf{v} + \frac{1}{\rho} \nabla p - \mathbf{F} = 0. \quad (2)$$

Above, ρ is the volume density of fluid mass, p is the pressure, \mathbf{v} is the velocity field, and \mathbf{F} the force per unit volume acting on the fluid. The cosmological principle requires ρ and p to be spatially constant; it also leads to the requirement that the velocity \mathbf{v} be everywhere proportional to the position vector \mathbf{r} . This latter requirement is nothing but Hubble's law, so the Hubble potential (1) arises naturally as a consequence of the cosmological principle. The gravitational self-attraction of the matter distribution and Hubble's repulsion are both taken care of by the force \mathbf{F} in the Euler equation.

Madelung long ago re-expressed Schrödinger quantum mechanics also in terms of an ideal fluid. Specifically, one separates the nonrelativistic wavefunction ψ into amplitude and phase,

$$\psi = A \exp\left(\frac{i}{\hbar} \mathcal{I}\right) = \exp\left(S + \frac{i}{\hbar} \mathcal{I}\right), \quad A =: e^S = \exp\left(\frac{\mathcal{S}}{2k_B}\right), \quad (3)$$

where \mathcal{I} is the classical mechanical action integral; we will later invoke Boltzmann's principle to regard \mathcal{S} as the Boltzmann entropy and $S := \mathcal{S}/2k_B$ as the dimensionless Boltzmann entropy. Substituting the Ansatz (3) into the Schrödinger equation for ψ , one is led to an expression containing a real part and an imaginary part. The imaginary part turns out to be the continuity equation for the quantum probability fluid,

$$\frac{\partial S}{\partial t} + \frac{1}{m} \nabla S \cdot \nabla \mathcal{I} + \frac{1}{2m} \nabla^2 \mathcal{I} = 0, \quad (4)$$

where the velocity field \mathbf{v} and the density ρ are defined by

$$\mathbf{v} := \frac{1}{m} \nabla \mathcal{I}, \quad \rho = A^2 = e^{2S}. \quad (5)$$

The real part turns out to be the quantum Hamilton–Jacobi equation:

$$\frac{\partial \mathcal{I}}{\partial t} + \frac{1}{2m} (\nabla \mathcal{I})^2 + V + \mathcal{Q} = 0, \quad (6)$$

where $V = mU$ is the external potential, and we have introduced the quantum potential [24]

$$\mathcal{Q} := -\frac{\hbar^2}{2m} \frac{\nabla^2 A}{A}. \quad (7)$$

Finally, a Euler equation for this quantum probability fluid is obtained by taking the gradient of the quantum Hamilton–Jacobi Equation (6):

$$\frac{\partial \mathbf{v}}{\partial t} + (\mathbf{v} \cdot \nabla) \mathbf{v} + \frac{1}{m} \nabla \mathcal{Q} + \frac{1}{m} \nabla V = 0. \quad (8)$$

We conclude that a one-to-one correspondence between the cosmological fluid on the one hand, and the quantum probability fluid on the other is provided by the following replacements:

$$\rho \mapsto e^{2S}, \quad \mathbf{v} \mapsto \frac{1}{m} \nabla \mathcal{I}, \quad \frac{1}{\rho} \nabla p \mapsto \frac{1}{m} \nabla Q, \quad \mathbf{F} \mapsto -\frac{1}{m} \nabla V. \quad (9)$$

The above correspondence suggests that, *given the cosmological fluid in the Newtonian approximation, we use nonrelativistic quantum mechanics as an equivalent description thereof*. The value of m entering Equation (9) is that of the overall matter contents of the Universe (baryonic and dark matter). This matter is subject to the repulsive effect of the dark energy, and to its own gravitational self-attraction, the combined effect of which is modelled by the effective Hubble potential (1).

2.2. Perturbative Estimate of the Entropy

2.2.1. Wavefunction of the Matter Distribution

We will model the ideal fluid of Newtonian cosmology by means of the probability fluid corresponding to a *scalar field ψ satisfying the Schrödinger equation*. Initially, the latter will be taken to be the free equation, for a perturbative treatment. That is, ψ will be used to compute $\langle \psi | U | \psi \rangle$, with U the Hubble potential (1). Alternatively, we can include the Hubble potential (1) in the Schrödinger equation already from the start; this nonperturbative treatment will be carried out in Section 2.3.

The squared modulus $|\psi|^2$ will equal the volume density ρ of mass. The cosmological principle requires the density ρ to be constant across space. In turn, the correspondence (9) implies that S must be a constant, so the quantum potential Q will vanish identically. Again by the correspondence (9), the pressure p must be spatially constant, which is also in agreement with the cosmological principle. The effective Hubble potential will be introduced later on, as a perturbation to the free field ψ .

The free Schrödinger equation admits the plane-wave solutions

$$\psi_{\mathbf{k}}(\mathbf{r}) = \frac{1}{R_0^{3/2}} \exp(i\mathbf{k} \cdot \mathbf{r}). \quad (10)$$

They have been normalised within a cubic box of side R_0 , the radius of the observable Universe. The cosmological principle is satisfied in its first formulation as given in Section 1. Moreover, the constant amplitude $A = R_0^{-3/2}$ leads to a vanishing quantum potential in Equation (7), in agreement with previous requirements.

The free Schrödinger equation can also be separated in spherical coordinates. The resulting free spherical waves $\psi_{\kappa lm}(r, \theta, \phi)$ are then labelled by κ (the modulus of the linear momentum \mathbf{k}) and l, m (the angular momentum quantum numbers). The cosmological principle imposes $l = 0$. We will therefore consider the free spherical waves

$$\psi_{\kappa 0 0}(r, \theta, \phi) = \frac{1}{\sqrt{4\pi R_0}} \frac{1}{r} \exp(i\kappa r). \quad (11)$$

They have been normalised within a sphere of radius R_0 , instead of a cubic box. Once the spherical Jacobian factor $4\pi r^2$ is taken into account, the second formulation of the cosmological principle given in Section 1 is satisfied. Moreover, the amplitude $A = 1/r$ also leads to a vanishing quantum potential in (7) because

$$\frac{\nabla^2 A}{A} = r \nabla^2 \left(\frac{1}{r} \right) = -4\pi r \delta(\mathbf{r}) = 0. \quad (12)$$

We will use both plane waves (10) and spherical waves (11) in order to model the distribution of the matter contents of the Universe. The results obtained from one or the other can differ at most by a dimensionless factor of geometrical origin, due to the use of a cubic box as opposed to a spherical box. Imposing boundary conditions on the wavefunction at the walls of the corresponding box only leads

to a quantisation of the energy levels—a possibility that we will disregard here (see Section 2.4 for a discussion of this point).

Since we are not imposing boundary conditions, we will work with a set of two linearly-independent solutions to the free Schrödinger equation. In Cartesian coordinates, a fundamental set of solutions is provided by the wavefunctions $\psi_{\pm\mathbf{k}}(x, y, z)$; in spherical coordinates, a fundamental set of solutions is provided by the wavefunctions $\psi_{\pm\kappa 00}(r, \theta, \phi)$.

2.2.2. Expectation Values

From what was said above, the operator $\mathbf{R}^2 = X^2 + Y^2 + Z^2$ —which is proportional to the effective potential (1)—is a measure of the amount of gravitational entropy enclosed by the Universe. Specifically, the combination

$$\mathcal{S}_g := \mathcal{N} \frac{k_B m H_0}{\hbar} \mathbf{R}^2 \tag{13}$$

is dimensionally an entropy; a *dimensionless* factor \mathcal{N} is of course left undetermined. We call \mathcal{S}_g the gravitational entropy operator. Its expectation value in the cubic-box state (10) equals

$$\langle \psi_{\mathbf{k}} | \mathcal{S}_g | \psi_{\mathbf{k}} \rangle = \mathcal{N} \frac{k_B m H_0}{\hbar} R_0^2, \tag{14}$$

while in the spherical-box state (11), it reads

$$\langle \psi_{\kappa 00} | \mathcal{S}_g | \psi_{\kappa 00} \rangle = \mathcal{N} \frac{k_B m H_0}{\hbar} \frac{R_0^2}{3}. \tag{15}$$

Substituting the known values of the cosmological data [25] into Equations (14) and (15), we find the estimate

$$\frac{\langle \mathcal{S}_g \rangle}{k_B} \simeq 10^{123}, \tag{16}$$

where we have (arbitrarily) set $\mathcal{N} = 1/2.6$ when using the plane-wave result (14), and $\mathcal{N} = 3/2.6$ when using the spherical-wave result (15), in order to keep only powers of 10. Our final result (16) saturates the upper bound set by the holographic principle [26].

We can also obtain an estimate for the entropy content of the matter described by the wavefunction ψ . Invoking Boltzmann’s principle, one regards the amplitude A of the wavefunction ψ as the exponential of the entropy (in units of k_B) of the particles described by the wavefunction ψ . This fact has been implicitly taken into account in the notation of Equation (3), from where we derive the entropy in terms of the amplitude:

$$\mathcal{S}_m = 2k_B \ln A. \tag{17}$$

Acting on the plane waves (10), the matter entropy operator \mathcal{S}_m is a constant,

$$\mathcal{S}_m = -3k_B \ln R_0. \tag{18}$$

Therefore, its expectation value in the state (10) equals

$$\langle \psi_{\mathbf{k}} | \mathcal{S}_m | \psi_{\mathbf{k}} \rangle = -3k_B \ln R_0. \tag{19}$$

The above is the correct behaviour for the entropy of an ideal gas, since the radius of the Universe is inversely proportional to its temperature.

For the spherical waves (11), we arrive at a matter entropy operator \mathcal{S}_m

$$\mathcal{S}_m = -2k_B \ln r - k_B \ln(4\pi R_0). \tag{20}$$

Its expectation value in the state (11) is found to be

$$\langle \psi_{\kappa 00} | \mathcal{S}_m | \psi_{\kappa 00} \rangle = -3k_B \ln R_0, \quad (21)$$

after dropping a constant independent of R_0 . We again find the expected (ideal-gas) logarithmic dependence of the entropy with respect to the temperature.

2.3. Nonperturbative Estimate of the Entropy

2.3.1. Exact Eigenfunctions

A nonperturbative evaluation requires solving the interacting Schrödinger equation $H\psi = E\psi$, where now

$$H = -\frac{\hbar^2}{2m} \nabla^2 - \frac{k_{\text{eff}}}{2} \mathbf{r}^2, \quad k_{\text{eff}} = mH_0^2. \quad (22)$$

Let us separate variables in Equation (22) using spherical coordinates. The standard factorisation $\psi(\mathbf{r}) = R(r)Y_{lm}(\theta, \phi)$ leads to a radial wave equation

$$\frac{1}{r^2} \frac{d}{dr} \left(r^2 \frac{dR}{dr} \right) - \frac{l(l+1)}{r^2} R + \frac{2m}{\hbar^2} \left(E + \frac{k_{\text{eff}}}{2} r^2 \right) R = 0. \quad (23)$$

Two linearly independent solutions with $l = 0$ are [27]

$$R_\lambda^{(1)}(r) = \exp\left(\frac{ia^2}{2}r^2\right) {}_1F_1\left(\frac{3}{4} - \frac{i\lambda}{4}, \frac{3}{2}; -ia^2r^2\right) \quad (24)$$

and

$$R_\lambda^{(2)}(r) = \frac{1}{r} \exp\left(\frac{ia^2}{2}r^2\right) {}_1F_1\left(\frac{1}{4} - \frac{i\lambda}{4}, \frac{1}{2}; -ia^2r^2\right). \quad (25)$$

Above, ${}_1F_1(a; \gamma; z)$ is the confluent hypergeometric function, and the parameters a , λ can be expressed in terms of the mechanical data m , k_{eff} , E , H_0 :

$$a^4 := \frac{mk_{\text{eff}}}{\hbar^2}, \quad \lambda := \frac{2E}{\hbar H_0}. \quad (26)$$

The complete interacting wavefunctions are (up to radial normalisation factors)

$$\psi_\lambda^{(j)}(r, \theta, \phi) = \frac{1}{\sqrt{4\pi}} R_\lambda^{(j)}(r), \quad j = 1, 2, \quad \lambda \in \mathbb{R}. \quad (27)$$

Since $\lambda \in \mathbb{R}$ is the (dimensionless) energy eigenvalue, it plays the same role that the quantum number $n \in \mathbb{N}$ plays in the standard harmonic oscillator. Our harmonic potential does not have quantised energy levels, but continuous energy levels λ instead. However, the range of values covered by λ , while unbounded above, is bounded below by

$$E_0 = -\frac{1}{2}mH_0^2R_0^2 \quad (28)$$

or, in terms of the dimensionless eigenvalue λ , by

$$\lambda_0 = -\frac{mH_0R_0^2}{\hbar} = -2.6 \times 10^{123}. \quad (29)$$

Substituting this value of λ_0 into Equation (27) produces the wavefunctions $\psi_{\lambda_0}^{(j)}$, with $j = 1, 2$, which are the analogues of the vacuum wavefunction of the usual oscillator. The bound (28) has been determined by a purely classical argument; although the uncertainty principle will shift the minimum

energy (28) by a positive amount, this correction can be discarded for our purposes, as it will be negligible compared to (28) itself.

As opposed to the free wavefunctions (10) and (11), the existence of zeroes of the confluent hypergeometric function ${}_1F_1$ is a sure sign that the cosmological principle will be violated by the wavefunctions (27), but the extent of this violation remains to be determined. We claim that:

(i) the expectation value of the quantum potential (7) is a measure of the violation of the cosmological principle. More precisely, small values of the dimensionless ratio $|\langle Q \rangle / \langle V \rangle|$ imply small violations of the cosmological principle, while large values imply large violations;

(ii) the ratio $|\langle Q \rangle / \langle V \rangle|$ achieves a minimum when evaluated in two states $\psi_{\lambda_0}^{(j)}$, because the numerator $|\langle Q \rangle|$ reaches a minimum while the denominator $|\langle V \rangle|$ reaches a maximum. That $|\langle V \rangle|$ achieves a maximum when $\lambda = \lambda_0$ is obvious. In what follows, we would like to argue that $|\langle Q \rangle|$ also reaches a minimum when $\lambda = \lambda_0$.

Evaluating the quantum potential (7) in terms of the eigenfunction ψ , with eigenvalue E , leads to

$$Q = E - V + \frac{\hbar^2}{8m} \left[\psi^{-2} (\nabla \psi)^2 + (\psi^*)^{-2} (\nabla \psi^*)^2 - 2(\psi^* \psi)^{-1} \nabla \psi^* \nabla \psi \right]. \quad (30)$$

Its expectation value in the eigenstate ψ equals

$$\langle Q \rangle = E - \langle V \rangle + \frac{\hbar^2}{8m} \int \left[\psi^* \psi^{-1} (\nabla \psi)^2 + (\psi^*)^{-1} \psi (\nabla \psi^*)^2 - 2 \nabla \psi^* \nabla \psi \right]. \quad (31)$$

Altogether, the ratio

$$\frac{\langle Q \rangle}{\langle V \rangle} = \frac{E - \langle V \rangle}{\langle V \rangle} + \frac{\hbar^2}{8m \langle V \rangle} \int \left[\psi^* \psi^{-1} (\nabla \psi)^2 + (\psi^*)^{-1} \psi (\nabla \psi^*)^2 - 2 \nabla \psi^* \nabla \psi \right] \quad (32)$$

is a dimensionless number. If it vanishes, the eigenfunction ψ satisfies the cosmological principle reasonably well. If the ratio (32) is nonvanishing but nevertheless small in absolute value, the eigenfunction ψ will satisfy the cosmological principle at least approximately, and our computation of the entropy will be on a sound basis.

Actually, the ratio (32) depends on the energy eigenvalue λ . We expect a regime of values to exist for λ such that within this regime, the dimensionless ratio $\langle Q \rangle / \langle V \rangle$ will be small enough to guarantee the validity of the replacement of the cosmological fluid with the quantum probability fluid. In order to justify this expectation, we first observe that for real eigenfunctions ψ , the ratio (32) simplifies considerably:

$$\frac{\langle Q \rangle}{\langle V \rangle} = \frac{E - \langle V \rangle}{\langle V \rangle}, \quad \psi^* = \psi. \quad (33)$$

Of course, our eigenfunctions (27) are not real. However, still assuming $\psi^* = \psi$, the best possible ratio $\langle Q \rangle / \langle V \rangle$ is attained for $E = \langle V \rangle$. This makes the following assumption plausible: *the complex wavefunction ψ_0 which minimises the ratio $|\langle Q \rangle / \langle V \rangle|$ is that for which the energy eigenvalue E_0 equals the expectation value $\langle \psi_0 | V | \psi_0 \rangle$.*

We therefore expect the two states $\psi_{\lambda_0}^{(j)}$ of Equation (27)—with λ_0 given in Equation (29)—to be those that *minimally* violate the cosmological principle. In other words, the correspondence put forth in this paper (the quantum probability fluid as an equivalent description of the ideal cosmological fluid) works best when applied to the states $\psi_{\lambda_0}^{(j)}$, while progressively becoming less and less reliable as the energy increases.

Unfortunately, the exact vacuum-state eigenfunctions $\psi_{\lambda_0}^{(j)}$ of Equations (24) and (25) contain the huge parameter λ_0 of Equation (29). Due to the oscillatory behaviour of the confluent hypergeometric function, this renders the exact radial eigenfunctions (27) extremely cumbersome to work with, both analytically and numerically. To simplify matters, we will replace the exact vacuum-state

eigenfunctions $\psi_{\lambda_0}^{(j)}$ of Equations (24) and (25) with a set of approximate radial eigenfunctions for the vacuum state. We will also see that these approximate eigenfunctions will be real, so they will only minimally violate the cosmological principle.

2.3.2. Approximate Eigenfunctions for the Vacuum State

We set $l = 0$ in Equation (23) and use $E = E_0$ from (28) to arrive at the eigenvalue equation for the vacuum state:

$$\frac{1}{r^2} \frac{d}{dr} \left(r^2 \frac{dR}{dr} \right) + \frac{m^2 H_0^2}{\hbar^2} (r^2 - R_0^2) R = 0. \quad (34)$$

The change of variables

$$r =: R_0 x, \quad R(r) =: f(x), \quad (35)$$

where $x \in [0, 1]$ is dimensionless, reduces Equation (34) to

$$\frac{1}{x^2} \frac{d}{dx} \left(x^2 \frac{df}{dx} \right) + \sigma_0^2 (x^2 - 1) f(x) = 0, \quad \sigma_0^2 := \frac{m^2 H_0^2 R_0^4}{\hbar^2}. \quad (36)$$

As compared to (34), the above equation is defined on the interval $x \in [0, 1]$, which is more manageable than the original $r \in [0, R_0]$; moreover, all large numbers present in the problem are contained within the *dimensionless* parameter σ_0 (the opposite of λ_0 in Equation (29)):

$$\sigma_0 = -\lambda_0 = 2.6 \times 10^{123}. \quad (37)$$

The parameter σ_0 equals the entropy of Equation (16) in units of k_B ; in fact, modulo the irrelevant factor 2.6, it equals the holographic bound [26]. We conclude that *the radial wave Equation (36) encodes information about the holographic principle.*

We have seen in Section 2.3.1 that Equation (36) is exactly soluble. However, the sheer size of σ_0 renders the exact wavefunctions (24) and (25) totally useless: analytical computations with them are out of the question, and numerical computations quickly get out of range. For this reason, we will consider an approximate solution in two steps. In the regime $x \rightarrow 0$, the radial wave Equation (36) can be approximated by

$$\frac{1}{x^2} \frac{d}{dx} \left(x^2 \frac{df}{dx} \right) - \sigma_0^2 f(x) = 0, \quad x \rightarrow 0, \quad (38)$$

while in the regime $x \rightarrow 1$, the approximate form of (36) reads

$$\frac{1}{x^2} \frac{d}{dx} \left(x^2 \frac{df}{dx} \right) = 0, \quad x \rightarrow 1. \quad (39)$$

Their respective solutions are

$$f_0^+(x) = \frac{1}{x} \cosh(\sigma_0 x), \quad f_0^-(x) = \frac{1}{x} \sinh(\sigma_0 x), \quad x \rightarrow 0 \quad (40)$$

and

$$f_1(x) = \frac{A}{x} + B, \quad x \rightarrow 1. \quad (41)$$

As announced above, these eigenfunctions are real; by the discussion following Equation (33), they violate the cosmological principle only minimally. The functions f_0^\pm must be joined smoothly to f_1 at some point $x_0 \in [0, 1]$; the joint function will be an approximate radial wavefunction for the vacuum state.

Beginning with the hyperbolic sine first, let us consider the radial wavefunction

$$f(x) = \begin{cases} \sinh(\sigma_0 x)/x & \text{if } 0 \leq x \leq x_0 \\ A/x + B & \text{if } x_0 \leq x \leq 1, \end{cases} \quad (42)$$

up to an overall normalisation factor $N(x_0)$. Dropping terms of order $\exp(-\sigma_0 x_0)$ and higher (this approximation is totally justified due to the sheer size of $\sigma_0 = 10^{123}$. For this approximation to break down, one would have to go to a regime where $\sigma_0 x_0 \simeq O(1)$, or equivalently, $x_0 \simeq 10^{-123}$. In turn, this would imply that the exponential part of the wavefunction should be strongly suppressed in favour of the term $A/x + B$. This, however, would be incompatible with the Hubble expansion), the matching conditions that f and its derivative f' be continuous at x_0 yield

$$A = -\frac{x_0 \sigma_0}{2} \exp(\sigma_0 x_0), \quad B = \frac{\sigma_0}{2} \exp(\sigma_0 x_0), \quad (43)$$

while for the normalisation factor $N(x_0)$ of f we find

$$N(x_0) = \frac{\sqrt{12} \sigma_0^{-1} \exp(-\sigma_0 x_0)}{(1 - x_0)^{3/2}}. \quad (44)$$

Equation (44) is singular at $x_0 = 1$; this results from dropping subdominant terms. Had we dropped *no* subdominant terms at all, then $N(x_0 = 1)$ would be perfectly regular. We can now compute the expectation value $\langle \mathcal{S}_g \rangle = \mathcal{N} k_B \sigma_0 \langle x^2 \rangle$ as a function of the matching point x_0 . We find

$$\langle x^2 \rangle(x_0) = \langle f | x^2 | f \rangle(x_0) = \frac{1}{10} (x_0^2 + 3x_0 + 6), \quad (45)$$

which no longer exhibits any singularity, since $\langle x^2 \rangle(x_0 = 1) = 1$. Some other values are

$$\langle x^2 \rangle(x_0 = 0.9) = 0.95, \quad \langle x^2 \rangle(x_0 = 0.5) = 0.77, \quad \langle x^2 \rangle(x_0 = 0.1) = 0.63. \quad (46)$$

This result is easily interpreted: the Hubble potential drives an exponential expansion that causes the Universe to concentrate mostly around the boundary at $x = 1$, even if the matching point x_0 is close to the origin. At the other end, when $x_0 = 1$, the corresponding entropy equals

$$\frac{\langle \mathcal{S}_g \rangle}{k_B} = \sigma_0 \langle x^2 \rangle = 10^{123}, \quad (47)$$

in complete agreement with the perturbative results of Section 2.2. In particular, the holographic bound continues to be saturated in this nonperturbative approach. The effect of having $x_0 < 1$ reduces this value somewhat, and the holographic bound is no longer saturated. However, the reduction thus attained is negligible, far from the necessary $\sim 10^{-19}$ that would be required to bring the entropy from the holographic bound $\sim 10^{123}$ down to its estimated value $\sim 10^{104}$ [28–31].

One readily verifies that Equations (45) and (47) continue to hold if one replaces the hyperbolic sine with a hyperbolic cosine in the wavefunction (42).

2.4. Concluding Remarks

In all three approaches considered here (perturbative using plane waves, perturbative using spherical waves, nonperturbative using approximate radial wavefunctions), we have abstained from applying boundary conditions to the wavefunction ψ . An obvious boundary condition to impose would be the vanishing of the wavefunction at R_0 , the boundary surface of the Universe. Now, requiring $\psi(R_0) = 0$ would quantise the allowed energy levels. This represents no problem per se, but it creates some difficulties without actually improving our analysis. One expects the quantised

energy levels to be so densely packed that, for all practical purposes, they will be indistinguishable from a continuous energy spectrum. On the other hand, the boundary condition $\psi(R_0) = 0$ reduces the two linearly-independent solutions of the Schrödinger equation to just one. For example, instead of the plane waves (10), one would now have a sinusoidal wave vanishing at R_0 , plus all of its higher harmonics. We do not gain much by this, but we *do* lose some consistency, because sinusoidal waves (as opposed to the complex exponentials (10)) no longer satisfy the cosmological principle. Analogous arguments hold in the cases of the spherical waves (11) and the hyperbolic functions (42). Altogether, these considerations justify *not* applying boundary conditions.

The dimensionless parameters λ_0 and σ_0 (Equations (29) and (37)) carry opposite signs—they have to, as λ_0 is the energy of the groundstate of a negative potential, while σ_0 is its corresponding entropy. However, they have the same absolute value. Given the physical constants at our disposal, σ_0 is the only (dimensionless) entropy and λ_0 is the only (dimensionless) energy that one can construct (up to dimensionless factors which our analysis cannot determine). So, the equality $\sigma_0 = -\lambda_0$ is inevitable. In turn, this equality reflects a physical property, namely: the equality of gravitational equipotential surfaces and isoentropic surfaces as dictated by the emergent spacetime scenario of Reference [12], used here.

One could turn the argument around and try to reason as follows. Starting from a knowledge of the actual entropy of the Universe $\sigma \sim 10^{104}$, one derives the radial wavefunction describing this nonmaximally entropic Universe: one simply substitutes the dimensionless eigenvalue $\lambda = -\sigma = -10^{104}$ into the eigenfunctions (24) and (25). Call the latter $\psi_{10^{104}}^{(j)}$ as in Equation (27). The expectation value of R^2 in the states $\psi_{10^{104}}^{(j)}$ should give back the initial entropy 10^{104} .

However, the above logic is flawed, because the eigenfunctions $\psi_{10^{104}}^{(j)}$ violate the cosmological principle substantially—and not just minimally, as argued in Section 2.3.1. We can get an idea of the order of magnitude of this violation. The *radius* R of the Universe described by $\psi_{10^{104}}^{(j)}$ can be inferred from Equation (36): write $\sigma = mH_0R^2/\hbar$, with R replacing R_0 , and solve for R . We find $R = 8 \times 10^{16}$ m—a far cry from the actual radius of the Universe, $R_0 = 4 \times 10^{26}$ m.

The notion of the emergence of spacetime put forward in Reference [12] demands that if the holographic bound is not to be saturated, then the quantum state of the Universe must be an excited state instead of the vacuum—it is only in a state of maximal entropy that minimal energy can be attained. Moreover, this must happen compatibly with the cosmological principle. Due to the limitations of our approach (the Newtonian approximation), the Universe described by our wavefunctions of Sections 2.2 and 2.3 has more entropy than necessary. On the positive side, the Universe described by our wavefunctions complies with the cosmological principle, with the holographic bound, and with the basic assumptions of emergent spacetime (*forces are entropy gradients*) put forth in Reference [12].

3. Discussion

In the nonrelativistic approximation, the cosmological fluid can be very conveniently described à la Madelung by separating the wavefunction of the matter contents of the Universe into amplitude and phase. This observation opens the gate to the application of quantum mechanics in order to obtain estimates of thermodynamical quantities of the Universe, such as the gravitational entropy.

In Section 2.2, we have carried out a perturbative computation. This perturbative analysis is based on a set of free wavefunctions which one uses to evaluate the expectation value of the Hubble potential. The nonperturbative computation performed in Section 2.3 is based on a set of interacting wavefunctions, obtained by solving the Schrödinger equation corresponding to the Hubble potential.

Both the perturbative and the nonperturbative analysis yield the same result: our estimates (16) and (47) saturate the upper bound established by the holographic principle [26]. Some estimates [28–31] place $\langle \mathcal{S}_g \rangle / k_B$ at around 10^{104} . While a somewhat lower value of our entropy would clearly be desirable, the fact is that the upper bound set by the holographic principle is respected by all of our

results. We are inclined to believe that the Newtonian approximation applied throughout is responsible for this saturation of the holographic bound, and that a fully relativistic treatment [18] will provide the necessary refinements that will reduce our entropy down to values better fitting with current estimates. Moreover, it is very rewarding to see the precise value of the holographic bound encoded in the wave equation as the parameter σ_0 (see Equations (36) and (37)). This means that our crude model bears an element of truth.

Our analysis can be regarded as a quantum-mechanical application of the theory of emergent spacetime presented in the celebrated paper [12]. We have made decisive use of the property of *emergence*, both of classical spacetime and of quantum theory. As concerns spacetime, the emergent property is used when regarding gravitational equipotentials as isoentropic surfaces. Concerning quantum theory, emergence is used when regarding the wavefunction amplitude as the exponential of the (matter) entropy, as dictated by Boltzmann's principle.

Admittedly, the assumptions made throughout automatically put black holes beyond our scope. Black holes are supposed to be the largest single contributors to the entropy budget of the Universe. Whether or not quantum mechanics as we know it remains applicable to black holes is of course a disputed question [30,31]. This understood, we would like to point out that our estimate is based on a *dynamical* model—a feature which, to the best of our knowledge, is entirely new.

Acknowledgments: It is a great pleasure to thank Sarira Sahu, Daniele Tommasini and Joan Vázquez Molina for interesting technical discussions. This research was supported by grant no. ENE2015-71333-R (Spain).

Author Contributions: All authors contributed equally to this paper. All authors have read and approved the final manuscript.

Conflicts of Interest: The authors declare no conflict of interest.

References

1. Adler, S. *Quantum Theory as an Emergent Phenomenon*; Cambridge University Press: Cambridge, UK, 2004.
2. Cabrera, D.; de Córdoba, P.F.; Isidro, J.M.; Vázquez Molina, J. Entropy, Topological Theories and Emergent Quantum Mechanics. *Entropy* **2017**, *19*, 87.
3. Cabrera, D.; Fernández de Córdoba, P.; Isidro, J.M. Amplitude, Phase, and Complex Analyticity. *arXiv* **2017**, arXiv:1702.06440.
4. Elze, H.-T. Symmetry Aspects in Emergent Quantum Mechanics. *J. Phys. Conf. Ser.* **2009**, *171*, 012034.
5. Fernández de Córdoba, P.; Isidro, J.M.; Vázquez Molina, J. Schroedinger vs. Navier–Stokes. *Entropy* **2016**, *18*, 34.
6. orromé, R.G. A Theory of Emergent Quantum Mechanics. *arXiv* **2014**, arXiv:1402.5070.
7. Khrennikov, A. Generalizations of Quantum Mechanics Induced by Classical Statistical Field Theory. *Found. Phys. Lett.* **2005**, *18*, 637.
8. Padmanabhan, T. General Relativity from a Thermodynamic Perspective. *Gen. Relativ. Grav.* **2014**, *46*, 1673.
9. Padmanabhan, T. Emergent Gravity Paradigm: Recent Progress. *Mod. Phys. Lett. A* **2015**, *30*, 1540007.
10. Padmanabhan, T. Gravity and/is Thermodynamics. *Curr. Sci.* **2015**, *109*, 2236.
11. Padmanabhan, T. The Atoms of Space, Gravity and the Cosmological Constant. *Int. J. Mod. Phys.* **2016**, *D25*, 1630020.
12. Verlinde, E. On the Origin of Gravity and the Laws of Newton. *JHEP* **2011**, *1104*, 029.
13. Eddington, A. *The Expanding Universe*; Cambridge Science Classics Series; Cambridge University Press: Cambridge, UK, 1987.
14. Hubble, E. A Relation between Distance and Radial Velocity among Extra–Galactic Nebulae. *Proc. Natl. Acad. Sci. USA* **1929**, *15*, 168.
15. Perlmutter, S.; Aldering, G.; Deustua, S.; Fabbro, S.; Goldhaber, G.; Groom, D.E.; Kim, A.G.; Kim, M.Y.; Knop, R.A.; Nugent, P.; et al. Cosmology from Type Ia Supernovae. *Bull. Am. Astron. Soc.* **1997**, *29*, 1351.
16. Riess, A.G.; Filippenko, A.V.; Challis, P.; Clocchiatti, A.; Diercks, A.; Garnavich, P.M.; Gilliland, R.L.; Hogan, C.J.; Jha, S.; Kirshner, R.P.; et al. Observational Evidence from Supernovae for an Accelerating Universe and a Cosmological Constant. *Astron. J.* **1998**, *116*, 1009.
17. Weinberg, S. *Cosmology*; Oxford University Press: Oxford, UK, 2008.

18. Cabrera, D.; Fernández de Córdoba, P.; Isidro, J.M. Boltzmann Entropy of the FLRW Universe. in preparation.
19. De Witt, B. Quantum Theory of Gravity. I. The Canonical Theory. *Phys. Rev.* **1967**, *160*, 1113.
20. Matone, M. Equivalence Postulate and Quantum Origin of Gravitation. *Found. Phys. Lett.* **2002**, *15*, 311.
21. Broadbridge, P. Problems in the Quantization of Quadratic Hamiltonians. *Hadron. J.* **1981**, *4*, 899.
22. Broadbridge, P.; Zulkowski, P. Dark Energy States from Quantization of Boson Fields in a Universe with Unstable Modes. *Rep. Math. Phys.* **2006**, *57*, 27.
23. Martínez-Merino, A.; Obregón, O.; Ryan, M. Newtonian Black Holes: Particle Production, “Hawking” Temperature, Entropies and Entropy Field Equations. *arXiv* **2016**, arXiv:1611.09654.
24. Matone, M. ‘Thermodynamique Cachée des Particules’ and the Quantum Potential. *Ann. Fond. Broglie* **2012**, *37*, 177, arXiv:1111.0270.
25. Planck Collaboration. Planck 2015 Results. XIII. Cosmological Parameters. *arXiv* **2015**, arXiv:1502.01589.
26. Bousso, R. The Holographic Principle. *Rev. Mod. Phys.* **2002**, *74*, 825.
27. Lebedev, N. *Special Functions and their Applications*; Dover Publications: New York, NY, USA, 1972.
28. Egan, C.; Lineweaver, C. A Larger Estimate of the Entropy of the Universe. *Astroph. J.* **2010**, *710*, 1825.
29. Frampton, P.; Hsu, S.; Kephart, T.; Reeb, D. What is the Entropy of the Universe? *Class. Quant. Grav.* **2009**, *26*, 145005.
30. Penrose, R. *The Road to Reality*; Jonathan Cape: London, UK, 2004.
31. Penrose, R. Black Holes, Quantum Theory and Cosmology. *J. Phys. Conf. Ser.* **2009**, *174*, 012001.



© 2017 by the authors. Licensee MDPI, Basel, Switzerland. This article is an open access article distributed under the terms and conditions of the Creative Commons Attribution (CC BY) license (<http://creativecommons.org/licenses/by/4.0/>).

Article

Entropy, Topological Theories and Emergent Quantum Mechanics

D. Cabrera, P. Fernández de Córdoba, J. M. Isidro * and J. Vazquez Molina

Instituto Universitario de Matemática Pura y Aplicada, Universidad Politécnica de Valencia, 46022 Valencia, Spain; dacabur@upvnet.upv.es (D.C.); pfernandez@mat.upv.es (P.F.d.C.); joavzmo@doctor.upv.es (J.V.M.)

* Correspondence: joissan@mat.upv.es; Tel.: +34-96-387-70-00

Academic Editors: Kevin H. Knuth and Giorgio Kaniadakis

Received: 29 November 2016; Accepted: 21 February 2017; Published: 23 February 2017

Abstract: The classical thermostatics of equilibrium processes is shown to possess a quantum mechanical dual theory with a finite dimensional Hilbert space of quantum states. Specifically, the kernel of a certain Hamiltonian operator becomes the Hilbert space of quasistatic quantum mechanics. The relation of thermostatics to topological field theory is also discussed in the context of the approach of the emergence of quantum theory, where the concept of entropy plays a key role.

Keywords: emergence of quantum theory; topological field theory

1. Motivation

The approach of the emergence of quantum mechanics has provided interesting clues into the deeper structure of the theory. The statement that *standard quantum mechanics is an emergent phenomenon* [1–4] has found further support in a series of papers, some of which have been reviewed in Reference [5]. Although this is a huge topic to summarize here, let us briefly mention some key points of this approach. The underlying notion is that it provides a coarse-grained version of some deeper theory, out of which quantum mechanics emerges as a kind of effective description. This effective description—in using variables that arise as averages over large collections of individual entities carrying the truly fundamental degrees of freedom—ignores the underlying fine structure. These fundamental degrees of freedom have been identified in References [3,4] as those of cellular automata.

This state of affairs is reminiscent of the relation between thermodynamics (as an emergent phenomenon) and statistical mechanics (the corresponding underlying theory). Based on this analogy, we have in previous publications (see [5] and references therein) established a bijective map that one can define between quantum mechanics, on the one hand, and the classical thermodynamics of irreversible processes, on the other [6,7]. It must be stressed that the classical thermodynamics of irreversible processes [6,7] is conceptually quite different from the usual *thermostatics of equilibrium* as presented in the standard textbooks [8]. Specifically, in the theory of irreversible processes, the continual production of entropy provides a rationale for the dissipation—or information loss—that has been argued to lie at the heart of quantum mechanics [3,4]. The relevance of thermodynamical concepts to quantum theory and gravity has been emphasized recently in references [9–13].

It might thus appear that the usual quasistatic thermodynamics [8] (i.e., the thermostatics of equilibrium processes) possesses no quantum mechanical dual theory at all. In this letter, we point out that such a conclusion is not true: the thermostatics of equilibrium processes *does* have a quantum mechanical dual; namely, a *quasistatic quantum mechanics*. By *quasistatic*, we mean that the kinetic term in the mechanical Lagrangian can be neglected compared to the potential term.

Neglecting the kinetic term in the Lagrangian function forces one to look elsewhere for the dissipative mechanism that is characteristic of quantum theory [3,4]. In particular, such a mechanism

can no longer be identified with the continual production of entropy associated with Onsager's kinetic term $L_{ij}\dot{q}^i\dot{q}^j$. The reciprocity theorem [6] ensures $L_{ij} = L_{ji}$, and dissipation requires that this matrix be positive definite; the latter two properties ensure that L_{ij} qualifies as a metric. The result of neglecting the kinetic term in the Lagrangian is a mechanics bearing some resemblance to topological field theory [14]. Indeed, once the metric represented by the kinetic term is neglected, correlation functions can no longer be metric dependent. Hence, while correlators can still depend on the topology of the underlying manifold, they can no longer depend on its metric structure. In our case, the underlying manifold will be given by the equipotential submanifolds (within configuration space) of the potential function.

2. A Quasistatic Mechanics

A quasistatic mechanics is obtained by neglecting the kinetic term K in the mechanical Lagrangian $L = K - U$, and keeping only the potential term U :

$$L = -U. \quad (1)$$

Since our Lagrangian does not depend on the velocities \dot{q} , this phase space is constrained by the requirement that all momenta vanish, $p = 0$, and the Hamiltonian equals

$$H = U. \quad (2)$$

We can now construct the reduced phase space corresponding to this reduced configuration space, and eventually quantise it (for our purposes, it will not be necessary to apply Dirac's theory of constrained quantisation [15]). When moving along equipotential submanifolds, the particle is effectively free; whenever motion takes place between neighbouring equipotentials, forces will cause the particle's kinetic energy to increase or decrease. However, the allowed motions must be quasistatic, so even for these motions, K must be negligible compared to U . In classical mechanics, motion along equipotential submanifolds plus a vanishing kinetic energy imply that a classical particle must forever stay at rest. Quantum mechanically, due to the uncertainty principle, a (more or less localised) free particle always carries a nonzero kinetic energy. So, neglecting the kinetic energy of a quantum particle implies a large uncertainty in the position. This large uncertainty is reflected in a large spread of the corresponding wavepacket: the latter encompasses a large interval of different classically allowed positions (or states), all of which coalesce into a single quantum state. It is only in the limit of complete delocalisation in space that a quantum particle can carry zero kinetic energy.

We have just described an information loss mechanism whereby different classical states (different spatial positions on an equipotential submanifold, corresponding to different classically allowed equilibrium states) are lumped together into just one quantum state. This information loss has been argued to be a key feature of the quantum world.

3. The Thermostatistics Dual to Quasistatic Mechanics

We claim that *the quasistatic quantum mechanical model described in Section 2 possesses a dual theory: the classical thermostatistics of equilibrium processes*. In what follows, we will exhibit the claimed duality explicitly.

The classical thermostatistics of equilibrium [8] is a theory of quasistatic processes. In particular, all kinetic energies are neglected; the processes described are either in thermal equilibrium, or at most differ infinitesimally from thermal equilibrium. This feature is in sharp contrast with the thermodynamics of irreversibility [6,7] that we described in previous publications [5] as a thermodynamical dual of quantum mechanics, *whenever the kinetic energies involved could not be neglected*.

Next we recall that classical thermostatistics is—like quantum mechanics—an emergent theory. By *emergent*, we mean that classical thermostatistics is the result of coarse graining over very many microscopic degrees of freedom; the resulting theory renounces the knowledge of detailed information

about its constituent degrees of freedom, retaining just a handful of relevant averages such as pressure, volume, and temperature. In other words, *an information loss mechanism is at work*. This situation is similar to that described in Section 2 for the passage from classical mechanics to quantum mechanics.

In the dual thermostatics considered here, the counterpart of the mechanical action $I = \int L dt$ is the entropy S . We will identify isoentropic submanifolds (of thermodynamical state space) with equipotential submanifolds (of mechanical state space). This is justified because in the approach of emergence, *forces are (proportional to) entropy gradients*. In the particular case of the gravitational force, this identification has been put forward in reference [16]; it coincides with the viewpoint applied in the theory of irreversibility [7], and indeed with the whole programme of the emergent physics paradigm. In this way, the quantum mechanical exponential

$$\exp\left(-\frac{i}{\hbar}I\right) \quad (3)$$

becomes, in the dual thermostatics,

$$\exp\left(\frac{S}{k_B}\right). \quad (4)$$

The correspondence between expressions (3) and (4) has been known for a long time, having been discussed more recently in reference [9] from the point of view of statistical mechanics. However, we would like to stress that the theory being considered here as dual to quantum mechanics is *not* statistical mechanics, but the thermostatics of equilibrium emerging from the latter.

Finally, the connection between the mechanical time variable t and the temperature T is as follows (this substitution is widely applied in thermal field theory; e.g., [17]):

$$\frac{i}{\hbar}t \longleftrightarrow -\frac{1}{k_B T}, \quad (5)$$

where \hbar and k_B are Planck's constant and Boltzmann's constant, respectively. The double arrow is to be understood as *replace every occurrence of i/\hbar in the mechanical theory with $-1/k_B T$ in the thermostatical dual, and vice versa*. Quasistatic mechanics therefore corresponds to isothermal processes in the dual thermostatics.

4. The Quasistatic Mechanics Dual to Thermostatics

Given some specific thermostatical systems, below we illustrate how to define their corresponding (quasistatic) quantum mechanical duals.

4.1. The Ideal Gas

An expression for the entropy of a system in terms of its thermodynamical variables is called a *fundamental equation* for the system [8]. To be specific, let us consider 1 mole of an ideal gas occupying a volume V at a fixed temperature T . Its fundamental equation reads

$$S(V) = S_0 + k_B \ln\left(\frac{V}{V_0}\right), \quad (6)$$

where S_0 is the entropy in the fiducial state specified by V_0 ; we take S_0 to contain a constant contribution from the fixed temperature T . The entropy depends only on the volume V ; the latter, running over $(0, \infty)$, can be regarded as the thermodynamical coordinate for the *isothermal* processes of an ideal gas.

In order to construct a kinetic energy operator K for the quantum theory, the standard rule is

$$K: = -\frac{\hbar^2}{2M}\nabla^2, \quad (7)$$

where ∇^2 is the Laplacian operator on functions. By definition, the Laplacian requires a metric g_{ij} :

$$\nabla^2 = \frac{1}{\sqrt{g}} \partial_i \left(\sqrt{g} g^{ik} \partial_k \right), \quad g = |\det(g_{ij})|. \quad (8)$$

The fundamental Equation (6) provides us with a clue as to which metric can be meaningfully chosen. We first observe that Equation (6) is valid in three-dimensional space, where the volume V scales like r^3 ; here r, θ, φ are spherical coordinates. This suggests using the Euclidean metric in \mathbb{R}^3 ,

$$ds^2 = dr^2 + r^2 d\theta^2 + r^2 \sin^2 \theta d\varphi^2, \quad (9)$$

and imposing the following two requirements. First, motion along the radial direction r must cause an increase or decrease of the entropy, as per the fundamental Equation (6), with $V = 4\pi r^3/3$; second, the sphere $r = r_0$ must define an isoentropic surface for each r_0 .

Further support for our argument follows from a classic result by H. Weyl: (we quote this result from reference [18]): let $R \subset \mathbb{R}^3$ be a bounded region with piecewise smooth boundary, and let $V(R) = \int_R \sqrt{g} d^3x$ denote its volume with respect to some Riemannian metric on \mathbb{R}^3 . Then, the eigenvalue equation for the Laplacian on R , $\nabla^2 f = \lambda f$, supplemented with some mild boundary conditions, has a countable infinity of real eigenvalues λ_n satisfying $0 \geq \lambda_1 \geq \lambda_2 \geq \lambda_3 \geq \dots$. These eigenvalues can be arranged into a partition function $Z(t)$,

$$Z(t) := \text{Tr} \exp \left(t \nabla^2 \right) = \sum_{n=1}^{\infty} \exp (t \lambda_n), \quad (10)$$

and it turns out that the small t asymptotics of $Z(t)$ is given by

$$Z(t) \simeq \frac{V(R)}{(4\pi t)^{3/2}}, \quad t \rightarrow 0. \quad (11)$$

An analogous result holds within \mathbb{R}^d (it is not necessary to assume that $d = 3$; it is not necessary that the metric be the Euclidean one; it is also not necessary to assume that R is a sphere). However, the Euclidean assumption is suggested by the fundamental Equation (6), while the assumption of spherical symmetry (in no way imposed by the ideal gas) provides a welcome simplification. *The volume V occupied by the ideal gas within Euclidean space is naturally related to the spectrum of the Laplacian operator within (and on the boundary surface of) V .*

We will initially define the Hilbert space \mathcal{H} of *quasistatic quantum mechanics* as the space of those states that minimise the expectation value of the kinetic energy, subject to the constraint that they be normalised (plus some boundary conditions to be specified below). Thus, introducing a Lagrange multiplier $-\lambda \in \mathbb{R}$, we need to solve

$$\frac{\delta}{\delta|\psi\rangle} (\langle\psi|K|\psi\rangle - \lambda\langle\psi|\psi\rangle) = 0, \quad \langle\psi|\psi\rangle = 1. \quad (12)$$

Since K is selfadjoint, Equation (12) leads to

$$K|\psi\rangle = \lambda|\psi\rangle, \quad (13)$$

so the Hilbert space \mathcal{H} is initially defined as

$$\mathcal{H} := \text{Ker} (K - \lambda_{\min}), \quad (14)$$

where λ_{\min} is the minimal kinetic energy; we have seen that $\lambda \geq 0$. We will presently see how the inclusion of a potential function U affects the definition (14) of the Hilbert space.

4.2. Motion along Isoentropic Surfaces

We first analyse motion along a given isoentropic surface, which we take to be the unit sphere S^2 . The angular part $\nabla_{S^2}^2$ of the Laplacian operator on \mathbb{R}^3 leads to the kinetic energy operator K_{S^2} :

$$K_{S^2}\psi := -\frac{\hbar^2}{2M}\nabla_{S^2}^2\psi = -\frac{\hbar^2}{2M}\frac{1}{\sin\theta}\left[\frac{\partial}{\partial\theta}\left(\sin\theta\frac{\partial\psi}{\partial\theta}\right) + \frac{1}{\sin\theta}\frac{\partial^2\psi}{\partial\varphi^2}\right]. \quad (15)$$

Within the space $L^2(S^2)$, the eigenvalues λ of Equation (13) are $\hbar^2 l(l+1)/(2M)$, with $l \in \mathbb{N}$; the least kinetic energy for motion on S^2 corresponds to the zeroth spherical harmonic $Y_{00} = (4\pi)^{-1/2}$:

$$K_{S^2}Y_{00} = 0. \quad (16)$$

The corresponding particle is completely delocalised on S^2 , as befits the fact that its momentum vanishes exactly. The Hilbert space \mathcal{H}_{S^2} is defined as the linear span of the spherical harmonic Y_{00} ; i.e.,

$$\mathcal{H}_{S^2} = \text{Ker}\left(\nabla_{S^2}^2\right). \quad (17)$$

On a compact connected manifold, the only harmonic functions are the constants; the specific value $(4\pi)^{-1/2}$ is determined by normalisation. Although we have computed $\dim \mathcal{H}_{S^2}$ explicitly, the finite dimensionality of $\text{Ker}\left(\nabla_{S^2}^2\right) \subset L^2(S^2)$ was already guaranteed on the basis of general results concerning the theory of elliptic operators on compact Riemannian manifolds [19] (in this particular case, one can more simply apply the Hodge theorem [20]: since the 2-sphere S^2 is a compact orientable Riemannian manifold, we have

$$\dim \text{Ker}\left(\nabla_{S^2}^2\right) = b^0(S^2) = 1,$$

where b^0 is the zeroth Betti number of the manifold in question). A finite dimensional Hilbert space is a feature of many topological theories [14]: although a metric was initially required to define a Laplacian operator, the metric dependence is softened in the end, through the requirement of quasistaticity (12).

Finally, we can add a potential function $U = U(r)$ depending only on the radial variable r , and the previous arguments remain entirely valid. We then get back to the situation described in Section 2: a particle moving quasistatically along the equipotential submanifolds of a certain potential.

4.3. Motion across Isoentropic Surfaces

Next, we analyse motion across isoentropic surfaces. The radial part ∇_r^2 of the Laplacian operator on \mathbb{R}^3 gives rise to the kinetic energy operator K_r :

$$K_r\psi := -\frac{\hbar^2}{2M}\nabla_r^2\psi = -\frac{\hbar^2}{2M}\left(\frac{d^2\psi}{dr^2} + \frac{2}{r}\frac{d\psi}{dr}\right). \quad (18)$$

By Equations (13) and (18), we need to solve

$$\frac{d^2\psi}{dr^2} + \frac{2}{r}\frac{d\psi}{dr} + c^2\psi = 0, \quad c^2 := \frac{2M\lambda}{\hbar^2} \geq 0; \quad (19)$$

a fundamental set of solutions is $\{\psi_{\pm}(r) = r^{-1}\exp(\pm icr)\}$. A vanishing kinetic energy is attained when $c = 0$. However, the corresponding wavefunction, $\psi(r) = 1/r$, is neither regular at $r = 0$, nor square integrable over the interval $(0, \infty)$. Imposing regularity of $\psi(r)$ at $r = 0$, one is left with the wavefunctions

$$\psi(r) = \frac{1}{r}\sin(cr), \quad (20)$$

while the wavenumber $c \in \mathbb{R}$ remains undetermined. We can determine c if we recall the relation between the squared wavefunction $|\psi|^2$ and the entropy [5]:

$$|\psi|^2 = \exp\left(\frac{S}{k_B}\right). \quad (21)$$

Collecting different microstates into a single pure quantum state is reminiscent of Von Neumann's density matrix formulation of the entropy of a mixed quantum state. However, even a pure state embodies a probability distribution; the latter has an associated Shannon entropy. The entropy of a pure state is not monotonic in time under Schrödinger evolution; this problem remains unsolved.

Let r_0 be the radius of the fiducial sphere in Equation (6). When evaluated at $r = r_0$, Equation (21) becomes (by Equation 20),

$$\frac{1}{r_0} \sin(cr_0) = \exp\left(\frac{S_0}{2k_B}\right). \quad (22)$$

Now the sine function is bounded between -1 and $+1$. This requires fine tuning the value of the fiducial entropy S_0 as a function of the fiducial radius r_0 , or vice versa, if Equation (22) is to have a real solution for c . The simplest choice is to formally set $S_0 = -\infty$. This choice has the added bonus that Equation (22) admits real solutions for c , without the need to fine-tune r_0 as a function of S_0 ; it corresponds to imposing the additional boundary condition $\psi(r_0) = 0$. Then, the admissible eigenfunctions, with their corresponding wavenumbers $c_n \in \mathbb{R}$, are given by

$$\psi_n(r) = \sqrt{\frac{2}{r_0}} \frac{1}{r} \sin(c_n r), \quad c_n = \frac{n\pi}{r_0} \quad n = 1, 2, \dots \quad (23)$$

We have normalised ψ_n within $L^2([0, r_0])$.

The least kinetic energy is attained when $n = 1$. Therefore, we define the Hilbert space \mathcal{H}_r as the kernel

$$\mathcal{H}_r = \text{Ker}\left(\nabla_r^2 + c_1^2\right). \quad (24)$$

This one-dimensional space is generated by the wavefunction $\psi_1(r)$. More generally, the finite dimensionality of $\text{Ker}\left(\nabla_r^2 + c_n^2\right) \subset L^2([0, r_0])$ for all $n = 1, 2, \dots$ is guaranteed by the theory of elliptic operators on compact Riemannian manifolds [19].

So far, the total Hilbert space \mathcal{H} is the tensor product of the spaces (17) and (24):

$$\mathcal{H} = \mathcal{H}_{S^2} \otimes \mathcal{H}_r. \quad (25)$$

We have up to now considered a free particle. If a potential function $U(r)$ is included, then the Hilbert space (24) must be redefined to be

$$\mathcal{H}_r = \text{Ker}\left(-\frac{\hbar^2}{2M} \nabla_r^2 - \frac{\hbar^2}{2M} c_1^2 + U(r)\right), \quad (26)$$

and the latter substituted back into Equation (25). The above kernel remains finite dimensional. This is because the addition of $U(r)$ does not alter the ellipticity of the Hamiltonian; hence, general theorems concerning the spectrum of elliptic operators on compact Riemannian manifolds continue to apply [19]. Of course, the presence of a potential on the quantum mechanical side modifies the fundamental Equation (6) of the corresponding thermostatics.

We close this section with some remarks.

- (i) The compact configuration space $[0, r_0] \times S^2$ has the advantage that, due to energy quantisation, one can univocally identify a *nonvanishing* state of least kinetic energy. On the noncompact

configuration space $[0, \infty) \times S^2$, the allowed energy eigenvalues run over $[0, \infty)$, and no *nonvanishing* state of least energy exists.

- (ii) Results analogous to those presented above would continue to hold if the free quantum particle were placed in a cubic box of volume L^3 , with vanishing boundary conditions for the wavefunction on the sides of the cube. The use of Cartesian coordinates renders isoentropic surfaces (now cubes) somewhat clumsier to work with than spheres, but the expectation value of the entropy (see Equation 28 below) remains metric independent, and also the Hilbert space continues to be one-dimensional.
- (iii) Analogous results would also hold if we worked in d -dimensional Euclidean space \mathbb{R}^d , viz: finite dimensionality of the Hilbert space, and metric independence of the expectation of the entropy.

4.4. A Metric Free Entropy

It is instructive to compute the expectation value of the entropy in the state (23). We set $V = 4\pi r^3/3$, $V_0 = 4\pi r_0^3/3$, and write the quantum mechanical operator corresponding to the classical entropy of Equation (6) as

$$\hat{S}(r) = S_0 + 3k_B \ln \left(\frac{\hat{r}}{r_0} \right). \tag{27}$$

The carets are meant to indicate quantum operators. Subtracting the infinite constant S_0 one finds an expectation value of the entropy

$$\langle \psi_n | \hat{S} | \psi_n \rangle = 3k_B \int_0^{r_0} r^2 |\psi_n(r)|^2 \ln \left(\frac{r}{r_0} \right) dr = 3k_B \left(\frac{\text{Si}(2\pi n)}{2\pi n} - 1 \right), \tag{28}$$

where $\text{Si}(x) := \int_0^x t^{-1} \sin t dt$ is the sine integral function. In particular, *all terms depending on r_0 drop out of Equation (28)*. This is in perfect agreement with the topological character [14] of our model: the entropy cannot depend on the radius r_0 of the fiducial sphere, because the latter requires a metric for its definition.

4.5. The Quantum Mechanical Partition Function

The quantum mechanical partition function $Z_{\text{qm}}(t)$ is defined by

$$Z_{\text{qm}}(t) = \sum_n \dim \mathcal{H}_n \exp \left(-\frac{i}{\hbar} E_n t \right), \tag{29}$$

where \mathcal{H}_n is the Hilbert eigenspace corresponding to the energy eigenvalue E_n . The above sum is usually divergent, but it can be made to converge by Wick rotating the time variable as per

$$Z_{\text{qm}}(\tau) = \sum_n \dim \mathcal{H}_n \exp \left(-\frac{1}{\hbar} E_n \tau \right). \tag{30}$$

In the quasistatic limit, the above sum is dominated by the least energy eigenvalue, E_{min} , and $Z_{\text{qm}}(\tau)$ becomes $Z_{\text{qqm}}(\tau)$, the subindex “qqm” standing for *quasistatic quantum mechanics*:

$$Z_{\text{qqm}}(\tau) = \dim \mathcal{H}_{\text{min}} \exp \left(-\frac{1}{\hbar} E_{\text{min}} \tau \right). \tag{31}$$

Therefore,

$$Z_{\text{qqm}}(0) = \dim \mathcal{H}_{\text{min}}, \tag{32}$$

and the partition function of quasistatic quantum mechanics computes the dimension of the Hilbert space of quantum states; also a conclusion that is reminiscent of topological models [14].

5. Conclusions and Outlook

The application of differential and Riemannian geometry to the theory of thermodynamical fluctuations has turned out to be extremely useful [21–23]. Thus, for example, the classical thermodynamics of irreversible processes [6,7] requires a metric on phase space for its formulation. This metric is provided by Onsager's matrix of kinetic coefficients L_{ij} . The metric enters the quantum mechanical dual theory [5] through the kinetic term in the mechanical Lagrangian.

On the contrary, the thermostatics of equilibrium processes [8] is genuinely metric free. Therefore, if thermostatics is to possess any quantum mechanical dual at all, this dual theory should be a topological theory [14], in the sense that it should be metric independent.

That the classical thermostatics of equilibrium processes should possess a quantum mechanical dual is suggested by two observations. First, by the claim that quantum mechanics is an emergent phenomenon [1–5,24]. Second, by the widespread opinion that thermodynamics (be it of equilibrium [8] or nonequilibrium [6,7]) is the paradigm of all emergent sciences. These conclusions remain unaltered even if—as argued in reference [25]—the emergent aspects of quantum mechanics can only become visible at very high energies.

Two guiding principles are at work here: the notion that forces are entropy gradients, and the requirement that all processes be quasistatic. Entropy gradients, while defining a direction for evolution, ignore microscopic structures, retaining only coarse-grained averages: this is a feature of emergent phenomena. Ignoring the metric structure of the underlying manifold amounts to ignoring the kinetic term in the Lagrangian. Quantum mechanically, due to the uncertainty principle, the effects of the kinetic term cannot be cancelled completely, unless one accepts a complete delocalisation of the particle in space. The result of following these two guiding principles is a quasistatic quantum mechanics, which is dual to the classical thermostatics of equilibrium processes, and shares a number of key properties in common with topological (i.e., metric free) models.

After completion of this work, there appeared reference [26], where the WKB expansion of quantum mechanics is developed from the point of view of topological string theory [27]. Reference [26] provides further evidence of the existing links between topological theories and quantum mechanics. Some of these links have been analysed in the present paper, from the alternative standpoint of the approach of emergence of quantum theory; further connections are being studied in an upcoming publication [28].

Acknowledgments: Research supported by grant No. ENE2015-71333-R (Spain).

Author Contributions: All coauthors contributed equally to this article. All authors have read and approved the final manuscript.

Conflicts of Interest: The authors declare no conflict of interest.

References

1. Elze, H.-T. Multipartite Cellular Automata and the Superposition Principle. *Int. J. Quantum Inf.* **2016**, *14*, 1640001.
2. Elze, H.-T. Quantum Models as Classical Cellular Automata. *arXiv* **2016**, arXiv:1701.02252.
3. Hooft, G. The Mathematical Basis for Deterministic Quantum Mechanics. *J. Phys. Conf. Ser.* **2007**, *67*, 012015.
4. Hooft, G. The Cellular Automaton Interpretation of Quantum Mechanics. In *Fundamental Theories of Physics*; Springer: Berlin/Heidelberg, Germany, 2016; Volume 185.
5. Fernández de Córdoba, P.; Isidro, J.M.; Vazquez Molina, J. The Holographic Quantum. *Found. Phys.* **2016**, *46*, 787–803.
6. Onsager, L.; Machlup, S. Fluctuations and Irreversible Processes. *Phys. Rev.* **1953**, *91*, 1505.
7. Prigogine, I. *Introduction to Thermodynamics of Irreversible Processes*; Interscience: New York, NY, USA, 1961.
8. Callen, H. *Thermodynamics and an Introduction to Thermostatistics*; Wiley: New York, NY, USA, 1985.
9. Baez, J.; Pollard, B. Quantropy. *Entropy* **2015**, *17*, 772–789.

10. Matone, M. Thermodynamique Cachée des Particules' and the Quantum Potential. *Ann. Fond. Broglie* **2012**, *37*, 177–185.
11. Padmanabhan, T. Thermodynamical Aspects of Gravity: New Insights. *Rep. Prog. Phys.* **2010**, *73*, 046901.
12. Penrose, R. Black Holes, Quantum Theory and Cosmology. *J. Phys. Conf. Ser.* **2009**, *174*, 012001.
13. Svozil, K. Space and Time in a Quantized World. *Int. J. Theor. Phys.* **2015**, *54*, 4376–4385.
14. Birmingham, D.; Blau, M.; Rakowski, M.; Thompson, G. Topological Field Theory. *Phys. Rep.* **1991**, *209*, 129–340.
15. Dirac, P. *Lectures on Quantum Mechanics*; Dover: New York, NY, USA, 2001.
16. Verlinde, E. On the Origin of Gravity and the Laws of Newton. *J. High Energy Phys.* **2011**, doi:10.1007/JHEP04(2011)029.
17. Kapusta, J.; Gale, C. *Finite-Temperature Field Theory: Principles and Applications*; Cambridge University Press: Cambridge, UK, 2006.
18. McKean, H.; Singer, I. Curvature and the Eigenvalues of the Laplacian. *J. Differ. Geom.* **1967**, *1*, 43–69.
19. Schwarz, A. Quantum Field Theory and Topology. In *Grundlehren der Mathematischen Wissenschaften*; Springer: Berlin/Heidelberg, Germany, 2010; Volume 307.
20. Schwarz, A. Topology for Physicists. In *Grundlehren der Mathematischen Wissenschaften*; Springer: Berlin/Heidelberg, Germany, 1994; Volume 308.
21. Ruppeiner, G. Riemannian Geometry in Thermodynamic Fluctuation Theory. *Rev. Mod. Phys.* **1995**, *67*, 605.
22. Bravetti, A.; López-Monsalvo, C.; Nettel, F. Conformal Gauge Transformations in Thermodynamics. *Entropy* **2015**, *17*, 6150–6168.
23. Fernández de Córdoba, P.; Isidro, J.M. Generalised Complex Geometry in Thermodynamical Fluctuation Theory. *Entropy* **2015**, *17*, 5888–5902.
24. Smolin, L. Quantum Mechanics and the Principle of Maximal Variety. *arXiv* **2015**, arXiv:1506.02938.
25. Calmet, X. Quantum Mechanics, Gravity and Modified Quantization Relations. *Philos. Trans. R. Soc.* **2015**, *A373*, 20140244.
26. Codesido, S.; Mariño, M. Holomorphic Anomaly and Quantum Mechanics. *arXiv* **2016**, arXiv:1612.07687.
27. Mariño, M. Chern–Simons Theory, Matrix Models, and Topological Strings. In *International Series of Monographs on Physics*; Oxford University Press: Oxford, UK, 2005; Volume 131.
28. Cabrera, D.; Fernández de Córdoba, P.; Isidro, J.M. Amplitude, phase, and complex analyticity. *arXiv* **2017**, arXiv:1702.06440.



© 2017 by the authors. Licensee MDPI, Basel, Switzerland. This article is an open access article distributed under the terms and conditions of the Creative Commons Attribution (CC BY) license (<http://creativecommons.org/licenses/by/4.0/>).

ϕ meson transparency in nuclei from ϕN resonant interactionsD. Cabrera,¹ A. N. Hiller Blin,^{2,3} M. J. Vicente Vacas,² and P. Fernández de Córdoba¹¹*Instituto Universitario de Matemática Pura y Aplicada, Universidad Politécnica de Valencia, E-46022 Valencia, Spain*²*Instituto de Física Corpuscular, Universidad de Valencia–CSIC, Institutos de Investigación, Ap. Correos 22085, E-46071 Valencia, Spain*³*Institut für Kernphysik and PRISMA Cluster of Excellence, Johannes Gutenberg-Universität Mainz, D-55128 Mainz, Germany*

(Received 3 July 2017; published 22 September 2017)

We investigate the ϕ meson nuclear transparency using some recent theoretical developments on the ϕ in medium self-energy. The inclusion of direct resonant ϕN scattering and the kaon decay mechanisms leads to a ϕ width much larger than in most previous theoretical approaches. The model has been confronted with photoproduction data from CLAS and LEPS and the recent proton induced ϕ production from COSY finding an overall good agreement. The results support the need of a quite large direct ϕN -scattering contribution to the self-energy.

DOI: [10.1103/PhysRevC.96.034618](https://doi.org/10.1103/PhysRevC.96.034618)**I. INTRODUCTION**

The light vector meson properties in dense/hot nuclear matter have been intensively studied the last decades in the search, among others, of any signal of chiral symmetry restoration. A good review of the related physics can be found in Refs. [1,2]. These mesons are particularly appealing because their dileptonic decays can provide a relatively clean information of the nuclear medium interior as opposed to strong decays undergoing a sizable final state interaction before the detection of the decay products. In addition, the ϕ -meson width is very narrow in vacuum and is well separated from the ρ and the ω mesons what could help in the experimental analysis and allow for the measurement of any modifications of its mass or width.

Experimentally, ϕ production and its decays, both hadronic and electromagnetic, have been investigated in heavy ion collisions by the STAR and ALICE collaborations [3,4]. In cold nuclei, ϕ production has been studied at Spring8 [5], KEK [6], Jefferson Laboratory [7], and Jülich [8]. One of the findings is that, whereas the ϕ mass in the medium is scarcely modified if at all, the width is much larger than in vacuum [5–9]. Actually, the in-medium ϕ width seems to be substantially larger than predicted by most theoretical models.

This width is expected to come mostly from the decay $\phi \rightarrow K \bar{K}$, which is dominant in vacuum. The medium effects modifying it have been much studied [10–15] and involve a quite rich dynamics. In nuclear matter, the kaons are just mildly repelled and will move out of the nucleus. However, antikaons are attracted by the nuclear medium and can also be absorbed leading to hyperons and resonances such as $\Lambda(1405)$ and others. These mechanisms are instrumental leading to a large ϕ width. For instance, in Ref. [13], we obtain $\Gamma_\phi \approx 30$ MeV at normal nuclear density to be compared to 4 MeV in vacuum. Still, that result is not large enough to describe the experimental data. This failure has been the cause for a search for additional mechanisms which could contribute to the meson decay.

In Ref. [16], we explored the ϕ self-energy pieces related to some direct ϕ -nucleon interaction channels not previously

considered. There, ϕ -nucleon elastic scattering proceeds via K^* -hyperon loops which give rise to a self-energy with real and imaginary parts. Our work was based in some recent studies analyzing the vector meson scattering with baryons in two different schemes. Both models account for a relatively strong ϕ -nucleon interaction. As a consequence of these mechanisms the ϕ meson gets an additional broadening up to 40–50 MeV and a mild attraction at normal nuclear density. Our purpose here is to test the results of the model of Ref. [16] comparing with the available data and check whether a satisfactory description of the ϕ self-energy in cold nuclear matter has been reached. We will focus on its controversial imaginary part, or equivalently the ϕ width.

A direct extraction of the in-medium width via the analysis of the invariant mass of the decay products poses some difficulties. For instance, in Ref. [6] the dilepton channel was measured in carbon and copper nuclei for 12 GeV $p + A$ reactions. With this kinematics, most of the ϕ mesons move very fast in the forward direction and escape from the nucleus before decaying. As a consequence, the observed width is frequently the free one. Nonetheless, a clear broadening was observed for the heavier nucleus and when only the slower ϕ mesons were selected. On the other hand, the dominant decay channel, $\phi \rightarrow K \bar{K}$, presents some additional challenges related to the final state interaction. The strong antikaon absorption restricts the visibility of decays that happen at high densities far from the surface. Also the real part of the optical potential, including Coulomb, modifies the kaon trajectories and distorts the invariant mass of the system.

Another observable, sensitive to the imaginary part of the ϕ self-energy is the nuclear transparency ratio given by the quotient of the cross sections for ϕ production on nuclei and on a free nucleon. This quantity depends on the loss of flux in the medium and thus on the width of the ϕ meson and its density dependence. The transparency has been measured in photoproduction by the LEPS and CLAS collaborations [5,7]. This process had been suggested in Ref. [17] and was also studied in Ref. [9]. Transparency for the case of proton induced ϕ production is more complicated due to the initial state interaction of the proton beam that leads to some secondary

production mechanisms such as $pN \rightarrow \pi NN$ followed by $\pi N \rightarrow \phi N$. This process had been studied in Refs. [18–21] and has been recently measured at Jülich [8,22].

In this paper, we present a study of the ϕ nuclear transparency for both photon and proton induced production on nuclei using the theoretical model from Ref. [16]. We will start by giving a brief reminder of the ϕ self-energy model and introduce the formalism used in the calculation. Then we proceed to the comparison with the experimental data.

II. THEORETICAL MODEL

Two sources of ϕ self-energy in nuclear matter are considered here, the mechanisms related to the $K\bar{K}$ decay, that will be denoted as kaon cloud, and those coming from $\phi N \rightarrow \phi N$ resonant scattering mediated by hyperon + vector meson and other intermediate coupled channels.

In vacuum, the largest decay channel (83%) is $\phi \rightarrow K\bar{K}$. At leading order, the ϕ self-energy is obtained by evaluating $K(\bar{K})$ loop and tadpole diagrams. The nuclear medium effects are incorporated by properly dressing the kaon and antikaon propagators with their self-energies originating from the $KN(\bar{K}N)$ s - and p -wave interactions. Details on the calculation of this contribution to the ϕ self-energy can be found in Ref. [13] and for the kaon/antikaon self-energy we use the results from Refs. [23,24].

The K self-energy is relatively simple. The KN amplitude is elastic and given the absence of resonances depends very slowly on the energy. To a good approximation the self-energy can be cast in the $T\rho$ form. The \bar{K} case is more involved. The p -wave part of the self-energy includes the coupling to several particle-hole excitations such as $\Lambda(1115)N^{-1}$, $\Sigma(1195)N^{-1}$, and $\Sigma^*(1385)N^{-1}$. The s -wave part of the self-energy is calculated in a unitarized chiral model and is dominated by the excitation of the $\Lambda(1405)$ resonance. A specially careful and self-consistent treatment of the many-body corrections is required in this case because of the vicinity to the $\bar{K}N$ threshold. As a result, a quite large width is obtained for the antikaons. Furthermore, the real part of the optical potential shows an attraction of -60 MeV at normal nuclear matter density for antikaons at rest in contrast to the mild repulsion in the kaon case.

The novelty of Ref. [16] was the calculation of the contribution to the ϕ self-energy in the medium related to the ϕN elastic scattering amplitude. We relied upon the results of two different schemes recently developed to describe the vector meson-baryon scattering. The first one [25–27] obtains the low-energy vector meson-baryon amplitude within the hidden local symmetry (HLS) approach. The second one [28] uses an SU(6) spin-flavor symmetry extension of the SU(3) chiral perturbation theory Lagrangian. This leads to the generalization of the Weinberg-Tomozawa interaction between pseudoscalar and vector mesons, and baryons from the light octet and decuplet. In both schemes the scattering amplitude is calculated in a coupled channels unitarized approach. These models have been successful in reproducing masses and decay widths of some negative parity resonances and the HLS one has also been tested and constrained in the analysis of the $\gamma p \rightarrow K\Sigma$ reaction [27]. At the lowest order, in these models,

there is no direct $\phi N \rightarrow \phi N$ interaction but that process happens via loops such as $\phi N \rightarrow K^*\Lambda \rightarrow \phi N$. These loops, on the other hand, produce an imaginary part for the scattering amplitude through the opening of some decay channels.

The contribution to the self-energy is then obtained by summing the scattering amplitude over the initial nucleon Fermi distribution. Also Pauli blocking is taken into account by replacing the vacuum nucleon propagators that appear in the calculation by single-particle propagators in the Fermi gas approximation. The new mechanisms produce a moderate momentum dependence of the ϕ self-energy reflecting the presence of some resonances on the ϕN amplitude. Furthermore, the predictions of the two theoretical models differ significantly at low momenta for both real and imaginary parts of the optical potentials. Close to threshold the attraction ranges from 5 to 40 MeV, what could strongly affect the existence and spectrum of possible ϕ meson nuclear bound states [29]. The imaginary part is stronger for the SU(6) model, though both models provide a larger contribution than the mechanisms related to the $K\bar{K}$ decay.

A. Nuclear transparency: Photoproduction

We start discussing the case of ϕ nuclear photoproduction reactions. In this case shadowing is negligible. Thus, the reaction takes place in the whole nucleus and the cross section can be approximated by

$$\frac{d\sigma_A}{d\Omega} = \int d^3r \rho(r) \frac{d\sigma_N}{d\Omega} F_{ABS}, \quad (1)$$

where $\frac{d\sigma_N}{d\Omega}$ and $\frac{d\sigma_A}{d\Omega}$ are the elementary-nucleon and nuclear differential cross section, respectively. F_{ABS} is an absorption factor accounting for the ϕ meson lost flux on its way out of the nucleus. Here, in the production itself, Fermi motion and Pauli blocking have not been considered. If we also set $F_{ABS} = 1$, omitting ϕ absorption in the nucleus, we would get the trivial result $\frac{d\sigma_A}{d\Omega} = A \frac{d\sigma_N}{d\Omega}$, where A is the number of nucleons.¹

On the other hand, for energies close to threshold, just for kinematic reasons, the ϕ meson goes forwards and is quite fast. The high momentum means that changes of trajectory because of the small real part of the optical potential can be neglected. Also, the quasielastic collisions are very improbable, as the imaginary part of the self-energy is fully dominated by inelastic channels according to our theoretical models. Therefore, to a good approximation, the ϕ meson will move forward until it gets out of the nucleus or it is absorbed. Thus, we can model the absorption factor in an eikonal form as [17]

$$F_{ABS} = \exp\left(-\int_0^\infty dl \frac{1}{p} \text{Im} \Pi(p, \rho(r'))\right), \quad (2)$$

where $\Pi(p, \rho(r))$ is the ϕ self-energy as a function of its momentum p and at the nuclear density ρ , \vec{r} is the ϕ production point. Finally, $\vec{r}' = \vec{r} + l \vec{p}/|\vec{p}|$. As long as the integrand of

¹Notice the implicit assumption, supported by the experiment [30], that the ϕ production cross section from protons and neutrons is very similar.

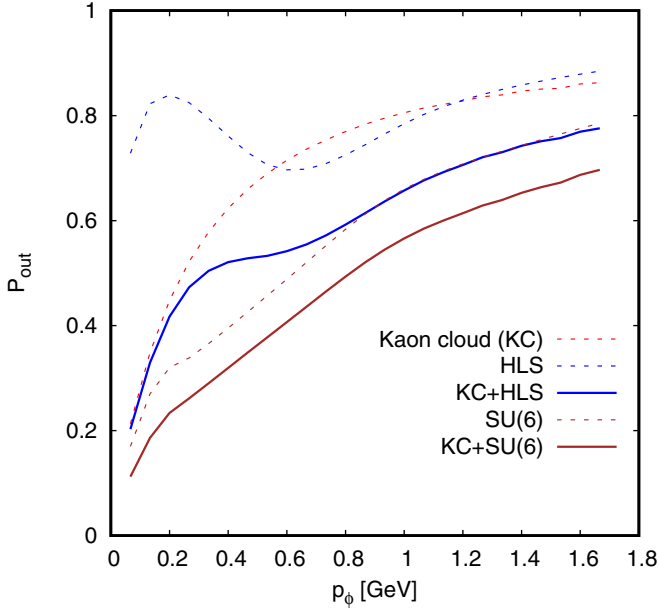


FIG. 1. Transparencies for the nucleus ^{20}Ne as a function of the ϕ momentum with kaon cloud self-energy only or adding the ϕ self-energies from the HLS [25,26] or the SU(6) model [28].

Eq. (1) does not depend on the direction of the ϕ momentum, other than via $\frac{d\sigma_N}{d\Omega}$, we can write the following ratio between the nuclear and the nucleon cross section:

$$P_{\text{out}} \equiv \frac{\sigma_A}{A \sigma_N} = \frac{1}{A} \int d^3r \rho(r) \exp\left(-\int_0^\infty dl \frac{1}{p} \text{Im} \Pi(p, \rho(r'))\right), \quad (3)$$

which measures the transparency of the nucleus to the ϕ meson.

The effect on the transparency observable for the ϕN resonant scattering is substantial, as expected from its large contribution to the ϕ self-energy [16]. In Fig. 1, we show this ratio between cross sections for ^{20}Ne as a function of the ϕ momentum for the theoretical models considered in this paper.

The nuclear density profiles for all cases have been taken from [31,32]. The inclusion of the new ϕN scattering mechanisms leads to a much stronger absorption for the whole momentum range explored than the kaon cloud alone. Additionally, the HLS model shows a strong energy dependence at relatively low (< 600 MeV) momenta. At higher momenta the nuclear transparency increases for all cases.

The only nuclear effects considered in this result and in Eq. (3) are those related to ϕ absorption, incorporated into the calculation of Π , the ϕ self-energy. Other nuclear effects affecting the production mechanism, rather than the ϕ propagation, are the Fermi motion of the initial nucleon and the Pauli blocking of the final one on the $\gamma N \rightarrow \phi N$ process. Pauli blocking will imply a reduction of the ϕ production cross section. The Fermi motion will distort the distribution of the final meson and nucleon and affect the Pauli blocking itself. The flux reduction due to these sources can be estimated for photon induced reactions by including in the integrand of Eq. (3) a factor considering a Fermi average of these

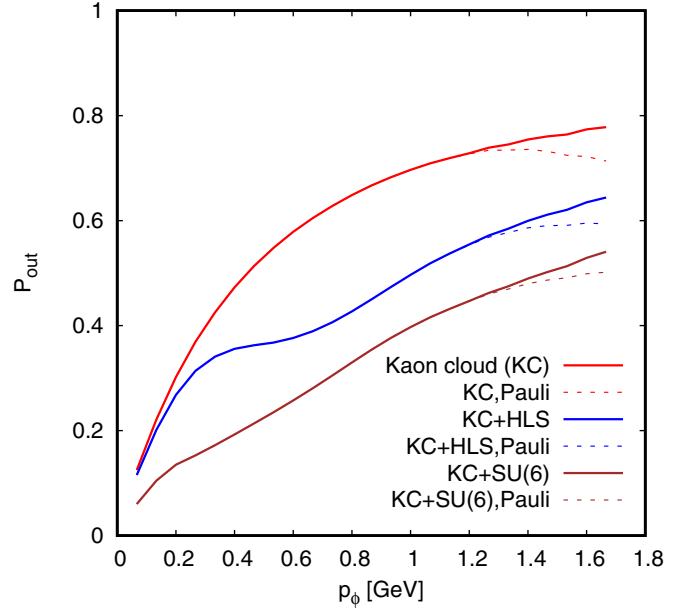


FIG. 2. Transparencies as a function of ϕ momentum for photoproduction processes, with ($\theta_\phi = 0$ degrees) and without Pauli blocking for ^{64}Cu .

effects [17,33]:

$$G(Q, \rho) = 1 - \Theta(2 - \tilde{Q}) \left(1 - \frac{3}{4} \tilde{Q} + \frac{1}{16} \tilde{Q}^3\right), \quad (4)$$

where $\tilde{Q} = |\vec{Q}|/k_F$, \vec{Q} is the momentum transfer and k_F is the Fermi momentum of the nucleons. In Fig. 2, we show how the transparency is modified by the Pauli blocking of the final nucleon. The result depends on the scattering angle. For the figure we have selected forward ϕ scattering that maximizes the change. Opening the angle increases the transfer momentum and as soon as it is above $2k_F$, Pauli blocking becomes ineffective. There is a small reduction at high ϕ momentum and practically no change below 1.2 GeV. This reduction will also affect transparency ratios comparing different nuclei because of the variation of the average density, and thus of the Fermi momentum. However, the dependence of the Pauli blocking correction on the nuclear size, beyond $A \approx 10$, is minimal as shown in Ref. [17].

In Fig. 3, we compare our model with data from LEPS [5] which measured the transparency detecting the ϕ mesons through their $K \bar{K}$ decay. The transparencies are normalized to that of lithium, the lightest nucleus measured in the experiment. In this way, some systematic errors could be reduced. Our presented results are obtained assuming forward scattering, thus maximizing the Pauli blocking effects. Removing Pauli blocking would push up by less than a 5% [5] the three curves. The photon spectrum had energies ranging from 1.5 to 2.4 GeV. We take an average momentum, $p_\phi = 1.8$ GeV as suggested in [5]. We find that the inclusion of the ϕN scattering mechanisms improves the agreement for both models. In principle, the largest absorption corresponding to the SU(6) model is favored. However, we find that it is very hard to reproduce the steep change in data from lithium to

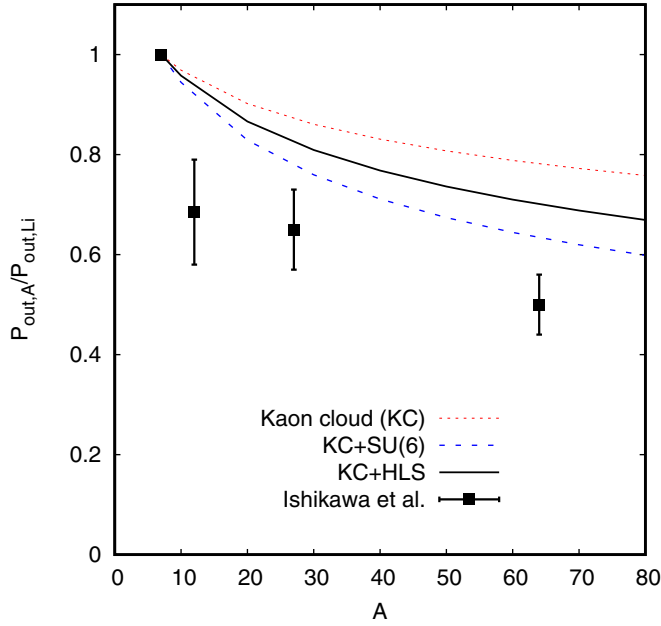


FIG. 3. Ratio of ϕ photoproduction transparencies as a function of the atomic number compared with data from LEPS [5].

carbon, even when artificially increasing the absorption by a large factor.

In Fig. 4, we compare our model with data from CLAS [7]. In this case, the ϕ meson was detected via the e^+e^- decay avoiding the complication of the final state kaon interactions and some other difficulties in the background subtraction and the experimental analysis. The average ϕ momentum is 2 GeV,

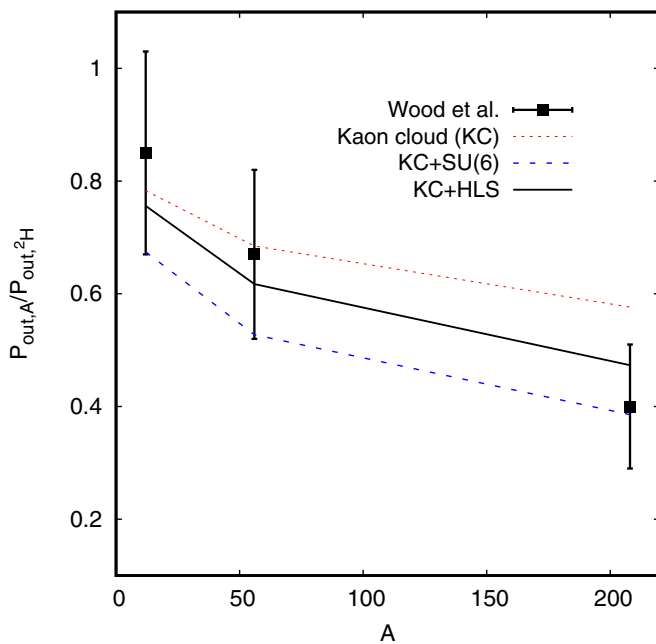


FIG. 4. Transparency ratios for ϕ photoproduction as a function of the atomic number compared with data from CLAS [7]. Curves to guide the eye.

only slightly larger than for LEPS. According to our model the transparencies at such close energies should be similar. The results here are consistent with data. Lead transparency, the one with the strongest nuclear effects, favors the inclusion of the new mechanisms and overall the best fit corresponds to the HLS model. Nonetheless, the large uncertainties prevent us from reaching strong conclusions. The much larger $\sigma_{\phi N}$ cross section that would be required to accommodate LEPS data would spoil the agreement with CLAS. Thus, the two available photoproduction experimental results seem hardly compatible.

As explained before, the LEPS data correspond to the $K\bar{K}$ decay of the ϕ meson. The complicated final-state interaction of the kaons could seriously affect the signal: the K^+ could modify its energy and direction because of quasielastic scattering, while the K^- can even be absorbed leading to hyperons. These effects could be included in a more complete theoretical calculation. However, there are further concerns related to the experimental separation of the ϕp and the $K^+\Lambda(1520)$ channels. Both of them could lead to the same pK^+K^- final state and thus, there are interferences which would require a more detailed theoretical and experimental analysis. There is some recent experimental progress along this line for the $\gamma p \rightarrow K^+K^-p$ reaction [34,35].

B. Nuclear transparency: proton induced production

The theoretical description of proton induced ϕ production is more complicated [18–20] even when assuming that the quasifree mechanism $pN \rightarrow pN\phi$ is dominant. First, we must consider the initial state interaction of the proton. A simple approximation is to include an additional factor to account for the proton flux reduction,

$$F_{IN} = \exp\left(-\int_{\infty}^{\vec{r}} \sigma_{NN} \rho(r') dl\right), \quad (5)$$

where σ_{NN} is the full nucleon-nucleon cross section. From here on, we adapt to the COSY/ANKE setup of Ref. [8]. There, the protons have a kinetic energy of 2.83 GeV. It is close to the reaction threshold and thus Pauli blocking is irrelevant for the primary reaction $NN \rightarrow NN\phi$ because the final nucleons have a too large momentum. On the other hand, for the initial distortion both σ_{pn} and σ_{pp} are around 42 mb [36]. A second change with respect to the photoproduction process is the sizable isospin asymmetry in the production cross section. According to both experimental data and theoretical models [37–39] the cross section for $pn \rightarrow pn\phi$ is substantially larger than for $pp \rightarrow pp\phi$. Also, the $pn \rightarrow d\phi$ process, which further enhances the relevance of neutrons, is of comparable size [37]. This isospin asymmetry is taken into account substituting σ_N in Eq. (1) by

$$\{N(\sigma_{pn \rightarrow pn\phi} + \sigma_{pn \rightarrow d\phi}) + Z\sigma_{pp \rightarrow pp\phi}\}/A \quad (6)$$

with Z and N the number of protons and neutrons and $A = N + Z$. We use for these cross sections the parametrizations from Ref. [19]. Obviously, this isospin asymmetry leads to a relatively larger ϕ production for heavier nuclei which have

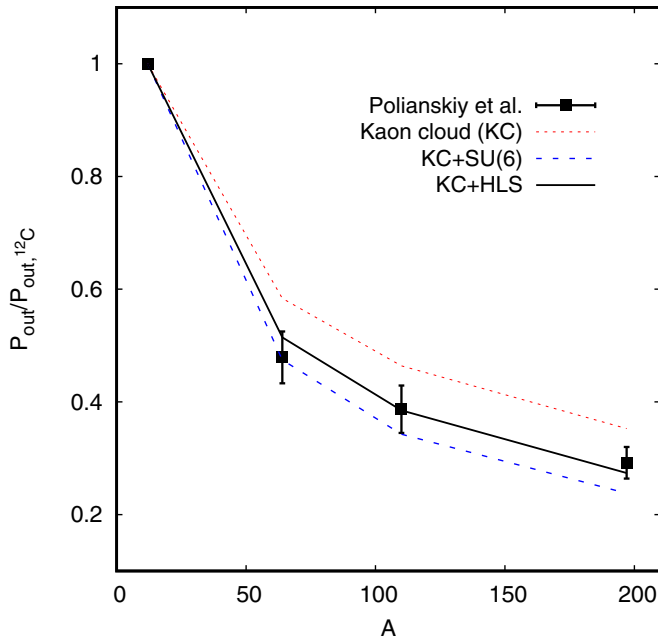


FIG. 5. Nuclear transparency ratios for the $pA \rightarrow \phi X$ reaction compared to data from Ref. [22].

more neutrons than protons. The effect is of the order of 10% for lead at the energy of Ref. [8].

Including the shadowing factor of Eq. (5) and the isospin correction from Eq. (6) we compare our results with data from Ref. [22] in Fig. 5. In the calculation we have taken an average ϕ momentum of 1.3 GeV, which approximately corresponds to the experimental peak of the ϕ production differential cross section for all nuclei [8] and also of the phase space distribution of the elementary $NN \rightarrow NN\phi$ process at the studied energy.

The agreement is fair for all models and a simple χ -squared analysis favors the HLS one. We should mention that in the proton induced process, a good part of the cross section reduction in nuclei comes from the initial state interaction of the proton. Thus, the process is more peripheral and there is less sensitivity to the ϕ meson absorption than in photoproduction [18].

Additionally, there are some caveats to be considered before giving too much weight to these results. The contribution of multistep processes to the ϕ production mechanism could also be important. For instance, the initial nucleon could undergo a quasielastic scattering loosing some energy, followed by ϕ production in a second step. Another possibility is the excitation of a Δ resonance followed by a $\Delta N \rightarrow NN\phi$ process. These two mechanisms were investigated in Ref. [18] finding that they were relevant modifying the nuclear cross sections, but hardly affected ratios such as that of Fig. 5. A third mechanism, π production followed by $\pi N \rightarrow N\phi$, has been studied in Ref. [19] leading to some enhancement of the

nuclear transparency ratios. Given the influence of all these mechanisms, with their large uncertainties, and the smaller sensitivity to the ϕ meson absorption, we find that proton induced production is less adequate than ϕ photoproduction to obtain information on the ϕ self-energy in nuclear matter.

III. CONCLUSIONS

We have investigated the ϕ meson nuclear transparency using the ϕ self-energy model developed in Ref. [16]. This self-energy includes direct ϕN -scattering mechanisms, evaluated in two different theoretical approaches, in addition to the terms due to the supposedly dominant kaon-cloud interactions. We find that the contribution associated to ϕN scattering is stronger than assumed in many previous theoretical calculations. With this self-energy, we reproduce well the nuclear transparency data obtained from ϕ photoproduction reactions at CLAS. Furthermore, the agreement with the LEPS photoproduction data is clearly improved when the ϕN -scattering effects are considered. However, an even stronger ϕ absorption would be required in this case. We find that CLAS and LEPS data are hardly reconcilable, since they seem to point to different in-medium ϕ absorption magnitudes.

The results also show a good reproduction of the proton induced transparency data. However, this case is less sensitive to the ϕ meson properties in the nuclear medium. Namely, large changes of the self-energy lead to small changes of the transparency which is dominated by shadowing effects. Furthermore, the theoretical modeling is necessarily more involved because of the importance of multistep production mechanisms.

This work supports the relevance of the direct ϕN -scattering mechanisms on the description of the ϕ meson width in the nuclear medium. However, there are still substantial uncertainties in the available theoretical models describing ϕN scattering. This calls for new, more precise experiments, which could help discriminating and constraining those theoretical models. In particular, the measurement of other observables, such as the spectrum of ϕ nuclear bound states, if they exist, would be instrumental to determine both the real and the imaginary part of the ϕ self-energy in nuclear matter.

ACKNOWLEDGMENTS

We acknowledge A. Ramos, E. Oset, L. Tolós, and J. Nieves for fruitful discussions and for providing us with numerical codes implementing their models. This research has been partially supported by the Spanish Ministerio de Economía y Competitividad (MINECO) and the European fund for regional development (FEDER) under Contracts No. FIS2014-51948-C2-2-P and No. SEV-2014-0398 and by Generalitat Valenciana under Contract No. PROMETEOII/2014/0068.

[1] R. Rapp and J. Wambach, *Adv. Nucl. Phys.* **25**, 1 (2000).
 [2] R. S. Hayano and T. Hatsuda, *Rev. Mod. Phys.* **82**, 2949 (2010).

[3] M. Wada (STAR Collaboration), *Nucl. Phys. A* **904–905**, 1019c (2013).

- [4] B. Abelev *et al.* (ALICE Collaboration), *Phys. Rev. C* **91**, 024609 (2015).
- [5] T. Ishikawa, D. S. Ahn, J. K. Ahn, H. Akimune, W. C. Chang, S. Date, H. Fujimura, M. Fujiwara *et al.*, *Phys. Lett. B* **608**, 215 (2005).
- [6] R. Muto *et al.* (KEK-PS-E325 Collaboration), *Phys. Rev. Lett.* **98**, 042501 (2007).
- [7] M. H. Wood *et al.* (CLAS Collaboration), *Phys. Rev. Lett.* **105**, 112301 (2010).
- [8] M. Hartmann, Y. T. Kiselev, A. Polyanskiy, E. Y. Paryev, M. Buscher, D. Chiladze, S. Dymov, A. Dzyuba *et al.*, *Phys. Rev. C* **85**, 035206 (2012).
- [9] P. Muhlich and U. Mosel, *Nucl. Phys. A* **765**, 188 (2006).
- [10] C. M. Ko, P. Lévai, X. J. Qiu, and C. T. Li, *Phys. Rev. C* **45**, 1400 (1992).
- [11] F. Klingl, T. Waas, and W. Weise, *Phys. Lett. B* **431**, 254 (1998).
- [12] E. Oset and A. Ramos, *Nucl. Phys. A* **679**, 616 (2001).
- [13] D. Cabrera and M. J. Vicente Vacas, *Phys. Rev. C* **67**, 045203 (2003).
- [14] P. Gubler and W. Weise, *Nucl. Phys. A* **954**, 125 (2016).
- [15] J. J. Cobos-Martínez, K. Tsushima, G. Krein, and A. W. Thomas, *Phys. Lett. B* **771**, 113 (2017).
- [16] D. Cabrera, A. N. Hiller Blin, and M. J. Vicente Vacas, *Phys. Rev. C* **95**, 015201 (2017).
- [17] D. Cabrera, L. Roca, E. Oset, H. Toki, and M. J. Vicente Vacas, *Nucl. Phys. A* **733**, 130 (2004).
- [18] V. K. Magas, L. Roca, and E. Oset, *Phys. Rev. C* **71**, 065202 (2005).
- [19] E. Y. Paryev, *J. Phys. G* **36**, 015103 (2009).
- [20] A. Sibirtsev, H.-W. Hammer, and U.-G. Meißner, *Eur. Phys. J. A* **37**, 287 (2008).
- [21] J. Steinheimer and M. Bleicher, *J. Phys. G* **43**, 015104 (2016).
- [22] A. Polyanskiy *et al.*, *Phys. Lett. B* **695**, 74 (2011).
- [23] A. Ramos and E. Oset, *Nucl. Phys. A* **671**, 481 (2000).
- [24] L. Tolós, A. Ramos, and E. Oset, *Phys. Rev. C* **74**, 015203 (2006).
- [25] E. Oset and A. Ramos, *Eur. Phys. J. A* **44**, 445 (2010).
- [26] E. Oset, A. Ramos, E. J. Garzon, R. Molina, L. Tolos, C. W. Xiao, J. J. Wu, and B. S. Zou, *Int. J. Mod. Phys. E* **21**, 1230011 (2012).
- [27] A. Ramos and E. Oset, *Phys. Lett. B* **727**, 287 (2013).
- [28] D. Gamermann, C. Garcia-Recio, J. Nieves, and L. L. Salcedo, *Phys. Rev. D* **84**, 056017 (2011).
- [29] J. J. Cobos-Martínez, K. Tsushima, G. Krein, and A. W. Thomas, *Phys. Rev. C* **96**, 035201 (2017).
- [30] W. C. Chang *et al.* (LEPS Collaboration), *Phys. Lett. B* **684**, 6 (2010).
- [31] H. De Vries, C. W. De Jager, and C. De Vries, *At. Data Nucl. Data Tables* **36**, 495 (1987).
- [32] C. W. De Jager, H. De Vries, and C. De Vries, *At. Data Nucl. Data Tables* **14**, 479 (1974).
- [33] C. Garcia-Recio, E. Oset, and L. L. Salcedo, *Phys. Rev. C* **37**, 194 (1988).
- [34] B. Dey *et al.* (CLAS Collaboration), *Phys. Rev. C* **89**, 055208 (2014); **90**, 019901(E) (2014).
- [35] S. Y. Ryu *et al.* (LEPS Collaboration), *Phys. Rev. Lett.* **116**, 232001 (2016).
- [36] C. Patrignani *et al.* (Particle Data Group), *Chin. Phys. C* **40**, 100001 (2016).
- [37] Y. Maeda *et al.*, *Phys. Rev. Lett.* **97**, 142301 (2006).
- [38] A. I. Titov, B. Kämpfer, and V. V. Shklyar, *Phys. Rev. C* **59**, 999 (1999).
- [39] L. P. Kaptari and B. Kämpfer, *Eur. Phys. J. A* **23**, 291 (2005).



Boltzmann Entropy, the Holographic Bound and Newtonian Cosmology [†]

Pedro Fernández De Córdoba * and Jose Maria Isidro San Juan

Instituto Universitario de Matemática Pura y Aplicada, Universidad Politécnica de Valencia, 46022 Valencia, Spain; joissan@mat.upv.es

* Correspondence: pfernandez@mat.upv.es

† Presented at the 4th International Electronic Conference on Entropy and Its Applications,

21 November–1 December 2017; Available online: <http://sciforum.net/conference/ecea-4>.

Published: 21 November 2017

Abstract: The holographic principle sets an upper bound on the total (Boltzmann) entropy content of the Universe at around $10^{123}k_B$ (k_B being Boltzmann's constant). In this work we point out the existence of a remarkable duality between nonrelativistic quantum mechanics on the one hand, and Newtonian cosmology on the other. Specifically, nonrelativistic quantum mechanics has a quantum probability fluid that exactly mimics the behaviour of the cosmological fluid, the latter considered in the Newtonian approximation. One proves that the equations governing the cosmological fluid (the Euler equation and the continuity equation) become the very equations that govern the quantum probability fluid after applying the Madelung transformation to the Schroedinger wavefunction. Under the assumption that gravitational equipotential surfaces can be identified with isoentropic surfaces, this model allows for a simple computation of the gravitational entropy of a Newtonian Universe.

Keywords: gravitational entropy; holographic principle; emergent spacetime

1. Introduction

There is a widespread certainty that the continuum description of spacetime as provided by general relativity must necessarily break down at very short length scales and/or very high curvatures. A number of very different approaches to an eventual theory of quantum gravity have been presented in the literature; these candidate theories are too varied and too extensive to summarise here. On the whole, the picture that emerges is that of a continuum description after some appropriate coarse graining of some underlying degrees of freedom. Even if the precise nature of the latter is unknown yet, one can still make progress following a thermodynamical approach: one ignores large amounts of detailed knowledge (say, the precise motions followed by the atoms of a gas) while concentrating only on a few coarse-grained averages (say, the overall pressure exerted by the atoms of a gas on the container walls). This way of approaching the problem has come to be called *the emergent approach*.

In the emergent approach to spacetime, gravity qualifies as an entropic force. This means that we do not know the fundamental degrees of freedom underlying gravity, but their overall macroscopic effect is that of driving the system under consideration in the direction of increasing entropy. If gravitational forces are entropy gradients, then gravitational equipotential surfaces can be identified with isoentropic surfaces. We will consider a density of particles representing the (baryonic and dark) matter contents of a hypothetical Newtonian Universe. This volume density will be identified with the squared modulus of a nonrelativistic wavefunction ψ satisfying the Schroedinger equation. Let U denote the gravitational potential. Once dimensions are corrected (using \hbar and k_B), the expectation value $\langle \psi | U | \psi \rangle$ becomes a measure of the gravitational entropy of the Universe when the matter is described by the wavefunction ψ .

2. Methods

In Newtonian cosmology, the Universe is regarded as being subject to a gravitational potential U satisfying the Poisson equation

$$\nabla^2 U = 4\pi G\rho. \tag{1}$$

The matter content (baryonic and dark matter) is modelled as an ideal fluid satisfying the continuity equation and the Euler equation,

$$\frac{\partial \rho}{\partial t} + \nabla \cdot (\rho \mathbf{v}) = 0, \quad \frac{\partial \mathbf{v}}{\partial t} + (\mathbf{v} \cdot \nabla) \mathbf{v} + \frac{1}{\rho} \nabla p - \mathbf{F} = 0. \tag{2}$$

The cosmological principle requires that the velocity field \mathbf{v} be everywhere proportional to the position vector \mathbf{r} . This requirement is equivalent to Hubble’s law [1–3], which can be described phenomenologically by the harmonic potential

$$U_{\text{Hubble}}(\mathbf{r}) = -\frac{H_0^2}{2} \mathbf{r}^2. \tag{3}$$

Hubble’s constant H_0 is an angular frequency; the negative sign implies that this potential is repulsive. Accordingly, U_{Hubble} satisfies the Poisson Equation (1) with a *negative* mass density.

Schroedinger quantum mechanics can also be understood in terms of an ideal fluid, the *quantum probability fluid*. Following Madelung one factorises the nonrelativistic wavefunction ψ into amplitude and phase:

$$\psi = \exp\left(\frac{\mathcal{S}}{2k_B} + i\frac{\mathcal{I}}{\hbar}\right). \tag{4}$$

The amplitude $\exp(\mathcal{S}/2k_B)$ is a real exponential; one can invoke Boltzmann’s principle to regard \mathcal{S} as a Boltzmann entropy of the matter described by ψ —not to be confused with the gravitational entropy \mathcal{S}_g in Equation (16) below. It will also be convenient to define a dimensionless Boltzmann entropy $S := \mathcal{S}/2k_B$. The phase $\exp(i\mathcal{I}/\hbar)$ is the complex exponential of the classical-mechanical action integral \mathcal{I} . Substituting the Ansatz Equation (4) into the Schroedinger equation for ψ , one arrives at a set of two equations. One of them is the continuity equation for the quantum probability fluid,

$$\frac{\partial S}{\partial t} + \frac{1}{m} \nabla S \cdot \nabla \mathcal{I} + \frac{1}{2m} \nabla^2 \mathcal{I} = 0, \tag{5}$$

where

$$\mathbf{v} := \frac{1}{m} \nabla \mathcal{I}, \quad \rho = e^{2S}. \tag{6}$$

The second equation obtained is known as the *quantum Hamilton-Jacobi equation*:

$$\frac{\partial \mathcal{I}}{\partial t} + \frac{1}{2m} (\nabla \mathcal{I})^2 + V + \mathcal{Q} = 0, \tag{7}$$

where V is the external potential present in the Schroedinger equation (we recall that the dimensions of U in Equations (1) and (3) are velocity squared, whereas those of V in Equation (7) are mass times velocity squared). Above,

$$\mathcal{Q} := -\frac{\hbar^2}{2m} [(\nabla S)^2 + \nabla^2 S] \tag{8}$$

is known as the *quantum potential*.

Finally we need to derive an Euler equation for the quantum probability. This is achieved by taking the gradient of Equation (7):

$$\frac{\partial \mathbf{v}}{\partial t} + (\mathbf{v} \cdot \nabla) \mathbf{v} + \frac{1}{m} \nabla \mathcal{Q} + \frac{1}{m} \nabla V = 0. \tag{9}$$

Comparison between Equations (2) and (9) produces a bijective correspondence between the quantum probability fluid and the cosmological fluid. Which suggests that, *given the cosmological fluid in the Newtonian approximation, we use nonrelativistic quantum mechanics as an equivalent description thereof.* In this description by means of a quantum wavefunction ψ , the amount of mass m_V contained within a volume V equals $m_V = m \int_V d^3x |\psi|^2$; the whole observable Universe is regarded as a sphere of radius R_0 . Considering the Universe as a sphere with finite radius has the added bonus that the instabilities [4] due to the negative sign of the potential Equation (3) are avoided naturally.

In view of Hubble’s law Equation (3) it is reasonable to consider the effective Hamiltonian

$$H_{\text{eff}} = -\frac{\hbar^2}{2m} \nabla^2 - \frac{k_{\text{eff}}}{2} \mathbf{r}^2, \quad k_{\text{eff}} = mH_0^2 \tag{10}$$

as governing the overall expansion of the Universe, at least within the Newtonian limit. As a first approximation it will also be useful to consider the free Hamiltonian

$$H_{\text{free}} = -\frac{\hbar^2}{2m} \nabla^2. \tag{11}$$

Their respective eigenfunctions are readily obtained in spherical coordinates. For Equation (11) we have the free spherical waves

$$\psi_{\kappa 00}(r, \theta, \varphi) = \frac{1}{\sqrt{4\pi R_0}} \frac{1}{r} \exp(i\kappa r), \quad \kappa \in \mathbb{R}, \tag{12}$$

normalised within a sphere of radius R_0 , and carrying zero angular momentum as required by the cosmological principle. For the Hubble Hamiltonian Equation (10) one finds the exact eigenfunctions [5]

$$\psi_{\alpha}^{(1)}(r, \theta, \varphi) = \frac{N_{\alpha}^{(1)}}{\sqrt{4\pi}} \exp\left(\frac{i\beta^2 r^2}{2}\right) {}_1F_1\left(\frac{3}{4} - \frac{i\alpha}{4}, \frac{3}{2}; -i\beta^2 r^2\right) \tag{13}$$

and

$$\psi_{\alpha}^{(2)}(r, \theta, \varphi) = \frac{N_{\alpha}^{(2)}}{\sqrt{4\pi}} \frac{1}{r} \exp\left(\frac{i\beta^2 r^2}{2}\right) {}_1F_1\left(\frac{1}{4} - \frac{i\alpha}{4}, \frac{1}{2}; -i\beta^2 r^2\right). \tag{14}$$

They also carry vanishing angular momentum, $N_{\alpha}^{(1)}$ and $N_{\alpha}^{(2)}$ being radial normalisation factors. Above, ${}_1F_1$ is the confluent hypergeometric function, and the parameters α, β are given by

$$\alpha := \frac{2E}{\hbar H_0}, \quad \beta^4 := \frac{m^2 H_0^2}{\hbar^2}, \tag{15}$$

with E the energy eigenvalue in $H_{\text{eff}}\psi = E\psi$.

3. Results and Discussion

Our previous reasoning leads naturally to the operator $\mathbf{R}^2 = X^2 + Y^2 + Z^2$ as a measure of the amount of gravitational entropy contained within a Newtonian Universe in which the Hubble repulsion arises as the net force. Specifically, the operator

$$\mathcal{S}_g := \mathcal{N} \frac{k_B m H_0}{\hbar} \mathbf{R}^2 \tag{16}$$

is dimensionally an entropy; a *dimensionless* factor \mathcal{N} is of course left undetermined. We call \mathcal{S}_g the gravitational entropy operator.

We can now compute the expectation value of the entropy \mathcal{S}_g in the free eigenstates Equation (12) and in the Hubble eigenstates Equations (13) and (14). For the free waves Equation (12) one finds

$$\langle \psi_{\kappa 00} | \mathbf{R}^2 | \psi_{\kappa 00} \rangle = \frac{R_0^2}{3}. \tag{17}$$

Substituting the known values [6] of the cosmological data m , H_0 , R_0 into Equations (16) and (17) we arrive at the estimate [7]

$$\langle \psi_{\kappa 00} | \mathcal{S}_g | \psi_{\kappa 00} \rangle = 10^{123} k_B. \tag{18}$$

Above we have set $\mathcal{N} = 3/2.6$. Our result Equation (18) saturates the upper bound set by the holographic principle. A finer estimate is obtained using the Hubble waves Equations (13) and (14). After some numerical approximations one finds

$$\langle \psi_\alpha^{(1)} | \mathbf{R}^2 | \psi_\alpha^{(1)} \rangle = \frac{R_0^2}{2 \ln(\beta R_0)} = \langle \psi_\alpha^{(2)} | \mathbf{R}^2 | \psi_\alpha^{(2)} \rangle. \tag{19}$$

This leads to [5]

$$\langle \psi_\alpha^{(1)} | \mathcal{S}_g | \psi_\alpha^{(1)} \rangle = 10^{120} k_B = \langle \psi_\alpha^{(2)} | \mathcal{S}_g | \psi_\alpha^{(2)} \rangle \tag{20}$$

upon taking $\mathcal{N} = 1/6$. This new theoretical estimate lies three orders of magnitude below the holographic bound, thus representing a considerable improvement on the estimate obtained from the free waves.

4. Conclusions

The holographic principle sets an upper bound of approximately $10^{123} k_B$ on the entropy content of the Universe. Some phenomenological estimates [8] place the actual value at around $10^{104} k_B$, gravitational entropy (and, in particular, black holes) representing the largest single contributors to the entropy budget of the Universe. Although Newtonian cosmology does allow for black holes, the many simplifications made by our elementary model necessarily leave out some essential physics of the Universe. Nevertheless, our toy model succeeds in capturing some key elements of reality. For example, the upper bound set by the holographic principle is always respected, even by such a crude approximation as the free waves Equation (12). The Hubble waves Equations (13) and (14) represent a considerable improvement on the free waves, as they reduce the expectation value of the entropy by three orders of magnitude.

Acknowledgments: This research was supported by grant no. ENE2015-71333-R (Spain).

Conflicts of Interest: The authors declare no conflict of interest.

References

1. Hubble, E. A Relation between Distance and Radial Velocity among Extra-Galactic Nebulae. *Proc. Nat. Acad. Sci. USA* **1929**, *15*, 168–173.
2. Perlmutter, S.; Aldering, G.; Deustua, S.; Fabbro, S.; Goldhaber, G.; Groom, D.E.; Kim, A.G.; Kim, M.Y.; Knop, R.A.; Nugent, P.; et al. Cosmology from Type Ia Supernovae. *Bull. Am. Astron. Soc.* **1997**, *29*, 1351.
3. Riess, A.G.; Filippenko, A.V.; Challis, P.; Clocchiatti, A.; Diercks, A.; Garnavich, P.M.; Gilliland, R.L.; Hogan, C.J.; Jha, S.; Kirshner, R.P.; et al. Observational Evidence from Supernovae for an Accelerating Universe and a Cosmological Constant. *Astron. J.* **1998**, *116*, 1009–1038.
4. Broadbridge, P.; Zulkowski, P. Dark Energy States from Quantization of Boson Fields in a Universe with Unstable Modes. *Rep. Math. Phys.* **2006**, *57*, 27–40.
5. Fernández de Córdoba, P.; Isidro, J.M. On the Holographic Bound in Newtonian Cosmology. *arXiv* **2017**, arXiv:1710.00507.
6. Ade, P.A.; Aghanim, N.; Arnaud, M.; Ashdown, M.; Aumont, J.; Baccigalupi, C.; Banday, A.J.; Barreiro, R.B.; Bartlett, J.G.; Bartolo, N.; et al. Planck 2015 Results. XIII. Cosmological Parameters. *Astron. Astrophys.* **2016**, *594*, A13.

7. Cabrera, D.; Fernández de Córdoba, P.; Isidro, J.M. Boltzmann Entropy of a Newtonian Universe. *Entropy* **2017**, *19*, 212, arXiv:1703.08082.
8. Egan, C.; Lineweaver, C. A Larger Estimate of the Entropy of the Universe. *Astrophys. J.* **2010**, *710*, 1825–1834.



© 2018 by the authors. Licensee MDPI, Basel, Switzerland. This article is an open access article distributed under the terms and conditions of the Creative Commons Attribution (CC BY) license (<http://creativecommons.org/licenses/by/4.0/>).

EMERGENCE FROM IRREVERSIBILITY

P. Fernández de Córdoba^{1,a}, J.M. Isidro^{1,b} and Milton H. Perea^{1,2,c}

¹Instituto Universitario de Matemática Pura y Aplicada,
Universidad Politécnica de Valencia, Valencia 46022, Spain

²Departamento de Matemáticas y Física, Universidad Tecnológica
del Chocó, Colombia

^apfernandez@mat.upv.es, ^bjoissan@mat.upv.es

^cmilpecr@posgrado.upv.es

Abstract The emergent nature of quantum mechanics is shown to follow from a precise correspondence with the classical theory of irreversible thermodynamics.

1 Introduction

The aim of this talk^[1] is to establish a correspondence between quantum mechanics, on the one hand, and the classical thermodynamics of irreversible processes, on the other. This we do in order to provide an independent proof of the statement that *quantum mechanics is an emergent phenomenon*. The emergent aspects of quantum mechanics have been the subject of a vast literature; a very incomplete list of refs. would include [\[1, 2, 3, 4, 5, 6, 7, 8, 9, 10, 11, 12, 13, 16, 17, 18, 19, 20, 21, 22, 25, 26, 31, 32, 33\]](#).

2 Basics in irreversible thermodynamics

We first summarise, for later use, some basic elements of the classical thermodynamics of irreversible processes in the linear regime [\[28\]](#).

Let a thermodynamical system be given, deviating only slightly from equilibrium. Assume that its entropy S depends on N extensive variables y^1, \dots, y^N , so we can write $S = S(y^1, \dots, y^N)$. The tendency of the system to seek equilibrium is measured by the *thermodynamic forces* Y_k , defined to be the components of the gradient of the entropy:

$$Y_k := \frac{\partial S}{\partial y^k}. \quad (1)$$

Now our system is away from equilibrium, but not too far away, so we can assume linearity between the fluxes \dot{y}^k and the forces Y_j :

$$\dot{y}^i := \frac{dy^i}{d\tau} = \sum_{j=1}^N L^{ij} Y_j, \quad Y_i = \sum_{j=1}^N R_{ij} \dot{y}^j, \quad R_{ij} = (L^{ij})^{-1}. \quad (2)$$

¹Work partially based on ref. [\[3\]](#) by some of the present authors (P. F. de C. and J.M.I.), presented by J.M.I. at the *Sixth International Workshop DICE 2012: Spacetime–Matter–Quantum Mechanics: from the Planck scale to emergent phenomena* (Castiglione, Italy, September 2012).

We use τ to denote thermodynamical time, and we suppose the above relation between forces and fluxes to be invertible. A well-known result is Onsager's reciprocity theorem: the matrix L is symmetric,

$$L^{ij} = L^{ji}. \quad (3)$$

By (2), the rate of entropy production can be written either as a quadratic form in the fluxes, or as a quadratic form in the forces:

$$\dot{S} = \sum_{j=1}^N \frac{\partial S}{\partial y^j} \dot{y}^j = \sum_{j=1}^N Y_j \dot{y}^j = \sum_{i,j=1}^N R_{ij} \dot{y}^i \dot{y}^j = \sum_{i,j=1}^N L^{ij} Y_i Y_j. \quad (4)$$

We can Taylor expand the entropy S around equilibrium and truncate the series at second order, to find

$$S = S_0 - \frac{1}{2} \sum_{i,j=1}^N s_{ij} y^i y^j + \dots, \quad (5)$$

where the matrix $s_{ij} = -\partial^2 S / \partial y^i \partial y^j|_0$ (the negative Hessian evaluated at equilibrium) is positive definite. This truncation has the consequence that fluctuations around equilibrium are Gaussian. Indeed, by Boltzmann's principle, the probability $P(y^1, \dots, y^N)$ of finding the values y^1, \dots, y^N of the extensive variables is given by

$$P(y^1, \dots, y^N) = Z^{-1} \exp\left(\frac{S}{k_B}\right) = Z^{-1} \exp\left(-\frac{1}{2k_B} \sum_{i,j=1}^N s_{ij} y^i y^j\right), \quad (6)$$

where Z is a normalisation factor.

For simplicity we set $N = 1$ in all that follows. Our aim is to calculate the probability of any path $y = y(\tau)$ in the thermodynamical configuration space. A *cumulative* distribution function $F_n \left(\begin{smallmatrix} y_1 \dots y_n \\ \tau_1 \dots \tau_n \end{smallmatrix} \right)$ is defined such that it yields the probability that the thermodynamical path $y(\tau)$ lie below the barriers y_1, \dots, y_n at times $\tau_1 < \tau_2 < \dots < \tau_n$:

$$F_n \left(\begin{smallmatrix} y_1 \dots y_n \\ \tau_1 \dots \tau_n \end{smallmatrix} \right) := P(y(\tau_k) \leq y_k, k = 1, \dots, n). \quad (7)$$

A stationary process is defined to be one such that F_n is invariant under time shifts $\delta\tau$:

$$F_n \left(\begin{smallmatrix} y_1 \dots y_n \\ \tau_1 \dots \tau_n \end{smallmatrix} \right) = F_n \left(\begin{smallmatrix} y_1 \dots y_n \\ \tau_1 + \delta\tau \dots \tau_n + \delta\tau \end{smallmatrix} \right). \quad (8)$$

In other words, the system that has been left alone long enough that any initial conditions have been forgotten. An *unconditional* probability density function $f_n \left(\begin{smallmatrix} y_1 \dots y_n \\ \tau_1 \dots \tau_n \end{smallmatrix} \right)$ is defined, such that the product

$$f_n \left(\begin{smallmatrix} y_1 \dots y_n \\ \tau_1 \dots \tau_n \end{smallmatrix} \right) dy_1 \dots dy_n \quad (9)$$

measures the probability that a thermodynamical path $y = y(\tau)$ pass through a gate of width dy_k at instant τ_k , for all $k = 1, \dots, n$. Similarly, the *conditional* probability density function $f_1 \left(\begin{smallmatrix} y_k & y_{k-1} \\ \tau_k & \tau_{k-1} \end{smallmatrix} \right)$ is such that the product

$$f_1 \left(\begin{smallmatrix} y_k & y_{k-1} \\ \tau_k & \tau_{k-1} \end{smallmatrix} \right) dy_k dy_{k-1} \quad (10)$$

gives the probability that $y = y(\tau)$ pass through dy_k at τ_k , given that it passed through dy_{k-1} at τ_{k-1} . Finally a Markov process is defined to be *one that has a short memory* or, more precisely, one such that its cumulative, conditional probability function satisfies

$$F_1 \left(\begin{smallmatrix} y_{n+1} & y_1 \dots y_n \\ \tau_{n+1} & \tau_1 \dots \tau_n \end{smallmatrix} \right) = F_1 \left(\begin{smallmatrix} y_{n+1} & y_n \\ \tau_{n+1} & \tau_n \end{smallmatrix} \right). \quad (11)$$

One can prove that, for a Markov process, the following factorisation theorem holds [28]:

$$f_n \left(\begin{smallmatrix} y_1 \dots y_n \\ \tau_1 \dots \tau_n \end{smallmatrix} \right) = f_1 \left(\begin{smallmatrix} y_n & y_{n-1} \\ \tau_n & \tau_{n-1} \end{smallmatrix} \right) \dots f_1 \left(\begin{smallmatrix} y_2 & y_1 \\ \tau_2 & \tau_1 \end{smallmatrix} \right) f_1 \left(\begin{smallmatrix} y_1 \\ \tau_1 \end{smallmatrix} \right). \quad (12)$$

Interesting about this factorisation theorem is the fact that $f_1 \left(\begin{smallmatrix} y_1 \\ \tau_1 \end{smallmatrix} \right)$ is known from Boltzmann's principle. Therefore, by stationarity, all we need to know is

$$f_1 \left(\begin{smallmatrix} y_2 & y_1 \\ \tau + \delta\tau & \tau \end{smallmatrix} \right), \quad (13)$$

and solving the n -gate problem $f_n \left(\begin{smallmatrix} y_1 \dots y_n \\ \tau_1 \dots \tau_n \end{smallmatrix} \right)$ nicely reduces to solving the 2-gate problem $f_1 \left(\begin{smallmatrix} y_2 & y_1 \\ \tau + \delta\tau & \tau \end{smallmatrix} \right)$.

Now, under the assumption that our irreversible thermodynamical processes is stationary, Markov and Gaussian, the conditional probability density (I3) has been computed in [28], with the result

$$f_1 \left(\begin{smallmatrix} y_2 & y_1 \\ \tau + \delta\tau & \tau \end{smallmatrix} \right) = \frac{1}{\sqrt{2\pi}} \frac{s/k_B}{\sqrt{1 - e^{-2\gamma\delta\tau}}} \exp \left[-\frac{s}{2k_B} \frac{(y_2 - e^{-\gamma\delta\tau} y_1)^2}{1 - e^{-2\gamma\delta\tau}} \right]. \quad (14)$$

Here we have defined the thermodynamical frequency γ ,

$$\gamma := \frac{s}{R}, \quad (15)$$

with R given as in (2) and $s = -d^2S/dy^2|_0$. Furthermore, one can reexpress the probability density (I4) in terms of path integrals over thermodynamical configuration space: up to normalisation factors one finds [28]

$$f_1 \left(\begin{smallmatrix} y_2 & y_1 \\ \tau_2 & \tau_1 \end{smallmatrix} \right) = \int_{y(\tau_1)=y_1}^{y(\tau_2)=y_2} Dy(\tau) \exp \left\{ -\frac{1}{2k_B} \int_{\tau_1}^{\tau_2} d\tau \mathcal{L} [\dot{y}(\tau), y(\tau)] \right\}. \quad (16)$$

Above we have defined the thermodynamical Lagrangian function \mathcal{L}

$$\mathcal{L} [\dot{y}(\tau), y(\tau)] := \frac{R}{2} [\dot{y}^2(\tau) + \gamma^2 y^2(\tau)], \quad (17)$$

whose actual dimensions are entropy per unit time.

3 Irreversible thermodynamics vs. quantum theory

We can now establish a precise map between quantum mechanics and classical, irreversible thermodynamics. Let t denote mechanical time, m the mass of the quantum particle under consideration, and ω the frequency of a harmonic potential experienced by the particle.

In the first place, the thermodynamical time variable τ must be analytically continued into it :

$$\tau \leftrightarrow it. \quad (18)$$

Second, the thermodynamical frequency γ becomes the mechanical frequency ω of the harmonic oscillator:

$$\gamma \leftrightarrow \omega. \quad (19)$$

Next we map the thermodynamical variable y onto the mechanical variable x :

$$y \leftrightarrow x. \quad (20)$$

As a rule, x will be a position coordinate. Hence there might be some dimensional conversion factor between x and y above, that we will ignore for simplicity. Bearing this in mind, we will finally make the identification

$$\frac{s}{2k_B} \leftrightarrow \frac{m\omega}{\hbar} \quad (21)$$

between thermodynamical and mechanical quantities. We have expressed all the above replacements with a double arrow \leftrightarrow in order to indicate the bijective property of our map between quantum mechanics and classical, irreversible thermodynamics.

On general grounds, applying the replacements (18), (19), (20) and (21), one expects thermodynamical conditional probabilities to map onto mechanical conditional probabilities².

$$f_1 \left(\begin{array}{c} y_2 \\ \tau_2 \end{array} \middle| \begin{array}{c} y_1 \\ \tau_1 \end{array} \right) \leftrightarrow K(x_2, t_2 | x_1, t_1), \quad (22)$$

while thermodynamical unconditional probabilities are expected to map onto mechanical unconditional probabilities:

$$f_1 \left(\begin{array}{c} y \\ \tau \end{array} \right) \leftrightarrow |\psi(x, t)|^2. \quad (23)$$

Here $K(x_2, t_2 | x_1, t_1)$ denotes the quantum–mechanical propagator, and $\psi(x, t)$ is the wavefunction. As in (20) above, one must allow for possible numerical factors between probabilities on the thermodynamical and on the mechanical sides; otherwise bijectivity is perfectly preserved.

Our expectations (22), (23) are borne out by experiment—experiment in our case being explicit computation. Indeed one finds the following. For $\gamma \rightarrow 0$, the irreversible thermodynamics corresponds to the free quantum–mechanical particle:

$$K^{(\text{free})}(x_2, t | x_1, 0) = \sqrt{\frac{k_B}{s}} f_1 \left(\begin{array}{c} x_2 \\ it \end{array} \middle| \begin{array}{c} x_1 \\ 0 \end{array} \right)_{\gamma \rightarrow 0}, \quad (24)$$

²While f_1 is a probability density, K is a probability density amplitude; see ref. [2] for a discussion of this issue.

while, for $\gamma \neq 0$, the irreversible thermodynamics corresponds to the quantum mechanics of a harmonic oscillator:

$$f_1 \left(\begin{matrix} x_2 & | & x_1 \\ it & | & 0 \end{matrix} \right) = \exp \left(\frac{i\omega t}{2} - \frac{\Delta V}{\hbar\omega} \right) \sqrt{\frac{2m\omega}{\hbar}} K^{(\text{harmonic})}(x_2, t|x_1, 0). \quad (25)$$

Above, $V = m\omega^2 x^2/2$ is the harmonic potential, and $\Delta V = V(x_2) - V(x_1)$. Moreover, if $\psi_0(x) = \exp(-m\omega x^2/2\hbar)$ is the harmonic oscillator groundstate, then it holds that, up to normalisation,

$$f_1 \left(\begin{matrix} x \\ it \end{matrix} \right) = \exp \left(-\frac{m\omega}{\hbar} x^2 \right) = |\psi_0^{(\text{harmonic})}(x)|^2, \quad (26)$$

as expected.

Finally the path–integral representation of quantum–mechanical propagators,

$$K(x_2, t_2|x_1, t_1) = \int_{x(t_1)=x_1}^{x(t_2)=x_2} \mathcal{D}x(t) \exp \left\{ \frac{i}{\hbar} \int_{t_1}^{t_2} dt L[x(t), \dot{x}(t)] \right\}, \quad (27)$$

has a nice reexpression in terms of classical, irreversible thermodynamics. Indeed, applying our dictionary (18), (19), (20) and (21) to the mechanical path integral (27), the latter becomes the thermodynamical path integral already seen in (16). This leads us to the following relation between the action integral I of the mechanical system and the entropy S of its thermodynamical counterpart:

$$\frac{i}{\hbar} I \leftrightarrow \frac{1}{k_B} S. \quad (28)$$

It should be remarked that both I and S independently satisfy an extremum principle. In the Gaussian approximation considered here, the respective fluctuations (measured with respect to the corresponding mean values of I and S as given by their extremals) are obtained upon taking the exponentials. We thus obtain the quantum–mechanical wavefunction and the Boltzmann distribution function:

$$\psi = \sqrt{\rho} \exp \left(\frac{i}{\hbar} I \right), \quad \rho_B = Z^{-1} \exp \left(\frac{1}{k_B} S \right). \quad (29)$$

As usual, Z denotes some normalisation factor. Since, by the Born rule, we must have $\rho_B = |\psi|^2$, this provides us with an elegant expression combining thermodynamics and quantum mechanics into a single equation:

$$\psi = Z^{-1/2} \exp \left(\frac{1}{2k_B} S \right) \exp \left(\frac{i}{\hbar} I \right). \quad (30)$$

Eqs. (28) and (30) are very inspiring, as they reveal a fundamental complementarity between the mechanical action integral (on the mechanical side) and the entropy (on the thermodynamical side). We will later on return to the complementarity between these two descriptions, a feature already foreseen by Prigogine [30]. For the moment let us simply remark the following consequence of this complementarity, namely, the symmetrical role played by Planck’s constant \hbar and Boltzmann’s constant k_B . This latter property, and the ensuing entropy quantisation, have been discussed at length in refs. [1, 2].

4 Emergence from irreversibility

It has been claimed that *quantisation is dissipation* [3, 4, 5, 6, 7, 8, 10, 18, 19, 31]—this claim is central to the emergence approach to quantum mechanics. In more precise terms, the previous statement implies that quantum behaviour can be expected from certain deterministic systems exhibiting information loss. One could compare this state of affairs to the relation between (equilibrium) thermodynamics and (classical) statistical mechanics. Namely, information loss in a microscopic theory (statistical mechanics) arises as the result of averaging out over many degrees of freedom; the emergent theory (thermodynamics) contains less information than its microscopic predecessor.

Thanks to the map established in section 3 the picture presented here features quantumness as an intrinsic property of dissipative systems. Conversely, by the same map, any quantum system features dissipation. In our picture, irreversibility and quantumness arise as the two sides of the same coin, thus becoming *complementary* descriptions of a given system (*complementarity* being understood here in Bohr’s sense of the word). As opposed to the emergence property discussed above, the two theories (quantum mechanics and irreversible thermodynamics) contain exactly the same amount of information. It is interesting to observe that closely related views regarding the complementarity between mechanics and thermodynamics were defended long ago by Prigogine [30].

Now it has been (rightly) pointed out that correspondence and emergence are not quite the same concept [23]. This notwithstanding, we can still argue that quantum mechanics continues to arise as an *emergent phenomenon* in our picture. This is so because Boltzmann’s dictum applies: *If something heats up, it has microstructure*. In other words, every thermodynamics is the coarse graining of some underlying statistical mechanics. Thus the mere possibility of recasting a given theory in thermodynamical language proves that the given theory is the coarse-grained version of some finer, microscopic theory.

5 Gaussianity

As a technical remark, we should point out that we have worked throughout in the Gaussian approximation. On the thermodynamical side of our map this corresponds to the linear response theory; on the mechanical side this refers to the harmonic approximation. Within the regime of applicability of this assumption we can safely claim to have provided a rigorous proof of the statement that *quantum mechanics is an emergent phenomenon, at least in the Gaussian approximation*.

Using the fact that any potential can be transformed into the free potential or into the harmonic potential by means of a suitable coordinate transformation (as in Hamilton–Jacobi theory [14, 15]), one would naively state that the Gaussian approximation is good enough to “prove” that quantum mechanics is an emergent phenomenon also beyond the Gaussian regime. However, this “proof” overlooks the fact that quantisation and coordinate changes do not generally commute. Therefore the previous reasoning invoking Hamilton–Jacobi can only be seen as a plausibility argument to support the statement that quantum mechanics must remain an emergent phenomenon *also beyond*

the Gaussian approximation. There is, however, abundant literature dealing with the emergent nature of quantum mechanics, *regardless of* the Gaussian approximation, using techniques that are very different from those presented here, and with a spectrum of applicability that ranges from the smallest [11, 24] to the largest [27, 29]. We will therefore content ourselves with the proof of emergence presented here, the expectation being that some suitable extension thereof (possibly using perturbative techniques) will also apply beyond the Gaussian approximation.

Acknowledgements J.M.I. would like to thank the organisers of the *Sixth International Workshop DICE 2012: Spacetime–Matter–Quantum Mechanics: from the Planck scale to emergent phenomena* (Castiglione, Italy, September 2012) for the invitation to present this talk, for stimulating a congenial atmosphere of scientific exchange, and for the many interesting discussions that followed.

*O muse, o alto ingegno, or m'aiutate;
o mente che scrivesti ciò ch'io vidi,
qui si parrà la tua nobilitate.*—Dante Alighieri.

References

- [1] D. Acosta, P. Fernández de Córdoba, J.M. Isidro and J.L.G. Santander, *An Entropic Picture of Emergent Quantum Mechanics*, Int. J. Geom. Meth. Mod. Phys. **9** (2012) 1250048, arXiv:1107.1898 [hep-th].
- [2] D. Acosta, P. Fernández de Córdoba, J.M. Isidro and J.L.G. Santander, *A Holographic Map of Action onto Entropy* J. Phys. Conf. Ser. **361** (2012) 012027, arXiv:1112.4353 [hep-th].
- [3] D. Acosta, P. Fernández de Córdoba, J.M. Isidro and J.L.G. Santander, *Emergent Quantum Mechanics as a Classical, Irreversible Thermodynamics*, arXiv:1206.4941 [math-ph].
- [4] M. Blasone, P. Jizba and G. Vitiello, *Dissipation and Quantization*, Phys. Lett. **A287** (2001) 205, arXiv:hep-th/0007138.
- [5] M. Blasone, P. Jizba and G. Vitiello, *Dissipation, Emergent Quantization, and Quantum Fluctuations*, in *Decoherence and Entropy in Complex Systems, Selected Lectures from DICE 2002*, H.-T. Elze (ed.), Lecture Notes in Physics **633**, Springer, Berlin (2004).
- [6] M. Blasone, P. Jizba and H. Kleinert, *Quantum Behavior of Deterministic Systems with Information Loss: Path Integral Approach*, Ann. Phys. **320** (2005) 468, arXiv:quant-ph/0504200.
- [7] M. Blasone, P. Jizba and F. Scardigli, *Can Quantum Mechanics be an Emergent Phenomenon?*, J. Phys. Conf. Ser. **174** (2009) 012034, arXiv:0901.3907 [quant-ph].

- [8] M. Blasone, P. Jizba, F. Scardigli and G. Vitiello, *Dissipation and Quantisation for Composite Systems*, Phys. Lett. **A373** (2009) 4106, 0905.4078 [quant-ph].
- [9] R. Carroll, *On the Emergence Theme of Physics*, World Scientific, Singapore (2010).
- [10] H.-T. Elze, *The Attractor and the Quantum States*, Int. J. Qu. Info. **7** (2009) 83, arXiv:0806.3408 [quant-ph].
- [11] H.-T. Elze, *Does Quantum Mechanics Tell an Atomistic Spacetime?*, J. Phys. Conf. Ser. **174** (2009) 012009, arXiv:0906.1101 [quant-ph].
- [12] H.-T. Elze, *Linear Dynamics of Quantum–Classical Hybrids*, Phys. Rev. **A85** (2012) 052109, arXiv:1111.2276 [quant-ph].
- [13] H.-T. Elze, *Four Questions for Quantum–Classical Hybrid Theory*, J. Phys. Conf. Ser. **361** (2012) 012004, arXiv:1202.3448 [quant-ph].
- [14] A. Faraggi and M. Matone, *Equivalence Principle, Planck Length and Quantum Hamilton–Jacobi Equation*, Phys. Lett. **B445** (1998) 77, arXiv: hep-th/9809125.
- [15] A. Faraggi and M. Matone, *The Equivalence Postulate of Quantum Mechanics: Main Theorems*, arXiv:0912.1225 [hep-th].
- [16] G. Groessing, S. Fussy, J. Mesa Pascasio and H. Schwabl, *The Quantum as an Emergent System*, J. Phys. Conf. Ser. **361** (2012) 012008, arXiv:1205.3393 [quant-ph].
- [17] G. Groessing, S. Fussy, J. Mesa Pascasio and H. Schwabl, *A Classical Framework for Nonlocality and Entanglement*, arXiv:1210.4406 [quant-ph].
- [18] G. 't Hooft, *Quantum Gravity as a Dissipative Deterministic System*, Class. Quant. Grav. **16** (1999) 3263, arXiv:gr-qc/9903084.
- [19] G. 't Hooft, *Emergent Quantum Mechanics and Emergent Symmetries*, AIP Conf. Proc. **957** (2007) 154, arXiv:0707.4568 [hep-th].
- [20] G. 't Hooft, *The Emergence of Quantum Mechanics*, AIP Conf. Proc. **1446** (2010) 341.
- [21] G. 't Hooft, *Quantum Mechanics from Classical Logic*, J. Phys. Conf. Ser. **361** (2012) 012024.
- [22] G. 't Hooft, *Relating the Quantum Mechanics of Discrete Systems to Standard Canonical Quantum Mechanics*, arXiv:1204.4926 [quant-ph].
- [23] B. Hu, *Gravity and Nonequilibrium Thermodynamics of Classical Matter*, Int. J. Mod. Phys. **D20** (2011) 697, arXiv:1010.5837 [gr-qc].

- [24] B. Hu, *Emergent/Quantum Gravity: Macro/Microstructures of Spacetime*, J. Phys. Conf. Ser. **174** (2009) 012015, arXiv:0903.0878 [gr-qc].
- [25] A. Khrennikov, “*Einstein’s Dream*” – *Quantum Mechanics as Theory of Classical Random Fields*, arXiv:1204.5172 [quant-ph].
- [26] A. Khrennikov, *Växjö Interpretation of Wave Function: 2012*, arXiv:1210.2390 [quant-ph].
- [27] C. Kiefer, *Can Quantum Theory be Applied to the Universe as a Whole?*, Found. Phys. **40** (2010) 1410.
- [28] L. Onsager and S. Machlup, *Fluctuations and Irreversible Processes*, Phys. Rev. **91** (1953) 1505.
- [29] R. Penrose, *Black Holes, Quantum Theory and Cosmology*, J. Phys. Conf. Ser. **174** (2009) 012001.
- [30] I. Prigogine, *Time, Structure and Fluctuations*, Nobel Prize Lecture (1977).
- [31] M. Sakellariadou, A. Stabile and G. Vitiello, *Noncommutative Spectral Geometry, Dissipation and the Origin of Quantization*, J. Phys. Conf. Ser. **361** (2012) 012025.
- [32] L. Smolin, *Could Quantum Mechanics be an Approximation to Another Theory?*, arXiv:quant-ph/0609109.
- [33] C. Wetterich, *Emergence of Quantum Mechanics from Classical Statistics*, J. Phys. Conf. Ser. **174** (2009) 012008, arXiv:0811.0927 [quant-ph].

Document downloaded from:

<http://hdl.handle.net/10251/64843>

This paper must be cited as:

Fernández De Córdoba Castellá, P.J.; Isidro San Juan, J.M.; Perea, M.H. (2014). Emergent quantum mechanics as a thermal ensemble. *International Journal of Geometric Methods in Modern Physics*. 11(8):1450068-1450084. doi:10.1142/S0219887814500686.



The final publication is available at

<http://dx.doi.org/10.1142/S0219887814500686>

Copyright World Scientific Publishing

Additional Information

EMERGENT QUANTUM MECHANICS AS A THERMAL ENSEMBLE

P. Fernández de Córdoba^{1,a}, J.M. Isidro^{1,b} and Milton H. Perea^{1,2,c}

¹Instituto Universitario de Matemática Pura y Aplicada,
Universidad Politécnica de Valencia, Valencia 46022, Spain

²Departamento de Matemáticas y Física, Universidad Tecnológica
del Chocó, Colombia

^apfernandez@mat.upv.es, ^bjoissan@mat.upv.es

^cmilpecr@posgrado.upv.es

Abstract It has been argued that gravity acts dissipatively on quantum–mechanical systems, inducing thermal fluctuations that become indistinguishable from quantum fluctuations. This has led some authors to demand that some form of time irreversibility be incorporated into the formalism of quantum mechanics. As a tool towards this goal we propose a thermodynamical approach to quantum mechanics, based on Onsager’s classical theory of irreversible processes and on Prigogine’s nonunitary transformation theory. An entropy operator replaces the Hamiltonian as the generator of evolution. The canonically conjugate variable corresponding to the entropy is a dimensionless evolution parameter. Contrary to the Hamiltonian, the entropy operator is not a conserved Noether charge. Our construction succeeds in implementing gravitationally–induced irreversibility in the quantum theory.

1 Introduction

It has been known for long that weak interactions violate CP–invariance [10]. By the CPT theorem of quantum field theory, time invariance must also be violated in weak interactions; recent observations [32] confirm this expectation. Now quantum field theory is an extension of quantum mechanics. Since time invariance is naturally implemented in the latter, it would appear that only CP–violating quantum field theories can also violate time invariance, because quantum mechanics as we know it is symmetric under time reversal.

Actually such is not the case. A number of firmly established quantum–gravity effects have been shown to be intrinsically irreversible; for background see, *e.g.*, [23, 30, 51, 52, 55] and references therein. From the independent perspective of statistical physics [40] it has also been suggested that time irreversibility should be taken into account at the more fundamental level of the differential equations governing mechanical processes. This is in sharp contrast with standard thinking, where irreversibility is thought to arise through *time–irreversible* initial conditions imposed on the solutions to *time–reversible* evolution equations. In view of this situation, a number of authors have called for the due modifications to the standard quantum–mechanical formalism (for a

detailed account and original references see, *e.g.*, [38]). Specifically, in this paper we tackle the problem of incorporating some form of time irreversibility at the level of the differential equation governing evolution [40].

Closely related to this viewpoint is the *emergent approach* to physics. The latter has been the subject of a vast literature (see [8] for a comprehensive review), but let us briefly mention some noteworthy aspects. The notion of an *emergent theory*, that is, the concept that a given physical theory could be an effective model of some deeper-level degrees of freedom, has been postulated of a number of existing theories, most notably of gravity and of quantum mechanics. In the particular case of the latter, refs. [3, 14, 15, 22, 24, 25, 26, 48] address this issue from a number of different perspectives. The paradigm that *quantisation is dissipation*, implicitly present in some of the above approaches, has been made precise in [6, 5]. Frequently, these takes on quantum physics can be completely recast in purely classical terms [4, 29, 53]. An alternative perspective, based on classical nonequilibrium thermodynamics [35], has been advocated in [1, 2, 16]. Beyond quantum mechanics, the relevance of nonequilibrium physics for quantum gravity and strings has been emphasised recently [18, 27].

The basic physical assumption we will make use of posits that *spacetime is not a fundamental concept, but rather an emergent phenomenon instead*. In fact this hypothesis is not at all new (for references and background see, *e.g.*, [30]), some of its most recent incarnations being [36, 37, 50]. Once spacetime is no longer regarded as a fundamental concept, but rather as a derived notion, then every theory that makes use of spacetime concepts automatically qualifies as emergent. Such is the case of quantum mechanics. For our purposes it will suffice to concentrate on the time variable and expose its emergent nature. We will therefore try to express time in terms of thermodynamical quantities, and explore the consequences for the quantum theory. Again, the notion of time as having a thermodynamical origin is not new [7, 11], having reappeared more recently in [19, 41, 44, 43]; see also [13, 17, 20, 21] for related views. New to our approach is the notion that *an emergent time variable automatically implies that quantum theory itself qualifies as an emergent phenomenon*. Specifically, the possibility of reexpressing the nonrelativistic Schrodinger equation in purely entropic terms (instead of its usual Hamiltonian language) implies that quantum mechanics involves some degree of coarse graining of microscopic information. In our approach, the very existence of an entropy operator replacing the Hamiltonian operator is an unequivocal clue of this coarse graining.

To begin with, we would like to draw attention to the following analogy. On one hand we have the quantum-mechanical time-energy uncertainty relation

$$\Delta E \Delta t \sim \hbar. \quad (1)$$

On the other hand, in the theory of irreversible thermodynamics [34, 35], one computes the average product of the fluctuations of the entropy and the temperature for a thermodynamical system slightly away from equilibrium (this is the linear regime, also called the Gaussian approximation). This product turns out to be given by [31]

$$\Delta S \Delta T = k_B T, \quad (2)$$

k_B being Boltzmann's constant. The change of variables

$$\tau := \ln \left[\frac{T}{T_0} \right], \quad (3)$$

where T_0 is some reference temperature, reduces (2) to

$$\Delta S \Delta \tau \geq k_B. \quad (4)$$

In (4) we have taken the liberty of replacing the equality sign of (2) with an inequality; the latter is saturated in the Gaussian approximation (used in the derivation of (2)). Beyond the Gaussian regime, one expects the inequality to hold strictly. As we will see, the analogy between (1) and (4) is more than just a happy coincidence—it is in fact anything but accidental.

2 Emergent time

Let t and T respectively denote nonrelativistic time and absolute temperature, as measured by an inertial observer that will be kept the same throughout. We posit that t^{-1} equals T modulo dimensional factors:

$$\frac{C}{t} = \frac{k_B}{k} T. \quad (5)$$

Here C is a dimensionless numerical factor, whose value we will pick presently in order to suit our needs. Modulo this C , which will play a prominent role in what follows, the relation (5) between time and temperature was postulated long ago by de Broglie [7]. A related change of variables has been used more recently in [45].

Beyond purely dimensional grounds, there are deeper motivations for Eq. (5). Specifically, in [2, 16] we have established a map between quantum mechanics (in the Gaussian approximation) and the classical theory of irreversible thermodynamics (in the linear regime).¹ In this latter theory [35] we have N independent thermodynamical coordinates y^1, \dots, y^N on which the entropy S depends, and N conjugate forces $Y_k := \partial S / \partial y^k$. Let t' denote thermodynamical time. The assumption of linearity between the velocities \dot{y}^k and the forces Y_j amounts to

$$\dot{y}^i = \frac{dy_i}{dt'} = \sum_{j=1}^N L^{ij} Y_j, \quad Y_i = \sum_{j=1}^N R_{ij} \dot{y}^j, \quad R_{ij} = (L^{ij})^{-1}. \quad (6)$$

Under the assumption that the underlying microscopic dynamics is time-reversible, the constant matrix L_{ij} turns out to be symmetric (Onsager's reciprocity theorem) [34]. By (6), the time rate of entropy production can be written either as a quadratic form in the velocities, or as a quadratic form in the forces:

$$\dot{S} = \sum_{i,j=1}^N R_{ij} \dot{y}^i \dot{y}^j = \sum_{i,j=1}^N L^{ij} Y_i Y_j. \quad (7)$$

¹As argued in [2, 16], the linear regime in irreversible thermodynamics is the analogue of the semiclassical, or Gaussian, approximation to quantum mechanics.

We see that it is not the entropy S , but its time rate of production \dot{S} , that plays the role of a (harmonic) Hamiltonian, because²

$$\dot{S} = \frac{dS}{dt} = \frac{1}{2} \sum_{i,j=1}^N R_{ij} \dot{y}^i \dot{y}^j + L^{ij} Y_i Y_j \dots \quad (8)$$

Here again we see that inverse time can be regarded as temperature. In Eqs. (6)–(8) above, the thermodynamical time t' and the mechanical time t are related as per the Wick rotation, $t' = it$ [2, 16]. Thus we expect a thermodynamical approach to quantum mechanics to involve the complexification of time. Multiplying (5) through by H/T , one realises that (5) is roughly equivalent to

$$C \frac{dS}{dt} = \frac{k_B}{k} H, \quad (9)$$

which bridges the gap between the mechanical point of view (the right-hand side of (9)) and the thermodynamical point of view (the left-hand side). The above is a handwaving argument to justify equating the time variation of the entropy with the energy (modulo dimensional constants); we will actually *derive* Eq. (9) later on (see (26)). Eq. (9) is also important because it holds beyond its Gaussian limit given in (8). In what follows we will work out in detail the relationship between the mechanical and the thermodynamical points of view expressed above.

3 Entropy vs. energy

3.1 The energy picture

For reasons that will become apparent presently let us call quantum mechanics, in its standard formulation, the *energy picture* of quantum mechanics; we will also use the term *H-picture*.³ The evolution of pure quantum states is governed by the Schroedinger equation,

$$ik \frac{d\psi}{dt} = H\psi. \quad (10)$$

The general solution to the above reads $\psi(t) = U(t)\psi(0)$, where

$$U(t) := T \exp \left[-\frac{i}{k} \int_0^t H(\tilde{t}) d\tilde{t} \right], \quad (11)$$

and T denotes the ordering operation along the evolution parameter \tilde{t} . When $t \in \mathbb{R}$, the time-evolution operators $U(t)$ define a 1-parameter group of unitary operators that ensure the reversibility of time flow in the *H-picture*.

² L^{ij} is positive definite for a dissipative process, hence also R_{ij} .

³We use the term *picture* instead of its synonym *representation* in order to avoid confusion with the technical meaning of the latter term in quantum-mechanical contexts such as *choice of basis in Hilbert space*, or *group representation*, or similar. Expressions such as *Schroedinger picture*, or *Heisenberg picture*, or related terms used in standard quantum mechanics should also not be confused with our use of the word *picture*.

3.2 The entropy picture

The purpose of this section is to develop *the entropy picture* of quantum mechanics, or the *S-picture* for short.

Under the combined changes of variables (5) and (3), the evolution equation (10) becomes

$$-\frac{ik_B d\psi}{C d\tau} = S\psi, \quad (12)$$

where we have defined the entropy operator S

$$S := \frac{H}{T}. \quad (13)$$

The new evolution parameter τ is dimensionless, while S carries the dimension of an entropy. Our time variable τ coincides with the thermal time of [11, 41, 44], the latter specified to the nonrelativistic limit corresponding to the Schroedinger wave equation.

We will see presently that $C \in \mathbb{C}$, so our evolution variable τ will actually be a complexified (or Wick-rotated), nonrelativistic, dimensionless, thermal-time variable.

The solution to the evolution equation (12) can be written as

$$\psi(\tau) = S_C(\tau)\psi(0), \quad \tau \geq 0, \quad (14)$$

where

$$S_C(\tau) := \mathbb{T} \exp \left[\frac{iC}{k_B} \int_0^\tau S(\tilde{\tau}) d\tilde{\tau} \right] \quad (15)$$

and \mathbb{T} denotes the ordering operation along the the evolution parameter $\tilde{\tau}$. If we now pick $C \in \mathbb{R}$, the evolution operators $\{S_C(\tau), \tau \in \mathbb{R}\}$ in (15) form a 1-parameter group of unitary operators.

As long as C remains real, Eqs. (12)–(15) above simply restate standard quantum mechanics using the alternative set of variables (τ, S) . It is only for $C \notin \mathbb{R}$ that time evolution can become irreversible. For this purpose let us set, dropping an irrelevant real normalisation,

$$C := e^{i\phi}, \quad \phi \in \mathbb{R}. \quad (16)$$

On the complex plane, (16) corresponds to Wick-rotating the time axis by an angle ϕ . Now certain special values of ϕ are known to correspond to specific physical situations. For example, $\phi = 0$ corresponds to standard quantum mechanics, while $\phi = \pi$ implements the time reverse of $\phi = 0$. The value $\phi = -\pi/2$ gives a positive real argument within the exponential of (15); we will see in section 3.3 that this corresponds to the case of maximal entropy production, or maximal dissipation. Finally, the value $\phi = \pi/2$ gives a negative real argument within the exponential of (15); this will turn out to correspond to the unphysical situation of maximal *antidissipation*. All other values of ϕ therefore correspond to intermediate situations between exactly unitary evolution (eventually, time-reversed) and maximal dissipation (eventually, antidissipation). For obvious reasons we must pick the quadrant corresponding to the forward time direction and positive dissipation, *i.e.*, $\phi \in [-\pi/2, 0]$. Let the dimensionless variable $x \in \mathbb{R}$ be a measure of the external gravitational field acting on the particle of mass m described by the Hamiltonian H , such that $x = 0$ describes the absence of gravitation, and $x \rightarrow \infty$

describes the case of a strong gravitational field acting on m . From what is known concerning the effects of gravitational fields on the quantum mechanics of particles we expect the phase ϕ to depend on x roughly as follows:

$$\phi(x) = -\frac{\pi}{2} \cdot \mathbf{1} - e^{-x}, \quad x \geq 0. \quad (17)$$

Indeed, for $x = 0$ we have a perfectly unitary evolution ($\phi = 0$) as befits quantum particles in the absence of gravitation, while for strong gravitational fields ($x \rightarrow \infty$) we have $\phi \rightarrow -\pi/2$, and unitarity gives way to dissipation. Of course, the precise profile (17) for the function $\phi(x)$ is just one out of many possible, but it captures the right physical behaviour, namely, that gravitational fields induce thermal dissipative effects in the quantum theory, in such a way as to render quantum uncertainties indistinguishable from statistical fluctuations [46, 47]. In the absence of a gravitational field, any inertial observer perceives a clear-cut separation between these two types of fluctuations.

Altogether, (16) and (17) yield

$$C(x) = \exp \left[-\frac{i\pi}{2} \cdot \mathbf{1} - e^{-x} \right]. \quad (18)$$

For the rest of this paper we will concentrate on the limiting case of a weak gravitational field. So we have⁴

$$C(\varepsilon) \simeq 1 + i\varepsilon, \quad \varepsilon = -\frac{\pi x}{2} \quad x \geq 0. \quad (19)$$

It remains to identify a dimensionless variable x that can provide a physically reasonable measure of a weak gravitational field acting on the quantum particle.⁵ It is standard to parametrise such a field by the metric $g_{\mu\nu} = \eta_{\mu\nu} + h_{\mu\nu}$, where $\eta_{\mu\nu}$ is the Minkowski metric, and $h_{\mu\nu}$ a small correction. It is also convenient to introduce the quantities $h^\alpha{}_\mu := \eta^{\lambda\alpha} h_{\mu\lambda}$ and $h := h^\alpha{}_\alpha = \eta^{\sigma\lambda} h_{\sigma\lambda}$. The linearised Einstein equations read

$$-16\pi T^{\nu}{}_{\mu} = \eta^{\sigma\lambda} \frac{\partial}{\partial x^\sigma} \frac{\partial}{\partial x^\lambda} h_{\mu}{}^{\nu} - \frac{1}{2} \eta^{\nu\mu} h, \quad (20)$$

and we can take $x = \langle h \rangle$ as a variable that satisfies our needs, at least in the weak field limit considered here. The angular brackets in $\langle h \rangle$ stand for the average value of the function h over the spacetime region of interest. That $\langle h \rangle$ is nonnegative follows from the fact that [49]

$$h = 4 \frac{[T_{\alpha\alpha}]}{r}, \quad T^{\alpha}{}_{\alpha} \geq 0. \quad (21)$$

The square brackets around the trace $T^{\alpha}{}_{\alpha}$ stand for the evaluation at a time earlier than that of interest by the interval needed for a signal to pass with unit velocity from the element $dx dy dz$ to a point a distance r apart.

Substitution of (19) into (15) leads to

$$S_{1+i\varepsilon}(\tau) := \mathbb{T} \exp \left[\frac{i - \varepsilon}{\kappa_B} \int_0^\tau S(\tilde{\tau}) d\tilde{\tau} \right], \quad (22)$$

⁴We will henceforth drop terms of order ε^2 and higher.

⁵In a sense, the situation analysed here is complementary to that described in ref. [28].

and the set $\{S_{1+i\varepsilon}(\tau), \tau \geq 0\}$ forms a 1-parameter *semigroup* of nonunitary operators. In the limit $\varepsilon = 0$, the set $\{S_1(\tau), \tau \in \mathbb{R}\}$ becomes again the 1-parameter group of unitary operators given in (15) (with $C = 1$). The parameter ε allows for a continuous transition between the unitary ($\varepsilon = 0$) and the nonunitary ($\varepsilon \neq 0$) regimes.

Our choice (19) yields in (12)

$$- (i + \varepsilon)k_B \frac{d\psi}{d\tau} = S\psi. \quad (23)$$

It makes sense to call (23) the *entropic Schroedinger equation*. Again, in the limit $\varepsilon = 0$ we recover a Schroedinger-like equation,

$$- ik_B \frac{d\psi}{d\tau} = S\psi. \quad (24)$$

The ε term on the left-hand side of (23) can be regarded as a perturbative correction to the derivative term in (24). We see that it breaks unitarity explicitly, already at the level of the differential equation governing evolution. The physical reason for this breakdown of unitarity is the presence of an external gravitational field, the strength of which is parametrised by ε .

Altogether, Eqs. (22) and (23) define the S -picture of quantum mechanics.

3.3 S rather than H

One might argue that there is no need for the S -picture because the H -picture suffices. Indeed it has been known for long that a simple, “phenomenological” implementation of nonunitarity within the H -picture consists in the addition of a nonvanishing imaginary part to the time variable t in (10):

$$(i + \varepsilon')k \frac{d\psi}{dt} = H\psi. \quad (25)$$

Here $\varepsilon' \in \mathbb{R}$ is a small (dimensionless) perturbation. What distinguishes (25) from its entropic partner (23), and why is the latter to be preferred over the former?

In terms of the variables (t, H) , invariance under translations in t is reflected in the conservation of the Noether charge H . There exists no preferred origin $t = 0$ for time. While (25) certainly leads to energy dissipation, the natural physical quantity to describe dissipation is the entropy, where one expects to find $dS/dt \geq 0$ instead of a conservation law. In the variables (τ, S) of (23), one expects to have no conservation law at all; one actually finds⁶

$$\frac{dS}{d\tau} = \frac{k_B}{k} (1 - i\varepsilon)H, \quad (26)$$

as anticipated in (9). Now, from (8) and the Wick rotation $t' = it$, we conclude that it is $\text{Im}(dS/dt)$, and not $\text{Re}(dS/dt)$, that accounts for dissipation. Indeed, recalling (5), the real part of (26) is the usual thermodynamical definition of temperature, $\partial S/\partial E =$

⁶Here we are assuming $dH/dt = 0$ for simplicity.

$1/T$. In other words, even if $\text{Re}(dS/dt) = k_B H/k \neq 0$, this latter equation alone does not account for dissipation. Since

$$\text{Im} \left[\frac{dS}{dt} \right] = -\varepsilon \frac{k_B}{k} H, \quad (27)$$

there will be no conservation law for S under evolution in t if $\varepsilon \neq 0$. The same conclusion applies to evolution in τ . Furthermore, dissipation vanishes in the limit $\varepsilon = 0$ as had to be the case. Finally, for Eq. (27) to be consistent with the second law of thermodynamics, we need to choose $\varepsilon < 0$, as anticipated in (19). This latter point is obvious in the Gaussian approximation (8), where H is a positive-definite quadratic form, but it also holds true beyond that approximation, because H is bounded from

below (if needed, one adds a constant to shift the energy of the groundstate, to make it nonnegative).

As already remarked, the operators (22) are unitary iff $\varepsilon = 0$. Here we see that their nonunitarity differs considerably in the two cases $\varepsilon > 0$ and $\varepsilon < 0$. Since $\tau \geq 0$, had ε been positive, this would have turned the $S_{1+i\varepsilon}(\tau)$ into a semigroup of *contraction operators* [54], which would describe an unphysical *antidissipative* world. On the contrary, the choice $\varepsilon < 0$ of (19) leads to the opposite behaviour, *dilatation*, which is in agreement with the second law of thermodynamics.

In the H -picture, whenever the Hamiltonian is time-independent, there exist energy eigenstates φ satisfying $H\varphi = E\varphi$; the wavefunction ψ then factorises as $\psi = \varphi \exp(-iEt/k)$. A similar property holds in the S -picture, assuming that H remains t -independent, hence also τ -independent. In this latter case one can readily check that the factorised wavefunctions

$$\psi = \varphi e^{(i-\varepsilon)\tau s}, \quad (28)$$

where φ does not depend on τ , lead to the eigenvalue equation

$$S\varphi = s k_B \varphi, \quad (29)$$

with $s \in \mathbb{R}$ playing the role of a dimensionless entropic eigenvalue. Again, eqs. (28) and (29) above are in perfect agreement with the second law of thermodynamics.

To summarise, unitarity is violated in the S -picture, where $\varepsilon < 0$ appears, but not in the H -picture, where the evolution equations (10) and (11) remain strictly valid. As such, this “change of picture” between H and S is an instance of Prigogine’s *nonunitary transformation* [40]. The apparent dilemma, “Is unitarity violated or not?”, will be resolved in section 3.6.

3.4 Uncertainty vs. the second law

It is common lore that, at least for large enough temperatures, quantum fluctuations are negligible compared to thermal statistical fluctuations [31]. When stating that, *in the presence of a gravitational field*, quantum fluctuations are inextricably linked with thermal statistical fluctuations, one is postulating a new kind of uncertainty principle: *the indistinguishability between quantum and statistical fluctuations* [9, 46, 47]. Here

we will provide an example of this indistinguishability. A look at Eq. (1) and a comparison of (23) with (10) leads one to conclude the following uncertainty relation:

$$\Delta S \Delta \tau \geq k_B. \quad (30)$$

It is rewarding to see the product of *thermal fluctuations* found in (4) nicely matched by the product of *quantum-mechanical uncertainties* (30). This is more than just a coincidence—it is an expression of the fact that, *in the presence of a gravitational field*, quantum uncertainties can be understood as statistical fluctuations possessing a thermal origin [46, 47]. The above uncertainty relation leads to the factor $2k_B$ replacing the quantum of action \hbar , in perfect agreement with the results of [45].

Since τ is dimensionless, we can safely set $\Delta \tau = 1$ in (30) with the certainty that this numerical value will not change upon changing units. This leads to

$$\Delta S \geq k_B > 0, \quad (31)$$

which becomes the familiar second law of thermodynamics when written as

$$\Delta S \geq 0. \quad (32)$$

Strictly speaking, the equality in (32) is never attained, as $k_B > 0$. However, in the limit $k_B \rightarrow 0$ we can saturate the inequality in (32) and have $\Delta S = 0$. The limit $k_B \rightarrow 0$ has been argued to correspond to the semiclassical limit $\hbar \rightarrow 0$ of quantum mechanics [1].⁷

We conclude that the quantum-mechanical uncertainty principle provides the refinement (31) of the second law of thermodynamics (32), to which it becomes strictly equivalent in the semiclassical limit $k_B \rightarrow 0$.

3.5 Commutators vs. fluctuations

In the standard quantum-mechanical formalism, nonvanishing commutators account for uncertainties. Fortunately for us, uncertainties can arise from fluctuations just as well as from commutators. In keeping with our previous arguments, here we will take statistical fluctuations as our starting point, in order to arrive at commutators.

We will illustrate our point by means of an example. Consider a thermodynamical system described by the temperature T , the pressure p , the volume V and the entropy S . Now, in the Gaussian approximation, the probability P of a fluctuation Δp , ΔV , ΔT , ΔS is given by [31]

$$P = Z^{-1} \exp \left[-\frac{1}{2k_B T} (-\Delta p \Delta V + \Delta T \Delta S) \right]. \quad (33)$$

If we have an equation of state $F(p, V, T) = 0$ we can solve for the temperature to obtain $T = g(p, V)$. This allows us to rewrite (33) as

$$P = Z^{-1} \exp \left[-\frac{1}{2k_B} \left(-\frac{\Delta p \Delta V}{g(p, V)} + \frac{\Delta T \Delta S}{T} \right) \right]. \quad (34)$$

⁷In order to conform to the conventions of ref. [50], in ref. [1] we have normalised the quantum of entropy to the value $2\pi k_B$ instead of the value $2k_B$ used here.

This somewhat clumsy expression can be further simplified if we assume our system to be an ideal gas, $pV = S_0 T$:⁸

$$P = Z^{-1} \exp \left[-\frac{1}{2k_B} \left(-S_0 \frac{\Delta p \Delta V}{pV} + \frac{\Delta T \Delta S}{T} \right) \right]. \quad (35)$$

Finally define the dimensionless variables

$$p_1 := -\ln \left[\frac{p}{p_0} \right], \quad q_1 := \ln \left[\frac{V}{V_0} \right], \quad p_2 := \ln \left[\frac{T}{T_0} \right], \quad q_2 := \frac{S}{S_0}, \quad (36)$$

where p_0, V_0, T_0, S_0 are fixed reference values, to arrive at

$$P = Z^{-1} \exp \left[-\frac{S_0}{2k_B} (\Delta p_1 \Delta q_1 + \Delta p_2 \Delta q_2) \right]. \quad (37)$$

The argument of the above exponential is very suggestive. Indeed, let q_1, q_2 be coordinates on the thermodynamical configuration space Y , and consider the (dimensionless) symplectic form on the cotangent bundle T^*Y given by

$$\Omega = dp_1 \wedge dq_1 + dp_2 \wedge dq_2. \quad (38)$$

We have

$$\Omega = d\theta, \quad \theta := p_1 dq_1 + p_2 dq_2. \quad (39)$$

Now $\Delta p_1 \Delta q_1 + \Delta p_2 \Delta q_2$ equals the (symplectic) area of a 2-dimensional open surface D within T^*Y ,

$$\Delta p_1 \Delta q_1 + \Delta p_2 \Delta q_2 = \int_D (dp_1 \wedge dq_1 + dp_2 \wedge dq_2) = \int_D d\theta, \quad (40)$$

the boundary of which is $\partial D \neq \emptyset$ (the surface D can be taken to be open precisely because D is caused by a fluctuation). Applying Stokes' theorem we can thus write for the probability (37)

$$\begin{aligned} P &= Z^{-1} \exp \left[-\frac{S_0}{2k_B} \int_D \Omega \right] \\ &= Z^{-1} \exp \left[-\frac{S_0}{2k_B} \int_D d\theta \right] = Z^{-1} \exp \left[-\frac{S_0}{2k_B} \int_{\partial D} \theta \right]. \end{aligned} \quad (41)$$

Starting from fluctuations, which render commutators unnecessary in the thermodynamical description, we have arrived back at a mechanical description in terms of a symplectic form. The inverse of the latter gives Poisson brackets and, upon quantisation, commutators. This simple example illustrates the thermodynamical analogue of quantum commutators.

⁸Here S_0 is the mole number n times the gas constant R . Whether or not our system is an ideal gas is immaterial, as the change of variables (36) can be modified appropriately without altering our conclusions.

3.6 Quantumness vs. dissipation

To round up our presentation of quantum theory in thermodynamical terms, let us see how suggestive Eq. (5) is of a closely related geometric construction.

Assume being given two copies of the complex plane \mathbb{C} , one parametrised by the complex coordinate z , the other by w . Then the set formed by the two coordinate charts $\{z \in \mathbb{C}\}$ and $\{w \in \mathbb{C}\}$ defines an (analytic) atlas covering the Riemann sphere S^2 , where $z = 0$ (respectively, $w = 0$) corresponds to the north pole (respectively, south pole). The transition between these coordinates is $w = -1/z$, which coincides with (5) up to dimensional constants.

In this way it is very tempting to identify (t, T) with (z, w) ; of course, the latter are real 2-dimensional variables, while the former are real 1-dimensional. We may thus regard the pair “time, temperature” as coordinates on a copy of the circle S^1 that one might call *the circle of time*, or *the circle of temperature* just as well [12]. Since the circle S^1 is a compact manifold, charting it smoothly requires at least two coordinate charts (in our case T and t). In physical terms, temperature is the physical variable that compactifies time, and viceversa [33]. The rotation (by 2π radians) of any circle S^1 joining the north and south poles spans the whole sphere S^2 . This same geometrical rotation (now by an angle ε) corresponds to the Wick rotation of (19). Thus Wick-rotating the circle of time S^1 by all possible angles generates the whole sphere S^2 .

Now, the H -picture discussed in section 3.1 corresponds to viewing quantum mechanics *in the absence of dissipation*. As already observed, this situation corresponds to *the absence of a gravitational field*. On the Riemann sphere S^2 , the H -picture describes quantum mechanics with respect to an evolution parameter t that runs over the real axis $\text{Im}(z) = 0$ within the coordinate chart $\{z \in \mathbb{C}\}$ around the north pole. Dissipation appears when Wick-rotating this axis by $\varepsilon < 0$ as done in (19) and changing variables as per (5), in order to work in the coordinate chart $\{w \in \mathbb{C}\}$ around the south pole; this is how the S -picture of section 3.2 arises. The H -picture is purely conservative (because it satisfies the conservation law $dH/dt = 0$), the S -picture is dissipative (because it satisfies the second law $\text{Im}(dS/dt) \geq 0$). We realise that the S -picture involves dissipation/gravity, while the H -picture involves neither. This is analogous to the equivalence principle of gravitation, whereby the action of a gravitational field can be (locally) turned off by an appropriate change of coordinates.

The foregoing arguments implement a relativity of the notion of *quantumness* vs. *dissipation* by means of $U(1)$ -transformations. However this $U(1)$ symmetry of Wick rotations is broken the very moment one selects a specific value for ε . Hence the distinction between quantumness and dissipation (falsely) appears to be absolute, while in fact it is not. In particular, just as gravity can be (locally) gauged away, so can dissipation. Turn this argument around to conclude that *quantumness, or alternatively dissipation, can be gauged away*, although never the two of them simultaneously. Quantumness is gauged away in the limit $\phi \rightarrow -\pi/2$, while dissipation is gauged away in the limit $\phi \rightarrow 0$.⁹ Moreover, our statement concerning the *relativity of dissipation* is equivalent to our statement concerning the *relativity of quantumness*. A concept closely related to this latter notion was put forward in [42]. Compare now the concept *relativ-*

⁹Since we have systematically dropped terms of order ε^2 and higher, some of our expressions may need amendments before taking the limit $\phi \rightarrow -\pi/2$, but this does not invalidate our reasoning.

ity of quantumness with its transpose *quantum relativity*, or *quantum gravity* as usually called: beyond the pun on words, these two concepts appear to be complementary, in Bohr’s sense of the term “complementarity”.

4 Discussion

Our approach to quantum mechanics is an attempt to meet the requirement (demanded *e.g.* in [39, 46, 47], among others) that gravity be incorporated into the foundations of quantum theory. The absence of a link between quantum and gravitational effects in the standard formulation of quantum theory is a feature that has been claimed to lie at the heart of some of the conceptual difficulties facing the foundations of quantum mechanics.

Specifically, in this paper we have presented a thermodynamical approach (following the classical theory of irreversible thermodynamics [34, 35, 40]) that provides a viable answer to this request, at least in a certain limit to be specified below. The incorporation of gravitational effects in a discussion of the principles of quantum mechanics is being addressed here through the appearance of dissipation as a gravitational effect. In this way the time–reversal symmetry of quantum mechanics is destroyed. Nonunitarity is implemented here by means of a Wick rotation; the latter is a consequence of gravitation. In fact Wick rotations of the time axis are the quantum–mechanical counterpart to the equivalence principle of gravitation. Just as gravity can be (locally) gauged away, so can dissipation/quantumness.

For ease of reference, below we present Eqs. (5), (22), (23), (27) and (30) again in order to summarise the relevant expressions of the S –picture of quantum mechanics developed in this paper. We have

$$\frac{e^{i\varepsilon}}{t} = \frac{k_B}{k} T, \quad \tau = \ln \left[\frac{T}{T_0} \right], \quad (42)$$

which relates inverse time and temperature through a Wick rotation by a small, dimensionless parameter $\varepsilon < 0$. The latter encodes the strength of an external gravitational field; in the absence of gravitation we have $\varepsilon = 0$. Applying the change of variables (42), the usual Schroedinger equation and the uncertainty principle become

$$k_B \frac{d\psi}{d\tau} = (i - \varepsilon) S \psi, \quad S = \frac{H}{T}, \quad \Delta S \Delta \tau \approx k_B, \quad (43)$$

where the Hamiltonian operator H is replaced with the entropy operator S . This entropic Schrodinger equation is solved by $\psi(\tau) = S(\tau)\psi(0)$, where the evolution operators $S(\tau)$ in the dimensionless parameter τ , defined as

$$S(\tau) := T \exp \left[\frac{i - \varepsilon}{k_B} \int_0^\tau S(\tilde{\tau}) d\tilde{\tau} \right], \quad (44)$$

satisfy a 1–parameter semigroup of nonunitary operators (above, T denotes operator ordering along the parameter $\tilde{\tau} \geq 0$). Finally the expression

$$\text{Im} \left[\frac{dS}{d\tau} \right] = -\varepsilon \frac{k_B}{k} H \quad (45)$$

relates the rate of entropy production to the Hamiltonian operator, while at the same time fixing the sign of ε to be negative, in compliance with the second law of thermodynamics.

The previous equations hold in the limiting case of a weak gravitational field acting on a quantum particle described by the same equations. In view of the smallness of ε in (44), it is only for large values of τ that one can hope to measure the appearance of unitarity loss. It is important to realise that, by just switching back and forth between the energy picture (standard quantum mechanics) and the entropy picture (as summarised in Eqs. (42), (43), (44) and (45)), either quantumness or dissipation can be gauged away, though never the two of them simultaneously. This fact we take as a reflection of the equivalence principle of relativity, whereby gravitational fields can be (locally) gauged away by means of coordinate changes.

The postulate (5) (first presented long ago by de Broglie [7] without the Wick rotation $e^{i\epsilon}$) leads to *considering time as emergent a property as temperature itself*. In this way unitarity violation can also be regarded as an emergent phenomenon.

Acknowledgements J.M.I. would like to thank the organisers of the *Sixth International Workshop DICE 2012: Spacetime – Matter – Quantum Mechanics: from the Planck scale to emergent phenomena* (Castiglioncello, Italy, September 2012), for stimulating a congenial atmosphere of scientific exchange, and for the many interesting discussions that followed.

Forse altro canterà con miglior plettro—L. Ariosto.

References

- [1] D. Acosta, P. Fernández de Córdoba, J.M. Isidro and J.L.G. Santander, *An Entropic Picture of Emergent Quantum Mechanics*, Int. J. Geom. Meth. Mod. Phys. **9** (2012) 1250048, arXiv:1107.1898 [hep-th].
- [2] D. Acosta, P. Fernández de Córdoba, J.M. Isidro and J.L.G. Santander, *Emergent Quantum Mechanics as a Classical, Irreversible Thermodynamics*, Int. J. Geom. Meth. Mod. Phys. **10** (2013) 1350007, arXiv:1206.4941 [math-ph].
- [3] S. Adler, *Quantum Theory as an Emergent Phenomenon*, Cambridge University Press, Cambridge (2004).
- [4] G. Bertoldi, A. Faraggi and M. Matone, *Equivalence Principle, Higher Dimensional Mobius Group and the Hidden Antisymmetric Tensor of Quantum Mechanics*, Class. Quant. Grav. **17** (2000) 3965, arXiv:hep-th/9909201.
- [5] M. Blasone, P. Jizba and F. Scardigli, *Can Quantum Mechanics be an Emergent Phenomenon?*, J. Phys. Conf. Ser. **174** (2009) 012034, arXiv:0901.3907 [quant-ph].
- [6] M. Blasone, P. Jizba and G. Vitiello, *Dissipation, Emergent Quantization, and Quantum Fluctuations*, in *Decoherence and Entropy in Complex Systems*, Se-

- lected Lectures from DICE 2002*, H.-T. Elze (ed.), Lecture Notes in Physics **633**, Springer, Berlin (2004).
- [7] L. de Broglie, *La Thermodynamique Cachée des Particules*, Ann. Inst. Poincaré (A) Physique Théorique **1** (1964) 1.
- [8] R. Carroll, *On the Emergence Theme of Physics*, World Scientific, Singapore (2010).
- [9] A. Caticha, *Entropic Dynamics, Time and Quantum Theory*, J. Phys. A: Math. Theor. **44** (2011) 225303, arXiv:1005.2357 [quant-ph].
- [10] J. H. Christenson, J. W. Cronin, V. L. Fitch and R. Turlay, *Evidence for the 2π Decay of the K_2^0 Meson*, Phys. Rev. Lett. **13** (1964) 138.
- [11] A. Connes and C. Rovelli, *Von Neumann Algebra Automorphisms and Time Thermodynamics Relation in General Covariant Quantum Theories*, Class. Quant. Grav. **11** (1994) 2899, arXiv:gr-qc/9406019.
- [12] D. Dolce, *Intrinsic Periodicity: the Forgotten Lesson of Quantum Mechanics*, arXiv:1304.4167 [quant-ph].
- [13] G. Ellis, *The Arrow of Time and the Nature of Spacetime*, arXiv:1302.7291 [gr-qc].
- [14] H.-T. Elze, *The Attractor and the Quantum States*, Int. J. Qu. Info. **7** (2009) 83, arXiv:0806.3408 [quant-ph].
- [15] H.-T. Elze, *Symmetry Aspects in Emergent Quantum Mechanics*, J. Phys. Conf. Ser. **171** (2009) 012034.
- [16] P. Fernández de Córdoba, J.M. Isidro and Milton H. Perea, *Emergence from Irreversibility*, arXiv:1210.7785 [math-ph].
- [17] R. Gambini, L. Garc'ia-Pintos and J. Pullin, *An Axiomatic Formulation of the Montevideo Interpretation of Quantum Mechanics*, Studies in History and Philosophy of Modern Physics **42** (2011) 256, arXiv:1002.4209 [quant-ph].
- [18] N. Gray, D. Minic and M. Pleimling, *On Non-Equilibrium Physics and String Theory*, Int. J. Mod. Phys. **A28** (2013) 1330009, arXiv:1301.6368 [hep-th].
- [19] H. Haggard and C. Rovelli, *Death and Resurrection of the Zeroth Principle of Thermodynamics*, arXiv:1302.0724 [gr-qc].
- [20] J. Hartle, *The Quantum Mechanical Arrows of Time*, arXiv:1301.2844 [quant-ph].
- [21] B. Hiley, *Time and the Algebraic Theory of Moments*, arXiv:1302.2323 [quant-ph].

- [22] T. Hollowood, *The Copenhagen Interpretation as an Emergent Phenomenon*, arXiv:1302.4228 [quant-ph].
- [23] G. 't Hooft, *Quantum Gravity as a Dissipative Deterministic System*, Class. Quant. Grav. **16** (1999) 3263, arXiv:gr-qc/9903084.
- [24] G. 't Hooft, *Emergent Quantum Mechanics and Emergent Symmetries*, AIP Conf. Proc. **957** (2007) 154, arXiv:0707.4568 [hep-th].
- [25] G. 't Hooft, *The Emergence of Quantum Mechanics*, AIP Conf.Proc. **1446** (2010) 341.
- [26] G. 't Hooft, *Relating the Quantum Mechanics of Discrete Systems to Standard Canonical Quantum Mechanics*, arXiv:1204.4926 [quant-ph].
- [27] B. Hu, *Gravity and Nonequilibrium Thermodynamics of Classical Matter*, Int. J. Mod. Phys. **D20** (2011) 697, arXiv:1010.5837 [gr-qc].
- [28] A. Kent, *Might Quantum Deviations from the Einstein Equations Detectably Affect Gravitational Wave Propagation?*, arXiv:1304.4981 [quant-ph].
- [29] A. Khrennikov, *“Einstein’s Dream” – Quantum Mechanics as Theory of Classical Random Fields*, arXiv:1204.5172 [quant-ph].
- [30] C. Kiefer, *Quantum Gravity*, Oxford University Press, Oxford (2012).
- [31] L. Landau and E. Lifshitz, *Statistical Physics, Part I*, vol. 5 of *Course of Theoretical Physics*, Pergamon Press, Oxford (1980).
- [32] J. Lees *et al.*, *Observation of Time Reversal Violation in the B^0 Meson System*, Phys. Rev. Lett. **109** (2012) 211801, arXiv:1207.5832 [hep-ex].
- [33] M. Matone, *‘Thermodynamique Cachée des Particules’ and the Quantum Potential*, Ann. Fond. Broglie **37** (2012) 177, arXiv:1111.0270 [hep-ph].
- [34] L. Onsager, *Reciprocal Relations in Irreversible Processes. I.*, Phys. Rev. **37** (1931) 405.
- [35] L. Onsager and S. Machlup, *Fluctuations and Irreversible Processes*, Phys. Rev. **91** (1953) 1505.
- [36] T. Padmanabhan, *Thermodynamical Aspects of Gravity: New Insights*, Rep. Prog. Phys. **73** (2010) 046901, arXiv:0911.5004 [gr-qc].
- [37] T. Padmanabhan, *Lessons from Classical Gravity about the Quantum Structure of Spacetime*, J. Phys. Conf. Ser. **306** (2011) 012001, arXiv:1012.4476 [gr-qc].
- [38] R. Penrose, *The Road to Reality*, Jonathan Cape, London (2004).
- [39] R. Penrose, *Black Holes, Quantum Theory and Cosmology*, J. Phys. Conf. Ser. **174** (2009) 012001.

- [40] I. Prigogine, *Time, Structure and Fluctuations*, Nobel Prize Lecture (1977).
- [41] C. Rovelli, *Statistical Mechanics of Gravity and the Thermodynamical Origin of Time*, *Class. Quant. Grav.* **10** (1993) 1549.
- [42] C. Rovelli, *Relational Quantum Mechanics*, *Int. J. Theor. Phys.* **35** (1996) 1637, arXiv:quant-ph/9609002.
- [43] C. Rovelli, *General Relativistic Statistical Mechanics*, arXiv:1209.0065 [gr-qc].
- [44] C. Rovelli and M. Smerlak, *Thermal Time and Tolman–Ehrenfest Effect: Temperature as the “Speed of Time”*, *Class. Quant. Grav.* **28** (2011) 075007, arXiv:1005.2985 [gr-qc].
- [45] A. Ruuge, *Pauli Problem in Thermodynamics*, arXiv:1208.2919 [math-ph].
- [46] L. Smolin, *On the Nature of Quantum Fluctuations and their Relation to Gravitation and the Principle of Inertia*, *Class. Quant. Grav.* **3** (1986) 347.
- [47] L. Smolin, *Quantum Gravity and the Statistical Interpretation of Quantum Mechanics*, *Int. J. Theor. Phys.* **25** (1986) 215.
- [48] L. Smolin, *A Real Ensemble Interpretation of Quantum Mechanics*, *Found. Phys.* **42** (2012) 1239, arXiv:1104.2822 [quant-ph].
- [49] R. Tolman, *Relativity, Thermodynamics and Cosmology*, Dover, New York (1987).
- [50] E. Verlinde, *On the Origin of Gravity and the Laws of Newton*, *JHEP* **1104** (2011) 029, arXiv:1001.0785 [hep-th].
- [51] R. Wald, *Quantum Gravity and Time Reversibility*, *Phys. Rev.* **D21** (1980) 2742.
- [52] R. Wald, *Gravitation, Thermodynamics and Quantum Theory*, *Class. Quant. Grav.* **16** (1999) A177, arXiv:gr-qc/9901033.
- [53] C. Wetterich, *Emergence of Quantum Mechanics from Classical Statistics*, *J. Phys. Conf. Ser.* **174** (2009) 012008, arXiv:0811.0927 [quant-ph].
- [54] K. Yosida, *Functional Analysis*, Springer, Berlin (1996).
- [55] H. Zeh, *The Physical Basis of the Direction of Time*, Springer, Berlin (2007).

Document downloaded from:

<http://hdl.handle.net/10251/78767>

This paper must be cited as:

Isidro San Juan, JM.; Fernández De Córdoba Castellá, PJ.; Vázquez Molina, J.; Perea-Córdoba, MH. (2015). The irreversible quantum. *International Journal of Geometric Methods in Modern Physics*. 12(1). doi:10.1142/S0219887815500139.



The final publication is available at

<http://dx.doi.org/10.1142/S0219887815500139>

Copyright World Scientific Publishing

Additional Information

THE IRREVERSIBLE QUANTUM

P. Fernández de Córdoba^{1,a}, **J.M. Isidro**^{1,b}, **Milton H. Perea**^{1,2,c} and **J. Vazquez Molina**^{1,d}

¹Instituto Universitario de Matemática Pura y Aplicada,
Universidad Politécnica de Valencia, Valencia 46022, Spain

²Departamento de Matemáticas y Física, Universidad Tecnológica
del Chocó, Colombia

^apfernandez@mat.upv.es, ^bjoissan@mat.upv.es

^cmilpecr@posgrado.upv.es, ^djoavzmo@etsii.upv.es

Abstract We elaborate on the existing notion that quantum mechanics is an emergent phenomenon, by presenting a thermodynamical theory that is dual to quantum mechanics. This dual theory is that of classical irreversible thermodynamics. The linear regime of irreversibility considered here corresponds to the semiclassical approximation in quantum mechanics. An important issue we address is how the irreversibility of time evolution in thermodynamics is mapped onto the quantum–mechanical side of the correspondence.

1 Introduction

In his Nobel Prize Lecture, Prigogine advocated an intriguing type of “complementarity between dynamics, which implies the knowledge of trajectories or wavefunctions, and thermodynamics, which implies entropy” [18]. Another Nobel Prize winner, ’t Hooft, has long argued that quantum mechanics must emerge from some underlying deterministic theory via information loss [11]. Entropy is of course intimately related to information loss, hence one expects some link to exist between these two approaches to quantum theory.

In an apparently unrelated venue, the Chapman–Kolmogorov equation [6]

$$F(z_1)F(z_2) = F(z_1 + z_2), \quad (1)$$

is a functional equation in the unknown F , where z_1, z_2 are any two values assumed by the complex variable z . It has the general solution

$$F_a(z) = e^{za}, \quad (2)$$

with $a \in \mathbb{C}$ an arbitrary constant. Implicitly assumed above is the multiplication rule for complex numbers. In other words, (2) solves (1) within a space of number–valued functions. If we allow for a more general multiplication rule such as matrix multiplication (possibly infinite–dimensional matrices), then the general solution (2) of the functional equation (1) can be allowed to depend parametrically on a z –independent, constant *matrix* or *operator* A acting on some linear space:

$$F_A(z) = e^{zA}. \quad (3)$$

The functional equation (1), in its different guises, will play an important role in what follows. We see that its solutions are by no means unique, depending as they do on the space where one tries to solve the equation. Moreover, we will see that the question of specifying one solution space or another will bear a close relation to the question posed at the beginning—namely, the duality between thermodynamics and mechanics, on the one hand, and the emergence property of quantum mechanics, on the other.

Let \mathcal{X} and \mathcal{Y} respectively stand for the configuration spaces of a mechanical system and a thermodynamical system, the latter taken slightly away from equilibrium. We will be interested in the quantum theory based on \mathcal{X} , and in the theory of irreversible thermodynamics in the linear regime based on \mathcal{Y} [16]. There exist profound analogies between these two theories [1, 8, 15, 19, 20]. Furthermore, seeming mismatches between the two actually have a natural explanation in the context of the emergent approach to quantum theory [2, 4]; closely related topics were analysed long ago in [3] and more recently in [5, 7, 9, 10, 12, 14, 17, 21, 22]. One of these mismatches concerns the irreversibility of time evolution in the thermodynamical picture, as opposed to its reversibility in the quantum–mechanical picture.

The standard quantum formalism is invariant under time reversal. This is reflected, *e.g.*, in the fact that the Hilbert space of quantum states $L^2(\mathcal{X})$ is complex and self-dual [23], so one can exchange the incoming state $|\phi\rangle$ and the outgoing state $\langle\psi|$ by Hermitean conjugation, without ever stepping outside the given Hilbert space $L^2(\mathcal{X})$. On the other hand, the thermodynamical space of states is the complex Banach space $L^1(\mathcal{Y})$ of complex-valued, integrable probability densities $\phi : \mathcal{Y} \rightarrow \mathbb{C}$. This is in sharp contrast to the square-integrable probability density *amplitudes* of quantum theory. Now the topological dual space to $L^1(\mathcal{Y})$ is the Banach space $L^\infty(\mathcal{Y})$ [23]. These two spaces fail to qualify as Hilbert spaces. In other words, for any $|\phi\rangle \in L^1(\mathcal{Y})$ and any $\langle\psi| \in L^\infty(\mathcal{Y})$ the respective norms $\|\phi\|_1$ and $\|\psi\|_\infty$ are well defined, but neither of these derives from a scalar product. All there exists is a nondegenerate, bilinear pairing

$$(\cdot|\cdot) : L^\infty(\mathcal{Y}) \times L^1(\mathcal{Y}) \longrightarrow \mathbb{C} \quad (4)$$

taking the covector $\langle\psi|$ and the vector $|\phi\rangle$ into the number $(\psi|\phi)$:

$$(\psi|\phi) := \int_{\mathcal{Y}} \psi^* \phi. \quad (5)$$

Under these circumstances there is no exchanging the incoming state $|\phi\rangle \in L^1(\mathcal{Y})$ and the outgoing state $\langle\psi| \in L^\infty(\mathcal{Y})$, as they belong to different spaces. Therefore time reversal symmetry is lost. We see that *dispensing with the scalar product in quantum theory is the same as dispensing with time reversal symmetry*.

We have in [1, 8] touched on several basic issues concerning a thermodynamical formalism for quantum theory. Specifically, a map has been constructed between the quantum mechanics of a finite number of degrees of freedom, on the one hand, and the theory of irreversible processes in the linear regime, on the other. The current paper elaborates further on the properties of a *thermodynamical dual theory* for emergent

¹We follow the notations of ref. [1]. In particular, the round brackets in $|\phi\rangle$ and $\langle\psi|$ refer to $L^1(\mathcal{Y})$ and its topological dual $L^\infty(\mathcal{Y})$, respectively, while the angular brackets of the quantum–mechanical ket $|\phi\rangle$ and bra $\langle\psi|$ refer to $L^2(\mathcal{X})$ and its topological dual $L^2(\mathcal{X})$. Concerning the measure on \mathcal{X} and \mathcal{Y} , see below.

quantum mechanics. The underlying logic might be briefly summarised as follows:

- i)* it has been claimed that thermodynamics is complementary, or dual, to mechanics;
- ii)* mechanics is symmetric under time reversal while thermodynamics is not;
- iii)* dispensing with time reversal symmetry is the same as dispensing with the scalar product in quantum theory;
- iv)* the representation of the Chapman–Kolmogorov equation (II) on the quantum mechanical Hilbert space $L^2(\mathcal{X})$ makes decisive use of the scalar product;
- v)* here we construct representations of (II) on the thermodynamical Banach spaces $L^1(\mathcal{Y})$ and $L^\infty(\mathcal{Y})$, where no scalar product is present.

For simplicity we will henceforth assume \mathcal{X} and \mathcal{Y} both equal to \mathbb{R} , the latter endowed with the Lebesgue measure.

The aim of our paper is not to reformulate the theory of irreversible thermodynamics as originally developed in [16]. Rather, *we intend to exhibit irreversibility as a key property of quantum–mechanical behaviour.*

2 Different representations for Chapman–Kolmogorov

2.1 The quantum–mechanical representation

In quantum mechanics it is customary to write (II) as

$$U(t_1)U(t_2) = U(t_1 + t_2), \quad t \in \mathbb{R}, \quad (6)$$

and to call it the *group property* of time evolution. If H denotes the quantum Hamiltonian operator (assumed time–independent for simplicity), then (6) is solved by matrices such as (3), here called time–evolution operators and defined as

$$U(t) := \exp\left(-\frac{i}{\hbar}tH\right). \quad (7)$$

The solutions of (6) satisfy the differential equation

$$i\hbar \frac{dU}{dt} = HU(t), \quad H = i\hbar \frac{dU}{dt} \Big|_{t=0}. \quad (8)$$

Comparing (7) with (3) we have $z = t$ and $A = -iH/\hbar$. The $U(t)$ are unitary on $L^2(\mathbb{R})$. In a basis of position eigenfunctions $|x\rangle$, the matrix elements of $U(t)$ equal the Feynman propagator: $\langle x_2|U(t_2 - t_1)|x_1\rangle = K(x_2, t_2|x_1, t_1)$. In terms of the latter, one rewrites the group property (6) as

$$K(x_3, t_3|x_1, t_1) = \int dx_2 K(x_3, t_3|x_2, t_2) K(x_2, t_2|x_1, t_1). \quad (9)$$

There is a path integral for the Feynman propagator K :

$$K(x_2, t_2|x_1, t_1) = \int_{x(t_1)=x_1}^{x(t_2)=x_2} Dx(t) \exp\left\{\frac{i}{\hbar} \int_{t_1}^{t_2} dt L[x(t), \dot{x}(t)]\right\}, \quad (10)$$

where L is the classical Lagrangian function.

To summarise, the operators (7) provide a unitary representation of the commutative group (6) on the Hilbert space $L^2(\mathbb{R})$.

2.2 Intermezzo

Here we recall some technicalities to be used later; a good general reference is [23].

$L^1(\mathbb{R})$ is the space of all Lebesgue measurable, absolutely integrable functions $\phi : \mathbb{R} \rightarrow \mathbb{C}$, *i.e.*, functions such that $\int_{\mathbb{R}} |\phi(y)| dy < \infty$. This is a complex Banach space with respect to the norm $\|\psi\|_1 := \int_{\mathbb{R}} |\phi(y)| dy$.² A *denumerable* basis (a Schauder basis) exists for $L^1(\mathbb{R})$.

The topological dual space to $L^1(\mathbb{R})$ is $L^\infty(\mathbb{R})$, a duality between the two being given in Eqs. (4), (5). $L^\infty(\mathbb{R})$ is the space of all Lebesgue measurable functions $\psi : \mathbb{R} \rightarrow \mathbb{C}$ that are essentially bounded, *i.e.*, functions that remain bounded on all \mathbb{R} except possibly on a set of measure zero. $L^\infty(\mathbb{R})$ is a Banach space with respect to the norm $\|\cdot\|_\infty$, defined as follows. A nonnegative number $\alpha \in \mathbb{R}$ is said to be an essential upper bound of ψ whenever the set of points $y \in \mathbb{R}$ where $|\psi(y)| \geq \alpha$ has zero measure. The norm $\|\psi\|_\infty$ is the infimum of all those α :

$$\|\psi\|_\infty := \inf \{ \alpha \in \mathbb{R}^+ : \alpha \text{ essential upper bound of } \psi \}. \quad (11)$$

A key property is that one can pointwise multiply $\psi \in L^\infty(\mathbb{R})$ with $\phi \in L^1(\mathbb{R})$ to obtain $\psi\phi \in L^1(\mathbb{R})$ because $\int_{\mathbb{R}} |\psi\phi| dy < \infty$; this is used decisively in the pairing (5). Another key property of $L^\infty(\mathbb{R})$ is that it admits no Schauder basis.

The space $L^1(\mathbb{R})$ is canonically and isometrically embedded into its topological bidual, *i.e.*, $L^1(\mathbb{R}) \subset L^1(\mathbb{R})^{**}$. Since $L^1(\mathbb{R})$ is nonreflexive, this inclusion is strict, a property that will be used later on.³ Finally, the absence of a scalar product on $L^1(\mathbb{R})$ and $L^\infty(\mathbb{R})$ does not prevent the existence of unitary operators on them, the latter being defined as those that preserve the corresponding norm.

2.3 The representation in irreversible thermodynamics

In statistics, the Chapman–Kolmogorov equation (1) was well known before the advent of quantum theory [6]. Here one is given a certain measure space \mathcal{Y} (here assumed equal to \mathbb{R} endowed with the Lebesgue measure) and the corresponding Banach spaces $L^1(\mathbb{R})$ and its topological dual $L^\infty(\mathbb{R})$. These two will become carrier spaces for representations of the Chapman–Kolmogorov equation (1).

One calls $f_1 \left(\begin{smallmatrix} y_2 & | & y_1 \\ \tau_2 & | & \tau_1 \end{smallmatrix} \right)$ the *conditional* probability that the random variable $y \in \mathbb{R}$ takes on the value y_2 at time τ_2 provided that it took on the value y_1 at time τ_1 . Then one usually writes the Chapman–Kolmogorov equation (1) in a manner similar to (9),

$$f_1 \left(\begin{smallmatrix} y_3 & | & y_1 \\ \tau_3 & | & \tau_1 \end{smallmatrix} \right) = \int dy_2 f_1 \left(\begin{smallmatrix} y_3 & | & y_2 \\ \tau_3 & | & \tau_2 \end{smallmatrix} \right) f_1 \left(\begin{smallmatrix} y_2 & | & y_1 \\ \tau_2 & | & \tau_1 \end{smallmatrix} \right), \quad (12)$$

which expresses the Bayes rule for conditional probabilities. A representation of this equation by means of linear operators $\mathcal{U}(\tau)$ on $L^1(\mathbb{R})$ and on $L^\infty(\mathbb{R})$ would thus have to satisfy the algebra

$$\mathcal{U}(\tau_1)\mathcal{U}(\tau_2) = \mathcal{U}(\tau_1 + \tau_2), \quad (13)$$

²Just for comparison, the norm on the Hilbert space $L^2(\mathbb{R})$ is $\|\phi\|_2 := (\int_{\mathbb{R}} |\phi(y)|^2 dy)^{1/2}$.

³The topological complementary space to $L^1(\mathbb{R})$, *i.e.*, the space Z such that $L^1(\mathbb{R})^{**} = L^1(\mathbb{R}) \oplus Z$, is known in the literature, but it will not be necessary here.

which is again a presentation of (11). We can immediately read off the matrix elements of $\mathcal{U}(\tau)$:

$$(y_2|\mathcal{U}(\tau_2 - \tau_1)|y_1) = f_1 \left(\begin{array}{c|c} y_2 & y_1 \\ \tau_2 & \tau_1 \end{array} \right). \quad (14)$$

As opposed to the quantum–mechanical case, the carrier space for the representation of the algebra (13) is Banach but not Hilbert. The reason for this is that one deals directly with probabilities rather than amplitudes.

The question arises: if one were to express the matrix (14) in the form given by the general solution (3), then clearly one would have $z = \tau$, but what would the operator A be? It is mathematically true, though physically unsatisfactory, to claim that A would be (proportional to) the logarithm of $\mathcal{U}(\tau)$. One of the purposes of this paper is to determine the operator A explicitly, and to interpret it in the terms stated in the introduction. However, in order to do this, a knowledge of the conditional probabilities $f_1 \left(\begin{array}{c|c} y_2 & y_1 \\ \tau_2 & \tau_1 \end{array} \right)$ is needed.

There are a number of instances in which the $f_1 \left(\begin{array}{c|c} y_2 & y_1 \\ \tau_2 & \tau_1 \end{array} \right)$ are known explicitly. An important example is that of *classical, irreversible thermodynamics of stationary, Markov processes in the linear regime*. For such processes one has (16)

$$f_1 \left(\begin{array}{c|c} y_2 & y_1 \\ \tau_2 & \tau_1 \end{array} \right) = \frac{1}{\sqrt{2\pi}} \frac{s/k_B}{\sqrt{1 - e^{-2\gamma(\tau_2 - \tau_1)}}} \exp \left[-\frac{s}{2k_B} \frac{(y_2 - e^{-\gamma(\tau_2 - \tau_1)}y_1)^2}{1 - e^{-2\gamma(\tau_2 - \tau_1)}} \right]. \quad (15)$$

The notation used here is that of (11). Specifically, k_B is Boltzmann’s constant, the entropy S is a function of the extensive parameter y , and we expand S in a Taylor series around a stable equilibrium point. Up to quadratic terms we have

$$S = S_0 - \frac{1}{2}sy^2 + \dots, \quad s := -\left. \frac{d^2S}{dy^2} \right|_0 > 0. \quad (16)$$

Moreover, the assumption of linearity implies the following proportionality between the thermodynamical force $Y := dS/dy$ and the flux $\dot{y} := dy/d\tau$ it produces (16):

$$\dot{y} = LY, \quad L > 0. \quad (17)$$

The Onsager coefficient L must be positive for the process to be dissipative. Finally $\gamma := sL$. Sometimes one also uses $R := L^{-1}$, so $\gamma = s/R$.

The following path–integral representation for the conditional probabilities (15) of these models is noteworthy (16):

$$f_1 \left(\begin{array}{c|c} y_2 & y_1 \\ \tau_2 & \tau_1 \end{array} \right) = \int_{y(\tau_1)=y_1}^{y(\tau_2)=y_2} \mathcal{D}y(\tau) \exp \left\{ -\frac{1}{2k_B} \int_{\tau_1}^{\tau_2} d\tau \mathcal{L}[\dot{y}(\tau), y(\tau)] \right\}. \quad (18)$$

The above exponential contains the *thermodynamical Lagrangian* \mathcal{L} , defined as

$$\mathcal{L}[\dot{y}(\tau), y(\tau)] := \frac{R}{2} [\dot{y}^2(\tau) + \gamma^2 y^2(\tau)], \quad \dot{y} := \frac{dy}{d\tau}. \quad (19)$$

The path integral (18) is the thermodynamical analogue of (10). The corresponding thermodynamical momentum p_y equals $Rdy/d\tau$, where R plays the role of a mass, and the *thermodynamical Hamiltonian* \mathcal{H} corresponding to (19) reads

$$\mathcal{H} = \frac{1}{2R}p_y^2 - \frac{R\gamma^2}{2}y^2. \quad (20)$$

It must be borne in mind, however, that the dimensions of \mathcal{L} and \mathcal{H} are entropy per unit time. With this caveat, we will continue to call \mathcal{H} a Hamiltonian.

2.4 Mapping irreversible thermodynamics into quantum mechanics

For the processes considered in (15) we claim that one can define operators on $L^1(\mathbb{R})$ and on $L^\infty(\mathbb{R})$

$$\mathcal{U}(\tau) := \exp\left(-\frac{1}{2k_B}\tau\mathcal{H}\right) \quad (21)$$

with \mathcal{H} suitably chosen, such that their matrix elements coincide with those given in (14). Hence the $\mathcal{U}(\tau)$ will provide a representation of the algebra (13). In what follows we construct $\mathcal{U}(\tau)$ explicitly, but one can already expect the argument \mathcal{H} of the exponential (21) to be some *operator* version of the thermodynamical Hamiltonian *function* given in (20). For this reason we have not distinguished notationally between the two. This operator \mathcal{H} will also turn out to be (proportional to) the unknown operator A mentioned after eq. (14). From (21) it follows that the thermodynamical analogue of the quantum–mechanical equation (8) is

$$-2k_B\frac{d\mathcal{U}(\tau)}{d\tau} = \mathcal{H}\mathcal{U}(\tau), \quad \mathcal{H} = -2k_B\frac{d\mathcal{U}(\tau)}{d\tau}\Big|_{\tau=0}. \quad (22)$$

We can resort to our previous work [1] in order to identify the operator \mathcal{H} in its action on $L^1(\mathbb{R})$ and on $L^\infty(\mathbb{R})$. In [1] we have established a map between quantum mechanics in the semiclassical regime, on the one hand, and the theory of classical, irreversible thermodynamics of stationary, Markov processes in the linear regime, on the other hand. In the mechanical picture, the relevant Lagrangian and Hamiltonian functions are

$$L = \frac{m}{2}\left(\frac{dx}{dt}\right)^2 - \frac{m\omega^2}{2}x^2, \quad H = \frac{1}{2m}p_x^2 + \frac{m\omega^2}{2}x^2. \quad (23)$$

Comparing them with their thermodynamical partners (19) and (20), we see that the mechanical and the thermodynamical functions can be transformed into each other if we apply the replacements⁴

$$\omega \leftrightarrow \gamma, \quad \frac{m\omega}{\hbar} \leftrightarrow \frac{s}{2k_B}, \quad x \leftrightarrow y, \quad (24)$$

⁴While the first two replacements of (24) are dimensionally correct without any further assumptions, the third identification also requires that x and y have the same dimensions. Since this need not always be the case, a dimensionful conversion factor must be understood as implicitly contained in the replacement $x \leftrightarrow y$, whenever needed.

as well as the Wick rotation

$$\tau = it. \quad (25)$$

Furthermore, Boltzmann's constant k_B is the thermodynamical partner of Planck's constant \hbar multiplied by 2 [19]:

$$\hbar \leftrightarrow 2k_B. \quad (26)$$

As a consistency check one can apply all the above replacements to (7) in order to arrive at

$$U(t) = \exp\left(-\frac{i}{\hbar}tH\right) \leftrightarrow \exp\left(-\frac{1}{2k_B}\tau\mathcal{H}\right) = \mathcal{U}(\tau). \quad (27)$$

However, we still have to identify the operator \mathcal{H} in its action on thermodynamical states. This will be done in section 3.1.

2.5 Incoming states vs. outgoing states

In principle, thermodynamical states are normalised probability densities, hence elements of $L^1(\mathbb{R})$. However, as we will see shortly, this viewpoint must be extended somewhat. For this purpose let us call the elements of $L^1(\mathbb{R})$ *incoming states*. Incoming linear operators \mathcal{O}_{in} are defined

$$\mathcal{O}_{\text{in}} : L^1(\mathbb{R}) \longrightarrow L^1(\mathbb{R}), \quad (28)$$

so as to map incoming states $|\phi\rangle \in L^1(\mathbb{R})$ into incoming states $\mathcal{O}_{\text{in}}|\phi\rangle \in L^1(\mathbb{R})$. Incoming states are postulated to evolve in time according to

$$-2k_B \frac{d|\phi\rangle}{d\tau} = \mathcal{H}_{\text{in}}|\phi\rangle, \quad (29)$$

where \mathcal{H}_{in} is an incoming linear operator, to be identified presently.

The space of outgoing states is the topological dual of $L^1(\mathbb{R})$, hence $L^\infty(\mathbb{R})$. Outgoing linear operators \mathcal{O}_{out} are similarly defined

$$\mathcal{O}_{\text{out}} : L^\infty(\mathbb{R}) \longrightarrow L^\infty(\mathbb{R}), \quad (30)$$

in order to map outgoing states $\langle\psi| \in L^\infty(\mathbb{R})$ into outgoing states $\langle\psi|\mathcal{O}_{\text{out}} \in L^\infty(\mathbb{R})$. The operator $\mathcal{O}_{\text{in}}^T$ that is transpose to an incoming operator \mathcal{O}_{in} is defined on the topological dual space:

$$\mathcal{O}_{\text{in}}^T : L^\infty(\mathbb{R}) \longrightarrow L^\infty(\mathbb{R}). \quad (31)$$

In this way $\mathcal{O}_{\text{in}}^T$ is actually an outgoing operator \mathcal{O}_{out} [5]. By definition the transpose satisfies

$$\langle\psi|\mathcal{O}_{\text{in}}^T|\phi\rangle = \langle\psi|\mathcal{O}_{\text{in}}|\phi\rangle, \quad \forall \langle\psi| \in L^\infty(\mathbb{R}), \forall |\phi\rangle \in L^1(\mathbb{R}). \quad (32)$$

⁵Since the topological bidual $(L^1(\mathbb{R}))^{**}$ contains more than just $L^1(\mathbb{R})$, we stop short of stating that “The transpose $\mathcal{O}_{\text{out}}^T$ to an outgoing operator \mathcal{O}_{out} is an incoming operator \mathcal{O}_{in} ”. The previous statement, trivially true in finitely many dimensions and still true on $L^2(\mathbb{R})$, no longer holds in our context, with the consequence that twice transposing does not give back the original operator. We will see in section 3.2 that this fact has far-reaching implications.

What equation should govern the time evolution of outgoing states? Clearly it can only be

$$-2k_B \frac{d(\psi)}{d\tau} = (\psi|\mathcal{H}_{\text{in}}^T = (\psi|\mathcal{H}_{\text{out}}, \quad (33)$$

therefore

$$-2k_B \frac{d}{d\tau}(\psi|\phi) = (\psi|\mathcal{H}_{\text{in}}^T|\phi) + (\psi|\mathcal{H}_{\text{in}}|\phi). \quad (34)$$

The right-hand side of the above is generally nonzero: it expresses the irreversibility property of time evolution in thermodynamics. This is a far cry from the time-symmetric case of standard quantum mechanics, where $i\hbar d(\langle\psi|\phi\rangle)/dt = 0$.

One further point deserves attention. In standard quantum mechanics on $L^2(\mathbb{R})$, the matrix element $\langle\psi|\mathcal{O}|\phi\rangle = \int dx \psi^*(x)\mathcal{O}\phi(x)$ naturally carries the dimensions of the operator \mathcal{O} ; here both $\psi^*(x)$ and $\phi(x)$ have the dimension $[x]^{-1/2}$ of a probability amplitude on \mathbb{R} . In the thermodynamical dual to quantum theory, the incoming state $|\phi\rangle \in L^1(\mathbb{R})$ carries the dimension $[y]^{-1}$ because it is a probability *density*, while the outgoing state $(\psi| \in L^\infty(\mathbb{R})$ is *dimensionless* because it is *not* meant to be integrated on its own. It is only upon taking the pairing (5) that $(\psi|$ will be integrated against $\mathcal{O}|\phi\rangle$. So the dimensions of $(\psi|\mathcal{O}|\phi)$ are again correct, although the dimensional balance between incoming and outgoing states that existed in $L^2(\mathbb{R})$ has disappeared.

Altogether, dispensing with the scalar product in quantum theory is the same as dispensing with time reversal symmetry. Moreover, dispensing with the scalar product has the consequence that, as thermodynamical states, one must regard not just the elements of $L^1(\mathbb{R})$ but also those of its topological dual $L^\infty(\mathbb{R})$.

3 The harmonic oscillator representation of irreversible thermodynamics

For mechanics we use the *dimensionless* coordinate $x \in \mathbb{R}$. Then the quantum harmonic oscillator equation on $L^2(\mathbb{R})$ reads

$$\left(-\frac{d^2}{dx^2} + x^2\right)w(x) = \varepsilon w(x), \quad \varepsilon \in \mathbb{R}, \quad (35)$$

where ε is a dimensionless energy eigenvalue.

3.1 The oscillator on the Banach spaces $L^1(\mathbb{R})$ and $L^\infty(\mathbb{R})$

For thermodynamics we use the *dimensionless* coordinate $y \in \mathbb{R}$. Then the dimensionless thermodynamical momentum is represented as $-id/dy$, and the equation for the thermodynamical oscillator reads

$$-\left(\frac{d^2}{dy^2} + y^2\right)w(y) = \sigma w(y) \quad \sigma \in \mathbb{R}. \quad (36)$$

Above, σ is a dimensionless eigenvalue (entropy per unit time), which we require to be real for physical reasons. With respect to (35), the only change in (36) is the sign of

the potential term (see (19) and (20)). Eq. (36) identifies the operator \mathcal{H} explicitly in its action on $L^1(\mathbb{R})$ and $L^\infty(\mathbb{R})$, a question posed in section 2.4. Specifically, for the action of the Hamiltonian on the initial states we have

$$\mathcal{H}_{\text{in}} = -\frac{d^2}{dy^2} - y^2 : L^1(\mathbb{R}) \longrightarrow L^1(\mathbb{R}). \quad (37)$$

The operator \mathcal{H}_{out} is formally the same as \mathcal{H}_{in} , but it acts on the dual space:

$$\mathcal{H}_{\text{out}} = -\frac{d^2}{dy^2} - y^2 : L^\infty(\mathbb{R}) \longrightarrow L^\infty(\mathbb{R}). \quad (38)$$

In order to solve (36) we first look for a factorisation of $w(y)$ in the form

$$w(y) = h(y) \exp(\alpha y^2), \quad \alpha \in \mathbb{C}, \quad (39)$$

where α is some constant to be picked appropriately. With (39) in (36) one finds

$$\frac{d^2}{dy^2} h(y) + 4\alpha y \frac{d}{dy} h(y) + [(2\alpha + \sigma) + (4\alpha^2 + 1)y^2] h(y) = 0. \quad (40)$$

The choice $\alpha = i/2$ simplifies (40) considerably:

$$\frac{d^2}{dy^2} h(y) + 2iy \frac{d}{dy} h(y) + (i + \sigma)h(y) = 0. \quad (41)$$

Finally the change of variables $z = e^{i\frac{3\pi}{4}} y$ reduces (41) to

$$\frac{d^2}{dz^2} \tilde{h}(z) - 2z \frac{d}{dz} \tilde{h}(z) - (1 - i\sigma)\tilde{h}(z) = 0, \quad (42)$$

where we have defined $\tilde{h}(z) := h\left(e^{-i\frac{3\pi}{4}} z\right) = h(y)$. Now (42) is a particular instance of the Hermite differential equation on the complex plane,

$$H''(z) - 2zH'(z) + 2\nu H(z) = 0, \quad \nu \in \mathbb{C}. \quad (43)$$

In our case we have $2\nu = -1 + i\sigma$ with $\sigma \in \mathbb{R}$, so $\nu \notin \mathbb{N}$. When $\nu \notin \mathbb{N}$ two linearly independent solutions to the Hermite equation are given by the Hermite functions $H_\nu(z)$ and $H_\nu(-z)$, where [13]

$$H_\nu(z) = \frac{1}{2\Gamma(-\nu)} \sum_{n=0}^{\infty} \frac{(-1)^n \Gamma\left(\frac{n-\nu}{2}\right)}{n!} (2z)^n. \quad (44)$$

The above power series defines an entire function of $z \in \mathbb{C}$ for any value of $\nu \in \mathbb{C}$. Its asymptotic behaviour is [13]:

$$H_\nu(z) \sim (2z)^\nu - \frac{\sqrt{\pi} e^{i\pi\nu}}{\Gamma(-\nu)} z^{-\nu-1} e^{z^2}, \quad |z| \rightarrow \infty, \quad \pi/4 < \arg(z) < 5\pi/4. \quad (45)$$

In (45) we have dropped subdominant terms, keeping only the leading contributions; the angular sector $\pi/4 < \arg(z) < 5\pi/4$ is imposed on us by the change of variables $z = e^{i\frac{3\pi}{4}}y$ made above for $y \in \mathbb{R}$.

Altogether, two linearly independent solutions to (36) corresponding to the eigenvalue $\sigma \in \mathbb{R}$ are given by $w_\sigma^\pm(y)$, where

$$w_\sigma^\pm(y) := H_{-\frac{1}{2} + \frac{i\sigma}{2}} \left(\pm e^{i\frac{3\pi}{4}}y \right) e^{iy^2/2}. \quad (46)$$

By (45), their asymptotic behaviour for $|y| \rightarrow \infty$ is

$$w_\sigma^\pm(y) \sim \left(\pm 2e^{i\frac{3\pi}{4}}y \right)^{-\frac{1}{2} + \frac{i\sigma}{2}} e^{iy^2/2} - \frac{\sqrt{\pi} e^{-\pi(\sigma+i)/2}}{\Gamma\left(\frac{1-i\sigma}{2}\right)} \left(\pm e^{i\frac{3\pi}{4}}y \right)^{-\frac{1}{2} - \frac{i\sigma}{2}} e^{-iy^2/2}. \quad (47)$$

We are looking for eigenfunctions within $L^1(\mathbb{R})$ and/or $L^\infty(\mathbb{R})$. Eqn. (47) proves that $w_\sigma^\pm(y) \in L^\infty(\mathbb{R})$ but $w_\sigma^\pm(y) \notin L^1(\mathbb{R})$.

3.2 The spectrum

Summarising, the operator $-d^2/dy^2 - y^2$ on $L^\infty(\mathbb{R})$ has an eigenvalue spectrum containing the whole real line \mathbb{R} ⁶. This spectrum is twice degenerate, the (unnormalised) eigenfunctions corresponding to $\sigma \in \mathbb{R}$ being given in Eq. (46). The same operator acting on $L^1(\mathbb{R})$ has a void spectrum. This latter conclusion is not as tragic as it might seem at first sight—on the contrary, everything fits together once one realises that evolution in thermodynamical time τ is irreversible, and that the space $L^1(\mathbb{R})$, which admits a Schauder basis, has a topological dual $L^\infty(\mathbb{R})$ admitting no Schauder basis. Let us analyse these facts from a physical and from a mathematical viewpoint.

Physically, an empty spectrum on $L^1(\mathbb{R})$ just means that *there can be no incoming eigenstates*. Moreover, no incoming state can ever evolve into an incoming *eigenstate* under thermodynamical evolution. This is an expression of irreversibility. However, as a result of evolution in τ , one can perfectly well obtain *outgoing* eigenstates. The latter remain outgoing *eigenstates* under thermodynamical evolution.

Mathematically, in standard quantum mechanics on $L^2(\mathbb{R})$ one is used to taking the transpose of a matrix by exchanging rows with columns. Implicitly understood here is the existence of Schauder bases in the space of $L^2(\mathbb{R})$ and in its topological dual (again $L^2(\mathbb{R})$). Once one diagonalises an operator, how can it be that its transpose is not diagonal as well? While this cannot happen in $L^2(\mathbb{R})$, *this can perfectly well be the case when dealing with the spaces $L^1(\mathbb{R})$ and $L^\infty(\mathbb{R})$, because $L^1(\mathbb{R})$ admits a Schauder basis while $L^\infty(\mathbb{R})$ does not*. In turn, this is a consequence of the fact that we are renouncing probability density *amplitudes* (elements of $L^2(\mathbb{R})$) in favour of probability *densities* (elements of $L^1(\mathbb{R})$), as befits a thermodynamical description of quantum theory.

One would like to identify the thermodynamical analogue of the quantum mechanical vacuum state; one expects to somehow map the quantum–mechanical state of least energy, or vacuum, into the thermodynamical state of maximal entropy. Let us recall

⁶Actually the eigenvalue spectrum of this operator on $L^\infty(\mathbb{R})$ also contains nonreal eigenvalues (see (48)), but here we are only interested in real eigenvalues.

that the (unnormalised) quantum–mechanical vacuum wavefunction is $\exp(-x^2/2)$. The Wick rotation (25) introduces the imaginary unit, giving us the term $\exp(iy^2/2)$ in (46). Now $\nu = -1/2 + i\sigma/2 = 0$ only when $\sigma = -i$, a possibility we have excluded per decree. Let us temporarily sidestep this decree and observe that

$$-\left(\frac{d^2}{dy^2} + y^2\right) e^{\pm iy^2/2} = \mp i e^{\pm iy^2/2} \quad (48)$$

is very reminiscent of the equation governing the quantum–mechanical vacuum. The thermodynamical density corresponding to the state $\exp(\pm iy^2/2)$ equals the constant unit function on \mathbb{R} , which is nonnormalisable under $\|\cdot\|_1$ in $L^1(\mathbb{R})$ but carries finite norm under $\|\cdot\|_\infty$ in $L^\infty(\mathbb{R})$. As a perfectly uniform probability distribution, $\exp(\pm iy^2/2)$ is the thermodynamical state that maximises the entropy. All the eigenstates in (46) are thermodynamical excitations thereof, hence they carry less entropy. Of course, we cannot allow the eigenvalues $\sigma = \pm i$ within our spectrum, but the above discussion is illustrative because, by (47), all our thermodynamical eigenstates (46) tend asymptotically to a linear combination of the states $y^{-1/2} \exp[\pm \frac{i}{2}(\sigma \ln(y) + y^2)]$. In other words, all our thermodynamical eigenstates can be interpreted as *fluctuations around a state of maximal entropy*.

3.3 Irreversibility vs. nonunitarity

A key consequence of irreversibility is nonunitarity. Contrary to the operators $U(t)$ of (7), which are unitary on $L^2(\mathbb{R})$, the operators $\mathcal{U}(\tau)$ of (21) are *nonunitary* on $L^\infty(\mathbb{R})$.

Nonunitarity is readily proved. Let $w_\sigma \in L^\infty(\mathbb{R})$ be such that $\mathcal{H}_{\text{out}} w_\sigma = \sigma w_\sigma$. Since $\sigma \in \mathbb{R}$ we have, by (21),

$$\mathcal{U}(\tau)w_\sigma = \exp\left(-\frac{\tau\sigma}{2k_B}\right) w_\sigma, \quad \tau\sigma \in \mathbb{R}, \quad (49)$$

hence

$$\|\mathcal{U}(\tau)w_\sigma\|_\infty = \exp\left(-\frac{\tau\sigma}{2k_B}\right) \|w_\sigma\|_\infty, \quad \tau\sigma \in \mathbb{R}, \quad (50)$$

which proves our assertion. To summarise: combining (21), (37) and (38) we find, after reinstating dimensional factors, that the operators

$$\mathcal{U}(\tau) = \exp\left[\frac{\tau}{2k_B} \left(\frac{1}{2R} \frac{d^2}{dy^2} + \frac{R\gamma^2}{2} y^2\right)\right], \quad \tau \geq 0, \quad (51)$$

provide a *nonunitary*, infinite–dimensional representation of the Chapman–Kolmogorov semigroup (13) on $L^\infty(\mathbb{R})$. The space $L^1(\mathbb{R})$ also carries an infinite–dimensional representation of (13) on which the operators (51) act.

It is interesting to observe that the eigenfunctions in (48), which we have discarded for reasons already explained, circumvent the above proof because their eigenvalues are purely imaginary. Each one of them actually provides a 1–dimensional, *unitary* representation of (13) on $L^\infty(\mathbb{R})$.

4 Discussion

Classical thermodynamics is the paradigm of emergent theories. It renounces the detailed knowledge of a large number of microscopic degrees of freedom, in favour of a small number of macroscopic averages that retain only some coarse-grained features of the system under consideration. It has been claimed in the literature that quantum mechanics must be an emergent theory [2, 4, 11]. As one further piece of evidence in support of this latter statement, in this paper we have developed a thermodynamical formalism for quantum mechanics.

In the usual formulation of quantum theory, one is concerned with the matrix elements $\langle \psi | \mathcal{O} | \phi \rangle$ of some operator \mathcal{O} , where the incoming state $|\phi\rangle$ belongs to $L^2(\mathbb{R})$ and the outgoing state $\langle \psi |$ belongs to the topological dual space, again $L^2(\mathbb{R})$.

In the thermodynamical theory that is dual to quantum mechanics one is again concerned with matrix elements of the type $(\psi | \mathcal{O} | \phi)$. However, now the incoming state is not square integrable but just integrable, $|\phi\rangle \in L^1(\mathbb{R})$, while the outgoing state $\langle \psi | \in L^\infty(\mathbb{R})$ belongs to a totally different space. Neither $L^1(\mathbb{R})$ nor its topological dual $L^\infty(\mathbb{R})$ qualify as a Hilbert space, because their respective norms do not derive from a scalar product; they are just Banach spaces. The absence of a scalar product is the hallmark of irreversibility. Indeed the thermodynamics that is dual to quantum mechanics is that of irreversible processes (considered here in the linear regime).

One is often interested in the case when the operator \mathcal{O} is the time evolution operator \mathcal{U} connecting the incoming and the outgoing states. Not being allowed to exchange the incoming and the outgoing *states* in the transition probability $(\psi | \mathcal{U} | \phi)$, because they belong to different spaces, emphasis falls on the *process* \mathcal{U} connecting these two. Irreversibility manifests itself through the nonunitarity of the representation constructed here for the Chapman–Kolmogorov equation. The latter is the functional equation satisfied by \mathcal{U} .

Incoming states $|\phi\rangle \in L^1(\mathbb{R})$ are probability densities, as opposed to the probability density *amplitudes* $|\phi\rangle \in L^2(\mathbb{R})$ of standard quantum theory. Outgoing states $\langle \psi | \in L^\infty(\mathbb{R})$ have a different physical interpretation. The norm $\| \cdot \|_\infty$ can be regarded as a probability density that is *not* meant to be integrated. Indeed a general function $\psi \in L^\infty(\mathbb{R})$ need not be normalisable under the norms $\| \cdot \|_1$ and $\| \cdot \|_2$ on $L^1(\mathbb{R})$ and $L^2(\mathbb{R})$ respectively. There is nothing unusual about this—scattering states in standard quantum theory also give rise to nonnormalisable probability densities.

As an example, in section 3.1 we have worked out the spectrum for the thermodynamical harmonic oscillator. This implies solving the Schroedinger equation for the *repulsive* potential $V(y) = -y^2$, the wrong sign being due to the Wick rotation connecting irreversible thermodynamics to mechanics. Not surprisingly, the spectrum is empty when diagonalising the Hamiltonian on the space $L^1(\mathbb{R})$, while exhibiting rich features on the space $L^\infty(\mathbb{R})$. In particular, all our eigenstates turn out to be nonnormalisable under the norms $\| \cdot \|_1$ and $\| \cdot \|_2$ on $L^1(\mathbb{R})$ and $L^2(\mathbb{R})$ respectively, hence they all are analogous to scattering states in standard quantum theory. However all our eigenstates are normalisable under the norm $\| \cdot \|_\infty$ of $L^\infty(\mathbb{R})$.

An apparently striking feature is the reluctance of incoming states to build *eigenstates* of the Hamiltonian, as seen in section 3.2. This apparent difficulty disappears once one realises that *outgoing* states make perfectly good eigenstates. Furthermore,

the existence of outgoing states that cannot be reached by the time evolution of any incoming state whatsoever is another sign of irreversibility. We cannot renounce irreversibility because we have programatically dispensed with time reversal symmetry. Hence incoming eigenstates must go.

Exeunt omnes.

References

- [1] D. Acosta, P. Fernández de Córdoba, J.M. Isidro and J.L.G. Santander, *Emergent Quantum Mechanics as a Classical, Irreversible Thermodynamics*, Int. J. Geom. Meth. Mod. Phys. **10** (2013) 1350007, [arXiv:1206.4941](#) [math-ph].
- [2] S. Adler, *Quantum Theory as an Emergent Phenomenon*, Cambridge University Press, Cambridge (2004).
- [3] L. de Broglie, *La Thermodynamique Cachée des Particules*, Ann. Inst. Poincaré (A) Physique Théorique **1** (1964) 1.
- [4] R. Carroll, *On the Emergence Theme of Physics*, World Scientific, Singapore (2010).
- [5] G. Chirco, H. Haggard and C. Rovelli, *Coupling and Thermal Equilibrium in General Covariant Systems*, [arXiv:1309.0777](#) [gr-qc].
- [6] J. Doob, *Stochastic Processes*, Wiley, New York (1953).
- [7] H.-T. Elze, *Discrete Mechanics, Time Machines and Hybrid Systems*, EPJ Web of Conferences **58** (2013) 01013, [arXiv:1310.2862](#) [quant-ph].
- [8] P. Fernández de Córdoba, J.M. Isidro and Milton H. Perea, *Emergent Quantum Mechanics as a Thermal Ensemble*, [arXiv:1304.6295](#) [math-ph].
- [9] F. Finster, *The Fermionic Projector, Entanglement and the Collapse of the Wavefunction*, J. Phys. Conf. Ser. **306** (2011) 012024, [arXiv:1011.2162](#) [quant-ph].
- [10] R. Gallego Torromé, *A Finslerian Version of 't Hooft Deterministic Quantum Models*, J. Math. Phys. **47** (2006) 072101, [arXiv:math-ph/0501010](#).
- [11] G. 't Hooft, *The Fate of the Quantum*, [arXiv:1308.1007](#) [quant-ph].
- [12] S. Kolekar and T. Padmanabhan, *Indistinguishability of Thermal and Quantum Fluctuations*, [arXiv:1308.6289](#) [gr-qc].
- [13] N. Lebedev, *Special Functions and their Applications*, Dover Publications, New York (1972).
- [14] M. Matone, *'Thermodynamique Cachée des Particules' and the Quantum Potential*, Ann. Fond. Broglie **37** (2012) 177, [arXiv:1111.0270](#) [hep-ph].

- [15] N. Olah, *Einsteins Trojanisches Pferd: eine Thermodynamische Deutung der Quantentheorie*, Springer, Wien (2011).
- [16] L. Onsager and S. Machlup, *Fluctuations and Irreversible Processes*, Phys. Rev. **91** (1953) 1505.
- [17] R. Penrose, *On the Second Law of Thermodynamics*, J. Stat. Phys. **77** (1994) 217.
- [18] I. Prigogine, *Time, Structure and Fluctuations*, Nobel Prize Lecture (1977).
- [19] A. Ruuge, *An Asymptotics of the Pauli Problem in Thermodynamics*, Doklady Akademii Nauk **450** (2013) 647; *A Tropical Analogue of the Pauli Problem and a Splitting of Quasithermodynamics*, Doklady Akademii Nauk, **451** (2013) 17, [arXiv:1208.2919](#) [math-ph].
- [20] A. Ruuge, *Fluctuations of Intensive Quantities in Statistical Thermodynamics*, [arXiv:1309.4439](#) [math-ph].
- [21] C. Ududek, N. Wiebe and J. Emerson, *Information-Theoretic Equilibration: the Appearance of Irreversibility under Complex Quantum Dynamics*, [arXiv:1208.3419](#) [quant-ph].
- [22] L. Velazquez Abad, *Principles of Classical Statistical Mechanics: a Perspective from the Notion of Complementarity*, Ann. Phys. **327** (2012) 1682, [arXiv:1203.1479](#) [cond-mat.stat-mech].
- [23] K. Yosida, *Functional Analysis*, Springer, Berlin (1996).

Article

Schroedinger *vs.* Navier–Stokes

P. Fernández de Córdoba [†], J. M. Isidro ^{*,†} and J. Vázquez Molina [†]

Received: 17 November 2015; Accepted: 13 January 2016; Published: 19 January 2016

Academic Editor: Ronnie Kosloff

Instituto Universitario de Matemática Pura y Aplicada, Universidad Politécnica de Valencia, Valencia 46022, Spain; pfernandez@mat.upv.es (P.F.d.C.); joavzmo@doctor.upv.es (J.V.M.)

* Correspondence: joissan@mat.upv.es; Tel.: +34-963-87-70-00

† These authors contributed equally to this work.

Abstract: Quantum mechanics has been argued to be a coarse-graining of some underlying deterministic theory. Here we support this view by establishing a map between certain solutions of the Schroedinger equation, and the corresponding solutions of the irrotational Navier–Stokes equation for viscous fluid flow. As a physical model for the fluid itself we propose the quantum probability fluid. It turns out that the (state-dependent) viscosity of this fluid is proportional to Planck’s constant, while the volume density of entropy is proportional to Boltzmann’s constant. Stationary states have zero viscosity and a vanishing time rate of entropy density. On the other hand, the nonzero viscosity of nonstationary states provides an information-loss mechanism whereby a deterministic theory (a classical fluid governed by the Navier–Stokes equation) gives rise to an emergent theory (a quantum particle governed by the Schroedinger equation).

Keywords: quantum mechanics; irreversible thermodynamics

1. Introduction

Interaction with an environment provides a mechanism whereby classical behaviour can emerge from a quantum system [1]. At the same time, however, dissipation into an environment can change this picture towards the opposite conclusion. Indeed certain forms of quantum behaviour have been *experimentally* shown to arise within classical systems subject to dissipation [2,3]. Now systems in thermal equilibrium are well described by classical thermostatics, while small deviations from thermal equilibrium can be described by the classical thermodynamics of irreversible processes [4]. It is sometimes possible to model long-wavelength dissipative processes through the dynamics of *viscous* fluids. Fluid viscosity provides a relatively simple dissipative mechanism, a first deviation from ideal, frictionless behaviour. Two relevant physical quantities useful to characterise viscous fluids are shear viscosity η and the entropy per unit 3-volume, s [5]. In a turn of events leading back to the Maldacena conjecture [6] it was found that, for a wide class of thermal quantum field theories in 4 dimensions, the ratio η/s for the quark–gluon plasma must satisfy the inequality [7]

$$\frac{\eta}{s} \geq \frac{\hbar}{4\pi k_B}. \quad (1)$$

The predicted value of the ratio η/s for the quark–gluon plasma has found experimental confirmation [8]. The simultaneous presence of Planck’s constant \hbar and Boltzmann’s constant k_B reminds us that we are dealing with theories that are both *quantum* and *thermal*.

One might be inclined to believe that these two properties, *quantum* on the one hand, and *thermal* on the other, are separate. One of the purposes of this paper is to show that this predisposition must be modified, at least partially, because the terms *quantum* and *thermal* are to a large extent linked

(see, e.g., [9–11] and refs. therein). In fact, that these two properties belong together follows from the analysis of refs. [1,3], even if the conclusions of these two papers seem to point in opposite directions.

In this article we elaborate on a theoretical framework that can accommodate the ideas of the previous paragraph. In plain words, this framework can be summarised in the statement *quantum = classical + dissipation*, although of course this somewhat imprecise sentence must be made precise. To begin with, we will restrict our analysis to quantum systems with a finite number of degrees of freedom. So we will be dealing not with theories of fields, strings and branes, but with plain quantum mechanics instead.

In the early days of quantum mechanics, Madelung provided a very intuitive physical interpretation of the Schroedinger wave equation in terms of a probability fluid [12]. Decomposing the complex wavefunction ψ into amplitude and phase, Madelung transformed the Schroedinger wave equation into an equivalent set of two: the quantum Hamilton–Jacobi equation, and the continuity equation. Further taking the gradient of the phase of ψ , Madelung arrived at a velocity field satisfying the Euler equations for an *ideal* fluid. In Madelung’s analysis, the quantum potential U is interpreted as being (proportional to) the pressure field within the fluid. It is important to stress that Madelung’s fluid was ideal, that is, *frictionless*. Independently of this analogy, Bohm suggested regarding the quantum potential U as a force field that the quantum particle was subject to, in addition to any external, classical potential V that might also be present [13].

There exists yet a third, so far unexplored alternative to Madelung’s and Bohm’s independent interpretations of the quantum potential. In this alternative, explored here, *the quantum potential is made to account for a dissipative term in the equations of motion of the probability fluid*. The velocity field no longer satisfies Euler’s equation for an ideal fluid—instead it satisfies the Navier–Stokes equation for a *viscous* fluid. It is with this viscosity term in the Navier–Stokes equation, and its physical interpretation as deriving from the Schroedinger equation, that we will be concerned with in this paper.

It has long been argued that quantum mechanics must emerge from an underlying classical, deterministic theory via some coarse-graining, or information-loss mechanism [14–20]; one refers to this fact as the *emergence property* of quantum mechanics [21]. Many emergent physical theories admit a thermodynamical reformulation, general relativity being perhaps the best example [22,23]. Quantum mechanics is no exception [24,25]; in fact our own approach [9,26] to the emergence property of quantum mechanics exploits a neat correspondence with the classical thermodynamics of irreversible processes [4].

In this article, the dissipation that is intrinsic to the quantum description of the world will be shown to be ascribable to the viscosity η of the *quantum probability fluid* whose density equals Born’s amplitude squared $|\psi|^2$. Moreover, the viscosity η will turn out to be proportional to \hbar , thus vanishing in the limit $\hbar \rightarrow 0$. Now mechanical action (resp. entropy) is quantised in units of Planck’s constant \hbar (resp. Boltzmann’s constant k_B), and Equation (1) contains these two quanta. (Concerning Boltzmann’s constant k_B as a quantum of entropy, see refs. [23,27]). Hence an important implication of our statement *quantum = classical + dissipation* is that quantum and thermal effects are inextricably linked.

Some remarks on conventions are in order; we follow ref. [5]. The viscosity properties of a fluid can be encapsulated in the viscous stress tensor σ'_{ik} ,

$$\sigma'_{ik} := \eta \left(\frac{\partial v_i}{\partial x_k} + \frac{\partial v_k}{\partial x_i} - \frac{2}{3} \delta_{ik} \frac{\partial v_l}{\partial x_l} \right) + \zeta \delta_{ik} \frac{\partial v_l}{\partial x_l}, \quad (2)$$

where η (shear viscosity) and ζ (bulk viscosity) are positive coefficients, and the v_i are the components of the velocity field \mathbf{v} within the fluid. Then the Navier–Stokes equation reads

$$\frac{\partial \mathbf{v}}{\partial t} + (\mathbf{v} \cdot \nabla) \mathbf{v} + \frac{1}{\rho} \nabla p - \frac{\eta}{\rho} \nabla^2 \mathbf{v} - \frac{1}{\rho} \left(\zeta + \frac{\eta}{3} \right) \nabla (\nabla \cdot \mathbf{v}) = 0. \quad (3)$$

Here p is the pressure, and ρ the density of the fluid. In the particular case of *irrotational* flow considered here, the Navier–Stokes equation simplifies to

$$\frac{\partial \mathbf{v}}{\partial t} + (\mathbf{v} \cdot \nabla) \mathbf{v} + \frac{1}{\rho} \nabla p - \frac{\eta'}{\rho} \nabla^2 \mathbf{v} = 0, \quad \eta' := \zeta + \frac{4\eta}{3}. \quad (4)$$

For notational simplicity, in what follows we will systematically write η for the viscosity coefficient η' just defined, bearing in mind, however, that we will always be dealing with Equation (4) instead of Equation (3).

The above must be supplemented with the continuity equation and the equation for heat flow. If T denotes the temperature and κ the thermal conductivity of the fluid, then the equation governing heat transfer within the fluid reads

$$\rho T \left(\frac{\partial s}{\partial t} + (\mathbf{v} \cdot \nabla) s \right) - \sigma'_{ik} \frac{\partial v_i}{\partial x_k} - \nabla \cdot (\kappa \nabla T) = 0. \quad (5)$$

We will use the notations \mathcal{I} and \mathcal{S} for mechanical action and entropy, respectively, while the dimensionless ratios \mathcal{I}/\hbar and $\mathcal{S}/2k_B$ will be denoted in italic type:

$$I := \frac{\mathcal{I}}{\hbar}, \quad S := \frac{\mathcal{S}}{2k_B}. \quad (6)$$

The factor of 2 multiplying k_B , although conventional, can be justified. By Boltzmann's principle, the entropy of a state is directly proportional to the logarithm of the probability of that state. In turn, this is equivalent to Born's rule:

$$\text{(Boltzmann)} \quad \mathcal{S} = k_B \ln \left(\left| \frac{\psi}{\psi_0} \right|^2 \right) \iff |\psi|^2 = |\psi_0|^2 \exp \left(\frac{\mathcal{S}}{k_B} \right) \quad \text{(Born)}. \quad (7)$$

Above, $|\psi_0|$ is the amplitude of a fiducial state ψ_0 with vanishing entropy. Such a fiducial state is indispensable because the argument of the logarithm in Boltzmann's formula must be dimensionless. It is convenient to think of ψ_0 as being related to a 3-dimensional length scale l defined through

$$l := |\psi_0|^{-2/3}. \quad (8)$$

One can also think of ψ_0 as a normalisation factor for the wavefunction.

2. The Physics of Navier–Stokes from Schroedinger

2.1. Computation of the Viscosity

Our starting point is Madelung's rewriting of the Schroedinger equation for a mass m subject to a static potential $V = V(\mathbf{x})$,

$$i\hbar \frac{\partial \psi}{\partial t} + \frac{\hbar^2}{2m} \nabla^2 \psi - V\psi = 0, \quad (9)$$

by means of the substitution

$$\psi = \psi_0 \exp \left(S + \frac{i}{\hbar} \mathcal{I} \right) = \psi_0 A \exp \left(\frac{i}{\hbar} \mathcal{I} \right), \quad A := e^S. \quad (10)$$

This produces, away from the zeroes of ψ , an equation whose imaginary part is the continuity equation for the quantum probability fluid,

$$\frac{\partial S}{\partial t} + \frac{1}{m} \nabla S \cdot \nabla \mathcal{I} + \frac{1}{2m} \nabla^2 \mathcal{I} = 0, \quad (11)$$

and whose real part is the quantum Hamilton–Jacobi equation:

$$\frac{\partial \mathcal{I}}{\partial t} + \frac{1}{2m}(\nabla \mathcal{I})^2 + V + U = 0. \tag{12}$$

Here

$$U := -\frac{\hbar^2}{2m} \frac{\nabla^2 A}{A} = -\frac{\hbar^2}{2m} [(\nabla S)^2 + \nabla^2 S] \tag{13}$$

is the quantum potential [13]. Next one defines the velocity field of the quantum probability fluid

$$\mathbf{v} := \frac{1}{m} \nabla \mathcal{I}. \tag{14}$$

Then the gradient of Equation (12) equals

$$\frac{\partial \mathbf{v}}{\partial t} + (\mathbf{v} \cdot \nabla) \mathbf{v} + \frac{1}{m} \nabla U + \frac{1}{m} \nabla V = 0. \tag{15}$$

The flow (14) is irrotational. We will sometimes (though not always) make the assumption of incompressibility, $\nabla \cdot \mathbf{v} = 0$. This reduces to the requirement that the phase \mathcal{I} satisfy the Laplace equation,

$$\nabla^2 \mathcal{I} = 0. \tag{16}$$

We will see in Equation (23) that the above Laplace equation is an equivalent restatement of the semiclassicality condition.

At this point we deviate from Madelung’s reasoning and compare Equation (15) not to Euler’s equation for an ideal fluid, but to the Navier–Stokes equation instead, Equation (4). For the correspondence to hold, we first identify $(\nabla p)/\rho$ with $(\nabla V)/m$. Second, it must hold that

$$\frac{1}{m} \nabla U + \frac{\eta}{\rho} \nabla^2 \mathbf{v} = 0. \tag{17}$$

That is, the gradient of the quantum potential must exactly compensate the viscosity term in the fluid’s equations of motion. Thus frictional forces within the fluid are quantum in nature. Altogether, we have established the following:

Statement 1. *Whenever condition (17) holds, the gradient of the quantum Hamilton–Jacobi equation, as given by Equation (15), is a Navier–Stokes equation for irrotational, viscous flow:*

$$\frac{\partial \mathbf{v}}{\partial t} + (\mathbf{v} \cdot \nabla) \mathbf{v} - \frac{\eta}{\rho} \nabla^2 \mathbf{v} + \frac{1}{\rho} \nabla p = 0. \tag{18}$$

Here the pressure p of the quantum probability fluid and the mechanical potential V are related as per

$$\frac{1}{\rho} \nabla p = \frac{1}{m} \nabla V, \tag{19}$$

while the density ρ of the fluid is given by

$$\rho = m|\psi|^2 = \frac{m}{l^3} e^{2S} = \frac{m}{l^3} A^2. \tag{20}$$

Given V , m and ρ , the equation $(\nabla p)/\rho = (\nabla V)/m$ defines a vector field $\mathbf{p} = \rho \nabla V/m$, that however need not be a gradient field ∇p . We will see later (statement 4) that, at least in the classical limit, the above equation is integrable, thus defining a scalar function p such that $\mathbf{p} = \nabla p$.

The order of magnitude of the viscosity coefficient η can be inferred from Equations (13), (14) and (17): since U is $O(\hbar^2)$ and \mathcal{I} is $O(\hbar)$, we conclude:

Statement 2. Whenever condition (17) holds, the viscosity coefficient η of the quantum probability fluid is proportional to Planck’s constant:

$$\eta = \frac{1}{l^3} O(\hbar). \tag{21}$$

It is worthwhile stressing that Equation (21) only provides an order of magnitude for η as a function of \hbar —namely, η is a linear function of \hbar . The denominator l^3 has been included for dimensional reasons, while a dimensionless factor multiplying the right-hand side of Equation (21) is allowed. (This dimensionless factor is undetermined, in the sense that our argument does not provide its precise value—not in the sense that the viscosity η is undetermined.) Moreover, this dimensionless factor will generally depend on the quantum state under consideration, because both U and \mathcal{I} are state-dependent. Although the viscosity of the quantum probability fluid depends, through an undetermined dimensionless factor, on the quantum state, the order of magnitude provided by Equation (21) is universal.

2.2. Viscous States vs. Dissipation-Free States

Condition (17) need not be satisfied by all wavefunctions, as the functions S and \mathcal{I} are already determined by the quantum Hamilton–Jacobi equation and by the continuity equation. Thus our next task is to exhibit a class of quantum-mechanical wavefunctions for which condition (17) is indeed satisfied, either exactly or at least approximately.

2.2.1. Exact Solutions

Equation (17) integrates to

$$U + \frac{\eta}{\rho} \nabla^2 \mathcal{I} = C_0(t), \quad C_0(t) \in \mathbf{R}, \tag{22}$$

where the integration constant $C_0(t)$ may generally depend on the time variable. Let us for simplicity set $C_0(t) = 0$. Using (13) and (20) the above becomes

$$\frac{2\eta l^3}{\hbar^2} \nabla^2 \mathcal{I} = e^{2S} \left[(\nabla S)^2 + \nabla^2 S \right]. \tag{23}$$

One can regard (23) as a Poisson equation $\nabla^2 \Phi = \varrho$, where the role of the electric potential Φ is played by the phase \mathcal{I} and that of the charge density ϱ is played by the right-hand side of Equation (23). The bracketed term, $(\nabla S)^2 + \nabla^2 S$, is actually proportional to the Ricci scalar curvature of the conformally flat metric $g_{ij} = e^{-S(x)} \delta_{ij}$, where δ_{ij} is the Euclidean metric on \mathbf{R}^3 . Equation (23) has been dealt with in ref. [28], in connection with the Ricci-flow approach to emergent quantum mechanics; it will also be analysed in a forthcoming publication. For the moment we will relax the requirement that Equation (17) hold exactly, and will satisfy ourselves with approximate solutions instead.

2.2.2. Approximate Solutions

Under the assumption that ρ is spatially constant, Equation (17) integrates to

$$U(\mathbf{x}, t) = C_1(t), \quad C_1(t) \in \mathbf{R}, \tag{24}$$

where Equations (14) and (16) have been used; the integration constant $C_1(t)$ may however be time-dependent. Equivalently, one may assume that S in Equation (23) is approximately constant as a function of the space variables, hence \mathcal{I} is an approximate solution of the Laplace Equation (16). Still another way of arriving at Equation (24) is to assume the flow to be approximately incompressible, $\nabla \cdot \mathbf{v} \simeq 0$. Of course, $\rho = mA^2/l^3$ is generally not spatially constant. However, in the semiclassical

limit, the amplitude $A = e^S$ is a slowly-varying function of the space variables. Under these assumptions, Equation (24) holds approximately:

Statement 3. *In the semiclassical limit, the sufficient condition (17) guaranteeing the validity of the Navier–Stokes equation is equivalent to Equation (24).*

We can now consider the effect of taking the semiclassical limit in the identification $(\nabla p)/\rho = (\nabla V)/m$ made in Equation (19). In this limit ρ is approximately constant, and the above identification defines an integrable equation for the scalar field p . Therefore:

Statement 4. *In the semiclassical limit, the identification $(\nabla p)/\rho = (\nabla V)/m$ made in Equation (19) correctly defines a scalar pressure field p within the probability fluid.*

In the stationary case, when $\psi = \phi(\mathbf{x}) \exp(-iEt/\hbar)$, the quantum potential becomes time-independent, and condition (24) reduces to the requirement that U be a constant both in space and in time:

$$U(\mathbf{x}) = C_2, \quad C_2 \in \mathbf{R}. \quad (25)$$

Statement 5. *In the semiclassical limit of stationary eigenfunctions, the sufficient condition (17) guaranteeing the validity of the Navier–Stokes equation is equivalent to Equation (25).*

One expects semiclassical stationary states to possess vanishing viscosity because, having a well-defined energy, they are dissipation-free. This expectation is borne out by a simple argument: Equation (17) and the (approximate) spatial constancy of U imply $\eta \nabla^2 \mathbf{v} = 0$. This reduces the Navier–Stokes Equation (4) to the Euler equation for a perfect fluid. Therefore:

Statement 6. *All semiclassical stationary states have vanishing viscosity: $\eta = 0$.*

Thus, as far as dissipation effects are concerned, the combined assumptions of stationarity and semiclassicality lead to a dead end. Furthermore, we cannot lift the requirement of semiclassicality because stationarity alone does not guarantee that the sufficient condition (17) holds. Even if we per decree assign a non-semiclassical but stationary state $\eta = 0$, that state need not satisfy condition (17)—the very assignment of a viscosity η would be flawed.

A physically reasonable assumption to make is that viscosity must be proportional to the density of the fluid:

$$\eta = C_3 \rho. \quad (26)$$

Here C_3 is some dimensional conversion factor that does not depend on the space variables: $C_3 \neq C_3(\mathbf{x})$. Then Equation (17) integrates to

$$U + mC_3 (\nabla \cdot \mathbf{v}) = C_4, \quad C_4 \in \mathbf{R}. \quad (27)$$

When the flow is incompressible, $\nabla \cdot \mathbf{v} = 0$, and Equation (27) reduces to the case already considered in Equations (24) and (25). Thus the proportionality assumption (26) provides an independent rationale for the semiclassical approximation made earlier, and viceversa. In turn, this shows that the semiclassicality condition can be recast as done in Equation (16). We conclude:

Statement 7. *In the semiclassical limit, the viscosity η is proportional to the density ρ of the quantum probability fluid. In particular, the viscosity η is approximately spatially constant for semiclassical states. Moreover, the proportionality factor C_3 in Equation (26) is linear in Planck's constant \hbar :*

$$C_3 = \frac{\hbar}{m} f. \quad (28)$$

Here $f \geq 0$ is an arbitrary dimensionless factor. By what was said previously, $f = 0$ when the state considered is an energy eigenstate, while $f > 0$ on all other states. Hence f is best thought of as a function $f : \mathcal{H} \rightarrow \mathbf{R}$ on the Hilbert space \mathcal{H} of quantum states.

Having exhibited the existence of approximate solutions to condition (17), whenever dealing with dissipation effects we will restrict our discussion to *nonstationary states*.

2.3. The Ratio of Viscosity to Entropy Density

We have interpreted dissipation as a quantum effect within the probability fluid. Hence the increase ds/dt in the volume density of entropy of the probability fluid also qualifies as a quantum effect. Here we will compute ds/dt in the semiclassical regime, both for stationary and nonstationary states.

Considering a stationary state first, we expect $ds/dt = 0$ because $\eta = 0$. This expectation is confirmed by the following alternative argument. We see that Equation (5) reduces to

$$\frac{ds}{dt} = \frac{\partial s}{\partial t} + (\mathbf{v} \cdot \nabla)s = \frac{\kappa}{\rho} \frac{\nabla^2 T}{T}, \quad (29)$$

because the dissipation term σ'_{ik} vanishes. On the other hand, by Boltzmann's principle (7) we can write the entropy \mathcal{S} in terms of the amplitude $A = e^{\mathcal{S}}$ as

$$\mathcal{S} = 2k_B \ln \left(\left| \frac{\psi}{\psi_0} \right| \right) = 2k_B \ln A. \quad (30)$$

This is reminiscent of the expression for the entropy of an ideal gas as a function of its temperature, *viz.* $\mathcal{S} = gk_B \ln(T/T_0)$, with g a dimensionless number and T_0 some fixed reference temperature. This suggests identifying the quantum-mechanical amplitude A with the thermodynamical temperature T , at least in the absence of friction—as is indeed the case for stationary states and for the ideal gas. So we set

$$A = \frac{T}{T_0}. \quad (31)$$

Thus $\nabla^2 A = 0$ implies $\nabla^2 T = 0$. In the semiclassical approximation, A is a slowly-varying function, and one can approximate $\nabla^2 A$ by zero. Thus substituting Equation (31) into Equation (29), we arrive at a counterpart to statement 5:

Statement 8. *In the semiclassical approximation, the entropy density of any stationary state is constant in time: $ds/dt = 0$.*

Our next task is to obtain an estimate for the order of magnitude of the entropy density s . This is readily provided by Equation (30):

Statement 9. *In the semiclassical approximation, the volume density of entropy s of the quantum probability fluid is proportional to Boltzmann's constant:*

$$s = \frac{1}{l^3} O(k_B). \quad (32)$$

As already mentioned regarding Equation (21), the denominator l^3 has been included for dimensional reasons, and an undetermined, dimensionless factor multiplying the right-hand side is allowed. Finally combining Equations (21) and (32) together we can state:

Statement 10. For the quantum probability fluid in the semiclassical approximation, the order of magnitude of the ratio of viscosity to entropy density is

$$\frac{\eta}{s} = O\left(\frac{\hbar}{k_B}\right). \quad (33)$$

Again an undetermined, dimensionless factor multiplying the right-hand side is allowed, but the dependence on the length scale l has dropped out.

2.4. Nonstationary States: Emergent Reversibility

Nonstationary states can be readily constructed as linear combinations of stationary eigenstates with different energy eigenvalues. The ratio η/s of the viscosity to the entropy density of a nonstationary state is important for the following reason. Any nonstationary state thermalises to a final equilibrium state. The time required for this transition is of the order of the Boltzmann time τ_B ,

$$\tau_B := \frac{\hbar}{k_B T}, \quad (34)$$

where T is the temperature of the final equilibrium state [29]. In Equation (31) we have related the temperature T to the amplitude $A = |\psi_{\text{eq}}|$ of the equilibrium state wavefunction ψ_{eq} . Therefore:

Statement 11. For semiclassical, nonstationary states of the quantum probability fluid, the Boltzmann time is directly proportional to the ratio η/s of the viscosity to the entropy density of the initial state, and inversely proportional to the amplitude of the final equilibrium state.

Out of this analysis there arises a nice picture of the thermalisation process, whereby a nonstationary state decays into a final stationary state. In this picture we have a slow dynamics superimposed on a fast dynamics. The latter corresponds to nonstationary states; the former, to stationary states. Viscous states correspond to the fast dynamics, while dissipation-free states pertain to the slow dynamics. Time reversibility emerges as a conservation law that applies only to the emergent, slow dynamics.

2.5. Stationary States: Emergent Holography

Turning now our attention to stationary states, let us see how an emergent notion of holography arises naturally in our context. For stationary states we first set $\partial S/\partial t = 0$ in the continuity Equation (11), then apply the semiclassicality condition (16), next divide through by \hbar and finally switch from \mathcal{I} to I as per Equation (6). This establishes:

Statement 12. For semiclassical stationary states we have

$$\nabla I \cdot \nabla S = O\left(l^{-2}\right). \quad (35)$$

For such states, Equations (25) and (35) are equivalent.

In the limit $l \rightarrow \infty$ we have $\nabla I \cdot \nabla S = 0$, and the foliation $I = \text{const}$ (This is abuse of language. Strictly speaking, the equation $I = \text{const}$ defines only one leaf of the foliation. The foliation itself is the union of all the leaves obtained by letting the constant run over the corresponding range.) intersects orthogonally the foliation $S = \text{const}$. That the length scale l , in our case of semiclassical stationary states, can be regarded as being sufficiently large, follows from Equation (8). Indeed a classical, perfectly localised state around $\mathbf{x} = \mathbf{x}_0$ carries a wavefunction $\delta(\mathbf{x} - \mathbf{x}_0)$, the amplitude of which is almost everywhere zero. As this localised state spreads out, ceasing to be perfectly classical, its width can be taken as an inverse measure of its localisation. In other words, the limit $\hbar \rightarrow 0$ is equivalent to the limit $l \rightarrow \infty$. Thus neglecting the right-hand side of Equation (35) we arrive at:

Statement 13. *Semiclassical stationary states provide two independent foliations of 3-dimensional space by two mutually orthogonal families of 2-dimensional surfaces, respectively defined by $I = \text{const}$ and by $S = \text{const}$.*

The foliation $I = \text{const}$ is well known since the early days of quantum theory. On the other hand the foliation $S = \text{const}$ was little used in mechanical contexts until the groundbreaking contributions of refs. [22,23] to the notion of *emergent spacetime*. Specifically, in ref. [23], isentropic surfaces $S = \text{const}$ are taken to be holographic screens, while also qualifying as equipotential surfaces $V = \text{const}$ of the gravitational field. We see immediately that:

Statement 14. *Under the above assumptions of stationarity and semiclassicality,*

- (i) *the vector field ∇I is parallel to the foliation $S = \text{const}$;*
- (ii) *the vector field ∇S is parallel to the foliation $I = \text{const}$;*
- (iii) *whenever $\nabla I \neq 0 \neq \nabla S$, the vector fields ∇I and ∇S define an integrable 2-dimensional distribution on \mathbf{R}^3 .*

The integrability of the distribution defined by the vector fields ∇I and ∇S follows from the semiclassicality property $\nabla I \cdot \nabla S = 0$. Then Frobenius' theorem guarantees the existence of a family of 2-dimensional integral manifolds for the distribution. (A purely differential-geometric proof of this statement can be found in ref. [30]; a related theorem by Liouville, in the context of classical integrability theory, can be found in ref. [31].) Each leaf of this integral foliation, that we denote by $F = \text{const}$, is such that its two tangent vectors ∇S and ∇I point in the direction of maximal increase of the corresponding quantities, S and I . Therefore:

Statement 15. *Under the above assumptions of stationarity and semiclassicality, the foliation $F = \text{const}$ is orthogonal to the two foliations $S = \text{const}$ and $I = \text{const}$ simultaneously.*

According to ref. [23], the leaves $S = \text{const}$ are holographic screens, enclosing that part of space that can be regarded as having emerged. We see that the leaves $I = \text{const}$ play an analogous role with respect to the time variable. Now the wavefunction contains both amplitude and phase. Hence the two foliations $S = \text{const}$ and $I = \text{const}$ must appear on the same footing—as is actually the case. Taken together, these facts can be renamed as the *holographic property of emergent quantum mechanics*. To be precise, this holographic property has been analysed here in the semiclassical regime only; we defer a full analysis until a forthcoming publication.

3. Discussion

To first order of approximation, any viscous fluid can be characterised by its viscosity coefficients and by its volume density of entropy. In this paper we have obtained an estimate for the order of magnitude of these quantities, in the case of irrotational flow, for the quantum probability fluid. Our analysis makes decisive use of Madelung's factorisation of the quantum wavefunction into amplitude and phase. However, we deviate substantially from Madelung on the following key issue: *Madelung's probability fluid is ideal, while ours is viscous*. Correspondingly, Madelung's fluid satisfies Euler's equation for a perfect fluid, while ours satisfies the Navier–Stokes equation. Consequently, the pressure within the fluid is also different: in Madelung's analysis, pressure is (proportional to) the quantum potential U , while our pressure is (proportional to) the external potential V in the Schrodinger equation. In our alternative approach, *the quantum potential is responsible for the appearance of viscosity*. Thus classical friction in the fluid can be regarded as the origin of quantum effects. Moreover, the dissipation that is inherent to quantum phenomena, under the guise of viscosity in our case, is a nonstationary phenomenon.

By letting the quantum potential account for the viscosity of the probability fluid, our analysis lends support to the emergent paradigm of quantum mechanics: the resulting theory, once dissipation has been taken into account, is no longer classical but quantum. We regard viscosity as the dissipation, or information-loss mechanism, whereby the fluid described by the Navier–Stokes equation

(a classical process) becomes the quantum wavefunction satisfying the Schroedinger equation (a quantum process). This mechanism illustrates the statement $quantum = classical + dissipation$ made in the introductory section.

Author Contributions: All coauthors contributed equally to this article. All authors have read and approved the final manuscript.

Conflicts of Interest: The authors declare no conflict of interest.

References

- Zurek, W. Decoherence, Einselection, and the Quantum Origins of the Classical. *Rev. Mod. Phys.* **2003**, *75*, doi:10.1103/RevModPhys.75.715.
- Couder, Y.; Protière, S.; Fort, E.; Boudaoud, A. Dynamical phenomena: Walking and orbiting droplets. *Nature* **2005**, *437*, doi:10.1038/437208a.
- Raftery, J.; Sadri, D.; Schmidt, S.; Türeci, H.; Houck, A. Observation of a Dissipation-Induced Classical to Quantum Transition. *Phys. Rev. X* **2014**, *4*, 031043.
- Onsager, L.; Machlup, S. Fluctuations and Irreversible Processes. *Phys. Rev.* **1953**, *91*, 1505–1512.
- Landau, L.; Lifshitz, E. *Course of Theoretical Physics Vol. 6: Fluid Mechanics*; Butterworth-Heinemann: Oxford, UK, 2000.
- Maldacena, J. The Large-N limit of Superconformal Field Theories and Supergravity. *Int. J. Theor. Phys.* **1998**, *38*, 1113–1133.
- Kovtun, P.; Son, D.; Starinets, A. Viscosity in Strongly Interacting Quantum Field Theories from Black Hole Physics. *Phys. Rev. Lett.* **2005**, *94*, 111601.
- Luzum, M.; Romatschke, P. Conformal Relativistic Viscous Hydrodynamics: Applications to RHIC Results at $\sqrt{s_{NN}} = 200$ GeV. *Phys. Rev. C* **2008**, *78*, 034915.
- Fernández de Córdoba, P.; Isidro, J.M.; Perea, M.H. Emergent Quantum Mechanics as a Thermal Ensemble. *Int. J. Geom. Meth. Mod. Phys.* **2014**, *11*, 1450068.
- Kolekar, S.; Padmanabhan, T. Indistinguishability of Thermal and Quantum Fluctuations. **2013**, arXiv:1308.6289v3.
- Kosloff, R. Quantum Thermodynamics: A Dynamical Viewpoint. *Entropy* **2013**, *15*, 2100–2128.
- Madelung, E. Quantentheorie in Hydrodynamischer Form. *Zeitschrift für Physik* **1927**, *40*, 322–326.
- Bohm, D. A Suggested Interpretation of the Quantum Theory in Terms of “Hidden” Variables. I. *Phys. Rev.* **1952**, *85*, doi:10.1103/PhysRev.85.166.
- Elze, H.-T. Symmetry Aspects in Emergent Quantum Mechanics. *J. Phys. Conf. Ser.* **2009**, *171*, 012034.
- Elze, H.-T. Discrete Mechanics, Time Machines and Hybrid Systems. *EPJ Web Conf.* **2013**, *58*, 01013.
- Gallego Torromé, R. A Finslerian Version of ‘t Hooft Deterministic Quantum Models. *J. Math. Phys.* **2006**, *47*, 072101.
- Torromé, R.G. A Theory of Emergent Quantum Mechanics. **2014**, arXiv:1402.5070.
- Hooft, G. Emergent Quantum Mechanics and Emergent Symmetries. **2007**, arXiv:0707.4568v1.
- Hooft, G. The Fate of the Quantum. **2013**, arXiv:1308.1007v1.
- Hooft, G. The Cellular Automaton Interpretation of Quantum Mechanics. **2015**, arXiv:1405.1548v3.
- Carroll, R. *On the Emergence Theme of Physics*; World Scientific: Singapore, Singapore, 2010.
- Padmanabhan, T. General Relativity from a Thermodynamic Perspective. *Gen. Rel. Grav.* **2014**, *46*, doi:10.1007/s10714-014-1673-7.
- Verlinde, E. On the Origin of Gravity and the Laws of Newton. *J. High Energy Phys.* **2011**, *2011*, doi:10.1007/JHEP04(2011)029.
- De Broglie, L. La Thermodynamique «Cachée» des Particules. *Ann. Inst. Henri Poincaré Sect. A Phys. Théor.* **1964**, *1*, 1–19. (In French)
- Matone, M. “Thermodynamique Cachée des Particules” and the Quantum Potential. **2012**, arXiv:1111.0270v4.
- Fernández de Córdoba, P.; Isidro, J.M.; Perea, M.H.; Vazquez Molina, J. The Irreversible Quantum. *Int. J. Geom. Meth. Mod. Phys.* **2014**, *12*, 1550013.
- Landauer, R. Irreversibility and Heat Generation in the Computing Process. *IBM J. Res. Dev.* **1961**, *5*, 183–191.

28. Abraham, S.; Fernández de Córdoba, P.; Isidro, J.M.; Santander, J.L.G. A Mechanics for the Ricci Flow. *Int. J. Geom. Meth. Mod. Phys.* **2009**, *6*, 759–767.
29. Goldstein, S.; Hara, T.; Tasaki, H. The Approach to Equilibrium in a Macroscopic Quantum System for a Typical Nonequilibrium Subspace. **2014**, arXiv:1402.3380v2.
30. Kobayashi, S.; Nomizu, K. *Foundations of Differential Geometry*; Wiley: New York, NY, USA, 1996.
31. Arnold, V. *Mathematical Methods of Classical Mechanics*; Springer: Berlin, Germany, 1989.



© 2016 by the authors; licensee MDPI, Basel, Switzerland. This article is an open access article distributed under the terms and conditions of the Creative Commons by Attribution (CC-BY) license (<http://creativecommons.org/licenses/by/4.0/>).

Document downloaded from:

<http://hdl.handle.net/10251/97603>

This paper must be cited as:

Fernández De Córdoba, P.; Isidro San Juan, JM.; J. Vazquez Molina (2016). The holographic quantum. *Foundations of Physics*. 46(7):787-803. doi:10.1007/s10701-015-9986-2



The final publication is available at

<https://doi.org/10.1007/s10701-015-9986-2>

Copyright Springer-Verlag

Additional Information

THE HOLOGRAPHIC QUANTUM

P. Fernández de Córdoba^a, J.M. Isidro^b and J. Vazquez Molina^c

Instituto Universitario de Matemática Pura y Aplicada,

Universidad Politécnica de Valencia, Valencia 46022, Spain

^apfernandez@mat.upv.es, ^bjoissan@mat.upv.es,

^cjoavzmo@etsii.upv.es

December 4, 2015

Abstract We present a map of standard quantum mechanics onto a dual theory, that of the classical thermodynamics of irreversible processes. While no gravity is present in our construction, our map exhibits features that are reminiscent of the holographic principle of quantum gravity.

Contents

1	Introduction	1
2	Basics in irreversible thermodynamics	2
3	Quantum mechanics vs. irreversible thermodynamics	6
4	Beyond the harmonic approximation	8
5	Quantum states as equivalence classes of classical trajectories	10
6	Quantum uncertainty vs. the second law	13
7	Discussion	13

1 Introduction

The holographic principle [3, 30, 31] has permeated wide areas of theoretical physics over the last twenty years. Stepping outside its initial quantum–gravity framework, it reached string theory [21, 33] as well as more established domains such as QCD [18] and condensed matter theory [15], to name but a few.

Another theoretical development of recent years is the recognition that *gravity arises as an emergent phenomenon* [24, 25, 32], a fact that has far-reaching consequences for our understanding of spacetime. Added to the dissipative properties already known to be exhibited by gravity [16, 26, 28, 29], this opens the gate to the application of thermodynamics to (supposedly) nonthermal physics. Indeed, thermodynamics is the paradigm of emergent theories. It renounces the knowledge of a vast

amount of detailed microscopic information, keeping just a handful of macroscopic variables such as volume, pressure and temperature—sufficient to state robust physical laws of almost universal applicability. These macroscopic variables are coarse-grained averages over the more detailed description provided by some underlying, microscopic degrees of freedom. Which brings us to yet another theoretical breakthrough of recent times that is worthy of mention: the notion of *emergence* [7].

The property of emergence has been postulated not only of gravity, but also of Newtonian mechanics [32] and of quantum mechanics [10, 17]; a key concept here is that of an *entropic force*. Equipped with thermodynamical tools as befits any emergent theory, we have in refs. [11, 12, 13] developed a framework that maps semiclassical quantum mechanics onto the classical thermodynamics of irreversible processes in the linear regime, the latter as developed by Onsager, Prigogine and collaborators [23, 27]. Within this framework, the statement often found in the literature, *quantisation is dissipation* [4], can be given a new interpretation.

In this paper we elaborate further on the above-mentioned map of semiclassical quantum mechanics onto the classical theory of linear, irreversible processes (sections 2 and 3); we call these two theories *dual* to each other. From there we move on to the nonlinear regime of the thermodynamics or, equivalently, to the quantum regime beyond the Gaussian approximation (section 4). Next we formulate a holographic-like principle for quantum mechanics (section 5) and place it in correspondence with the second law of thermodynamics (section 6). The term *holographic-like* is meant to stress that, while it is true that no gravity is present in our framework, an undeniable conceptual similarity with the holographic principle of quantum gravity underlies the principle postulated here. We summarise our conclusions in section 7.

A word on notation is in order. Rather than using natural units, we will explicitly retain Planck's constant \hbar and Boltzmann's constant k_B in our expressions, in order to better highlight the properties of the map presented here between quantum mechanics and irreversible thermodynamics. In particular, the role that \hbar plays on the mechanical side of our correspondence will be played by k_B on the thermodynamical side. If we were to set $\hbar = 1 = k_B$, the fact that they are counterparts under our correspondence [8, 19] would be somewhat obscured.

2 Basics in irreversible thermodynamics

The following is a very brief summary of some notions of irreversible thermodynamics [23, 27] that we will make use of.

Let an irreversible thermodynamical system be characterised by its entropy function S . Assume that the thermodynamical state of the system is determined by just one extensive variable $x = x(\tau)$, where τ is time variable. We can thus write $S = S(x(\tau))$. At any instant of time, the probability P of a state is given by Boltzmann's principle,

$$k_B \ln P = S + \text{const.} \quad (1)$$

Let S_0 denote the maximum (equilibrium) value of S , and let us redefine the coordinate x so it will vanish when evaluated at equilibrium: $S_0 = S(x = 0)$. Irreversible thermodynamics [23] analyses the response of the system when driven away from equilibrium.

For this purpose one introduces the *thermodynamical force* X ,

$$X = \frac{dS}{dx}, \quad (2)$$

which measures the tendency of the system to restore equilibrium. Nonequilibrium causes fluxes to appear in the system, that is, nonvanishing time derivatives $dx/d\tau$ and $dS/d\tau$. Further one supposes that the irreversible process considered is *linear*. This amounts to the assumption that the flux is proportional to the force,

$$\frac{dx}{d\tau} = LX, \quad L > 0, \quad (3)$$

where L is a positive constant, independent of x and τ . One also writes (3) under the form

$$X = R \frac{dx}{d\tau}, \quad R = L^{-1} > 0, \quad (4)$$

where the dimensions of R are time \times entropy $\times x^{-2}$. Eq. (4) is often termed a *phenomenological law*. Indeed numerous dissipative phenomena, at least to first order of approximation, take on the form of a linear relation between a driving force X and the corresponding flux $dx/d\tau$: Ohm's law in electricity, Fourier's law of heat transfer, etc, are familiar examples. In linear irreversible thermodynamics, the time rate of entropy production is the product of those two:

$$\frac{dS}{d\tau} = X \frac{dx}{d\tau}. \quad (5)$$

On the other hand, Taylor–expanding the entropy around its (maximum) equilibrium value and keeping terms up to second–order we have

$$S = S_0 - \frac{1}{2}sx^2 + \dots, \quad s := - \left(\frac{d^2S}{dx^2} \right)_0 > 0. \quad (6)$$

Three consequences follow from truncating the expansion (6) at second order. First, the force X is a linear function of the coordinate x :

$$X = -sx. \quad (7)$$

Second, in conjunction with Boltzmann's principle (1), the expansion (6) implies that the probability distribution for fluctuations is a Gaussian in the extensive variable x :

$$P(x) = Z^{-1} \exp\left(\frac{S}{k_B}\right) = Z^{-1} \exp\left(-\frac{1}{2k_B}sx^2\right), \quad (8)$$

where Z is some normalisation¹. Third, the phenomenological law (4) specifies a linear submanifold of thermodynamical phase space:

$$R \frac{dx}{d\tau} + sx = 0. \quad (9)$$

¹We will henceforth omit all normalisation factors, bearing in mind that all probabilities are to be normalised at the end.

Fluctuations around the deterministic law given by Eq. (9) can be modelled by the addition of a random force F_τ . This turns the deterministic equation (9) into the stochastic equation

$$R \frac{dx}{d\tau} + sx = F_\tau. \quad (10)$$

We are interested in computing the path $x = x(\tau)$ under the influence of these random forces, under the assumption that F_τ has a vanishing average value. While mimicking random fluctuations, this assumption ensures that the net force continues to be given as in the deterministic Eq. (9). Now our aim is to calculate the probability of any path in configuration space. For this purpose we need to introduce some concepts borrowed from ref. [9].

The *unconditional probability density function* $f\left(\frac{x}{\tau}\right)$, also called *one-gate function*, is defined such that the product $f\left(\frac{x}{\tau}\right) dx$ equals the probability that the random trajectory $x = x(\tau)$ pass through a gate of width dx around x at the instant τ . The *conditional probability density function* $f\left(\frac{x_2}{\tau_2} \middle| \frac{x_1}{\tau_1}\right)$, also called the *two-gate function*, is defined such that $f\left(\frac{x_2}{\tau_2} \middle| \frac{x_1}{\tau_1}\right) dx_2 dx_1$ equals the probability that a thermodynamical path pass through a gate of width dx_2 around x_2 at time τ_2 , given that it passed through a gate of width dx_1 around x_1 at time τ_1 . The assumption that our stochastic process (10) satisfies the Markov property ensures that the unconditional probability $f\left(\frac{x_2}{\tau_2}\right)$ can be obtained from the conditional probability $f\left(\frac{x_2}{\tau_2} \middle| \frac{x_1}{\tau_1}\right)$ by letting $\tau_1 = -\infty$ in the latter and setting a fixed value of x_1 , say $x_1 = 0$. Informally speaking: Markov systems have a short-lived memory.

Let us consider a time interval (τ_1, τ_{n+1}) , which we divide into n subintervals of equal length. Then the conditional probabilities obey the Chapman–Kolmogorov equation,

$$f\left(\frac{x_{n+1}}{\tau_{n+1}} \middle| \frac{x_1}{\tau_1}\right) = \int dx_n \cdots \int dx_2 f\left(\frac{x_{n+1}}{\tau_{n+1}} \middle| \frac{x_n}{\tau_n}\right) \cdots f\left(\frac{x_2}{\tau_2} \middle| \frac{x_1}{\tau_1}\right), \quad (11)$$

where all $n - 1$ intermediate gates at x_2, x_3, \dots, x_n are integrated over. In particular, the unconditional probability density $f\left(\frac{x}{\tau}\right)$ propagates according to the law

$$f\left(\frac{x_2}{\tau_2}\right) = \int dx_1 f\left(\frac{x_2}{\tau_2} \middle| \frac{x_1}{\tau_1}\right) f\left(\frac{x_1}{\tau_1}\right). \quad (12)$$

It turns out that, for a Markovian Gaussian process, the conditional probability function $f\left(\frac{x_2}{\tau_2} \middle| \frac{x_1}{\tau_1}\right)$ that solves the Chapman–Kolmogorov equation is given by [23]

$$f\left(\frac{x_2}{\tau_2} \middle| \frac{x_1}{\tau_1}\right) = \frac{s}{2k_B} \frac{e^{s(\tau_2 - \tau_1)/2R}}{\sqrt{\pi \sinh [s(\tau_2 - \tau_1)/R]}} \quad (13)$$

$$\times \exp \left\{ -\frac{s}{2k_B} \frac{[e^{s(\tau_2 - \tau_1)/2R} x_2 - e^{-s(\tau_2 - \tau_1)/2R} x_1]^2}{2 \sinh [s(\tau_2 - \tau_1)/R]} \right\}.$$

As a consistency check we observe that, in the limit $\tau_2 \rightarrow \infty$, the conditional probability (13) reduces to the unconditional probability (8). Using the Chapman–Kolmogorov equation (11) one can reexpress the conditional probability (13) as

$$f \left(\begin{matrix} x_{n+1} \\ \tau_{n+1} \end{matrix} \middle| \begin{matrix} x_1 \\ \tau_1 \end{matrix} \right) = \exp \left[-\frac{1}{4k_B} \int_{\tau_1}^{\tau_{n+1}} d\tau R \left(\frac{dx}{d\tau} + \gamma x \right)^2 \right]_{\min}, \gamma := \frac{s}{R}, \quad (14)$$

subject to the boundary conditions $x(\tau_1) = x_1$ and $x(\tau_{n+1}) = x_{n+1}$. Above, γ carries the dimension of inverse time, while the subscript *min* reminds us that the integral is to be evaluated along that particular path which minimises the integral.

Now $f \left(\begin{matrix} x_2 \\ \tau_2 \end{matrix} \right)$ can be obtained from $f \left(\begin{matrix} x_2 \\ \tau_2 \end{matrix} \middle| \begin{matrix} x_1 \\ \tau_1 \end{matrix} \right)$ by letting $\tau_1 = -\infty$ and $x_1 = 0$ in the latter. In order to take this limit in Eq. (14) we first define the *thermodynamical Lagrangian* \mathcal{S} to be

$$\mathcal{S} := \frac{R}{2} \left(\frac{dx}{d\tau} + \gamma x \right)^2, \quad (15)$$

or, dropping a total derivative,

$$\mathcal{S} = \frac{R}{2} \left[\left(\frac{dx}{d\tau} \right)^2 + \gamma^2 x^2 \right]. \quad (16)$$

The dimensions of \mathcal{S} are entropy per unit time. The corresponding Euler–Lagrange equation reads

$$\frac{d^2x}{d\tau^2} - \gamma^2 x = 0, \quad (17)$$

while

$$x(\tau) = x_2 e^{\gamma(\tau - \tau_2)} \quad (18)$$

is the particular solution to (17) that satisfies the boundary conditions $x(\tau = -\infty) = 0$ and $x(\tau = \tau_2) = x_2$. Thus evaluating (14) along this extremal path yields

$$f \left(\begin{matrix} x_2 \\ \tau_2 \end{matrix} \middle| \begin{matrix} 0 \\ -\infty \end{matrix} \right) = f \left(\begin{matrix} x_2 \\ \tau_2 \end{matrix} \right) = \exp \left[-\frac{s}{2k_B} (x_2)^2 \right]. \quad (19)$$

This is again in agreement with Boltzmann’s principle (1) in the Gaussian approximation (6). Moreover, the conditional probability density $f \left(\begin{matrix} x_2 \\ \tau_2 \end{matrix} \middle| \begin{matrix} x_1 \\ \tau_1 \end{matrix} \right)$ admits the path–integral representation [23]‡

$$f \left(\begin{matrix} x_2 \\ \tau_2 \end{matrix} \middle| \begin{matrix} x_1 \\ \tau_1 \end{matrix} \right) = \int_{x(\tau_1)=x_1}^{x(\tau_2)=x_2} Dx(\tau) \exp \left\{ -\frac{1}{2k_B} \int_{\tau_1}^{\tau_2} d\tau \mathcal{S} \right\}. \quad (20)$$

In fact, a saddle–point evaluation of the path integral (20) is readily seen to yield the two–gate function (14).

The above Eqs. (2)–(20) have obvious generalisations to a case with D independent thermodynamical coordinates.

²What quantum theorists call the Feynman path integral was independently developed in ref. [23] by Onsager and collaborators, who appear to have arrived at the notion of a path integral all by themselves, without previous knowledge of Feynman’s earlier work [14].

3 Quantum mechanics vs. irreversible thermodynamics

The attentive reader will have noticed the striking similarity between Eqs. (2)–(20) and the quantum mechanics of the harmonic oscillator. The corresponding Lagrangian is

$$\mathcal{L} = \frac{m}{2} \left(\frac{dx}{dt} \right)^2 - \frac{k}{2} x^2. \quad (21)$$

Mechanical time is denoted by the variable t ; it is related to thermodynamical time τ through the Wick rotation

$$\tau = it. \quad (22)$$

We define as usual the angular frequency ω through $\omega^2 = k/m$. Let us for simplicity assume that the thermodynamical extensive coordinate x of the dual irreversible thermodynamics is a length. In this way no dimensionful factor is needed to reinterpret it as the coordinate of the harmonic oscillator in the mechanical dual theory. Then the Wick rotation (22) and the replacements³

$$\frac{m\omega}{\hbar} = \frac{s}{2k_B}, \quad \omega = \gamma \quad (23)$$

provide us with a dictionary to establish a 1-to-1 map between the linear, irreversible thermodynamics of section 2 and the quantum mechanics of the harmonic oscillator.

Specifically, let us spell out the entries of this map, one by one [2]. The mechanical Lagrangian (21) is readily obtained from its thermodynamical counterpart (16) upon application of the replacements (22), (23):

$$\frac{\mathcal{S}}{2k_B} = -\frac{\mathcal{L}}{\hbar}. \quad (24)$$

The above also makes it clear that the thermodynamical analogue of Planck's constant \hbar is twice Boltzmann's constant, $2k_B$. In this way the thermodynamical path integral (20) becomes its usual quantum-mechanical expression. Unconditional probabilities $f\left(\frac{x}{\tau}\right)$ in thermodynamics become wavefunctions squared $|\psi(x, t)|^2$ in quantum mechanics. Thus the 1-gate distribution function (19) gives the squared modulus of the oscillator groundstate,

$$f\left(\frac{x}{it}\right) = \exp\left(-\frac{m\omega}{\hbar} x^2\right). \quad (25)$$

The thermodynamical conditional probability (13) becomes proportional to the quantum-mechanical Feynman propagator. Away from the caustics, the latter is given by

$$K(x_2, t_2 | x_1, t_1) = \sqrt{\frac{m\omega}{2\pi i \hbar \sin(\omega(t_2 - t_1))}} \quad (26)$$

³Implicit in the replacements (23) is the assumption that the thermodynamical extensive variable x , and the mechanical variable x , both have units of length. A dimensionful conversion factor is to be understood in case the dimensions do not match.

$$\times \exp \left\{ \frac{im}{2\hbar} \frac{\omega}{\sin(\omega(t_2 - t_1))} [(x_2^2 + x_1^2) \cos(\omega(t_2 - t_1)) - 2x_2x_1] \right\}$$

and one actually finds

$$f \left(\begin{matrix} x_2 & | & x_1 \\ it & | & 0 \end{matrix} \right) = \exp \left(\frac{i\omega t}{2} - \frac{\Delta V}{\hbar\omega} \right) \sqrt{\frac{2m\omega}{\hbar}} K(x_2, t | x_1, 0), \quad (27)$$

where $\Delta V = V(x_2) - V(x_1)$, with $V(x) = kx^2/2$ the harmonic potential. The Chapman–Kolmogorov equation (11) becomes the group property of propagators, while the propagation law (12) exactly matches that for wavefunctions ψ under propagators K . Altogether, the promised 1–to–1 map is complete.

Our Eqs. (21)–(27) have obvious generalisations to higher dimensions. Since the concept of *equipotential submanifolds* will play a key role in our duality between quantum mechanics and irreversible thermodynamics, it will be useful to consider the lowest dimension in which equipotential manifolds are *2–dimensional surfaces*. Configuration space is then 3–dimensional, which we take to be \mathbb{R}^3 , coordinatised by x, y, z . For simplicity we will assume the harmonic potential to be isotropic, so the harmonic force is $\mathbf{F}_h = -k(x, y, z)$. On the thermodynamical side of our correspondence, this translates into the fact that Onsager’s (inverse) coefficients R_x, R_y, R_z in Eq. (4) are all equal, so the dissipative force acting on the system is $\mathbf{F}_d = R(dx/d\tau, dy/d\tau, dz/d\tau)$. We then have a thermodynamical Lagrangian

$$\mathcal{S} = \frac{R}{2} \left[\left(\frac{dx}{d\tau} \right)^2 + \left(\frac{dy}{d\tau} \right)^2 + \left(\frac{dz}{d\tau} \right)^2 + \gamma^2(x^2 + y^2 + z^2) \right] \quad (28)$$

and a mechanical Lagrangian

$$\mathcal{L} = \frac{m}{2} \left[\left(\frac{dx}{dt} \right)^2 + \left(\frac{dy}{dt} \right)^2 + \left(\frac{dz}{dt} \right)^2 - \omega^2(x^2 + y^2 + z^2) \right]. \quad (29)$$

The latter has the family of 2–dimensional spheres $x^2 + y^2 + z^2 = \rho^2$ as equipotential surfaces within the mechanical configuration space \mathbb{R}^3 . We claim that the thermodynamical counterpart of this family of spheres is the family of 5–dimensional submanifolds

$$\left(\frac{dx}{d\tau} \right)^2 + \left(\frac{dy}{d\tau} \right)^2 + \left(\frac{dz}{d\tau} \right)^2 + \gamma^2(x^2 + y^2 + z^2) = \rho^2 \quad (30)$$

within the thermodynamical phase space \mathbb{R}^6 ; we may call the above hypersurfaces *isoentropic submanifolds*. Although we seem to have a dimensional mismatch between isoentropic submanifolds and equipotential surfaces, this mismatch disappears if we restrict to those thermodynamical trajectories that satisfy the equation of motion of the thermodynamical Lagrangian (28). This equation was given in (17) and solved in (18); we see that, *on shell*, the velocity $dx/d\tau$ is proportional to the coordinate x . This property effectively allows us to replace the term $(dx/d\tau)^2 + (dy/d\tau)^2 + (dz/d\tau)^2$ in Eq. (30) with a constant multiple of $x^2 + y^2 + z^2$. In turn, this reduces the family of 5–dimensional submanifolds (30) to a family of 2–dimensional spheres—exactly as in the mechanical case.

We conclude that *equipotential surfaces for the mechanical problem become isentropic surfaces for the thermodynamical problem, and viceversa*. This is in nice agreement with the results of ref. [32] for the gravitational potential, in the context of a theory of emergent spacetime.

4 Beyond the harmonic approximation

While explicit expressions for our map between quantum mechanics and irreversible thermodynamics are difficult to obtain beyond the harmonic approximation considered so far, some key physical ideas can be extracted from the previous analysis and generalised to an arbitrary potential. On the thermodynamical side, this generalisation implies going beyond the Gaussian approximation made in Eq. (6) or, equivalently, beyond the assumption (7) of linearity between forces and fluxes.

Let a mechanical system be described by a Lagrangian function $\mathcal{L} = \mathcal{L}(q_i, \dot{q}_i)$. For simplicity we assume our configuration space to be \mathbb{R}^D ; an additional \mathbb{R} stands for the time axis. The mechanical time variable t , initially real, will be complexified presently.

We will equate certain spacetime concepts (on the left-hand side of the equations below) to certain thermodynamical quantities (on the right). To begin with, we observe that the two physical constants \hbar and k_B allow one to regard time t and temperature T as mutually inverse, through the combination

$$\frac{1}{t} = \frac{k_B}{\hbar} T. \quad (31)$$

Admittedly, this observation is not new [5].

Corresponding to the mechanical system governed by the Lagrangian $\mathcal{L}(q_i, \dot{q}_i)$ there will be a thermodynamical system whose dynamics will be governed by an entropy $S = \int \mathcal{S} dt$. Following our previous result (24), let us postulate the following differential relation between the two of them:

$$\frac{1}{\hbar} \mathcal{L} dt = \frac{C}{2k_B} dS = \frac{C}{2k_B} \mathcal{S} dt, \quad C \in \mathbb{C}. \quad (32)$$

Again, dimensionality arguments basically fix the two sides of the above relation, but leave room for a dimensionless number C . Agreement with the Wick rotation (22) requires that we set $C = -i$. Now Eq. (32) overlooks the fact that the right-hand side contains the exact differential dS , while the differential $\mathcal{L} dt$ on the left-hand side is generally *not* exact. In other words, while there exists a well-defined entropy *function* $S = \int \mathcal{S} dt$, the line integral $I = \int \mathcal{L} dt$ generally depends on the trajectory in \mathbb{R}^D being integrated along.

The mechanical action I , however, *can* define a path-independent function of the integration endpoint if we restrict to a certain class of trajectories in \mathbb{R}^D . Let us see how this comes about. Let $V = V(q_i)$ be the potential function of the mechanical system under consideration. The equation

$$V(q_i) = \text{const} \quad (33)$$

defines, as the constant on the right-hand side is varied, a family of $(D-1)$ -dimensional, *equipotential submanifolds* of \mathbb{R}^D . An elementary example, when $D = 3$, is the case of the Newtonian potential generated by a point mass located at the origin O . Then the above family of equipotential surfaces is a family of concentric spheres \mathbb{S}_ρ of increasing radii $\rho > 0$, all centred at O . This family of equipotentials, singular only at O , defines a foliation of $\mathbb{R}^3 - \{O\}$, so the latter space equals the union $\cup_{\rho>0}\mathbb{S}_\rho$ of all leaves \mathbb{S}_ρ . This foliation can also be used to define a coordinate system on $\mathbb{R}^3 - \{O\}$. Namely, one splits $\mathbb{R}^3 - \{O\}$ into 2 tangential directions to the spheres of the foliation, and 1 normal direction. For example, the standard spherical coordinates ρ, θ, φ centred at O qualify as such a coordinate system, ρ being the normal coordinate and θ, φ the tangential coordinates.

Returning now to the general case when both D and $V(q_i)$ are arbitrary, Eq. (33) defines, for each particular value of the constant on the right-hand side, one equipotential leaf \mathbb{L}_n of a foliation $\cup_n \mathbb{L}_n$ of \mathbb{R}^D . Here the subindex n stands for a certain (local) coordinate n on \mathbb{R}^D that is normal to all the leaves. The $D - 1$ tangential coordinates thus span the $(D - 1)$ -dimensional leaves \mathbb{L}_n , each one of them being located at a specific value of the normal coordinate n . We will assume that all the leaves \mathbb{L}_n are compact.

Trajectories within \mathbb{R}^D that run exclusively along this normal coordinate n , thus being orthogonal to the leaves, are such that the action integral I *does* defines a function I_n of the integration endpoint; the subindex n reminds us of the restriction to these normal trajectories. Independence of path is merely a consequence of the 1-dimensionality of the normal directions to the equipotential leaves \mathbb{L}_n . This is the particular class of trajectories mentioned above: along them, $\mathcal{L}dt$ defines an exact differential, dI_n . For these normal trajectories, the differential equation (32) makes perfect sense as an equality between two exact differentials. For these normal trajectories we can write

$$\frac{1}{\hbar}I_n - \frac{C}{2k_B}S = \text{const.} \quad (34)$$

Now the sought-for thermodynamics *cannot* be the standard thermodynamics of equilibrium processes as presented in any standard textbook, say, ref. [6]. Among other reasons for this not being the case, standard equilibrium thermodynamics does not include time as one of its variables. We have already in section 3 produced evidence that it must in fact be the *explicitly time-dependent, classical thermodynamics of irreversible processes* as developed by Onsager, Prigogine *et al* [23, 27]. We will present arguments in section 5 to the effect that quantum states arise through a dissipative mechanism. For completeness the thermodynamical dual to quantum mechanics must be supplemented with the relation

$$\frac{1}{T} = \frac{\partial S}{\partial U}, \quad (35)$$

which must always be satisfied. So we take (35) to *define* the internal energy U of the thermodynamical theory, given that T and S have already been defined.

5 Quantum states as equivalence classes of classical trajectories

A key consequence of using normal and tangential coordinates in \mathbb{R}^D is that quantum states ψ , to be constructed presently, will factorise as

$$\psi = \psi_t \psi_n, \quad (36)$$

or sums thereof. Here, the normal wavefunction ψ_n depends exclusively on the normal coordinate n , while ψ_t is a function of the tangential coordinates. For example, in the case of the Coulomb potential, the wavefunction ψ_t would be a spherical harmonic $Y_{lm}(\theta, \varphi)$, while ψ_n would be a radial wavefunction $R_{nl}(\rho)$. This construction contains elements that are very reminiscent of those present in ref. [32]. In this latter paper, *equipotential surfaces of the gravitational potential are identified as isoentropic surfaces*. Our equipotential leaves are the counterpart of the *holographic screens* of ref. [32].

Moreover, the classical mechanics exhibits a precise mechanism whereby *different classical trajectories coalesce into a single equivalence class that can, following ref. [17], be identified as a single quantum state* ψ . So the presence of Planck's constant \hbar in Eq. (32) obeys not just dimensional reasons—it is the sure sign of an information-loss mechanism, a dissipative process that is truly quantum in nature.

Let us see how this dissipation comes about. In order to do this we need to explain why many different classical trajectories coalesce into one single quantum state ψ . A quantum of area on the leaf \mathbb{L}_n measures L_P^2 , where L_P denotes the Planck length. According to the holographic principle, at most 1 bit of information fits into this quantum of area L_P^2 . One classical trajectory traversing this quantum of area corresponds to 1 bit of information. Classically one can regard the surface density of trajectories as being correctly described by a smooth distribution function: there fit some 1.4×10^{69} classical trajectories into each square meter of area on the leaf \mathbb{L}_n [3]. Although this is a huge number, it sets an upper limit on the potentially infinite number of classical trajectories that can traverse one quantum of area L_P^2 .

The holographic principle alone would suffice to account for the lumping together of many different classical trajectories into one equivalence class. One equivalence class, or quantum state, would be comprised by all those different classical trajectories crossing one given quantum of area L_P^2 .

Of course, the *actual* number of quantum particles traversing one square meter of area on the leaf \mathbb{L}_n is much smaller than the above 1.4×10^{69} . The reason is simple: quantum effects become nonnegligible on matter well before quantum-gravity effects become appreciable on the geometry. Again, the existence of a (now particle-dependent) quantum of area is responsible for this. This can be seen as follows.

Let m be the mass of the particle under consideration. Its Compton wavelength $\lambda_C = \hbar/(mc)$ imposes a fundamental limitation on its position, that we can call a *quantum of length*, denoted Q_1 . This Q_1 , which is particle-dependent, is of a fundamentally different nature than the *geometric* quantum of length L_P . On configuration space \mathbb{R}^D , this gives rise to a quantum Q_{D-1} of $(D-1)$ -dimensional volume within

the leaf \mathbb{L}_n , with measure (proportional to) λ_C^{D-1} , and to a quantum of length Q_1 along the normal coordinate.

In the presence of more than one particle species with different masses, each mass m_i defines one value of the quantum $Q_{D-1}^{(i)}$. Then a quantum of volume that remains valid for all particles is the largest value of all those $Q_{D-1}^{(i)}$. This is the quantum of volume determined by the lightest particle.

Let us now elucidate how quantum states ψ can arise as equivalence classes of different classical trajectories. By Eq. (36) we have to account for the appearance of the normal wavefunction ψ_n and of the tangential wavefunction ψ_t .

Starting with ψ_t , let us consider all the different classical trajectories traversing any one quantum of volume Q_{D-1} within a leaf \mathbb{L}_n . The allowed values of the momentum carried by those trajectories are those compatible with the uncertainty principle. Since the particle has been spatially localised to an accuracy of λ_C along each tangential coordinate, the corresponding momentum can be specified to an accuracy of \hbar/λ_C . Therefore, corresponding to a spatial quantum of volume Q_{D-1} in the leaf, we have a quantum of volume $P_{D-1} = (\hbar/\lambda_C)^{D-1}$ in momentum space.

We are now in a position to state a postulate:

All the different classical trajectories traversing any quantum of volume Q_{D-1} in the leaf \mathbb{L}_n , and simultaneously traversing a quantum P_{D-1} in tangential momentum space, are to be regarded as different representatives of just one tangential state ψ_t .

An analogous postulate for the normal coordinate reads:

All classical trajectories traversing any quantum of length Q_1 along the normal coordinate n , and simultaneously traversing the corresponding quantum P_1 in normal momentum space, make up one normal state ψ_n .

In support of the above postulate, let us return to Eq. (23), where the mechanical combination $m\omega/\hbar$ has been identified with the thermodynamical quotient $s/(2k_B)$. The constant s , defined in Eq. (6), carries the dimensions of entropy $\times x^{-2}$, so $s/(2k_B)$ has the dimensions x^{-2} . Thus $s/(2k_B)$ is homogeneous to the inverse square of the Compton wavelength, λ_C^{-2} .

On the other hand, the constant s (and the frequency γ in (23)) are all the data one needs in order to univocally specify the irreversible thermodynamics that is dual to the given quantum mechanics. The previous statement, which holds exactly true in the harmonic approximation of section 3, is raised to the category of a principle in the above postulate. Indeed, let us assume going beyond the harmonic approximation in mechanics. In the thermodynamical dual theory, this is equivalent to considering terms beyond quadratic in the Taylor expansion (6). Higher derivatives d^3S/dx^3 , d^4S/dx^4 , etc, evaluated at the equilibrium point, simply introduce new constants s_3 , s_4 , etc, which can be dimensionally accounted for in terms of just two physical constants, namely k_B and λ_C . Up to a set of *dimensionless* coefficients, all the data we need in the irreversible thermodynamics can be constructed in terms of k_B and powers of λ_C .

These arguments render our above postulate a very plausible statement. Moreover, they provide an estimate of the entropy increase (*i.e.*, of the amount of information loss) involved in the lumping together of many classical trajectories into just one quantum state. Namely, *the increase in entropy ΔS due to the formation of one equivalence*

class of classical trajectories is a positive multiple of λ_C^2 times the coefficient s ,

$$\Delta S = ns\lambda_C^2, \quad n > 0, \quad (37)$$

where n is a dimensionless number. (Admittedly, our arguments leave n undetermined, although one could resort to Landauer’s principle [20] in order to argue that n must be of order unity). More importantly, the surface density of entropy s can be naturally identified, via Eq. (37), with the entropy increase ΔS due to the formation of quantum states as equivalence classes [16, 17]. In other words, *the dissipation that is inherent to irreversible thermodynamics has a natural counterpart in quantum mechanics.*

Having described the dissipative mechanism whereby classical trajectories organise into quantum states, we go next to a counting of the number of quantum states. Since the leaf \mathbb{L}_n has been assumed compact, it encloses a finite number N_n of volume quanta Q_{D-1} . Tentatively identifying this number N_n with the (complex) dimension of the tangential Hilbert space \mathcal{H}_t , we immediately realise that the quantum of momentum P_{D-1} is contained an infinite number of times within tangential momentum space (this is however a *countable* number of times). Indeed the momenta may grow to arbitrarily large values. Therefore, the tangential Hilbert space \mathcal{H}_t is infinite-dimensional, and separable.

On the other hand, the dimension of the normal Hilbert space \mathcal{H}_n is infinite already from the start (again a countable infinity, hence \mathcal{H}_n is separable). The reason for this is the noncompactness of \mathbb{R}^D : the normal coordinate n must cover an interval of infinite length.⁴ This implies that the normal coordinate encloses an infinite (though countable) number of length quanta Q_1 . Multiplication by the number of independent momentum quanta P_1 does not alter this separable, infinite-dimensional, of \mathcal{H}_n .

Altogether, the complete Hilbert space \mathcal{H} of quantum states is the tensor product $\mathcal{H}_t \otimes \mathcal{H}_n$. However, because it singles out the normal coordinate n , one might worry that our construction depends on the particular choice of a leaf \mathbb{L}_n within the foliation. Now the only possible difference between any two leaves \mathbb{L}_{n_1} and \mathbb{L}_{n_2} is the value of their $(D - 1)$ -dimensional volume. Hence the numbers of volume quanta N_{n_1} and N_{n_2} they enclose may be different—but they are both finite. This possible difference is washed away upon multiplication by the (countably infinite) number of momentum quanta P_{D-1} corresponding to each leaf. The dimension of \mathcal{H}_t is therefore countably infinite regardless of the point, n_1 or n_2 , along the radial coordinate—that is, regardless of which leaf is considered.⁵

As explained in ref. [11], determining the tangential wavefunctions ψ_t does not require a knowledge of the specific dynamics under consideration. Instead, this tangential dependence is univocally fixed by the geometry of the leaves \mathbb{L}_n . In more

⁴In case more than just one normal coordinate is needed, this statement is to be understood as meaning the sum of all the lengths so obtained.

⁵We should remark that the assumption of compactness of the leaves \mathbb{L}_n can be lifted without altering our conclusions. A noncompact leaf encloses an infinite (yet countable) number of volume quanta Q_{D-1} . Upon multiplication by an infinite (yet countable) number of momentum-space quanta P_{D-1} , the dimension of the tangent Hilbert space \mathcal{H}_t remains denumerably infinite. This form of holography in which the leaves are noncompact replaces the notion of *inside vs. outside* the leaf with the equivalent notion of *one side of the leaf vs. the other side*. One should not dismiss this possibility as unphysical: the constant potential, for example, can be regarded as having either compact or noncompact equipotential submanifolds.

technical terms, the wavefunctions ψ_t must provide a complete orthonormal set for a unitary, irreducible representation of the isometry group of the leaves \mathbb{L}_n . Moreover, as argued in ref. [1], the modulus squared $|\psi|^2$, evaluated at the value n , is proportional to the surface density of entropy flux across the leaf \mathbb{L}_n .

6 Quantum uncertainty vs. the second law

Just as Planck's constant \hbar represents a coarse-graining of phase space into cells of minimal volume, or quanta of action, so does Boltzmann's constant k_B represent a *quantum of entropy*. This implies that any process must satisfy the condition

$$\Delta S = Nk_B, \quad N \in \mathbb{N}. \quad (38)$$

The above expresses a quantised form of the second law of thermodynamics. The extreme smallness of the numerical value of k_B in macroscopic units makes this quantisation macroscopically unobservable. In particular, unless $N = 0$, the second law becomes

$$\Delta S \geq k_B. \quad (39)$$

In this form, the second law is actually a rewriting of the quantum-mechanical uncertainty principle for the canonical pair E, t :

$$\Delta E \Delta t \geq \frac{\hbar}{2}. \quad (40)$$

Of course, this derivation of the uncertainty relation $\Delta E \Delta t \geq \hbar/2$ is heuristic, because time is a parameter in quantum mechanics. It is only in the limit $k_B \rightarrow 0$ that the second law (39) reduces to its classical formulation $\Delta S \geq 0$. The limit $k_B \rightarrow 0$ is the thermodynamical counterpart of the usual semiclassical limit $\hbar \rightarrow 0$ of quantum mechanics.

We conclude that the equivalence between Eqs. (39) and (40) is a consequence of our basic postulate (32). In other words, the second law (39) expresses, in the thermodynamical theory, the same statement as the uncertainty principle (40) expresses in the quantum-mechanical theory.

Our correspondence implies that, while one needs two canonical variables E, t in order to express the uncertainty principle in the quantum theory, just one variable S is needed in order to write the second law. An equivalent way of saying this is that *entropy is a selfconjugate variable*: one does not have to multiply it with a canonical variable (say, ξ) in order to obtain a product ξS carrying the dimensions of the quantum k_B . The variable S already carries the dimensions of its corresponding quantum k_B .

7 Discussion

The holographic principle of quantum gravity states that there fits at most 1 bit of information into each quantum of area L_P^2 in configuration space, where L_P is Planck's length. For quantum mechanics, in section 5 we have postulated that

There fits at most 1 quantum state into each quantum of volume $(\lambda_C)^{2D}$ in phase space, whereby the Compton length λ_C of the particle in question extends once along each coordinate q and once along each conjugate momentum p in a $2D$ -dimensional phase space.

Thus our postulate is conceptually analogous to the holographic principle of quantum gravity. We should stress, however, that our postulate does not follow from, nor does it imply, the holographic principle of quantum gravity.

We can summarise our construction as follows. Let a quantum-mechanical system be given in configuration space \mathbb{R}^D . Let this latter space be foliated as per $\cup_n \mathbb{L}_n$, where each leaf \mathbb{L}_n is an equipotential submanifold, in dimension $D-1$, of the given mechanical potential function $V(q_i)$. Assume that each leaf \mathbb{L}_n encloses a finite D -dimensional volume \mathbb{V}_n , so $\partial\mathbb{V}_n = \mathbb{L}_n$. Then quantum states in \mathbb{V}_n are equivalence classes of different classical trajectories. These equivalence classes comprise all those classical trajectories that fit into one given quantum of volume in configuration space, with the corresponding momenta inside the corresponding quantum in momentum space. No quantum particle can be located to an accuracy better than its Compton wavelength.⁶ Hence a physically reasonable unit for defining this quantum of length (and thus areas and volumes) is the Compton wavelength. Configuration space is subdivided into many such elementary volume quanta, each one of them (with the corresponding quanta in momentum space) defining one different quantum state.

The quantisation of phase-space area by Planck's constant \hbar proceeds along lines that are somewhat similar to ours, although not exactly identical. We recall that, semi-classically, the (symplectic) area element $dp \wedge dq$, divided by \hbar , gives the number of different quantum states fitting into that area element. However, the coordinate width dq may be arbitrarily squeezed, provided the momentum dp is correspondingly enlarged, and viceversa.

On the contrary, our construction makes use of the Compton wavelength λ_C as a fundamental quantum of length (for the specific particle considered), below which no sharper localisation is possible: there is no squeezing the particle below this lower limit. This gives rise to an arrangement of different classical trajectories into equivalence classes that, following ref. [17], we identify with quantum states. This is an irreversible, dissipative mechanism that exhibits the emergent nature of quantum mechanics. The Hilbert space of quantum states is determined as described in section 5.

Under our correspondence, an irreversible thermodynamics can be mapped into a quantum mechanics, and viceversa. This correspondence may be regarded as *dictionary* that allows one to switch back and forth between a *quantum-mechanical picture* and a *thermodynamical picture* of one and the same physics.

A key point to remark is the following. Thermodynamical approaches to quantum theory are well known [5, 22]. In particular, the link between (complex-time) quantum mechanics, on the one hand, and the *equilibrium* statistical mechanics of the Gibbs ensemble, on the other, has been known for long. We should stress that we have *not* dwelled on this long-established connection. Rather, the new correspondence

⁶Unless, of course, one is willing to allow for pair creation out of the vacuum, thus quitting quantum mechanics and entering field theory.

explored here is that between (complex–time) quantum mechanics, and the *classical* thermodynamics of *irreversible* processes. *Classicality* of the thermodynamics means that \hbar does not appear on the thermodynamical side of the correspondence, its role being played instead by Boltzmann’s constant k_B . *Irreversibility* implies the existence of dissipation, as befits the presence of quantum effects.

References

- [1] D. Acosta, P. Fernández de Córdoba, J.M. Isidro and J. Santander, *An Entropic Picture of Emergent Quantum Mechanics*, Int. J. Geom. Meth. Mod. Phys. **9** (2012) 1250048, [arXiv:1107.1898](#) [hep-th].
- [2] D. Acosta, P. Fernández de Córdoba, J.M. Isidro and J.L.G. Santander, *Emergent Quantum Mechanics as a Classical, Irreversible Thermodynamics*, Int. J. Geom. Meth. Mod. Phys. **10** (2013) 1350007, [arXiv:1206.4941](#) [math-ph].
- [3] R. Bousso, *The Holographic Principle*, Rev. Mod. Phys. **74** (2002) 825, [arXiv:hep-th/0203101](#).
- [4] M. Blasone, P. Jizba and G. Vitiello, *Quantization and Dissipation*, Phys. Lett. **A287** (2001) 205, [arXiv:hep-th/0007138](#).
- [5] L. de Broglie, *La Thermodynamique Cachée des Particules*, Ann. Inst. Poincaré (A) Physique Théorique **1** (1964) 1.
- [6] H. Callen, *Thermodynamics*, Wiley, New York (1960).
- [7] R. Carroll, *On the Emergence Theme of Physics*, World Scientific, Singapore (2010).
- [8] G. Cohen-Tannoudji, *An Interpretive Conjecture for Physics Beyond the Standard Models: Generalized Complementarity*, [arXiv:1402.0823](#) [gr-qc].
- [9] J. Doob, *Stochastic Processes*, Wiley, New York (1953).
- [10] H.-T. Elze, *Symmetry Aspects in Emergent Quantum Mechanics*, J. Phys. Conf. Ser. **171** (2009) 012034.
- [11] P. Fernández de Córdoba, J.M. Isidro and Milton H. Perea, *Emergent Quantum Mechanics as a Thermal Ensemble*, Int. J. Geom. Meth. Mod. Phys. **11** (2014) 1450068, [arXiv:1304.6295](#) [math-ph].
- [12] P. Fernández de Córdoba, J.M. Isidro, Milton H. Perea, J. Vazquez Molina, *The Irreversible Quantum*, Int. J. Geom. Meth. Mod. Phys. **12** (2015) 1550013, [arXiv:1311.2787](#) [quant-ph].
- [13] P. Fernández de Córdoba, J.M. Isidro, J. Vazquez Molina, *Schroedinger vs. Navier–Stokes*, [arXiv:1409.7036](#) [math-ph].

- [14] R. Feynman, *Space–Time Approach to Non–Relativistic Quantum Mechanics*, Rev. Mod. Phys. **20** (1948) 367.
- [15] S. Hartnoll, *Lectures on Holographic Methods for Condensed Matter Physics*, Class. Quant. Grav. **26** (2009) 224002, [arXiv:0903.3246](#) [hep-th].
- [16] G. 't Hooft, *Quantum Gravity as a Dissipative Deterministic System*, Class. Quant. Grav. **16** (1999) 3263, [arXiv:gr-qc/9903084](#).
- [17] G. 't Hooft, *Emergent Quantum Mechanics and Emergent Symmetries*, AIP Conf. Proc. **957** (2007) 154, [arXiv:0707.4568](#) [hep-th].
- [18] Y. Kim, I. Shin and T. Tsukioka, *Holographic QCD: Past, Present, and Future*, Prog. Part. Nucl. Phys. **68** (2013) 55, [arXiv:1205.4852](#) [hep-ph].
- [19] S. Kolekar and T. Padmanabhan, *Indistinguishability of Thermal and Quantum Fluctuations*, Class. Quant. Grav. **32** (2015) 202001, [arXiv:1308.6289](#) [gr-qc].
- [20] R. Landauer, *Irreversibility and Heat Generation in the Computing Process*, IBM Journal of Research and Development **5** (1961) 183.
- [21] J. Maldacena, *The Large N Limit of Superconformal Field Theories and Supergravity*, Adv. Theor. Math. Phys. **2** (1998) 231, [arXiv:hep-th/9711200](#).
- [22] M. Matone, *'Thermodynamique Cachée des Particules' and the Quantum Potential*, Ann. Fond. Broglie **37** (2012) 177, [arXiv:1111.0270](#) [hep-ph].
- [23] L. Onsager and S. Machlup, *Fluctuations and Irreversible Processes*, Phys. Rev. **91** (1953) 1505.
- [24] T. Padmanabhan, *Thermodynamical Aspects of Gravity: New Insights*, Rep. Prog. Phys. **73** (2010) 046901, [arXiv:0911.5004](#) [gr-qc].
- [25] T. Padmanabhan, *General Relativity from a Thermodynamic Perspective*, Gen. Rel. Grav. **46** (2014) 1673, [arXiv:1312.3253](#) [gr-qc].
- [26] R. Penrose, *The Road to Reality*, Jonathan Cape, London (2004).
- [27] I. Prigogine, *Introduction to Thermodynamics of Irreversible Processes*, Interscience, New York (1961).
- [28] L. Smolin, *On the Nature of Quantum Fluctuations and their Relation to Gravitation and the Principle of Inertia*, Class. Quant. Grav. **3** (1986) 347.
- [29] L. Smolin, *Quantum Gravity and the Statistical Interpretation of Quantum Mechanics*, Int. J. Theor. Phys. **25** (1986) 215.
- [30] C. Stephens, G. 't Hooft and B. Whiting, *Black Hole Evaporation Without Information Loss*, Class. Quant. Grav. **11** (1994) 621, [arXiv:gr-qc/9310006](#).

- [31] L. Susskind, *The World as a Hologram*, J. Math. Phys. **36** (1995) 6377, [arXiv:hep-th/9409089](#).
- [32] E. Verlinde, *On the Origin of Gravity and the Laws of Newton*, JHEP **1104** (2011) 029, [arXiv:1001.0785](#) [hep-th].
- [33] E. Witten, *Anti-de Sitter Space and Holography*, Adv. Theor. Math. Phys. **2** (1998) 253, [arXiv:hep-th/9802150](#).

Article

Generalised Complex Geometry in Thermodynamical Fluctuation Theory

P. Fernández de Córdoba and J. M. Isidro *

Instituto Universitario de Matemática Pura y Aplicada, Universidad Politécnica de Valencia, Valencia 46022, Spain; E-Mail: pfernandez@mat.upv.es

* Author to whom correspondence should be addressed; E-Mail: joissan@mat.upv.es.

Academic Editor: George Ruppeiner

Received: 29 May 2015 / Accepted: 19 August 2015 / Published: 20 August 2015

Abstract: We present a brief overview of some key concepts in the theory of generalized complex manifolds. This new geometry interpolates, so to speak, between symplectic geometry and complex geometry. As such it provides an ideal framework to analyze thermodynamical fluctuation theory in the presence of gravitational fields. To illustrate the usefulness of generalized complex geometry, we examine a simplified version of the Unruh effect: the thermalising effect of gravitational fields on the Schroedinger wavefunction.

Keywords: differential-geometric techniques; fluctuation theory; Unruh effect

1. Introduction

The theory of thermodynamical fluctuations provides a solid link between macroscopic and microscopic physics. Classical fluctuation theory [1] often sheds light on counterintuitive quantum-mechanical phenomena, thus helping to bridge the gap between the classical world and the quantum world. For example, Heisenberg's uncertainty principle can be nicely illustrated resorting to the theory of Gaussian fluctuations around thermal equilibrium [2].

On the other hand, the theory of thermodynamical fluctuations can be recast using the geometric language of differential manifolds [3–9]. This reexpression of a physical discipline in more abstract mathematical language goes a long way beyond a mere rewriting of the concepts involved. It renders the theory more versatile, enlarging its scope. Moreover, since the advent of Einstein's general relativity

a century ago, (pseudo) Riemannian geometry belongs to the technical skills that any physicist has to master (at least at a working level). This places (pseudo) Riemannian geometry at a vantage point. In the opposite direction (*i.e.*, thermodynamics as applied to geometry) one should mention at least two developments. The first one is a whole body of knowledge on the thermodynamics of black holes [10,11]. More recently, the reexpression of Einstein's relativity as a thermodynamics [12,13] has had far-reaching consequences for our understanding of spacetime.

Here we would like to report on another recent development in geometry with implications on the thermodynamics of fluctuations: the theory of generalized complex manifolds [14,15].

In trying to understand the thorny relationship between gravity and the quantum [16–19] it has been argued that gravity acts dissipatively on quantum systems [20]. Specifically, in the presence of a gravitational field, thermal fluctuations become indistinguishable from quantum fluctuations [21–23]. This raises the fundamental question: How is one to treat thermal and quantum fluctuations on the same footing? Is it altogether possible? We will see here that generalized complex manifolds provide one viable answer to this question, one that appears not to have been explored yet in the geometrical approach to thermodynamics.

2. Geometry and Fluctuations

2.1. Riemannian Geometry

As a very elementary example, consider a thermodynamical system in an equilibrium state described by the following variables: temperature T , pressure P and volume V . In the Gaussian approximation, choosing T and V as independent variables, the probability W of a fluctuation ΔT , ΔV around equilibrium is given by [24]

$$W = W_0 \exp \left[-\frac{C_V}{2k_B T^2} \Delta T^2 + \frac{1}{2k_B T} \left(\frac{\partial P}{\partial V} \right)_T \Delta V^2 \right] \quad (1)$$

The thermodynamic inequalities $C_V > 0$ and $(\partial P/\partial V)_T < 0$ ensure that the argument of the above exponential is negative definite. This suggests considering the following (positive definite) Riemannian metric on the 2-dimensional manifold coordinatised by T, V :

$$ds^2 := \frac{C_V}{2k_B T^2} dT^2 - \frac{1}{2k_B T} \left(\frac{\partial P}{\partial V} \right)_T dV^2 =: g_{ij} dx^i dx^j \quad (2)$$

The metric coefficients g_{ij} are of course (T, V) -dependent functions. This Riemannian structure encodes all the relevant information. For example, the average value $\langle f(T, V) \rangle$ of an arbitrary function $f = f(T, V)$,

$$\langle f(T, V) \rangle = Z^{-1} \int f(T, V) \exp(-g_{TT}T^2 - g_{VV}V^2) \sqrt{g} dT dV \quad (3)$$

where $Z := \int \sqrt{g} \exp(-g_{TT}T^2 - g_{VV}V^2) dT dV$, naturally involves the metric. The role of Riemannian geometry in fluctuation theory is well known and has been reviewed at length in [8].

2.2. Symplectic Geometry

As our starting point here we will consider a certain thermodynamical system in equilibrium, in order to arrive at a corresponding symplectic structure.

Again in the Gaussian approximation, the probability W of a fluctuation $\Delta P, \Delta V, \Delta T, \Delta S$ is given by [24]

$$W = W_0 \exp \left[-\frac{1}{2k_B T} (-\Delta P \Delta V + \Delta T \Delta S) \right] \tag{4}$$

Assume an equation of state $F(P, V, T) = 0$ that can be solved for the temperature to obtain $T = g(P, V)$. For simplicity let us consider an ideal gas, $PV = S_0 T$:

$$W = W_0 \exp \left[-\frac{1}{2k_B} \left(-S_0 \frac{\Delta P \Delta V}{PV} + \frac{\Delta T \Delta S}{T} \right) \right] \tag{5}$$

It is convenient to define the dimensionless variables

$$p_1 := -\ln \left(\frac{P}{P_0} \right), \quad q_1 := \ln \left(\frac{V}{V_0} \right), \quad p_2 := \ln \left(\frac{T}{T_0} \right), \quad q_2 := \frac{S}{S_0} \tag{6}$$

where P_0, V_0 and T_0 are reference values. Then Equation (5) becomes

$$W = W_0 \exp \left[-\frac{S_0}{2k_B} (\Delta p_1 \Delta q_1 + \Delta p_2 \Delta q_2) \right] \tag{7}$$

We can regard q_1 and q_2 as coordinates on a thermodynamical configuration space \mathbf{S} , with p_1 and p_2 as their conjugate momenta. Thus the q_1, p_1, q_2, p_2 are Darboux coordinates for the symplectic form

$$\omega = dp_1 \wedge dq_1 + dp_2 \wedge dq_2 \tag{8}$$

In this way we identify $\Delta p_1 \Delta q_1 + \Delta p_2 \Delta q_2$ in Equation (7) as the symplectic area of a 2-dimensional surface \mathbf{F} induced by the fluctuation:

$$\Delta p_1 \Delta q_1 + \Delta p_2 \Delta q_2 = \int_{\mathbf{F}} (dp_1 \wedge dq_1 + dp_2 \wedge dq_2) \tag{9}$$

Finally substituting Equation (9) into Equation (7) we find

$$W = W_0 \exp \left(-\frac{S_0}{2k_B} \int_{\mathbf{F}} \omega \right) \tag{10}$$

i.e., the probability of this thermal fluctuation is proportional to the exponential of the symplectic area of the fluctuation surface \mathbf{F} .

The importance of symplectic structures in classical mechanics is widely recognized and need hardly be recalled [25]. In fact not just Riemannian geometry, but also symplectic geometry, pertains to the realm of thermal fluctuations: the first law of thermodynamics endows the thermodynamic phase space with a contact structure, which includes symplectic geometry as a sub-case [3,4,6,7].

A real $2n$ -dimensional manifold \mathbf{M} is symplectic if there exists a closed, non-degenerate, rank 2 antisymmetric tensor field ω_{ij} defined everywhere on \mathbf{M} . Let x^i be local coordinates around $x \in \mathbf{M}$, so $\omega = \frac{1}{2} \omega_{ij} dx^i \wedge dx^j$ with $\omega_{ji} = -\omega_{ij}$. Since the matrix ω_{ij} is nonsingular, an inverse π^{jk} exists such that

$\omega_{ij}\pi^{jk} = \delta_i^k$. The Poisson brackets of two functions f, g are defined as $\{f, g\} := \pi^{jk}\partial_j f \partial_k g$, and the integrability condition $d\omega = 0$ turns out to be equivalent to the Jacobi identity for these Poisson brackets.

In this way the following symplectic analogue of Equation (3) allows one to compute the average value $\langle f \rangle$ of the function f on M :

$$\langle f \rangle = Z^{-1} \int_M f \exp(-\omega) \tag{11}$$

Above, the exponential $e^{-\omega}$ is defined by Taylor expansion, powers being taken with respect to the wedge product. Then the $2n$ -dimensionality of the symplectic manifold picks out just one differential form that can be integrated against M , namely the $2n$ -form $(-1)^n \omega^n / n!$; all other terms in the Taylor expansion give a vanishing contribution when integrated. The factor $(-1)^n / n!$ has been included in the normalization Z . As had to be the case, this average involves the data concerning the symplectic structure on M .

One can also regard a symplectic structure as providing an isomorphism from the tangent space $T_x M$ into the cotangent space $T_x^* M$ at each $x \in M$. Specifically, the tangent vector $X = X^i \partial_i$ is mapped into the 1-form $\omega(X) = \xi = \xi_i dx^i$, with $\xi_i = \omega_{ij} X^j$. This viewpoint motivates the following definition (equivalent to the above, but more useful for later applications): a symplectic structure over a $2n$ -dimensional manifold M is an isomorphism ω_x between the tangent and the cotangent fibers over each point $x \in M$,

$$\omega_x : T_x M \longrightarrow T_x^* M \tag{12}$$

such that, under the operation of taking the linear dual (denoted by an asterisk),

$$\omega_x^* = -\omega_x, \quad \forall x \in M \tag{13}$$

Moreover, the integrability condition $d\omega = 0$ must be satisfied.

2.3. Complex Geometry and Kähler Geometry

Informally one could say that the imaginary unit is the hallmark of quantum mechanics. That $i = \sqrt{-1}$ pertains to the quantum world has been very interestingly argued recently in [26,27]. More standard arguments have been known for long; such as the heat equation in imaginary time it , or the fact that quantum commutators $[\cdot, \cdot]$ formally equal $\sqrt{-1}$ times classical Poisson brackets $\{\cdot, \cdot\}$. Here we will briefly recall the role played by complex structures in the theory of coherent states [28,29].

Let M be a real $2n$ -dimensional phase space endowed with the symplectic form ω . For simplicity let us also assume that M admits a holomorphic atlas compatible with the symplectic structure (this compatibility condition is called the Kähler property). In plain words, the real and imaginary parts of the holomorphic coordinates z^j are Darboux coordinates for ω (here assumed dimensionless for simplicity):

$$z^j = \frac{1}{\sqrt{2}} (q^j + ip_j), \quad j = 1, \dots, n \tag{14}$$

Upon quantisation, the Darboux coordinates q^j and p_j become operators Q^j and P_j on Hilbert space satisfying the Heisenberg algebra $[Q^j, P_k] = i\delta_k^j$. Creation and annihilation operators are defined in the standard fashion: $A_j^\dagger := (Q^j - iP_j)/\sqrt{2}$, $A_j := (Q^j + iP_j)/\sqrt{2}$, and quantum excitations are measured

with respect to a vacuum state $|0\rangle$ satisfying $A_j|0\rangle = 0$, for all $j = 1, \dots, n$. Coherent states $|z^j\rangle$ are eigenvectors of A_j , the eigenvalues being the holomorphic coordinates (14):

$$A_j|z^j\rangle = z^j|z^j\rangle, \quad j = 1, \dots, n \tag{15}$$

(No sum over j implied). In order to illustrate our point let us consider a 1-dimensional harmonic oscillator. The expectation value of the Hamiltonian operator $H = A^\dagger A + 1/2$ in the state $|z\rangle$ equals $\langle z|H|z\rangle = |z|^2 + 1/2$. Since the energy fluctuation in the state $|z\rangle$ equals

$$(\Delta H)_z = |z|, \quad z \in \mathbf{C} \tag{16}$$

the relative fluctuation goes, for large enough $|z|$, like

$$\frac{(\Delta H)_z}{\langle z|H|z\rangle} \simeq \frac{1}{|z|}, \quad |z| \rightarrow \infty \tag{17}$$

But $1/|z|$ is the inverse of the square root of the Kähler potential $K(z, \bar{z}) := |z|^2$ for the Euclidean metric on the complex plane \mathbf{C} . This simple example illustrates the important role played by complex manifolds in the quantum theory.

Every complex manifold \mathbf{M} admits a (positive definite) Hermitian metric $h_{ij}d\bar{z}^i dz^j$ that is compatible with the complex structure [30]. Then an analogue of Equations (3) and (11) gives us the average value $\langle f \rangle$ of a function f on \mathbf{M} :

$$\langle f \rangle = Z^{-1} \int_{\mathbf{M}} f \exp(-h_{ij}\bar{z}^i z^j) \sqrt{h} \prod_{k=1}^n d\bar{z}^k \wedge dz^k \tag{18}$$

The normalization Z includes all factors of $i = \sqrt{-1}$ coming from the volume element, and $h := |\det h_{ij}|$. As had to be the case, this average involves the data concerning the complex structure on \mathbf{M} .

Formally, a complex structure J over a real $2n$ -dimensional manifold \mathbf{M} is an endomorphism of the tangent fibre over each point $x \in \mathbf{M}$

$$J_x: T_x\mathbf{M} \longrightarrow T_x\mathbf{M} \tag{19}$$

satisfying

$$J_x^2 = -\mathbf{1}, \quad \forall x \in \mathbf{M} \tag{20}$$

as well as the integrability condition that the Nijenhuis tensor N vanish identically. (We will not write down the Nijenhuis tensor explicitly; see reference [30] for details). Roughly speaking, Equation (20) expresses the existence of the imaginary unit $i = \sqrt{-1}$ locally around the point $x \in \mathbf{M}$. The integrability condition $N = 0$ ensures that the complex coordinates thus constructed locally truly transform holomorphically across different coordinate patches on the manifold \mathbf{M} . (The Kähler property assumed in Equation (14) above is an additional hypothesis, that an arbitrary complex manifold may, but need not, satisfy in general).

2.4. Generalized Complex Geometry

Our original motivation was the statement [21–23] that, in the presence of a gravitational field, quantum fluctuations become indistinguishable from thermal fluctuations. We have argued that thermal fluctuations are associated with symplectic structures, while quantum fluctuations come along with complex structures. How, then, is one to treat thermal and quantum fluctuations on the same footing? This is trivially achieved by those phase spaces M that qualify as Kähler manifolds. However, the Kähler condition is very restrictive: not only does M have to be simultaneously complex and symplectic; these two independent structures also have to be compatible.

In references. [3,4] the geometry of the thermodynamic phase space (including fluctuations) results in a para-Sasakian manifold, which is the contact-geometry equivalent of a Kähler manifold in symplectic geometry. This means that if one restricts to a proper even-dimensional subspace, the geometry is indeed that of a Kähler manifold. This geometry achieves the goal of treating thermal and quantum fluctuations on the same footing.

Generalized complex structures (GCS) also achieve the goal of providing a unified framework for thermal and quantum fluctuations. The following is a brief summary of GCS extracted from [14], duly tailored to meet our needs. For simplicity we prefer to work locally around a point $x \in M$. Global issues can be taken care of by the corresponding integrability conditions, to be mentioned along the way whenever necessary. For our purposes the $2n$ -dimensional manifold M is assumed to be a phase space, that is, $M = T^*S$, for a certain n -dimensional configuration space S .

Rather than considering the fibres T_xM or T_x^*M separately, in generalized complex geometry one considers their direct sum: over each point $x \in M$ one erects the fibre $T_xM \oplus T_x^*M$. The total space of the bundle so constructed is $6n$ -dimensional: $2n$ dimensions for the base M , $4n$ dimensions for the fibre.

An inner product is defined on the fibre $T_xM \oplus T_x^*M$:

$$\langle X + \xi, Y + \eta \rangle := \frac{1}{2} (\xi(Y) + \eta(X)) \tag{21}$$

Above, $X, Y \in T_xM$ are tangent vectors, while $\xi, \eta \in T_x^*M$ are 1-forms, all evaluated at $x \in M$. It turns out that this inner product is pseudo-Riemann with signature $(2n, 2n)$. Hence the Lie group $SO(2n, 2n)$ acts on $T_xM \oplus T_x^*M$ by isometries. It is convenient to block-decompose the Lie algebra $so(2n, 2n)$ as follows:

$$\begin{pmatrix} A & \beta \\ B & -A^* \end{pmatrix} \tag{22}$$

The diagonal blocks A and A^* are endomorphisms of their respective (sub)fibers, $A \in \text{End}(T_xM)$ and $A^* \in \text{End}(T_x^*M)$, while the offdiagonal blocks B and β connect these two (sub)fibers as per

$$B : T_xM \longrightarrow T_x^*M, \quad \beta : T_x^*M \longrightarrow T_xM \tag{23}$$

Moreover, upon taking the dual we have $B^* = -B$, $\beta^* = -\beta$. This antisymmetry allows us to regard the block B as a 2-form in $\Lambda^2 T_x^*M$ if we set

$$B(X) = i_X B \tag{24}$$

For illustrative purposes let us express Equation (24) in local coordinates x^i around a point $x \in M$, so B becomes the matrix B_{ij} . Given the vector $X = X^j \partial_j \in T_xM$, the object $i_X B$ is defined to be the

covector whose components are $B_{ij}X^j \in T_x^*\mathbf{M}$. We see that this is exactly the way a symplectic form ω behaves. Since ω can be regarded as an element of $\Lambda^2 T_x^*\mathbf{M}$, so can B . (Contrary to ω , however, B need neither be closed nor non-degenerate).

The particular isometries of the fibre $T_x\mathbf{M} \oplus T_x^*\mathbf{M}$ obtained by setting $A = 0 = \beta$ in Equation (22) and exponentiating,

$$\exp \begin{pmatrix} 0 & 0 \\ B & 0 \end{pmatrix} = \begin{pmatrix} \mathbf{1} & 0 \\ B & \mathbf{1} \end{pmatrix} \tag{25}$$

are the pseudo-orthogonal transformations

$$X + \xi \longrightarrow X + \xi + i_X B \tag{26}$$

The isometries (26), called B -transformations, will play an important role.

A generalized complex structure over \mathbf{M} , denoted \mathcal{J} , is an endomorphism of the fibre over each $x \in \mathbf{M}$,

$$\mathcal{J}_x : T_x\mathbf{M} \oplus T_x^*\mathbf{M} \longrightarrow T_x\mathbf{M} \oplus T_x^*\mathbf{M} \tag{27}$$

such that the following two conditions hold. First,

$$\mathcal{J}_x^2 = -\mathbf{1}, \quad \forall x \in \mathbf{M} \tag{28}$$

Second,

$$\mathcal{J}_x^* = -\mathcal{J}_x, \quad \forall x \in \mathbf{M} \tag{29}$$

The above two conditions are formulated locally around any $x \in \mathbf{M}$; as usual they need not be compatible with changes of coordinate charts on \mathbf{M} . The Courant integrability condition, whose validity we will henceforth assume without stating its contents explicitly, ensures this compatibility; see [14,15] for details.

Comparing now Equations (29) and (13), we are led to the particular case when \mathcal{J} at $x \in \mathbf{M}$ is given by

$$\mathcal{J}_{\omega_x} = \begin{pmatrix} 0 & -\omega_x^{-1} \\ \omega_x & 0 \end{pmatrix} \tag{30}$$

where ω is a symplectic form. One says that this \mathcal{J}_ω defines a GCS of symplectic type.

Similarly, the comparison of Equations (28) and (20) suggests the particular case of a GCS given by

$$\mathcal{J}_{J_x} = \begin{pmatrix} -J_x & 0 \\ 0 & J_x^* \end{pmatrix} \tag{31}$$

where J is a complex structure. We say that the above \mathcal{J}_J defines a GCS of complex type.

Furthermore, GCS succeed at interpolating between the above opposite types, the symplectic type and the complex type; let us explain this more carefully. A point $x \in \mathbf{M}$ is said to be regular if it possesses a neighborhood \mathcal{N}_x on which there exists a Poisson structure ω^{-1} with constant rank. In a neighborhood \mathcal{N}_x of any regular point $x \in \mathbf{M}$ one can define a diffeomorphism and a B -transformation, the combined action of which maps \mathcal{N}_x into the product $\mathcal{C}_x \times \mathcal{R}_x \subset \mathbf{C}^k \times \mathbf{R}^{2n-2k}$. Here \mathcal{C}_x is an open set within the standard complex manifold \mathbf{C}^k , and \mathcal{R}_x is an open set within the standard symplectic manifold \mathbf{R}^{2n-2k} .

The nonnegative integer k is called the *type* of the GCS \mathcal{J} , the limiting cases of Equations (30) and (31) respectively corresponding to $k = 0$ and $k = n$. As described in [14,15], the type k need not be constant across M : it may vary from one point to another in M .

In plain words, any generalized complex manifold factorizes locally as the product of a complex manifold times a symplectic manifold.

Finally assume that M is a linear space. Then any generalized complex structure of type $k = 0$ is the B -transform of a symplectic structure. This means that any generalized complex structure of type $k = 0$ can be written as

$$e^{-B} \mathcal{J}_\omega e^B = \begin{pmatrix} -\omega^{-1} B & -\omega^{-1} \\ \omega + B\omega^{-1} B & B\omega^{-1} \end{pmatrix} \quad (32)$$

for a certain 2-form B ; use has been made of Equations (25) and (30). Similarly any generalized complex structure of type $k = n$ over a linear manifold M is the B -transform of a complex structure,

$$e^{-B} \mathcal{J}_J e^B = \begin{pmatrix} -J & 0 \\ BJ + J^* B & J^* \end{pmatrix} \quad (33)$$

after using Equations (25) and (31). When M is an arbitrary smooth manifold, not necessarily a linear space, statements (32) and (33) remain basically true, with some minor modifications required; see references [14,15] for details.

The consequences of the above become immediately apparent. Let us for simplicity assume that the type k is constant across M . Then any GCS with an extremal value of k , *i.e.*, either $k = 0$ or $k = n$, can always be reduced to the corresponding canonical form (30) or (31) by means of a B -transformation. Thus $k = 0$ corresponds to a thermal description of phenomena, while $k = n$ corresponds to a quantum description of phenomena, no interpolation existing between the two descriptions. Nonextremal values of the type, *i.e.*, such that $0 \neq k \neq n$, contain both thermal and quantum descriptions simultaneously.

Average values $\langle f \rangle$ of functions f on generalized complex manifolds are defined by an obvious modification of the product of the right-hand sides of Equations (11) and (18).

3. When “Quantum” Becomes “Thermal”

Any gravitational field is locally equivalent to an accelerated frame. In an accelerated frame, quantum becomes thermal; this is basically the content of the Unruh effect [31] (in an admittedly lax formulation that is however precise enough for our purposes). Without using the full apparatus of relativistic quantum field theory, let us see how quantum can become thermal in the simplified setup of the quantum mechanics of a nonrelativistic particle. This understood, we will analyse the role played by the GCS on phase space under the passage from an inertial frame to an accelerated frame. We will conclude that the transformation law for the Schroedinger wavefunction under the passage to a noninertial frame (as in the Unruh effect) is governed by a B -transformation of the GCS on phase space.

A remark is in order. The gravitational field considered here must be weak in order to rule out effects such as, *e.g.*, relativistic speeds, or the likely breakdown of standard quantum mechanics in the presence of very strong gravitational fields [20]. Such phenomena lie beyond our scope.

3.1. Inclusion of a Gravitational Field

In flat Euclidean space \mathbf{R}^3 , let K denote an inertial frame with origin O and axes Ox , Oy and Oz . Let K' denote a uniformly accelerated frame, with origin O' and axes $O'x'$, $O'y'$ and $O'z'$ respectively parallel to Ox , Oy and Oz . For simplicity we will assume that, at $t = 0$, the two origins O and O' coincide, their relative velocity also vanishing at $t = 0$. Let the acceleration $\vec{\alpha}$ of K' with respect to K be $(\alpha, 0, 0)$, with α a constant. Coordinates (x, y, z) with respect to K are related to coordinates (x', y', z') with respect to K' as per

$$x = x' + \frac{1}{2}\alpha t^2, \quad y = y', \quad z = z', \quad t = t' \quad (34)$$

We consider a point particle of mass m fixed to the origin O' , thus at rest with respect to K' . If H denotes the Hamiltonian of the particle as seen from the inertial frame K , then the Hamiltonian H' in K' reads

$$H' = H - p_x \alpha t + \frac{m}{2} \alpha^2 t^2 \quad (35)$$

with the momenta p_x and p'_x related as per $p'_x = p_x - m\alpha t$. In the inertial frame K we have a Schroedinger equation $i\hbar\partial\psi/\partial t = H\psi$. Our aim is to derive a transformation law for the wavefunction ψ such that, in the accelerated frame K' , the Schroedinger equation will read $i\hbar\partial\psi'/\partial t = H'\psi'$. For this purpose let us make the Ansatz

$$\psi' = \psi \exp [f(t)] \quad (36)$$

$f(t)$ being an undetermined function of the time variable. In this way we arrive at the following differential equation for the unknown function f :

$$i\hbar \frac{df}{dt} = -p_x \alpha t + \frac{1}{2} m \alpha^2 t^2 \quad (37)$$

Dropping an irrelevant integration constant and substituting the result into Equation (36) leads to

$$\psi' = \exp \left[-\frac{i}{\hbar} \left(\frac{1}{6} m \alpha^2 t^3 - \frac{1}{2} p_x \alpha t^2 \right) \right] \psi \quad (38)$$

Classically, the particle is at rest in the frame K' , so $p'_x = 0$ implies $p_x = m\alpha t$. Quantum-mechanically we can only state that the centre of mass remains at rest at $x' = 0$, the wavepacket spreading around this average position. With this understanding we can also set $\langle p_x \rangle = p_x = m\alpha t$ in Equation (38). We conclude that, taking the wavefunction in the accelerated frame to be

$$\psi' = \exp \left(\frac{i}{\hbar} \frac{1}{3} m \alpha^2 t^3 \right) \psi \quad (39)$$

ensures the form invariance of the Schroedinger equation under the transformation from an inertial frame to an accelerated frame. For time lapses that are short enough, and/or for accelerations that are weak enough, the speeds attained will never become relativistic. Within this limited range, Newtonian mechanics (and its quantum counterpart, the Schroedinger equation) can be trusted.

3.2. The Unruh Effect

The next step is to invoke de Broglie [32] in order to write an inverse proportionality between time t and temperature T :

$$-\frac{i}{t} = \frac{k_B T}{\hbar} \quad (40)$$

Thus substituting Equation (40) into Equation (39) we find

$$\psi' = \exp\left(-\frac{1}{3} \frac{m\alpha^2 \hbar^2}{k_B^3 T^3}\right) \psi. \quad (41)$$

Moreover, from the above we can read off what power law must relate the acceleration to the temperature of the accelerated frame: α must be proportional to T , while dimensional analysis provides the necessary conversion factors. Specifically,

$$\alpha = 2\pi \frac{ck_B}{\hbar} T \quad (42)$$

The dimensionless normalization factor 2π , that cannot be derived using our simplified treatment, comes from a full quantum-field-theoretical analysis [31]. Finally substituting Equation (42) into Equation (41) we arrive at

$$\psi' = \exp\left(-\frac{4\pi^2}{3} \frac{mc^2}{k_B T}\right) \psi \quad (43)$$

Equations (43) and (39) are equivalent, the equivalence between the two being guaranteed by the de Broglie relation Equation (40) and the Unruh relation Equation (42).

The Boltzmann-like factor present in Equation (43) bears out the fact that the effect of the gravitational field on the Schrodinger wavefunction is of thermal nature. Due to the assumptions made in our derivation, Equation (43) is valid only for intermediate temperatures. The limit $T \rightarrow \infty$ is excluded (because this would require strong gravitational fields); so is the limit $T \rightarrow 0$ (because of the inverse proportionality Equation (40) between time and temperature).

3.3. Transformation to an Accelerated Frame as a B-Transformation

Classical phase space is spanned by the coordinates x, y, z and their conjugate momenta p_x, p_y, p_z . For the rest of the discussion, the dimensions y, p_y, z, p_z can be ignored, as they are unaffected by the change of frame Equation (34). Thus, for our purposes, the manifold M of Section 2.4 can be taken to be that subspace of classical phase space spanned by x and p_x , i.e., \mathbf{R}^2 .

Now the manifold \mathbf{R}^2 can be endowed with a GCS. This can be done in two equivalent ways. One can consider the GCS of complex type defined on $\mathbf{R}^2 = \mathbf{C}$ by the complex coordinates Equation (14). Alternatively, one can consider the GCS of symplectic type defined on \mathbf{R}^2 by the standard symplectic form $\omega = dx \wedge dp_x / \hbar$. Since our interest lies in considering the effect of B -transformations, and $\mathbf{R}^2 = \mathbf{C}$ is a Kähler manifold, the type of the CGS considered is immaterial.

We claim that the transformation law for the Schrodinger wavefunction under the passage to an accelerated frame, Equation (39), follows from a B -transformation of the GCS on phase space \mathbf{R}^2 , Equation (26). In other words, the Schrodinger wavefunction keeps track of which frame is being used, the bookkeeping device being the GCS on phase space. Verifying that such is indeed the case requires, so to speak, translating the geometer's language into the physicist's language. This we do next.

Tangent vectors X at the point $(x, p_x) \in \mathbf{R}^2$ are objects

$$X = a\partial_x + b\partial_{p_x} \in T_{(x,p_x)}\mathbf{R}^2, \quad a, b \in \mathbf{R} \tag{44}$$

Similarly, tangent covectors ξ at the point $(x, p_x) \in \mathbf{R}^2$ are objects

$$\xi = cdx + ddp_x \in T^*_{(x,p_x)}\mathbf{R}^2, \quad c, d \in \mathbf{R} \tag{45}$$

As the basepoint $(x, p_x) \in \mathbf{R}^2$ is moved around, we obtain a vector field X and a field of differential 1-forms ξ on \mathbf{R}^2 . This amounts to promoting the numbers a, b, c, d to real-valued functions $a(x, p_x), b(x, p_x), c(x, p_x), d(x, p_x)$ on \mathbf{R}^2 . Finally, an object such as $X + \xi$ in Equation (26) is the direct sum of a vector field and a field of differential 1-forms on \mathbf{R}^2 —a section of the direct sum bundle $T\mathbf{R}^2 \oplus T^*\mathbf{R}^2$.

Next we reexpress the B -transformation (26) as the variation

$$\delta(X + \xi) = \delta X + \delta\xi = \delta\xi = i_X B \tag{46}$$

Above we have used the fact that, under a B -transformation, X remains unchanged. The B -field is a 2-form on \mathbf{R}^2 ,

$$B = B(x, p_x)dx \wedge dp_x \tag{47}$$

with a certain coefficient function $B(x, p_x)$. Now

$$\delta\xi = i_X B = a(x, p_x)B(x, p_x)dp_x + b(x, p_x)B(x, p_x)dx \tag{48}$$

The above is a 1-form field, so it can be added to $X + \xi$ as required by Equation (26). Let us now make the following specific choice for the vector field X :

$$a(x, p_x) = x, \quad b(x, p_x) = p_x \tag{49}$$

In the physicist’s language, this X is just the position vector on phase space \mathbf{R}^2 . Substituted into Equation (48), this choice for X yields

$$\delta\xi = i_X B = xB(x, p_x)dp_x + p_xB(x, p_x)dx \tag{50}$$

Along the motion of the particle located at O' we can write, using Equation (34),

$$dp_x = m\alpha dt, \quad dx = \alpha t dt \tag{51}$$

Substitution of Equations (34) and (51) into (50) leads to

$$\delta\xi = i_X B = \frac{3}{2}B(x(t), p_x(t))m\alpha^2 t^2 dt \tag{52}$$

The above is a 1-form, that can be integrated along the trajectory followed by the particle between $\tau = 0$ and $\tau = t$. We denote by $\Delta\xi(t)$ the number so obtained:

$$\Delta\xi(t) := \int_0^t \delta\xi = \frac{3}{2}m\alpha^2 \int_0^t B(x(\tau), p_x(\tau))\tau^2 d\tau \tag{53}$$

When B is a constant, the integral can be evaluated explicitly:

$$\Delta\xi(t) = \frac{1}{2}Bm\alpha^2t^3 \tag{54}$$

That the function $B(x(t), p_x(t))$ is actually constant on \mathbf{R}^2 implies that the 2-form B in Equation (47) becomes a mere scalar multiple of the canonical symplectic form on phase space. Specifically, picking $B = 2/3$ we find in Equation (54)

$$\Delta\xi(t) = \frac{1}{3}m\alpha^2t^3 \tag{55}$$

The right-hand side of the above equals ($-i\hbar$ times) the argument of the exponential in the Unruh transformation law Equation (39). Therefore the latter can be reexpressed as

$$\psi' = \exp\left(\frac{i}{\hbar}\Delta\xi(t)\right)\psi \tag{56}$$

Summarising, we may say that the Unruh effect acts on the wavefunction by multiplication with the exponential of (i/\hbar times) the integral of a B -field along the particle’s trajectory on phase space. The vector field X involved in this B -transformation is just the position vector on phase space, while the B -field considered is a mere scalar multiple of the canonical symplectic form on phase space.

3.4. A Nonuniform Gravitational Field

The relation just derived between the Unruh effect and the B -transformation of the GCS on phase space was based on the assumption that the gravitational field was static and spatially constant. In turn, this assumption made it possible to choose a constant B -field on phase space (actually a scalar multiple of the symplectic form). A nonstatic and/or nonuniform gravitational field can be mimicked by a nonstatic and/or nonuniform acceleration vector $\vec{\alpha}$. This lends plausibility to the following hypothesis:

Hypothesis 1. *Regard classical phase space as a generalized complex manifold. In the presence of a nonstatic and/or nonuniform, but nevertheless weak, gravitational field, the inertial-frame Schroedinger wavefunction ψ remains form-invariant under a transformation to a locally accelerated frame, where its value is ψ' , provided that ψ and ψ' are related according to the law*

$$\psi' = \exp\left(\frac{i}{\hbar}\Delta\xi(t)\right)\psi \tag{57}$$

Above,

$$\Delta\xi(t) := \int_0^t i_X B(x(\tau), p_x(\tau))d\tau \tag{58}$$

is a line integral along the particle’s trajectory in phase space, while X is the position vector of the particle along the said trajectory. Moreover, whenever the generalised complex structure on classical phase space is of symplectic type, the 2-form B is an appropriate scalar multiple of the symplectic form ω .

We defer analysis of the above hypothesis for further study.

4. Conclusions

We have presented a brief review of some recent developments in differential geometry with applications to thermodynamical fluctuation theory. Standard wisdom draws a clear frontier between thermal fluctuations and quantum fluctuations. While this separation is perfectly consistent in the absence of gravitational fields, this border becomes fuzzy in the presence of gravity [20–23]. A well-known example of this mixing is the Unruh effect [31,33,34]. Another instance of a gravitational incursion into the thermal realm is the Ehrenfest-Tolman effect [35]. One can expect an eventual theory of quantum gravity to enhance, rather than diminish, this mixing of thermal and quantum phenomena.

In this article we have examined the thermalising effect of weak, classical gravitational fields on the Schroedinger wavefunction from the point of view of generalised complex geometry on classical phase space. Using the transformation law for the Schroedinger wavefunction under the passage to an accelerated frame, we have derived the nonrelativistic Unruh effect. As expected, the latter establishes a linear dependence law between the acceleration of the noninertial frame and the temperature thereby generated. Within the scope of the techniques presented here lie other interesting physical systems, to be treated in an upcoming publication. Such are quantum-classical hybrids [36,37] and the thermalising properties of nonuniform (but still weak and classical) gravitational fields.

Altogether, we conclude that generalised complex geometry provides a powerful tool to analyse fluctuation theory and thermal phenomena in the presence of gravity.

Author Contributions

Both authors contributed equally to this article. Both authors have read and approved the final manuscript.

Conflicts of Interest

The authors declare no conflict of interest.

References

1. Callen, H. *Thermodynamics*; Wiley: New York, NY, USA, 1960.
2. Velazquez, L. Principles of Classical Statistical Mechanics: A Perspective from the Notion of Complementarity. *Ann. Phys.* **2012**, *327*, 1682–1693.
3. Bravetti, A.; Lopez-Monsalvo, C. Para-Sasakian Geometry in Thermodynamic Fluctuation Theory. *J. Phys. A* **2015**, *48*, 125206.
4. Bravetti, A.; Lopez-Monsalvo, C.S.; Nettel, F. Contact Symmetries and Hamiltonian Thermodynamics. *Ann. Phys.* **2015**, *361*, 377–400.
5. Quevedo, H.; Vázquez, A. The Geometry of Thermodynamics. *AIP Conf. Proc.* **2008**, *977*, 165, doi:10.1063/1.2902782.
6. Rajeev, S. Quantization of Contact Manifolds and Thermodynamics. *Ann. Phys.* **2008**, *323*, 768–782.
7. Rajeev, S. A Hamilton–Jacobi Formalism for Thermodynamics. *Ann. Phys.* **2008**, *323*, 2265–2285.

8. Ruppeiner, G. Riemannian Geometry in Thermodynamic Fluctuation Theory. *Rev. Mod. Phys.* **1995**, *67*, 605.
9. Velazquez, L. Curvature of Fluctuation Geometry and its Implications on Riemannian Fluctuation Theory. *J. Phys. A* **2013**, *46*, 345003.
10. Bardeen, J.M.; Carter, B.; Hawking, S.W. The Four Laws of Black Hole Mechanics. *Comm. Math. Phys.* **1973**, *31*, 161–170.
11. Ruppeiner, G. Thermodynamic Curvature and Black Holes. In *Breaking of Supersymmetry and Ultraviolet Divergences in Extended Supergravity*, Proceedings of the INFN-Laboratori Nazionali di Frascati School 2013; Springer: Switzerland, 2014; Springer Proceedings in Physics, Volume 153; pp. 179–203.
12. Padmanabhan, T. Thermodynamical Aspects of Gravity: New Insights. *Rept. Prog. Phys.* **2010**, *73*, 046901.
13. Padmanabhan, T. General Relativity from a Thermodynamic Perspective. *Gen. Rel. Grav.* **2014**, *46*, 1673.
14. Gualtieri, M. Generalized Complex Geometry. *Ann. Math.* **2011**, *174*, 75–123.
15. Hitchin, N. Generalized Calabi–Yau Manifolds. *Q. J. Math.* **2003**, *54*, 281–308.
16. Calmet, X. Quantum Mechanics, Gravity and Modified Quantization Relations. *High Energy Phys. Theory* **2015**, doi: 10.1098/rsta.2014.0244.
17. Elze, H.-T. Are Nonlinear Discrete Cellular Automata Compatible with Quantum Mechanics? *Quantum Phys.* **2015**, *631*, 012069.
18. 't Hooft, G. The Cellular Automaton Interpretation of Quantum Mechanics. A View on the Quantum Nature of our Universe, Compulsory or Impossible? **2015**, arXiv:1405.1548.
19. Matone, M. Equivalence Postulate and Quantum Origin of Gravitation. *Found. Phys. Lett.* **2002**, *15*, 311–328.
20. Penrose, R. *The Road to Reality: A Complete Guide to the Laws of the Universe*; Alfred A. Knopf: London, UK, 2004.
21. Kolekar, S; Padmanabhan, T. Indistinguishability of Thermal and Quantum Fluctuations. **2013**, arXiv:1308.6289.
22. Smolin, L. On the Nature of Quantum Fluctuations and their Relation to Gravitation and the Principle of Inertia. *Class. Quant. Grav.* **1986**, *3*, 347, doi:10.1088/0264-9381/3/3/009.
23. Smolin, L. Quantum Gravity and the Statistical Interpretation of Quantum Mechanics. *Int. J. Theor. Phys.* **1986**, *25*, 215–238.
24. Landau, L; Lifshitz, E. *Statistical Physics, Part 1*; Pergamon Press: Oxford, UK, 1980.
25. Arnold, V. *Mathematical Methods of Classical Mechanics*; Springer: Berlin, Germany, 1989.
26. Kauffman, L. Eigenforms and Quantum Physics. *Cybern. Human Knowing. V.* **2011**, *18*, 111–121.
27. Kauffman, L. Iterants, Fermions and the Dirac Equation. **2014**, arXiv:1406.1929.
28. Florentino, C.; Matias, P.; Mourão J.; Nunes, J.P. Geometric Quantization, Complex Structures and the Coherent State Transform. **2005**, arXiv:math/0402313.
29. Perelomov, A. *Generalized Coherent States and their Applications*; Springer: Berlin, Germany, 1986.

30. Kobayashi, S; Nomizu, K. *Foundations of Differential Geometry*; Wiley: New York, NY, USA, 1996.
31. Unruh, W. Notes on Black-Hole Evaporation. *Phys. Rev. D* **1976**, *14*, 870.
32. De Broglie, L. La thermodynamique «Cachée» des particules. *Ann. Inst. Henri Poincaré* **1964**, *1*, 1–19. Available online: <https://drive.google.com/file/d/0B0xb4crOvCgTemNOektLV25Kc0U/edit> (accessed on 20 August 2015).
33. Davies, P. Scalar Production in Schwarzschild and Rindler Metrics. *J. Phys. A* **1975**, *8*, 609.
34. Fulling, S. Nonuniqueness of Canonical Field Quantization in Riemannian Space-Time. *Phys. Rev. D* **1973**, *7*, 2850.
35. Tolman, R. *Relativity, Thermodynamics and Cosmology*; Dover: New York, NY, USA, 1987.
36. Elze, H.-T. Linear Dynamics of Quantum-Classical Hybrids. *Phys. Rev. A* **2012**, *85*, 052109.
37. Elze, H.-T. Action Principle for Cellular Automata and the Linearity of Quantum Mechanics. *Phys. Rev. A* **2014**, *89*, 012111.

© 2015 by the authors; licensee MDPI, Basel, Switzerland. This article is an open access article distributed under the terms and conditions of the Creative Commons Attribution license (<http://creativecommons.org/licenses/by/4.0/>).

Modeling nonlinear waves in photonics, plasmonics and cold atoms

Modelado de ondas no lineales en fotónica, plasmónica y átomos fríos

A. Ferrando^(1,*S), C. Milián⁽²⁾, D. Ceballos⁽³⁾, N. González⁽³⁾, I. Orquín⁽⁴⁾,
M. A. García-March⁽⁵⁾, M. Zacarés⁽⁶⁾, Ll. Monreal⁽⁴⁾, J. M. Isidro⁽⁴⁾,
P. Fernández de Córdoba⁽⁴⁾

1. Departament d'Òptica, Universitat de València, Dr Moliner 50, 46100 Burjassot (València), Spain.
2. Instituto de Instrumentación para Imagen Molecular, Universidad Politécnica de Valencia, Camino de Vera S/N, 46022 Valencia, Spain.
3. Centro de Investigaciones en Óptica, A.C., Guanajuato (León), México.
4. Instituto Universitario de Matemática Pura y Aplicada, Universidad Politécnica de Valencia, Camino de Vera S/N, 46022 Valencia, Spain.
5. Department of Physics, Colorado School of Mines, Golden (Colorado), USA.
6. Departamento de Ciencias Experimentales y Matemáticas, Universidad Católica de Valencia, C/ Guillem de Castro 94, 46003, Valencia, Spain.

^(*) Email: albert.ferrando@uv.es

S: miembro de SEDOPTICA / SEDOPTICA member

Recibido / Received: 30/10/2010. Aceptado / Accepted: 15/12/2010

ABSTRACT:

We review the present status of the different lines of research in the area of Photonics at the Interdisciplinary Modeling Group, InterTech (www.intertech.upv.es) paying special attention to new topics that we have recently incorporated to our research interests: temporal solitons and design of supercontinuum generation, plasmon-soliton interaction, nonlinear effects of the quantum electrodynamics vacuum, and, finally, cold atoms in the mean-field and quantum regimes.

Keywords: Nonlinear Optics, Plasmonics, Cold Atoms.

RESUMEN:

En este artículo presentamos el estado actual de las diferentes líneas de investigación desarrolladas en el área de Fotónica del Grupo de Modelización Interdisciplinar, InterTech (www.intertech.upv.es) prestando especial atención a aquellas que han sido incorporadas recientemente: solitones temporales y diseño de la generación de supercontinuo, interacción plasmón-soliton, efectos no lineales del vacío en electrodinámica cuántica y, finalmente, átomos fríos en el régimen de campo medio y en el régimen cuántico

Palabras clave: Óptica No Lineal, Plasmónica, Átomos Fríos.

REFERENCES AND LINKS

- [1]. Yu. S. Kivshar, G. P. Agrawal, *Optical Solitons. From Fibers to Photonic Crystals*, Academic Press, Burlington (2003).
- [2]. M. A. García-March, A. Ferrando, M. Zacarés, J. Vijande, L. D. Carr, "Angular pseudomomentum theory for the generalized nonlinear Schrödinger equation in discrete rotational symmetry media", *Physica D* **15**, 1432-1438 (2009).
- [3]. A. Ferrando, M. Zacarés, P. F. De Córdoba, D. Binosi, J. A. Monsoriu, "Spatial soliton formation in photonic crystal fibers", *Opt. Express* **11**, 452-459 (2003).
- [4]. A. Ferrando, M. Zacarés, P. F. De Córdoba, D. Binosi, J. A. Monsoriu, "Vortex solitons in photonic crystal fibers", *Opt. Express* **12**, 817-822 (2004).

- [5]. A. Ferrando, M. Zacarés, P. Andrés, P. Fernández De Córdoba, J. A. Monsoriu, "Nodal solitons and the nonlinear breaking of discrete symmetry", *Opt. Express* **13**, 1072-1078 (2005).
- [6]. A. Ferrando, M. Zacarés, M.-Á. García-March, J. A. Monsoriu, P. F. De Córdoba, "Vortex transmutation", *Phys. Rev. Lett.* **95**, 123901(2005).
- [7]. A. S. Desyatnikov, Yu. S. Kivshar, L. Torner, "Optical vortices and vortex solitons", *Prog. Optics* **47**, 291-391 (2005).
- [8]. A. Ferrando, M. Zacarés, M. A. García-March, "Vorticity cutoff in nonlinear photonic crystals", *Phys. Rev. Lett.* **95**, 043901 (2005).
- [9]. A. Ferrando, "Discrete-symmetry vortices as angular Bloch modes", *Phys. Rev. E* **72**, 036612 (2005).
- [10]. M. A. García-March, A. Ferrando, M. Zacarés, S. Sahu, D. E. Ceballos-Herrera, "Symmetry, winding number, and topological charge of vortex solitons in discrete-symmetry media", *Phys. Rev. A* **79**, 053820 (2009).
- [11]. M. Zacarés, M. A. García-March, J. Vijande, A. Ferrando, E. Merino, "Topological charge selection rule for phase singularities", *Phys. Rev. A* **80**, 043812 (2009).
- [12]. G. P. Agrawal, *Nonlinear Fiber Optics*, Academic Press, San Diego, California (1995).
- [13]. J. Dudley, G. Genty, S. Coen, "Supercontinuum generation in photonic crystal fiber", *Rev. Mod. Phys.* **78**, 1135-1184 (2006).
- [14]. G. Moltó, M. Arevalillo-Herráez, C. Milián, M. Zacarés, V. Hernández, A. Ferrando, Proceedings of the 3rd Iberian Grid Infrastructure Conference (IberGrid 2009), pp. 137-147 (2009).
- [15]. I. C. Khoo, *Liquid Crystals: Physical Properties and Nonlinear Optical Phenomena*, John Wiley & Sons, New York (1992).
- [16]. S. A. Maier, *Plasmonics: Fundamentals and Applications*, Springer, New York (2007).
- [17]. K. Y. Bliokh, Y. P. Bliokh, A. Ferrando, "Resonant plasmon-soliton interaction", *Phys. Rev. A* **79**, 041803 (2009).
- [18]. V. M. Pérez-García, M. A. García-March, A. Ferrando, "Symmetry-assisted vorticity control in Bose-Einstein condensates", *Phys. Rev. A* **75**, 033618 (2007).
- [19]. <http://optics.uvigo.es/>
- [20]. A. Ferrando, H. Michinel, M. Seco, D. Tommasini, "Nonlinear phase shift from photon-photon scattering in vacuum", *Phys. Rev. Lett.* **99**, 150404 (2007).
- [21]. D. Tommasini, A. Ferrando, H. Michinel, M. Seco, "Detecting photon-photon scattering in vacuum at exawatt lasers", *Phys. Rev. A* **77**, 042101(2008).
- [22]. D. Tommasini, A. Ferrando, H. Michinel, M. Seco, "Precision tests of QED and non-standard models by searching photon-photon scattering in vacuum with high power lasers", *J. High Energy Phys.* **11**, 043 (2009).

1. Introduction

Nonlinear waves are fundamental objects in media characterized by a nonlinear response. Their modeling and understanding is a fascinating object of study shared by different disciplines. This broad spectrum of topics in which nonlinear waves play a key role makes this subject especially suitable for the characteristic InterTech interdisciplinary approach based on advanced mathematical / physical modeling, demanding computational methods, and the development of new technological applications. We will present here the main lines of research developed in the area of photonics at InterTech during the last years

and the present time which include contributions in the following topics: spatial solitons in discrete media, singular optics, temporal solitons and supercontinuum generation, non-paraxial nonlinear optics in photonic crystals, nonlinear liquid crystals, nonlinear plasmonics, cold atoms in the mean-field and quantum regimes and nonlinear effects of the QED vacuum.

2. Spatial solitons in discrete-symmetry media

Spatial solitons are nonlinear light structures that are able to propagate without diffraction

due to an exact compensation between diffraction and nonlinear effects. They are mathematically described by Nonlinear Schrödinger Equations (NLSE) or alike [1]. The propagation of spatial solitons in discrete-symmetry media such as periodic dielectric structures provides them with special properties absent in ordinary propagation in homogenous media. The richness and complexity of nonlinear solutions in discrete-symmetry media is highly remarkable. Our group has worked intensively in this topic in the last years. Our main contribution has been to introduce a powerful theoretical tool to classify this panoply of nonlinear solutions in a systematic manner. This mathematical tool is the generalization of discrete group theory to nonlinear equations of the type given by NLSE [2]. In particular, our group showed the possibility of generating spatial solitons solutions (of the fundamental, vortex and dipole type) in photonic crystal fibers [3-5] and nontrivial phenomena involving nonlinear photonic crystals as that of vortex transmutation [6].

3. Nonlinear singular optics

The mathematical tools developed for the study of solutions of NLS-like equations were especially well suited for the study of phase singularities. In general, complex scalar solutions of wave equations can present dislocations similar to those found in crystals. The essential mathematical property of these complex scalar functions in the point or line where a dislocation is localized is that its phase is increased or decreased in a multiple of 2π along a closed curve around it. In these points or lines, also known as phase singularities or, in a wide sense, as vortices, the amplitude of the function vanishes and its phase is undetermined. In the case of nonlinear optics, the study of such singularities or vortices is often enclosed in a separated branch called nonlinear singular optics [7]. An important category of optical vortices is that of discrete vortices (DV), or vortices in discrete-symmetry media. We have developed a series of powerful theorems and rules to predict the behaviour of phase singularities propagating in optical media owning discrete rotational symmetry. This includes a vorticity cut-off theorem [8], the demonstration of DV as angular Bloch modes [9], the essential relation between symmetry, winding number and topological charge of DV [10] and the existence of selection rules for the topological charge of DV in interfaces breaking rotational symmetry [11].

4. Nonlinear temporal optics and design of supercontinuum spectra

The behavior of optical pulses in optical fibers and optical fiber devices in the nonlinear regime is also given by an effective NLSE in the time domain for the pulse envelope [12]. Generalized versions of NLSEs are used to include higher order nonlinear effects. Among them, supercontinuum generation, the spectacular enhancement of the spectral width of a pulse in a PCF, is likely the most relevant phenomenon in nonlinear fiber optics in the last years [13]. Supercontinuum generation is a complex phenomenon that strongly depends on the dispersion features of the fiber and the characteristic of the input pulse. This generates

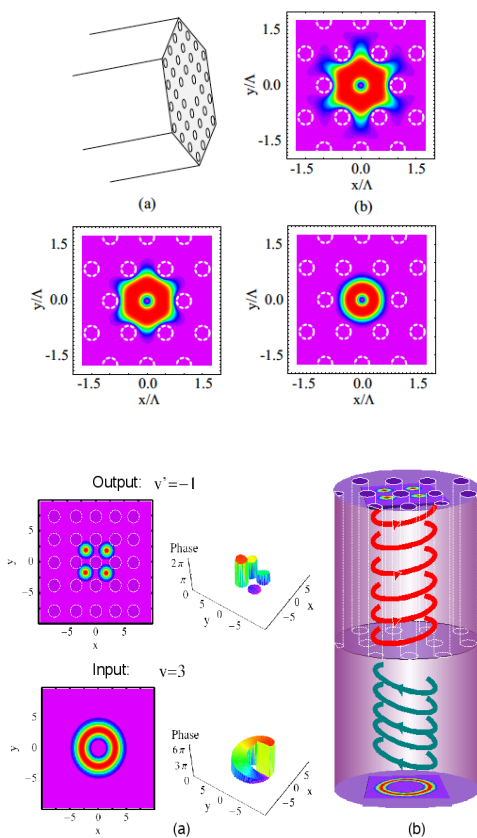


Fig. 1. Vortex soliton solutions for different powers in a photonic crystal fiber (up) as in Ref. [5] and a characteristic example of vortex transmutation (down) as in Ref. [6].

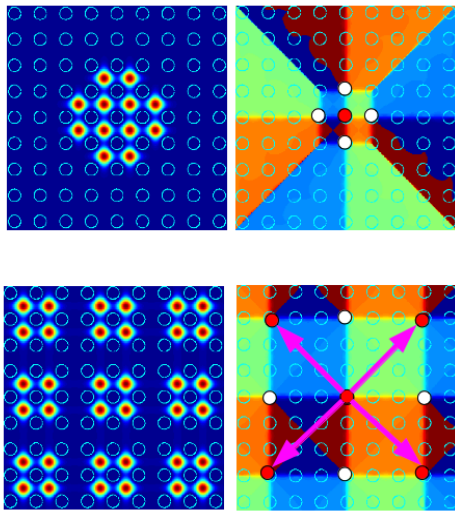


Fig. 2. Examples of the amplitude (left column) and phase (right column) of DV solitons with same rotational behavior under $\pi/2$ discrete rotations: they both have identical angular pseudo-momentum $m=-1$ (see [9]), but different total topological charge: $v=-3$ in the upper case and $v=-1$ in the lower case. White circles in phase figures indicate phase singularities with topological charge +1 whereas red circles correspond to charge -1. Classification and behavior of these solutions are given in Ref. [10].

an enormous variety of available output spectra by suitable tuning of these parameters. However, the computational cost to explore all the parameter space is unaffordable. Thus, in order to design useful PCF-based devices yielding spectra for useful applications, a combination of optimization techniques and large computational resources is needed. In this context, we have developed a new computational scheme to design supercontinuum spectra “à la carte” by means of genetic algorithms [14]. Due to the potentially large amount of computations required by this strategy, the deployment of these heuristic algorithms is performed using distributed computing in the form of a Grid platform. The optimization procedure is automated within the Grid platform and permits escalation to large computational Grids. Some examples of designed supercontinua are given in Fig. 3. Potential applications for the design of future photonic devices include the fabrication of light sources for specific targets in nonlinear microscopy and biomedicine.

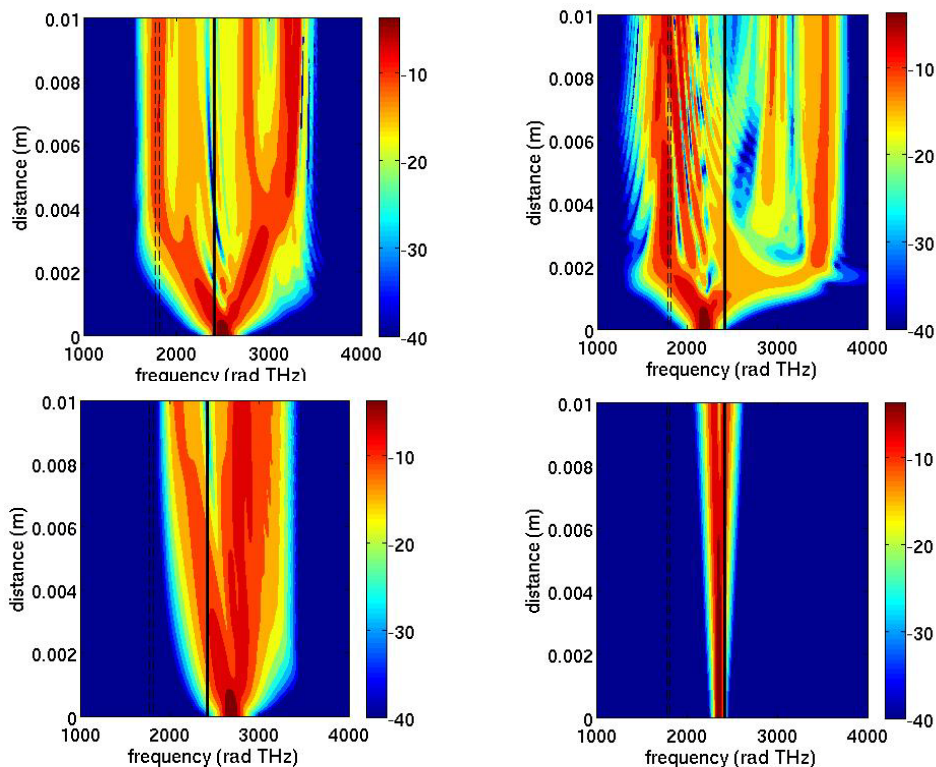


Fig. 3. Spectral evolution examples that belong to the parameter space. Full vertical lines mark the zero GVD and dashed show the targeted spectrum in the anomalous GVD regime. Figs. (a) and (b) correspond to far non optimized results, whereas Figs. (c) and (d) show two optimized cases.

5. Nonlinear liquid crystals

Nematic Liquid Crystal (NLC) devices are being widely studied in the field of Nonlinear Optics due to its large nonlinear response [15]. It allows to generate nonlinear solutions with no change of shape, the so called nematons at very low optical powers. Its interest range from all optical communication devices to computation. Besides, the nonlocality exhibited by NLC cells has been shown as an efficient mechanism for stabilizing optical complex structures which cannot exist in local nonlinear homogeneous media. The aim of this line of research is presenting a complete realistic model for NLC devices that permits realistic simulations of nonlinear propagation of light in these structures. This model provides new effects absent in ordinary simplified nonlinear nonlocal models.

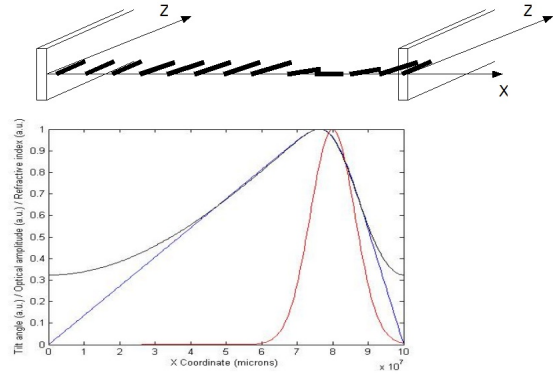


Fig. 4. Calculated angle of rotation of the NLC molecules versus horizontal position for a typical configuration at an arbitrary z axial position (blue line and descriptive figure above), effective refractive induced in light by this molecular distribution (black line) and light field distribution at the same axial slice (red line).

6. Nonlinear plasmonics

Plasmonics is an important and quickly developing area of modern physics which offers promising applications in nano-optics and electronics. It deals with the so-called surface-plasmon polaritons (SPP), i.e., collective oscillations of the electromagnetic field and electrons which propagate along a metal-dielectric surface and decay exponentially away from the surface [16]. SPPs are characterized by their frequency and their propagation constant along the interface. SPPs can only interact resonantly with evanescent electromagnetic waves in the dielectric medium. Accordingly, there are two main methods for excitations of plasmons: (i) via the evanescent wave generated at the total internal reflection and (ii) via a periodic structure producing evanescent modes. In this context, we have shown the possibility of resonant interaction between a SPP at a metal surface and a parallel self-focusing beam, in the form of a spatial soliton, in a nonlinear dielectric [17]. A simple two-level model reveals hybridized plasmon-soliton eigenmodes, we refer to as soliplasmon excitations, and their complex nonlinear dynamics which offers plasmon excitation and control using spatial solitons.

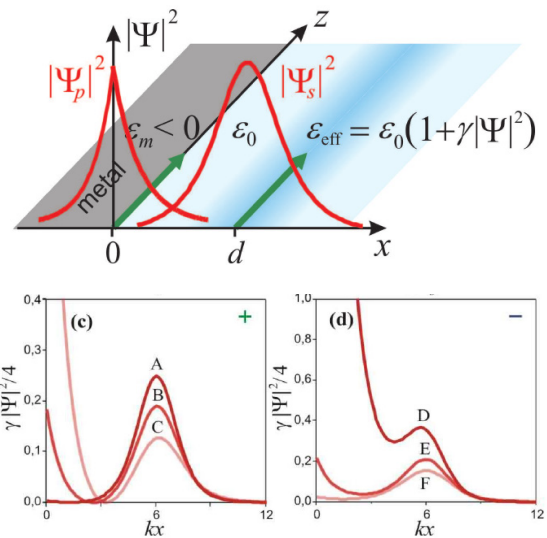


Fig. 5. Characteristic metal/dielectric/Kerr structure supporting soliplasmon excitations (up). Two examples of “antisymmetric” and “symmetric” soliplasmon excitations as appearing in Ref. [17].

7. Cold atoms in the mean-field and quantum regimes

Ultracold matter can be represented by a coherent state, constituted by many atoms, called a Bose-Einstein condensate (BEC). This quantum state can be, in turn, represented by a mean-field wave function that fulfills the so-called Gross-Pitaevskii equation (GPE). The GPE is a temporal equation that describes the dynamics of the BEC wave function and is formally identical to the NLSE in different dimensions. In the particular case of BEC in 2D traps the GPE is identical to NLSE describing the

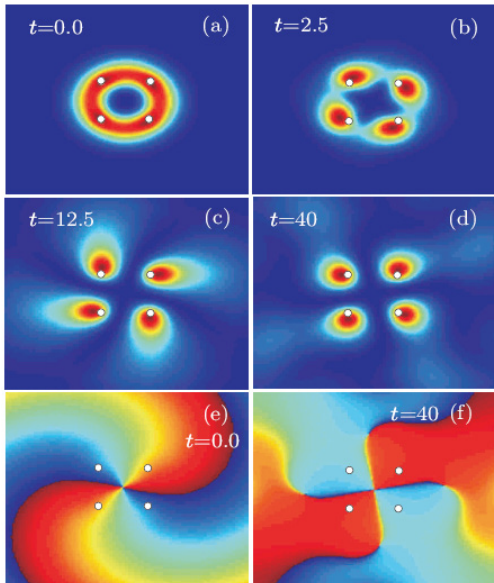


Fig. 6. Different snapshots of the evolution of a charge 2 matter wave vortex under the action of a symmetry breaking potential of order 4. This behavior is consistent with the discrete group theory rules developed in Ref [18].

propagation of light in 2D optical media. For this reason, all our results based on discrete group theory previously applied in optical systems can be translated to the ultracold matter formalism in a straightforward manner. In this way, the symmetry rules governing the behavior of optical vortices under the presence of discrete-symmetry media also hold for matter vortices when the full continuous rotational symmetry of the potential is broken by the presence of an

instantaneous discrete-symmetry potential [18]. Further studies initiated in our group indicates that our symmetry rules are also preserved in the quantum limit, i.e., that in which the number of atoms is so small that the usual GPE approach start to fail because of quantum fluctuations in the atom number. Modeling in this case is performed using the full quantum Bose-Hubbard model for atom traps in the form of a ring showing discrete rotational symmetry.

8. Nonlinear effects of the QED vacuum

This line of research is developed together with Daniele Tommasini and Humberto Michinel from the Optics Laboratory of the Universidad de Vigo at Ourense [19]. This line is devoted to light nonlinearities induced by the QED vacuum, that is, in the absence of any form of matter. Surprisingly, in terms of classical Nonlinear Optics, vacuum excitations, in the form of the quantum generation of virtual electron-positron pairs, can induce effective nonlinearities. However, despite it is a well-known result since long time ago, photon-photon scattering in vacuum has not yet been detected using standard high-energy experiments where the probability of this effect to occur, given by the photon-photon cross section, is maximized. An alternative approach is to perform experiments using ultrahigh power optical lasers, such as

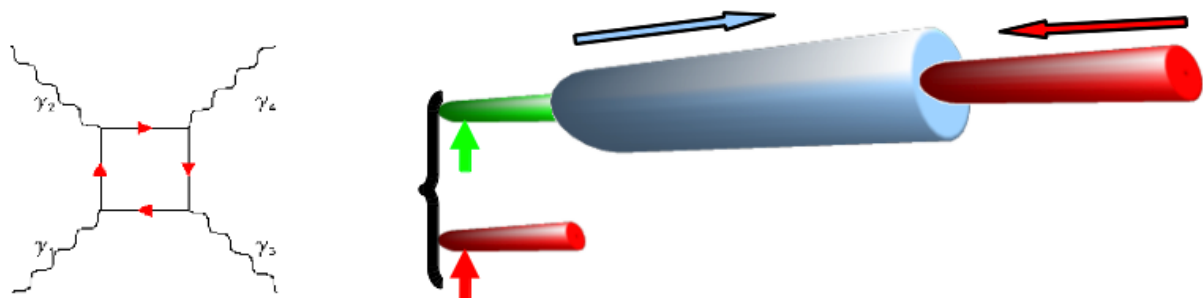


Fig. 7. Characteristic box diagram of photon-photon scattering in vacuum generating effective nonlinearity (left). Schematic representation (right) of a proposed experiment with a high-intensity laser (green) interacting with a low-intensity one (red beam above); nonlinearities induced by the high-intensity laser generate a nonlinear shift in the low-intensity laser that can be measured by interferometric methods using a non-shifted reference low-intensity beam (red beam below).

those that will be available in the near future, in such a way that the high density of photons will compensate the smallness of the cross section. In this case, the small energies characteristic of optical photons (a few eVs) and the effect of photon-photon collisions due to the interchange of virtual electron-positron pairs can be expressed in terms of the effective Euler-Heisenberg nonlinear Lagrangian. This modifies Maxwell's equations transforming them into a Lorentz covariant set of nonlinear equations. Our mixed group has proposed optical

experiments based on ultrahigh intensity lasers in which this small effective nonlinearities can be unveiled thus showing for the first time the presence of photon-photon scattering in vacuum [20-22].

Acknowledgements

This work was partially supported by the Government of Spain No. TIN2006-12890.

Issues regarding the implementation of sliding controls for thermal regulation

Frank Florez
Universidad Nacional de Colombia
Manizales, Colombia
frflorezmo@unal.edu.co

Pedro Fernández de Córdoba
Universitat Politècnica de València
Valencia, Spain
pfernandez@mat.upv.es

Gerard Olivar Tost
Universidad Nacional de Colombia
Manizales, Colombia
golivart@unal.edu.co

Abstract—In this work a sliding modes controller is designed and implemented to regulate the temperature in a closed space. The system is represented with a lumped parameter model of 18R13C, initially the model is evaluated in simulation and tuned with experimental data, for the design of the controller is used the Monte Carlo method to simplify, and later calculate the equilibriums and main parameters, finally the controller is tested in a reduced scale model.

Index Terms—sliding modes controller, lumped parameter model, Monte Carlo, Full Scale Model.

I. INTRODUCTION

The reduction of the energy consumption in cities and different human environments is a very important study field in the last century [1]. Has been identified that the urban zones concentrate close to the 50% and consume almost the 85% of annual energy production on developed countries, and of all these energy required in cities almost the 40% is used on HVAC (Heating, Ventilation and Air Conditioning) systems to achieve the thermal comfort in offices and residential spaces [2], [3].

To decrease the energetic consumption of a thermal zone is necessary analyse all the possible sources or lakes of heat, and try to reduce his impact on the thermodynamic of the space, for this is necessary the use of accurate mathematical models and simulators, that allow to the researchers execute deeper and different experiments [4].

The mathematical models used to analyse a thermal zone can be classified in black, grey or white box according with the grade of configuration and knowledge allowed to the researcher, the commercial simulator such as TRNSYS® and ENERGY+® usually implements black or grey models, and are widely used in research and industry, for this reason in any investigation is necessary take in account the response of these simulators and realize comparison for guarantee the good behaviour of the used models [5]–[7].

Otherwise, the use of the accurate mathematical models that allow understand the thermodynamic of a building is just a part of the problem of high energy consumption, is necessary implement control actions that regulate the thermal conditions and look for energy savings, in literature many controllers has

been proposed and investigated in this ambit, but is necessary continue investigating new strategies that can achieve the aims and for his nature can be adapted to the thermal scope.

The sliding modes control is a technique used widely in power converters and mechanical applications [8], [9], using his good characteristics as the quick response to disturbances, stability and easy tuning, besides can be adapted to new applications, such as the thermal regulation, but his implementation on real buildings is a challenge for different reasons, such as the interruption of human activities, economic costs and aleatory environmental conditions between others, for avoid these elements in the evaluation of new control strategies is helpful practice the use of scale reduced models.

In this work we present the process of verification in simulation and experimentally of a lumped parameter model, described mathematically and adjusted to represent the thermodynamic of a wooden box used as scale reduced model with an internal gain, later a sliding modes controller is designed and implemented for regulate the internal temperature.

The rest of the article is organized as follow: in section II is described the structure of the lumped parameters model. The section III used to present the simulation and experimental tests. In section IV the controller is designed and evaluated theoretical and experimentally. Finally, in section V are showed the conclusions.

II. MATHEMATICAL MODEL

To evaluate the control sliding method is needed count with a mathematical model accurate and tuned to the study case, in this research we select the lumped parameter model presented in figure II, in literature this structure is called Full Scale Model (FSM) [10], [11], and use the subscripts i, j , where $i = 1, 2, \dots, 6$ corresponds to the wall of the thermal space, and the subscript $j = in, med, ex$ indicate the position of the element, in and ex corresponds to the internal and external surfaces, and mid is used for the conduction resistance of the walls, the state variables of the models are the internal temperature T , and the 12 superficial internal and external temperature $T_{i,in}$ y $T_{i,ex}$, the environmental temperature is represented as T_a , additionally is considered the thermal capacity of the air in the room represented with the capacitor

C_r , the internal gains are included with the variable I_L and controlled with the binary variable u [7].

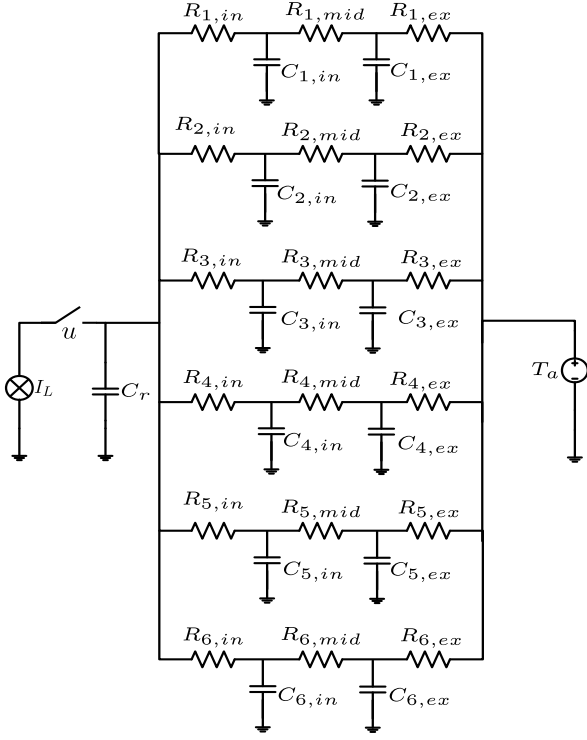


Fig. 1. Full scale model

$$C_{i,ex} \frac{dT_{i,ex}}{dt} = \frac{T_i}{R_{i,ex}} - T_{i,ex} \left(\frac{1}{R_{i,ex}} + \frac{1}{R_{i,mid}} \right) + \frac{T_{i,in}}{R_{i,mid}} \quad (1)$$

$$C_{i,in} \frac{dT_{i,in}}{dt} = \frac{T_{i,ex}}{R_{i,mid}} - T_{i,in} \left(\frac{1}{R_{i,mid}} + \frac{1}{R_{i,in}} \right) + \frac{T}{R_{i,in}} \quad (2)$$

$$C_r \frac{dT}{dt} = \frac{T_{1,in} - T}{R_{1,in}} + \frac{T_{2,in} - T}{R_{2,in}} + \frac{T_{3,in} - T}{R_{3,in}} + \frac{T_{4,in} - T}{R_{4,in}} + \frac{T_{5,in} - T}{R_{5,in}} + \frac{T_{6,in} - T}{R_{6,in}} + uI_L \quad (3)$$

It is necessary clarify that the internal and external resistances is considered the heat transfer process for radiation and convection, meanwhile the conduction heat process is calculated with the physical characteristics of the wall [12].

III. TUNING AND SIMULATION

For guarantee the efficiency of the mathematical model it was planted a theoretical study case with a constant temperature, the same situation it was model with the commercial program TRNSYS®, the model planted was a empty cube of edges $2m$, the material in the walls is the medium concrete, with the following thermal characteristics: conductivity= $4.14 \frac{KJ}{hm^\circ K}$, specific heat= $1 \frac{KJ}{kg^\circ K}$ and

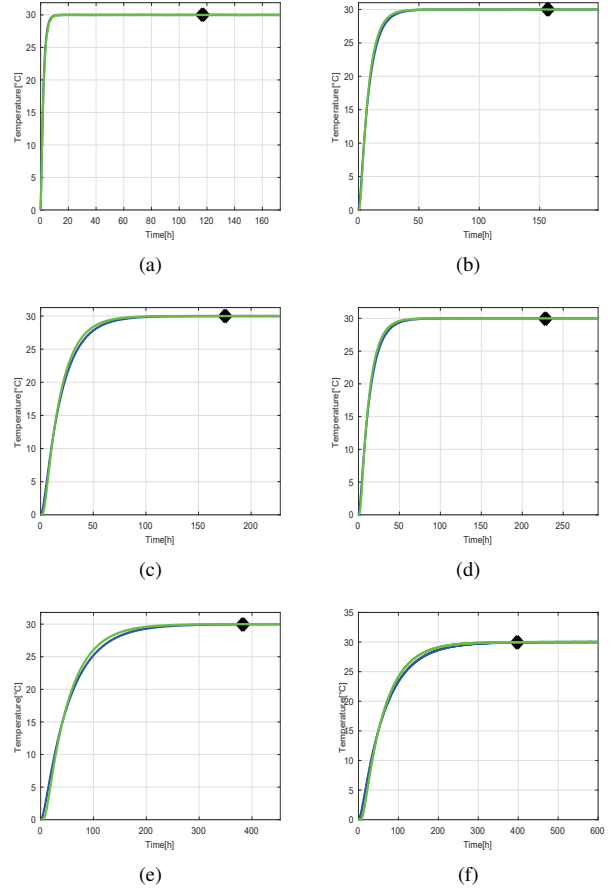


Fig. 2. Comparison between FSM and TRNSYS

density= $1800 \frac{kg}{m^3}$. The simulators results were compared using the root mean square error (RMSE), the aim of this test is analyse the difference between the simulators changing the thickness of the walls, the results are presented in figure 2, where the blue green line corresponds to the TRNSYS data and the blue is for the FSM, the black point is the time taken for achieve the stationary state. In table I is resumed the thickness values used and his corresponding time of the establishment and error calculated, with this first simulation is possible appreciate the good behaviour of the FSM especially for thermal spaces with walls of low thickness.

TABLE I
FSM AND TRNSYS ERRORS

Espesor[m]	RMSE[C]	Muestra[h]	Gráfica
0.05	0.5314	117	2(a)
0.15	0.9131	157	2(b)
0.25	1.5991	175	2(c)
0.35	2.0028	243	2(d)
0.45	2.1316	383	2(e)
0.5	2.4331	397	2(f)

The next step in the investigation was tuning the model with experimental data, for this aim was built a wooden box with

TABLE II
WOODEN BOX PARAMETERS

Material	Parameter	Value
Wood	Conductivity	$0.645 \frac{KJ}{hmK}$
	Density	$700 \frac{kg}{m^3}$
	Especific heat	$1.6 \frac{KJ}{kgK}$
Air	Density	$1.2 \frac{kg}{m^3}$
	Especific heat	$1.007 \frac{KJ}{kgK}$

the dimensions $70cm \times 40cm \times 58cm$ with $15.8mm$ of walls thickness, the thermal characteristics are resumed on the table II; in the interior was set a infrared lamp of $60W$ to stimulate the heat flux, this experiment was executed indoor to minimise the changes on the environmental temperature, and consisted on consecutive periods of charge and discharge of 4h duration. The experiment taken almost 3 days, and the internal temperature experimentally recorded were used to adjust the transfer heat coefficients between the air internal and external and the box walls, this results are presented on figure 3, showing with the red line the experimental data, blue line is for simulated internal temperature and green line for environmental temperature.

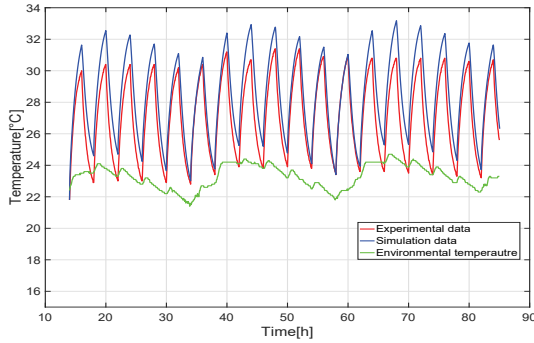


Fig. 3. Circuito equivalente

IV. CONTROL DESIGN

The basic theory on the the sliding modes controller start defining a nonlinear time-dependent system $\dot{x} = g(x(t)) + \phi(x(t))u(t)$, where x is a vector of state variables, $g(\cdot)$ and $\phi(\cdot)$ are smooth vector fields [13], and $u(t)$ is a binary equation depending on the next relation:

$$u = \begin{cases} u = 0 & \text{para } s > 0 \\ u = 1 & \text{para } s < 0 \end{cases} \quad (4)$$

The variable s is the system trajectory, usually defined as a linear arrangement with form $s = \sum_{i=1}^m \alpha_i x_i = Jx$, $J = [\alpha_1, \alpha_2, \dots, \alpha_m]$ is a vector of constants of the controller α_i to be tuned [14].

The state variables defined for this case are the temperature error about a reference temperature T_{ref} i.e. $(x_1 = T_{ref} - T)$ and the incoming heat flux x_2 , but initially the FSM counts

with 13 state variable related to the internal temperature an superficial temperatures, and must be reduced or discarded according with his importance on the model, for this process was developed a Monte Carlo analysis with the coefficients of the convection internal and external, the radiation internal and external, and the conduction process. The analysis allow know the impact of little variations in the nominal value of an initial coefficient over the internal temperature and classify the importance of the parameter and phenomenon according to the slope of the line final, the disturbances on the input parameters were generated with 1000 aleatory numbers with different distributions, the range of disturbances used in each case is from 2.5% until 12.5% [15].

In figure 4 is presented the result of this analysis, in this picture is evident that the radiation process has low impact on the internal temperature, and the system can be simplified to a model that only considers the conduction and convection process.

The next step on the controls design is the establishment of the

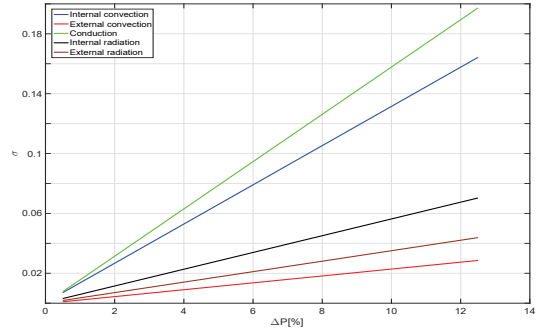


Fig. 4. Monte Carlo analysis results

system equilibriums, these points must be stable attractors with fixed input and infinite time, in figure 5 is showed the theoretic equilibriums and the sliding manifold taking the controllers coefficients $J = [\alpha 1]$, the constants a, b, c and d are positive values calculated with the walls characteristics according with the equations 5-9.

$$R_{i,s} = R_{i,ex} + \frac{R_{i,med}}{2} \quad (5)$$

$$R_{i,m} = R_{i,in} + \frac{R_{i,med}}{2} \quad (6)$$

$$\frac{1}{R_{st}} = \sum_{i=1}^6 \frac{1}{R_{i,s}} \quad (7)$$

$$\frac{1}{R_{mt}} = \sum_{i=1}^6 \frac{1}{R_{i,m}} \quad (8)$$

$$C_w = \sum_{i=1}^6 C_{i,in} + C_{i,ex} \quad (9)$$

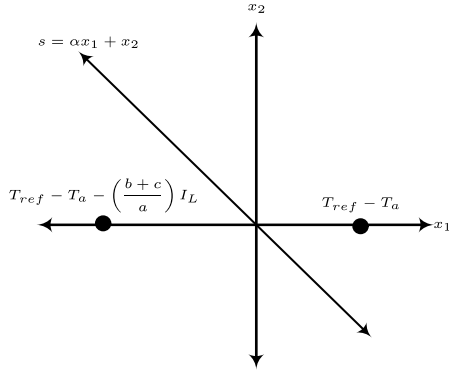


Fig. 5. Theoretic equilibrium

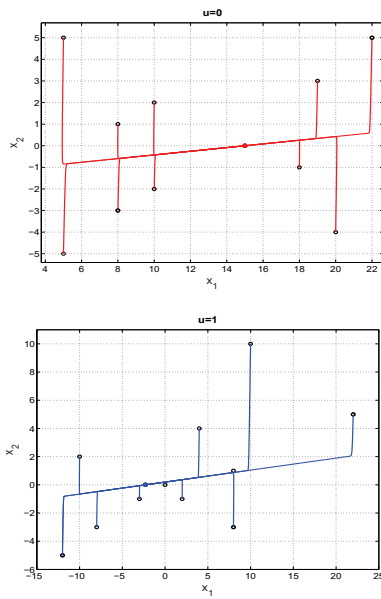


Fig. 6. Equilibriums in simulation

$$a = \frac{1}{R_{st}R_{mt}C_w} \quad (10)$$

$$b = \frac{1}{R_{st}C_w} \quad (11)$$

$$c = \frac{1}{R_{mt}C_w} \quad (12)$$

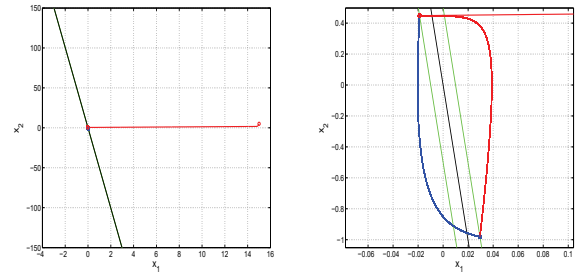
$$d = \frac{1}{R_{mt}C_r} \quad (13)$$

Figure 4 shows the simulation results for the both states of the variable u , in these pictures the black circles represents the initial point, and the the circle blue and red are the equilibrium in each case. After find the equilibriums system is necessary define the surface sliding $s = \alpha x_1 + x_2$ and his derivative \dot{s} expressed on equation 14, this equation is

expressed function of the the state variables, the reference temperature and environmental temperature [16].

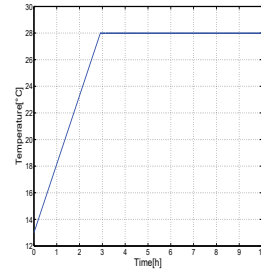
$$\dot{s} = ax_1 - (b+c+d - \frac{\alpha}{C_r})x_2 - bT_{ref} + uI_L(b+c) + bT_a \quad (14)$$

Based on the equation 14 is possible determine the critic value of α , for this case is planted of $\alpha = Cr \left(\frac{1}{R_{st}C_w} + \frac{1}{R_{mt}C_w} + \frac{1}{R_{mt}C_r} \right)$, it must be selected a close value higher o lower, the chosen value taken is $\alpha = 48.3198$. The hysteresis bandwidth is defined with the establishment of two lines λ_1 and λ_2 , these lines corresponds to the inclusions of one positive constants chosen arbitrary, in this case is $\epsilon = 0.5$, i.e. $\lambda_1 = \alpha x_1 + x_2 - \epsilon$ and $\lambda_2 = \alpha x_1 + x_2 + \epsilon$.



(a) Searching stage

(b) Tracking stage



(c) Internal temperature

Fig. 7. Sliding modes control in simulation

In figure 8 are presented the simulations results, the black line represents the sliding surfaces $s = 0$, the green line are used for represent λ_1 and λ_2 , the red line is used for represent the system evolution with $u = 1$, and the blue line the evolution with $u = 0$, specifically in 7(c) is presented the internal temperature, and after the transitory period the temperature achieve the reference of $28^\circ C$ satisfying the 2% criteria.

The experimental test was implemented with a electronic card ESP32 LOLIN, and temperature sensors DS18B20, the system was programmed to sampling temperature every three minutes, in this experiment the initial conditions were very close to the sliding surface as is presented on figure 8(a), but as in theory the system achieve the stable point in $x_1 = x_2 = 0$, in that moment the duty cycle is very stable (figure 8(b)), finally in figure 8(c) is showed the internal temperature recorded, in this picture is evident the good behaviour of the controller

regulating the internal temperature even with a increasing environmental temperature.

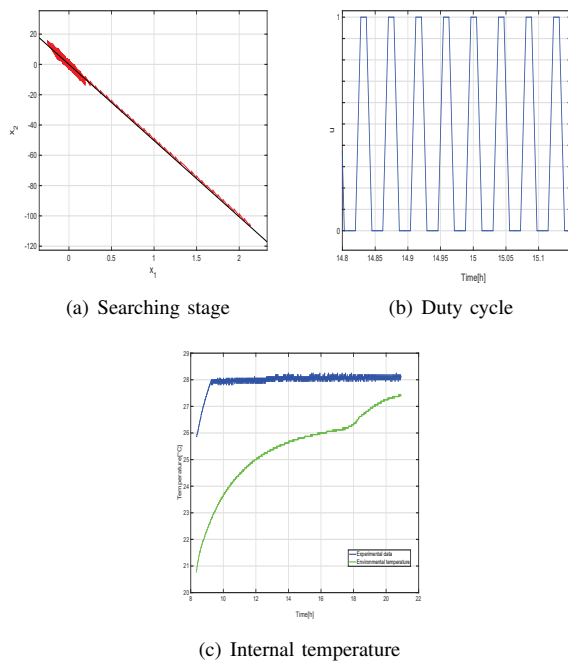


Fig. 8. Sliding modes control experimental results

V. CONCLUSIONS

In this paper was designed and tested experimentally a sliding modes control for regulate temperature in a closed space. In first stages of the investigations the Full Scale Model was compared with the commercial software TRNSYS®, giving low errors values, especially on thermal zones with low thickness walls.

The experimental tests were done with a reduced scale models, giving a set of experimental data that allowed adjust the simulator and minimise the difference between the experimental and the simulation in open loop.

The Monte Carlo analysis was used to discard parameters on the model on the beginning of transitory stages, in this period the radiation heat transfer has low impact over the internal temperature.

Following the theory of sliding control strategy, it was design the operation rule, and founded the main control parameters, in experimental and simulation tests the controller satisfied the 2% criteria, allowing conclude that the strategy can works without problem with the thermal variables.

VI. ACKNOWLEDGMENT

This investigation was supported by national doctoral program of the Colombian Administrative Department of Science Technology and Innovation (Colciencias), and the agreement "Analysis of the properties, applications and market opportunities of Coatings G-COVER".

REFERENCES

- [1] R. Forgiarini, N. Giraldo, and R. Lamberts, "A review of human thermal comfort in the built environment," vol. 105, pp. 178–205, 2015.
- [2] N. Delgarm, B. Sajadi, and S. Delgarm, "Multi objective optimization of building energy performance and indoor thermal A new method using artificial bee colony ABC," vol. 131, pp. 42–53, 2016.
- [3] X. Zheng, H. Li, M. Yu, G. Li, and Q. Shang, "Benefit analysis of air conditioning systems using multiple energy sources in public buildings," vol. 107, pp. 709–718, 2016.
- [4] O. M. Brastein, D. W. U. Perera, C. Pfeifer, and N. Skeie, "Energy and Buildings Parameter estimation for grey-box models of building thermal behaviour R," vol. 169, pp. 58–68, 2018.
- [5] K. Perini, A. Chokhachian, S. Dong, and T. Auer, "Modeling and simulating urban outdoor comfort: Coupling ENVIMet and TRNSYS by grasshopper," *Energy Build.*, vol. 152, pp. 373–384, 2017.
- [6] A. Scherba, D. J. Sailor, T. N. Rosenstiel, and C. C. Wamser, "Modeling impacts of roof reflectivity, integrated photovoltaic panels and green roof systems on sensible heat flux into the urban environment," *Build. Environ.*, vol. 46, no. 12, pp. 2542–2551, 2011.
- [7] F. Macdonald, I. Beausoleil-Morrison, A. Ferguson, M. Kummert, T. McDowell, and R. Jost, "Demonstration of the new ESP-r and TRNSYS co-simulator for modelling solar buildings," *Energy Procedia*, vol. 30, pp. 505–514, 2012.
- [8] H. Ding, A. Khajepour, Y. Huang, M. Bahrami, and F. Bagheri, "An energy-saving set-point optimizer with a sliding mode controller for automotive air-conditioning/refrigeration systems," *Appl. Energy*, vol. 188, pp. 576–585, 2016.
- [9] A. Mironova, P. Mercorelli, and A. Zedler, "Robust Control using Sliding Mode Approach for Ice-Clamping Device activated by Thermoelectric Coolers," *IFAC-PapersOnLine*, vol. 49, no. 25, pp. 470–475, 2016.
- [10] Y. Lin, T. Middelkoop, and P. Barooah, "Issues in identification of control-oriented thermal models of zones in multi-zone buildings," pp. 6932–6937, 2012.
- [11] P. Fazenda, P. Lima, and P. Carreira, "Context-based thermodynamic modeling of buildings spaces," *Energy Build.*, vol. 124, pp. 164–177, 2016.
- [12] Y. A. Cengel, *Transferencia de Calor y Masa*, Third edit. Mexico D.F.: McGraw-Hill, 2007.
- [13] V. Utkin, *Sliding Mode Control Design Principles and Applications to Electric Drives*. IEEE Transactions on Industrial Electronics, pp. 23–36, 1993.
- [14] T. Siew-Chong, L. Yuk-Ming, and T. Chi Kong, *Sliding Mode Control of Switching Power Converters*. 2012.
- [15] R. Robledo Fava, M. C. Hernandez Luna, P. Fernandez de Cordoba, H. Michinel, S. Zaragoza, A. Castillo Guzman and R. Selvas Aguilar, "Analysis of the Influence Subjective Human Parameters in the Calculation of Thermal Comfort and Energy Consumption of Buildings". *Energies*, 12(8), 1531, 2019.
- [16] F. Florez, P. Fernandez de Córdoba, J. Higón, G. Olivar, and J. Taborda. "Modeling, Simulation, and Temperature Control of a Thermal Zone with Sliding Modes Strategy". *Mathematics*, 1–13, 2019.

Article

Modeling, Simulation, and Temperature Control of a Thermal Zone with Sliding Modes Strategy

Frank Florez ^{1,*}, Pedro Fernández de Córdoba ², José Luis Higón ³, Gerard Olivar ⁴ and John Taborda ⁵

¹ Faculty of Engineering and Architecture, Universidad Nacional de Colombia, Campus la Nubia, 170003 Manizales, Colombia

² Instituto Universitario de Matemática Pura y Aplicada, Universitat Politècnica de València, Camino de Vera s/n, 46022 Valencia, Spain; pfernandez@mat.upv.es

³ Department of Architectural Graphic Expression, Universitat Politècnica de València, Camino de Vera s/n, 46022 Valencia, Spain; jhigonc@ega.upv.es

⁴ Faculty of Exact and Natural Sciences, Universidad Nacional de Colombia, Campus la Nubia, 170003 Manizales, Colombia; golivart@unal.edu.co

⁵ Faculty of Engineering, Universidad del Magdalena, 470003 Santa Marta, Colombia; jtaborda@unimagdalena.edu.co

* Correspondence: frfloresmo@unal.edu.co; Tel.: +57-300-349-6229

Received: 27 March 2019; Accepted: 29 May 2019; Published: 2 June 2019



Abstract: To reduce the energy consumption in buildings is necessary to analyze individual rooms and thermal zones, studying mathematical models and applying new control techniques. In this paper, the design, simulation and experimental evaluation of a sliding mode controller for regulating internal temperature in a thermal zone is presented. We propose an experiment with small physical dimensions, consisting of a closed wooden box with heat internal sources to stimulate temperature gradients through operating and shut down cycles.

Keywords: building modeling; lumped parameter model; sliding control mode; reduced scale model

1. Introduction

In recent decades, building modeling and energy consumption in thermal zones have become a growing field of study for engineers and researchers [1]. These studies have been impelled by different countries thanks to international agreements such as the Kyoto Protocol and the implementation of the sustainable development goals of the United Nations (UN). It has been realized that the high energetic consumption of HVAC systems in buildings, which in developed countries can account for 40% of the annual energy production, is a key factor in climatic change [2].

To minimize consumption in buildings, it is necessary to understand the main factors of energy waste, such as thermal comfort and human habits. Different tools have been developed to simulate thermodynamic processes in buildings [3,4]. For example, commercial programs such as TRNSYS and ENERGY PLUS allow representing an entire building and analyzing the effects of specific actions. Another important tool is mathematical modeling, which permits deeper numerical analysis and contributes to the development of new strategies and controllers for temperature regulation. At the same time, this allows reducing energy consumption [5].

The representation of a entire building consisting of different levels and a large number of rooms in each level, is a complex task especially if geometrical and physical characteristics, environmental conditions and relations with external bodies are taken into account. To simplify the problem, only individual and closed rooms are analyzed, and in subsequent stages the results are extrapolated to the entire building. The analysis of a single room as a thermal zone is reduced to capturing the

thermodynamic processes in the room. This includes evaluating the different heat sources, both external and internal. Examples of external heat sources include sun radiation and surrounding bodies at different temperatures. Possible internal heat sources include electronic equipment and occupants. Some factors and phenomena are easily handled, while others require important mathematical modeling in order to be captured. In order to meet these requirements without increasing the complexity of the mathematical model one makes simplifications that maintain the predominant dynamics of the problem [6].

There are many choices of a mathematical model, depending on factors such as accuracy, computational cost and adaptability. In many cases, high accuracy needs powerful electronic equipment for sensing and processing. If implemented, this often drives costs beyond the budget. Additionally, the more specific a mathematical model is, the more difficult its electronic implementation will be, including modifications and variations in a case study. Another important factor is the tuning of parameters in the model. Tuning strategies based on large databases or combinations of modeling strategies in order to obtain the maximum amount of information about the study case are found in [7–9].

Some modeling options are mentioned below: Ref. [5] presents a method for modeling room temperature based on the laws of thermodynamics resulting in an Armax model for control purposes. Ref. [10] uses the Zokolov mathematical model, which is based on heat balance with quasi-steady-state approximations to determine the average internal temperature. For more detailed models, it is possible to include different thermal phenomena such as infiltration and thermal inertia, as in [11], where the mass and energy conservation principle was used. However, in the majority of research it is acceptable to use reduced order models. The Lumped Parameter Methods (LPM) allow a choice among a large variety of structures and orders. Refs. [6,12] use circuits of 4th and 7th order to model single thermal zones, while Refs. [13,14] use simplifications and apply different control techniques.

An aspect as important as the mathematical model itself is the control strategy. This is so because some of the thermal zones inputs are constantly changing. Thus it becomes necessary to rely on a central controller that regulates the internal variables to achieve the objectives of thermal comfort and energy savings. Strategies such as the model predictive control (MPC) are accepted within the scientific community as a good alternative in thermal applications [15–18]. This technique has been compared with classic controllers such as PID [19] and been shown to perform better. Refs. [20,21] propose cooperative work with fuzzy controllers that exhibits an energy savings of about 20%, demonstrating that the study of other techniques cannot be disregarded.

However, the study of alternative control techniques is not a easy task, especially in experimental investigations. To minimize problems in the evaluation of new control strategies, some researchers have been using reduced scale models. The latter allow the creation of sensed thermal zones with minimal resources and minimize the effect of environmental conditions. This effect is typically one of the most common factors in the failure of new control strategies [22–25].

In this article, we show how to use the Sliding Control strategy for regulation of the temperature in a thermal zone. This technique is normally used for commuted systems as power converters, but it is robust enough to be implemented in different applications [26–30]. For the evaluation of the control technique, an experiment with a scale reduced model was planned. The experiment consisted of a wooden box equipped with an internal lamp to simulate a heater in a room, in a cold climate environment. In the first stages of the experiment, a mathematical modeling technique was built and tuned with an experimental database. This allowed the development of a simulator that reproduced the experimental results with high accuracy. Subsequently we programmed an electronic card to drive the internal lamp according to the control rule.

This article is organized as follows: Section 2 presents the mathematical models used to represent the proposed experiment. Section 3 describes in detail the elements and places used in the tests. In Section 4 the process for tuning parameters is shown and the experimental and simulation results are compared. Finally, in Section 5, we present the control technique and the mathematical description

necessary to simulate and complete the experimental test. Section 6 presents conclusions and suggests future work.

2. Mathematical Model

The lumped parameter technique is a methodology for modeling buildings, based on an analogy between thermal and electrical phenomena. Temperature is represented by voltage, heat flux by electric current, and thermal resistance is defined as the resistance to heat transfer through walls, and represented by an electrical resistance [31]. The resulting circuit must include a series of resistances associated with the different heat transfer processes, and capacitors that represent the wall's capacity to accumulate energy. In the literature it is possible to find different configurations and circuits, which allows choosing different models to solve the problem according to information quantity, physical characteristics, internal gains and others factors [32].

In the Lumped Parameter Models the heat flux is assumed in one direction, the orientation is defined by the difference between the environmental and internal temperature. In case of a higher external temperature, the sequence followed for the thermal energy is as follows: first, transfer from the external air to the exterior surface of each wall; next, conduction through the walls; finally, transfer from the interior surface wall to the interior air in the zone. The reverse process takes place when the internal temperature is higher than the environmental temperature.

2.1. Full Scale Model

Figure 1 shows a RC circuit equivalent to one closed room with four walls, a roof and a floor. This configuration of the LPM is called Full Scale Model [6–33]. It is characterized by including branches for the different surfaces, each branch incorporating resistances for the convection, radiation and conduction processes. The nomenclature uses two subscripts i and j ; the first one indicates the surface $i = 1, \dots, 6$, and the second one indicates the position $j = in, med, ex$. The subscript "in" corresponds to the interior elements, "mid" to conduction resistances, and "ex" represents the exterior elements. Thus, e.g., the resistance $R_{1,in}$ corresponds to the heat transfer process between the interior face and the interior air.

The conduction resistance for the corresponding wall is calculated according to Equation (1), the interior and exterior resistances are calculated with Equation (2). Here ϵ denotes the emissivity coefficient of the material, and h denotes the convection coefficient which must be tuned experimentally. The thermal capacity of each wall and the air contained in the zone is defined by Equation (3):

$$R_{i,med} = \frac{L_i}{k_i A_i} \tag{1}$$

$$R_{i,in-ex} = \frac{1}{A(h_{in-ex} + \epsilon_{in-ex} \sigma (T_{sup}^2 + T_a^2)(T_{sup} + T_a))} \tag{2}$$

$$C_{i,in-ex} = \frac{\rho_i C e_i A_i L_i}{2} \tag{3}$$

The whole model contains 31 fixed parameters: capacitors, resistances, one single time variant input (the environmental temperature $T_a(t)$), and finally 13 state variables associated with the internal and external surface temperatures together with the internal air temperature. All temperatures are calculated as the voltage over the capacitors, connecting the temperature $T_{i,j}$ with the capacitor $C_{i,j}$, and the internal air temperature T with the capacitor C_r . Applying circuit theory it is possible to determine one set of differential equations to calculate the temperature evolution:

$$\frac{dT_{i,ex}}{dt} = \frac{T_i}{R_{i,ex} C_{i,ex}} - T_{i,ex} \left(\frac{1}{R_{i,ex} C_{i,ex}} + \frac{1}{R_{i,mid} C_{i,ex}} \right) + \frac{T_{i,in}}{R_{i,mid} C_{i,ex}} \tag{4}$$

$$\frac{dT_{i,in}}{dt} = \frac{T_{i,ex}}{R_{i,mid}C_{i,in}} - T_{i,in} \left(\frac{1}{R_{i,mid}C_{i,in}} + \frac{1}{R_{i,in}C_{i,in}} \right) + \frac{T}{R_{i,in}C_{i,in}} \tag{5}$$

$$\frac{dT}{dt} = \frac{T_{1,in} - T}{R_{1,in}C_r} + \frac{T_{2,in} - T}{R_{2,in}C_r} + \frac{T_{3,in} - T}{R_{3,in}C_r} + \frac{T_{4,in} - T}{R_{4,in}C_r} + \frac{T_{5,in} - T}{R_{5,in}C_r} + \frac{T_{6,in} - T}{R_{6,in}C_r} + \frac{uI_L}{C_r} \tag{6}$$

Above, I_L represents the power of the internal gains and u their state (active or inactive).

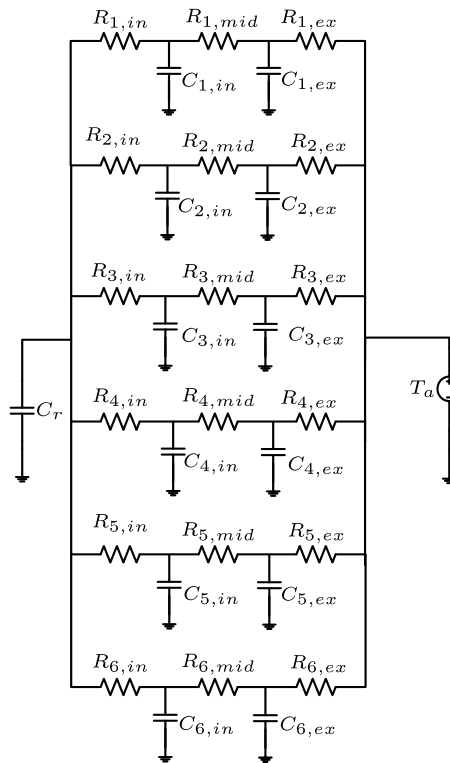


Figure 1. Circuit for a thermal zone using the full scale model.

2.2. Simplified Model

Another useful structure is presented in Figure 2; this circuit provides a simplified model and, in many cases, is enough to analyze a thermal zone with minimal parameters. This model requires 18 fixed parameters, one single input and only two state variables, corresponding to the wall temperature and the internal temperature (T_w and T respectively). In this case, the conduction resistance is denoted with only one subscript i , and the internal and external resistances carry one additional subscript j to indicate their positions. Important elements are the calculation of R_i and C_w ; in this structure, the resistance is calculated with one half of the wall's thickness, and the capacitor uses the entire superface area. The order reduction in this model is given by disregarding the radiation process that, in transitional states, hardly contributes to the general dynamics. Thus, the internal and external resistances are calculated with the convection coefficient.

In order to calculate the set of differential equations, the circuit must be simplified by reducing the resistors; the external face is calculated by the parallel resistor as $\frac{1}{R_{st}} = \sum_1^i \frac{1}{R_{s,i}}$, where $R_{s,i}$ is the linear addition of the conduction and convection resistors $R_{s,i} = R_i + R_{i,ex}$. Similarly, the internal face resistor R_{mt} is calculated using the corresponding convection coefficient for the resistor $R_{m,i} = R_i + R_{i,in}$. The final results are shown in Equations (7) and (8):

$$\frac{dT_w}{dt} = \frac{T}{R_{st}C_w} - T_w \left(\frac{1}{R_{st}C_w} + \frac{1}{R_{mt}C_w} \right) + \frac{T_a}{R_{st}C_w} \tag{7}$$

$$\frac{dT}{dt} = \frac{T_w - T}{R_{mt}C_r} \tag{8}$$

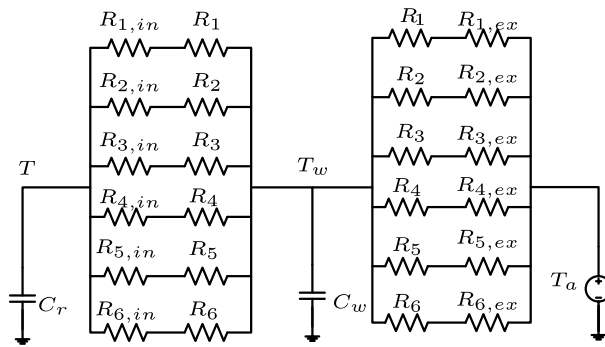


Figure 2. Circuit for a thermal zone using the simplified model.

3. Experimental Setup

Using the concept of reduced scale models for the evaluation of the controller, a closed container was built with a chipboard working as a thermal zone. Such elements are regularly used in kitchen furniture. The dimensions of the container are 70 cm × 40 cm × 58 cm with 15.8 mm of wall thickness; additionally, it is lifted 10 cm from the ground with plastic legs that limit heat transmission by contact with the ground. In Table 1 additional data associated with the materials used in the experiment are presented.

Table 1. Parameters of the materials used in the experiment.

Material	Parameter	Value
Wood	Conductivity	$0.645 \frac{KJ}{hmK}$
	Density	$700 \frac{kg}{m^3}$
	Specific heat	$1.6 \frac{KJ}{kgK}$
Air	Density	$1.2 \frac{kg}{m^3}$
	Specific heat	$1.007 \frac{KJ}{kgK}$

The box was equipped with: one 60 W incandescent internal lamp with infrared light to simulate a heater in a closed room; one temperature and humidity sensor (Data Logger Wöhler CDL 210) inside the box, and another one outside the box for registering environmental conditions.

Figure 3 shows the wooden box with the lamp and temperature sensor ready to start the experiment. All the tests were carried out in closed spaces (in order to minimize the effect of environmental changes) at Polytechnic University of Valencia (Spain). The first two data recomputations were done in open loop, with the objective of generating enough information to adjust the models and calculate the control parameters [34].



Figure 3. Wooden box used as scale reduced model.

4. Adjusting the Models

For the dynamical analysis of the thermal zone built, it was necessary to develop a simulator to reproduce the experimental results. The mathematical model described in Section 2.1 needs to be adjusted to the situation of the system. That is, the convection and radiation coefficients for internal and external faces had to be determined as functions of the state of the lamp. The activation state is called “charge” and the deactivation stage is called “discharge” in the rest of this work. The tuning is based on the experimental records obtained in open loop. Our strategy uses the registered data of the internal temperature and an optimization algorithm to minimize the error between simulation and experimental results.

The first test was done on 15 March 2018 and lasted 24 h (only the first 6 h were on charge). With the data compiled, the Pattern Search algorithm from the OptimTool of MATLAB was used. This tool requires a mathematical model, one objective function, and a set of output parameters. In this case, the mathematical model used is presented in Section 2.1. The objective function $F_o(T)$ is shown in Equation (9). Finally, the set of output parameters defined are the internal convection coefficient h_i , the external convection h_o , the internal emissivity ϵ_i and the external emissivity ϵ_o .

$$F_o(T) = \min \left\{ E(T) \right\} \tag{9}$$

$$E(T) = \frac{\sqrt{\int_{t_0}^{t_f} |T_{measured} - T|^2}}{\sqrt{\int_{t_0}^{t_f} |T_{measured}|^2}} \times 100 \tag{10}$$

As mentioned previously, the charge and discharge phases were analyzed individually, with the resulting coefficients presented in Table 2. With these parameters, the simulator was compared with the experimental results. This produced the results shown in Figure 4. The model’s accuracy with the adjusted parameters was tested by calculating the relative error shown in Equation (10). This led to an approximate error of 2.7%.

Table 2. convection and radiation coefficients.

Phase/Parameter	$h_i [\frac{KJ}{hm^2K}]$	$h_o [\frac{KJ}{hm^2K}]$	ϵ_i	ϵ_o
Charge	44.6875	11.1250	0.9430	0.9
Discharge	0	9.7324	0.0211	0.8805

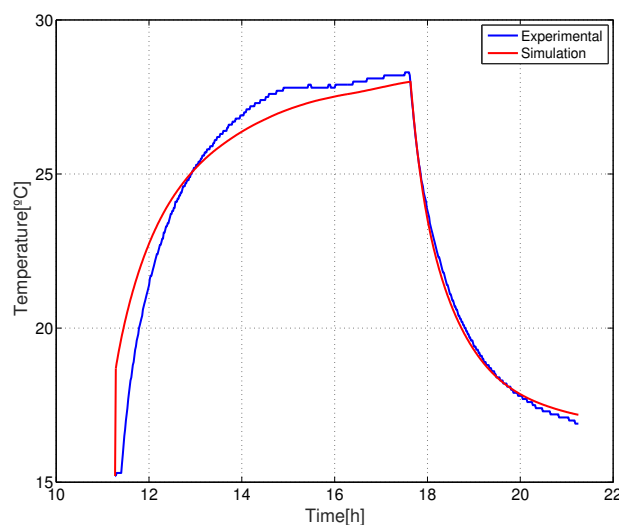


Figure 4. Simulated and experimental results in the first test.

The second test in open loop was done on 13 April 2018 and lasted 11 days (10 days were on charge phase). The comparison between experimental and simulation is shown in Figure 5. In this case the relative error was about 2.3%. This figure was plotted using a total amount of 4756 data. Among these, only in six cases does the difference between experimental and theoretical values exceed 2 degrees. It exceeds 1.5 degrees in 97 cases, while exceeding 1 degree in 461 cases. In all remaining 4295 cases the error lies below 1 degree.

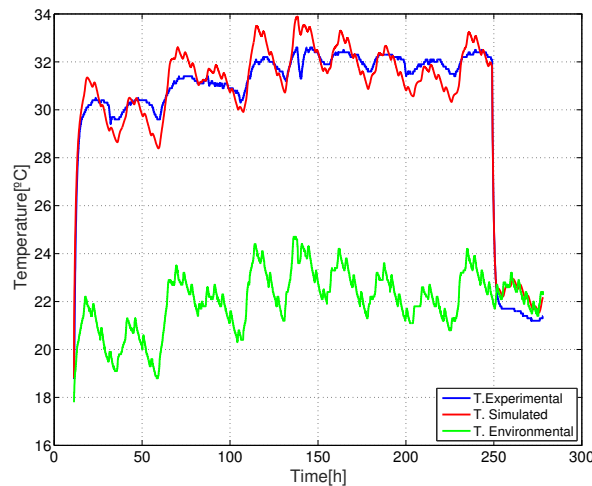


Figure 5. Simulated and experimental results in the second test.

5. Control Application

For the evaluation of the Sliding Control (SC) on the thermal zone, it was decided to use the second order model (presented in Section 2.2) because this scheme is easier to adapt to the control structure. In Figure 6, a reduction of the second order circuit is presented, with the internal gain I_L driven by the SC to handle the internal temperature in the thermal zone.

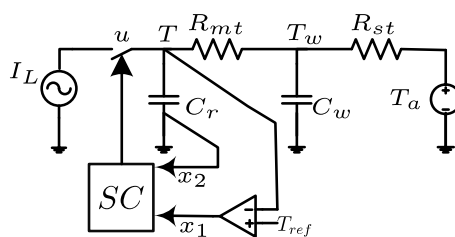


Figure 6. Reduced circuit of the simplified model with sliding modes control structure.

The state variables defined by the controller are the temperature error x_1 and the heat flux x_2 shown in Equations (11) and (12). Here the desired temperature for the closed room is called reference temperature T_{ref} , and the switch u represents the internal gain state. With these variables and differentiating with respect to time, the state-space model can then be implemented by Equations (13) and (14):

$$x_1 = T_{ref} - T \tag{11}$$

$$x_2 = i_{C_r} \tag{12}$$

$$\dot{x}_1 = \frac{-x_2}{C_r} \tag{13}$$

$$\dot{x}_2 = \dot{i}_{C_r} \tag{14}$$

To simplify the mathematical equations, the following parameters are defined:

$$a = \frac{1}{R_{mt}R_{st}C_w} \tag{15}$$

$$b = \frac{1}{R_{st}C_w} \tag{16}$$

$$c = \frac{1}{R_{mt}C_w} \tag{17}$$

$$d = \frac{1}{R_{mt}C_r} \tag{18}$$

The state variables are defined as functions of the constants previously defined (the ambient temperature, reference temperature, and the internal power source):

$$\begin{bmatrix} \dot{x}_1 \\ \dot{x}_2 \end{bmatrix} = \begin{bmatrix} 0 & -\frac{1}{C_r} \\ a & -(b+c+d) \end{bmatrix} \begin{bmatrix} x_1 \\ x_2 \end{bmatrix} + \begin{bmatrix} 0 \\ I_L(b+c) \end{bmatrix} u + \begin{bmatrix} 0 \\ a(T_a - T_{ref}) \end{bmatrix} \tag{19}$$

The SC determines the switch position with a trajectory function s based on the state variables,

$$s = \alpha x_1 + x_2 = Jx \tag{20}$$

Above, J and x are the vectors $J = [\alpha, 1]$ and $x = [x_1, x_2]^T$, and α is the parameter to be adjusted by the controller designer. The objective of this constant is to divide the space state in two sectors by a line with slope α . This line is generated by the state variables that satisfy $s = 0$. In each zone, one system equilibrium ($\dot{x}_1 = \dot{x}_2 = 0$) must be located, corresponding to the switch position (active/inactive).

The first case analyzed is the internal active source, with $u = 1$ equilibrium coordinates presented in Equations (21) and (22). In this point the trajectory function is fulfilling the condition $s > 0$.

$$x_1 = T_{ref} - I_L\left(\frac{b+c}{a}\right) - T_a \tag{21}$$

$$x_2 = 0 \tag{22}$$

For the second case, the internal source is deactivated. The $u = 0$ equilibrium conditions are shown in Equations (23) and (24). This point satisfies the condition $s < 0$:

$$x_1 = T_{ref} - T_a \tag{23}$$

$$x_2 = 0 \tag{24}$$

Once the equilibrium analysis is done, the control laws can be established. Equation (25) shows the actions in the searching period. Equation (26) defines the control laws when the system is approaching the stability ($x_1 = x_2 = 0$) tracking the sliding line. Here ϵ is a positive small constant arbitrarily determined.

$$u = \begin{cases} u = 0 & \text{if } s > 0 \\ u = 1 & \text{if } s < 0 \end{cases} \tag{25}$$

$$\dot{s} = \begin{cases} J\dot{x} & \text{if } 0 < s < \epsilon \\ J\dot{x} & \text{if } -\epsilon < s < 0 \end{cases} \tag{26}$$

To determine the slope of the sliding line (α) the evolution of the trajectory function must be evaluated with respect to time. Equation (28) shows that only the sliding parameter affects the incoming heat flux. Enforcing $\dot{s} = 0$, the critical value α can be determined as presented in Equation (29):

$$\dot{s} = \alpha \dot{x}_1 + \dot{x}_2 \tag{27}$$

$$\dot{s} = -\alpha \frac{x_2}{C_r} + \alpha x_1 - x_2(b + c + d) - aT_{ref} + uI_L(b + c) + aT_a \tag{28}$$

$$\alpha = C_r \left(\frac{1}{R_{st}C_w} + \frac{1}{R_{mt}C_w} + \frac{1}{R_{mt}C_r} \right) \tag{29}$$

Based on the previous analysis, the slope of the sliding line was $\alpha = 48.3192$. With this constant and the system parameters defined, it was possible to develop the simulation of the thermal zone under the sliding control technique.

The simulation was designed with an ambient temperature of 16 °C, a reference temperature of $T_{ref} = 28$ °C, and the hysteresis band with a fixed constant of $\varepsilon = 0.5$. The results are presented in Figure 7. Here the black line represents the sliding surface, the green lines limits the hysteresis band, and the red and blue lines in Figure 7a correspond to the evolution of the state variables x_1 and x_2 as a function of the switch position; blue is for the active $u = 1$ and red for the inactive $u = 0$. This first figure shows the search stage. Figure 7b shows the tracking stage and the oscillation of the system around the stability point ($\dot{x}_1 = \dot{x}_2 = 0$). Finally, Figure 7c presents the internal temperature that achieves the reference temperature and maintains its value satisfying the 2% criteria.

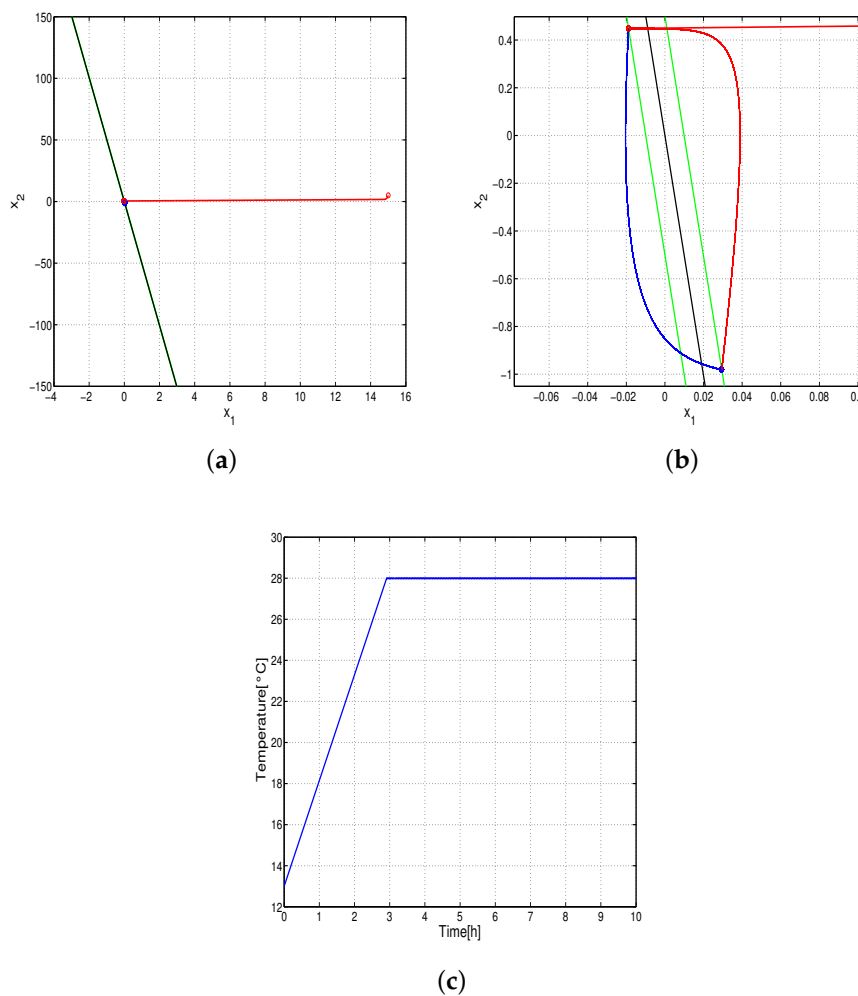


Figure 7. simulation results. (a) Theoretical development of the search stage. (b) Theoretical development of the tracking stage. (c) Theoretical internal temperature with the sliding mode control.

We performed different experimental tests by programming the electronic card ESP32 LOLIN lite and measuring internal and external temperatures using a sensor DS18B20 with a sampling rate of 3 min. Figure 8 presents the results obtained after 65 h of experimentation. The first two pictures present the x_1 and x_2 variable evolution (searching and tracking stages). Figure 8c shows that the internal temperature achieves the reference temperature of 28 °C. As in the case of the simulated results, this reference temperature (output variable) is achieved and it maintained the 2% criterion.

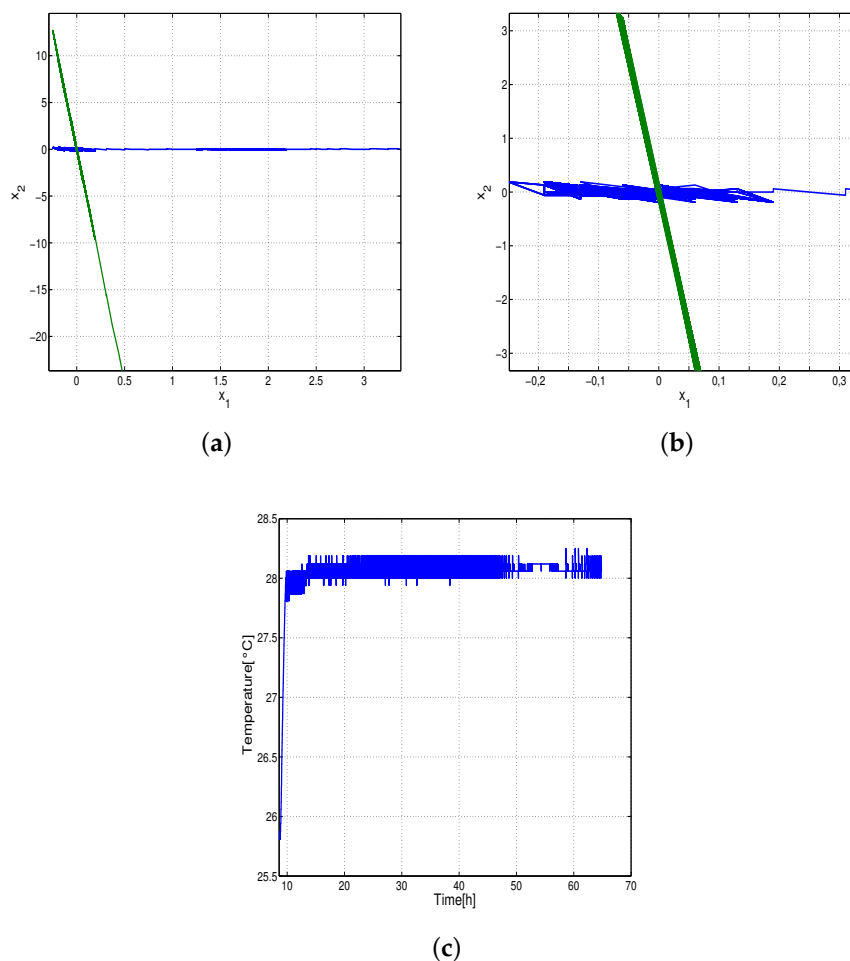


Figure 8. Experimental results. (a) Experimental development of the search stage. (b) Experimental development of the tracking stage. (c) Experimental internal temperature with the sliding mode control.

6. Conclusions

An appropriate mathematical model can capture the thermodynamical behavior of a closed room, allowing analyzing its characteristics and determining the most important factors in energy consumption. In the energetic analysis of buildings, it is important to rely on algorithms and methods to estimate the heat transfer parameters that contribute to thermal leaks. In this work we proposed an experiment based on a piece of kitchen furniture with one internal lamp. Using the lumped parameter technique for modeling, it was possible to build a simulator to reproduce the internal temperature in the thermal zone.

In order to adjust the main parameters for the simulator, different tuning strategies were used. The best results were obtained by the algorithm called Pattern Search, in MATLAB. With this tool, and using the experimental data, we determine the transfer coefficients between the walls and the surrounding air. The full scale model to reproduce the experimental results with a relative error of less than 3%.

To summarize, in this paper we tested the ability of the sliding control technique to regulate temperature in a thermal zone. The goals were achieved through the implementation of reduced scale models, through a set of important tools to experimentally verify the theories, and through new techniques of simulation and control in buildings. It is even possible to avoid many error sources in the mathematical models, such as environmental conditions and random disturbances. Furthermore, the test can be done with a low budget and without interrupting regular conditions in a real building.

The simulation and experimental results show that the technique control can be used to regulate the internal temperature of a thermal zone in regions with a low ambient temperature. This procedure can be extrapolated to different and bigger zones.

Future work to be done would be the introduction of disturbances test and the random opening of doors or windows. This could help to test the robustness of the controller. Furthermore, the evaluation of the energetic consumption in closed loop is necessary to define the savings in comparison with other control strategies.

Author Contributions: Conceptualization and methodology design: P.F.d.C. and J.L.H.; experiment development and data collection: F.F., J.L.H. and G.O.; data analysis and simulations: P.F.d.C., F.F. and J.T.; writing—original draft preparation: G.O. and F.F.; validation and writing—review and editing: P.F.d.C. and J.T.; funding acquisition: G.O., P.F.d.C. and J.L.H.

Funding: This investigation was supported by national doctoral program of the Colombian Administrative Department of Science Technology and Innovation (Colciencias), and the agreement “Analysis of the properties, applications and market opportunities of G-cover Coatings” closed between the Universitat Politècnica de València (Spain) and the Mexican company G-cover.

Acknowledgments: The authors thank to the Journal editors and the reviewers for their worthwhile suggestions and comments.

Conflicts of Interest: The authors declare no conflict of interest.

Nomeclature

α	Sliding constant
σ	Stefan-Boltzman contant
ρ	Material density
ε_{in-ex}	Radiation coefficient
ϵ	Hysteresis band amplitude
L_i	Thickness of the walls
k_i	Material's conductivity
A_i	Surface area
h_{in-ex}	Convection coefficient
s	Sliding trajectory
J	Sliding constants vector
x	State variables vector
$R_{i,j}$	Thermal resistance
$C_{i,j}$	Surface thermal capacity
C_r	Air thermal capacity
C_w	Envelope thermal capacity
Ce_i	Specific heat
$T_{i,j}$	Surface temperature
T	Zone temperature
T_a	Ambient temperature
T_{sup}	Superficial temperature
T_{ref}	Reference temperature
i_{cr}	Incoming heat flux
u	Lamp state

I_L	Internal gain power
$F_0(T)$	Objective function
$E(T)$	Temperature error
$\ f\ _2$	L_2 norm of function f : $\sqrt{\int_a^b f(x) ^2 dx}$

References

1. Forgiarini, R.; Giraldo, N.; Lamberts, R. A review of human thermal comfort in the built environment. *Energy Build.* **2015**, *105*, 178–205. [[CrossRef](#)]
2. Delgarm, N.; Sajadi, B.; Delgarm, S. Multi-objective optimization of building energy performance and indoor thermal comfort: A new method using artificial bee colony (ABC). *Energy Build.* **2016**, *131*, 42–53. [[CrossRef](#)]
3. Underwood, C.; Yik, F. *Modelling Methods for Energy in Buildings*; Blackwell Science: Oxford, UK, 2004. [[CrossRef](#)]
4. Park, H. Dynamic Thermal Modeling of Electrical Appliances for Energy Management of Low Energy Buildings. Ph.D. Thesis, University of Cergy-Pontoise, Cergy-Pontoise, France, 2014.
5. Gorni, D.; Castilla, M.; Visioli, A. An efficient modelling for temperature control of residential buildings. *Build. Environ.* **2016**, *103*, 86–98. [[CrossRef](#)]
6. Fazenda, P.; Lima, P.; Carreira, P. Context-based thermodynamic modeling of buildings spaces. *Energy Build.* **2016**, *124*, 164–177. [[CrossRef](#)]
7. Bacher, P.; Madsen, H. Identifying suitable models for the heat dynamics of buildings. *Energy Build.* **2011**, *43*, 1511–1522. [[CrossRef](#)]
8. Mba, L.; Meukam, P.; Kémajou, A. Application of Artificial Neural Network for Predicting the Indoor Air Temperature in Modern Building in Humid Region. *Energy Build.* **2016**, *121*, 32–42. [[CrossRef](#)]
9. Lin, Y.; Middelkoop, T.; Barooah, P. Issues in identification of control-oriented thermal models of zones in multi-zone buildings. In Proceedings of the IEEE Conference on Decision and Control, Maui, HI, USA, 10–13 December 2012; pp. 6932–6937. [[CrossRef](#)]
10. Anisimova, E.Y. Building Thermal Regime Modeling. *Procedia Eng.* **2017**, *206*, 795–799. [[CrossRef](#)]
11. Ryzhov, A.; Ouerdane, H.; Gryazina, E.; Bischi, A.; Turitsyn, K. Model predictive control of indoor microclimate: Existing building stock comfort improvement. *Energy Convers. Manag.* **2019**, *179*, 219–228. [[CrossRef](#)]
12. Bagheri, A.; Feldheim, V.; Thomas, D.; Ioakimidis, C. Energy Efficiency from to The walls The adjacent effects in simplified thermal model of buildings. In Proceedings of the ScienceDirect CISBAT 2017 International Conference, Lausanne, Switzerland, 6–8 September 2017.
13. Luzi, M.; Vaccarini, M.; Lemma, M. A tuning methodology of Model Predictive Control design for energy efficient building thermal control. *J. Build. Eng.* **2019**, *21*, 28–36. [[CrossRef](#)]
14. Fiorentini, M.; Wall, J.; Ma, Z.; Braslavsky, J.H.; Cooper, P. Hybrid model predictive control of a residential HVAC system with on-site thermal energy generation and storage. *Appl. Energy* **2017**, *187*, 465–479. [[CrossRef](#)]
15. Massa Gray, F.; Schmidt, M. Thermal building modelling using Gaussian processes. *Energy Build.* **2016**, *119*, 119–128. [[CrossRef](#)]
16. Ascione, F.; Bianco, N.; De Stasio, C.; Mauro, G.M.; Vanoli, G.P. Simulation-based model predictive control by the multi-objective optimization of building energy performance and thermal comfort. *Energy Build.* **2015**, *111*, 131–144. [[CrossRef](#)]
17. Acosta, A.; González, A.I.; Zamarreño, J.M.; Álvarez, V. Energy savings and guaranteed thermal comfort in hotel rooms through nonlinear model predictive controllers. *Energy Build.* **2016**, *129*, 59–68. [[CrossRef](#)]
18. Afram, A.; Janabi-shari, F. Theory and applications of HVAC control systems—A review of model predictive control (MPC). *Build. Environ.* **2014**, *72*, 343–355. [[CrossRef](#)]
19. Nagarathinam, S.; Doddi, H.; Vasani, A.; Sarangan, V.; Venkata Ramakrishna, P.; Sivasubramanian, A. Energy efficient thermal comfort in open-plan office buildings. *Energy Build.* **2017**, *139*, 476–486. [[CrossRef](#)]
20. Smarra, F.; Jain, A.; de Rubeis, T.; Ambrosini, D.; D’Innocenzo, A.; Mangharam, R. Data-driven model predictive control using random forests for building energy optimization and climate control. *Appl. Energy* **2018**, *226*, 1252–1272. [[CrossRef](#)]

21. Killian, M.; Mayer, B.; Kozek, M. Cooperative fuzzy model predictive control for heating and cooling of buildings. *Energy Build.* **2016**, *112*, 130–140. [[CrossRef](#)]
22. Brastein, O.M.; Perera, D.W.; Pfeifer, C.; Skeie, N.O. Parameter estimation for grey-box models of building thermal behaviour. *Energy Build.* **2018**, *169*, 58–68. [[CrossRef](#)]
23. Lirola, J.M.; Castañeda, E.; Lauret, B.; Khayet, M. A review on experimental research using scale models for buildings: Application and methodologies. *Energy Build.* **2017**, *142*, 72–110. [[CrossRef](#)]
24. Coutinho, C.P.; Baptista, A.J.; Dias Rodrigues, J. Reduced scale models based on similitude theory: A review up to 2015. *Eng. Struct.* **2016**, *119*, 81–94. [[CrossRef](#)]
25. Chew, L.W.; Glicksman, L.R.; Norford, L.K. Buoyant flows in street canyons: Comparison of RANS and LES at reduced and full scales. *Build. Environ.* **2018**, *146*, 77–87. [[CrossRef](#)]
26. Chen, S.Y.; Gong, S.S. Speed tracking control of pneumatic motor servo systems using observation-based adaptive dynamic sliding-mode control. *Mech. Syst. Signal Process.* **2017**, *94*, 111–128. [[CrossRef](#)]
27. Huang, Y.; Khajepour, A.; Ding, H.; Bagheri, F.; Bahrami, M. An energy-saving set-point optimizer with a sliding mode controller for automotive air-conditioning/refrigeration systems. *Appl. Energy* **2017**, *188*, 576–585. [[CrossRef](#)]
28. Mironova, A.; Mercorelli, P.; Zedler, A.; Mironova, A.; Mercorelli, P. Robust Control using Sliding Mode Approach for Ice-Clamping Device activated by Thermoelectric Coolers. *Int. Fed. Autom. Control* **2016**, *25*, 470–475. [[CrossRef](#)]
29. Norton, M.; Khoo, S.; Kouzani, A.; Stojcevski, A. Adaptive fuzzy multi-surface sliding control of multiple-input and multiple-output autonomous flight systems. *IET Control Theory Appl.* **2015**, *9*, 587–597. [[CrossRef](#)]
30. He, T.; Li, L.; Zhu, J.; Zheng, L. A Novel Model Predictive Sliding Mode Control for AC/DC Converters with Output Voltage and Load Resistance Variations. In Proceedings of the 2016 IEEE Energy Conversion Congress and Exposition (ECCE), Milwaukee, WI, USA, 18–22 September 2016; pp. 1–6.
31. Cengel, Y. *Transferencia de Calor y Masa*; McGraw Hill: Mexico City, Mexico, 2007.
32. Fux, S.F.; Ashouri, A.; Benz, M.J.; Guzzella, L. EKF based self-adaptive thermal model for a passive house. *Energy Build.* **2014**, *68*, 811–817. [[CrossRef](#)]
33. Lin, Y.; Middelkoop, T.; Barooah, P. Identification of control-oriented thermal models of rooms in multi-room buildings. In Proceedings of the 2012 IEEE 51st Annual Conference on Decision and Control (CDC), Maui, HI, USA, 10–13 December 2012.
34. Florez, F.; Higón, J.; Conejero, J.A.; Córdoba, P.F.D. Modeling and Experimental verification of thermal properties of Thermo Sköld coating solutions. In Proceedings of the International Congress on Industrial and Applied Mathematics, Valencia, Spain, 15–19 July 2019; Volume 9.



Neutrino mixing and masses in a left-right model with mirror fermions

R. Gaitán², A. Hernández-Galeana¹, J. M. Rivera-Rebolledo¹
and P. Fernández de Córdoba³

”Interdisciplinary Modeling Group, InterTech.”

1. Departamento de Física,
Escuela Superior de Física y Matemática, I.P.N.,
U.P. Adolfo L. Mateos, México D.F., 07738, México

2. Centro de Investigaciones Teóricas, FES, UNAM,
Apartado Postal 142, Cuatitlán-Izcalli, Estado de México,
Código postal 54700, México.

November 10, 2018

Abstract

In the framework of a left-right model containing mirror fermions with gauge group $SU(3)_C \otimes SU(2)_L \otimes SU(2)_R \otimes U(1)_{Y'}$, we estimate the neutrino masses, which are found to be consistent with their experimental bounds and hierarchy. We evaluate the decay rates of the Lepton Flavor Violation (LFV) processes $\mu \rightarrow e\gamma$, $\tau \rightarrow \mu\gamma$ and $\tau \rightarrow e\gamma$. We obtain upper limits for the flavor-changing branching ratios in agreement with their present experimental bounds. We also estimate the decay rates of heavy Majorana neutrinos in the channels $N \rightarrow W^\pm l^\mp$, $N \rightarrow Z\nu_l$ and $N \rightarrow H\nu_l$, which are roughly equal for large values of the heavy neutrino mass. Starting from the most general Majorana neutrino mass matrix, the smallness of active neutrino masses turns out from the interplay of the hierarchy of the involved scales and the double application of seesaw mechanism. An appropriate parameterization on the structure of the neutrino mass matrix imposing a symmetric mixing of electron neutrino with muon and tau neutrinos leads to Tri-bimaximal mixing matrix for light neutrinos.

PACS numbers: 12.60.Cn, 12.60.Fr, 13.35.Bv, 13.35.Dx, 13.35.Hb, 14.60.Pq

1 Introduction

The evidences for neutrino oscillations obtained in experimental results from atmospheric, solar, reactor and accelerator neutrinos lead to conclude that the neutrinos have a mass different from zero. The current neutrino experimental data (SuperKamiokande, SNO, Kamland, K2K, GNO, CHOOZ) can be described by neutrino oscillations via three neutrino mixings [1]. The present data give the solar neutrino lepton mixing angle $\tan^2 \theta_{12} = 0.45 \pm 0.05$, the atmospheric angle $\sin^2 2\theta_{23} = 1.02 \pm 0.04$ and $\sin^2 2\theta_{13} = 0 \pm 0.05$ [2]. The complex phase has not yet been measured.

The experimental information on neutrino masses and mixing points out new physics beyond the Standard Model (SM) of particle physics, with a great activity on the consequences. Among the possible mechanisms of neutrino mass generation, the most simple and attractive one is the seesaw mechanism [3, 4], which explains the smallness of the observed light neutrino masses through the exchange of superheavy particles; an alternative explanation is given by extra dimensions beyond the usual three ones [5]. It has been suggested [ref.] that right-handed (RH) neutrinos experience one or more of these extra dimensions, such that they only spend part of their time in our world, with apparently small masses. At the present, it is not known whether neutrinos are Dirac or Majorana fermions.

Models with heavy neutrinos of mass of order 1 TeV can give rise to significant light-heavy mixing and deviation from unitarity of the Pontecorvo-Maki-Nakagawa-Sakata (PMNS) matrix [6]. The nonunitarity nature of the neutrino mixing matrix due to mixing with fields heavier than $\frac{M_Z}{2}$ can manifest in tree level processes like $\pi \rightarrow \mu\nu$, $Z \rightarrow \bar{\nu}\nu$, $W \rightarrow l\nu$ or in charged lepton decays $\mu \rightarrow e\gamma$, $\tau \rightarrow \mu\gamma$, etc. which are flavor violating and rare and proceed at one loop level [6, 7]. The TeV scale seesaw models are interesting because they can have signatures in the CERN Large Hadron Collider (LHC) in the near future [8].

Neutrinos also are important in astrophysics and cosmology [9] and probably they contribute to hot dark matter in the Universe and in its evolution.

Parity P violation was one of the greatest discoveries of particle physics [10]. Before this observation, according to Fermi's hypothesis it was believed that weak interactions have purely vectorial V or axial vectorial (V-A) parity conserving Lorentz structure [11]. The theory of Lee and Yang in 1956 [12] proposed a fermion current with V and A structure. It is known that in the standard model (SM) the electroweak interactions have a V-A form, with only left-handed (LH) (ordinary) fermions coupling to the weak gauge boson W^\pm . But one can include also mirror fermions [13] with a $V + A$ coupling, such that P is conserved. In this sense, the term "mirror fermion" is equivalent to "vector-like fermion", where for a theory with gauge group G , in a representation R one has sets of LH and RH fermions.

In the literature a second meaning of that term is used. G is extended to a $G \times G$ gauge theory, and for every multiplet $(R, 1)$ a mirror partner $(1, R)$ is added, such that there is no gauge invariant mass term connecting the LH and RH multiplets [14]. Thus it is natural to consider the existence of mirror generations.

Masses of mirror particles arise from symmetry breaking; for mirror generation they may lie below one TeV , and feasible to be discovered in Fermilab Tevatron Collider and LHC.

A solution to the strong CP problem has been proposed within a L-R symmetric context [16]. The electroweak group is extended to $SU(2)_L \otimes SU(2)_R \otimes U(1)$ including mirror fermions. These fermions are conjugated to the ordinary ones with respect to the gauge symmetry group such

that a fermion representation including both of them is real and the cancellation of anomalies is automatic [17].

In this paper we consider a L-R model with mirror fermions (LRMM) with gauge group $G \equiv SU(3)_C \otimes SU(2)_L \otimes SU(2)_R \otimes U(1)_{Y'}$. We discuss in section 2 the formalism of mixing between standard and new exotic fermions. In Sec. 3 we present the model and discuss the symmetry breaking process with two scalar doublets.

In Sec. 4 we write the gauge invariant Yukawa couplings which after spontaneous symmetry breaking give the most general Majorana neutrino mass matrix. With a double application of the type I seesaw approximation we estimate the light neutrino masses in terms of free Yukawa couplings assuming textures for the light and mirror matrices, obtaining consistent normal hierarchical values for masses and a tribimaximal mixing for light neutrinos. We discuss in section 4 the mixing between standard and mirror fermions. In Sec. 5 we include the radiative decays $\mu \rightarrow e\gamma$, $\tau \rightarrow \mu\gamma$ and $\tau \rightarrow e\gamma$ and estimate bounds for their branching ratios. Finally, we calculate such ratios for the heavy Majorana neutrinos decays $N \rightarrow W^+l^-$, $N \rightarrow Z\nu_l$ and $N \rightarrow H\nu_l$, getting a smooth variation with the heavy neutrino mass, even when it is much larger than any of the involved masses.

2 Fermion mixing and flavor violation

To consider the mixing of fermions, we shall follow Ref. [6], grouping all fermions of electric charge q and helicity $a = L, R$ into $n_a + m_a$ vector column of n_a ordinary (o) and m_a exotic (e) gauge eigenstates, i.e. $\psi_a^o = (\psi_{n_a}^o, \psi_{m_e}^o)_a^T$. The ordinary fermions include the SM ones, whereas the exotics include any new fermion with sequential (mirror or singlet) properties beyond the SM.

The relation between the gauge eigenstates and the corresponding light (l) and heavy (h) charged mass eigenstates $\psi_a = (\psi_l, \psi_h)_a^T$, $a = L, R$ is given by the transformation

$$\psi_a^o = V_a \psi_a \quad , \quad a = L, R \quad (1)$$

where

$$V_a = \begin{pmatrix} A_a & E_a \\ F_a & G_a \end{pmatrix} \quad (2)$$

In the Eq. (2), A_a is a matrix relating the ordinary weak states and the light-mass eigenstates, while G_a relates the exotic and heavy states. E_a and F_a describe the mixing between the two sectors.

From the unitary of V

$$V_a V_a^+ = 1, a = L, R \quad (3)$$

it follows that the submatrix A_a is not unitary. The term $F_a^+ F_a$, which is second order in the small light-heavy fermion mixing, will induce flavor-changing transitions in the light-light sector.

The vacuum expectation values (VEV) of the neutral scalars produce the SM fermion mass terms, which together with the exotic mass and mixing matrices lead to the mass matrix M which takes the form

$$M = \begin{pmatrix} K & \hat{\mu} \\ \mu & \hat{K} \end{pmatrix} \quad (4)$$

where K denotes the SM fermion mass matrix and \hat{K} corresponds to the fermion mass matrices associated with the exotic sector, while $\mu, \hat{\mu}$ correspond to the mixing terms between ordinary and exotic fermions.

The diagonal mass matrix M_d can be obtained through a biunitary rotation acting on the L and R sectors, namely

$$M_d = V_L^+ M V_R = \begin{pmatrix} m_l & 0 \\ 0 & M_h \end{pmatrix} \quad (5)$$

where m_l, m_h denote the light and heavy diagonal mass matrices, respectively. The form of the mass matrix will depend on the type of exotic fermion considered.

The scalar-fermion couplings within some specific Higgs sector are not diagonal in general, and one can see that the couplings are not diagonal in general; thus new phenomena associated with flavor-changing neutral currents (FCNC) will be present in such model.

3 The Model

In this and next sections we follow closely [15]. The LRMM formulation is based on the gauge group $SU(2)_L \otimes SU(2)_R \otimes U(1)_{Y'}$. In order to solve different problems such as the hierarchy of quark and lepton masses or the strong CP problem, different authors have enlarged the fermion content to the form

$$\begin{aligned} l_{iL}^0 &= \begin{pmatrix} \nu_i^0 \\ e_i^0 \end{pmatrix}_L, \quad e_{iR}^0, \nu_{iR}^0, & ; & \quad \hat{l}_{iR}^0 = \begin{pmatrix} \hat{\nu}_i^0 \\ \hat{e}_i^0 \end{pmatrix}_R, \quad \hat{e}_{iL}^0, \hat{\nu}_{iL}^0, \\ Q_{iL}^0 &= \begin{pmatrix} u_i^0 \\ d_i^0 \end{pmatrix}_L, \quad u_{iR}^0, d_{iR}^0, & ; & \quad \hat{Q}_{iR}^0 = \begin{pmatrix} \hat{u}_i^0 \\ \hat{d}_i^0 \end{pmatrix}_R, \quad \hat{u}_{iL}^0, \hat{d}_{iL}^0, \end{aligned} \quad (6)$$

where the index i runs over the three fermion families and the superscripts 0 denote gauge eigenstates. The quantum numbers of these fermions under the gauge group G defined above are given by

$$\begin{aligned} l_{iL}^0 &\sim (1, 2, 1, -1)_{iL} \quad , \quad \nu_{iR}^0 \sim (1, 1, 1, 0)_{iR} \quad , \quad e_{iR}^0 \sim (1, 1, 1, -2)_{iR} \\ \hat{\nu}_{iL}^0 &\sim (1, 1, 1, 0)_{iL} \quad , \quad \hat{e}_{iL}^0 \sim (1, 1, 1, -2)_{iL} \quad , \quad \hat{l}_{iR}^0 \sim (1, 1, 2, -1)_{iR} \\ u_{iR}^0 &\sim (3, 1, 1, \frac{4}{3})_{iR} \quad , \quad d_{iR}^0 \sim (3, 1, 1, \frac{2}{3})_{iR} \\ \hat{u}_{iL}^0 &\sim (3, 1, 1, \frac{4}{3})_{iL} \quad , \quad \hat{d}_{iL}^0 \sim (3, 1, 1, \frac{2}{3})_{iL} \\ Q_{iL}^0 &\sim (3, 2, 1, \frac{1}{3})_{iL} \quad , \quad \hat{Q}_{iR}^0 \sim (3, 1, 2, \frac{1}{3})_{iR} \end{aligned}$$

respectively, and the last entry corresponds to the hypercharge (Y') with the electric charge defined as $Q = T_{3L} + T_{3R} + \frac{Y'}{2}$.

A model with gauge group $SU(2)_L \times SU(2)_R \times U(1)_V \times SU(3)_H$ and the fermion content (6) was originally suggested in Z. G. Berezhiani [18] as the "universal seesaw" model which generated masses of charged fermions as well as of the neutrinos. He also worked on a $SU(5) \times SU(3)_H$ model for extension to $SO(10)$ or Pati-Salam [19], predicting for instance $m_{\nu_e} = O(10)$ eV. At low (electroweak scale) energies the model simulates the standard $SU(3)_C \times SU(2)_L \times U(1)_Y$ model, and FCNC are suppressed naturally.

3.1 Symmetry breaking

The "Spontaneous Symmetry Breaking" (SSB) is achieved following the stages:

$$G \longrightarrow G_{SM} \longrightarrow SU(3)_C \otimes U(1)_Q \quad (7)$$

where $G_{SM} = SU(3)_C \otimes SU(2)_L \otimes U(1)_Y$ is the "Standard Model" group symmetry, and $\frac{Y}{2} = T_{3R} + \frac{Y'}{2}$. The Higgs sector to induce the SSB in Eq. (7) involves two doublets of scalar fields:

$$\Phi = (1, 2, 1, 1) \quad , \quad \hat{\Phi} = (1, 1, 2, 1) \quad (8)$$

where the entries correspond to the transformation properties under the symmetries of the group G , with the "Vacuum Expectation Values" (VEV's)

$$\langle \Phi \rangle = \frac{1}{\sqrt{2}} \begin{pmatrix} 0 \\ v \end{pmatrix} \quad , \quad \langle \hat{\Phi} \rangle = \frac{1}{\sqrt{2}} \begin{pmatrix} 0 \\ \hat{v} \end{pmatrix} . \quad (9)$$

The most general potential that develops this pattern of VEVs is

$$V = -(\mu\Phi^\dagger\Phi + \hat{\mu}\hat{\Phi}^\dagger\hat{\Phi}) + \frac{\lambda_1}{2}[(\Phi^\dagger\Phi)^2 + (\hat{\Phi}^\dagger\hat{\Phi})^2] + \lambda_2(\Phi^\dagger\Phi)(\hat{\Phi}^\dagger\hat{\Phi}). \quad (10)$$

In the last expression the terms with μ , $\hat{\mu}$ are included so that the parity symmetry (P) is broken softly, i. e., only through the dimension-two mass terms of Higgs potential.

The scalar Lagrangian for the model is written as

$$\mathcal{L}_{sc} = (D_\mu\Phi)^\dagger(D^\mu\Phi) + (\hat{D}_\mu\hat{\Phi})^\dagger(\hat{D}^\mu\hat{\Phi}) \quad (11)$$

where D_μ and \hat{D}_μ are the covariant derivatives for the SM and the mirror parts, respectively. The gauge interactions of quarks and leptons can be obtained from the Lagrangian

$$\mathcal{L}^{int} = \bar{\psi}i\gamma^\mu D_\mu\psi + \hat{\psi}i\gamma^\mu \hat{D}_\mu\hat{\psi} \quad (12)$$

The VEV's v and \hat{v} are related to the masses of the charged gauge bosons W and \hat{W} by $M_W = \frac{1}{2}g_L v$ and $M_{\hat{W}} = \frac{1}{2}g_R \hat{v}$, where g_L and g_R are the coupling constants of $SU(2)_L$ and $SU(2)_R$, and $g_L = g_R$ if we demand L - R symmetry.

4 Generic Majorana neutrino mass matrix

With the fields of fermions introduced in the model, we may write the gauge invariant Yukawa couplings for the neutral sector¹:

$$\begin{aligned}
& h_{ij} \bar{\nu}_{iL} \nu_{jR} + \lambda_{ij} \bar{l}_{iL} \tilde{\Phi} \nu_{jR} + \eta_{ij} \bar{l}_{iR} \tilde{\Phi} \hat{\nu}_{jL} \\
& + \hat{M}_{ij} \bar{\nu}_{iL} (\hat{\nu}_{jL})^c + \sigma_{ij} \bar{l}_{iL} (\hat{\nu}_{jL})^c \tilde{\Phi} \\
& + \chi_{ij} \bar{\nu}_{iR} (\nu_{jR})^c + \pi_{ij} \bar{l}_{iR} (\nu_{jR})^c \tilde{\Phi} + h.c.
\end{aligned} \tag{13}$$

where $i, j = 1, 2, 3$, $\tilde{\Phi} = i\sigma_2 \Phi^*$, $\hat{\Phi} = i\sigma_2 \hat{\Phi}^*$, h_{ij} , \hat{M}_{ij} , χ_{ij} have dimensions of mass, and σ_{ij} , η_{ij} , λ_{ij} and π_{ij} are dimensionless Yukawa coupling constants. When Φ and $\hat{\Phi}$ acquire VEV's we get the neutrino mass terms

$$\begin{aligned}
& h_{ij} \bar{\nu}_{iL} \nu_{jR} + \frac{v}{\sqrt{2}} \lambda_{ij} \bar{\nu}_{iL} \nu_{jR} + \frac{\hat{v}}{\sqrt{2}} \eta_{ij} \bar{\nu}_{iR} \hat{\nu}_{jL} \\
& + \hat{M}_{ij} \bar{\nu}_{iL} (\hat{\nu}_{jL})^c + \frac{v}{\sqrt{2}} \sigma_{ij} \bar{\nu}_{iL} (\hat{\nu}_{jL})^c \\
& + \chi_{ij} \bar{\nu}_{iR} (\nu_{jR})^c + \frac{\hat{v}}{\sqrt{2}} \pi_{ij} \bar{\nu}_{iR} (\nu_{jR})^c + h.c.
\end{aligned} \tag{14}$$

which are written in the generic Majorana matrix form

$$(\bar{\Psi}_{\nu L}, \bar{\Psi}_{\nu L}^c) \begin{pmatrix} M_L & M_D \\ M_D^T & M_R \end{pmatrix} \begin{pmatrix} (\Psi_{\nu}^c)_R \\ (\Psi_{\nu})_R \end{pmatrix} \tag{15}$$

where

$$(\Psi_{\nu})_{L,R} = \begin{pmatrix} \nu_i \\ \hat{\nu}_i \end{pmatrix}_{L,R}, \quad (\Psi_{\nu}^c)_{L,R} = \begin{pmatrix} (\nu_i^c) \\ (\hat{\nu}_i^c) \end{pmatrix}_{L,R} \tag{16}$$

$$M_L = \begin{pmatrix} 0 & \frac{v}{\sqrt{2}} \sigma \\ \frac{v}{\sqrt{2}} \sigma^T & \hat{M} \end{pmatrix}, \quad M_R = \begin{pmatrix} \chi & \frac{\hat{v}}{\sqrt{2}} \pi \\ \frac{\hat{v}}{\sqrt{2}} \pi^T & 0 \end{pmatrix}, \tag{17}$$

$$M_D = \begin{pmatrix} \frac{v}{\sqrt{2}} \lambda & 0 \\ h & \frac{\hat{v}}{\sqrt{2}} \eta \end{pmatrix}, \tag{18}$$

¹To simplify notation we drop the "0" superscript

with $h, \hat{M}, \chi, \sigma, \eta, \lambda$ and π unknown matrices of 3×3 dimension. By assuming the natural hierarchy $|(M_L)_{ij}| \ll |(M_D)_{ij}| \ll |(M_R)_{ij}|$ for the mass terms, the mass matrix in Eq. (15) can approximately be diagonalized, yielding

$$(\overline{\Psi}'_{\nu L}, \overline{\Psi}'^c_{\nu L}) \begin{pmatrix} M_\nu & 0 \\ 0 & M_R \end{pmatrix} \begin{pmatrix} (\Psi'_{\nu R})^c \\ (\Psi'_{\nu R}) \end{pmatrix}, \quad (19)$$

where, neglecting $\mathcal{O}(M_D M_R^{-1})$ terms, we may write in good approximation [20] $\Psi'_{\nu L,R} \approx \Psi_{\nu L,R}$, and $\Psi'^c_{\nu L,R} \approx \Psi^c_{\nu L,R}$. The Majorana mass matrix for the left handed neutrinos may be written in this seesaw approximation as

$$M_\nu \approx M_L - M_D M_R^{-1} M_D^T. \quad (20)$$

We assume a scenario where the dominant contribution for the active known neutrinos comes from the M_L matrix having the same structure of a Type I seesaw. Then in this scenario the eigenvalues for the light neutrinos may be obtained by applying again the seesaw approximation, that is:

$$M^{\text{light}} = -\left(\frac{v}{\sqrt{2}} \sigma\right) \hat{M}^{-1} \left(\frac{v}{\sqrt{2}} \sigma\right)^T. \quad (21)$$

Taking advantage of the fact that all σ_{ij} and \hat{M}_{ij} entries in Eq. (21) are free parameters, we propose the following parameterizations for \hat{M} and M^{light} neutrino mass matrices:

$$M^{\text{light}} = \frac{Y^2 v^2}{2 \hat{m}} \begin{pmatrix} 1+b & b & b \\ b & 1+b+c & b-c \\ b & b-c & 1+b+c \end{pmatrix}, \quad \hat{M} = \hat{m} \text{Diag}(Y_1, Y_2, Y_3). \quad (22)$$

where Y, Y_1, Y_2, Y_3, b, c are dimensionless coupling constants and \hat{m} represents the mirror scale. This parameterization for the light neutrinos mass matrix imposes a symmetric mixing of electron neutrino with muon and tau neutrinos in the first row and column of $(M^{\text{light}})_{ij}$, and the 2×2 submatrix $i, j = 2, 3$ generate maximal mixing for muon and tau neutrinos. This structure for M^{light} makes possible the diagonalization of light neutrinos by the so called "Tri-bimaximal mixing matrix" [26], i. e.

$$U_{\text{TB}}^T M^{\text{light}} V_{\text{TB}} = -U_{\text{TB}}^T \left(\frac{v}{\sqrt{2}} \sigma\right) \hat{M}^{-1} \left(\frac{v}{\sqrt{2}} \sigma\right)^T U_{\text{TB}} = \text{Diag}(m_1, m_2, m_3), \quad (23)$$

with

$$U_{\text{TB}} = \begin{pmatrix} \frac{2}{\sqrt{6}} & \frac{1}{\sqrt{3}} & 0 \\ -\frac{1}{\sqrt{6}} & \frac{1}{\sqrt{3}} & -\frac{1}{\sqrt{2}} \\ -\frac{1}{\sqrt{6}} & \frac{1}{\sqrt{3}} & \frac{1}{\sqrt{2}} \end{pmatrix} \quad (24)$$

and the light neutrino mass eigenvalues

$$(m_1, m_2, m_3) = \frac{Y^2 v^2}{2 \hat{m}} (1, 1 + 3b, 1 + 2c) . \quad (25)$$

The suppression by the mirror scale \hat{m} in Eq.(25) provides a natural explanation for the smallness of neutrino masses. The allowed range of values for the square neutrino mass differences reported in PDG [22]:

$$m_2^2 - m_1^2 \approx 7.6 \times 10^{-5} \text{ eV}^2 \quad , \quad m_3^2 - m_2^2 \approx 2.43 \times 10^{-3} \text{ eV}^2 , \quad (26)$$

with the input for normal hierarchy of the neutrino masses

$$(m_1, m_2, m_3) = (0.0865, 0.0870, .1) \text{ eV} , \quad (27)$$

fix the parameter values as $b = 0.00168$ and $c = 0.07757$. These neutrino masses are consistent with the bounds $m_\nu < 2 \text{ eV}$ [22], and set the mass differences

$$m_3^2 - m_1^2 \approx 2.5 \times 10^{-3} \text{ eV}^2 . \quad (28)$$

So, from Eqs.(25, 27)

$$\frac{Y^2 v^2}{2 \hat{m}} \approx 8.65 \times 10^{-2} \text{ eV} . \quad (29)$$

Therefore, assuming $\hat{m} = m_{\hat{\nu}} = 100 \text{ GeV}$ and $v = 246 \text{ GeV}$ we obtain

$$Y \approx 5.34 \times 10^{-7} \quad (30)$$

The matrix M_L in Eq.(17), may be diagonalized by using a unitary transformation

$$U^\dagger M_L U = \text{Diag}(m_1, m_2, m_3, \hat{m}_1, \hat{m}_2, \hat{m}_3) , \quad (31)$$

where the mixing matrix U compatible with our framework is written in good approximation as

$$U_{6 \times 6} \approx \begin{pmatrix} U_{TB} & \frac{v}{\sqrt{2}} \sigma \hat{M}^{-1} \\ -(\frac{v}{\sqrt{2}} \sigma \hat{M}^{-1})^T & I_{3 \times 3} \end{pmatrix} , \quad (32)$$

The particular numerical solution congruent with the above scenario for the neutrino masses and mixing is

$$\frac{v}{\sqrt{2}} \sigma \approx 93041.9 \text{ eV} \begin{pmatrix} -1.2001 & 0.6355 & 1.2952 \\ 0.6355 & -1.2702 & 1.3006 \\ 1.2952 & 1.3006 & 0.5389 \end{pmatrix}, \quad (33)$$

$$\hat{M} = 100 \text{ GeV Diag} (3.4918, 3.2643, 3.6043) , \quad (34)$$

and

$$\frac{v}{\sqrt{2}} \sigma \hat{M}^{-1} \approx 9.3 \times 10^{-7} \begin{pmatrix} -0.3437 & 0.1946 & 0.3593 \\ 0.1819 & -0.3891 & 0.3608 \\ 0.3709 & 0.3984 & 0.1495 \end{pmatrix} \quad (35)$$

for light ν - mirror mixing. Since the light-mirror mixing is very small, the mixing matrix for light neutrinos behaves in good approximation as the U_{TB} , Eq.(24). It is worth to mention here that in the limit of very small light-mirror charged lepton mixing, $(F_L^\dagger F_L)_{ij}$, $(E_L^\dagger E_L)_{ij} \ll 1$, we may approach U_{TB} as the usual U_{PMNS} lepton mixing matrix for three generations. Then, we obtain $(U_{PMNS})_{e2} \simeq \frac{1}{\sqrt{3}}$, $(U_{PMNS})_{e3} \simeq 0$, and $(U_{PMNS})_{\mu 3} \simeq \frac{1}{\sqrt{2}}$, which give for the solar and the atmospheric neutrino mixing angles $\theta_{12} \simeq 35.2^\circ$ and $\theta_{23} \simeq 45^\circ$, with $\theta_{13} \simeq 0$ in good agreement with current data, although recent evidences [27] show that θ_{13} may have a value different from zero.

In earlier papers on the study of neutrinos and left-right symmetry [28] appear similar representations of the fermions and mass matrices as our in Eq.(18), but these authors obtain masses for the standard and mirror neutrinos some orders of magnitude different from ours. On the other hand, the mass generation in the LRMM here considered is achieved with the scalar fields Φ and $\hat{\Phi}$, Eqs.(3,4), transforming as doublets under $SU(2)_L$ and $SU(2)_R$, respectively, with a mirror scale much lower than 10^{12} - 10^{13} GeV's.

5 Radiative decays

In this section we analyze the lepton flavor violation processes $\mu \rightarrow e\gamma$, $\tau \rightarrow \mu\gamma$ and $\tau \rightarrow e\gamma$ arising in the model by the existence of gauge invariant mixing terms between ordinary leptons and with the mirror counterparts. The lower order contribution to these decays mediated by the neutral scalar fields comes from the Feynman diagrams where the photon is radiated from an internal line. The corresponding amplitude is proportional to the operator $\overline{u(p_2)}\sigma^{\mu\nu}q_\nu\epsilon_\mu u(p_1)$, where $q = p_1 - p_2$ and ϵ_μ is the photon polarization [21].

In the limit $m_e \ll m_\mu \ll m_\tau$ the rate decay is given by

$$\Gamma(l_i \rightarrow l_j + \gamma) = \frac{\alpha}{512\pi^4} (G_F m_{l_i}^2)^2 \frac{m_{l_i}^5}{M_H^4} \left| \left(\ln \frac{M_H^2}{m_{l_i}^2} - \frac{4}{3} \right) \epsilon_{ij} - \sum_k x_{\nu_k} V_{L,jk} V_{R,ki}^+ \right|^2 \quad (36)$$

where $x_{\nu_k} \equiv \frac{m_{\nu_k}^2}{M_W^2}$, $\epsilon_{ij} = |A_L^+ A_R|_{ij}$ represents the flavor-changing couplings, and the second term is the very small contribution from the light neutrino propagating inside the loop.

In the limit $\alpha \ll 1$ and $M_H \ll M_{\hat{H}}$ the branching ratios are respectively

$$B_1(\mu \rightarrow e + \gamma) = \frac{3\alpha m_\mu^4}{8M_H^4} \left| \left(\ln \frac{M_H^2}{m_\mu^2} - \frac{4}{3} \right) \epsilon_{e\mu} - \sum_k x_{\nu_k} V_{L,ek} V_{R,k\mu}^+ \right|^2 \quad (37)$$

$$B_2(\tau \rightarrow \mu + \gamma) = \frac{3\alpha m_\tau^4}{8M_H^4} \left| \left(\ln \frac{M_H^2}{m_\tau^2} - \frac{4}{3} \right) \epsilon_{\mu\tau} - \sum_k x_{\nu_k} V_{L,\mu k} V_{R,k\tau}^+ \right|^2 \quad (38)$$

and

$$B_3(\tau \rightarrow e + \gamma) = \frac{3\alpha m_\tau^4}{8M_H^4} \left| \left(\ln \frac{M_H^2}{m_\tau^2} - \frac{4}{3} \right) \epsilon_{e\tau} - \sum_k x_{\nu_k} V_{L,ek} V_{R,k\tau}^+ \right|^2 \quad (39)$$

By using the constraints $\epsilon_{ij} < 1$, $i \neq j$ for the parameters in Eqs. (37,39), required by unitarity of V , see Eqs. (23), one gets for the above branching ratios:

$$B_1 < 2.2 \times 10^{-13} \quad , \quad B_2 < 5 \times 10^{-9} \quad \text{and} \quad B_3 < 5 \times 10^{-9} \quad (40)$$

which is congruent with the experimental bounds [22] $B(\mu \rightarrow e + \gamma) < 1.2 \times 10^{-11}$, $B(\tau \rightarrow \mu + \gamma) < 4.4 \times 10^{-8}$ and $B(\tau \rightarrow e + \gamma) < 3.3 \times 10^{-8}$ PDG [22].

6 Heavy Neutrino signals

Possible new neutrinos can be detected in various ways in colliders. If these neutrinos are heavy they will be unstable and may be detected directly in their decay products.

Next generation of large colliders will probe Nature up to TeV scales with high precision, probably discovering new heavy particles. Thus, it will be a window to any new physics near the electroweak scale which couples to the SM. Such colliders can be used to produce new heavy neutrinos at an observable level to improve present limits on their masses and mixings [29]. These fermions with new interactions, like in the left-right models [30], can be produced by gauge couplings suppressed by small mixing angles. For the analysis of the heavy neutrinos signals it is necessary to know their decay modes, which are different in the Dirac and Majorana cases.

Heavy Majorana neutrino singlets can be produced in the process [31]

$$q\bar{q}' \rightarrow W^* \rightarrow l^\pm H \quad (41)$$

with $l = e, \mu, \tau$, which cross sections depend on M_N and the small mixing V_{lN} . Heavy Majorana neutrino decays in the channels $N \rightarrow W^\pm l^\mp$, $N \rightarrow Z\nu_l$ and $N \rightarrow H\nu_l$. The partial widths for the N decays are

$$\Gamma(N \rightarrow W^+ l^-) = \Gamma(N \rightarrow W^- l^+) = \frac{e^2}{64\pi s_{\theta_w}^2} |U_{lN}|^2 \frac{m_N^3}{M_W^2} \left(1 - \frac{M_W^2}{m_N^2}\right) \left(1 + \frac{M_W^2}{m_N^2} - 2\frac{M_W^4}{m_N^4}\right) \quad (42)$$

$$\Gamma(N \rightarrow Z\nu_l) = \frac{e^2}{64\pi s_{\theta_w}^2 c_{\theta_w}^2} |U_{lN}|^2 \frac{m_N^3}{M_Z^2} \left(1 - \frac{M_Z^2}{m_N^2}\right) \left(1 + \frac{M_Z^2}{m_N^2} - 2\frac{M_Z^4}{m_N^4}\right) \quad (43)$$

$m_N(\text{GeV})$	B_{W^\pm}	B_Z	B_H
100	0.34	0.1	0.2
390	0.3	0.306	0.09
780	0.3	0.297	0.107
$\gg M_W, M_Z, M_H$	0.293	0.3	0.111

Table 1: Branching ratios for different values of m_N

$$\Gamma(N \rightarrow H\nu_l) = \frac{e^2}{64\pi s_{\theta_w}^2} |U_{lN}|^2 \frac{m_N^3}{M_W^2} \left(1 - \frac{M_H^2}{m_N^2}\right)^2 \quad (44)$$

where U_{lN} is the light-mirror neutrino mixing $\frac{v}{\sqrt{2}} \sigma \hat{M}^{-1}$, Eq.(35). From Eqs. (32,35) the contributions come from terms of the order $|V_{lN}| \lesssim 10^{-7}$. From these expressions we can conclude that the total branching for each of the four channels is independent of the heavy neutrino mixing, determined only by m_N and the gauge and Higgs boson masses.

Heavy neutrino signals are limited by the small mixing of the heavy neutrino required by precision constraints [33] and masses of order 100 GeV are accessible at LHC. For this mass range, SM backgrounds are larger and, since production cross sections are relatively small, heavy neutrino singlets are rather difficult to observe.

The branching ratios for different values of m_N reads as Table I ($M_H = 130$ GeV); and in all these cases $\sum B_i \approx 1$. Here

$$B_{W^\pm} = B_r(N \rightarrow W^\pm l^\mp) \quad , \quad B_Z = B_r(N \rightarrow Z\nu_l) \quad , \quad B_H = B_r(N \rightarrow H\nu_l) \quad (45)$$

Table I shows that these decays are not so sensitive to the heavy neutrino mass, such that for heavy neutrino signals it is not necessary to have center of mass energies much larger than a hundred GeV.

Among the possible final states given by Eqs.(42,44), only charged current decays give final states which may in principle be detected. For $m_N < M_W$ these two body decays are not possible and N decays into three fermions, mediated by off-shell bosons.

Other simple production processes like

$$q\bar{q}' \rightarrow Z^* \rightarrow \nu N \quad (46)$$

$$gg \rightarrow H^* \rightarrow \nu N \quad (47)$$

give l^\pm and l^+l^- final states which are unobservable due to the huge backgrounds. For the pair production

$$q\bar{q} \rightarrow Z^* \rightarrow NN \quad (48)$$

the cross section is suppressed by $|V_{lN}|^4$, phase space and the Z propagator, and is thus negligible.

Three signals are produced in the two charged current decay channels of the heavy neutrino

$$l^+N \rightarrow l^+l^-W^+ \rightarrow l^+l^-l^+\bar{\nu} \quad (49)$$

$$l^+ N \rightarrow l^+ l^+ W^- \rightarrow l^+ l^+ l^- \nu \quad (50)$$

and small additional contributions from τ leptonic decays.

Heavy neutrino signals in the final state $l^\pm l^\pm$ are given in the lepton number violating neutrino decay and subsequent hadronic W decay, or leptonic decay when the lepton is missed. LHC present energies are enough to discover heavy Majorana neutrino with very small V_{eN} [32].

7 Conclusions

Here the LRMM with gauge group $SU(3)_C \otimes SU(2)_L \otimes SU(2)_R \otimes U(1)_{Y'}$ is applied in order to find closer values for neutrino masses fitted to experimental data. We have worked with Majorana neutrinos, which mass matrix was written in terms of blocks that stand for standard and mirror mass terms. The large number of parameters involved induces to make some simplifications on the structure of the matrix. A double seesaw approach method is used and diagonalization is performed, and with the help of neutrino data we accommodate neutrino masses with normal hierarchy of the order of $(m_1, m_2, m_3) \approx (0.0865, 0.0870, 0.1)$ eV. So, we have found a consistent smallness hierarchy for the neutrino masses. With the LRMM we have also analyzed the radiative decays $\mu \rightarrow e + \gamma$, $\tau \rightarrow e + \gamma$ and $\tau \rightarrow \mu + \gamma$ for a Higgs mass of 130 GeV , obtaining bounds for the branching ratios congruent with the experimental ones. Decay rates for heavy neutrinos N were calculated for different channels, and we found that their BR are nearly equal for $M_N \gg M_W, M_Z, M_H$ and also that they do not change too much for other values of M_N . To find heavy Majorana neutrinos one has only a few parameter dependence (for neutrino singlets, the heavy neutrino mass and its mixing angle) and also the mass scale could be accessible at the LHC.

8 Acknowledgments

The author R. Gaitán wishes to thank to the "Sistema Nacional de Investigadores" (SNI) in Mexico for partial support. and also acknowledges support by PAPIIT project IN104208. A. Hernandez-Galeana is thankful for partial support from the "Instituto Politécnico Nacional", (Grants from EDI and COFAA) and "Sistema Nacional de Investigadores" (SNI) in Mexico, and J. M. Rivera-Rebolledo wishes to thank to COFAA-IPN and the "Sistema Nacional de Investigadores" (SNI) in Mexico for partial support.

References

- [1] Y. Fukuda et al. [Super-Kamiokande Collaboration], Phys. Rev. Lett. 81, 1562 (1998); The SNO Collaboration, Phys. Rev. Lett. 87, 71301 (2001); K. Eguchi et al. [KamLAND Collaboration], Phys. Rev. Lett. 90, 021801 (2003); E. Aliu et al. [K2K Collaboration], Phys. Rev. Lett. 94, 081802 (2005); Y. Ashie et al. [SK Collaboration], Phys. Rev. D71 (2005); M. Altmann et al. [GNO Collaboration], Phys. Lett. B616, 174(2005), M. Apolonio et al. [CHOOZ Collaboration], Eur. Phys. J. C27, 331 (2003).

- [2] M. Maltoni, T. Schwetz, M. A. Tortotola and J. W. F. Valle, Phys. Rev. D **68**, 113010 (2003); G. L. Fogli, E. Lisi, A. Marrone, A. Palazzo, Prog. Part. Nucl. Phys. **57**, 742-795 (2006); A. Strumia and F. Vissani, [arXiv:hep-ph/0606054](https://arxiv.org/abs/hep-ph/0606054).
- [3] P. Minkowski, Phys. Lett. **B67**, 421 (1977); T. Yanagida, in *Proceedings of the Workshop on the Unified Theory and the Baryon Number in the Universe*, (O. Sawada and A. Sugamoto, eds.), KEK, Tsukuba, Japan, 1979, p. 95; M. Gell-Mann, P. Ramond, and S. Slansky, *Complex spinors and unified theories in Supergravity* (P. van Nieuwenhuizen and D. Z. Freedman, eds.), North Holland, Amsterdam, 1979, p. 315; S. L. Glashow, in *Quarks and Leptons* (Plenum, New York, 1979), p. 687; R. N. Mohapatra and G. Senjanovic, Phys. Rev. Lett. **44**, 912 (1980).
- [4] M. Magg and C. Wetterich, Phys. Lett. **94B**, 61 (1980); G. Lazarides, Q. Shafi, and C. Wetterich, Nucl. Phys. **B181**, 287 (1981); J. Schechter and J. W. F. Valle, Phys. Rev. D **22**, 2227 (1980); R. N. Mohapatra and G. Senjanovic, Phys. Rev. D **23**, 165 (1981); J. Schechter and J. W. F. Valle, Phys. Rev. D **25**, 774 (1982).
- [5] A. Aranda and J. L. Díaz-Cruz, Mod. Phys. Lett. **A20**, 203 (2005).
- [6] P. Langacker and D. London, Phys. Rev. **D38**, 907 (1988); S. Antusch, C. Biggio, E. Fernández-Martínez, M. B. Gavela, and J. López-Pavon, J. High Energy Phys. **10**, 084 (2006); A. Abada, C. Biggio, F. Bonnet, M. B. Gavela, and T. Hambye, J. High Energy Phys. **12** 061 (2007).
- [7] E. Nardi, E. Roulet, and D. Tommasini, Phys. Lett. **B344**, 225 (1995); D. Tommasini, G. Barenboim, J. Bernabeu, and C. Jarlskog, Nuc. Phys. B **444**, 451 (1995).
- [8] J. Kersten and A. Y. Smirnov, Phys. Rev. **D76**, 073005 (2007); S. Bray, J. S. Lee, and A. Pilaftsis, Nucl. Phys. **B786**, 95 (2007); F. del Aguila, J. A. Aguilar-Saavedra, and R. Pittau, J. High Energy Phys. **10**, 047 (2007).
- [9] M. Fukugita and T. Yanagida, Phys. Lett. **B174**, 45 (1986).
- [10] C. S. Wu, E. Ambler, R. Hayward, D. Hopes, and Hudson, Phys. Rev. **105** (1957) 1413; R. Garwin, L. Lederman, and M. Weinrich, Phys. Rev. **105** (1957) 1415; J. Friedman and V. Telegdi, Phys. Rev. **105** (1957) 1681.
- [11] E. Fermi, Nuovo Cimento **11** (1934)1; Z. Phys. **88** (1934) 161.
- [12] T.D. Lee and C.N. Yang, Phys. Rev. (1956) 104. 254.
- [13] J. Maalampi and M. Roos, Phys. Rep. **186** (1990) 53.
- [14] Yu. Kobzarev, L. B. Okun, and I. Ya. Pomeranchuk, Sov. J. Nucl. Phys. **3** (1966) 837; L.B. Okun, [hep-ph/0606202](https://arxiv.org/abs/hep-ph/0606202) VI, 19 jun 2006; R. Foot and R.R. Volkas, Phys. Rev. D. **52** (1995) 6595; Z.G. Berezhiani and R.N. Mohapatra, Phys. Rev.D **52** (1995) 6607.

- [15] V. E. Ceron, U. Cotti, J. L. Díaz-Cruz, and M. Maya, Phys. Rev. D **57**, 1934 (1998); U. Cotti, J. L. Díaz-Cruz, R. Gaitán, H. Gonzalez, and A. Hernández-Galeana, Phys. Rev. D **66**, 015004 (2002); R. Gaitán, O. G. Miranda, and L. G. Cabral-Rosetti, Phys. Rev. D **72**, 034018 (2005); R. Gaitán, S. Rodríguez-Romo, A. Hernández-Galeana, J. M. Rivera-Rebolledo and P. Fernández de Córdoba, Int. J. Mod. Phys. A **22** (2007) 2935.
- [16] S. M. Barr, D. Chang, and G. Senjanovic, Phys. Rev. Lett. **67** (1991)2765; K. S. Babu and R. N. Mohapatra, Phys. Rev. D **41** (1990) 1286.
- [17] J. C. Pati and A. Salam, Phys. Rev. D **11** (1975) 1137.
- [18] Z. G. Berezhiani, Phys. Lett. B **129** (1983) 99.
- [19] Z. G. Berezhiani, Phys. Lett. B **150** (1985) 177; Z. G. Berezhiani, Sov. J. Nucl. Phys. **42** (1985) 825.
- [20] See for instance: S. Antusch and S.F. King, Nucl. Phys. B **705** (2005) 239.
- [21] B. W. Lee and R. E. Schrock, Phys. Rev. D **16** (1977) 1444; A. Abada, C. Biggio, F. Bonnet, M. B. Gavela, and T. Hambye, Phys. Rev D **78** (2008) 033007; P. Q. Hung, Phys. Lett. B **659** (2008) 585.
- [22] K. Nakamura *et al.*, Particle Data Group, J. Phys. G: Nucl. Part. Phys. **37** (2010) 075021.
- [23] Rabindra N. Mohapatra and Palash B. Pal, *Massive neutrinos in Physics and astrophysics*, Third Ed., World Scientific, 2004.
- [24] Yara Do Amaral Coutinho, Jose Antonio Martins Simoes, and C. M. Porto, Eur. Phys. **C18**,(2001) 779.
- [25] B. Pontecorvo, *Mesonium and antimesonium*, Sov. Phys. JETP **6**, 429 (1957); *Inverse beta processes and nonconservation of lepton charge*, Sov. Phys. JETP **7**, 172 (1958); Z. Maki, M. Nakagawa and S. Sakata, *Remarks on the unified model of elementary particles*, Prog. Theor. Phys. **28**, 870 (1962).
- [26] F. Harrison, D. H. Perkins and W. G. Scott, Phys. Lett. **B520**, 167 (2002).
- [27] A.B. Balantekin, arXiv: 1106.5021 [hep-ph]; S. F. King, arXiv: 1106.4239 [hep-ph].
- [28] C. H. Albright and J. Oliensis, Phys. Rev. D **33**, 2602 (1986); J. Oliensis and C. H. Albright, Phys. Lett. B **160**, 121 (1985); D. Chang and R. N. Mohapatra, Phys. Rev. Lett. **58**, 1600 (1987); S. Bertolini and J. Liu, Nucl. Phys. B **297**, 401 (1988).
- [29] A. Datta, M. Guchai and A. Pilaftsis, Phys. Rev. D **50**, 3195 (1994); J. Almeida, F. M. L., Y. D. A. Coutinho, J. A. Martins Simoes and M. A. B. do Vale, Phys. Rev. D **62**, 075004 (2000); O. Panella, M. Cannoni and Y. N. Srivastava, Phys. Rev. D **65**, 035005 (2002); T. Han and B. Zhang, Phys. Rev. Lett. **97**, 171804 (2006).
- [30] P. Langacker, R. W. Robinett and J. L. Rosner, Phys. Rev. D **30**, 1470 (1984).

- [31] F. del Aguila and J. A. Aguilar-Saavedra, Phys. Lett. B **672**, 158 (2009); F. del Aguila and J. A. Aguilar-Saavedra, Nucl. Phys. B **813**, 22 (2008).
- [32] A. Datta, M. Guchai and A. Pilaftsis, Phys. Rev. D **50**, 3195 (1994); F. del Aguila, J. A. Aguilar-Saavedra, and R. Pittau, J. High Energy Phys. **10**, 047 (2007).
- [33] F. Del Aguila, J. de Blas, M Peres-Victoria, Phys. Rev. D **78**, 013010 (2008).

Document downloaded from:

<http://hdl.handle.net/10251/152279>

This paper must be cited as:

Gamermann, D.; Montagud Aquino, A.; Aparicio, P.; Navarro-Peris, E.; Triana, J.; Villatoro, F.; Urchueguía Schölzel, JF.... (2012). A Modular Synthetic Device to Calibrate Promoters. *Journal of Biological System*. 20(1):37-55. <https://doi.org/10.1142/S0218339012500015>



The final publication is available at

<https://doi.org/10.1142/S0218339012500015>

Copyright WORLD SCIENTIFIC PUBL CO PTE LTD

Additional Information

A modular synthetic device to calibrate promoters

D. Gamermann^{a,b}, A. Montagud^b, P. Aparicio^c, E. Navarro^d, J. Triana^e, F. R. Villatoro^d, J. F. Urchueguía^b, P. Fernández de Córdoba^b

^a*Cátedra Energesis de Tecnología Interdisciplinar, Universidad Católica de Valencia San Vicente Mártir,*

Guillem de Castro 94, E-46003, Valencia, Spain.

^b*Instituto Universitario de Matemática Pura y Aplicada, Universidad Politécnica de Valencia,*

Camino de Vera 14, 46022 Valencia, Spain.

^c*Departament de Química Física i Inorgànica,*

Universitat Rovira i Virgili, 43007, Tarragona, Spain.

^d*Departamento de Lenguajes y Ciencias de la Computación,*

E.T.S.I Industriales, Universidad de Málaga,

Campus El Ejido, S/n 29013, Málaga, Spain.

^e*Departamento de Química,*

Universidad Pinar del Río “Hermanos Saíz Montes de Oca”,

Martí 270, 20110, Pinar del Río, Cuba.

Abstract

In this contribution, a design of a synthetic calibration genetic circuit to characterize the relative strength of different sensing promoters is proposed and its specifications and performance are analyzed via an effective mathematical model. Our calibrator device possesses certain novel and useful features like modularity (and thus the possibility of being used in many different biological contexts), simplicity, being based on a single cell, high sensitivity and fast response. To uncover the critical model parameters and the corresponding parameter domain at which the calibrator performance will be optimal, a sensitivity analysis of the model parameters was carried out over a given range of sensing protein concentrations (acting as input). Our analysis suggests that the half saturation constants for repression, sensing and difference in binding cooperativity (Hill coefficients) for repression are the key to the performance of the proposed device. They furthermore are determinant for the sensing speed of the device, showing that it is possible to produce de-

Email address: daniel.gamermann@ucv.es (D. Gamermann)

tectable differences in the repression protein concentrations and in turn in the corresponding fluorescence in less than two hours. This analysis paves the way for the design, experimental construction and validation of a new family of functional genetic circuits for the purpose of calibrating promoters.

Keywords: synthetic genetic circuits, synthetic biology, calibration, gene promoter, effective modeling of gene circuits, parameter analysis

1. Introduction

One of the fundamental principles of synthetic biology is the construction of biological standardized parts and devices which are interchangeable. A proper characterization of these parts and devices appears as a key issue in order to make them reusable in a predictive way. In the recent past scientists have witnessed several initiatives towards the design and fabrication of synthetic biological components and systems as a promising way to explore, understand and obtain beneficial applications from nature. For instance, in the post genomic era one of the most fascinating challenges scientists are facing is to understand how the phenotypic behaviour of living cells arise out of the properties of their complex network of signalling proteins. While the interacting biomolecules perform many essential functions in these systems, the underlying design principles behind the functioning of such intracellular networks still remain poorly understood [3, 13]. Several initiatives have been reported in this line of thought to uncover some key working principles of such genetic regulatory networks via quantitative analysis of some relatively simple, experimentally well characterized, artificial genetic circuits. It has been shown that custom made gene-regulatory circuits with any desired property can be constructed from simple regulatory elements [4]. These properties include bistability, multistability or oscillatory behaviour of genetic circuits in various microorganisms such as bacteriophage switch [5] or the cyanobacterium circadian oscillator [6]. As one example, the genetic *toggle switch*, a synthetic, bi-stable gene-regulatory network in *Escherichia coli*, was shown to provide a simple theory that uncovers the conditions necessary for bi-stability [11, 12]. Further, artificial positive feedback loops (PFLs) have been used as genetic amplifiers in order to enhance the responses of weak promoters and in the creation of eukaryotic gene switches [14]. Sayut et al. demonstrated the construction and directed evolution of two PFLs based on the LuxR transcriptional activator and its cognate promoter, Pluxl

[8]. These circuits may have application in metabolic engineering or gene therapy that requires inducible gene expressions [9, 10].

The desired performance of these synthetic networks and in turn the resultant phenotype is strongly dependent on the expression level of the corresponding genes, which is further controlled by several factors such as promoter strength, cis- and trans-acting factors, cell growth stage, the expression level of various RNA polymerase-associated factors and other gene-level regulation characteristics [11, 13]. Thus, one important ingredient to elucidate gene function and genetic control on phenotype would be to have access to well-characterized promoter libraries. These promoter libraries would be in turn useful for the design and construction of novel biological systems. There have been several initiatives to control gene expression through the creation of promoter libraries [2, 7]. Alper et al., [1] have reported a methodology to develop a completely characterized, homogeneous, broad-range, functional promoter library with the demonstration of its applicability to analysis of genetic control.

Since Miller published [16] a proposal for a measurement standard for β -galactosidase assays, yet much work has been done with no conclusive standard being established [17, 18, 19]. The main goal in calibration is measuring a *query* value up to an established *standard*. A good *device* should be unique, reliable and easy to use; additionally it should circumvent, to all possible extent, any noise that could alter the measurement. Recently a methodology [20] has been reported to characterize the activity of promoters by using two different cell strains. In the present study we propose the use of a synthetic gene regulatory network as a framework to characterize different promoter specifications by using a single-cell strategy. In this context characterization stands for evaluating the parameters of a *query* promoter as compared to a standard promoter acting as a scale. The proposed device, the promoter calibrator, works on the principle of comparing a specific input signal which will be sensed by promoters of different sensing strengths and, as an output, produces fluorescence of specific colours which allows quantifying the relative strength of the promoters. Analyses were carried out in order to find out relevant model parameters and the corresponding range of model parameter values which are compatible with the performance of this calibrating biological design over a spectrum of given input .

This contribution is organized as follows: in the first part, “Design”, the structure and working principle are explained and the mathematical model resulting from the construction is established. In section 3, “Numerical Anal-

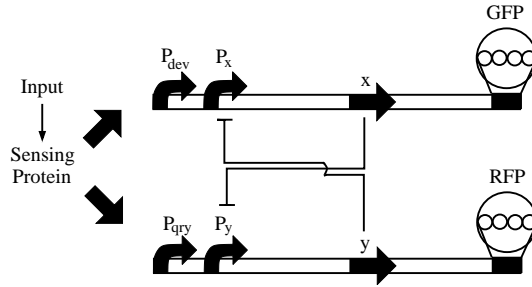


Figure 1: Design of the proposed promoter calibrator. It is composed of two promoters (with two parts each: a sensing and a repressed domain) one of the sensing promoters is the *device* promoter and the other is the *query* promoter. The repressed domains are controlled by the two repressors proteins (x and y). Each promoter is inhibited by the repressor which is transcribed from the opposing promoter. Fluorescence proteins levels will be proportional to repressor protein levels, which, in turn, will be promoted by the sensing promoters.

ysis of the System”, we analyze the dynamics of the model equations in regard to its stability, functional parameter regions and sensitivity or robustness vs. the change in certain key parameter values. In the following section, a proof of concept design is proposed in order to choose the right parameters to actually perform the experimental validation of our concepts and have a system that gives a clear and stable signal that can be interpreted. Finally, the conclusions resulting from our paper are exposed.

2. Design

2.1. Biological principles

Our promoter calibrator is composed of two promoters (each with two parts: a sensing and a repressed domain), two repressors proteins and two fluorescent protein outputs (see Fig. 1). Each promoter is inhibited by the repressor, transcription of which is promoted by the opposing promoter. Fluorescence protein levels will be directly related to repressor protein levels, activated in turn by their sensing promoters. Hence, different sensing strengths will cause a difference in the expression of the fluorescence proteins, detectable by means of single cell fluorescence as changes in the color patterns of the individual cell or cell sample.

In our scheme, one of the sensing promoters acts as the *device* promoter to which the strength of a given *query* promoter is quantitatively compared.

The main use of this device is to characterize different promoter specifications (sensing affinities and cooperativities) compared to some standard. One of the main usefulness of this design lies in the potential modularity of the system: by changing the sensing part of the promoters, other sensing promoters could be calibrated; this change can be carried out by a simple, straightforward cloning step. Modularity also boasts the potential of this device as it can be implemented in a potentially unlimited set of systems.

2.2. Mathematical model

The behaviour of the proposed promoter calibrator can be understood via an effective mathematical model. The model is considered to be effective as transcription and translation have been modeled as a lumped reaction. The separation of transcription and translation otherwise involves a response delay. We seek to classify dynamic behaviors depending upon the change in model parameters and determine which experimental parameters should be fine-tuned in order to obtain a satisfactory performance of our device.

The time dependent changes in repressor and sensing protein (input) concentrations is shown in equations (1-3). Subsequent to the biological design, reporter protein concentrations are directly related to repressor protein concentrations.

$$\frac{dx}{dt} = \alpha_1 \frac{\left(\frac{p_s}{k_1}\right)^{n_1}}{1 + \left(\frac{p_s}{k_1}\right)^{n_1}} \frac{1}{1 + \left(\frac{y}{k_y}\right)^{n_y}} - \beta_x x + \gamma_x, \quad (1)$$

$$\frac{dy}{dt} = \alpha_2 \frac{\left(\frac{p_s}{k_2}\right)^{n_2}}{1 + \left(\frac{p_s}{k_2}\right)^{n_2}} \frac{1}{1 + \left(\frac{x}{k_x}\right)^{n_x}} - \beta_y y + \gamma_y, \quad (2)$$

$$\frac{dp_s}{dt} = -\beta_{p_s} p_s. \quad (3)$$

The *device* and *query* promoters activate the production of repressor protein x and y , respectively, and their concentration is related directly to the concentration of fluorescence proteins. Thus these variables will be treated as equivalent from the modelling point of view. Parameters α_1 and α_2 represent the effective rate of synthesis of repressor proteins x and y , respectively; α is a lumped parameter that takes into account the net effect of various activities such as RNA polymerase binding, RNA elongation and termination of

transcript, ribosome binding and polypeptide elongation and will be modified by repression and sensing effects. The β_x , β_y and β_{p_s} are the degradation constants of repressor protein x , repressor protein y and sensing protein p_s , respectively. The sensing protein concentration p_s will depend on the sensed input, will be easy to change in a given experiment and is used as the main input variable in our calibrator experiments. It is important to note that a slow rate of degradation is assumed for the sensing protein, implying a nearly constant level over a reasonable experimental time interval. Basal level rates of synthesis of proteins x and y are denoted by γ_x and γ_y , respectively.

Repressor and sensing responses are assumed to follow Hill equation dynamics: promoter-binding monomers form multimers by positive allosterism and attach to its cognate promoter with saturating behaviour. Binding cooperativities are described by Hill coefficients n_x and n_y for repressor domains corresponding to x and y respectively, and n_1 and n_2 for sensing domains corresponding to *device* and *query* promoter respectively. The extent of the saturation rate is described by half saturation constants or Michaelis constants, denoted by parameter k_x and k_y for repressor domains corresponding to x and y respectively and k_1 and k_2 for sensing domains corresponding to *device* and *query* promoter respectively. The total number of promoter sites is assumed to be conserved and the total concentration of both promoters is chosen to be identical.

In our construction, the crossrepressing part will be kept unchanged while different sensing domains may be attached to it. The aim is to establish a protocol to accurately quantify differences between the sensing promoter parameters $(\alpha_{1,2}, k_{1,2})$. Crossrepression parameters $(k_{x,y}, \beta_{x,y}$ and $n_{x,y})$ are structural parameters that must be chosen in such a way that the fluorescence response of the system gives us stable, sensitive and robust indication about the quantitative relations between the sensing promoter parameters. The dynamic analysis of the system will help us to take the right decisions on which are the most appropriate values for these structural parameters. The next sections are devoted to the dynamical analysis in order to determine the sensitivity and robustness of the system for different ranges of the structural parameters.

The commercial software package Mathematica (Wolfram), was used for model development and simulation. In the numerical calculations we have used the following dimensionless variables:

$$X = \frac{x}{k_x} \quad (4)$$

$$Y = \frac{y}{k_y} \quad (5)$$

$$\tau = t\beta_x \quad (6)$$

$$\bar{\alpha}_{1,2} = \frac{\alpha_{1,2}}{\beta_x k_{x,y}} \quad (7)$$

$$\bar{\gamma}_{x,y} = \frac{\gamma_{x,y}}{\beta_x k_{x,y}} \quad (8)$$

therefore, the units in the plots of the figures in this work are given in units of k_x or k_y for the x and y repressor proteins concentrations and time in units of $\frac{1}{\beta_x}$. For the adimensional variables, Equations (4-8) take the form:

$$\frac{dX}{d\tau} = \bar{\alpha}_1 \frac{\left(\frac{p_s}{k_1}\right)^{n_1}}{1 + \left(\frac{p_s}{k_1}\right)^{n_1}} \frac{1}{1 + Y^{n_y}} - X + \bar{\gamma}_x, \quad (9)$$

$$\frac{dY}{d\tau} = \bar{\alpha}_2 \frac{\left(\frac{p_s}{k_2}\right)^{n_2}}{1 + \left(\frac{p_s}{k_2}\right)^{n_2}} \frac{1}{1 + X^{n_x}} - RY + \bar{\gamma}_y, \quad (10)$$

where R is the ratio $\frac{\beta_y}{\beta_x}$.

3. Numerical analysis of the system

The simplifying assumption of considering sensing proteins for which the degradation constant β_{p_s} is much smaller than the rest ($\beta_{p_s} \ll \beta_x, \beta_y$) was made in order to classify the possible dynamic scenarios of our model. Given this assumption, in a first order of approximation we have,

$$\frac{dp_s}{dt} = -\beta_{p_s} p_s \approx 0. \quad (11)$$

In such approach, the concentration of sensing protein p_s is constant during the evolution time of the rest of the internal variables of the system. This assumption leads to a system of two autonomous coupled non-linear

ordinary differential equations dependent on the variables x and y , eqs. (9-10), in which p_s is fixed although it can be easily changed within a given experiment. This is not true for the rest of parameters which are more difficult to modify in a given experiment. This approximation transforms the system into:

$$\frac{dX}{d\tau} = \bar{\alpha}'_1 \frac{1}{1 + Y^{n_y}} - X + \bar{\gamma}_x, \quad (12)$$

$$\frac{dY}{d\tau} = \bar{\alpha}'_2 \frac{1}{1 + X^{n_x}} - RY + \bar{\gamma}_y. \quad (13)$$

where the new parameters $\bar{\alpha}'_i$ (effective transcription factors) are given by the following expression:

$$\bar{\alpha}' = \alpha \frac{\left(\frac{p_s}{k}\right)^n}{1 + \left(\frac{p_s}{k}\right)^n}. \quad (14)$$

In the limit in which the constants $k_{x,y}$, $\beta_{x,y}$, $\gamma_{x,y}$ are equal, this equations describe the biological equivalent of an electronic *comparator*, that is, a device which compares two voltages or currents and switches its output to the larger signal. In the biological equivalent, our comparator would select for the larger of the two $\bar{\alpha}$'s, as exemplified in Fig. 2, which represent the evolution of the system for the cases in which the *query* promoter has a higher and lower effective transcription factor compared to the device promoter, respectively.

In any case, our aim is to construct a device, termed a *calibrator*, which not only selects the stronger affinity but also allows quantifying the relative strength of both promoters. Although the comparator is a fundamental part of this device, a deeper understanding of the dynamics of the system is required for its application as a calibrator device in real biological environments.

3.1. Dynamic analysis of the calibrator

The dynamical analysis of the system given by Eqs. (12-13) requires the determination of its steady state solutions and their linear stability. The steady states (x_{ss}, y_{ss}) are given by the intersection of the null clines:

$$F_1(X, Y) = \bar{\alpha}'_1 \frac{1}{1 + Y^{n_y}} - X + \bar{\gamma}_x = 0, \quad (15)$$

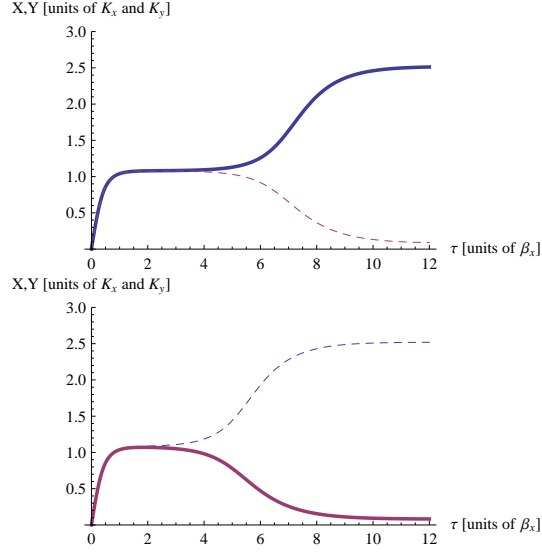


Figure 2: Typical response of the proposed promoter calibrator. In the upper figure the concentration of the x protein (solid line) in the steady state is higher while in the figure below the concentration of the y protein (dashed line) is higher.

and

$$F_2(X, Y) = \bar{\alpha}'_2 \frac{1}{1 + X^{n_x}} - RY + \bar{\gamma}_y = 0. \quad (16)$$

The analytical solution of Eqs. (15-16) cannot be obtained, hence numerical methods must be used. The linear stability of the steady states is determined by the sign of the eigenvalues of the Jacobian matrix,

$$M = \begin{pmatrix} \frac{\partial F_1}{\partial X} & \frac{\partial F_1}{\partial Y} \\ \frac{\partial F_2}{\partial X} & \frac{\partial F_2}{\partial Y} \end{pmatrix}_{X=X_{ss}, Y=Y_{ss}} \quad (17)$$

which are given by

$$\lambda_{\pm} = -\frac{1+R}{2} \pm \frac{1}{2} \sqrt{(R-1)^2 + 4\Delta}, \quad (18)$$

$$\Delta = \frac{n_x n_y (X_{ss} - \bar{\gamma}_x) (\bar{\alpha}'_1 + \bar{\gamma}_x - X_{ss}) (Y_{ss} R - \bar{\gamma}_y) (\bar{\alpha}'_2 + \bar{\gamma}_y - Y_{ss} R)}{\bar{\alpha}'_1 \bar{\alpha}'_2 X_{ss} Y_{ss}}. \quad (19)$$

From the analysis of the previous equations (15-16), we deduce that, for the positive steady state solutions ($X_{ss} > 0$ and $Y_{ss} > 0$), the following mathematical constraints hold: $\bar{\alpha}'_1 > X_{ss} - \bar{\gamma}_x > 0$ and $\bar{\alpha}'_2 > Y_{ss}R - \bar{\gamma}_y > 0$, respectively. Thus, taking into account (18-19), we observe that $\Delta > 0$ and λ_- is always negative. However, λ_+ can be either negative, for $\Delta > R$, or positive, for $\Delta < R$, resulting in either stable nodes (sinks) or unstable saddles, respectively. The condition $\Delta = R$ is satisfied at certain critical values of the parameters at which precisely one of the steady state solutions of the system changes its stability.

In order to highlight the specific aspects of the calibrator dynamics, we will in the following sections consider a number of special cases. Specifically we will examine the (fully) symmetrical calibrator, $\bar{\alpha}'_1 = \bar{\alpha}'_2 = \bar{\alpha}'$, $n_x = n_y = n$, $k_x = k_y = k$, $\beta_x = \beta_y \Rightarrow R = 1$ and $\bar{\gamma}_x = \bar{\gamma}_y = \bar{\gamma}$, and the partially symmetrical calibrator, with the same specifications except that $\bar{\alpha}'_1$ and $\bar{\alpha}'_2$ may differ. At the end of the section some general considerations about dynamics of the system in the most general case will be made.

3.2. The fully symmetrical calibrator ($\bar{\alpha}'_1 = \bar{\alpha}'_2 = \bar{\alpha}'$)

From the analysis of Eqs. (15-16) it is shown that there is always a fixed point with $Y_{ss} = X_{ss}$ and that there exists a minimum value of X_m such that for parameters resulting in $X_{ss} > X_m$, three steady states exist, otherwise only one.

Using $\bar{\alpha}'$ as free parameter and taking fixed values for the rest, i.e., n , R and $\bar{\gamma}$, the condition $\Delta = R = 1$, together with Eq. (15), allows to obtain the critical values $\bar{\alpha}'_m$ and X_m that characterize the appearance of the bifurcation, namely:

$$1 = \frac{n^2(\bar{\gamma} - X_m)^2(\bar{\gamma} - X_m + \bar{\alpha}'_m)^2}{X_m^2 \bar{\alpha}'_m{}^2} \quad (20)$$

whose values can be obtained by numerical methods. For example, for $n = 2$, $k = 80$, $\beta = 0.069$ and $\bar{\gamma} = 0.1$, yields $\bar{\alpha}'_m = 11.24$ and $x_m = 81.46$ or, in the dimensionless variables: $X = 1.018$ and $\bar{\alpha}' = 2.036$. Figure 3 shows the bifurcation diagram for X_{ss} as function of $\bar{\alpha}$ showing that for $\bar{\alpha} > \bar{\alpha}_m$ there are three steady states.

This analysis shows that the (fully) symmetrical calibrator possesses three fixed points for $\bar{\alpha}'_1 > \bar{\alpha}'_m$: a saddle (x_M) with $X_{ss} = Y_{ss}$, and two sinks, one with $X_{ss} > Y_{ss}$ and another one with $X_{ss} < Y_{ss}$, referred to as \vec{x}_R and \vec{x}_L ,

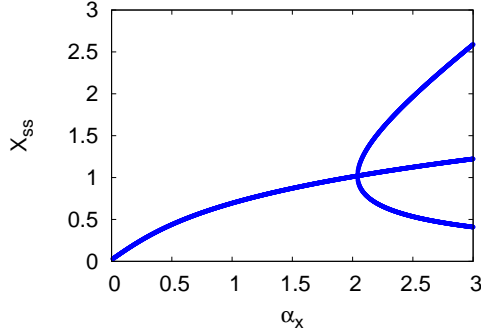


Figure 3: Bifurcation diagram for X_{ss} .

respectively. This behaviour is typical of the occurrence of a (supercritical) pitchfork bifurcation and bistable behaviour.

Regarding the possible trajectories of the dynamic variables, Figure 4 illustrates the phase plane of Eqs. (12-13), where the steady states are located at the intersection of the null clines eqs. (15-16) represented by dashed lines. The solid lines are the stable (W^S) and unstable (W^U) manifolds of the saddle fixed point \vec{x}_M . The stable manifold W^S divides the phase plane in two regions, the first and second octants corresponding to the attraction basins of the sinks \vec{x}_R and \vec{x}_L , respectively. Different possible trajectories in the phase plane are depicted for a given number of initial conditions, where the arrows indicate the flow direction.

In a calibrator experiment the initial value of the repressor protein concentrations x and y would be zero and hence the phase plane trajectories would depart from the origin in Figure 4. For values of $\bar{\alpha}'$ larger than $\bar{\alpha}'_m$, the system becomes unpredictable, as small perturbations in the trajectories would potentially push the system into any of the attraction basins of the sinks \vec{x}_R and \vec{x}_L .

3.3. The partially symmetrical calibrator

We consider now the more general scenario in which $\bar{\alpha}'_1$ and $\bar{\alpha}'_2$ may differ being the rest of variables equal ($n_x = n_y = n$, $k_x = k_y = k$, $\beta_x = \beta_y = \beta$ and $\bar{\gamma}_x = \bar{\gamma}_y = \bar{\gamma}$). The condition $\Delta = R$ which characterizes the occurrence of the pitchfork bifurcations now reads:

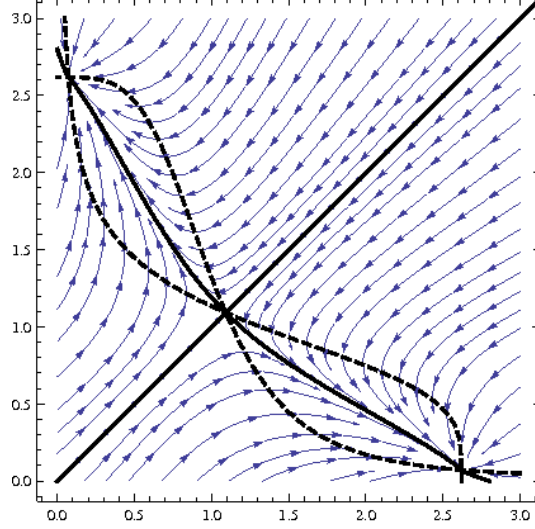


Figure 4: Phase plane, showing the unstable equilibrium point (the point where the two dashed lines touch in the center) and the two steady state solutions (points where the dashed lines touch close to each axis). The arrows show the path the system would do starting from any point in the phase space.

$$1 = \frac{n^2(\bar{\gamma} - X_{ss})(\bar{\gamma} - Y_{ss})(\bar{\gamma} - X_{ss} + \bar{\alpha}'_1)(\bar{\gamma} - Y_{ss} + \bar{\alpha}'_2)}{X_{ss}Y_{ss}\bar{\alpha}'_x\bar{\alpha}'_y} \quad (21)$$

that shall be solved together with Eqs. (15-16) for the fixed points of the system.

Fig. 5 shows the result of the numerical simulation of the resulting system of equations (with initial conditions $X = Y = 0$) by slightly changing the value of $\bar{\alpha}'_2$ with respect to $\bar{\alpha}'_1$. The figure shows the results of different simulations for $\bar{\alpha}'_1 = 3.0$, $n = 3$ and $\bar{\alpha}'_2 = \epsilon\bar{\alpha}'_1$ with $\epsilon = 0.5, 0.6, 0.7, \dots, 1.0, \dots, 1.5$. The results for $\epsilon < 1$ are the points in the right down corner of the plot. One can see that these points positions are very insensitive to the value of $\bar{\alpha}'_2$. There is only one point in the center of the plot, which corresponds to $\bar{\alpha}'_1 = \bar{\alpha}'_2$, it is the unstable saddle, and small perturbations in the system will drive the system away from this solution to either of the other two steady state solutions. Once $\epsilon > 1$, the system goes to the solutions where $Y_{ss} > X_{ss}$ which are represented by the points in the upper left corner. For these points the maximum value of $\bar{\alpha}'$ is growing and one can observe that the solution

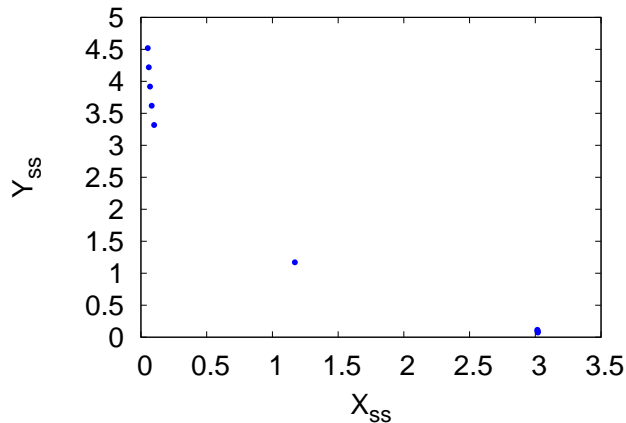


Figure 5: Results for the simulation of the partially symmetric calibrator. On the right, close to the x-axis ($\bar{\alpha}'_2 < \bar{\alpha}'_1$ for these points), there are many points at the same position, showing that, for the parameter region where a bifurcation happens, the solution is insensitive to the value of the weakest between the two $\bar{\alpha}'$ s.

is sensitive to this value. So the steady state solution into which the system falls is only sensitive to the bigger value between $\bar{\alpha}'_1$ and $\bar{\alpha}'_2$ and changes in the smaller among these two parameters has no sensible effect in the final solution.

For the case in which the calibrator falls within the region of bistability, if $\bar{\alpha}'_2 < \bar{\alpha}'_1$ the orbits departing from the origin of Fig. 5 would fall within the attraction basin of solution \vec{x}_R . It is nevertheless observed that \vec{x}_R is quite insensitive to the actual $\bar{\alpha}'_2/\bar{\alpha}'_1$ ratio. In consequence, the system would show a stable but rather insensitive response to different *query* promoters. On the other hand, if $\bar{\alpha}'_1 < \bar{\alpha}'_2$, the orbits departing from the origin would fall within the attraction basin of solution \vec{x}_L , which changes appreciably as a function of the $\bar{\alpha}'_2/\bar{\alpha}'_1$ ratio. Thus the system would not only be stable, but also rather sensitive to changes in the effective *query* promoter affinity. It should be kept in mind that the sensing protein concentration, p_s , can be used to modify $\bar{\alpha}'_1$, $\bar{\alpha}'_2$, which changes from unity to $\bar{\alpha}_{1,2}$ as p_s changes from zero to infinity and therefore the ratio $\bar{\alpha}'_2/\bar{\alpha}'_1$ changes with p_s .

We can also define the fluorescence ratio as the ratio of X/Y if $X < Y$ and Y/X if $Y > X$. This will be the intensity ratio of the two fluorescences once the system reaches stability. In Fig. 6 we show a plot of this ratio for

different values of $\bar{\alpha}'_2/\bar{\alpha}'_1$. This ratio grows until it reaches its maximum when $\bar{\alpha}'_2 = \bar{\alpha}'_1$ and then it decreases. Another observation about this parameter is that the bigger $\bar{\alpha}'_1$ is, the less sensible to the ratio $\bar{\alpha}'_2/\bar{\alpha}'_1$ the fluorescence ratio will be.

3.4. The calibrator dynamics in the general case

The theorem of Andronov and Pontryagin [21] states that Eqs. (12-13) in the symmetrical case are structurally stable, since every fixed point is hyperbolic (its eigenvalues have a non-null real part) and there are no orbits connecting two saddles (since there is only one). Structural stability implies that the phase plane topology is preserved under small perturbations of the parameters. Hence, the phase plane of Eqs. (12-13) in the case that $\bar{\alpha}'_x \approx \bar{\alpha}'_y$, $n_x \approx n_y$, $k_x \approx k_y$, $\beta_x \approx \beta_y$ and $\bar{\gamma}_x \approx \bar{\gamma}_y$, is topologically equivalent to that shown in Fig. 4, meaning that there is a continuous function (homeomorphism) between both phase planes.

Changing the ratio of other structural parameters of the calibrator has similar results as in the partially symmetrical case. For a given range close to the value 1 for the ratio of each parameter ratio ($n_{x/y}$, $\beta_{x/y}$, ...) the bifurcation appears while far from the value 1 the bifurcation cannot be seen. The range is usually bigger, the bigger the values for $\bar{\alpha}'_{1,2}$ are. In Fig. 7 we show, as an example, the range where the bifurcation appears for different values of β_x/β_y .

If $R < 1$ the orbits departing from the origin ($X = Y = 0$) would fall within the attraction basin of solution \vec{x}_L , on the other hand if $R > 1$ the orbits departing from the origin would fall within the attraction basin of solution \vec{x}_R .

3.5. Calibrator performance analysis: robustness and response time

In order to use this system to measure the relative strength between two promoters, one should keep in mind two factors. The first important factor is the right choice for the parameters of the repressor proteins and *device* promoter in order to have a robust system, that gives a stable response that can be easily interpreted. Second, is the time response of the device, that means, how long does the system needs to reach its steady state solution.

When the equations are written in the dimensionless form, the parameters k_x and k_y do not appear explicitly, see eqs. (9-10). These parameters appear implicit in the definition of the variables X and Y and in the $\bar{\gamma}$ parameters (which have small influence in the dynamics of the system). By choosing

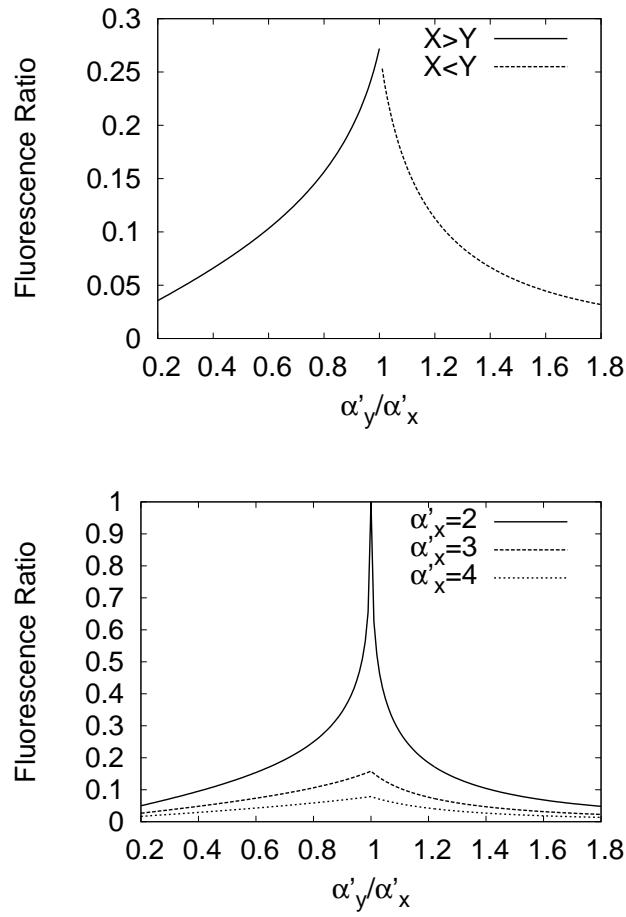


Figure 6: Upper plot: Fluorescence ratio for different values of $\bar{\alpha}'_y/\bar{\alpha}'_x$ ($\bar{\alpha}'_x = 2.5$). The blue points are solutions where $X > Y$ and in the red points $Y > X$. Lower plot: Fluorescence ratio for different values of $\bar{\alpha}'_y/\bar{\alpha}'_x$ and for different values of $\bar{\alpha}'_x$ (Solid line: $\bar{\alpha}'_x = 2$, dashed line: $\bar{\alpha}'_x = 3$, dotted line: $\bar{\alpha}'_x = 4$).

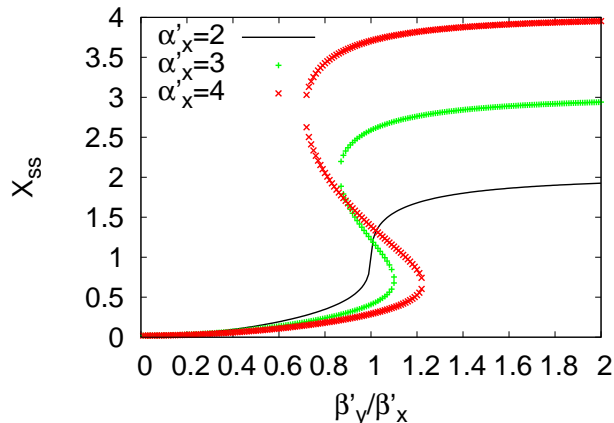


Figure 7: (Color online) Position of X_{ss} for different values of β_y/β_x . In the black curve $\bar{\alpha}'_x = \bar{\alpha}'_y = 2$, in the blue curve $\bar{\alpha}'_x = \bar{\alpha}'_y = 3$ and in the red one $\bar{\alpha}'_x = \bar{\alpha}'_y = 4$.

$k_x = k_y$ the results will be easier to interpret since the fluorescence is directly related to the concentrations of the proteins x and y and, by setting $k_x = k_y$, the fluorescence intensity ratio (X/Y and Y/X) and the fluorescence intensity difference ($|X - Y|$) will be directly proportional to these parameter calculated with the real protein concentrations.

An experiment made with the calibrator would consist of cloning a plasmid with the calibrator genetic circuit assembled with the *device* promoter (whose parameters one have to choose) among known ones and with a *query* promoter whose parameters are unknown. The plasmid should be inserted in cells in solutions of the signaling protein at different concentrations p_s . Each promoter is modeled through two parameters, $\bar{\alpha}_{1/2}$ and $k_{1/2}$, $1/2$ stand for *device/query* promoter. While at low p_s concentrations both promoters are weak and give a weak fluorescence response, at high p_s concentrations, both promoters are saturated and their strength is maximal. From the fluorescence intensities at these high concentrations of the signaling protein it is possible to establish the relative strength of the two promoters $\bar{\alpha}_2/\bar{\alpha}_1$. In figures 8 and 9 we show plots of the fluorescence difference defined as $|X - Y|$ and the fluorescence ratio X/Y for three different values of $\bar{\alpha}_1$ and varying $\bar{\alpha}_2$ at high signaling protein concentrations (the effective strength of both promoters is maximum).

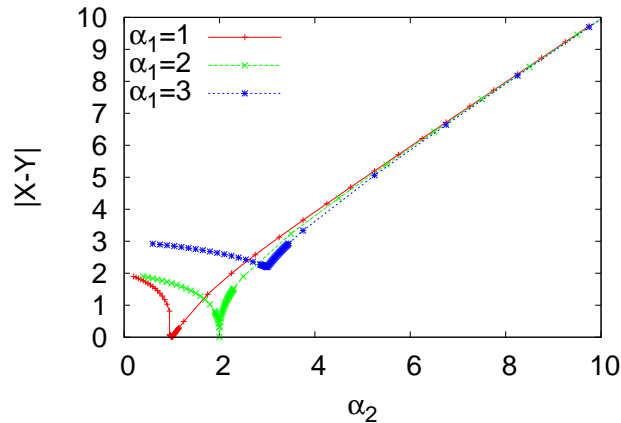


Figure 8: (Color online) The fluorescence difference for different values of $\bar{\alpha}_1$ as a function of $\bar{\alpha}_2$. Note that for values of $\bar{\alpha}_2$ sufficiently higher than $\bar{\alpha}_1$ the fluorescence difference increases linearly with the value of $\bar{\alpha}_2$.

The first thing to note from figures [8](#) and [9](#) is that, if the *query* promoter is stronger than the *device* one, the *device* fluorescence (X) will be strongly suppressed, and the fluorescence intensity coming from the *query* promoter is proportional to its strength (the response of the system is linear). That means, choosing a weak *device* promoter, one can establish the relative strength of other promoters by a simple proportionality law given by the linear response plotted in figure [8](#).

At each different p_s concentration, the effective strength of the *device* and *query* promoters is different, see eq. [\(14\)](#). The parameter that distinguishes two promoters, with respect to the p_s concentration, is their Michaelis constants, $k_{1,2}$. The parameters $k_{1,2}$ mark the rhythm at which the effective strength of each promoter grows. If a promoter has a small value of k , at low p_s concentrations of the signaling protein, the promoter is already acting at full strength, while for high values of k the promoter saturates only at high values of p_s . We have already established to choose a small value for the *device* promoter $\bar{\alpha}_1$, so we expect the *query* promoters to have $\bar{\alpha}_2 > \bar{\alpha}_1$. If $k_2 < k_1$, the effective strength of the *query* promoter is always bigger than the relative strength of the *device* one, and in the experiment one observes that the luminosity associated with the *query* promoter is stronger for any value of the signaling protein concentration p_s . On the other hand, if one

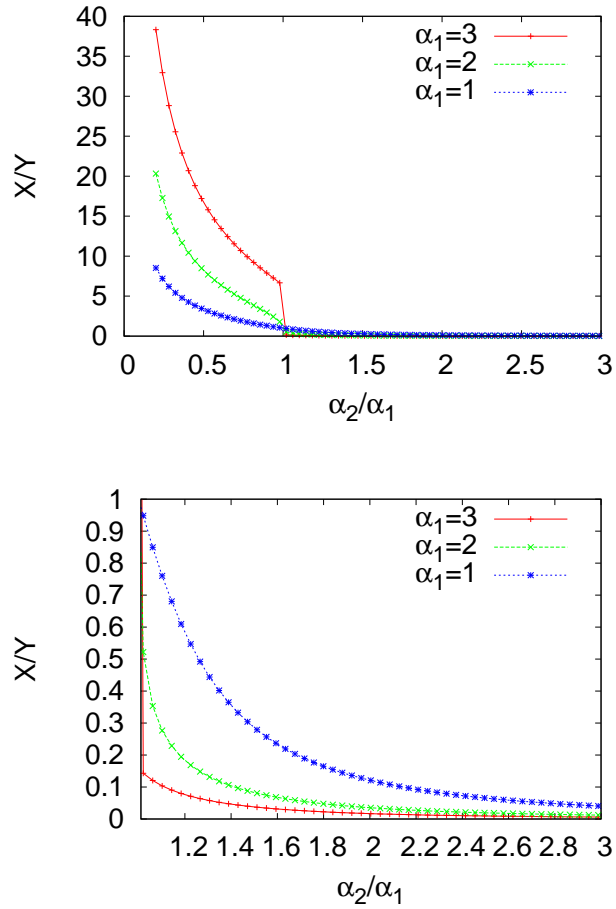


Figure 9: (Color online) Upper plot: the fluorescence ratio X/Y as a function of $\bar{\alpha}_2/\bar{\alpha}_1$ for different values of $\bar{\alpha}_1$. One can clearly see that for similar values of $\bar{\alpha}_1$ and $\bar{\alpha}_2$, when the bifurcation occurs, the system goes to a state where the repressor protein of the stronger promoter completely dominates the system. Lower plot: Detail of the region where $\bar{\alpha}_2 > \bar{\alpha}_1$.

chooses a small value for k_1 , already at low p_s concentrations the strength of the *device* promoter saturates, and if k_1 is small enough it saturates before the effective strength of the *query* promoter reaches a value bigger than $\bar{\alpha}_1$. In this situation one would observe at low concentrations of p_s the luminosity of the *device* promoter stronger than the one coming from the *query* promoter. Then, at some critical value of $p_s = p_{sc}$ both strength are equal and for $p_s > p_{sc}$ the stronger fluorescence is the one from the *query* promoter. For $n_1 = n_2$, the value of k_2 given in units of k_1 as a function of p_{sc} (also in units of k_1) is given by:

$$k_2 = \sqrt[n]{p_{sc}^n \left(\frac{\bar{\alpha}_2}{\bar{\alpha}_1} - 1 \right) - \frac{\bar{\alpha}_2}{\bar{\alpha}_1}}, \quad (22)$$

$$p_{sc} = \sqrt[n]{\left(k_2^n - \frac{\bar{\alpha}_2}{\bar{\alpha}_1} \right) \left(\frac{\bar{\alpha}_1}{\bar{\alpha}_2 - \bar{\alpha}_1} \right)}. \quad (23)$$

In figure [10](#) we show a few examples of results one might expect for different values of k_2 .

So, the construction of the calibrator device, as we present it, would be the following: first one chooses a very weak promoter which has a small Michaelis constant to act as the *device* promoter in the calibrator. Second step is to define a standard, to choose a known promoter, clone the calibrator device with it as *query* promoter and perform a measurement of the fluorescence intensity of this standard promoter at high p_s concentrations. This fluorescence intensity is the standard one, to which we can compare other promoters. Now performing the experiment with another promoter acting as *query* promoter one obtains another value for the luminosity that we can compare with the standard one. The higher or lower this luminosity is with respect to the standard, the stronger or weaker the promoter is compared with the standard, so one can establish the value of α_2 . Knowing α_2 one can perform the same measurement for different p_s concentrations in order to establish the critical value of p_s where the *query* fluorescence becomes higher than the *device* one. Knowing the value of p_{sc} it is possible to establish the value of k_2 by means of eq. [22](#) (assuming both promoters have the same n).

Now that we have established the ideal parameters for the *device* promoter (weak strength and small Michaelis constant) and set $k_x = k_y$ and $\beta_x = \beta_y$ the last important factor is the time response of the system.

In figure [III](#) we show plots for the t_f , the time the systems needs to reach its steady state¹ for different values of $\bar{\alpha}_1$. One observes that the time response of the system has a peak with the maximum around $30\beta_x^{-1}$ when the effective strength of both promoters is equal and then it goes to a rather stable value close to $7\beta_x^{-1}$. For a realistic value of β_x like 0.069 min^{-1} the peak value for t_f is 7 hours, while for most of the measurements (the calibrator at different p_s concentrations) this time should be around two hours.

4. Conclusions

In the present study we have proposed a biological device that works as a promoter calibrator in which the strength of a collection of *query* promoters can be measured against the strength of a *device* promoter. Some of the key features of the proposed design are its single cell character, high modularity and handy construction: a unique molecular cloning permits the change of the promoter ready to be calibrated. The designed performance of the proposed biological device has been demonstrated by means of an effective mathematical model. The sensitivity analysis of the model shows that there is a sensible relation between the relative promoter strengths and the final steady fluorescences measured by the system.

Furthermore, a response time analysis shows that the device can produce a large difference in the repression protein concentrations and in turn in the corresponding fluorescence in approximately two hours.

Finally our promoter calibrator principle may lead to an improvement in the modeling and characterizations of systems in Synthetic Biology, which frequently rely on arbitrarily characterized, or even non-characterized, promoters.

acknowledgements

This work has been funded by MICINN TIN2009-12359 project ArtBio-Com, the Spanish Ministerio de Educacin y Ciencia through the program Juan de la Cierva, the FPI grant program of the Generalitat Valenciana and the Beca de recerca predoctoral from the Universitat Rovira i Virgili.

¹The system actually goes asymptotically to its steady state without really reaching it. What we have calculated is the time needed so that the sum of the absolute values of the derivatives of X and Y reach a small value (0.01).

The authors would also like to thank the Valencia iGEM 2007 team and Enrique O'Connor for useful discussions.

References

- [1] Alper et al., Tuning genetic control through promoter engineering., PNAS. 102 (36), 12678-12683 (2005).
- [2] Kumar A and Snyder M., Genome-Wide Transposon Mutagenesis in Yeast., Current Protocols in Molecular Biology., 13, 13.3 (2001).
- [3] Elowitz MB and Leibler S., A synthetic oscillatory network of transcriptional regulators., Nature, 403, 335-338 (2000).
- [4] Monod, J. and Jacob, General conclusions: teleonomic mechanisms in cellular metabolism, growth and differentiation., Cold spring Harb. Symp. Quant. Biol., 26, 389-401 (1961).
- [5] Ptashne, M., A genetic switch: phage λ and Higher Organisms. (1992).
- [6] Ishiura, M et al., Expression of gene cluster kaiABC as a circadian feedback process in cyanobacteria., Science, 281, 1519-1523 (1998)
- [7] Santos CN and Stephanopoulos G., Combinatorial engineering of microbes for optimizing cellular phenotype., Current Opinion in Chemical Biology., 12, 168-176 (2008)
- [8] Sayut DJ, Niu Y, and Sun L., Construction and Engineering of Positive Feedback Loops., JACS chemical Biology., 1(11), 692-696 (2006)
- [9] Weber, W., and Fussenegger, M., Pharmacologic transgene control systems for gene therapy, J. Gene Med., 8, 535-556 (2006).
- [10] Walz, D., and Caplan, S. R., Chemical oscillations arise solely from kinetic nonlinearity and hence can occur near equilibrium, Biophys. J., 69, 1698-1707 (1995).
- [11] Gardner T, Cantor CR and Collins JJ., Construction of genetic toggle switch in Escherichia coli., Nature., 403, 339-342 (2000).
- [12] J. Stricker et. al., A fast, robust and tunable synthetic gene oscillator., Nature., 456, 516-519 (2008).

- [13] Becskei A and Serrano L., Engineering stability in gene networks by autoregulation., *Nature* 405, 590-593 (2000).
- [14] Becskei A, Seraphin B and Serrano L., Positive feedback in eukaryotic gene networks: cell differentiation by graded to binary response conversion., *The EMBO Journal*, 20(10), 2528-2535 (2001).
- [15] Cox, Surette, Elowitz., Programming gene expression with combinatorial promoters., *Mol Syst Biol.*, 3, 145(2007).
- [16] J. Miller., *Experiments in molecular genetics*, Cold Spring Harbor Laboratory (1972).
- [17] Liang et al., Activities of Constitutive Promoters in *Escherichia coli.*, *J Mol Biol.*, 292, 19-37, (1999).
- [18] Smolke & Keasling., Effect of Gene Location, mRNA Secondary Structures, and RNase Sites on Expression of Two Genes in an Engineered Operon., *Biotech Bioeng.*, 80, 762-776 (2002).
- [19] Khlebnikov et al., Modulation of gene expression from the arabinose-inducible araBAD promoter., *J Ind Microb Biotec.*, 29, 34-37 (2002).
- [20] J. R. Kelly et. al., Measuring the activity of BioBrick promoters using an in vivo standard., *Journal of Biological Engineering*, 3, 1-13 (2009).
- [21] Guckenheimer, J., and Holmes, P., *Nonlinear oscillations, dynamical systems, and bifurcations of vector fields.*, Springer Berlin (1990).

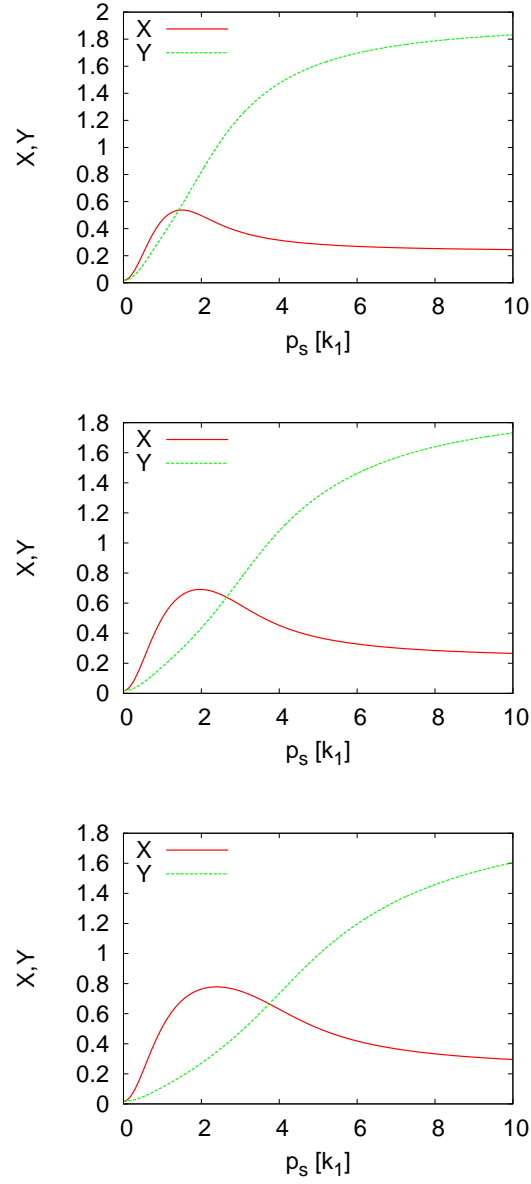


Figure 10: In all plots $\bar{\alpha}_1=k_1=1$ and $\bar{\alpha}_2=2$. In the upper plot $k_2=2$, in the center $k_2=3$ and in the bottom plot $k_2=4$. The values for p_{sc} are respectively: $\sqrt{2}$, $\sqrt{7}$ and $\sqrt{14}$.

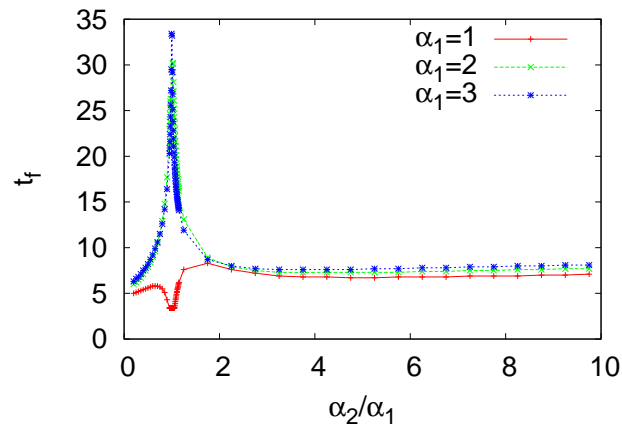


Figure 11: Response time of the system for different values of $\bar{\alpha}_1$ and $\bar{\alpha}_2$. For values of the $\bar{\alpha}$'s that the system presents a bifurcation, the response time can be large because the system spend time in its non-equilibrium solution.

New Approach for Phylogenetic Tree Recovery Based on Genome-Scale Metabolic Networks

DANIEL GAMERMANN,^{1,2} ARNAUD MONTAGUD,² J. ALBERTO CONEJERO,²
JAVIER F. URCHUEGUÍA,² and PEDRO FERNÁNDEZ DE CÓRDOBA²

ABSTRACT

A wide range of applications and research has been done with genome-scale metabolic models. In this work, we describe an innovative methodology for comparing metabolic networks constructed from genome-scale metabolic models and how to apply this comparison in order to infer evolutionary distances between different organisms. Our methodology allows a quantification of the metabolic differences between different species from a broad range of families and even kingdoms. This quantification is then applied in order to reconstruct phylogenetic trees for sets of various organisms.

Key words: connectivity, genome-scale metabolic models, networks, phylogeny.

1. INTRODUCTION

METABOLIC MODELS AT THE GENOME SCALE ARE one of the prerequisites for obtaining insight into the operation and regulation of metabolism as a whole (Barrett et al., 2006; Morange, 2009; Patil et al., 2004; Stephanopoulos et al., 1998). Uses of metabolic models embrace all aspects of biotechnology, from food (Nielsen, 2001) to pharmaceutical (Boghigian et al., 2010) and biofuels (Montagud et al., 2010, 2011a). Genome-scale metabolic network reconstruction is, in essence, a systematic assembly and organization of all reactions that build up the metabolism of a given organism. It usually starts with genome sequences to identify reactions and network topology. This methodology also offers an opportunity to systematically analyze *omics* datasets in the context of cellular metabolic phenotype.

Reconstructions have now been built for a wide variety of organisms and have been used toward five major ends (Oberhardt et al., 2009): contextualization of high-throughput data (Stephanopoulos et al., 1998; Montagud et al., 2010; Edwards et al., 1999), guidance of metabolic engineering (Angermayr et al., 2009), directing hypothesis-driven discovery (Nevoigt, 2008), interrogation of multi-species relationships (Stolyar et al., 2007), and network property discovery (Guimera and Nunes Amaral, 2005).

Nowadays, phylogeny has become so popular that it's being used in almost every branch of biology (Yang and Rannala, 2012). Beyond representing the relationships among species in the tree of life, phylogeny is used to describe relationships between paralogues in a gene family (Maser et al., 2001), histories of populations (Edwards, 2009), the evolutionary and epidemiological dynamics of pathogens (Marra et al.,

¹Cátedra Energesis de Tecnología Interdisciplinar, Universidad Católica de Valencia San Vicente Mártir, Valencia, Spain.

²Instituto Universitario de Matemática Pura y Aplicada, Universidad Politécnica de Valencia, Valencia, Spain.

2003; Grenfell et al., 2004), the genealogical relationship of somatic cells during differentiation and cancer development (Salipante and Horwitz, 2006), and even the evolution of language (Gray et al., 2009). More recently, molecular phylogenetics has become an indispensable tool for genome comparisons (Brady and Salzberg, 2011; Kellis et al., 2003; Green et al., 2010).

A phylogeny is a tree containing vertices that are connected by branches. Each branch represents the persistence of a genetic lineage through time, and each vertex represents the birth of a new lineage. If the tree represents the relationships among a group of species, then the vertices represent speciation events. Phylogenetic trees are not directly observed and are instead inferred from sequence or other data. Phylogeny reconstruction methods are either distance-based or character-based. In distance matrix methods, the distance between every pair of sequences is calculated, and the resulting distance matrix is used for tree reconstruction. For a very instructive review, please refer to Yang and Rannala (2012).

This work is organized as follows. In the next section, we explain the genome-scale models with which we work, how we define a parameter for comparing two models, and how we recover the phylogenetic tree from the comparison matrix obtained for many metabolic models. Additionally, we will account for the minimum spanning tree of a nondirected, connected, weighted network associated with these metabolic models. In the subsequent section, we present the results, a brief study of the sensibility of the comparison parameter, and a summary and overview.

2. COMPARISON BETWEEN METABOLIC MODELS

In a recent article (Reyes et al., 2012), a method has been presented for automatically generating genome-scale metabolic models from data contained in the KEGG database (Kanehisa and Goto, 2000). The method consists of searching the database for genes and pathways present in an organism and downloading the corresponding set of chemical reactions. The algorithm filters isoenzymes, or other repeated reactions, and may add missing reactions to a given pathway using a probabilistic criterion based on the comparison of the organism's pathway with the same pathway in other organisms. In this work, we use data obtained from this platform, but the method described can, in principle, be used with any set of metabolic models given that the compound names in the models follow the same standard (the same compound has the same name in all models).

The methodology we are about to describe will make use of two fundamentally different networks. One is the metabolic network build-up from the chemical reactions contained in an organism's metabolism. In this network, each metabolite represents a node (or vertex), and each link (or edge) is associated with a pair of nodes if their respective metabolites are connected as a substrate and product by some reaction. The second kind of network is the complete weighted network where each vertex represents an organism and each edge connecting two nodes is weighted by the parameter measuring the metabolic distance between the organisms' metabolism (note that this will be a complete network, where all vertices are connected to all others). In order to distinguish clearly the two networks in the text, we will talk about nodes and links for the metabolic network while for the organisms' network we will use the terms vertices and edges. As for the notation, we use capital letters (N, V, E) for the network, nodes, and links in the metabolic networks and curly letters ($\mathcal{N}, \mathcal{V}, \mathcal{E}$) for the network, vertices, and edges in the organisms' network. In the metabolic network we will use roman lowercase letters for indices representing single metabolites in sums, while for the organisms network we use Greek letters for the indices representing single organisms.

The first step in our work is to construct for every metabolic model A a nondirected connected network $N_A = (V_A, E_A)$ from the information contained in it. Here, V_A stands for the set of nodes of A , and E_A stands for its set of links. A metabolic model comprises a set of chemical reactions. Each chemical reaction associates a set of substrates with a set of products. For constructing the network, first we define the set of nodes V_A as the set of compounds in A (metabolites present in the model), assigning a node to each metabolite. The chemical reactions in the model will define the links of the network. If two metabolites appear as a substrate and as a product, respectively, in a chemical reaction, a link connecting the correspondent nodes is added to the network. A typical metabolic model of a prokaryote, with around 1000 metabolites and the same number of chemical reactions, becomes through this process a nondirected connected network with 1000 nodes and approximately 3000 links.

The problem at hand is to elaborate a method to systematically compare and quantify the differences between two metabolic networks. For this purpose, we define a parameter that scales between zero and

infinity, zero meaning identical networks and infinity for networks that either share no node or no link in common. The definition of this parameter is based on the identity of the nodes (the compounds) but not directly on the chemical reactions of the metabolic models, only indirectly through the links of the network.

Here we start with the metabolic networks of two organisms $A = (V_A, E_A)$ and $B = (V_B, E_B)$. The set of all metabolites in between the two organisms $A \cup B = (V_A \cup V_B, E_A \cup E_B)$ can be divided into a partition of three disjoint sets: the set of metabolites only present in A , the set of metabolites only present in B , and the set of metabolites common to both organisms:

$$V_{A \cup B} = \underbrace{(V_A \setminus V_B)}_{\text{Only in A}} \cup \underbrace{(V_A \cap V_B)}_{\text{Common}} \cup \underbrace{(V_B \setminus V_A)}_{\text{Only in B}} \quad (1)$$

where \setminus stands for the difference of sets. A representation of this situation is shown in Figure 1. As it is represented there, each metabolite may have connections to metabolites within its set and connections to metabolites in the other sets.

Suppose that $V_A \cup V_B = \{v_1, \dots, v_n\}$. Fix an arbitrary node v_i , $1 \leq i \leq n$. We can consider its degree in $A \cup B$, that is, the total number of connections of v_i to the rest of the metabolites of $V_A \cup V_B$, that we denote by $\text{deg}(v_i)$. We can also consider the degree of v_i when we restrict ourselves to the subnetwork generated by the node in $(V_A \setminus V_B)$, which we will call $\text{deg}_{A \setminus B}(v_i)$. Similarly, we can also define $\text{deg}_{A \cap B}(v_i)$ and $\text{deg}_{B \setminus A}(v_i)$. With these degrees we can define, for each metabolite $v_i \in V_A \cup V_B$, the rate $p_{A \setminus B, i}$ of connections of v_i to metabolites inside A and not in B with respect to the total number of connections of v_i , that is:

$$p_{A \setminus B, i} = \frac{\text{deg}_{A \setminus B}(v_i)}{\text{deg}(v_i)}.$$

Analogously, we can define

$$p_{B \setminus A, i} = \frac{\text{deg}_{B \setminus A}(v_i)}{\text{deg}(v_i)} \quad \text{and} \quad p_{A \cap B, i} = \frac{\text{deg}_{A \cap B}(v_i)}{\text{deg}(v_i)}.$$

The following weighted sum of the rates $p_{A \setminus B, i}$ provides a parameter of the differentiation of $A \cup B$ with respect to A :

$$\alpha = \left(\frac{1}{|V_A \setminus V_B|} \sum_{v_j \in V_A \setminus V_B} \text{deg}(v_j) \right) \sum_{v_i \in V_A \setminus B} \frac{p_{A \setminus B, i}}{\text{deg}(v_i)}$$

On the one hand, the rates $p_{A \setminus B, i}$ are multiplied by the inverse of the total number of connections of v_i to give more importance to the metabolites with fewer connections. The reason to do this is that metabolic networks of all organisms usually share their hubs (metabolites with many connections), so in order to establish differences and similitude for different networks, one should focus on specific metabolites particular to only some organisms sharing common features. This weighting of $p_{A \setminus B, i}$ with the inverse of $\text{deg}(v_i)$ will reduce the importance of very connected metabolites (hubs) that are common to most organisms and adds weight to specific metabolites that might be particular for a branch in the tree of life, helping in this way to differentiate the branches. Removing this inverse weighting results in a very mild difference between the organisms, which makes the second step in the reconstruction very hard, because the differences will appear as a small noise in the parameters.

On the other hand, the factor $\frac{1}{|V_A \setminus V_B|} \sum_{v_j \in V_A \setminus V_B} \text{deg}(v_j)$ gives an average of the number of connections of the metabolites only present in A with respect to the whole network. This is done in order to rescale the size

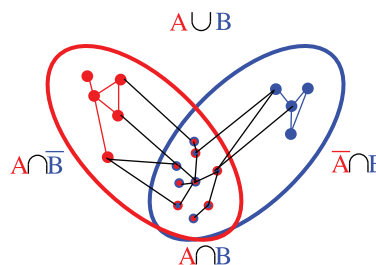


FIG. 1. Representation of the sets of metabolites between two organisms.

of the network and normalize (balance) the parameter after the inverse weighting done by the factor $\deg(v_i)$ for each metabolite in the set.

Analogously, we can define β and γ from the metabolites in the other two sets.

$$\beta = \left(\frac{1}{|V_B \setminus V_A|} \sum_{v_j \in V_B \setminus V_A} \deg(v_j) \right) \sum_{v_i \in V_B \setminus A} \frac{P_{B \setminus A, i}}{\deg(v_i)}$$

$$\gamma = \left(\frac{1}{|V_A \cap V_B|} \sum_{v_j \in V_A \cap V_B} \deg(v_j) \right) \sum_{v_i \in V_A \cap B} \frac{P_{A \cap B, i}}{\deg(v_i)}$$

For illustrating the process, let's consider three organisms, the *Synechocystis* sp. PCC 6803 (which we refer to as syn), *Synechococcus elongatus* PCC7942 (referred to as syf), and the *Escherichia coli* K-12 MG1655 (referred to as eco). In Table 1, you can see the number of metabolites and links in the networks of these organisms, and in Table 2, we show the number of elements in each one of the three sets of the partition in which we split the set of nodes of the network obtained from each pair of these three organisms.

Now let's focus on a few metabolites to see their contribution to the differentiation parameters (i.e., to the parameters α , β , and γ). For this, we chose pyruvate (PYR), glyoxylate (GXL), and 2-dehydro-3-deoxy-6-phospho-D-gluconate (6PDG), which are respectively very, medium, and poorly connected metabolites present in these three organisms. In Table 3, we show the contribution of these metabolites to the parameters α , β , and γ . Column δ_i of Table 3 shows, for each one of these metabolites, the value of

$$\delta_i = \left(\frac{\frac{1}{\deg(v_i)}}{\sum_{v_j \in V_A \cap V_B} \frac{1}{\deg(v_j)}} \right), \tag{2}$$

which is the weight proportion associated with the metabolite (with respect to all others) discussed above in the text. Note that this weight for PYR is very small, since pyruvate has many connections and is a very common metabolite in the metabolism of virtually any organism, and therefore is not a good candidate to help differentiate branches in the tree of life. On the other hand, 6PDG has few connections and they are different in cyanobacteria than in the *E. Coli*, potentially helping, in this way, to differentiate these two branches.

Finally, the comparison between the networks A and B , namely $\zeta_{A,B}$, is defined as:

$$\zeta_{A,B} = \frac{\frac{|V_B|}{|V_A|} \alpha + \frac{|V_A|}{|V_B|} \beta}{2\gamma}$$

The parameters α and β are balanced since some organisms have much smaller metabolic networks than others. If this is not corrected, it results in a disproportionate size between subnetworks generated by $V_{A \setminus B}$ and $V_{B \setminus A}$. In order to weaken this difference, the parameter factors $\frac{|V_B|}{|V_A|}$ and $\frac{|V_A|}{|V_B|}$ are introduced. For two identical networks, α and β are zero, and so that $\zeta = 0$. For two networks that do not have a single metabolite in common we have $\gamma = 0$ and so $\zeta = \infty$.

3. CONSTRUCTION OF THE PHYLOGENETIC TREE

Given a set of n organisms $\{A_1, A_2, \dots, A_n\}$, we will see how to construct their phylogenetic tree taking into account the degrees of similarity between every pair of metabolic models.

TABLE 1. SETS OF NODES AND LINKS

Organism	No. nodes	No. links
syn	1001	2891
syf	979	2810
eco	1227	3801

Nodes and links in the networks of syn, syf, and eco.

TABLE 2. METABOLITES IN THE PARTITIONS

	<i>syf</i>	<i>eco</i>
syn	$ V_A \cap V_B = 911$	$ V_A \cap V_B = 778$
	$ V_A \setminus V_B = 90$	$ V_A \setminus V_B = 223$
	$ V_B \setminus V_A = 68$	$ V_B \setminus V_A = 449$
syf	-	$ V_A \cap V_B = 775$
	-	$ V_A \setminus V_B = 204$
	-	$ V_B \setminus V_A = 452$

Metabolites in the three sets of the partition when comparing three organisms.

Firstly, let $\mathcal{N} = (\mathcal{V}, \mathcal{E}, w)$ be a nondirected, connected, complete weighted network, where $\mathcal{V} = \{A_1, A_2, \dots, A_n\}$ is the set of vertices that represent the metabolic models of the aforementioned organisms, \mathcal{E} is the set of edges (A_μ, A_ν) , $1 \leq \mu, \nu \leq n$, $\mu \neq \nu$, and $w : \mathcal{E} \rightarrow \mathbb{R}$ is a function that assigns to every edge (A_μ, A_ν) , the amount $w_{\mu, \nu} = \zeta_{A_\mu, A_\nu}$. Looking at the definition of ζ , we observe that this network \mathcal{N} must be symmetric. In particular, all the weights in our study are strictly positive.

Secondly, we will compute a minimum spanning tree of \mathcal{N} , that is, a tree that has \mathcal{V} as the set of vertices, and such that the sum of the weights associated with the edges of this tree is minimum. In these trees, every vertex $A_\mu \in \mathcal{V}$ is connected with at least one of the other vertex of $\mathcal{V} \setminus \{A_\mu\}$ by an edge that has minimum weight among all the edges incident to A_μ . The well-known Kruskal algorithm gives us a procedure for finding these trees (see, for instance, Gross and Yellen, 2005). We just have to follow the trace of the Kruskal algorithm in order to recover the phylogenetic tree of the organisms represented by the models A_1, \dots, A_n .

In order to compute the phylogenetic tree of the models $\{A_1, A_2, \dots, A_n\}$, consider the minimum spanning tree of \mathcal{N} , namely $\mathcal{T} = (\mathcal{V}, \mathcal{E}', w|_{\mathcal{E}'})$, where $\mathcal{E}' \subset \mathcal{E}$ and $w|_{\mathcal{E}'}$ denotes the restriction of the function w to the elements in \mathcal{E}' . Let us take all the elements of \mathcal{E}' in decreasing order of weights, that is, $\mathcal{E}' = \{e'_1, e'_2, \dots, e'_{n-1}\}$ with $w(e'_1) \geq w(e'_2) \dots \geq w(e'_{n-1})$. We are going to remove edges from \mathcal{T} following this order. Every time an edge is removed, the number of connected components of the resulting graph is increased in one respect to the previous one. We can represent this division of connected components by a binary tree. The phylogenetic tree is generated taking into account how we divide \mathcal{T} .

There are two different situations depending on the size of the (new) connected components (if any of them consists on a single vertex or not). Let us start with the edge with maximum weight in \mathcal{T} which we have denoted as e'_1 . Suppose that e'_1 is adjacent to two vertices A_{μ_0} and A_{ν_0} , with $1 \leq \mu_0, \nu_0 \leq n$, $\mu \neq \nu$. Then two possibilities can occur:

- (a) One of these vertices, for instance A_{μ_0} , is a leaf (vertex of degree 1),

TABLE 3. METABOLITE WEIGHTING

Metabolite	Organisms in comparison	$p_{A \cap B, i}$	δ_i	Contribution (%)
PYR	syn and syf	0.98	0.127	0.0064
	syn and eco	0.73	0.117	0.0044
	syf and eco	0.75	0.113	0.0044
GXL	syn and syf	0.86	0.454	0.020
	syn and eco	0.87	0.550	0.024
	syf and eco	0.80	0.439	0.018
6PDG	syn and syf	1.00	3.176	0.16
	syn and eco	0.80	1.762	0.072
	syf and eco	0.80	1.757	0.072

Contributions of different metabolites to the differentiation parameter (ζ) between two networks. The column δ_i shows the weight of the metabolite in the calculation of $p_{A \cap B, i}$, which is the inverse of the degree of the metabolite divided by the sum of the inverses of the degrees of all metabolites contributing to the parameter.

TABLE 4. COMPARISON MATRIX

<i>org</i>	<i>syf</i>	<i>syn</i>	<i>syc</i>	<i>mge</i>	<i>lpl</i>	<i>cbe</i>	<i>bcj</i>	<i>eco</i>	<i>tma</i>	<i>ypk</i>
syf	0.0	0.019	0.0061	0.1628	0.1493	0.1239	0.1083	0.106	0.1567	0.1155
syn	0.019	0.0	0.0177	0.1821	0.1524	0.1269	0.1079	0.1116	0.161	0.1213
syc	0.0061	0.0177	0.0	0.1779	0.1616	0.1318	0.1067	0.1032	0.1572	0.112
mge	0.1628	0.1821	0.1779	0.0	0.1179	0.1351	0.1257	0.1252	0.1159	0.1266
lpl	0.1493	0.1524	0.1616	0.1179	0.0	0.0711	0.1098	0.1194	0.0668	0.111
cbe	0.1239	0.1269	0.1318	0.1351	0.0711	0.0	0.0979	0.0926	0.0674	0.1049
bcj	0.1083	0.1079	0.1067	0.1257	0.1098	0.0979	0.0	0.0592	0.1167	0.0557
eco	0.106	0.1116	0.1032	0.1252	0.1194	0.0926	0.0592	0.0	0.102	0.0294
tma	0.1567	0.161	0.1572	0.1159	0.0668	0.0674	0.1167	0.102	0.0	0.1044
ypk	0.1155	0.1213	0.112	0.1266	0.111	0.1049	0.0557	0.0294	0.1044	0.0

Comparison matrix for 10 organisms.

(b) Neither of these two vertices is a leaf (each vertex is still connected with the other vertex). This happens only if the former connected component has three or more vertices.

We point out that our phylogenetic tree will have two types of vertices: the leaves, which represent metabolic models, and the inner vertices, which represent two branches that each have more than one vertex.

We start our phylogenetic tree with a vertex v_0 that will be its root. Then two vertices v_1, v_2 are hanged from v_0 . Each one of these vertices represents one of the two connected components of the network $T \setminus \{e'_1\}$. Let us see what to do with v_1 and v_2 according to the case.

- If we are in case (a), one of these two vertices, for instance v_1 , represents the vertex A_{μ_0} , and v_2 represents the other connected component of T which is a subgraph of T generated by the vertex of $V \setminus \{A_{\mu_0}\}$.
- If we are in case (b), one of the vertices, for instance v_1 , represents the connected component of $T \setminus \{e'_1\}$ that contains A_{μ_0} , and the other vertex, v_2 , represents the connected component of $T \setminus \{e'_1\}$ that contains A_{v_0} .

This procedure is repeated again with v_1 and v_2 and by removing e'_2 from $T \setminus \{e'_1\}$. When we remove e'_2 , then either the connected component that represents v_1 or v_2 is split into two smaller ones, and the vertex associated with this component plays again the role of v_0 . This process is repeated until we remove all the edges.

Let us see with two examples how it works:

1. In Table 4, we have the weights associated with a set of 10 organisms. We can represent them by a complete weighted network in which every organism is connected with the others. This is a weighted network, so that we can apply the Kruskal algorithm in order to get a minimum spanning tree of this network, which is represented in Figure 2. Following the aforementioned

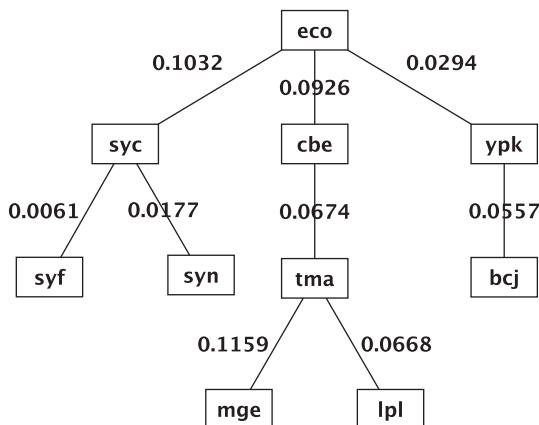
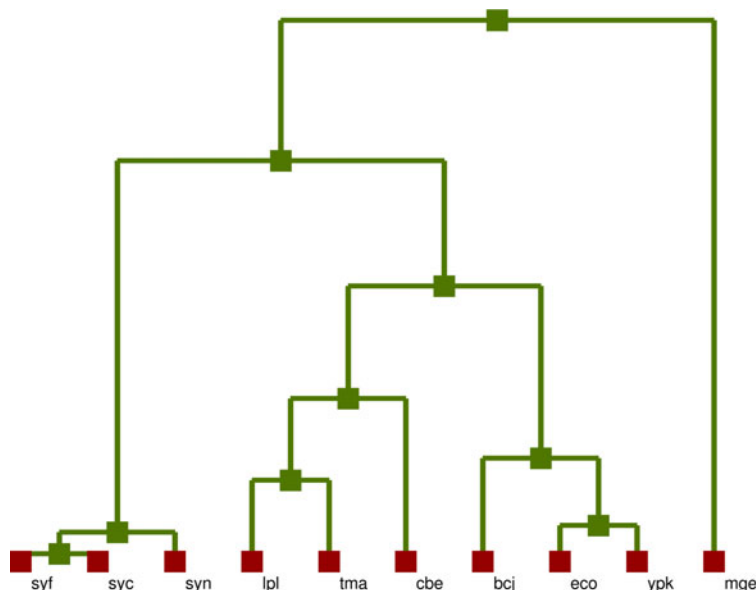


FIG. 2. A minimum spanning tree associated with 10 organisms.

FIG. 3. A phylogenetic tree with 10 organisms.



notation, e'_1 corresponds to the edge that connects *mge* with *tma*, weighting 0.1159. We can see in Figure 3 that two vertices are hanging from the root of the tree. The one on the left represents the *mge*; the one on the right represents the subgraph associated with the rest of vertices, where *tma* can be found.

2. In the case of 38 organisms, when we remove from the minimum spanning tree the edge with maximum weight, we split this tree into two connected components: the one associated with the pair *mge* and *mpm*, and the one associated to the other vertices.

Finally, the vertices in the phylogenetic tree can keep more information concerning the aforementioned minimum spanning tree. Suppose that the height of our phylogenetic tree is $w(e'_1)$, which represents the maximum weight in the minimum spanning tree (i.e., the weight associated with e'_1). We place the root of our phylogenetic tree at height $y = w(e'_1)$. Now, two vertex are hanged from the root. If one is associated with a single vertex, for instance, v_1 in case (a), then we place this vertex at height $y = 0$. We remember that this vertex represents the organism $A_{\mu 0}$. If not, for instance, v_2 in case (a) and either v_1 or v_2 in case (b), each one of these vertices represents a connected component with more than one vertex in which the minimum spanning tree is split. In order to know at which height we should put these vertices, we have to continue removing edges from the former tree. After removing e'_2 , one of these connected components, for instance, the one represented by v_2 , is split again into two smaller connected components. So we place the vertex v_2 at height $w(e'_2)$. We repeat this process recursively until the initial tree is just reduced to isolated vertices.

4. RESULTS AND DISCUSSION

We have reconstructed two phylogenetic trees, one with 10 bacteria and another one with both prokaryotes and eukaryotes. In Table 4 we show the parameter ζ for the pairwise comparison of the 10 prokaryotes in the first tree. The data for the comparison of the 33 organisms in the second tree is given in the Supplementary Material (available online at www.liebertonline.com/cmb).

The organisms in each comparison are:

- 10 organisms tree \rightarrow *Mycoplasma genitalium* (*mge*), *Lactobacillus plantarum* WCFS1 (*lpl*), *Synechocystis* sp. PCC 6803 (*syn*), *Synechococcus elongatus* PCC7942 (*syf*), *Synechococcus elongatus* PCC6301 (*syc*), *Clostridium beijerinckii* (*cbe*), *Burkholderia cenocepacia* J2315 (*bcj*), *Escherichia coli* K-12 MG1655 (*eco*), *Thermotoga maritima* (*tma*), and *Yersinia pestis* KIM10 (*ypk*).

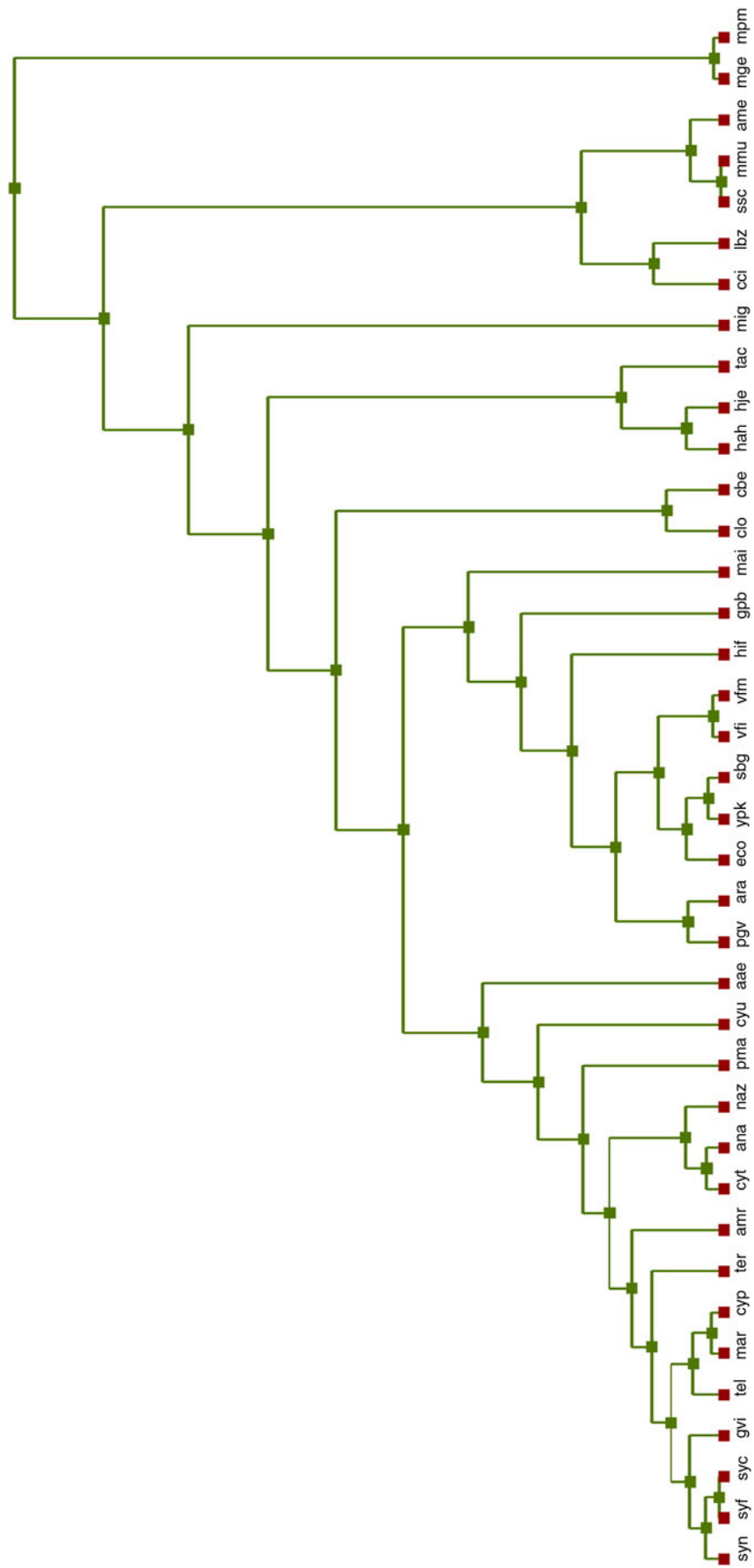


FIG. 4. A phylogenetic tree with 38 organisms.

TABLE 5. SENSIBILITY STUDY 1

<i>org</i> \ <i>org</i>	<i>syn</i>	<i>syf</i>	<i>eco</i>	<i>mge</i>
<i>syn</i>	0.0002 ± 0.0003	0.0184 ± 0.0005	0.0893 ± 0.0005	0.1600 ± 0.0014
<i>syf</i>	0.0184 ± 0.0004	0.0002 ± 0.0003	0.0857 ± 0.0006	0.1527 ± 0.0014
<i>eco</i>	0.0892 ± 0.0005	0.0856 ± 0.0005	0.0001 ± 0.0002	0.1278 ± 0.0009
<i>mge</i>	0.1597 ± 0.0025	0.1527 ± 0.0026	0.1283 ± 0.0015	0.0014 ± 0.0016

Sensibility calculation for $N_t = 500$ and $n_K = 5$. Each element in the table is the average of the parameter ζ in an ensemble plus (minus) its standard deviation ($\bar{\zeta} \pm \sigma_{\zeta}$).

- 38 organisms tree → *Mycoplasma genitalium* (mge), *Mycoplasma pneumoniae* 309 (mpm), *Synechocystis* sp. PCC 6803 (syn), *Synechococcus elongatus* PCC7942 (syf), *Synechococcus elongatus* PCC6301 (syc), *Clostridium beijerinckii* (cbe), *Salmonella bongori* (sbg), *Escherichia coli* K-12 MG1655 (eco), *Aquifex aeolicus* (aae), *Yersinia pestis* KIM 10 (ypk), *Cyanobacterium* UCYN-A (cyu), *Thermosynechococcus elongatus* (tel), *Microcystis aeruginosa* (mar), *Cyanothece* sp. ATCC 51142 (cyt), *Cyanothece* sp. PCC 8801 (cyp), *Gloeobacter violaceus* (gvi), *Anabaena* sp. PCC7120 (ana), *Anabaena azollae* 0708 (naz), *Prochlorococcus marinus* SS120 (pma), *Trichodesmium erythraeum* (ter), *Acaryochloris marina* (amr), *Halophilic archaeon* (hah), *Polymorphum gilvum* (pgv), *Micavibrio aeruginosavorus* (mai), *Agrobacterium radiobacter* K84 (ara), *Clostridiales genomsp.* BVAB3 (clo), *Gamma proteobacterium* HdN1 (gpb), *Vibrio fischeri* ES114 (vfi), *Vibrio fischeri* MJ11 (vfm), *Haemophilus influenzae* F3031 (hif), *Coprinopsis cinerea* (cci), *Sus scrofa* (ssc) and *Leishmania braziliensis* (lbz), *Mus musculus* (mmu), *Apis mellifera* (ame), *Methanotorris igneus* (mig), *Halalkalicoccus jeotgali* (hje), and *Thermoplasma acidophilum* (tac).

In Figures 3 and 4 we present the two phylogenetic trees that we have constructed. In the first tree, the only organism displaced in relation to what is expected from standard methods of phylogenetic tree reconstruction is the tma. In both trees mge (and mpm in the second one) diverges from other organisms at the beginning of the tree. This happens because of their minimalistic genomes, with only a couple hundred metabolites in their metabolomes. As a result, when compared with an organism without a reduced genome with almost a thousand metabolites, several hundred metabolites will not have a correspondent one, increasing hugely the value of α in the calculation of the parameter ζ , and therefore distancing these organisms from the rest. The problem with these parasitic organisms has been noticed elsewhere (Fukami-Kobayashi et al., 2007), but unfortunately the solution found in this article did not yield better results in our present study. One should keep in mind that the present approach only considers genes (and proteins) associated with metabolic reactions and moreover, considers only the existence/absence of the enzymes (reactions). Our work yields results that are very close to the tree of life, in spite of using only a subset of all genome's information. It was not our intention to build trees that would address properly minimal organisms' phylogenies, but to prove the feasibility of building those trees using only reactome data. In any case, for the second study we used organisms from very different origins in the evolutionary history, and we found that the method is able to separate bacteria, archaea, and eukaryotes. Different strains of the same species also appear closely related and share branches with organisms from the same family and order.

We have also studied the sensibility of the parameter ζ . For this we performed a Monte Carlo analysis of ζ . The procedure for this analysis is explained as follows. Given two organisms, one of them remains the wild type while, with the other, one builds an ensemble with N_t elements, where each element is the result

TABLE 6. SENSIBILITY STUDY 2

<i>org</i> \ <i>org</i>	<i>syn</i>	<i>syf</i>	<i>eco</i>	<i>mge</i>
<i>syn</i>	0.0005 ± 0.0005	0.0186 ± 0.0006	0.0896 ± 0.0007	0.1604 ± 0.0018
<i>syf</i>	0.0187 ± 0.0006	0.0005 ± 0.0005	0.0860 ± 0.0007	0.1532 ± 0.0019
<i>eco</i>	0.0893 ± 0.0008	0.0857 ± 0.0007	0.0003 ± 0.0003	0.1281 ± 0.0011
<i>mge</i>	0.1602 ± 0.0035	0.1531 ± 0.0032	0.1288 ± 0.0023	0.0028 ± 0.0023

Sensibility calculation for $N_t = 500$ and $n_K = 10$. Each element in the table is the average of the parameter ζ in an ensemble plus (minus) its standard deviation ($\bar{\zeta} \pm \sigma_{\zeta}$).

TABLE 7. SENSIBILITY STUDY 3

<i>org</i> \ <i>org</i>	<i>syn</i>	<i>syf</i>	<i>eco</i>	<i>mge</i>
<i>syn</i>	0.0028 ± 0.0011	0.0209 ± 0.0014	0.0915 ± 0.0017	0.1652 ± 0.0045
<i>syf</i>	0.0207 ± 0.0013	0.0029 ± 0.0011	0.0879 ± 0.0016	0.1575 ± 0.0044
<i>eco</i>	0.0903 ± 0.0017	0.0868 ± 0.0016	0.0016 ± 0.0007	0.1301 ± 0.0029
<i>mge</i>	0.1638 ± 0.0080	0.1577 ± 0.0077	0.1343 ± 0.0055	0.0170 ± 0.0053

Sensibility calculation for $N_t = 500$ and $n_K = 50$. Each element in the table is the average of the parameter ζ in an ensemble plus (minus) its standard deviation ($\bar{\zeta} \pm \sigma_\zeta$).

of n_K knock-outs (removal of n_K randomly selected reactions from the metabolic model) in the organism. Then the calculation of ζ is performed between the wild-type organism and each organism in the knock-out ensemble. From this process one obtains an ensemble of N_t values of ζ for the comparison (one from each version of the organism in the knock-out ensemble), from which one calculates its average and standard deviation. This standard deviation is treated as an indicator of the sensibility of the parameter (as a function of the number of knock-outs).

We performed this sensibility analysis for four organisms (*syn*, *syf*, *eco*, and *mge*) with ensembles of sizes $N_t = 500$ for $n_K = 5, 10, 50,$ and 100 . The results are shown in Tables 5 through 8. These four organisms have been chosen to observe the sensibility in the comparison between very similar organisms (*syn* and *syf*), more distant ones (*syn* and *eco*), and very different ones (*syn* and *mge*).

This sensibility analysis mainly reflects the uncertainties in the calculation of the metabolic distances. Since the distance parameter is based on metabolic models, one relies in the genome annotations for each organism and any annotation is usually faulty. One may miss enzymes or wrongly annotate existing ones. The models used in this study have been automatically generated from a database constructed from information downloaded from the KEGG database (Kanehisa and Goto, 2000), and since the beginning of this study the databases have been updated and most models have to be changed as well. The “knocked-out” models used for the sensibility parameter analysis simulate such imperfect annotations: one might consider the situation with $n_K = 5$ as the model constructed from a well-annotated genome, while the case with $n_K = 100$ is the model resulting from a very poor annotation. One can see that when only a few enzymes might be missing from the annotation, the error in the parameter can be expected to be less than 1%, except for the case of the minimalistic genomes like the parasitic *mge*, that has an error more than five times bigger than the other organisms. This error increases as the number of knock-outs increase, but it keeps below 5% even for 100 knockouts (or missing enzymes), except again in the case of the *mge*, but even for the *mge* it is below 10%. This shows that the methodology is robust and that one works here with an uncertainty of less than 5% in most of the cases.

5. CONCLUSIONS AND OVERVIEW

In this work, we have developed a methodology for comparing organisms based on their metabolic networks. This methodology has been successfully applied for the reconstruction of phylogenic trees for several organisms from a broad range of families and kingdoms. Resulting trees stand up well to their comparison with the so-called “tree of life.” The great majority of the branches in the tree fit their expected

TABLE 8. SENSIBILITY STUDY 4

<i>org</i> \ <i>org</i>	<i>syn</i>	<i>syf</i>	<i>eco</i>	<i>mge</i>
<i>syn</i>	0.0058 ± 0.0016	0.0239 ± 0.0020	0.0942 ± 0.0024	0.1715 ± 0.0062
<i>syf</i>	0.0238 ± 0.0018	0.0061 ± 0.0017	0.0907 ± 0.0023	0.1630 ± 0.0066
<i>eco</i>	0.0919 ± 0.0024	0.0883 ± 0.0022	0.0033 ± 0.0011	0.1329 ± 0.0040
<i>mge</i>	0.1694 ± 0.0120	0.1648 ± 0.0131	0.1433 ± 0.0092	0.0460 ± 0.0076

Sensibility calculation for $N_t = 500$ and $n_K = 100$. Each element in the table is the average of the parameter ζ in an ensemble plus (minus) its standard deviation ($\bar{\zeta} \pm \sigma_\zeta$).

positions well and their distance is in good correlation with evolutionary distances. The discrepancies found can be explained by particularities in these very few organisms not fitting the tree, such as tremendous genome reductions that caused reduced metabolisms.

Our methodology is innovative for it is not directly based on the structure and evolution of proteins or DNA but on the metabolism and the organisms' components and metabolic capabilities, allowing one to compare organisms very distant from the evolutionary point of view or organisms for which orthologs' comparison is difficult. In order to accomplish this, we make use of the correlation between evolutionary distances and metabolic network likelihood and propose our methodology as a starting point to study it.

Metabolism information is retrieved as a subset of the whole genome information. We hereby show that metabolic network connectivity can be used to build phylogenetic trees that are in accordance with gene-directed trees. It can be argued whether the selected construction parameter (ζ) is the optimal one for this purpose (or even if there is an optimal one), but it stands clear that this is an innovative application for metabolic models, their curation, and cross-species evolutionary studies.

We have also performed a sensibility study in which we show that the methodology is robust even if the annotation information used to construct the metabolic models is faulty. This study also suggests an upper-bound for the uncertainty in the distance parameter of approximately 5%.

ACKNOWLEDGMENT

The research leading to these results has received funding from the European Union Seventh Framework Program (FP7/2007-2013) under grant agreement number 308518 (CyanoFactory).

AUTHOR DISCLOSURE STATEMENT

The authors declare that no competing financial interests exist.

REFERENCES

- Angermayr, S.A., Hellingwerf, K.J., Lindblad, P., and de Mattos, M.J. 2009. Energy biotechnology with cyanobacteria. *Curr. Opin. Biotechnol.* 20, 257–263.
- Barrett, C.L., Kim, T.Y., Kim, H.U., et al. 2006. Systems biology as a foundation for genome-scale synthetic biology. *Curr. Opin. Biotechnol.*, 17, 488–492.
- Boghigian, B.A., Seth, G., Kiss, R., and Pfeifer, B.A. 2010. Metabolic flux analysis and pharmaceutical production. *Metab. Eng.* 12, 81–95.
- Brady, A., and Salzberg, S. 2011. PhymmBL expanded: confidence scores, custom databases, parallelization and more. *Nat. Methods* 8, 367.
- Edwards, J., Ramakrishna, R., Schilling, C., and Palsson, B. 1999. *Metabolic Flux Balance Analysis*. In *Metabolic Engineering*. Marcel Dekker Inc., New York.
- Edwards, S.V. 2009. Is a new and general theory of molecular systematics emerging? *Evolution* 63, 1–19.
- Fukami-Kobayashi, K., Minezaki, Y., Tateno, Y., and Nishikawa, K. 2007. A tree of life based on protein domain organizations. *Mol. Biol. Evol.* 24, 1181–1189.
- Gray, R.D., Drummond, A.J., and Greenhill, S.J. 2009. Language phylogenies reveal expansion pulses and pauses in Pacific settlement. *Science* 323, 479–483.
- Green, R.E., Krause, J., Briggs, A.W., 2010 A draft sequence of the Neandertal genome. *Science* 328, 710–722.
- Grenfell, B.T., Pybus, O.G., Gog, J.R., 2004. Unifying the epidemiological and evolutionary dynamics of pathogens. *Science* 303, 327–332.
- Gross, J.L., and Yellen, J. 2005. *Graph Theory and Its Applications, Second Edition (Discrete Mathematics and Its Applications)*. Chapman and Hall/CRC.
- Guimera, R., and Nunes Amaral, L.A., 2005. Functional cartography of complex metabolic networks. *Nature* 433, 895–900.
- Kanehisa, M., and Goto, S. 2000. KEGG: kyoto encyclopedia of genes and genomes. *Nucleic Acids Res.* 28, 27–30.
- Kellis, M., Patterson, N., Endrizzi, M., et al. 2003. Sequencing and comparison of yeast species to identify genes and regulatory elements. *Nature* 423, 241–254.
- Marra, M.A., Jones, S.J., Astell, C.R., et al. 2003. The genome sequence of the SARS-associated coronavirus. *Science* 300, 1399–1404.

- Maser, P., Thomine, S., Schroeder, J.I., et al. 2001. Phylogenetic relationships within cation transporter families of *Arabidopsis*. *Plant Physiol.* 126, 1646–1667.
- Montagud, A., Navarro, E., Fernandez de Cordoba, P., et al. 2010. Reconstruction and analysis of genome-scale metabolic model of a photosynthetic bacterium. *BMC Syst. Biol.* 4, 156.
- Montagud, A., Zelezniak, A., Navarro, E., et al. 2011a. Flux coupling and transcriptional regulation within the metabolic network of the photosynthetic bacterium *Synechocystis* sp. PCC6803. *Biotechnol. J.*, 6, 330–342.
- Morange, M. 2009. A new revolution? The place of systems biology and synthetic biology in the history of biology. *EMBO Rep.* 10, S50–S53.
- Nevoigt, E. 2008. Progress in metabolic engineering of *Saccharomyces cerevisiae*. *Microbiol. Mol. Biol. Rev.* 72, 379–412.
- Nielsen, J. 2001. Metabolic engineering. *Appl. Microbiol. Biotechnol.* 55, 263–283.
- Oberhardt, M.A., Palsson, B.O., and Papin, J.A. 2009. Applications of genome-scale metabolic reconstructions. *Mol. Syst. Biol.* 5, 320.
- Patil, K.R., Akesson, M., and Nielsen, J. 2004. Use of genome-scale microbial models for metabolic engineering. *Curr. Opin. Biotechnol.* 15, 64–69.
- Reyes, R., Gamermann, D., Montagud, A., 2012. Automation on the generation of genome-scale metabolic models. *J. Comput. Biol.* 19, 1295–1306.
- Salipante, S.J., and Horwitz, M.S. 2006. Phylogenetic fate mapping. *Proc. Natl. Acad. Sci. U.S.A.* 103, 5448–5453.
- Stephanopoulos, G.N., Aristidou, A.A., and Nielsen, J. 1998. *Metabolic Engineering: Principles and Methodologies*. Academic Press.
- Stolyar, S., Van Dien, S., Hillesland, K.L., et al. 2007. Metabolic modeling of a mutualistic microbial community. *Mol. Syst. Biol.* 3, 92.
- Yang, Z., and Rannala, B. 2012. Molecular phylogenetics: principles and practice. *Nat. Rev. Genet.* 13, 303–314.

Address of correspondence:

Dr. Daniel Gamermann
Instituto de Física
Universidade Federal do Rio Grande do Sul
Av. Bento Gonçalves 9500
Caixa Postal 15051, 91501-970
Porto Alegre RS, Brazil

E-mail: daniel.gamermann@ucv.es